

EBONE



European Biodiversity Observation Network:

Design of a plan for an integrated biodiversity observing system
in space and time

Assessing the role of EO in biodiversity monitoring. Options for integrating *in-situ* observations with EO within the context of the EBONE concept.

Deliverable 5.5¹

Ver 2.0

Document date: 2012-04-24

Document Ref.: EBONE-D5.5-2.0

Authors: F. Gerard¹, L. Blank³, R.G.H. Bunce⁴, Y. Carmel³, G. Caudullo⁵, N. Clerici⁵, M. Deshayes⁶, L. Erikstad⁷, C. Estreguil⁵, E. Framstad⁷, A-H. Granholm¹⁰, A. Halabuk⁸, L. Halada⁸, R. Harari-Kremer⁹, G.W. Hazeu⁴, S.M. Hennekens⁴, J. Holmgren¹⁰, T. Kikas¹¹, V. Kuusemets¹¹, M. Lang¹¹, N. Levin⁹, M. Luck-Vogel¹², D. Morton¹, C.A Mùcher⁴, M. Nilsson¹⁰, K. Nordkvist¹⁰, H. Olsson¹⁰, L. Olsvig-Whittaker¹³, J. Raet¹¹, W. Roberts¹², G.J. Roerink⁴, K. Sepp¹¹, P. Scholefield¹, A. Vain¹¹, H. Van Calster², C. J. Weissteiner⁵.

Reviewer: H. Olsson¹⁰

¹ Centre for Ecology and Hydrology (CEH), UK; ² Research Institute for Nature and Forest (INBO), Belgium; ³ Faculty of Civil and Environmental Engineering, Technion – Israel Institute of Technology, Israel; ⁴ ALTERRA, The Netherlands; ⁵ Joint Research Centre - Institute for Environment and Sustainability, EC-DG, Italy; ⁶ L'institut de recherche en sciences et technologies pour l'environnement (CEMAGREF), France; ⁷ Norwegian Institute for Nature Research (NINA), Norway; ⁸ Institute of Landscape Ecology, Slovak Academy of Sciences (ILE-SAS), Slovak Republic; ⁹ Department of Geography, The Hebrew University of Jerusalem, Israel; ¹⁰ Department of forest resource management, Swedish University of Agricultural Sciences (SLU), Sweden; ¹¹ Institute of Agricultural and Environmental Sciences, Estonian University of Life Sciences, Estonia; ¹² Council for Scientific and Industrial Research (CSIR), S-Africa; ¹³ Israel Nature and Parks Authority (INPA), Israel

EC-FPV Contract Ref: ENV-CT-2008-212322

¹ The original title of the D5.5 report as listed in the EBONE DoW was: *Report on the technical best integration in GEO data streams of current and future EO data sources in and outside EU.*



Table of Contents

1. Introduction	4
2. Habitat extent - The link between <i>in-situ</i> observations and Earth observation.	6
2.1. Mapping according to a habitat classification system	6
2.2. Introducing physical environmental variables	10
2.3. EO mapping of GHC, summary of test cases	11
<i>LiDAR – airborne (Annex-2, 3, 4)</i>	12
<i>Hyperspectral – airborne (Annex-5)</i>	12
<i>Thematic Mapper – satellite (Annex-6, 7, 8)</i>	15
<i>MODIS – satellite (deliverable D5.2, Annex-2)</i>	15
2.4. Landscape complexity	16
3. Habitat extent - Methods for integrating <i>in-situ</i> and EO	17
3.1. Inter-calibration of EO and <i>in-situ</i> monitoring.....	17
3.2. Post stratification (Deliverable 5.4).....	18
3.3. Training the classification of EO imagery using <i>in-situ</i> samples.....	19
3.4. Sampling strategies (Deliverable 5.4).....	20
4. Habitat extent - The impact of spatial and thematic detail on change detection (Annex-9)....	23
5. Habitat extent - EO in support of the field work.....	25
6. Habitat - pattern related measures (Deliverable D5.3).....	27
7. Conclusions and recommendations.....	29
8. References.....	31
9. Annexes	34

1. Introduction

The **European Biodiversity Observation Network (EBONE)** is a European contribution on terrestrial monitoring to GEO BON, the Group on Earth Observations Biodiversity Observation Network. EBONE's aims are to develop a system of biodiversity observation at regional, national and European levels by assessing existing approaches in terms of their validity and applicability starting in Europe, then expanding to regions in Africa. The objective of EBONE is to deliver:

1. A sound scientific basis for the production of statistical estimates of stock and change of key indicators;
2. The development of a system for estimating past changes and forecasting and testing policy options and management strategies for threatened ecosystems and species;
3. A proposal for a cost-effective biodiversity monitoring system.

There is a consensus that **Earth Observation (EO) has a role to play in monitoring biodiversity**. With its capacity to observe detailed spatial patterns and variability across large areas at regular intervals, our instinct suggests that EO could deliver the type of spatial and temporal coverage that is beyond reach with *in-situ* efforts. Furthermore, when considering the emerging networks of *in-situ* observations, the prospect of enhancing the quality of the information whilst reducing cost through integration is compelling. This report gives a **realistic assessment** of the role of EO in biodiversity monitoring and the options for integrating *in-situ* observations with EO within the context of the EBONE concept (cfr. EBONE-ID1.4). The assessment is mainly based on a set of targeted pilot studies. Building on this assessment, the report then presents a series of **recommendations** on the best options for using EO in an effective, consistent and sustainable biodiversity monitoring scheme.

The **issues** that we faced were many:

1. Integration can be interpreted in different ways. One possible interpretation is: the combined use of independent data sets to deliver a different but improved data set; another is: the use of one data set to complement another dataset.
2. The targeted improvement will vary with stakeholder group: some will seek for more efficiency, others for more reliable estimates (accuracy and/or precision); others for more detail in space and/or time or more of everything.
3. Integration requires a link between the datasets (EO and *in-situ*). The strength of the link between reflected electromagnetic radiation and the habitats and their biodiversity observed *in-situ* is function of many variables, for example: the spatial scale of the observations; timing of the observations; the adopted nomenclature for classification; the complexity of the landscape in terms of composition, spatial structure and the physical environment; the habitat and land cover types under consideration.
4. The type of the EO data available varies (function of e.g. budget, size and location of region, cloudiness, national and/or international investment in airborne campaigns or space technology) which determines its capability to deliver the required output.

EO and *in-situ* could be combined in different ways, depending on the type of integration we wanted to achieve and the targeted improvement. We aimed for an improvement in accuracy (i.e. the reduction in error of our indicator estimate calculated for an environmental zone). Furthermore, EO would also provide the spatial patterns for correlated *in-situ* data.

EBONE in its initial development, focused on three main indicators covering:

- (i) the extent and change of habitats of European interest in the context of a general habitat assessment;
- (ii) abundance and distribution of selected species (birds, butterflies and plants); and
- (iii) fragmentation of natural and semi-natural areas.

For **habitat extent**, we decided that it did not matter how *in-situ* was integrated with EO as long as we could demonstrate that acceptable accuracies could be achieved and the precision could consistently be improved. The nomenclature used to map habitats *in-situ* was the General Habitat Classification. We considered the following options where the EO and *in-situ* play different roles:

- using *in-situ* samples to re-calibrate a habitat map independently derived from EO;
- improving the accuracy of *in-situ* sampled habitat statistics, by post-stratification with correlated EO data;
- using *in-situ* samples to train the classification of EO data into habitat types where the EO data delivers full coverage or a larger number of samples.

For some of the above cases we also considered the impact that the **sampling strategy** employed to deliver the samples would have on the accuracy and precision achieved.

Restricted access to European wide species data prevented work on the indicator '**abundance and distribution of species**'.

With respect to the indicator '**fragmentation**', we investigated ways of delivering EO derived **measures of habitat patterns** that are meaningful to sampled *in-situ* observations.

2. Habitat extent - The link between *in-situ* observations and Earth observation.

2.1. Mapping according to a habitat classification system

EO instruments record reflected, scattered or emitted electromagnetic signals which vary in function of the physical and chemical properties of the viewed surface type. Two types of information can be derived from EO data (Figure 1): quantitative estimates of physical or chemical properties (i.e. a map of for example soil moisture, surface temperature or canopy cover) or a map of thematic classes representing areas with similar reflected, scattered or emitted electromagnetic signals, texture, patterns or shapes. EO derived products of land cover, habitats and species (flora) belong to the second category.

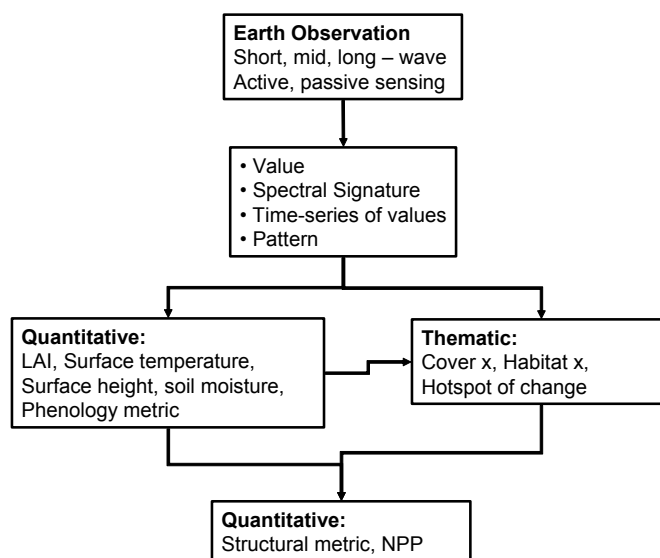


Figure 1: Schematic illustrating the difference between the quantitative and thematic measures derived from Earth Observation.

The observation and recording of land cover, habitats and species require classification systems. Their design results from a compromise between scope of use, level of detail and spatial application. EO introduces not only full area and frequent coverage, but also a new and unique set of classification parameters, such as, reflectance, texture, height or patterns. The degree in which a relationship can be established between electromagnetic signals and the thematic classes (e.g. physiognomic, floristic or ecological) required by the biodiversity monitoring community, will determine the usefulness of the EO derived thematic maps. However, depending on the role EO is being assigned the strength of this relationship needed for a successful outcome will vary (see section 3).

The quality and detail achieved when mapping land cover using EO is primarily limited by the manner in which the electromagnetic radiation interacts with the physical and chemical properties of the land surface. In other words, if habitat classes of interest respond similarly across the whole spectrum in terms of visible and near-infrared reflectance, thermal emission, and microwave scattering, separating these into distinct classes on a map using EO is not feasible. By adopting an EO based perspective of habitats it is possible to predict the EO mapping success for classes of existing habitat nomenclatures (Medcalf et al. 2011). For example, in the case of grassland types, spectral variability is expected to be influenced by, amongst others, the ratio of living plant material to dead plant material; the proportion of plants with horizontal leaves as opposed to upright leaves; the productivity of the vegetation; the wetness of the vegetation and underlying soil; and the density and height of the sward.

This general knowledge can be used to develop a framework, such as that of Mark Crick, for assessing the mapping potential of a habitat class by EO (Tables 1 and 2).

Table 1: The Crick Framework describing the options for mapping habitats as a tiered system (Source: Medcalf et al. 2011). VHR = Very High Resolution.

Tier 1						Likely to be identified solely using EO											
Likely to be identified using EO and ancillary data																	
Tier 2 ¹		Tier 2a - Likely to be identified using EO together with ancillary data		Tier 2b - Likely to be identified using VHR EO together with ancillary data		Tier 2c ² - Likely to be identified using EO data (in some cases VHR) but ID dependent on good geological data		Tier 2d - Likely to be identified using EO methods such as fuzzy membership values		Tier 2e - Likely to be identified using EO including LiDAR to give detailed information about vegetation structure							
Likely to be identified using EO and ancillary data but also dependant on availability of time series of imagery																	
Tier 3		Tier 3a - Likely to be identified using EO together with ancillary data				Tier 3b - Likely to be identified using VHR EO together with ancillary data				Tier 3c - Likely to be identified using EO data (in some cases VHR) but ID dependent on good geological data							
Currently unlikely to be determined using EO																	
Tier 4		Tier 4a - Habitats distinguished by low frequency or small features				Tier 4b - Habitat hidden from above for most of the year											
Tier 5												Cannot be identified using EO					

Table 2: The Crick Framework applied to 2 Nomenclatures: total number of classes detectable per mapping option (Source: Medcalf et al. 2011)

		UK BAP Priority Habitats	EC Habitats Directive Annex I habitats
Tier 1		0	0
Tier 2	2a	6	6
	2b	7	2
	2c	2	5
	2d	1	1
	2e	1	1
Tier 3	3a	6	5
	3b	9	11
	3c	4	6
Tier 4	4a	3	26
	4b	12	9
Tier 5		0	3
Total		51	75

A similar framework could be used to design a more ‘EO friendly’ habitat nomenclature. The work of Paradella et al. (1994) suggested that physiognomy may be the most important attribute which influences the EO response of vegetation. Jakubauskas et al. (2002), Moody and Johnson (2001) and Hill et al. (submitted) used time series of EO, exploiting differences in phenology to successfully map crop types, vegetation types or tree species.

The BioHab General Habitat Categories (GHC) classification system, adopted by EBONE for *in-situ* monitoring, is based on 21 or 34 plant life forms (Bunce et al. 2008), their % covers within a mapping element and a number of optional qualifiers (life form, environmental and management). The use of plant life forms enables the recording of habitats with comparable structures within contrasting bio-geographical zones. Based on the hypothesis that habitat structure is related to the environment, the GHC are also expected to correspond to phytosociological classes at high level. This makes the classification system not only applicable throughout the world, but also more amenable to EO’s sensitivity to vegetation physiognomy

and cover. A set of EBONE test cases provide an insight into the EO mapping accuracies that could be achieved when using the GHC and further confirm the existence of a tier system as described in the Crick Framework (see section 2.3).

When continental or global consistency in EO methodology is imposed, the variety of EO data types and approaches available is greatly reduced. As a result, the current global, continental and national land cover maps produced from EO have been limited to reporting the extent of major vegetation types or 'broad habitats' at pixel sizes ranging from 1km to 25m with total number of vegetation classes ranges between 7 and 36 (Table 3). An investigation carried out by UNEP-WCMC found that although these land cover maps are a useful resource for indicating the distribution of broad habitats, they are inadequate for detailed biodiversity or habitat monitoring by land managers (Strand et al. 2007). The main reason is that the class number and type and the spatial detail of these products do not come anywhere near the thematic and spatial detail produced from a classification system such as the GHC (minimum mapping unit of 400m²; total of 160 GHC with the average of classes found ranging substantially between zones), the UK BAP priority habitats (51 classes) or European Annex I habitats (75 classes). Reducing the spatial extent of a land cover map, is likely to enable more spatially and/or thematically detailed analysis, as relatively more resources can be made available for the task at hand (i.e. cost/km²).

A mapping effort of special relevance for European level monitoring is the recently started GIO project (GMES Initial Operations), which will produce pan-European data sets. The exact definitions are not determined yet, but the current plans for the forest part is to produce 20m pixel raster data sets with canopy coverage and forest type, based on data from IRS LISS3 and SPOT, complemented with data from RapidEye and AWIFS for improved phenology data.

Table 3: The spatial and thematic detail provided by the global, international and national land cover maps derived from Earth observation.

Land cover map	Pixel size or * MMU ²	N° Classes Total	N° Classes Vegetation + Arable
IGBP (Loveland and Belward, 1997)	1 km	17	10+2
GLC2000 (Bartholome and Belward, 2005)	1 km	22	15+3
MOD12Q1 PFT (Friedl et al., 2002)	1 km	11	5+2
GLOBCOVER (Arino et al., 2005)	300 m	22	10+4
Land cover map of South America (Eva et al., 2004)	1km	31	21+4
CORINE Land Cover level 3, Europe	250,000 m ² *	44	14+11
Vegetation cover map of India (Kumar Joshi et al., 2004)	188 m	35	20+2
USGS National land cover, US (USGS, 2010)	30 m	43	36+1
National Land Cover Database, US (Homer et al., 2007)	30 m	20	11+2
Land Cover map of UK (Fuller et al., 2005)	25 m	23	13+1
The Netherlands (Thunnissen and deWit, 2000)	25 m	39	19+9
GSD Land cover map, Sweden (Engberg, 2005)	25 m	57	na
Land Cover of Catalonia, Spain (http://www.creaf.uab.es/mcsc)	500 m ² *	61	15+11

One way of testing the suitability of the thematic and spatial information provided by EO derived land cover maps is through correspondence matrices (see D5.1) calculated from co-registering the *in-situ* habitat sample observations with the EO land cover map.

Correspondence matrices are a standard method for assessing mapping accuracy. However, by assessing the clusters of one-to-one, one-to-many and many-to-many relationships within the matrix, this same information can be used to interpret patterns of correspondence or lack-off between *in-situ* habitat and EO land cover classes, helping to understand what

² MMU: minimum mapping unit

makes certain EO derived land cover maps more suitable than others for integration with *in-situ* habitat observations. The preferred outcome would be a near perfect match which would show high correspondence values between individual or small groups of classes, shown as example A of the idealised correspondence tables (Figure 2). The worst case scenario is shown in example B, where there is no clear pattern of correspondence. The reality will be somewhere in between (example C; Source: Deliverable 5.1) and will be function of a variety of factors:

- the strength of the match between the habitat class definitions implemented in the field and the EO-based habitat classes (i.e. the degree in which a relationship can be established between electromagnetic signals and the thematic classes identified in the field);
- mismatches introduced by a less than perfect spatial co-registration of the two layers;
- mismatches associated to differences in spatial scale between the two layers; and finally
- mismatches caused by an element of miss-classification in either or both of the layers (classification errors of EO imagery could be caused by, for example, the use of an unsuitable classification algorithm, or unsuitable or incomplete training sites).

Idealised correspondence tables

Example A:						Example B:					
	A	B	C	D	E		A	B	C	D	E
1	0	3826	0	0	0	1	630	630	630	630	630
2	0	4832	0	0	0	2	630	630	630	630	630
3	0	0	0	557	26	3	630	630	630	630	630
4	0	0	0	1195	752	4	630	630	630	630	630
5	0	0	7599	0	0	5	630	630	630	630	630
6	5328	0	0	0	0	6	630	630	630	630	630
7	0	0	445	0	0	7	630	630	630	630	630
8	667	0	0	0	0	8	630	630	630	630	630

Example C: correspondence table between *in-situ* habitat and EO land cover map layer for 1km² sample

Broad Habitat (CS1998) for 1km ² sample	Land Cover Map UK for 1km ² sample				
	Dwarf Shrub Heath	Fen, Marsh, Swamp	Bog	Acid Grassland	Bracken
Bog (shrub)	57	15	87	13	57
Bog (grass/shrub)	31	79	0	20	4
Bog (grass/herb)	3	5	0	8	15
Inland Rock (Semi natural)	0	0	0	3	13
Coniferous Woodland	8	0	13	0	0
Acid Grassland	1	1	0	57	11

Figure 2: Tables demonstrating how correspondence can help reveal how well the class definitions and classification methods of two products (EO and *in-situ*) match up.

EBONE looked into this further by exploring the correspondence between the following *in-situ* and EO derived layers (Deliverable D5.1):

- the UK 2000 *in-situ* countryside survey samples (591 1km² *in-situ* samples) and the UK land cover map 2000 (25m grid cell resolution) both of which show the same habitat classes.
- the UK 2000 *in-situ* countryside survey samples (591 1km² *in-situ* samples) translated to GHC (Metzger et al, 2005) compared with the CORINE Land Cover 2000 classes (100m grid cell resolution).

The main findings were that fewer and more generic thematic classes result in higher correspondences, whilst increased discrepancies in spatial scale between *in-situ* and EO derived habitats maps (i.e. using a low spatial resolution and generalised EO map) will reduce the correspondences that can be achieved.

2.2. Introducing physical environmental variables

Physical environmental variables defining site conditions in detail (e.g. climate, topography, soil type and condition) can to some extent determine the types of habitats present and in some cases, their condition. This is often referred to as ecological modelling. There is evidence that adding environmental variables to the classification of EO imagery improves accuracy and precision. For example, in the UK Land cover map, a soil map was used to separate spectrally similar grassland habitat classes. The USGS national cover map achieves 43 classes (Table 1) by introducing data on elevation and climate. EBONE achieved promising results when implementing a decision tree to predict the location of two Annex I habitat types across Europe using a combination of the existing EO derived European land cover map (CORINE land cover), altitude and soils data and a bioclimatic zonation (Annex-1). Still, the predictive power of environmental variables is expected to decrease where the landscape has had a long history of human intervention or land management. Also, the spatial detail and quality of the environmental data used will heavily influence the detail and quality of the ensuing habitat map. Currently, these spatially detailed (1-10m resolutions) environmental data often do not exist.

In the future, some of these environmental variables could become available. A recently launched satellite pair will soon (2014) deliver a 12 m global digital elevation model (http://www.infoterra.de/tandem-x_dem) from SAR data. Surface height models or elevation models, derived from airborne LiDAR data, are for an increasing number of countries, available at 1 to 5m resolutions. But other operational satellite EO products, such as, rainfall, relative soil moisture and land surface temperature are currently delivering at unsuitable spatial resolutions of 5 degrees, 0.5 degrees to 1km and 1km respectively. Technical bottlenecks need resolving before the acquisition of higher spatial resolution observations of such type of data will become possible. The alternative could be the use of regional land surface atmosphere interaction models to predict environmental variables such as soil moisture and land surface temperature. The quality and the spatial detail of their outputs are determined by (i) the quality and detail of the climate variables used to drive the models and (ii) the quality and suitability of the models. GEO-BON is taking the lead in developing Essential Biodiversity Variables which are required to track future changes in biodiversity. The definition of the EBVs should catalyze the efforts of the EO industry and academics to deliver data that is relevant and useful for monitoring biodiversity.

When available at coarser spatial resolutions, physical environmental variables can form the basis for environmental stratifications (WP3). As demonstrated by work carried out under the EU funded project BIOPRESS (Table 4), introducing such an environmental stratification greatly reduces the one to many relationships between EO Land Cover classes and *in-situ* habitat classes and so refines the thematic links between the two mapping systems.

Table 4: Example showing the importance of using an environmental classification to reduce the number of habitat classes in relation with an EO-based class: a global (Moss & Davies, 2002) versus regional approach for the CLC 3.2.2 ‘Moors and Heathland’ and the corresponding EUNIS classes. The regional approach used quantitative correspondence data produced from Natura2000 sites located within BIOPRESS transect samples (See Biopress45 report). As a result not all EUNIS habitat classes that were linked to CLC 3.2.2 by Moss and Davies (2002) were found. Still, although not representative for the whole area of Europe it demonstrates the potential of a regional approach, (%) is percentage of quantified links (area correspondences), that are attributed to the EUNIS habitat type.

EO-based Class		Corresponding EUNIS habitats
CLC 3.2.2 without a regional approach (From Moss & Davies, 2002)		B1.5, B1.6, B2.5, B2.6, , B3.3, E5.3, F2.2, F2.3, F2.4, F3.1, F3.2, F4.1, F4.2, F4.3, F5.2, F5.4, F6.7, F6.8, F9.1, F9.2, F9.3, G5.6, G5.7
CLC 3.2.2 with a regional approach	Atlantic	F4.2 Wet heath (49%) F7.4 Hedgehog heath (27%) F2.2 Alpine and subalpine heath (11%)
	Continental	F3.1 Temperate thicket and scrub (54%) F2.2 Alpine and subalpine heath (18%) F9.1 Riverine scrub (9%)
	Alpine	F2.2 Alpine and subalpine heath (75%) F2.3 Subalpine and oroboreal bush communities (10%) F2.4 Pinus mugo scrub (9%)
	Mediterranean	F5.1 Arborescent matorral (36%) F7.4 Hedgehog heath (31%) Minor: F3.2 Mediterraneo-montane thickets, F2.2 Alpine and subalpine heath, F3.1 Temperate thicket and scrub , F6.7 Mediterranean gypsum scrub, F9.3 Southern riparian thickets.

2.3. EO mapping of GHC, summary of test cases

The test cases looked into five EO data options for mapping the GHC (Table 5).

- Lidar (Airborne; 26 - 0.45 pts /m²; digital elevation and surface height model, signal intensity derived from NIR signal; single date);
- Hyperspectral (Airborne; 5 m pixel; 127 bands covering the visible, NIR and SWIR; single date);
- Thematic Mapper (Satellite; 25 - 30 m pixel; 7 spectral bands covering the visible, NIR and SWIR; single date);
- Spot Image (Satellite; 10 m and 20 m pixel; 4 spectral bands covering visible, NIR and SWIR; single date);
- MODIS (Satellite; 0.25 – 1 km pixel; Vegetation index derived from visible and NIR spectrum; time-series).

Almost all test cases had a similar setup: the 1km² field samples, surveyed following the protocols described in the GHC handbook (D4.3), were used to train and validate the mapping success. Different EO data types were tested in different environmental zones. The choice of EO data was determined by the availability of the data to the EBONE team.

Table 5: overview of test case locations and EO data used

Country	MODIS series	TM	SPOT Image	Hyper-spectral	Lidar
The Netherlands		X		X	X
Estonia		X			X
Sweden			X		X
Slovakia	X				
Spain		X		X	
Europe	X				
Israel	X	X			X
South Africa			X		

Although the test cases do not represent a comprehensive assessment of all possible EO data for all possible landscapes and habitats, they provide a reasonable evaluation of how well certain EO data types could deliver the General Habitat Categories. The data types which are missing in this analysis are radar and thermal imagery.

LiDAR – airborne (Annex-2, 3, 4)

LiDAR (Light Detection and Ranging) is an active remote sensing system sending light pulses in the NIR. The time for the pulses to return back to the LiDAR sensor is used to calculate the distance to a target. The LiDAR sensor also records signal intensity. Four test cases investigated the LiDAR's potential (Table 5 of Annex-2). The general consensus is that LiDAR will reliably separate LPH, MPH, TPH, FPH, and GPH of the 'trees and shrubs' GHCs (Table 6). As a matter of fact, using LiDAR produces more accurate estimates of height and of the % cover of height classes than those acquired through field surveying (Annex-2). The LiDAR height information was also shown to improve the GHC mapping accuracies achieved with multi-spectral imagery (Annex-3).

Table 6: The GHC under the heading 'Trees and Shrubs' are separated using height thresholds

DCH	SCH	LPH	MPH	TPH	FPH	GPH
Dwarf Chamaephytes, dwarf shrubs	Shrubby Chamaephytes, under shrubs	Low Phanerophytes, low shrubs	Mid Phanerophytes, mid shrubs	Tall Phanerophytes, tall shrubs	Forest Phanerophytes, trees	Mega Forest Phanerophytes, trees
<0.05m	0.05-0.30m	0.30-0.60m	0.60-2.00m	2.00-5.00m	5.00-40.00m	>40.00m

The vertical accuracy of current LiDAR systems varies with ground surface condition and canopy density but is generally below 10 cm (Annex-4), so relying on LiDAR to identify and separating life forms with height ranges around and below 10 cm (i.e. DCH and SCH) is not advisable. Further separation of the TRS GHC based on their qualifiers DEC, EVR, CON, NLE, SUM was not tested. Separating DEC, EVR and SUM should be possible with multi-spectral imagery provided the timing of the EO data was chosen correctly or multi-date imagery was used (Boyd and Danson, 2005). Identifying CON and NLE may prove more difficult (Yang et al., 2007). One area not evaluated by EBONE but demonstrated in other studies, is the use of LiDAR to deliver indicators of vegetation structure and woody habitat condition which have been successfully used to predict bird species richness in grasslands and forests (see review in Annex-2).

Hyperspectral – airborne (Annex-5)

Hyperspectral sensors are passive systems which record the surface reflectance in continuous and very narrow spectral bands (~3 a 18 nm) across the visible, near- and mid-infrared spectrum (from ~ 450 nm to ~2400 nm). Hyperspectral observations make it possible to detect most of the absorption features found in the spectra of vegetation (Ustin et al. 2004). This is in contrast to multi-spectral observations (for example, Thematic Mapper or MODIS, Spot Image) where a limited number of discrete spectral bands are recorded, focussing around main absorption features.

The HyMap (Hyperspectral Mapper) airborne sensor used in the EBONE test cases (The Netherlands and Spain) recorded reflectances in 126 spectral bands from 450 nm to 2480 nm at a spatial resolution of 5 m. The standard method for using hyperspectral data is to use spectral signature matching procedures using typical reflectance spectra of the 'pure end-member' to determine the composition of both homogeneous or heterogeneous (i.e. mixed) pixels. Hyperspectral imagery is particularly suited for an end-member based classification as the many narrow spectral bands increase the likelihood of finding features in the spectral signature which are unique to the end-members of interest which in the case of EBONE are the life forms defining the GHCs.

The manner in which the GHCs are being mapped, i.e. parcels are being assigned % coverages of life forms, makes the GHC nomenclature potentially very suitable for end-member classifications and spectral unmixing approaches. The critical requirement is that the plant life forms present in the mapping area (maximum 34, but generally fewer) have distinct spectra. Experimental and modeling studies (Gates et al., 1965; Thomas et al., 1971; Ross, 1981; Goel, 1988; Myneni et al., 1989; Wessman, 1990; Walter-Shea and Norman, 1991; Curran et al., 1992; Jacquemoud et al., 1992, Gitelson and Merzlyak 1997, Peñuelas et al. 1997, Asner et al., 1998) have amply demonstrated that vegetation reflectance is mainly a function of tissue optical properties (leaf, woody stem, and standing litter), canopy structure (e.g., leaf and stem area, leaf and stem orientation, and clumping), soil reflectance and viewing geometry, where the tissue optical properties are function of biochemicals, water content and intra-cellular structure and soil reflectance is function of soil moisture, roughness and texture, organic matter content, and mineralogical composition. Figure 3 shows the outcome of a study by Asner (1998), evaluating the contribution of each of these factors relative to all the other factors for a series of grassland, shrubland, and woodland sites in Colorado, New Mexico, Texas and the Cerrado region of Brazil. It shows that most of the reflectance variability is explained by one or two dominant factors and that these vary with cover type. The potential for a successful GHC life form separation using reflectance values will depend on whether the life form definition includes traits (e.g. vegetation height, leaf area, leaf clumping) which are directly or indirectly related to the most contributing factors.

The review by Ustin et al (2004) highlights the unique value of airborne hyperspectral data. Its capability of detecting very narrow absorption bands which are indicative of, for example, canopy water content and specific canopy biochemicals enables it to be used for a wide range of applications at local level, including detailed habitat and vegetation species mapping. However it is clear from the examples provided that what is achievable is very much specific to the site and its conditions.

The conclusions from the EBONE test case in The Netherlands confirms the above (Annex-5). The success of the GHC classification is dependent on the life forms being spectrally distinct and their spectral signature ranges (variance) showing low overlap. Overall site mapping successes achieved ranged from 64% to 78%. The accuracies achieved for specific life forms varied substantially. Better classification results could be obtained by combining hyperspectral imagery with LiDAR data which would deliver the height based life forms at high accuracy. Because of the manner in which the GHC classes are defined, achieving a GHC map requires, depending on the spatial resolution of the imagery, either the unmixing of image pixels to % coverages of life forms, or imposed parcel outlines for which % coverages of life forms are calculated and translated to GHC. In the latter case, determining the parcel boundaries will have to be the first step to classification. This aspect is discussed further under heading 4.

The conclusions from the EBONE test case in Spain mainly highlighted the importance of increasing the spatial detail whilst maintaining the spectral range: the 4 m airborne HyMap imagery delivered more spatially detailed and consequently thematically more accurate (evaluated visually) GHC maps than the 30m Thematic Mapper image.

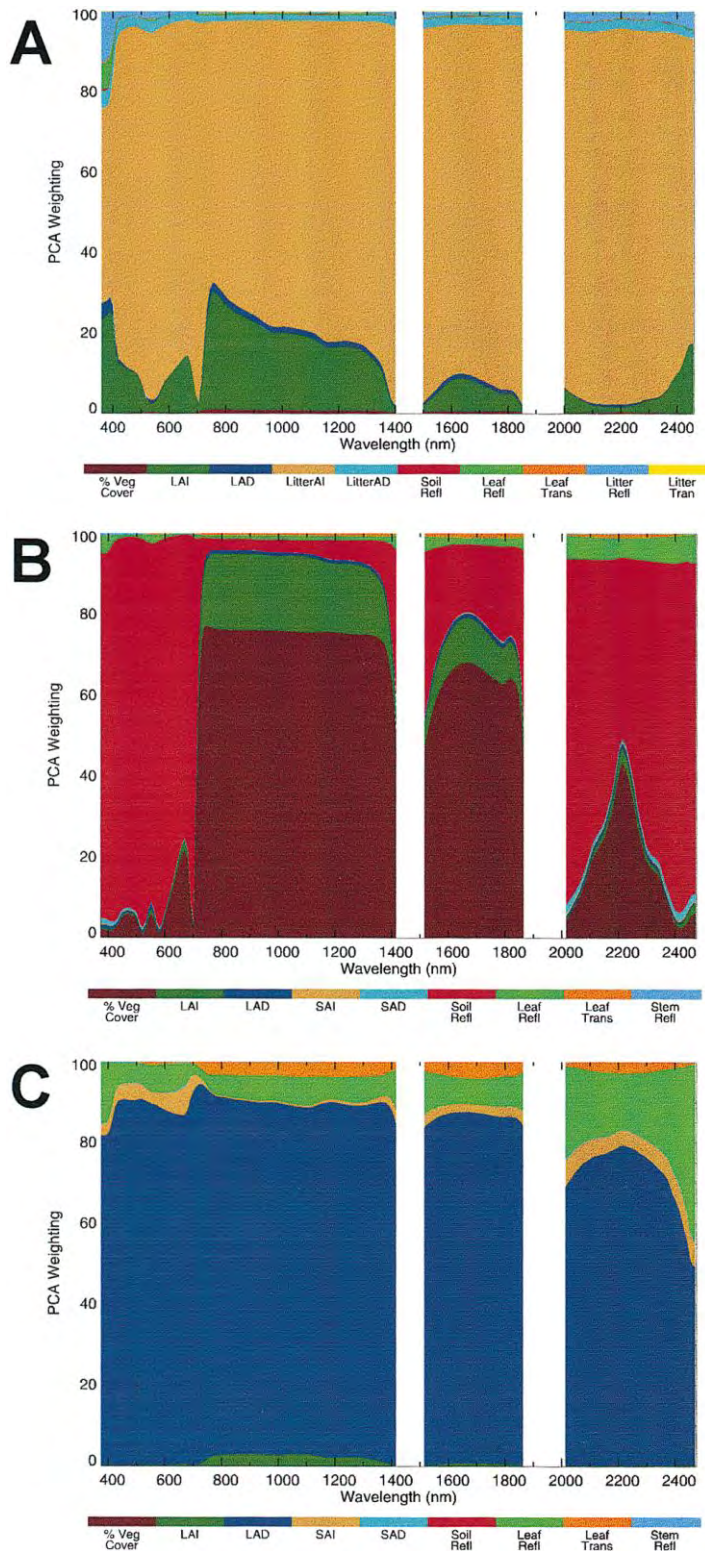


Figure 3: Diagram showing the relative contribution of the main structural vegetation parameters to the variability in reflectance across the spectrum of a hyperspectral sensor for a grassland (A), shrubland (B) and woodland(C) site. (Source : Asner 1998). LAD = leaf angle distribution; LAI = Leaf area index; LitterAD= litter angle distribution; LitterAI = litter area index; SAD= Woody stem angle distribution; SAI= Woody stem area index; leaf litter and stem reflectance and transmittance are determined by their optical and biochemical properties.

Thematic Mapper – satellite (Annex-6, 7, 8)

The Thematic Mapper, and variants (e.g. SPOT-image; Linear Imaging Self-scanning Sensor – LISS; Advanced Spaceborne Thermal Emission and Reflection Radiometer – ASTER; and the planned sensor on Sentinel-2) are satellite borne passive sensors which record the surface reflectance in 4 a 7 discrete and broad spectral bands (~ 50 nm a 200 nm) across the visible, near- and mid-infrared spectrum (from ~ 450 nm to ~2600 nm) at a spatial resolution ranging from 10m to 30m. It is widely known that multi-spectral information will separate vegetated from non-vegetated areas. This data is also generally good at differentiating coniferous from broadleaved vegetation and arable and grasslands from woody vegetation provided the timing of the EO data is such that it enhances the spectral differences. Many national and continental land cover maps are based on this type of imagery (e.g. US, The Netherlands, Sweden, UK, Europe - see Table 1). The capability of delivering the GHC was tested through test cases in Estonia, Spain and Israel.

The general conclusion is that this type of imagery contains many mixed pixels which impacts on the mapping accuracies especially when the landscape is complex and heterogeneous. Pan-sharpening the TM imagery with higher spatial resolution imagery helps resolve this problem to some extent (e.g. Spain and Israel). In the case of Estonia where the test sites were located in an arable landscape with many large fields the accuracies achieved varied from 75% to almost 100% (Annex-6). For the Mediterranean sites in Israel the overall classification accuracies were between 30% and 60%, after merging some of the GHC classes. Among classes, trees (including maquis) were mapped well (accuracies between 60% and 90%), whereas the success in mapping the shrubs and herbaceous classes was lower (Annex-8). The classifications of the test sites in Spain delivered disappointingly low correspondences with the *in-situ* data (no quantitative data available) (Annex-7). For both Spain and Israel it was clear that the classification success was dependent on the timing of the image acquisition coinciding with the dry or rainy season.

MODIS – satellite (deliverable D5.2, Annex-2)

MODIS, and variants (SPOT VEGETATION, MERIS, AVHRR) are satellite borne passive sensors which revisit the same spot every day and record the surface reflectance in discrete and broad spectral bands (~ 10 nm a 30nm) across the visible, near- and mid-infrared spectrum (from ~ 450 nm to ~2600 nm) at a spatial resolution ranging from 250 m to 1000 m. Their main feature is the provision of time-series of daily vegetation indices data which opens up the potential to exploit the information to capture habitat leaf phenology (Figure 4). The main disadvantage of such data is the reduced spatial resolution which means that often a single pixel represents a mixture of land cover.

Four EBONE test cases investigated the use of time-series of data. The first case focussed on grassland GHCs in Slovakia, the second on forest GHCs in Austria and Slovakia, the third on two Annex I habitats and the final on Israel in general. Both the forest, grassland and Annex I habitat test cases found that the variability in phenology behaviour between and within GHC classes is too great to enable an effective separation of classes using phenometrics (i.e. metrics describing the phenological signal such as growing season length and amplitude). The spatial scale of the observations (250 m – 1 km), which results in many mixed pixels, is one of the confounding factors. The other factor is that phenology is only a secondary attribute in the GHC classification system, as illustrated by Figure 5 (Annex-8). Still, the grassland case study demonstrated the value of phenology information for separating grassland types and monitoring their condition, provided that the location of the grasslands is known a priori. Increasing the spatial resolution of time-series of vegetation indices to match the spatial scale of grassland or woodland patches would substantially reduce the occurrence of mixed pixels and bring about this potential.

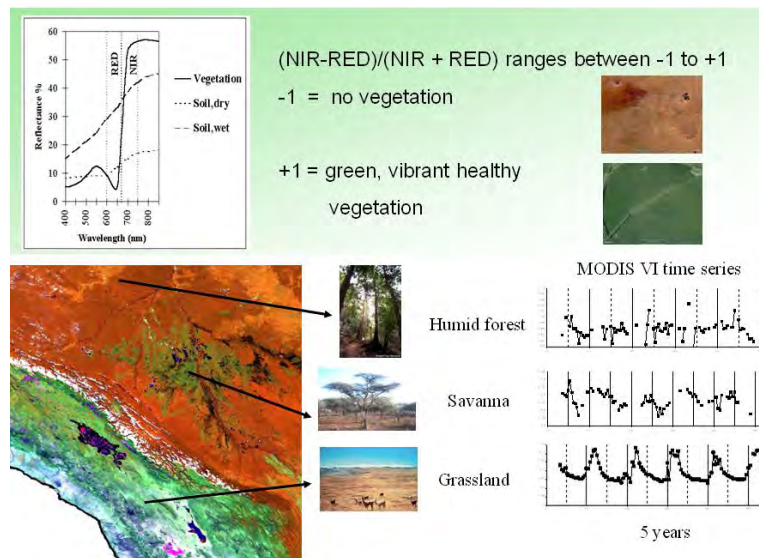


Figure 4: Schematic illustrating how time-series of vegetation indices (VI) can capture vegetation leaf phenology. The example 1200km x 1200km MODIS image (left) shows the Altiplano grasslands, lowland savannas and tropical forests of parts of Bolivia and Peru.

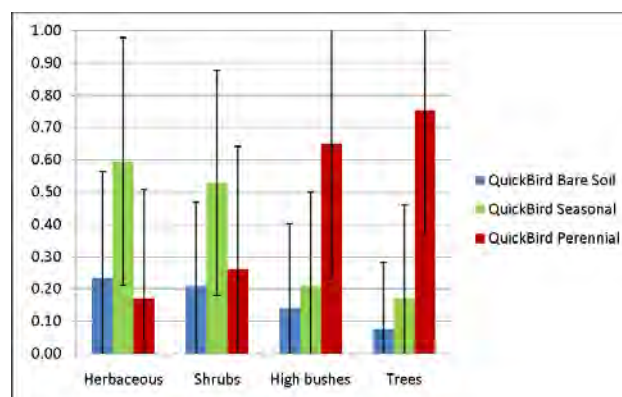


Figure 5: Representation of percent coverage of phenology classes (bare soil, seasonal and perennial vegetation) for each of the four combined EBONE GHC categories in Ramat Ha'Nadiv, Israel (herbaceous, shrubs, high bushes, and trees) (Source: Annex-8).

2.4. Landscape complexity

When the EO mapping performance of habitats is assessed and the spectral detectability of a particular habitat is discussed, the environmental context of the study area is often only briefly mentioned. Nevertheless, it is important to understand how the spectral properties of the area surrounding a habitat influence the detectability of that habitat. Andrew and Ustin (2008) suggested that EO mapping successes are influenced by site complexity. This was tested as part of the HyMap case study in The Netherlands (Annex-5). The general finding was that mapping success decreases with an increase in Biological Complexity (i.e. species richness as measured through the Simpson's diversity and Shannon diversity indices). The EBONE test case involved 4 sites so the results are indicative only. The work of Andrew and Ustin (2008) also demonstrated an inverse relationship between the Spectral Complexity and mapping success.

High spatial resolution (centimeter to meter resolution) can result in high within patch spectral variability which, as is the case in the work of Andrew and Ustin (2008), can be treated as a source of mapping error. Others, however, have used it as a source of information and have suggested that, spectral complexity could be linked to biodiversity. It is based on the spectral variation hypothesis, i.e., spatial variation, expressed as a standard deviation of reflectance, is likely to be correlated with spatial variation of the environment, which in turn is likely to be correlated with plant species richness (Palmer et al. 2002). Oldeland et al. (2010) tested this hypothesis in a savanna ecosystem with positive results, while Schmidteitn and Sassin (2004), working in Alpine meadows, found that although heterogeneous reflectances were always a sign of heterogeneous species composition, homogeneous reflectances did not always indicate a homogeneous plant species composition. In the tropics Asner et al. (2011) have developed the concept of spectranomics where spectral diversity is being linked to the chemical diversity of the tropical forest canopy which in turn is linked to plant trait diversity. Considerable uncertainty remains about the utility of these approaches for biodiversity monitoring, and, given their potential, further research is needed to determine whether the main factors that contribute to spectral heterogeneity could also be indicators of biodiversity.

3. Habitat extent - Methods for integrating *in-situ* and EO

Using a strict interpretation, the idea of integrating *in-situ* with EO data is that the combination of the two data set types will deliver information which is more accurate or precise than either of the two data sets used independently. A more relaxed interpretation of integration is the use of one type of data to improve the accuracy or precision of the information of the other data, or alternatively to make the collection of the other data more efficient.

We considered the following options where the EO and *in-situ* play different roles:

- using *in-situ* samples to re-calibrate a habitat map independently derived from EO; this is referred to as 'inter-calibration';
- using an independent but less accurate EO layer characterising the general spatial variability in cover to post-stratify the *in-situ* samples;
- using *in-situ* samples to train the classification of EO data into habitat types where the EO data delivers full coverage or a larger number of samples.

3.1. Inter-calibration of EO and *in-situ* monitoring

Inter-calibration refers to an integration approach developed for the UK (Fuller et al. 1998; Hill and Smith, 2004). Inter-calibration uses correspondence matrices (Lillesand and Kiefer, 1994) that are created to calculate the classification accuracy of EO derived land cover maps. For each 1 km square Countryside survey 2000 field data (CS2000) a correspondence matrix was produced with the land cover map 2000 (LCM2000). Correspondence matrices were averaged within strata (the ITE Land Classes) to produce stratum specific calibration matrices. These calibration matrices are then used to adjust the stock estimates per 1 km square produced by LCM2000 for each stratum (Figure 6). Although this approaches reduced the original spatial resolution of the land cover map from 25 m to 1 km, Fuller et al. (1998) and Hill and Smith (2004) found that, at national level, the habitat statistics produced from the calibrated land cover map closely matched those extrapolated from the field samples. Confidence intervals for adjusted stock were produced using a Monte-Carlo bootstrapping procedure and it was concluded in Fuller et al. (1998) that in most cases the calibrated results produced more precise stock estimates than either the LCM2000 or CS2000 alone. However, a closer assessment of the publication and report showed no clear evidence that the revised stock estimates were closer to the truth. Moreover, the report inter-calibration increased the uncertainty of national stock for 16 of 19 land cover types. In their own conclusions Hill and Smith (2004) did acknowledge that their work posed more questions than answers. They identified weaknesses in both the FS and

EO approaches to stock estimation and made nine recommendations about how to conduct future surveys, so that the integration of FS and EO approaches could lead to improved estimates of stock. The main points have been condensed to a shorter list below:

- Timing of surveys: Due to the dynamic nature of some of the habitats (for example agricultural and coastal) the time difference between products should be minimised.
- Spatial resolution of products: The minimal mappable units (MMUs) of products should be normalised (most likely to the largest) prior to any correspondence analysis to prevent features that could not exist at the coarser MMU being seen as error.
- Thematic differences: Thematic differences between products should be avoided.
- Rarity: Rarity and patch structure should be considering. Classes with limited extent compared to the largest MMU should be avoided.
- Knowledge Base Enhancements and Validation: The use of additional spatial data is necessary in order to disable calibrations that worsen the results and also for validation. Care should be taken to select datasets with suitable thematic and spatial specifications, temporal similarity and appropriate uncertainty information.

It is worth noting that the work of Hill and Smith was delivered as a contract report and was never subjected to peer review. Inter-calibration was not tested in EBONE. Future work should consider evaluating this option rigorously.

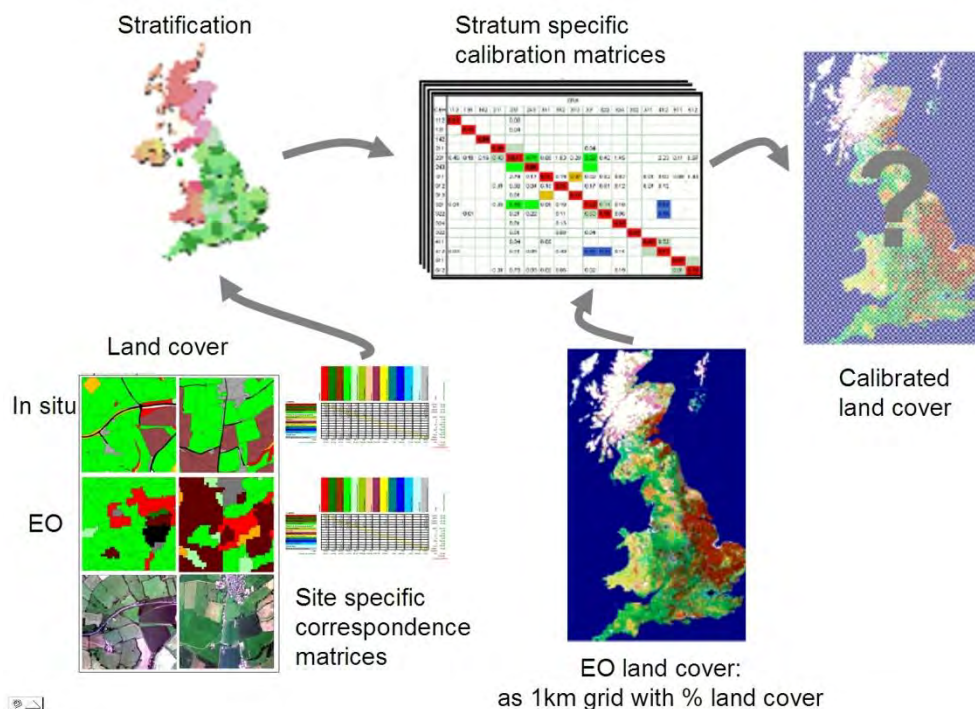


Figure 6: Diagram illustrating inter-calibration as implemented by Fuller et al (1998)

3.2. Post stratification (Deliverable 5.4)

When only statistics and not wall-to-wall maps describing the spatial pattern of different habitats or categories are needed, the combined use of EO data and data from sample-based inventories can provide accurate area estimates for various categories. Almost unbiased area estimates of habitats or classes can, for example, be obtained by combining EO data and *in-situ* data using post-stratification. The main requirement is that there is a reasonably correlation between the classes of the EO map and the and the *in-situ*

determined categories to be finally estimated, but the EO-derived classes do not need to be the same as the *in-situ* derived classes. Previous work has shown that post-stratification, where satellite images or classified satellite images are used for stratifying existing sample based forest inventories, improves the accuracy of estimated forest characteristics (McRoberts et al., 2002 and 2006; Nilsson et al., 2003 and 2009). Similarly, CORINE land cover data was used to post-stratify *in-situ* data from the LUCAS sample based land inventory to improve the accuracy of area estimates for various coastal land cover classes (Galego and Bamps, 2008).

EBONE tested this approach for one of the nine environmental strata of Sweden combining the comprehensive NILS inventory data (NILS; <http://nils.slu.se/>) with the EO derived Swedish GSD land cover map (Engberg, 2005). The results obtained in this study also show an increase in precision when using classified satellite images for post-stratification, further confirming that post-stratification is an easy and straight forward method that can be used to derive improved area statistics for habitats. One important advantage of using products like the GSD Land Cover map or the CLC2000 map for the stratification is that they already exist. The increase in precision obtained using post-stratification also means that estimates of the area covered by different habitat classes can be presented for smaller areas than possible from estimates based on a sparse sample of *in-situ* data alone, without any reduction in precision.

An important future research task is to test if the use of other EO derived map products can improve the estimation accuracy for selected habitats and whether similar results can be achieved in other landscapes (e.g. Mediterranean). In particular the usefulness for post stratification of the upcoming GMES pan-European map layers should be evaluated. Also the more specialised follow-on products derived from these pan-European data sets could be of relevance for post-stratification. It will also be of interest to investigate how the gain in efficiency for post-stratified estimates (RE) is affected by the number of *in-situ* observations used.

3.3. Training the classification of EO imagery using *in-situ* samples

The most relaxed definition for integration is to use the *in-situ* field samples to train and validate the classification of the EO data into habitat types. The EO data could either deliver full coverage or a larger number of samples.

Traditionally, the collection of training data for any EO classification algorithm would focus on identifying spectrally homogeneous areas of the cover classes of interest, ensuring that the within and between class spectral variability is represented. To avoid unclassified areas in the imagery it is important to ensure that the full range of spectral signatures found in the imagery have been identified and allocated to a cover class. Unsupervised image classifications are often used as a tool to explore the spectral information content of an image and help guide the field work. Field work is organised to capture and confirm the cover identity of the spectral classes observed on the imagery as effectively as possible. A sampling strategy designed to train and validate an image classification will not only have to take into account the spatial distribution of the cover classes of interest, but also the within class spectral variability found across the imagery. Consequently a sampling strategy designed for EO image training, classification and validation is unlikely to suit the purpose of delivering unbiased and precise estimates of habitat extend and vice versa. The EBONE team investigated this when assessing the use of TM imagery in Estonia (Annex-6) and Spain (Annex-7) and found that '*Single central monitoring square can be non-representative for surrounding squares*'; '*Supervised classifications of satellite imagery are only possible when targeted training samples have been collected in the field*'; and '*unsupervised image classification was useful to examine the spectral variation in the image, within field mapped*

GHC areas and to locate those areas for which the supervised classifier did not have a like training area in the monitoring square.'

3.4. Sampling strategies (Deliverable 5.4)

'Going *in-situ*' is the only way to collect detailed information on the flora and fauna present. Also *in-situ* land cover or habitat observations, when benefiting from a well designed field survey approach and protocol, have the advantage of providing high thematic and spatial detail. *In-situ* work is intensive and costly and is therefore limited in the area it can cover and the revisit frequency. One question EBONE looked at, using a statistical simulation experiment, was whether using EO to increase the number of samples to increase precision, is a viable option. This option only makes sense if EO can be made to deliver local habitat maps at an acceptable accuracy using a variety of more expensive and sophisticated EO data (high spatial, spectral and temporal resolution imagery, Lidar), an option which would be a very expensive proposition if acquired at national or continental scale to deliver a wall to wall coverage, but potentially cheaper than field work if limited to sample areas.

The take home messages from this work are that:

- the effect that EO sample has on precision or bias will depend crucially on differences in user (omission) and producer (commission) accuracy (WP8 provides further details about the statistical procedure to estimate precision and bias);
- unbiased estimates are obtained when user accuracy (omission) = producer accuracy (commission);
- it is possible to correct for possible systematic bias if and only if the EO sample and the *in-situ* sample partly overlap so that user and producer accuracy can be estimated. This overlap, however, should be sufficiently large to ensure that user and producer accuracy themselves can be estimated precisely and without bias. In this respect, it is also crucial that the overlapping part of both samples is a spatially balanced, random sample to avoid bias.

The figures 7 and 8 below (Source D5.4) illustrate how the bias and precision of habitat area estimates are affected by the habitat mapping (producers and users) accuracy achieved with EO.

When exploring for a cost-effective monitoring design, the problem that needs solving is how to achieve a good balance between the output quality of the design and the available monetary budget (or alternatively, the constraint could be formulated in terms of time). The effectiveness can often be related to statistical concepts, such as the margin of error or the sampling variance. Which measure for effectiveness will be most useful will depend on the question at hand. For estimation of a mean or a total, higher effectiveness is related to a narrower confidence interval. For trend detection, the effectiveness will depend on the power to detect a trend, and so this will depend on the magnitude of the trend that needs to be detected. For a given sample size, we can thus assess effectiveness.

Establishing relative differences in cost between *in-situ* sampling and EO is the other essential ingredient. However, although estimates of the cost associated with field work were available (through the EBONE pilot studies) those associated with the EO work were lacking. This situation is not uncommon and for it to improve it is important that we all actively encourage the documentation and reporting of costs associated to EO mapping activities and field work.

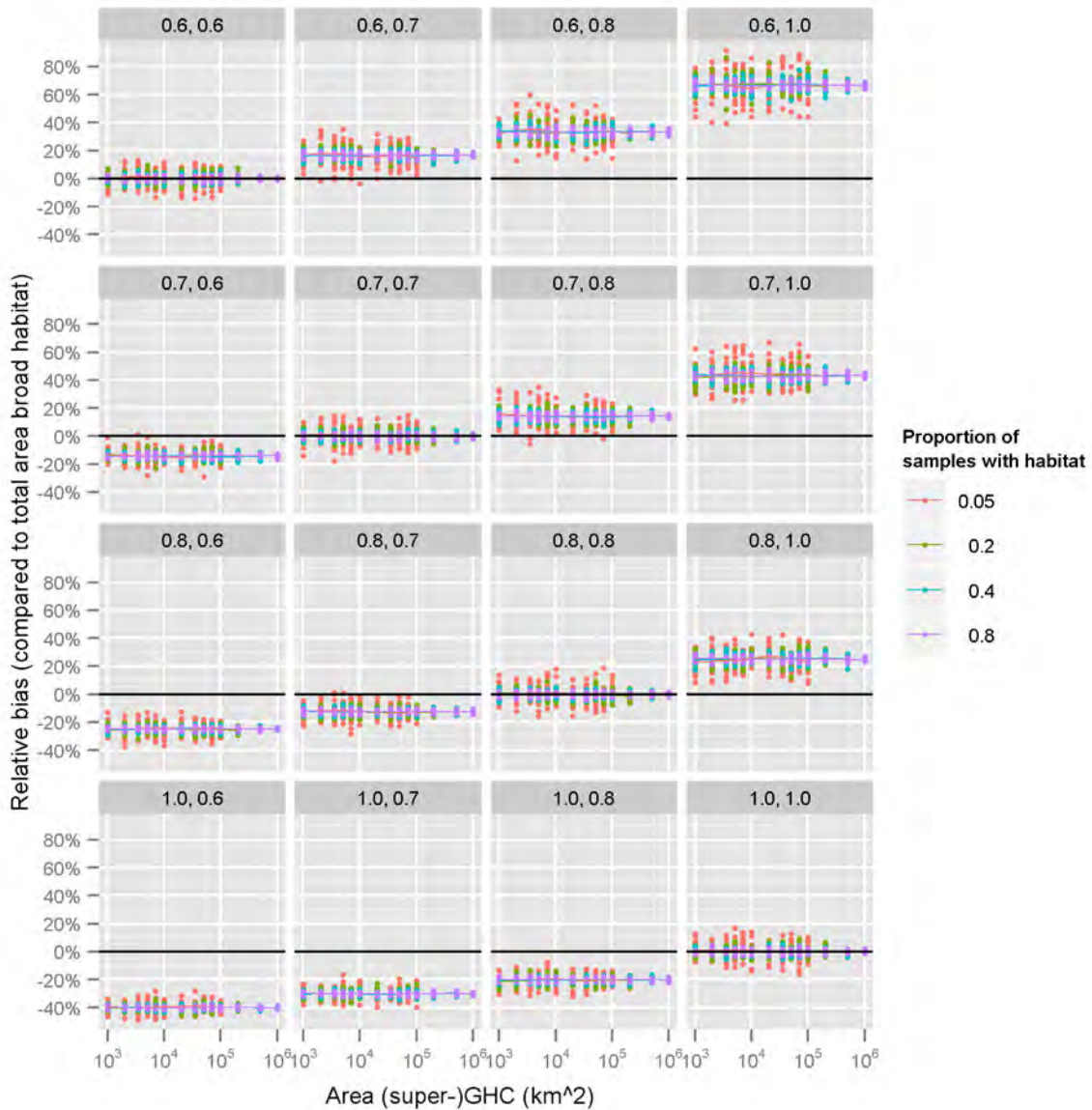


Figure 7: Relative bias as a function of user and producer accuracy. The heading above each panel gives user accuracy and producer accuracy respectively. The lower right panel corresponds with the situation where *in-situ* samples and Earth observation samples give identical results (i.e. 100% accuracy; for comparison purposes only). The sample size is equal to 10000.

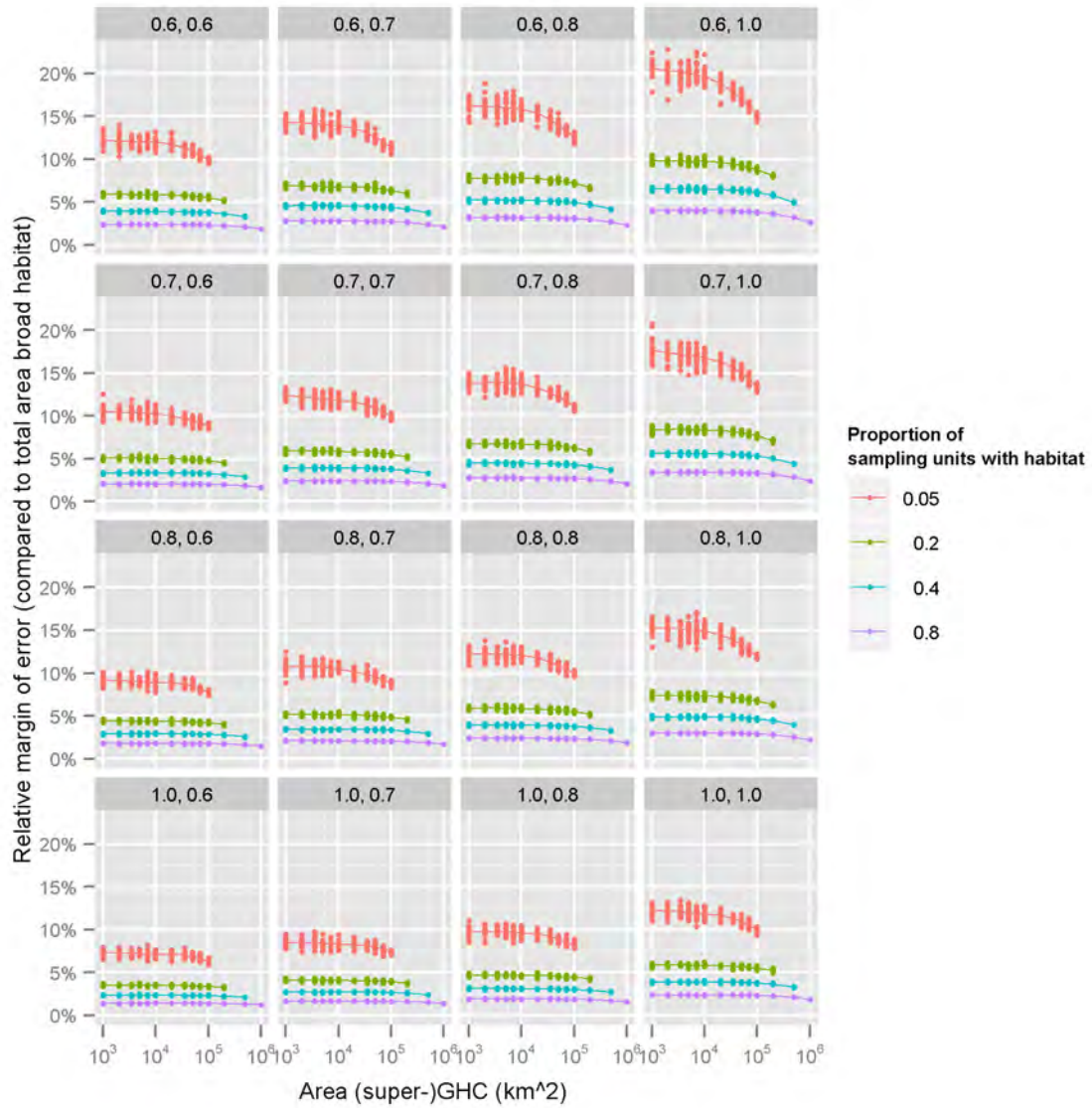


Figure 8: Relative margin of error as a function of user and producer accuracy. The heading above each panel gives user accuracy and producer accuracy respectively. The lower right panel corresponds with the situation where *in-situ* samples and Earth observation samples give identical results (i.e. 100% accuracy; for comparison purposes only). Sample size used was 10000.

4. Habitat extent - The impact of spatial and thematic detail on change detection (Annex-9)

The level of spatial and thematic detail at which habitats are being mapped and monitored is expected to have a direct impact on the resulting change statistics that can be obtained. Through a test case in Slovakia, EBONE tried to quantify the impact of reduced spatial detail (i.e. spatial generalisation) and thematic detail on the resulting estimates of habitat extent and changes in habitat extent. For this study EBONE used the land cover and habitat data obtained for eight test sites at three spatial scales (25 ha, 0.5 ha, 0.04 ha) and two different nomenclatures (the CORINE Land Cover nomenclature and the General Habitat Categories) (see Figure 9). To study change EBONE looked at the time period between 1949 and 2011. During this period substantial land cover and land use changes occurred in Slovakia, enabling us to highlight differences in statistics that would have been less evident if a shorter period was examined.

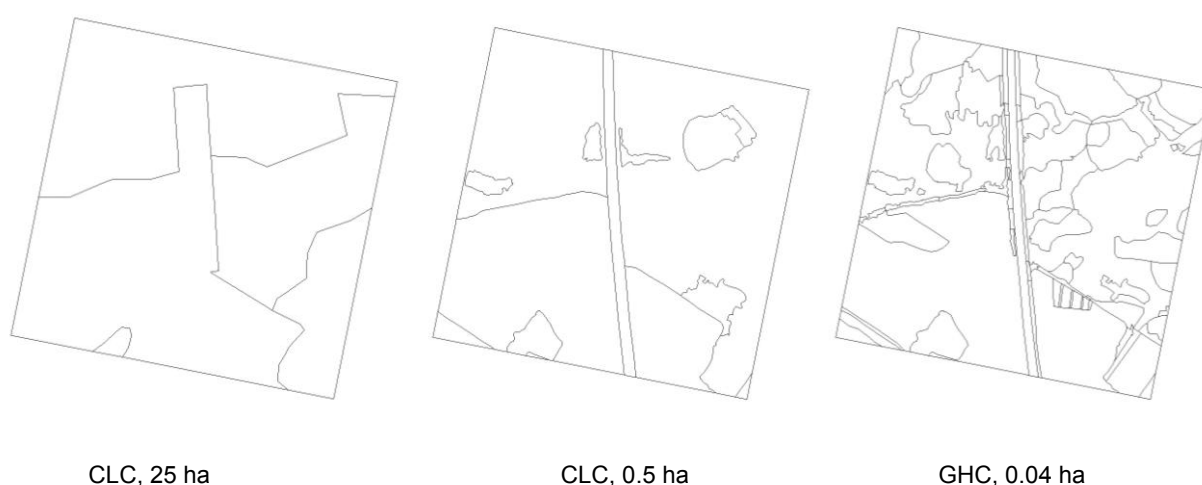


Figure 9: Habitat information obtained for site 8 (Malacky) when implementing the Corine Land Cover nomenclature at a 25 ha MMU, a 0.5 ha MMU and when implementing the General habitat categories nomenclature at a 0.04 ha MMU.

As expected, an increase in thematic and spatial detail leads to the identification of a larger number of classes and polygons which in turn leads to the detection of a larger number of changes (Table 7). Using a different nomenclature will also lead to the detection of different types of changes which when interpreted into, for example, land cover or land use change processes can result in different conclusions (Figure 10). Generally when EO is used to produce full coverage maps at continental and global scales both the spatial and thematic detail of the resulting product is greatly reduced (see Table 3 in Section 2.1). The results from this exercise emphasises the importance of a common denominator to establish a link between the EO and *in-situ* derived estimates of extent and trend. This common denominator could be (1) the habitat nomenclature; (2) the spatial scale (i.e. the minimum mapping unit); or (3) both. Lengyel et al. (2008) go even further listing, amongst others, the following criteria as key for a successful integration between EO and *in-situ*:

- comparable areas and spatial scales used in each scheme,
- compatibility of habitat nomenclatures, compatible depth of habitat nomenclature hierarchy, exhaustiveness of field mapping,
- comparable thematic precision,
- comparable monitoring/mapping accuracy.

It is clear that the success rate of achieving the same habitat classification with EO as delivered through *in-situ* will vary in space and time. At the other hand, the minimum mapping unit which can be achieved through EO is determined by the technical specification of the sensor used and current technology is capable of delivering meter resolution multi-spectral imagery from which we can reliably deliver the universal top level thematic classes (i.e. not vegetated; non-woody vegetation; woody vegetation; crops; and water). On that basis the logical and most practical conclusion would be to aim for EO mapping products which match the spatial scale of the *in-situ* observations (for GHC: 0.04 ha MMU) and are linked thematically through the top level classes of the habitat classification system (for GHC: Urban, Crops, Sparsely Vegetated, Vegetated Herbaceous, Vegetated Tree or Shrub).

Table 7: Summary of change statistics (1949-2011) as detected by CLC, 0.5 ha and GHC, 0.04 ha for eight 1km2 test sites in Slovakia

Site	No of change types			Changed area (%)		
	CLC, 0.5 ha	GHC, 0.04 ha	Difference	CLC, 0.5 ha	GHC, 0.04 ha	Difference
1 Klin	7	27	20	93.07	47.99	45.08
2 Gôtovany	11	33	22	74.87	37.43	37.44
3. Lipt. Teplička	6	27	21	74.85	48.79	26.06
4. Tisovec	6	57	51	65.19	62.96	2.23
5. Tachty	22	51	29	73.54	63.32	10.22
6. Súdovce	24	82	58	79.03	61.21	17.82
7. Oponice	24	67	43	54.78	63.83	-9.05
8. Malacky	8	54	46	66.92	59.36	7.56
Average	13.5	49,75	36.25	72.78	55.61	17.17

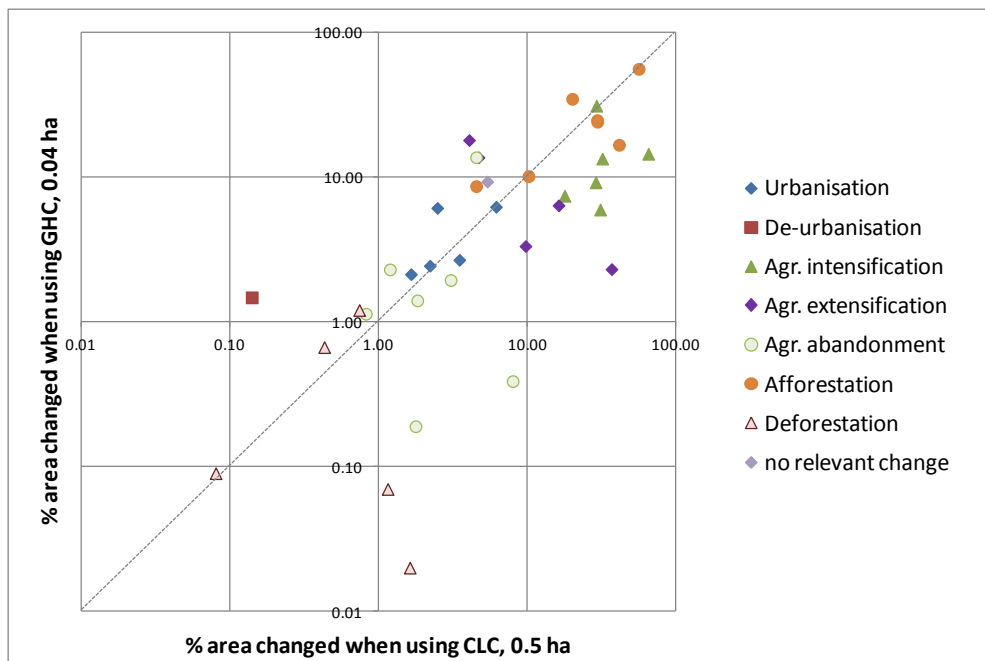


Figure 10: The land cover and use change (1949-2011) processes derived from maps interpreted at different spatial scales using different nomenclatures for eight 1km2 test sites in Slovakia.

5. Habitat extent - EO in support of the field work

The GHC system is based on determining the composition of individual plant life forms for habitat mapping units with a minimum area of 400 m². In the field, the identification of these habitat mapping units is a major challenge especially when the transitions between mapping units are gradual. BIOHAB's protocol strongly recommends the use aerial photography to identify and manually digitise habitat mapping units which can then be subsequently labelled in the field (Figure 9). This approach reduces the time spent in the field and ensures a more accurate spatial delineation of the habitat units. Forest managers and nature conservation agencies are well aware of the value of aerial photography and have for some time now fully incorporated aerial photo interpretation into their operational field surveying activities (for example, UK Country Side Survey (Barr et al., 1993)).

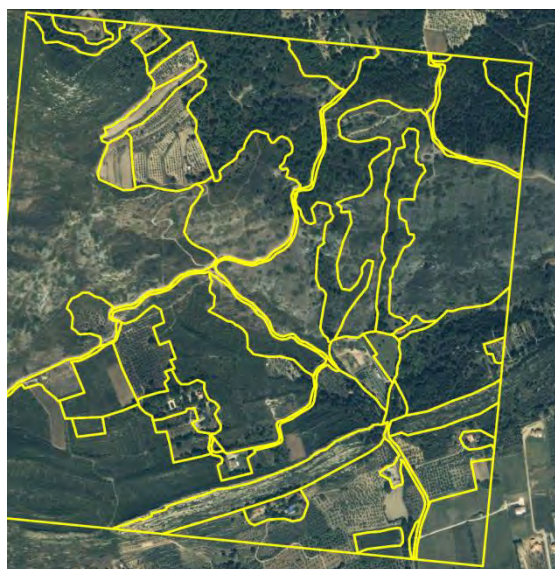


Figure 9: Example of the manual digitisation of an aerial photo for a 1km² sample prior to the field survey.

Manual digitisation benefits from the human ability to recognise spatial patterns and, in some cases, the local knowledge of the interpreter. The main disadvantage is the subjective nature of manual interpretation which impacts on the consistency of the interpretation in space and time. Steps can be taken to reduce this impact, such as, provide clear and complete interpretation rules which have been thoroughly tried and tested; train and regularly re-train the interpreters and; use people who are familiar with the local or regional landscape. Still quantifying consistency remains difficult and manual digitisation takes time.

The general consensus among the EBONE team was that automated image segmentation of the aerial photographs would reduce the time spent digitising mapping units and ensure consistency. This was not tested within the project. Image segmentation is the process of partitioning a digital image into parcels or segments which contain neighbouring pixels that are similar in terms of reflectance value (colour, intensity) or texture. The main potential problem with image segmentation is that the underlying algorithms require user defined input parameters which prescribe 'when to stop adding to or growing the segment' and subsequently determine the number and size of the resulting segments. Optimising these input parameters is an iterative and interactive process which will be partly function of the landscape. Figure 11, taken from Gerard et al. (2003) illustrates this issue, showing how the choice of 2 input parameters can drastically change the number (and size) of resulting segments.

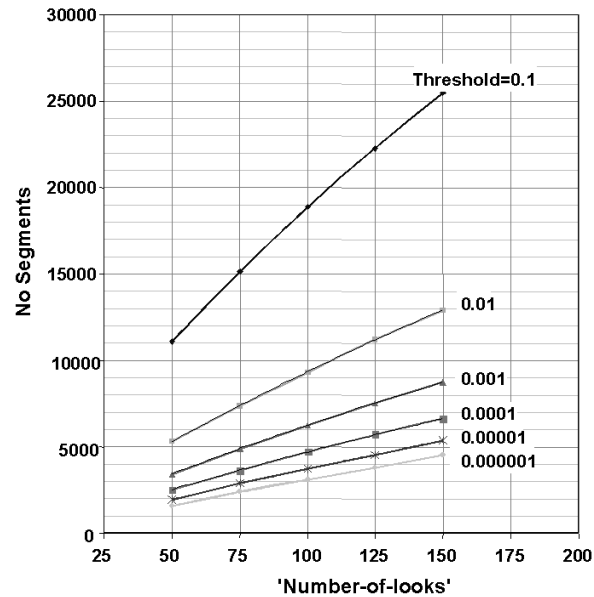


Figure 11: Variation in number of segments produced for a 700 km x 700 km area from a 1 km resolution NDSWIR SPOT-VEGETATION image by the CAESAR MUM image segmentation procedure as a function of the input parameters “threshold” and “number of looks.” (Source: Gerard et al 2003).

Nevertheless the advantage of being able to quickly produce digitisations based on relatively consistent clustering rules which are repeatable and easy to document, are likely to outweigh this problem. Another advantage is that such an approach can easily be implemented on multiple layers of imagery, enabling a segmentation based on a combination of, for example, spectral reflectance, height information and image texture. Figure 12 shows the results of a small EBONE study that explored how the segmentation of combined LiDAR and aerial photography could be used to deliver habitat mapping units for field surveying (see Annex-3). The potential of image segmentation is clearly demonstrated, however a more thorough study involving a range of test cases which represent a variety of landscape types is required to establish if image segmentation is not only more cost effective but also more consistent and precise than manual interpretation.

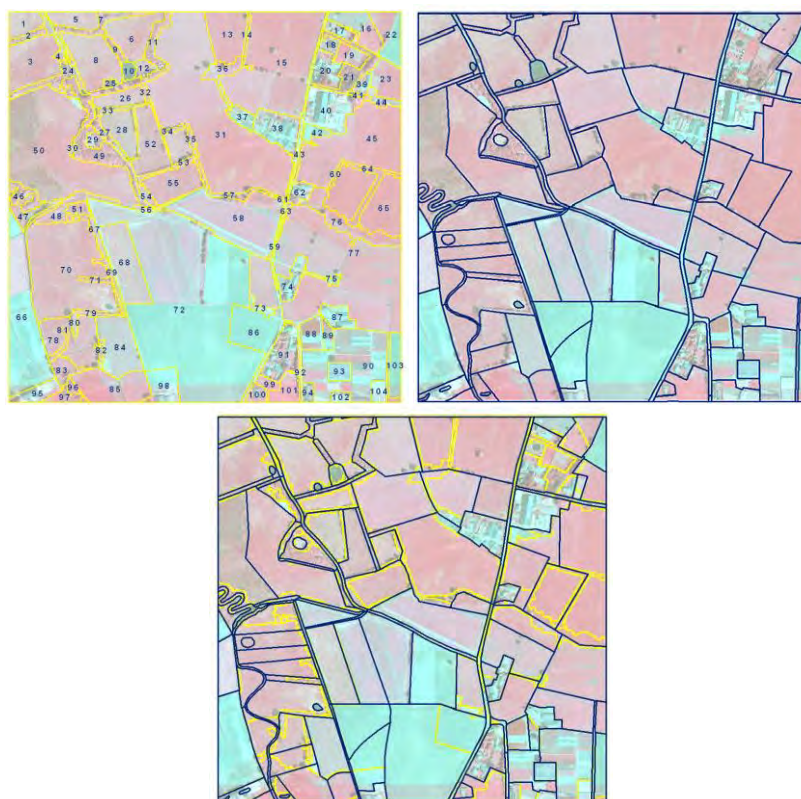


Figure 12: The habitat mapping units created through (a) segmentation of combined LIDAR and aerial photo data; (b) manual interpretation of the aerial photo and (c) an overlay of both approaches (from Annex-3).

6. Habitat - pattern related measures (Deliverable D5.3)

Landscape ecology is based on the premise that there are strong links between patterns, functions and processes and a number of studies have explored the utility of spatial metrics in landscape analysis since the 1980s. As a result, the number of pattern related indices has proliferated. Nowadays, the potential (non-expert) user, either from landscape planning or environmental local, regional or national agencies or from international agencies, who is looking for one measure of pattern, is left alone in front of this plethora of indices. The test case in EBONE was an attempt to respond to this need of guidelines and standardization to measure pattern. It also investigated how to deliver pattern measures which provide context for the *in-situ* field observations.

The EBONE test case focussed on the customisation, integration and automation of available and well selected pattern models. Its final aim was to derive a system of standardised ecologically meaningful characterisation of pattern.

The example GHC of interest was arbitrarily decided to be forest phanerophyte. The three models considered (GUIDOS/MSPA, Landscape mosaic and connectivity models) were revisited to present new indices characterising morphology, interface mosaic context and connectivity. User information requirements were assumed to be about

- the landscape share of anthropogenic versus more natural habitats;
- the availability of interior habitat and connecting linear features;
- the presence of isolated features;
- the mosaic interface context at edges; and
- the habitat connectivity at landscape level.

The models were successfully applied to the available EO based land cover maps and the sixty 1km² field samples available in the EBONE project. The samples represented areas in France, Austria and Sweden. Each field sample was easily and quickly characterised in a standardised manner for the forest GHC. The methods could easily be applied to other focal GHC provided that the habitat is accurately identify in the field and using EO. The sample based results showed a high level of within stratum variability across all three types of indices (morphology, interface mosaic context and connectivity).

Due to insufficient sample size (1km²) and sample population for certain environmental zones, a proper multi-scale and multi-source data assessment could not be done and only an illustration of the scale dependency of the results was provided over few samples (Figure13). Connectivity analyses were implemented using 25km x 25km analysis units providing macro-connectivity information context to the available habitat samples, which in turn were characterized by their micro-connectivity level.

Quantifying spatial pattern is not an end in itself, rather it should be the first step to understanding ecological processes. Spatial pattern analysis is of limited value if not used to explain structural changes in landscapes and predict how they influence ecological processes (Li and Wu, 2004). It should also be kept in mind that spatial indices are influenced by the image material used and the processing carried out to deliver the input habitat maps. The spatial and temporal dimensions as well as field recording of ecological condition of habitats should be integrated in monitoring programs to increase our understanding of pattern-process relationship. This standardised pattern characterisation will probably facilitate such studies (which are too often restricted to basic patch area measures such as in Krauss et al, 2010) and the comparison of pattern processes across regions.

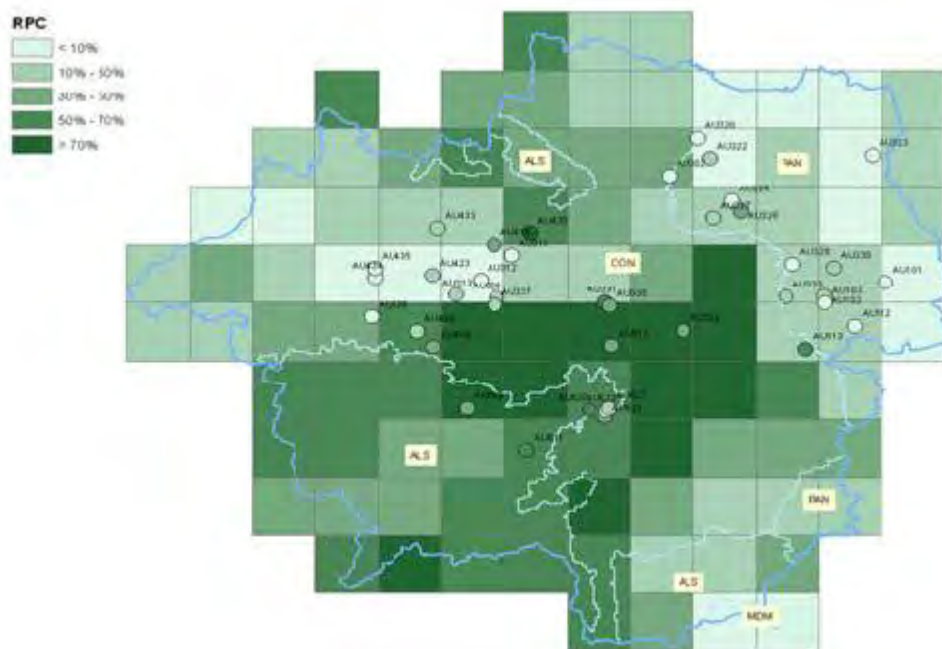


Figure 13. Macro and micro connectivity information (RPC) in Austria case study. Macro-connectivity is derived from the analysis of 25km x 25km units. Micro-connectivity is available for each 1km² sample (circles shade according to their RPC values)

7. Conclusions and recommendations

A measure of the biodiversity indicator 'Habitat extent' could be delivered in two formats: as sample-based estimates for a region, country or zone or as a wall to wall map showing the distribution and extent of the habitats. *In-situ* observations will deliver the former whilst EO based observations are expected to deliver the latter. General expectations are that a combination of the traditional *in-situ* surveys and EO-derived land cover/habitat products could deliver better maps and/or estimates more efficiently.

When considering wall to wall habitat mapping, it has become clear that, at the moment, even with the various types of EO data and EO mapping techniques currently available, the level of thematic and spatial detail required for habitat and biodiversity monitoring cannot be achieved for all the habitat types of interest. When considering EO, one should always bear in mind that the quality and detail achieved when mapping land cover or habitats using EO is primarily limited by the manner in which the electromagnetic radiation interacts with the physical and chemical properties of the land surface and the manner in which the electromagnetic radiation is being recorded (spatial resolution, spectral range and resolution, temporal resolution, active or passive system). Still, the upcoming GMES pan-European data layers should be evaluated with respect to their contribution to habitat mapping, including their potential for producing area statistics through post-stratification.

The EO mapping success of habitats varies with landscape and habitat type, so although a detailed wall to wall coverage showing the distribution of all habitat types of interest may not be possible, EO can produce good quality distribution maps of selected habitats. Adopting an EO based perspective of habitats (e.g. Crick Framework) to predict the EO mapping success of the habitat classes at the start of a mapping project, would not only help direct the effort towards the mappable habitats but also help manage stakeholder expectations.

Introducing physical environmental variables to improve EO mapping success is widely accepted as the way forward. An environmental stratification will increase the thematic link between EO land cover and *in-situ* habitat nomenclatures. However, the spatial resolution of the data and models, that deliver most of these environmental variables, needs to drastically increase for these variables to directly improve the EO mapping of habitats. A thorough review to establish in which circumstances the added environmental information is likely to make a significant difference in habitat mapping is still required.

When considering the combination of the traditional *in-situ* surveys and EO-derived land cover/habitat products, a couple of potential options were identified.

- One option was using *in-situ* samples to re-calibrate a habitat map independently derived from EO ('inter-calibration'). Here a good thematic match between the habitat classes observed *in-situ* and those mapped through EO and limiting the difference in spatial resolution (minimum mappable unit) between the *in-situ* and EO products appeared to be important. A thorough testing of this option across a variety of landscapes is recommended.
- The most promising option was to use an independent but less accurate EO layer to post-stratify the *in-situ* samples. This option delivers a more precise sample-based estimates without requiring a good thematic match between the *in-situ* and EO layer or a very accurate EO land cover map. The next steps would be to test this option further across a variety of landscapes using a range of *in-situ* sample sizes.
- Using the *in-situ* samples to train the classification of EO data, initially appeared to be an attractive proposition, however it became clear that a sampling strategy designed for EO image training, classification and validation is unlikely to suit the purpose of delivering

unbiased and precise estimates of habitat extent and vice versa. An unsupervised classification of the EO imagery will quickly help establish whether the planned *in-situ* sampling strategy is representing the spectral range found in the imagery.

- Using EO to increase the number of *in-situ* samples to increase precision, is a viable option only if the EO sample and the *in-situ* sample partly overlap so that omission error, commission error and bias can be estimated. It is also crucial that the overlapping part of both samples is a spatially balanced, random sample to avoid bias. Finally, the best results (i.e. no bias and enhanced precision) will be achieved when omission and commission errors are kept the same or if the omission error is slightly larger than the commission error.

There is a critical need to accurately document costs associated to field surveying and, more urgently, the EO mapping effort. Without this information it is not possible to assess the cost-effectiveness of the options considered. Related to this is the need for the monitoring community and their stakeholders to agree on the minimum acceptable levels of accuracy and precision required for the indicator 'extent and change of habitats'.

The level of spatial and thematic detail at which habitats are being mapped and monitored has a direct impact on the resulting change statistics that can be obtained. If the discrepancy between EO and *in-situ* is too great, the task of reconciling or consolidating change statistics from both sources may become insurmountable. For a successful integration of EO and *in-situ* observations, the impact of spatial and thematic generalisation has to be either quantified or minimised. One option would be to develop a hierarchical habitat classification system where the cover classes that are easily and accurately mapped through EO form the top level (generic) of the habitat classification system (e.g. GHC: Urban, Crops, Sparsely Vegetated, Vegetated Herbaceous, Vegetated Tree or Shrub). These are further subdivided through an environmental stratification and the *in-situ* samples surveyed at the more detailed sublevels. The GHC or FAO LCCS are very well suited for such an approach. To avoid issues of spatial generalisation, the EO layer is delivered at a spatial resolution matching the minimum mapping unit of the *in-situ* habitat mapping. The issue of spatial mismatches between parcel delineation from EO and *in-situ* observations at sample level is still outstanding. Further work to develop and test the viability of this option is recommended.

High spatial resolution EO imagery (aerial photography, hyperspectral airborne imagery and LiDAR) can be used very effectively to delineate parcel boundaries prior to the surveying of the *in-situ* sample. A thorough study involving a range of test cases which represent a variety of landscape and habitat types is required to establish whether automated approaches to delineate the parcels are more cost effective, consistent and precise than manual interpretation.

In terms of the future requirements from Earth Observation for habitat monitoring, the following general recommendation can be drawn from the EBONE experience.

- EBONE has clearly demonstrated the great potential LiDAR holds. The main limitations are the costs associated to building up national and continental coverages and making the data available and affordable to the user communities.
- The biodiversity community works at meter spatial resolutions and requires multi-temporal coverage and spectral information in the NIR and SWIR to differentiate habitats and monitor their change. In addition the provision of time-series of very high spatial resolution (1 m – 10 m) physical environmental variables such as soil moisture and surface temperature combined with high spatial resolution topography would greatly enhance habitat mapping and the monitoring of their condition. The only current option available is multispectral airborne data. However, it is nearly impossible to achieve

successful and affordable single year multi-temporal airborne campaigns for large areas. Sentinel-2 will deliver 10 m visible-NIR and 20 m SWIR at best every 5 days. These specifications are expected to improve the spatial scale of current regional, national and international land cover mapping activities and will undoubtedly make these more suitable for habitat mapping and monitoring. Still the spatial resolution provided falls short of what is required to ensure a workable integration between *in-situ* and EO habitat observations. The next generation satellite-sensor setups should aim towards the provision of time-series of affordable meter resolution spaceborne multi-spectral imagery.

8. References

- Arino, O., Trebossen, H., Achard, F., Leroy, M., Brockman, C., Defourny, P. (2005) The GLOBCOVER Initiative, Proceedings of the MERIS (A)ATSR Workshop 2005 (ESA SP-597). 26 - 30 September 2005 ESRIN, Frascati, Italy. Editor: H. Lacoste. Published on CDROM., pp.36.
- Asner, G. P., Wessman, C. A., Schimel, D. S., and Archer, S. (1998), Variability in leaf and litter optical properties: implications for BRDF model inversions using AVHRR, MODIS, and MISR. *Remote Sens. Environ.*, 63:243–257.
- Asner, G.P., Martin, R.E. (2011) Canopy phylogenetic, chemical and spectral assembly in a lowland Amazon forest, *New Phytologist*, 189, 999-1012.
- Barr, C. J.; Bunce, R. G. H.; Clarke, R. T.; Fuller, R. M.; Furse, M. T.; Gillespie, M. K.; Groom, G. B.; Hallam, C. J.; Hornung, M.; Howard, D. C.; Ness, M. J.. 1993 Countryside Survey 1990: main report. (Countryside 1990 vol.2). London, Department of the Environment, 174pp. (ITE Project No:T02051m5)
- Bartholomé, E., Belward, A. S. (2005) GLC2000: a new approach to global land cover mapping from Earth observation data, *International Journal of Remote Sensing*, 26(9): 1959-1977.
- Boyd, D.S. Danson, F.M.(2005) Satellite remote sensing of forest resources: three decades of research development, *Progress in Physical Geography*, 29(1): 1–26.
- Bunce et al. 2008 *Landscape Ecology*, 23:11–25
- Curran, P. J., Dungan, J. L., Macler, B. A., Plummer, S. E., and Peterson, D. L. (1992), Reflectance spectroscopy of fresh whole leaves for the estimation of chemical concentration. *Remote Sens. Environ.*, 39:153–166.
- Delbart N, Le Toan T, Kergoat L and Fedotova V (2006). Remote sensing of spring phenology in boreal regions: A free of snow-effect method using NOAA-AVHRR and SPOT-VGT data (1982-2004). *Remote Sensing of Environment*, 101, 52-62
- Di Gregorio, A.; Jansen, L.J.M. (2000) *Land Cover Classification System: Classification Concepts and User Manual*. FAO, Rome,
- Estreguil C., Vogt, P., Ostapowick (submitted) European level assessment of the status and trends of forest spatial patterns, *Environmental Monitoring and Assessment Journal*.
- Engberg, A., 2005. Produktspecifikation av Svenska CORINE Marktäckedata (in Swedish). Lantmäteriet, Gävle, Document No SCMD-0001. Available online at: http://www.lantmateriet.se/upload/filer/kartor/kartor_och_geografisk_info/GSD-Produktbeskrivningar/SCMDspec.pdf
- Eva, H.D., Belward, A.S., De Mirandaw, E.E., Di Bellaz, C.D., Gond, V.R., Hub Er, O., Onesk, S.J., Sgrenzaroli, M. and Steffenfritz (2004) A land cover map of South America *Global Change Biology* (2004) 10, 1–14.
- Friedl, M.A., D. K. McIver, J. C. F. Hodges, X. Y. Zhang, D. Muchoney, A. H. Strahler, C. E. Woodcock, S. Gopal, A. Schneider, A. Cooper, A. Baccini, F. Gao, C. Schaaf (2002) Global land cover mapping from MODIS: algorithms and early results, *Remote Sensing of Environment*, Vol. 83 (1-2): 287-302.
- Fuller, R.M., Wyatt, B.K., Barr, C.J., 1998. Countryside survey from ground and space: different perspectives, complementary results. *J. Environ. Manag.* 54, 101–126.
- Fuller, R. M.; Cox, R.; Clarke, R. T.; Rothery, P.; Hill, R. A.; Smith, G. M.; Thomson, A. G.; Brown, N. J.; Howard, D. C.; Stott, A. P.. 2005 The UK land cover map 2000: Planning, construction and calibration of a remotely sensed, user-oriented map of broad habitats. *International Journal of Applied Earth Observation and Geoinformation*, 7, 202-216
- Gates, D. M., Keegan, H. J., Schleiter, J. C., and Wiedner, V. R. (1965), Spectral properties of plants. *Appl. Opt.* 4:11–20.

- Galego, J and Bamps, C., 2008. Using CORINE land cover and the point survey LUCAS for area estimation. *International Journal of Applied Earth Observation and Geoinformation* 10: 467–475.
- Gerard, F., Plummer, S., Wadsworth, R., Ferreruella, A., Iliffe, L., Balzter, H. and Wyatt, B., 2003. Forest Fire Scar Detection in the Boreal forest with multi-temporal SPOT-VEGETATION data. *IEEE transactions on Geoscience and Remote Sensing*, 41, 2575- 2585.
- Gitelson, A. A. and M. N. Merzlyak. 1997. Remote estimation of chlorophyll content in higher plant leaves. *International Journal of Remote Sensing*, 18:2691–2697
- Goel, N. S. (1988), Models of vegetation canopy reflectance and their use in estimation of biophysical parameters from reflectance data. *Remote Sens. Rev.* 4:1–212.
- Hill R, Wilson A, George M (submitted) Mapping tree species in temperate deciduous woodland using time-series multi-spectral data, *Journal of Applied Vegetation Science*.
- Hill, R. A.; Smith, G. M.. 2004 CS2000 Module 9. Data integration for localised results and support for indicators of countryside character and quality. Reports A4 - February 2004. NERC/Centre for Ecology and Hydrology, 34pp. (C02124) (Unpublished)
- Hill R, Thomson A. (2005) Mapping woodland species composition and structure using airborne spectral and LiDAR data, *International Journal of Remote Sensing*, 26, 3763–377
- Homer, C., Dewitz, J., Fry, J., Coan, M., Hossain, N., Larson, C., Herold, N., McKerrow, A., VanDriel, J.N. & Wickham, J., 2007. Completion of the 2001 National Land Cover Database for the conterminous United States. *Photogrammetric Engineering and Remote Sensing* 73: 337-341.
- Jacquemoud, S., Baret, F., and Hanocq, J. F. (1992), Modeling spectral and bidirectional soil reflectance, *Remote Sens. Environ.* 41:123–132.
- Jakubauskas M, Legates D, Kastens J (2002) Crop identification using harmonic analysis of time-series AVHRR NDVI data, *Computers and Electronics in Agriculture*, 37,127-139
- Krauss, J., Bommarco, R., Guardiola, M., Heikkinen, R.K., Helm, A., Kuussaari, M., Lindborg, R., Ockinger, E., Meelis, M., Pino, J., Poyry, J., Raatikainen, K.M., Sang, A., Stefanescu, C., Teder, T., Zobel, M., and Steffan-Dewenter, S. 2010. Habitat fragmentation causes immediate and time delayed biodiversity loss at different trophic levels. *Ecology Letters*, (2010) 13: 597–605
- Kumar Joshi, P.K. , Roy, P.S., Singh, S., Agrawal, S., and Yada, D. (2006) Vegetation cover mapping in India using multi-temporal IRS Wide Field Sensor (WiFS) data *Remote Sensing of Environment* 103:190–202.
- Lengyel, S., Kobler, A., Kutnar, L., Framstad, E., Henry, P.-Y., Babij, V., Gruber, B., Schmeller, D., & Henle, K. (2008). A review and a framework for the integration of biodiversity monitoring at the habitat level. *Biodiversity and Conservation*, 17, 3341-3356.
- Li, H., Wu, J., 2004. Use and misuse of landscape indices. *Landscape Ecology* 19, 389–399.
- Lillesand T, Kiefer R (2008) *Remote Sensing and Image Interpretation*, Sixth Edition: John Wiley and Sons Inc. pp 804.
- Loveland, T. R. and A. S. Belward, 1997, The IGBP-DIS global 1km land cover data set, DISCover: first results *International Journal of Remote Sensing*, 18, 3289-3295.
- McRoberts, R.E., Wendt, D.G., Nelson, M.D. & Hansen, M.H., 2002. Using a land cover classification based on satellite imagery to improve the precision of forest inventory area estimates. *Remote Sensing of Environment* 81: 36-44.
- McRoberts, R.E., Holden, G.R., Nelson, M.D., Liknes, G.C., and Gormanson, D.D, 2006, Using satellite imagery as ancillary data for increasing the precision of estimates for the Forest Inventory and Analysis program of the USDA Forest service. *Canadian Journal of Forest Research*, 36: 2968-2980.
- Medcalf, K., Turton, N., Finch C. (2011) Making Earth observation work for UK biodiversity conservation. DEFRA/JNCC project report EnvSys/TEO_07-A, pp.83.
- Metzger, M. J., Bunce, R. G. H., Jongman, R. H. G., Múcher, C. A. and Watkins, J. W. (2005), A climatic stratification of the environment of Europe, *Global Ecology and Biogeography*, 14(6): 549-563.
- Moody A, Johnson D (2001) Land-surface phenologies from AVHRR using the discrete fourier transform, *Remote Sensing of Environment*, 75, 305-323
- Moss, D. & Davies, C.E. 2002. Cross-references between the EUNIS Habitat Classification and the nomenclature of CORINE Land Cover European Topic Centre on Nature Protection and Biodiversity, Paris.
- Myneni, R. B., Ross, J., and Asrar, G. (1989), A review on the theory of photon transport in leaf canopies. *Agric. For. Meteorol.* 45:1–153.
- Nilsson M., Folving, S., Kennedy, P., Puumalainen, J., Cincinati, G., Corona, P., Marchetti, M., Olsson, H., Ricotta, C., Ringvall, A., Ståhl, G., and Tompoo, E., 2003. Combining remote sensing and field data for deriving unbiased estimates of forest parameters over large regions. In: Corona, P.,

- Köhl, M., and Marchetti, M. (eds.) *Advances in Forest Inventory and for Sustainable Forest Management and Biodiversity Monitoring*. Kluwer Academic Publishers, Forestry Sciences pp. 19-32
- Nilsson, M., Holm, S., Wallerman, J., Reese, H. and Olsson, H., 2009. Estimating annual cuttings using multi-temporal satellite data and field data from the Swedish NFI. *International Journal of Remote Sensing*, 30:5109-5116.
- Oldeland, J., Wesuls, D., Rocchini, D., Schmidt, M., Jürgens, N. , 2010. Does using species abundance data improve estimates of species diversity from remotely sensed spectral heterogeneity? *Ecological Indicators* 10: 390-396.
- Palmer, M.W., Earls P.G., Hoagland B.W., White P.S., Wohlgemuth T. (2002) Quantitative tools for perfecting species lists, *Envirometrics*, 13: 121-137.
- Paradella W, Da Silva M, Rosa N. Kushigbor C (1994). A geobotanical approach to the tropical rain forest environment of the Carajas mineral province (Amazon region, Brazil), based on digital TM-Landsat and DEM data. *International Journal of Remote Sensing*, 15, 1633-1648.
- Peñuelas, J., J. Piñol, R. Ogaya, and I. Filella. 1997. Estimation of plant water concentration by the reflectance Water Index WI (R900/R970). *International Journal of Remote Sensing* 18:2869–2875
- Reese, H.M., Lillesand, T.M., Nagel, D.E., Stewart, J.S., Goldmann, R.A., Simmons, T.E., Chipman, J.W. & Tessar, P.A., 2002. Statewide land cover derived from multiseasonal Landsat TM data - A retrospective of the WISCLAND project. *Remote Sensing of Environment* 82: 224-237.
- Ross, J. K. (1981), *The Radiation Regime and Architecture of Plant Stands*, Kluwer Boston, Hingham, MA.
- Schmidtein, S., & Sassin, J. (2004) Mapping of continuous floristic gradients in grasslands using hyperspectral imagery, *Remote Sensing of Environment*, 92: 126-138
- Strand, H., Höft, R., Stritholt, J., Miles, L., Horning, N., Fosnight, E., eds. (2007). *Sourcebook on Remote Sensing and Biodiversity Indicators*. Secretariat of the Convention on Biological Diversity, Montreal, Technical Series no. 32: pp. 201.
- Thomas, J. R., Namken, L. M., Oerther, G. F., and Brown, R. G. (1971), Estimating leaf water content by reflectance measurements. *Agron. J.* 63:845–847.
- Thunnissen, H., de Wit, A. (2000) *The National Land Cover Database of The Netherlands* , ISPRS, Vol. XXXIII, Amsterdam, 2000
- US Geological Survey, Gap Analysis Program (GAP). February 2010. National Land Cover, Version 1.
- Ustin, S.L., Roberts D.A., Gamon, J.A., Asner, G.P. and Green, R.O. 2004, Using imaging spectroscopy to study ecosystem processes and properties, *BioScience*, 54(6):523-534.
- Walter-Shea, E. A., and Norman, J. M. (1991), Leaf optical properties. In *Photon–Vegetation Interactions* (R. B. Myneni and J. Ross, Eds.), Springer-Verlag, Berlin: 229–252.
- Wessman, C. A. (1990), Evaluation of canopy biochemistry. In *Remote Sensing of Biosphere Functioning* (R. J. Hobbs and H. A. Mooney, Eds.), Springer-Verlag, New York, pp.
- Yang, X., Skidmore, A.K., Melick, D., Zhou, Z., Xu, J. (2007) Towards an efficacious method of using Landsat TM imagery to map forest in complex mountain terrain in Northwest Yunnan, China, *Tropical Ecology* 48(2): 227-239

9. Annexes

Annex-1

EBONE



European Biodiversity Observation Network:

Design of a plan for an integrated biodiversity observing system
in space and time

Task 5.1.3 Intercalibration between SYNBIOSYS data and spatial data

Predictive habitat distribution modelling using RS proxy indicators, environmental data sets and in-situ data

Ver 3.0

Document date: 2011-04-05

A contribution to Document Ref.: EBONE-D5.5-2.0

Authors:

C.A Mùcher, S.M. Hennekens, M.H.G.I. Danes, G.W. Hazeu, G.J.
Roerink, A.J.W de Wit, S.B. Hoek, R.G.H. Bunce

EC-FPV Contract Ref: ENV-CT-2008-212322

Task5.1.3: a contribution to Report D5.5 Predictive habitat distribution modelling using RS proxy indicators, environmental data sets and in-situ data

Authors:

C.A Mücher, S.M. Hennekens, M.H.G.I. Danes, G.W. Hazeu, G.J.
Roerink, A.J.W de Wit, S.B. Hoek, R.G.H. Bunce



Table of Contents

1.	INTRODUCTION.....	4
2.	SELECTION OF HABITAT TYPES	5
2.1.	Habitat and vegetation typology.....	5
3.	VEGETATION RELEVÉS.....	9
4.	DATA SOURCES TO ESTABLISH KNOWLEDGE RULES.....	13
4.1.	Sources of documentation	14
4.2.	CORINE land cover manual.....	15
4.3.	Annex I habitat description.....	15
5.	SPATIAL MODELLING OF EUROPEAN HABITATS	17
5.1.	Alpine and Boreal heaths (H4060)	19
5.2.	Bushes with <i>Pinus mugo</i> and <i>Rhododendron hirsutum</i> (H4070)	23
5.3.	Siliceous alpine and boreal grasslands (H6150).....	27
5.4.	H6170 Alpine and subalpine calcareous grasslands.....	31
5.5.	H6210 Semi-natural dry grasslands and scrubland facies on calcareous substrates (Festuco-Brometalia) (* important orchid sites).....	35
5.6.	Species-rich <i>Nardus</i> grasslands, on siliceous substrates in (sub) mountain areas (H6230).....	41
5.7.	H6240. Sub-pannonic steppic grasslands	45
5.8.	H6250. Pannonic loess steppic grasslands	49
5.9.	H7110. Active raised bogs.....	53
5.10.	H7130 Blanket bogs (* if active bog).....	57
5.11.	H9150. Medio-European limestone beech forests of the Cephalanthero-Fagion..	61
5.12.	H9410. Acidophilous <i>Picea</i> forests of the montane to alpine levels (Vaccinio-Piceetea).....	65
5.13.	H9420. Alpine <i>Larix decidua</i> and/or <i>Pinus cembra</i> forests	69
5.14.	H9510. Southern Apennine <i>Abies alba</i>	73
6.	INTERCALIBRATION OF IN-SITU DATA WITH ENVIRONMENTAL DATA	75
6.1.	The decision tree experiment.....	75
7.	EO TIME-SERIES ANALYSIS TO IDENTIFY HABITATS.....	81
7.1.	Introduction	81
7.2.	Classifications.....	86
7.3.	Material.....	87
7.4.	Methodology.....	87
7.5.	Results	88
7.6.	Assessment of results.....	90
7.7.	Discussion.....	93
8.	REFERENCES.....	94
	Annex I Criteria used to classify the SynBioSys vegetation releves into the relevant Annex I habitat types for the various countries for which in-situ data were obtained.....	96

1. INTRODUCTION

For many reasons, amongst others the design of ecological networks and monitoring the status of habitats, there is need for information about the ‘wall-to-wall’ spatial distribution of habitats and species in Europe, both inside and outside protected areas. For example, to determine the spatial cohesion of habitat networks for viable populations in the landscape (Opdam et al., 2003, 2006) it is necessary to obtain information about the exact extent and spatial distributions of habitats. Information about the spatial distribution of species is being collected by many international organisations (e.g. Birdlife International). However, there are currently no pan-European habitat maps available. In response to this need, we present a methodology for the assessment and mapping of the distribution of habitats at pan-European scales.

A first step is to develop a refinement of land cover information into relevant ecological classes, as demonstrated in Figure 1. A second step is the integration with in-situ data, e.g. vegetation relevés. These relevés can not only be used to validate the modelled habitat maps based on the refinement of land cover information, but could also be exploited to calibrate the in-situ data with existing environmental layers to find new knowledge rules (inter-calibration). A last step is to enhance to spatial identification of European habitats based on their phenology using time-series of satellite imagery.

The ecological refinement concerns the land cover information as produced by for example CORINE and GLOBCOVER or GLOBCORINE. The developed methodology is a follow-up from former experiences (Mücher et al., 2009). Land cover information next to environmental data sets play a crucial role in this methodology. Since it became clear that in-situ information is often crucial next to information derived from remotely sensed information (Mücher, 2009) much effort was put in the collection of vegetation relevés across Europe. The land cover refinements will focus especially on the forest and grassland ecosystems, since they are under serious decline as reported by organisations like the European Environment Agency (EEA) and European Topic Centre Biological Diversity (ETC/BD). At first a selection of interesting vegetation types and related Annex I habitat types (European Commission, 2007) was made, which could be modelled in terms of their probability in actual distribution across Europe.

Chapter 1 is a general introduction. Chapter 2 treats the selection of vegetation types and habitats. Chapter 3 concerns the in-situ data. Chapter 4 deals with the knowledge rules to identify the selected habitats spatially across Europe. Chapter 5 provides the results and shows the correspondence with the independent in-situ data. Chapter 6 concerns the tree classification experiment for the intercalibration of in-situ data from SynBioSys with the spatial environmental data sets. Chapter 7 focusses on the analysis of MODIS time series to enhance to spatial identification of European habitats based on their phenology.

2. SELECTION OF HABITAT TYPES

The following sections will discuss the selection of Annex I habitat types and related vegetation types, since it is impossible to implement the methodology for all Annex I habitat types in this study.

2.1. *Habitat and vegetation typology*

The use of the Natura 2000 habitat types seems to be logical since the European policies on nature and biodiversity conservation are strongly linked to the Habitat Directive. However, the Annex I of the Habitat directive is not a hierarchical system and cannot be applied at various scales. Since aggregation and disaggregation of land cover, habitats and vegetation types is a strong requirement for the EBONE project, we suggest to use the European vegetation classification next to the Annex I of the Habitat Directive. The European vegetation classification is a hierarchical unifying system for habitats in Europe (Rodwell et al., 2002). It consists of 930 alliances, grouped into 237 alliances and 80 classes. In most cases the alliances can be linked to General Habitat Categories (Bunce et al. 2011), EUNIS and Annex I types. On the basis of the European classification of vegetation types (Rodwell et al., 2002), and as implemented in SynBioSys Europe with a serious collection of vegetation relevés across Europe, see www.synbiosys.alterra.nl/synbiosyseu/ (Schaminée et al., 2007), and a set of well-defined criteria, a preliminary set of 18 vegetation types have been selected. This will be discussed in the next sections. Chapter 3 will discuss more the vegetation relevés.

The criteria for the selecting of vegetation types have been defined as follows by us:

- Sensitive to climatic change
 - salt marsh vegetation along the coast;
 - snow bed vegetation and tall forbs vegetation in alpine and sub alpine regions
 - bog vegetation
- Sensitivity to land use change
 - Grassland and heath types in sub alpine and alpine regions
 - Mediterranean shrub vegetation
- Availability of computerized plot observation data.

Three tables will be presented. One with the selected vegetation types (called Alliances in the hierarchical system of the European vegetation classification, see Rodwell et al., 2002). For each type there is a short description and an indication of their sensitivity. The higher order level (Class) to which the selected types belong is mentioned each time above. The second table presents a list of potential species for each of the vegetation types. This list is created by linking the vegetation types to Natura 2000 habitat types and to extract the species listed for the habitat types.

ANNEX-1
Annex 1-EBONE Task 513 Report Mucher version-3

Table 1 Preliminary list of 15 selected vegetation types (plant communities), according to the European Vegetation Classification. The types in grey represent the orders or alliances.

Code	Scientific name	Description	Sensitivity
25	<i>Oxycocco-Sphagnetea</i>	<i>Ombrotrophic bog and wet heathland vegetation of acid oligotrophic peats</i>	
25A01	Ericion tetralicis	Wet heath and bog vegetation on drying deeper peats or winter-waterlogged peaty intergrades (Atlantic and sub-atlantic distribution)	Representative of heathlands and susceptible to changes in ground water levels and land use.
25C02	Ledo-Pinion	Pine-dominated swampy woodlands (East-European distribution)	Representative of heathlands and susceptible to changes in ground water levels and land use.
26	<i>Molinio-Arrhenatheretea</i>	<i>Anthropogenic pastures and meadows on deeper, more or less fertile soils in lowland regions</i>	
26I03	Trisetio-Polygonion bistortae	Meadows of well-drained, relatively fertile mineral soils in low-input agricultural systems of montane regions	Very sensitive to changes in agricultural practice.
28	<i>Festuco-Brometea</i>	<i>Steppes, rocky steppes and sandy grasslands of the sub-continental temperate and sub-boreal regions</i>	
28F05	Festucion valesiaca	Sub-continental closed fescue pastures and swards of central Europe	Sensitive to changes in agricultural practice.
42	<i>Mulgedio-Aconitetea</i>	<i>Scrub and tall-herb vegetation at high altitudes, moistened and fertilised by percolating water</i>	
42A01	Adenostylion alliariae	Tall-herb communities of central European mountains	Sensitive to climate change and maybe land use.
43	<i>Salicetea herbaceae</i>	<i>Vegetation of long-lasting snow-beds and slopes irrigated by melt waters</i>	
43A04	Salicion herbaceae	Dwarf-willow and moss dominated communities of snow-beds on lime-poor soils and rocks	Wide spread at high altitudes in the Alps and southern Norway, progressively lower in the North of Norway. Distribution can be accurately estimated and is very sensitive to climatic change
44	<i>Elyno-Seslerietea</i>	<i>Alpine and sub-alpine calcareous grasslands</i>	
44D08	Seslerion albicantis	Alpine and sub-alpine calcareous blue-grass swards	In the mountains this is one of highest grazed pastures susceptible to declining grazing pressure.
46	<i>Juncetea trifidi</i>	<i>Pastures, rush-heaths and fjell-field on lime-poor soils above the forest belt in alpine and sub-alpine zones</i>	

ANNEX-1
Annex 1-EBONE Task 513 Report Mucher version-3

46A04	Caricion curvulae	Alpine acid swards of the Alps and eastern and southern Carpathians	Sensitive to climate change, likely to be colonized by trees and shrubs (possibly by <i>Pinus mugo</i> and <i>Juniperus</i> species)
46A08	Juncion trifidi	Rush-heaths of Scandinavia, the Alps and the western Carpathians	Sensitive to climate change, likely to be colonized by trees and shrubs (possibly by <i>Pinus mugo</i> and <i>Juniperus</i> species)
46B05	Nardion strictae	Dense chionophilous grassy swards of the subalpine and alpine belts of the Alps, Carpathians and northern Apennines	Sensitive to land use
59	<i>Quercio-Fagetea</i>	<i>Mixed broadleaved woodland of more temperate climates in central and western Europe</i>	
59B05	Cephalanthero-Fagion	Thermophilous beech forests mostly on limestone	Sensitive to climate change
62	<i>Loiseleurio-Vaccinietea</i>	<i>Arctic-boreal and (sub)alpine dwarf-shrub heathlands</i>	
62A02	Loiseleurio-Diapension	Arctic-boreal chionophilous tundra scrub	Sensitive to change in climate (snow cover and temperature). Not affected by agricultural activities
62A05	Rhododendro-Vaccinion	Subalpine chionophilous wind-swept dwarf shrub heath of the Alps and Carpathians	Alpine low scrub mainly sensitive to grazing pressure
63	<i>Erico-Pinetea</i>	<i>Calcareous relict montane pine woods of the Balkans, the Alps and Carpathians</i>	
63A01	Erico-Pinion sylvestris	Relict open pine woods of the Alps, Carpathians and northern Dinarides	Will probably expand due to climatic change and/or abandonment.
66	<i>Vaccinio-Piceetea</i>	<i>Coniferous forest communities, and related heaths, of more acidic soils</i>	
66B01	Pinion mugo	Subalpine silicicolous krummholz of mountains of central and southwestern Europe	Might expand due to changes in climate and agricultural abandonment

Finally, it lead to the selection of 14 Annex I habitat types (see Table 2), for which European distribution maps were produced.

ANNEX-1
Annex 1-EBONE Task 513 Report Mucher version-3

Table 2 Table of selected Natura 2000 habitat types and their relation to vegetation types, according to the European Vegetation Classification.

Nr.	Natura 2000 code	Natura 2000 description	Code	Vegetation type
1	4060	Alpine and Boreal heaths	62A02	Loiseleurio-Diapension
			62A05	Rhododendro-Vaccinion
			63A01	Erico-Pinion sylvestris
2	4070	Bushes with <i>Pinus mugo</i> and <i>Rhododendron hirsutum</i> (<i>Mugo-Rhododendretum hirsuti</i>)	66B01	Pinion mugo
			25C02	Ledo-Pinion
3	6150	Siliceous alpine and boreal grasslands	46A04	Caricion curvulae
			46A08	Juncion trifidi
			46B05	Nardion strictae
4	6170	Alpine and subalpine calcareous grasslands	44D08	Seslerion albicantis
5	6210	Semi-natural dry grasslands and scrubland facies on calcareous substrates (<i>Festuco-Brometalia</i>) (* important orchid sites)	28C02	Bromion erecti
6	6230	Species-rich <i>Nardus</i> grasslands, on siliceous substrates in mountain areas (and submountain areas, in Continental Europe)	46A04	Caricion curvulae
7	6240	Sub-pannonic steppic grasslands	28F	Festucetalia valesiaca
8	6250	Pannonic loess steppic grasslands	28E	Festucetalia vaginatae
9	7110	Active raised bogs	25A01	Ericion tetralicis
10	7130	Blanket bogs (* if active bog)	25A01	Ericion tetralicis
11	9150	Medio-European limestone beech forests of the <i>Cephalanthero-Fagion</i>	59B05	Cephalanthero-Fagion
12	9410	Acidophilous <i>Picea</i> forests of the montane to alpine levels (<i>Vaccinio-Piceetea</i>)	66C01	Dicrano-Pinion
13	9420	Alpine <i>Larix decidua</i> and/or <i>Pinus cembra</i> forests		
14	9510	Southern Apennine <i>Abies alba</i>	66A01	Abieti-Piceion

3. VEGETATION RELEVÉS

To perform the various analyses within EBONE the availability of in situ vegetation data (plot observations or relevés) is highly required. It is estimated that throughout Europe there are more than one million computerized plot observations stored in numerous local databases. Most of these observations are available in so-called Turboveg databases. Turboveg (Gijbels et al., 2011) is a software package that was developed in The Netherlands for the processing of plot observations. It's an easy-to-use data base management system and provides methods for input, import, selection, and export of plot data. In 1994, Turboveg was accepted as the standard computer package for the European Vegetation Survey. Currently it has been installed in most European countries with more than a thousand users.

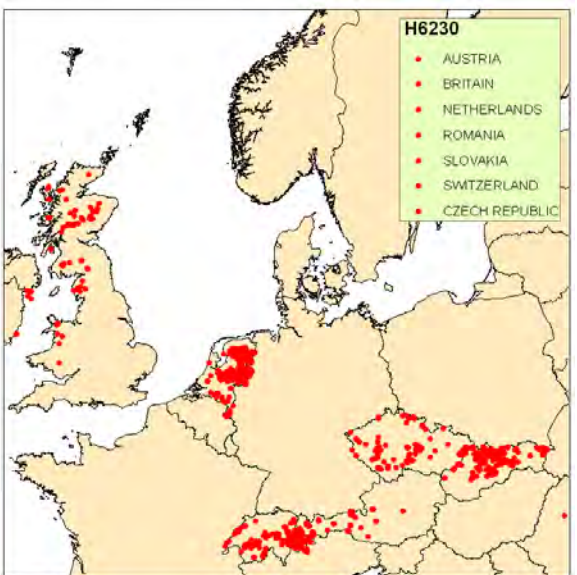
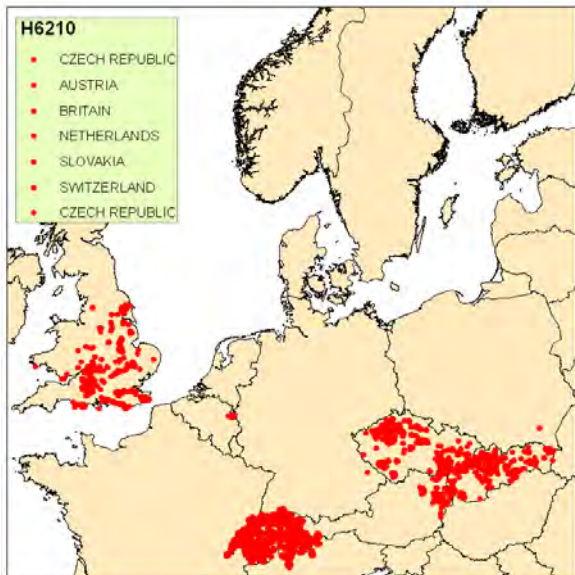
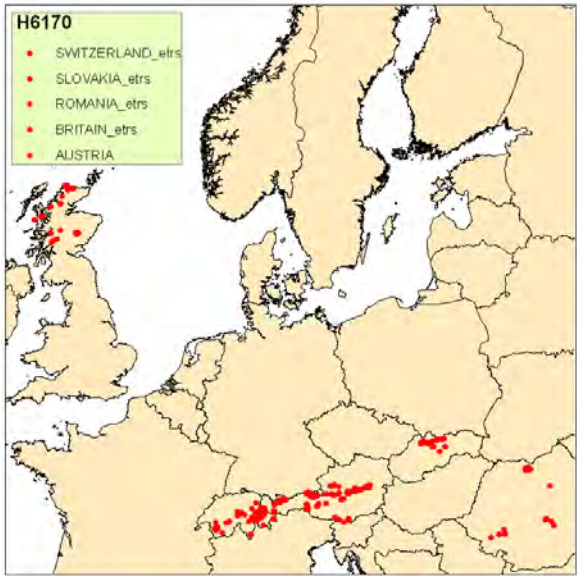
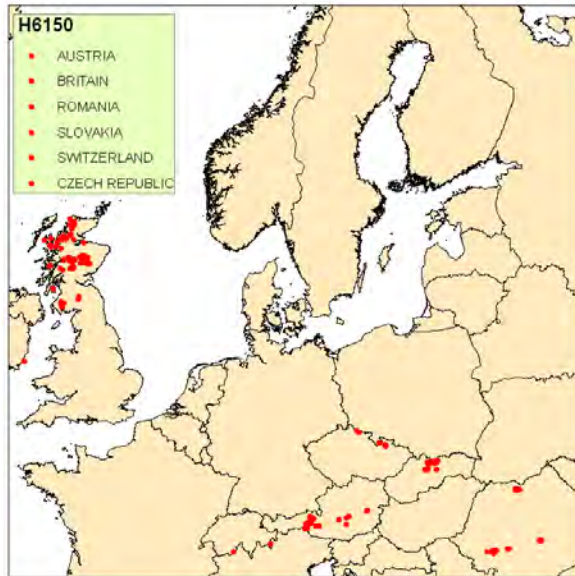
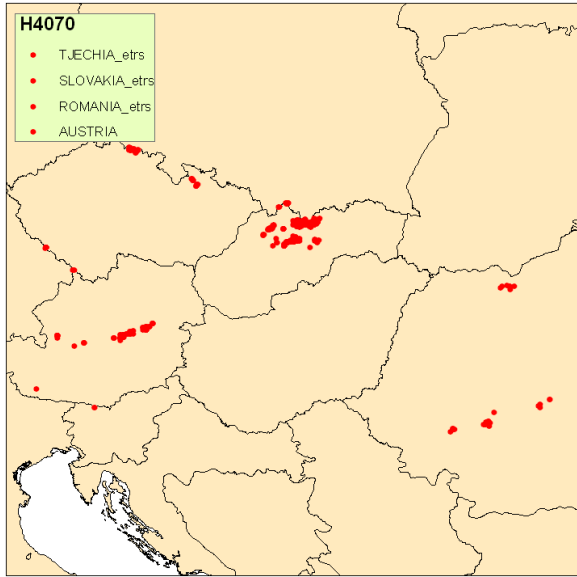
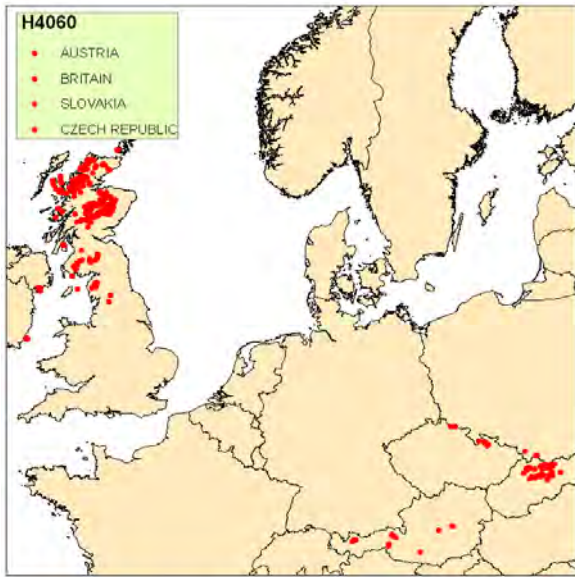
For the EBONE project in-situ vegetation data (stored in Turboveg databases) have been obtained through the network of SynBioSys Europa (Schaminée et al., 2007). In Table 3 an overview is given of all the collected vegetation relevés. Unfortunately, there are still a lot of EU countries for which we did not succeed yet to obtain vegetation plot data, although we know that they exist.

Table 3 Overview of collected vegetation relevés in the various countries

Country	Contact person	# of relevés	Selected	Long/Lat	Precision	Vegetation types	Remarks
Netherlands	stephan.hennekens@wur.nl	420,000	890	yes	point & 5x5 km	All requested delivered	
Britain		28,536	2,900	yes	100x100m	All requested delivered	
Germany	dengler@uni-lueneburg.de						Data expected soon
Belgium	Heidi.DEMOLDER@inbo.be	856	856	yes	point	Acid+Basic grasslands	
Austria	wolfgang.willner@vinca.at	917	4,300	yes	35km ²	All requested delivered	
Tjech republic	chytry@sci.muni.cz	5,985	8,762	yes	point	All requested delivered	
Slovakia	jozef.sibik@savba.sk	17,910	15,003	yes	point	All requested delivered	
Bulgaria	iva@bio.bas.bg	137	137	yes	point	Acid+Basic grasslands	
Slovenia	urban@zrc-sazu.si	0	0	no			Approached, but no geo refer
Frankrijk	brisse.henry@orange.fr	0	0				Databank Sophie, H. Brisse
Spain	idoia.biurrun@ehu.es	190	190	yes	10x10km	Acid+Basic grasslands	
	mcaceres@ub.edu	1900					No yet approached
Roemenia	popanamarca19@yahoo.com	2000		yes	500 * 500 m	All types	
Switzerland	niklaus.zimmermann@wsl.ch	14,900	14,900	yes	mostly 10x10m	All grassland types	
Poland		0	0				Approached, but no response
Estonia		0	0				?
Latvia		0	0				?
Lithuania		0	0				?
Italy		0	0				?
Hungary	bdz@botanika.hu	0	0				Approached, but no response
Norway	Nigel.Yoccoz@ib.uio.no	0	0				Approached, but no response
Sweden		0	0				?
Denmark		0	0				?
		493,331	47,938				

The vegetation relevés were classified into the relevant vegetation classes of Table 2, which are related to the specific Annex I habitat types of interest, using the TurboVeg software and additional specific criteria are mentioned in Annex I.

ANNEX-1
Annex 1-EBONE Task 513 Report Mucher version-3



ANNEX-1
Annex 1-EBONE Task 513 Report Mucher version-3

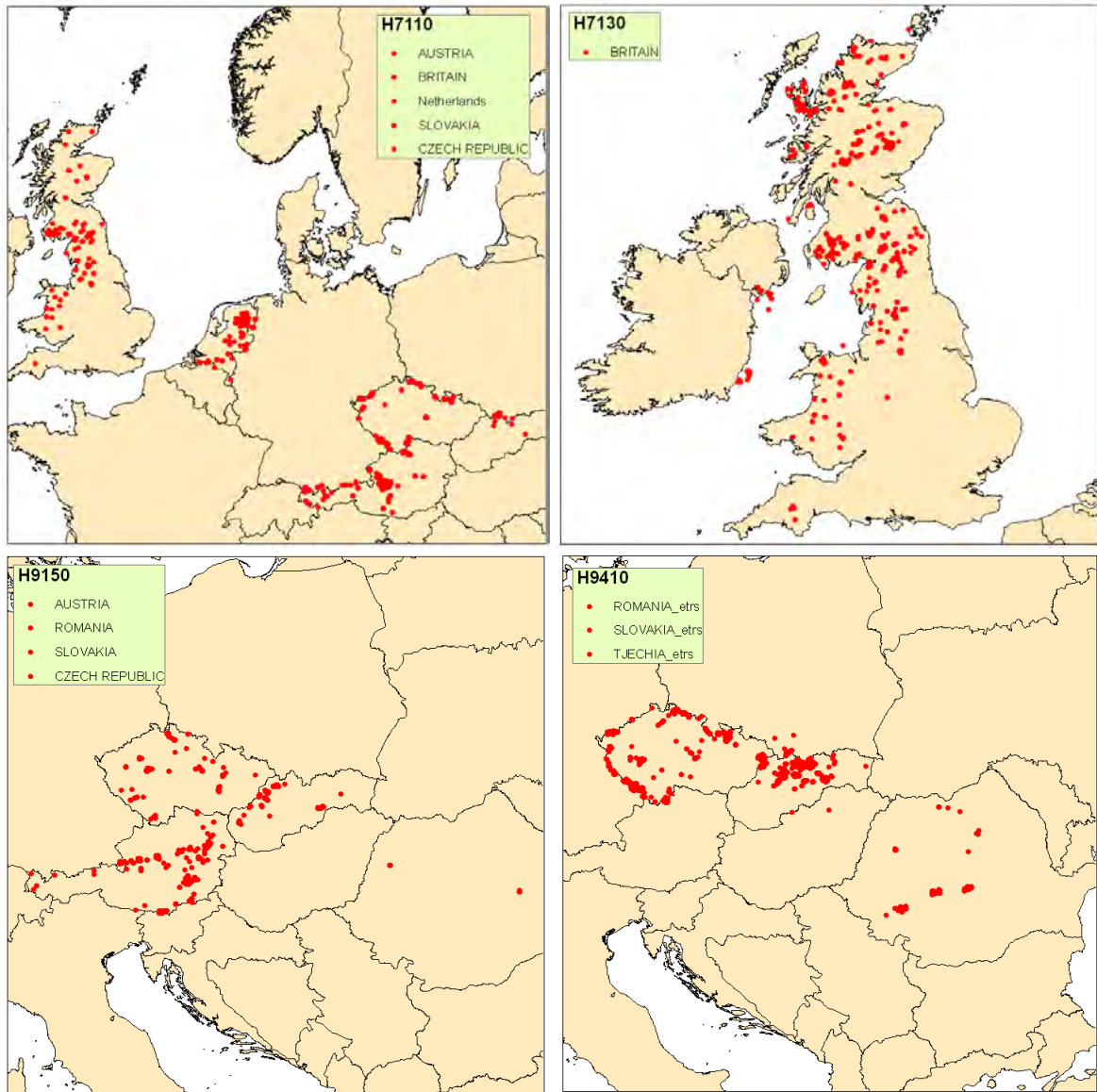


Figure 1 Locations of the selected vegetation relevés in relation to the specific Habitat Directive Annex I habitat types.

4. DATA SOURCES TO ESTABLISH KNOWLEDGE RULES

Much effort was made on the establishment of the knowledge rules for the relationship between CORINE land cover classes (CEC, 1994; Bossard et al., 2000; Büttner et al., 2004) and the Annex 1 Habitats (European Commission, 2007). The knowledge rules were largely based on the ecological knowledge of Dr R.G.H. Bunce who was responsible for this specific part in the report.

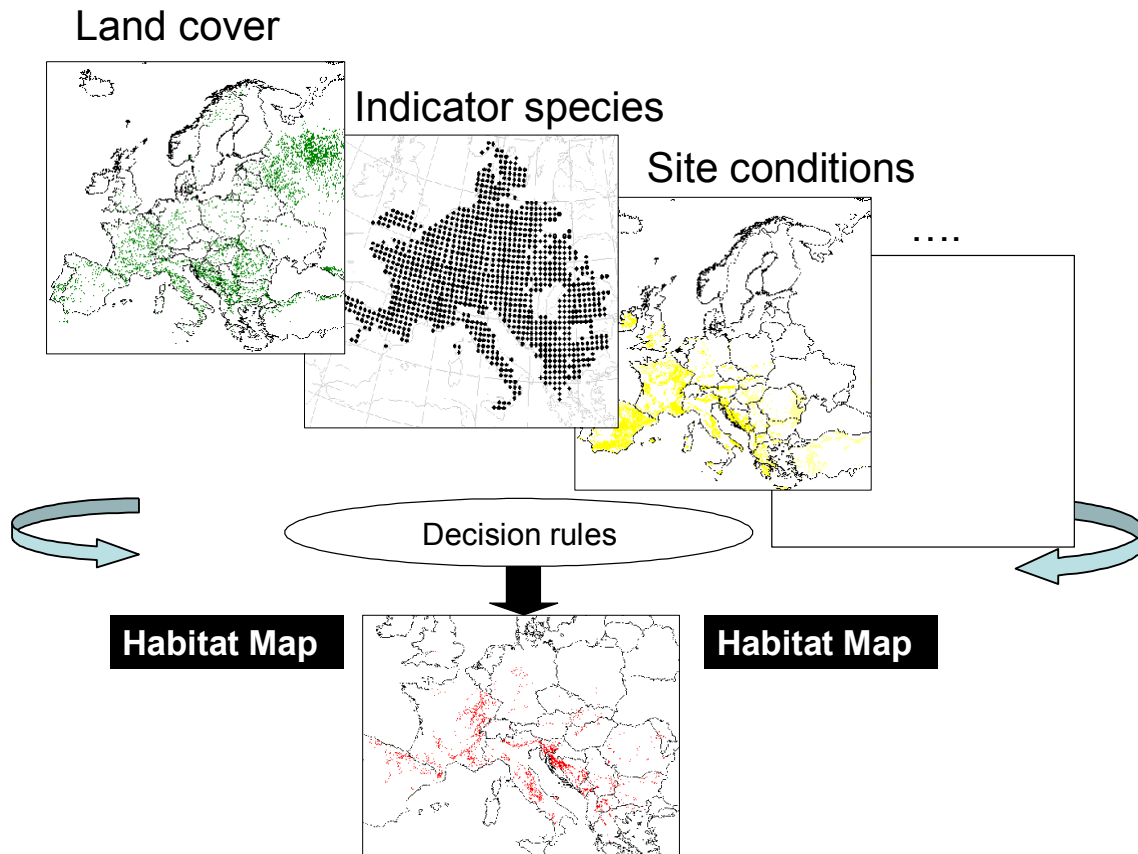


Figure 2 Flowchart of the methodological approach (Mücher et al 2009) to identify the spatial distribution of European Habitats.

A first formal relation between the Annex I habitats and CORINE land cover (CEC, 1994; Bossard et al, 2000; Büttner et al, 2004) was made in the PEENHAB project (Mücher et al., 2004, Mücher et al., 2009). The relationship between CORINE land cover (CLC) and Natura 2000 habitats is now being improved per biogeographic region (Metzger et al., 2005) So the EBONE knowledge rules provides now additional information about the mapping rules, the indicator species, the relationship to the General Habitat Categories (Bunce et al., 2011), the field identification and its occurrence, direct threats to the habitat, its relation to climate change, and the distribution of Annex I sites over the environmental zones.

In the following section the sources of information are listed that have been used in preparing the current document.

4.1. Sources of documentation

The following data sources have been used to establish the knowledge rules for habitat modelling:

1. Interpretation Manual of European Union Habitats
2. EUNIS website (<http://eunis.eea.europa.eu/index.jsp>)
3. Tables of Annex 1 habitats by Biogeographic regions
4. CORINE land cover technical report
5. PEENHAB report (Mücher et al., 2005)
6. Consultation with *Doug Evans* (ETC/BD) and some local experts

Evans (2006) describes in detail how the Annex 1 Habitats were constructed. The Interpretation manual of European Union Habitats is a living document. Evans also indicates that the names are much more difficult to change than their descriptions. The present document is a scientific amplification and interpretation of those descriptions, and will subsequently be discussed.

The Annex 1 and its Priority Habitats are determined by an ongoing series of meetings held under the auspices of the EU. There has been no intention to complete a land cover key for the Annex I habitat types with total coverage of the land surface of Europe nor to provide a hierarchy for the classes. Because Annex 1 is legally binding it is essential that in the long term the habitats must be mapped in a consistent and reproducible way.

The descriptions in the Interpretation manual of European Habitats varies a lot in level of detail, from three pages for species rich *Nardus* grasslands, to three lines for *Castanea sativa* forests (but even in the former case there is no definition as to the number of species as a threshold for the class). Although some habitats are point features e.g. Tufa springs, it is unlikely that small patches of other habitats would be considered as valid records of that habitat. As Evans (2006) has pointed out the majority of Annex 1 habitats are based on vegetation associations with the principal exceptions of the landscape units, of which there are about 20. The response of many countries has been to use broad interpretations of the Annex 1 descriptions e.g. in north-west Spain acidophilous beech forests (9120) are included in the biogeographic information submitted on Natura 2000 sites although the region is not mentioned as containing 9120 in the Annex I descriptions. Doug Evans has emphasized that the Annex I descriptions are not exhaustive as to their regional distributions. Furthermore it is recognized that the biogeographic references in the habitat names do not preclude that habitat from occurring outside that region.

In other cases, as in the Netherlands, closely linked associations have been added to the Annex I habitats present in Natura 2000 sites. The implications of this process are that a given list of habitats from different countries may not involve the same range of characteristics. The only way to determine the actual situation is to take stratified random samples of Annex I habitats in different Environmental Zones and actually record in the field what is present. Highly managed habitats e.g. species rich fallow and cropland, are not included in Annex I although they may be present in habitat complexes such as Machair. Many red data book species are present in such habitats and will therefore not be included under the current Annex I list. Similarly agricultural land which is in the process of being abandoned is not included because the main objective of Annex 1 is to : “identify undisturbed/semi-natural habitats for protection”. The Annex 1 habitats are not hierarchical but such a structure is currently being prepared for the expert system in EBONE. Habitats may occur at several spatial levels, e.g. points, linear features, patches, and landscapes. The implication of these comments is that the majority of lowland agricultural landscapes do not have Annex 1 habitats present, hence there is a need to identify residual biodiversity in such

areas by using other habitat categories (e.g. Bunce et al., 2011). Including linear and point elements.

There are many possibilities for refinement of the relationships identified in the present document, especially by consulting the available literature, e.g. on tree lines and the range of altitudes occupied by different vegetation associations. Many of the terms used in Annex 1 are not defined which leads to differences in interpretation. For example, Fennoscandia may include the Baltic coast of Germany or not, whereas concepts like alpine and montane are notoriously difficult to define. Evans (2006) states that the names of Annex 1 Habitats can only be altered by a decision from the Council of Ministers, whereas the descriptions can be changed by agreement of the Habitats Committee. The present document is only concerned with the interpretation of those descriptions.

4.2. CORINE land cover manual

The English text contains many words e.g. briars and hortillonage that are not in general use in the ecological literature. Some terms e.g. heathland are incorrectly used and some species e.g. *Ostrya carpinifolia* do not belong to the land covers concerned. The English names of some species are also given the wrong Latin names e.g. briars are given as *Rubus* species. Some of the descriptions are very general so that it is difficult to know what is included. The text in the present document includes commentaries on the manual and is designed to support the interpretation given as well as to help future users because the assumptions are described eg that briars probably do not mean *Rosa* spp which are only rarely seen as a dominant member of scrub habitats, whereas *Rubus* is widespread in this role throughout Europe. Their information has been included in the present report. As with Annex 1 of the Habitat Directive the only way to obtain more reliable quantitative data is to visit actual locations or use extant data like vegetation relevés. For example the boundaries between raised bog and blanket bogs is clear in well developed situations and in many regions, but in Ireland and Scotland there are many overlaps and further confusion with valley bogs which do not fit into either of the other two categories. The interpretation of some classes means that a given Annex 1 habitat may appear in different places but with different rules being used to identify it. Some land cover types may have a wide range of biodiversity linked to them e.g. vineyards and olive groves so that local rules could be developed to define potential biodiversity more accurately. Thus in mountain foothills and on shallow soils in the Gredos mountains the vineyards are rich whereas in much of Andalusia they are intensively managed.

4.3. Annex I habitat description

Each of the Annex I habitats has the following description fields in this document:

1. Mapping rules: these mapping rules are constructed from the information provided in the Interpretation manual of European habitats on where the habitat occurs. This information is supplemented by field experience of prof. R.G.H. Bunce and by discussions with phytosociologists in the EBONE project. Consultation was also held with Doug Evans of the European Environment Agency Topic Centre on Biological Diversity in Paris to further check the descriptions.

2. Indicator species: the indicator species are in most cases a subset of the Annex I plant species. A subset has been made since the selected species are the most characteristic and stable species present within the habitat.

3. GHC. The General Habitat Classes (GHC) are defined within the EBONE project (Bunce et al., 2011). The basis of the General Habitat Categories is the classification of plant Life forms produced by the Danish botanist Raunkiaer early in the 20th Century. These Life forms e.g. annuals or trees. They are based on the scientific hypothesis that habitat structure is related to the environment. The General Habitat Categories cover the Pan-European region (except Turkey) with 160 GHC's derived from 16 plant life forms and 18 non-life forms (Bunce et al., 2011). The Codes for the General Habitat Categories are in this document: **LHE** = leafy hemicryptophytes(herbs), **CHE** = caespitose hemicryptophytes (grasses), **SUC** = succulents, **THE** = therophytes (annuals), **HEL** =helophytes (marsh plants) **CRY** = mosses, liverworts and lichens, **DCH** = espaliers below 5cm, **SCH**=dwarf scrub 5-30cm, **LPH** = low scrub,30-60cm, **MPH** = mid scrub 60cm-2.0 m, **TPH** = tall scrub2m-5m., **FPH** = forest over 5 m, **CON** = conifer, **DEC** = deciduous, **EVR** = evergreen, **NLE** = non leafy evergreen, **SPI** = spiny/summer deciduous

4. Field identification: comments on the probable ease of identification of the habitat in the field.

5. Occurrence: three categories are used: rare, where the habitat is present in isolated patches, usually small, common, where it is distributed widely but does not cover large areas in the landscape and abundant where it is not only widespread but is also dominant. These are qualified where necessary.

6. Direct threats: based on the knowledge of the vegetation and literature . The information could also be supplemented later by other experts.

7. Potential impacts of climate change: based on knowledge of the vegetation, literature and the change in Environmental Zones described by Metzger et al. (2005).

8. Vegetation succession due to abandonment: conversion of the present composition into plant lifeform categories followed by an interpretation of likely successional changes together with possible timescales.

9. Distribution. This is the distribution of the specific habitat over the various Environmental Zones (Metzger et al., 2005). The codes, based on the EBONE handbook (Bunce et al 2011) are as follows for the Environmental Zones:

ALS = Alpine South, **BOR** = Boreal, **NEM** = Nemoral, **ATN** = Atlantic North, **ATC** = Atlantic Central, **ALS** = Alpine South, **PAN** = Pannonian, **CON** = Continental, **LUS** = Lusitanian, **MDM**- Mediterranean Mountains, **MDN** = Mediterranean North, **MDS** = Mediterranean South

Distribution (sites) has been obtained directly from the Natura 2000 database intersected with the Environmental Zones. Distribution (Bunce) is based on expert knowledge from Bob Bunce. Besides, note that the code **CLC** refers to the CORINE land cover class. **Annex I** is standing for the Annex I of the Habitat Directive.

For the selected habitats the knowledge rules are given in the sections below. For all other habitat types, the knowledge rules are given in Annex II.

5. SPATIAL MODELLING OF EUROPEAN HABITATS

The following sections will give the results of the habitat distribution modelling for each specific habitat type. All models were implemented within ARCGIS 9.3 model builder. An example of such a model is given below. All resulting habitat distribution maps have a spatial resolution of 100 meters. Since this spatial resolution can hardly be visualised in this document for entire Europe, the results are also highlighted for specific details of the European habitat distribution maps.

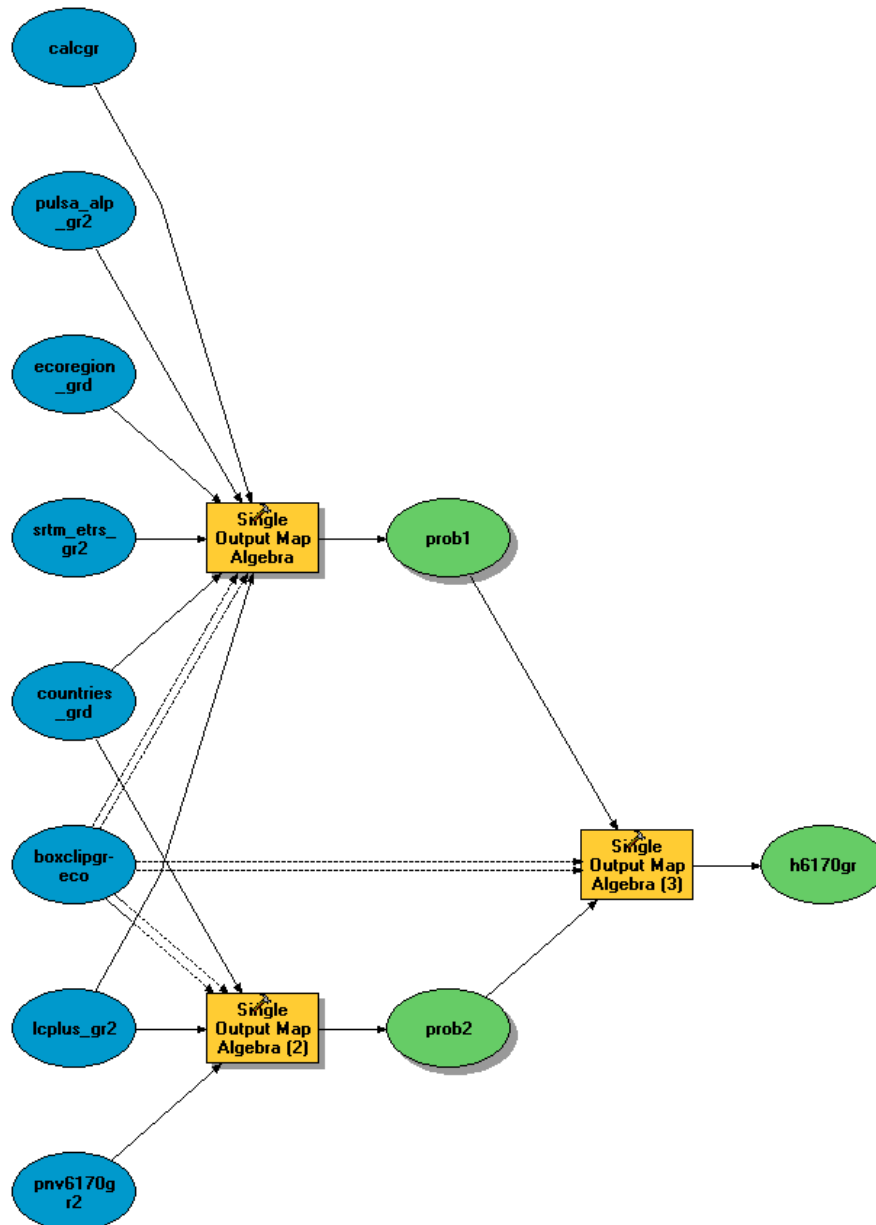


Figure 3 Example of the constructed distribution model for Annex I habitat type H6170 "Alpine and subalpine calcareous grasslands" made with the modelbuilder in ARCGIS 9.2. In the blue boxes the input data sets are mentioned, in the orange boxes the knowledge rules are implemented. Intermediate results are probability 1 based on actual land cover information and abiotic conditions, probability 2 is based on information from the potential natural vegetation map confronted with actual land cover information. H6170gr is the final result as an ARCGIS grid file for Annex I habitat type 617.

The following sections demonstrate the results of the spatial modelling exercises for the 14 selected Annex I habitat types and provides also inside to the established knowledge rules.

5.1. Alpine and Boreal heaths (H4060)

Annex I description

Alpine and Boreal heaths
Natura 2000 habitat type code 4060
Palaearctic habitat code (and Corine Biotopes) 31.4
Priority habitat: No
Parent: Temperate heath and Scrub (4000)
Description
<p>Small, dwarf or prostrate shrub formations of the alpine and subalpine zones of the mountains of Eurasia dominated by ericaceous species, [<i>Dryas octopetala</i>], dwarf junipers, brooms or greenweeds; [<i>Dryas</i>] heaths of the British Isles and Scandinavia.</p> <p>Sub-types :</p> <ul style="list-style-type: none"> • 31.41 - Alpine dwarf ericoid wind heaths. <i>Loiseleurio-Vaccinion</i>. Very low, single-stratum, carpets of trailing azalea, <i>Loiseleuria procumbens</i>, prostrate <i>Vaccinium</i> spp. or other prostrate ericoid shrublets, accompanied by lichen, of high windswept, mostly snowfree, localities in the alpine belt of the high mountains of the Alpine system. • 31.42 - Acidocline alpenrose heaths. <i>Rhododendro-Vaccinion</i>. <i>Rhododendron</i> spp.-dominated heaths of acid podsols in the Alps, the Pyrenees, the Dinarids, the Carpathians, the Balkan Range, the Pontic Range, the Caucasus and the Himalayan system, often with <i>Vaccinium</i> spp., sometimes with dwarf pines. • 31.43 - Mountain dwarf juniper scrub. <i>Juniperion nanae</i>, <i>Pino-Juniperion sabinae</i> p., <i>Pino-Cytision purgantis</i> p. Usually dense formations of prostrate junipers of the higher levels of southern Palaearctic mountains. • 31.44 - High mountain <i>Empetrum-Vaccinium</i> heaths. <i>Empetro-Vaccinietum uliginosi</i>. Dwarf heaths dominated by <i>Empetrum hermaphroditum</i>, <i>Vaccinium uliginosum</i>, with <i>Arctostaphylos alpina</i>, <i>Vaccinium myrtillus</i>, <i>Vaccinium vitis-idaea</i> and lycopodes (<i>Huperzia selago</i>, <i>Diphasiastrum alpinum</i>), mosses (<i>Barbilophozia lycopodioides</i>, <i>Hylocomium splendens</i>, <i>Pleurozium schreberi</i>, <i>Rhythidiadelphus triquetrus</i>) and lichens (<i>Cetraria islandica</i>, <i>Cladonia arbuscula</i>, <i>Cladonia rangiferina</i>, <i>Cladonia stellaris</i>, <i>Cladonia gracilis</i>, <i>Peltigera aphthosa</i>) of the sub-alpine belt of the Alps, the Carpathians, the Pyrenees, the Central Massif, the Jura, the Northern Apennines, characteristic of relatively windswept, snow-free stations, in frost-exposuresituations that are, however, less extreme than those prevailing where communities of 31.41 dominate. Unlike the formations of 31.41, those of 31.44 are clearly two-layered. • 31.45 - Boreo-alpine heaths Alpine heaths of the highlands and islands of Scotland, alpine and lowland boreal heaths of Iceland, alpine heaths of boreal mountains, in particular of the mountains of Scandinavia, of the Urals, of the mountains of Siberia, alpine heaths of Far Eastern mountains at, or just south of, the limits of the boreal zone, with <i>Juniperus nana</i>, <i>Loiseleuria procumbens</i>, <i>Empetrum hermaphroditum</i>, <i>Arctostaphylos uva-ursi</i>, <i>Arctostaphylos alpina</i> and elements of Alpine flora. • 31.46 - <i>Bruckenthalia</i> heaths: only outside the European Union. • 31.47 - Alpine bearberry heaths. <i>Mugo-Rhodoretum hirsuti</i> p., <i>Juniperion nanae</i> p., i.a. Interpretation Manual - EUR25 Page 44 Mats of <i>Arctostaphylos uva-ursi</i> or <i>Arctostaphylos alpina</i> of the alpine, sub-alpine and locally, montane, belts of the Alps, the Pyrenees, the northern and central Apennines, the Dinarids, the Carpathians, the Balkan Range, the Rhodopides (south to the Slavianka-Orvilos, the Menikion, the Pangeon, the Falakron and the Rhodopi), the Moeso-Macedonian mountains (including Athos), the Pelagonides (south to the Greek Macedonian border ranges Tzena, Pinovon and Kajmakchalan) and Olympus, in the Thessalian mountains, mostly on calcareous substrates. • 31.48 - Hairy alpenrose-erica heaths. <i>Mugo-Rhodoretum hirsuti</i> p. Forest substitution heaths, treeline fringe formations and alpine heaths or mats of calcareous soils in the Alps and the Dinarides, with <i>Rhododendron hirsutum</i>, <i>Rhododendron intermedium</i>, <i>Rhodothamnus chamaecistus</i> and <i>Erica herbacea</i>, often accompanied by <i>Clematis alpina</i>, <i>Daphne striata</i>, <i>Daphne mezereum</i>, <i>Globularia cordifolia</i>, <i>Arctostaphylos uva-ursi</i>. <i>Rhododendron hirsutum</i> and, mostly in the Austrian Alps, <i>Erica herbacea</i> are the most frequent dominants; other shrubs can locally play that role. <i>Arctostaphylos</i> spp.-dominated facies have, however, been included in 31.47. • 31.49 - Mountain Dwarf heaths formed by mats of the woody <i>Dryas octopetala</i> in high Palaearctic mountains, in boreal regions and in isolated Atlantic coastal outposts. • 31.4A - High mountain dwarf bilberry heaths <i>Vaccinium</i>-dominated dwarf heaths of the sub-alpine belt of southern mountains, in particular, of the northern and central Apennines, the Balkan Range, the Helenides, the Pontic Range and the Caucasus, with <i>Vaccinium myrtillus</i>, <i>Vaccinium uliginosum</i> s.l., <i>Vaccinium vitis-idaea</i> and, locally, <i>Empetrum nigrum</i>. They are richer in grassland species than the communities of 31.44 and often take the appearance of alpine grassland with dwarf shrubs. <i>Vaccinium myrtillus</i> also plays a much more dominant role, in lieu of <i>Vaccinium uliginosum</i> and <i>Empetrum hermaphroditum</i>.

ANNEX-1

Annex 1-EBONE Task 513 Report Mucher version-3

- 31.4B - High mountain greenweed heaths Low *Genista* spp. or *Chamaecytisus* spp. heaths of the sub-alpine, low alpine or montane belts of high southern nemoral mountains, in particular of the southern Alps, the Apennines, the Dinarides, the southern Carpathians, the Balkan Range, the Moeso-Macedonian mountains, the Pelagonides, the northern Pindus, the Rhodopides, the Thessalian mountains.

Plants

31.41 - *Loiseleuria procumbens*, *Vaccinium* spp.; 31.42 - *Rhododendron ferrugineum*; 31.44 - *Empetrum hermaphroditum*, *Vaccinium uliginosum*; 31.45 - *Juniperus nana*, *Loiseleuria procumbens*, *Empetrum hermaphroditum*, *Arctostaphylos uva-ursi*, *Arctostaphylos alpina*; in Fennoscandia also *Betula nana*, *Cassiope tetragona*, *Cornus suecica*, *Juniperus communis*, *Phyllodoce caerulea*, *Vaccinium myrtillus* and *Cladonia alpestris*; 31.47 - *Arctostaphylos uva-ursi*, *Arctostaphylos alpina*; 31.48 - *Rhododendron hirsutum*, *Rhododendron intermedium*, *Rhodothamnus chamaecistus* and *Erica herbacea*; 31.49 - *Dryas octopetala*; 31.4A - *Vaccinium myrtillus*, *Vaccinium uliginosum* s.l., *Vaccinium vitis-idaea*; 31.4B - *Genista radiata*, *G. holopetala*, *G. hassertiana*, *Chamaecytisus eriocarpus*, *C. absinthioides*.

Geographic distribution

Austria, Finland, France, Germany, Greece, Ireland, Italy, Portugal, Spain, Sweden, United Kingdom. Sub-type distribution: 31.41 alpine belt of the high mountains of the Alpine system; 31.42 the Alps, the Pyrenees, the Dinarids, the Carpathians, the Balkan Range, the Pontic Range, the Caucasus and the Himalayan system; 31.43 the higher levels of southern Palaeartic mountains; 31.44 the sub-alpine belt of the Alps, the Carpathians, the Pyrenees, the Central Massif, the Jura, the Northern Apennines; 31.45 Scotland, Iceland, boreal mountains, in particular of the mountains of Scandinavia, of the Urals, of the mountains of Siberia, Far Eastern mountains at, or just south of, the limits of the boreal zone; 31.47 alpine, sub-alpine and locally, montane, belts of the Alps, the Pyrenees, the northern and central Apennines, the Dinarids, the Carpathians, the Balkan Range, the Rhodopides (south to the Slavianka-Orvilos, the Menikion, the Pangeon, the Falakron and the Rhodopi), the Moeso-Macedonian mountains (including Athos), the Pelagonides (south to the Greek Macedonian border ranges Tzena, Pinovon and Kajmakchalan) and Olympus, in the Thessalian mountains, mostly on calcareous substrates; 31.48 the Alps and the Dinarides; 31.49 high Palaeartic mountains, in boreal regions and in isolated Atlantic coastal outposts; 31.4A the sub-alpine belt of southern mountains, in particular, of the northern and central Apennines, the Balkan Range, the Helenides, the Pontic Range and the Caucasus; 31.4B the sub-alpine, low alpine or montane belts of high southern nemoral mountains, in particular of the southern Alps, the Apennines, the Dinarides, the southern Carpathians, the Balkan Range, the Moeso-Macedonian mountains, the Pelagonides, the northern Pindus, the Rhodopides, the Thessalian mountains;

<http://eunis.eea.europa.eu/habitats-factsheet.jsp?tab=0&idHabitat=10087>

EBONE rules

CLC:	322 - Moors and heath lands
Annex I:	4060 - Alpine and Boreal heaths
Mapping rules:	Alpine North / Boreal over 800m , Atlantic North over 900 m small patches on exposed coastal areas in the north), Alpine South over 1800 m. No soils as highly variable, although skeletal soils eg rankers predominate.
Indicator species:	-
GHC:	- SCH/EVR but locally DCH/EVR/DEC + Moist acid soils + upto 30% bare ground/rocks + key indicators. Also LPH/CON MPH/EVR
Field identification:	Although highly variable because this class has a well recognisable landscape context and consistent life form structure it will probably be readily identified.
Occurrence:	-Occurs in large areas in the centre of its range – small patches on edge

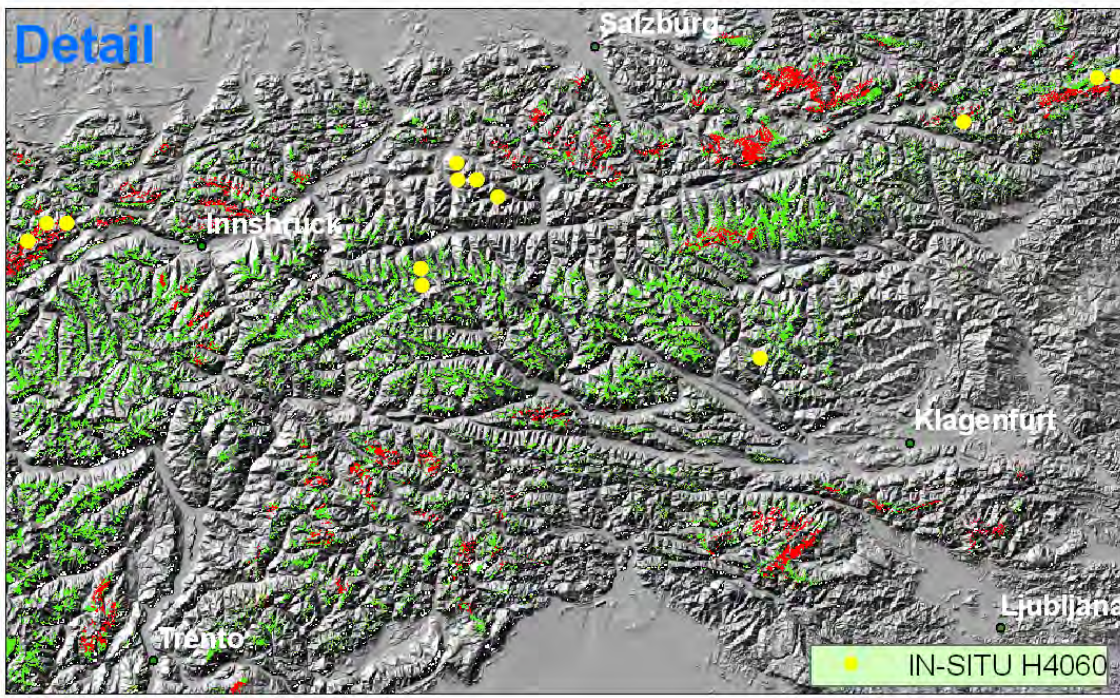
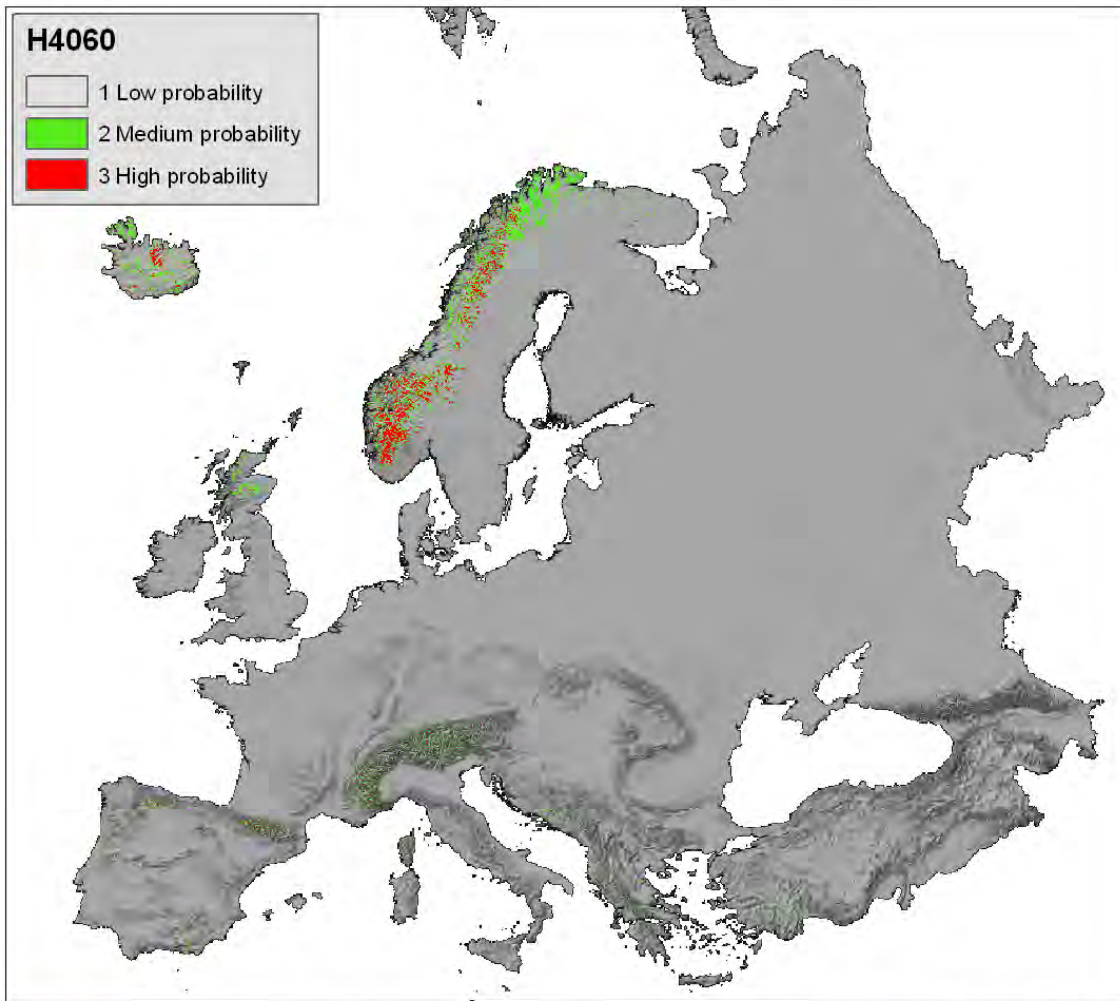
ANNEX-1
Annex 1-EBONE Task 513 Report Mucher version-3

Direct threats:	At low altitudes overgrazing locally although in some areas grazing may have halted scrub invasion. decline in grazing can therefore lead to quite rapid changes. Reindeer grazing can cause erosion in Scandinavia.											
Climate change:	The increased temperatures likely in many of these mountains will favour scrub expansion at lower levels as shown by Kienast. However the class may well be able to move higher except where it is caused by extreme exposure.											
Succession:	Colonisation: status Shrubby chamaephytes or L PH or even Mid phanerophytes in some situations. May remain as Shrubby chamaephytes in extreme situations and especially in the Scandinavian mountains at mid altitudes Low phanerophytes to Mid phanerophytes 10 and Tall phanerophytes 15 at low altitudes Low phanerophytes to Mid phanerophytes 10 Tall phanerophytes 15 possibly Forest phanerophytes 20.											
Distribution (sites):	ALN	BOR	<i>nem</i>	ATN	ALS	CON	ATC	<i>pan</i>	LUS	MDM	<i>mdn</i>	<i>mds</i>
Distribution (Bunce):	ALN	BOR	<i>nem</i>	<i>atn</i>	ALS	CON	<i>atc</i>	<i>pan</i>	<i>lus</i>	<i>mdm</i>	<i>mdn</i>	<i>mds</i>



Photo 1 H4060 Alpine and boreal heath in Mountains Sweden (photo Bob Bunce, 2005).

RESULT H4060 ALPINE AND BOREAL HEATHS



5.2. Bushes with *Pinus mugo* and *Rhododendron hirsutum* (H4070)

Annex I description

Bushes with <i>Pinus mugo</i> and <i>Rhododendron hirsutum</i> (Mugo-Rhododendretum hirsuti)
Natura 2000 habitat type code 4070
Paleartic habitat code (and Corine Biotopes) 31.5
Priority habitat: Yes
Parent: Temperate heath and Scrub (4000)
Description
<i>Pinus mugo</i> formations usually with <i>Rhododendron</i> spp. of the dry eastern inner Alps, the northern and southeastern outer Alps, the southwestern Alps and the Swiss Jura, the eastern greater Hercynian ranges, the Carpathians, the Apennines, the Dinarides and the neighbouring Pelagonides, the Pirin, the Rila and the Balkan Range.
Plants
<i>Pinus mugo</i> , <i>Rhododendron hirsutum</i> , <i>R. ferrugineum</i> . <i>Rhodothamnus chamaecistus</i>
Geographic distribution
Alps (Austria, France, Germany, Italy) and Apennines
http://eunis.eea.europa.eu/habitats-factsheet.jsp?idHabitat=10088

EBONE rules

CLC:	322 - Moors and heath lands											
Annex I:	4070 - Bushes with <i>Pinus mugo</i> and <i>Rhododendron hirsutum</i> (Mugo-Rhododendretum hirsuti)											
Mapping rules:	Alpine South over 1800 m plus distribution of <i>Pinus mugo</i> .											
Indicator species:	<i>Pinus mugo</i> , <i>Rhododendron chamaecistus</i> , <i>Rhododendron hirsutum</i> .											
GHC:	-MPH/EVR/CON + moist acid soils + montane situation + indicators											
Field identification:	:straightforward if a minimal cover of 30% is assumed.											
Occurrence:	-often in large units but locally in small patches											
Direct threats:	Burning and clearance for grazing.											
Climate change:	Likely to expand upwards with higher temperatures.											
Succession:	Colonisation: climax in most cases.											
Distribution (sites):	<i>aln</i>	<i>bor</i>	<i>nem</i>	<i>atn</i>	ALS	CON	<i>atc</i>	<i>pan</i>	<i>lus</i>	MDM	<i>mdn</i>	<i>mds</i>
Distribution (Bunce):	<i>aln</i>	<i>bor</i>	<i>nem</i>	<i>atn</i>	ALS	<i>con</i>	<i>atc</i>	<i>pan</i>	<i>lus</i>	<i>mdm</i>	<i>mdn</i>	<i>mds</i>

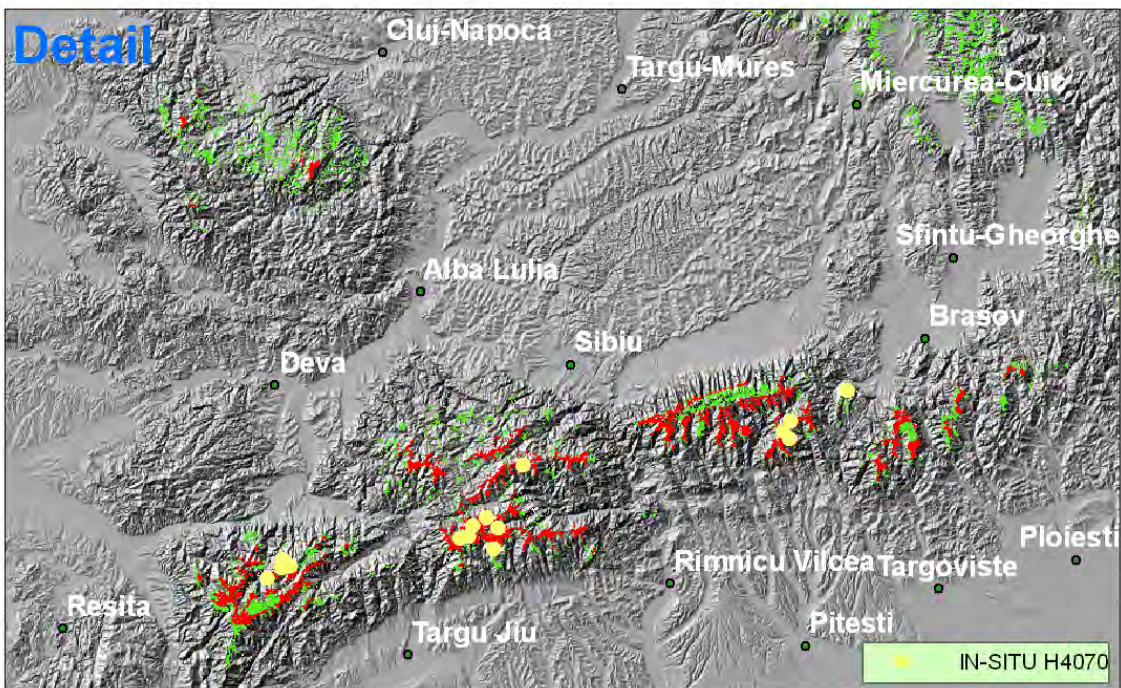
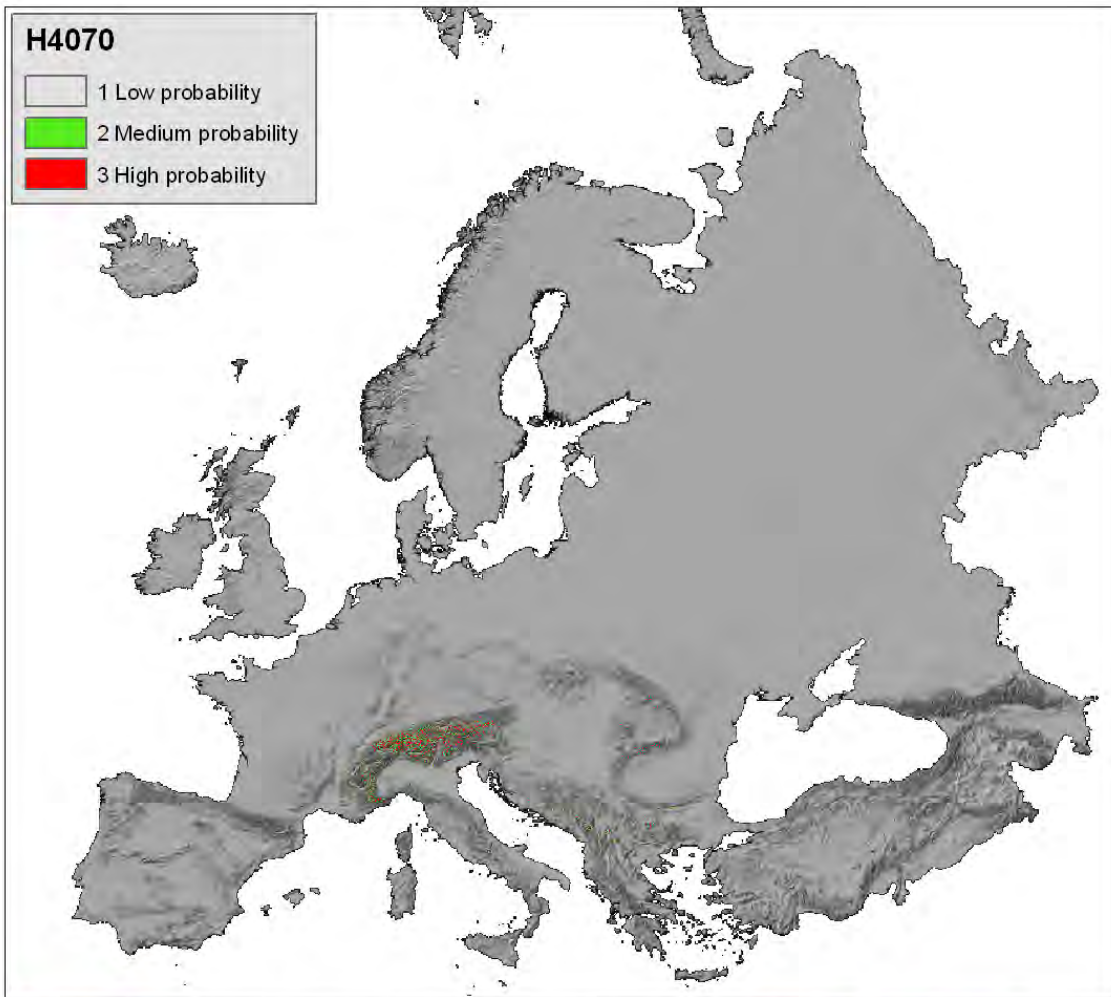


Photo 2 H4070 - Bushes with Rhododendron hirsutum (Mugo-Rhododendretum hirsuti) on Schneeberg, Austria (Photo Thomas Wrбка)



Photo 3 H4070 - Bushes with Pinus mugo (Mugo-Rhododendretum hirsuti) on Schneeberg, Austria (Photo Thomas Wrбка)

RESULT H4070 BUSHES WITH PINUS MUGO AND RHOD. HIRSUTUM



5.3. Siliceous alpine and boreal grasslands (H6150)

Annex I Description

Siliceous alpine and boreal grasslands
Natura 2000 habitat type code 6150
Palaearctic habitat code (and Corine Biotopes) 36.32 (36.11, 36.32, 36.34)
Priority Habitat: No
Parent: Natural grasslands (6100)
Description
Boreo-alpine formations of the higher summits of mountains in the Alps and Scandanavia with outliers elsewhere such as the Tatra, with <i>Juncus trifidus</i> , <i>Carex bigelowii</i> , mosses and lichens. Also included are associated snowbed communities.
Plants
<i>Juncus trifidus</i> , <i>Carex bigelowii</i> , <i>Cassiope tetragona</i> .
Geographic distribution
Boreo-alpine formations of the higher summits of the boreal mountains of northern Finland and Sweden, of Scotland, northern England and northern Wales, with [<i>Juncus trifidus</i> , <i>Carex bigelowii</i>], mosses and lichens.
Austria (Alpine), Czech Republic (Continental), Germany (Alpine, Continental), Finland (Alpine, Boreal), France (Alpine), Italy (Alpine), Poland (Alpine), Sweden (Alpine, Boreal), Slovenia (Alpine), Slovakia (Alpine), United Kingdom (Atlantic)
http://eunis.eea.europa.eu/habitats-factsheet.jsp?idHabitat=10115

EBONE rules

CLC:	321 - Natural grasslands (incl. Pastures)
Annex I:	6150 - Siliceous alpine and boreal grasslands
Mapping rules:	Acid rocks / soils. Look at adjacency of 332 and 333. Alpine South over 1500m./ Alpine north/Boreal over 700m, Atlantic North over 900m
Indicator species:	<i>Juncus trifidus</i> , <i>Carex bigelowii</i> .
GHC:	-CHE/CRY + some dwarf chamaephytes + shallow acidic soils + mud bare rock + indicator species
Field identification:	Needs instructions to separate from related vegetation, but readily identifiable
Occurrence:	-Except in Atlantic North occurs in large units above the critical altitude
Direct threats:	-Overgrazing
Climate change:	Will allow tree / shrub growth to higher altitudes.
Succession:	Colonisation. Status: Ceaspitose hemicryptophytes / Cryptogames –Dwarf chamaephytes 5-10 years Shrubby chamaephytes 5-10 years maybe to Low phanerophytes 5-10 years.

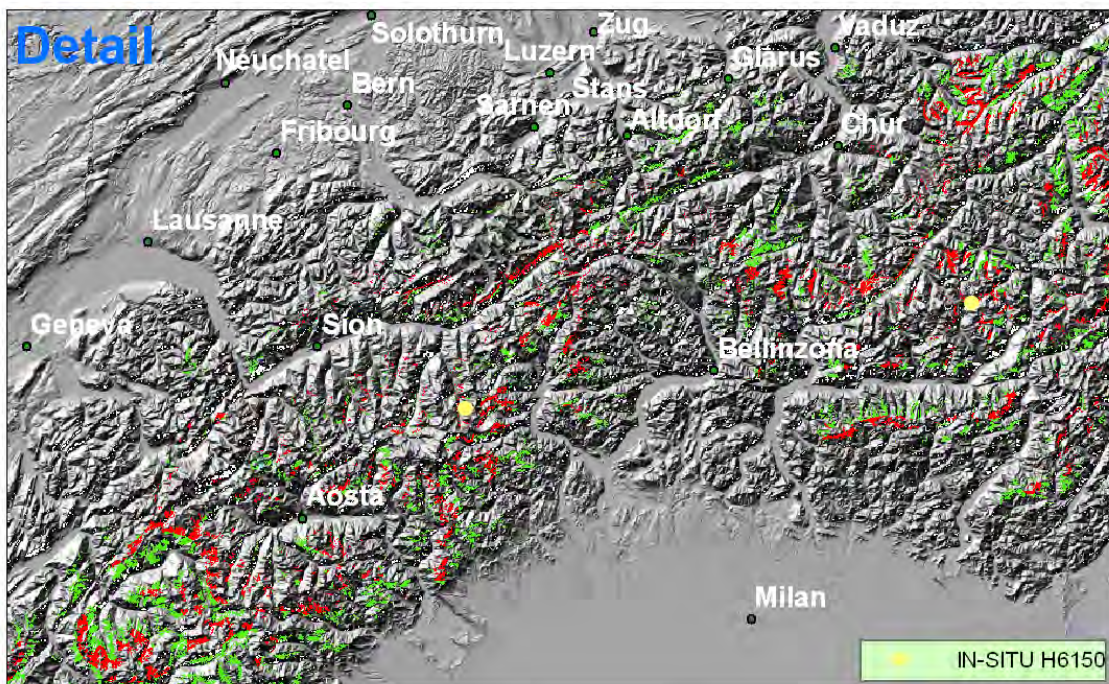
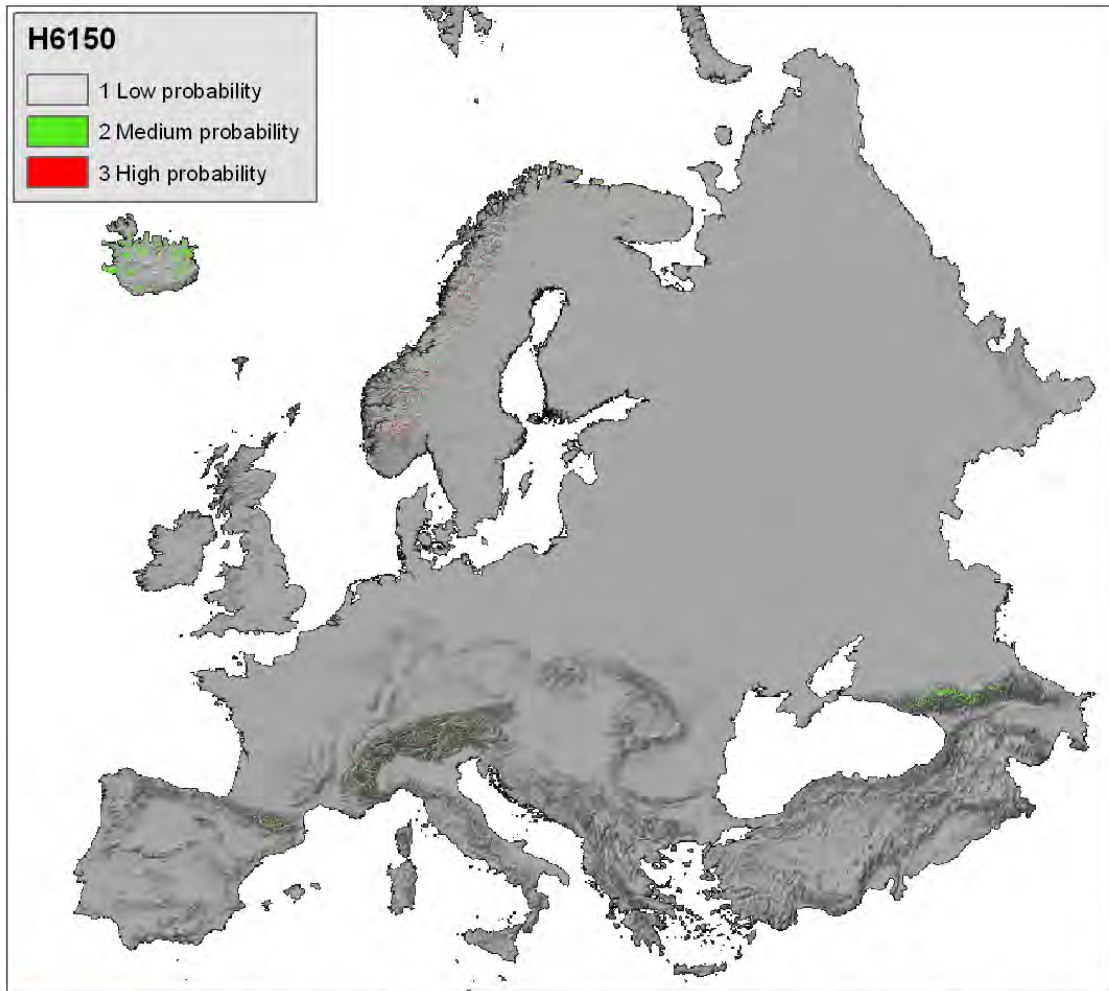
ANNEX-1
Annex 1-EBONE Task 513 Report Mucher version-3

Distribution (s)	ALN	BOR	<i>nem</i>	ATN	ALS	CON	<i>atc</i>	<i>pan</i>	<i>lus</i>	<i>mdm</i>	<i>mdn</i>	<i>mds</i>
Distribution	ALN	BOR	<i>nem</i>	ATN	ALS	<i>CON</i>	<i>atc</i>	<i>pan</i>	<i>lus</i>	<i>mdm</i>	<i>mdn</i>	<i>mds</i>



Photo 4 H6150: Alpine Carex curvula turf on siliceous parent material; Mannlibode (ca. 2400 m) south of Reckingen, Obervallis/ Switzerland (Photo U. Bohn).

RESULT H6150 SILICEOUS ALPINE AND BOREAL GRASSLANDS



5.4. H6170 *Alpine and subalpine calcareous grasslands*

Annex I description

Alpine and subalpine calcareous grasslands
Natura 2000 habitat type code 6170
Palaearctic habitat code (and Corine Biotopes) 36.41 -> 36.45
Priority habitat: No
Parent: Natural grasslands (6100)
Description
<p>Alpine and subalpine grasslands of base-rich soils, with <i>Dryas octopetala</i>, <i>Gentiana nivalis</i>, <i>Gentiana campestris</i>, <i>Alchemilla hoppeana</i>, <i>Alchemilla conjuncta</i>, <i>Alchemilla flabellata</i>, <i>Anthyllis vulneraria</i>, <i>Astragalus alpinus</i>, <i>Aster alpinus</i>, <i>Draba aizoides</i>, <i>Globularia nudicaulis</i>, <i>Helianthemum nummularium</i> ssp. <i>grandiflorum</i>, <i>Helianthemum oelandicum</i> ssp. <i>alpestre</i>, <i>Pulsatilla alpina</i> ssp. <i>alpina</i>, <i>Phyteuma orbiculare</i>, <i>Astrantia major</i>, <i>Polygala alpestris</i> (36.41 to 36.43) of mountain ranges such as the Alps, Pyrenees, Carpathians and Scandinavia. Also included are the grasslands of the subalpine (oro-Mediterranean) and alpine levels of the highest mountains of Corsica (36.37), and the Mesophile, closed, short turfs of the subalpine and alpine levels of the southern and central Apennines, developed locally above treeline, on calcareous substrates (36.38). Can also include associated snowpatch communities (e.g. <i>Arabidion coeruleae</i>).</p> <p>Sub-types :</p> <ul style="list-style-type: none"> • 36.41 - Closed calciphile alpine grasslands Mesophile, mostly closed, vigorous, often grazed or mowed, grasslands on deep soils of the subalpine and lower alpine levels of the Alps, the Pyrenees, the mountains of the Balkan peninsula, and, locally, of the Apennines and the Jura. • 36.42 - Wind edge naked-rush swards Meso-xerophile, relatively closed and unsculptured swards of <i>Kobresia myosuroides</i> (<i>Elynamyosuroides</i>) forming on deep, fine soils of protruding ridges and edges exposed to strong winds in the alpine and nival levels of the Alps, the Carpathians, the Pyrenees, the Cantabrian Mountains, Scandinavian mountains and, very locally, the Abruzzi and the mountains of the Balkan peninsula, with <i>Oxytropis jacquinii</i> (<i>Oxytropis montana</i>), <i>Oxytropis pyrenaica</i>, <i>Oxytropis carinthiaca</i>, <i>Oxytropis foucaudii</i>, <i>Oxytropis halleri</i>, <i>Antennaria carpatica</i>, <i>Dryas octopetala</i>, <i>Draba carinthiaca</i>, <i>Draba siliquosa</i>, <i>Draba fladnizensis</i>, <i>Draba aizoides</i>, <i>Gentiana tenella</i>, <i>Erigeron uniflorus</i>, <i>Dianthus glacialis</i>, <i>Dianthus monspessulanus</i> ssp. <i>stembergii</i>, <i>Potentilla nivea</i>, <i>Saussurea alpina</i>, <i>Geranium argenteum</i>, <i>Sesleria sphaerocephala</i>, <i>Carex atrata</i>, <i>Carex brevicollis</i>, <i>Carex foetida</i>, <i>Carex capillaris</i>, <i>Carex nigra</i>, <i>Carex curvula</i> ssp. <i>rosae</i> and <i>Carex rupestris</i>. Scandinavian <i>Kobresia</i> grasslands with <i>Carex rupestris</i> are included. • 36.43 - Calciphilous stepped and garland grasslands Interpretation Manual - EUR25 Page 59 Xero-thermophile, open, sculptured, stepped or garland grasslands of the Alps, the Carpathians, the Pyrenees, the mountains of the Balkan peninsula and the Mediterranean mountains, with very local outposts in the Jura. • 36.44 - Alpine heavy metal communities: included in habitat 6130 'Calaminarian grasslands (<i>Violetalia calaminariae</i>)', • 36.37 - Oro-Corsican grasslands Grasslands of the subalpine (oro-Mediterranean) and alpine levels of the highest mountains of Corsica. • 36.38 - Oro-Apennine closed grasslands Mesophile, closed, short turfs of the subalpine and alpine levels of the southern and central Apennines, developed locally above treeline, on calcareous substrates.
Plants
<p>36.41 to 36.43 - <i>Dryas octopetala</i>, <i>Gentiana nivalis</i>, <i>Gentiana campestris</i>, <i>Alchemilla hoppeana</i>, <i>Alchemilla conjuncta</i>, <i>Alchemilla flabellata</i>, <i>Anthyllis vulneraria</i>, <i>Astragalus alpinus</i>, <i>Aster alpinus</i>, <i>Draba aizoides</i>, <i>Globularia nudicaulis</i>, <i>Helianthemum nummularium</i> ssp. <i>grandiflorum</i>, <i>Helianthemum oelandicum</i> ssp. <i>alpestre</i>, <i>Pulsatilla alpina</i> ssp. <i>alpina</i>, <i>Phyteuma orbiculare</i>, <i>Astrantia major</i>, <i>Polygala alpestris</i>; 36.37 - <i>Plantago subulata</i> ssp. <i>insularis</i>, <i>Saginapilifera</i>, <i>Armeria multiceps</i>, <i>Paronychia polygonifolia</i>, <i>Bellardiochloa violacea</i>, <i>Phleum brachysrachyum</i>, <i>Geum montanum</i>, <i>Sibbaldia procumbens</i>, <i>Veronica alpina</i>; 36.38 - <i>Festucaviolacea</i> ssp. <i>macrathera</i>, <i>Trifolium thalii</i>.</p>

ANNEX-1
Annex 1-EBONE Task 513 Report Mucher version-3

Geographic distribution
Austria (Alpine), Germany (Alpine), Spain (Alpine, Atlantic, Mediterranean) France (Alpine, Continental, Mediterranean), Greece (Mediterranean) Italy (Alpine, Continental, Mediterranean), Poland (Alpine), Sweden (Alpine) Slovenia (Alpine), Slovakia (Alpine), United Kingdom (Atlantic)
http://eunis.eea.europa.eu/habitats-factsheet.jsp?idHabitat=10117

EBONE rules

CLC:	321 - Natural grasslands (incl. Pastures)											
Annex I:	6170 - Alpine and subalpine calcareous grasslands											
Mapping rules:	Calcareous soils / rocks probably mainly skeletal but also deeper soils given in the description. Alpine North / Boreal over 700m, Atlantic North over 800m, Lusitanian / Mediterranean mountains over 2000m, Alpine South / Continental over 1000m.											
Indicator species:	Dryas octopetala, Gentiana nivalis, Draba aizoides.											
GHC:	-CHE/LHE + moist calcareous soils + open ground upto 3-% + montane situations + indicator species											
Field identification:	Contains many vegetation classes and experience probably needed for exact allocation.											
Occurrence:	-occurs in large units in the centre of its distributions – small patches towards the edge											
Direct threats:	Decline or cessation in grazing. Rate of change determines rate of development.											
Climate change:	May move higher but threatened at lower levels by increased tree / shrub growth., and limited by the distribution of calcareous soils/rocks											
Succession:	Colonisation. Status: Ceaspitose hemicryptophytes / Leafy hemicryptophytes to Ceaspitose hemicryptophytes if not grazed Shrubby chamaephytes 5-10 Low phanerophytes 5-10 Tall phanerophytes 5-10 but only with climate change otherwise only Low phanerophytes. .											
Distribution (sites):	ALN	<i>bor</i>	<i>nem</i>	ATN	ALS	CON	<i>atc</i>	<i>pan</i>	LUS	MDM	MDN	MDS
Distribution (Bunce):	ALN	BOR	<i>nem</i>	ATN	ALS	CON	<i>atc</i>	<i>pan</i>	<i>lus</i>	<i>mdm</i>	<i>mdn</i>	<i>mds</i>



Photo 5 H6170 Alpine acalcareous grasslands at Ötztal Mountains, Austria (Photo Thomas Wrbka)



*Photo 6 H6170 Alpine acalcareous grassland with *Dryas octopetala* and *Anthyllis vulneraria* at Ötztal Mountains, Austria (Photo Thomas Wrbka).*

5.5. H6210 Semi-natural dry grasslands and scrubland facies on calcareous substrates (*Festuco-Brometalia*) (* important orchid sites)

Annex I Description

Semi-natural dry grasslands and scrubland facies on calcareous substrates (<i>Festuco-Brometalia</i>) , (* important orchid sites)
Natura 2000 habitat type code 6210
Palaearctic habitat code (and Corine Biotopes) 34.31 -> 34.34
Priority habitat: Yes
Parent: Semi-natural dry grasslands and scrubland facies (6200)
Description
<p>Dry to semi-dry calcareous grasslands of the <i>Festuco-Brometea</i>. This habitat is formed on the one hand by steppic or subcontinental grasslands (<i>Festucetalia valesiaca</i>) and, on the other, by the grasslands of more oceanic and sub-Mediterranean regions (<i>Brometalia erecti</i>); in the latter case, a distinction is made between primary <i>Xerobromion</i> grasslands and secondary (semi-natural) <i>Mesobromion</i> grasslands with <i>Bromus erectus</i>; the latter are characterised by their rich orchid flora. Abandonment results in thermophile scrub with an intermediate stage of thermophile fringe vegetation (<i>Trifolio-Geranietea</i>). Interpretation Manual - EUR25 Page 61.</p> <p>Important orchid sites should be interpreted as sites that are important on the basis of one or more of the following three criteria:</p> <p>(a) the site hosts a rich suite of orchid species</p> <p>(b) the site hosts an important population of at least one orchid species considered not very common on the national territory</p> <p>(c) the site hosts one or several orchid species considered to be rare, very rare or exceptional on the national territory.</p>
Plants
<p><i>Mesobromion</i> - <i>Anthyllis vulneraria</i>, <i>Arabis hirsuta</i>, <i>Brachypodium pinnatum</i>, <i>Bromus inermis</i>, <i>Campanula glomerata</i>, <i>Carex caryophylla</i>, <i>Carlina vulgaris</i>, <i>Centaurea scabiosa</i>, <i>Dianthus carthusianorum</i>, <i>Eryngium campestre</i>, <i>Koeleria pyramidata</i>, <i>Leontodon hispidus</i>, <i>Medicago sativa</i> ssp. <i>falcata</i>, <i>Ophrys apifera</i>, <i>O. insectifera</i>, <i>Orchis mascula</i>, <i>O. militaris</i>, <i>O. morio</i>, <i>O. purpurea</i>, <i>O. ustulata</i>, <i>O. mascula</i>, <i>Polygala comosa</i>, <i>Primula veris</i>, <i>Sanguisorba minor</i>, <i>Scabiosa columbaria</i>, <i>Veronica prostrata</i>, <i>V. teucrium</i>. <i>Xerobromion</i> - <i>Bromus erectus</i>, <i>Fumana procumbens</i>, <i>Globularia elongata</i>, <i>Hippocrepis comosa</i>. <i>Festucetalia valesiaca</i>: <i>Adonis vernalis</i>, <i>Euphorbia seguierana</i>, <i>Festuca valesiaca</i>, <i>Silene otites</i>, <i>Stipa capillata</i>, <i>S. joannis</i>.</p>
Geographic distribution
<p>Austria (Alpine Continental), Belgium (Atlantic Continental), Czech Republic (Continental Pannonian), Germany (Alpine Atlantic Continental), Denmark (Atlantic Continental), Estonia (Boreal), Spain (Alpine Atlantic Mediterranean), Finland (Boreal), France (Alpine Atlantic Continental Mediterranean), Greece (Mediterranean), Hungary (Pannonian), Ireland (Atlantic), Italy (Alpine Continental Mediterranean), Lithuania (Boreal), Luxembourg (Continental), Latvia (Boreal)</p> <p>Netherlands (Atlantic), Poland (Alpine Continental), Portugal (Mediterranean), Sweden (Alpine Boreal Continental), Slovenia (Alpine), Slovenia (Continental)</p> <p>Slovakia (Alpine), Slovakia (Pannonian), United Kingdom (Atlantic)</p>

ANNEX-1
Annex 1-EBONE Task 513 Report Mucher version-3

<http://eunis.eea.europa.eu/habitats-factsheet.jsp?idHabitat=10120>

EBONE rules

CLC:	321 - Natural grasslands (incl. Pastures)											
Annex I:	6210 - Semi-natural dry grasslands and scrubland facies on calcareous substrates(Festuco-Brometalia) (* important orchid sites)											
Mapping rules:	Calcareous soils. Boreal / Nemoral Below 200m Atlantic North below 300m All Atlantic Central Continental / Alpine South below 700m Mediterranean mountains below1400m.											
Indicator species:	Arabis hirsuta, Dianthus carthusianorum, Ophrys apifera, Orchis mascula, Bromus erecta, Adonis vernalis.											
GHC:	-LHE/CHE + dry calcareous soils + indication											
Field identification:	Difficult as many vegetation associations are included-instructions as to local conditions therefore needed for regional surveyors. Also a definition of important orchid sites is required.											
Occurrence:	-Could be large patches locally but often fragmented											
Direct threats:	Decline in grazing.											
Climate change:	Could expand into mesic grasslands on south facing slopes but rate likely to be slow because of closed swards.											
Succession:	Colonisation. Status: Ceaspitose hemicryptophytes / Leafy hemicryptophytes to Ceaspitose hemicryptophytes 5 without grazing Shrubby chamaephytes 10 Low phanerophytes 5 Mid phanerophytes 5 Tall phanerophytes 10 Forest phanerophytes 10. .											
Distribution (sites):	<i>aln</i>	BOR	NEM	ATN	ALS	CON	ATC	PAN	LUS	MDM	MDN	<i>mds</i>
Distribution (Bunce):	<i>aln</i>	BOR	NEM	ATN	<i>als</i>	CON	ATC	PAN	LUS	MDM	<i>mdn</i>	<i>mds</i>



Photo 7 H6210: Chalk grassland in South Limburg (Gerendal, The Netherlands) with *Orbis purpurea* and *Orchis militaris* (C.A.J. Kreuth)



Photo 8 H6210 Orchid rich calcareous grassland on slope of Wrakeler berg, South-Limburg, the Netherlands (Photo Sander Mucher).

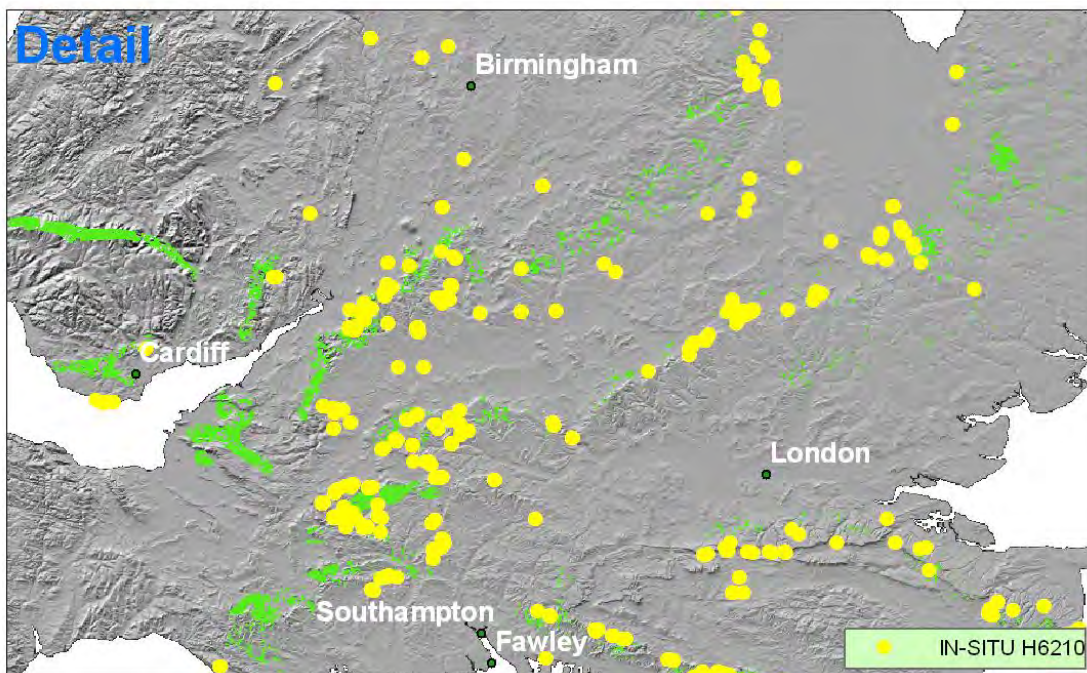
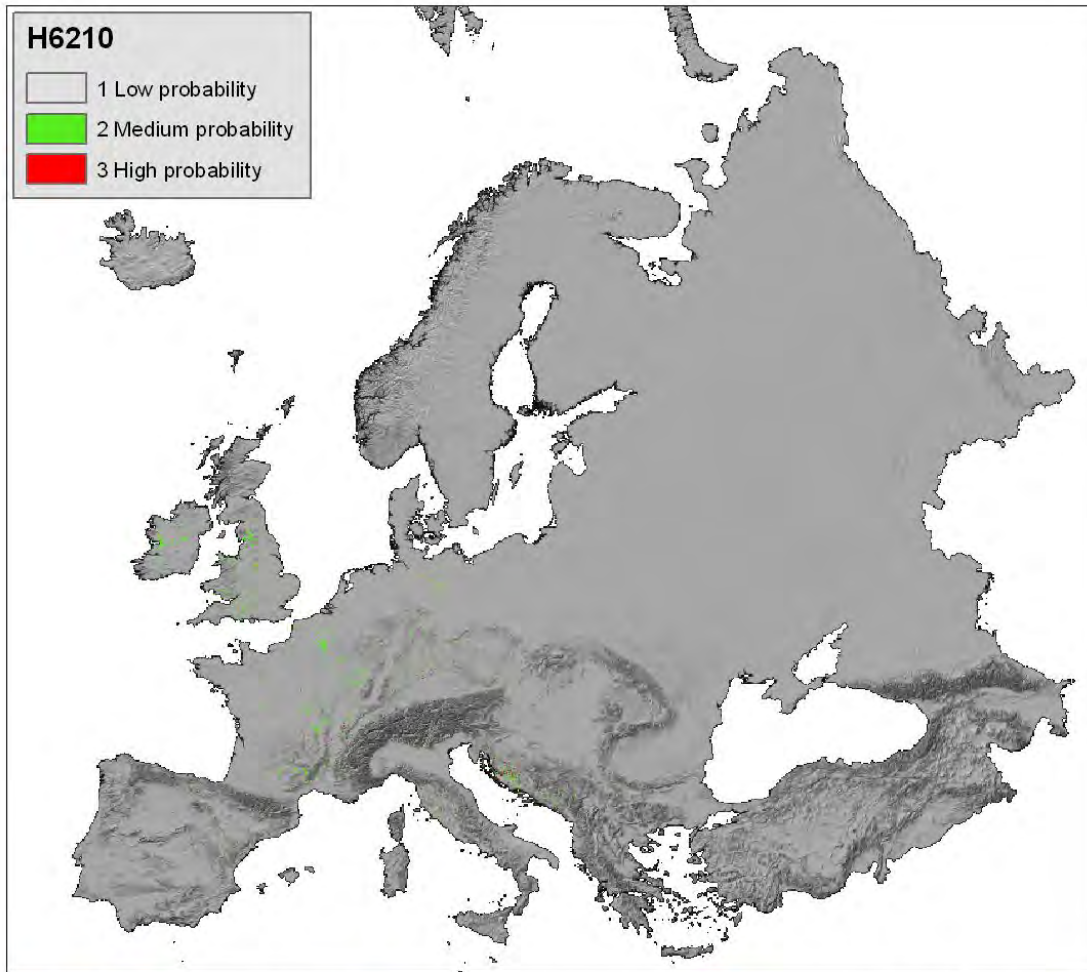


*Photo 9 6210: Chalk grassland in South Limburg (Wrakelberg, The Netherlands) with several thousand of individuals of *Gymnadenia conopsea* (J.H.J. Schaminée)*



Photo 10 H6210. Calcareous grassland in a groundwater protection area in South Limburg, the Netherlands (Photo Sander Mucher)

RESULT H6210 SEMI-NATURAL DRY GRASSLANDS AND SCRUBLAND FACIES ON CALCAREOUS SUBSTRATES



5.6. Species-rich *Nardus* grasslands, on siliceous substrates in (sub) mountain areas (H6230)

Annex I description

Species-rich <i>Nardus</i> grasslands, on siliceous substrates in mountain areas (and submountain areas, in Continental Europe)	
Natura 2000 habitat type code 6230	
Palearctic habitat code (and Corine Biotopes) 35.1	
Priority Habitat: Yes	
Parent: Semi-natural dry grasslands and scrubland facies (6200)	
Description	
Closed, dry or mesophile, perennial <i>Nardus</i> grasslands occupying siliceous soils in Atlantic or sub-Atlantic or boreal lowland, hill and montane regions. Vegetation highly varied, but the variation is characterised by continuity. <i>Nardetalia</i> : 35.1- <i>Violo-Nardion</i> (<i>Nardo-Galion saxatilis</i> , <i>Violion caninae</i>); 36.31- <i>Nardion</i> . Species-rich sites should be interpreted as sites which are remarkable for a high number of species. In general, the habitats which have become irreversibly degraded through overgrazing should be excluded.	
Plants	
<i>Antennaria dioica</i> , <i>Arnica montana</i> , <i>Campanula barbata</i> , <i>Carex ericetorum</i> , <i>C. pallescens</i> , <i>C. panicea</i> , <i>Festuca ovina</i> , <i>Galium saxatile</i> , <i>Gentiana pneumonanthe</i> , <i>Hypericum maculatum</i> , <i>Hypochoeris maculata</i> , <i>Lathyrus montanus</i> , <i>Leontodon helveticus</i> , <i>Leucorchis albida</i> , <i>Meum athamanticum</i> , <i>Nardus stricta</i> , <i>Pedicularis sylvatica</i> , <i>Platanthera bifolia</i> , <i>Polygala vulgaris</i> , <i>Potentilla aurea</i> , <i>P. erecta</i> , <i>Veronica officinalis</i> , <i>Viola canina</i> .	
Geographic distribution	
Alps, Pyrenees, Apennines, Jura, Hercynian ranges, Netherlands, British Isles, Iberia peninsula, Luxembourg, Finland, Sweden.	
Entire EU	
http://eunis.eea.europa.eu/habitats-factsheet.jsp?idHabitat=10122	

EBONE rules

CLC:	321 - Natural grasslands (incl. Pastures)
Annex I:	6230 - Species-rich <i>Nardus</i> grasslands, on siliceous substrates in mountain areas (and submountain areas, in Continental Europe)
Mapping rules:	Making rules for this class is difficult because it depends on interpretation of the term species rich. If it is assumed that the extensive generally species poor <i>Nardus</i> grasslands of the Atlantic zone are included then it is widespread. More species rich grasslands with <i>Nardus</i> are rare in GB but are rather common at quite high elevations in the Alps. The comment in the text suggests that irreversibly degraded grasslands should be excluded which probably means many of those in GB. The rules below cover the whole range but mean that very different frequencies are likely to be involved. Siliceous soils / rocks Alpine North / Boreal below 700m Nemoral / Atlantic Central all altitudes Atlantic North below 900 m, Continental / Alpine South / Pannonian over 700 m but under 2000m, Lusitanian over 1000 m, Mediterranean mountains over 1500 m.
Indicator species:	<i>Antennaria dioica</i> , <i>Galium saxatile</i> .
GHC:	-CHE/LHE + moist neutral/acidic soils + <i>Nardus</i> + wide range of species
Field	Depends on the definition of species rich but the associations are well defined.

ANNEX-1
Annex 1-EBONE Task 513 Report Mucher version-3

identification:												
Occurrence:	-often occurs in large units in the centre of its range, smaller patches elsewhere											
Direct threats:	Mostly maintained by grazing but some of the higher sites may be above the tree line.											
Climate change:	The class covers a high of altitude so probably robust although tree / shrub colonization at higher levels would be favoured if grazing declines. The proportion of montane species may also decline as more competitive species are likely to expand.											
Succession:	Colonisation: status Ceaspitose hemicryptophytes / Leafy hemicryptophytes- Nardus will expand with less grazing and will therefore change to Ceaspitose hemicryptophytes , further development depends on altitude, low altitudes will end up as Forest phanerophytes ,mid Tall phanerophytes high Shrubby chamaephytes. .											
Distribution (sites):	ALN	BOR	NEM	ATN	ALS	CON	ATC	pan	LUS	MDM	MDN	mds
Distribution (Bunce):	ALN	BOR	NEM	ATN	ALS	CON	ATC	PAN	LUS	mdm	mdn	mds

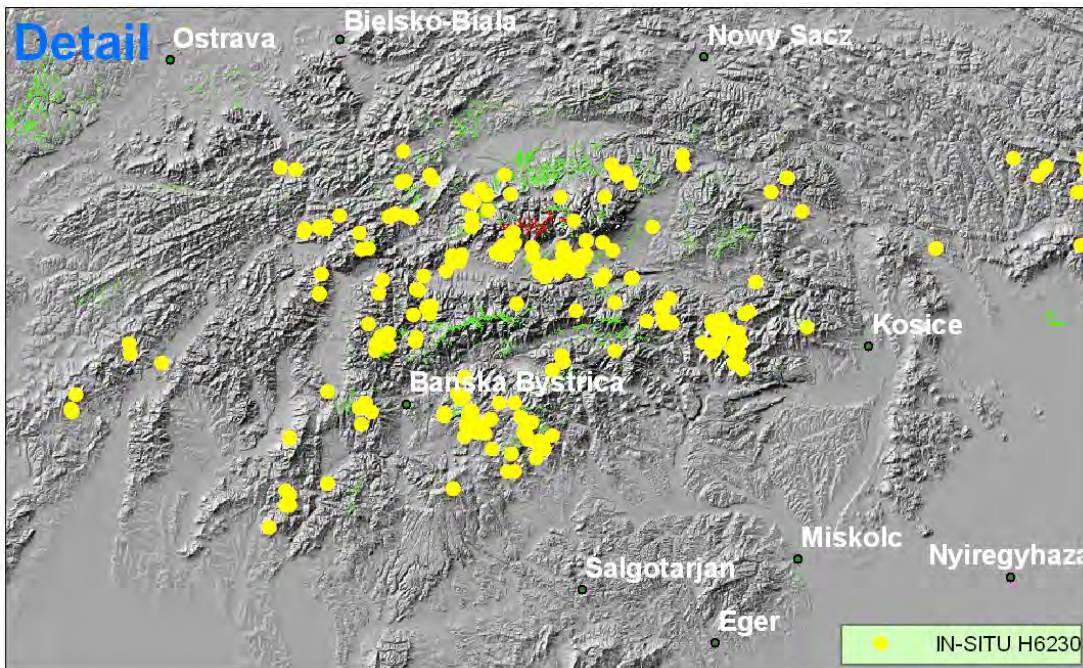
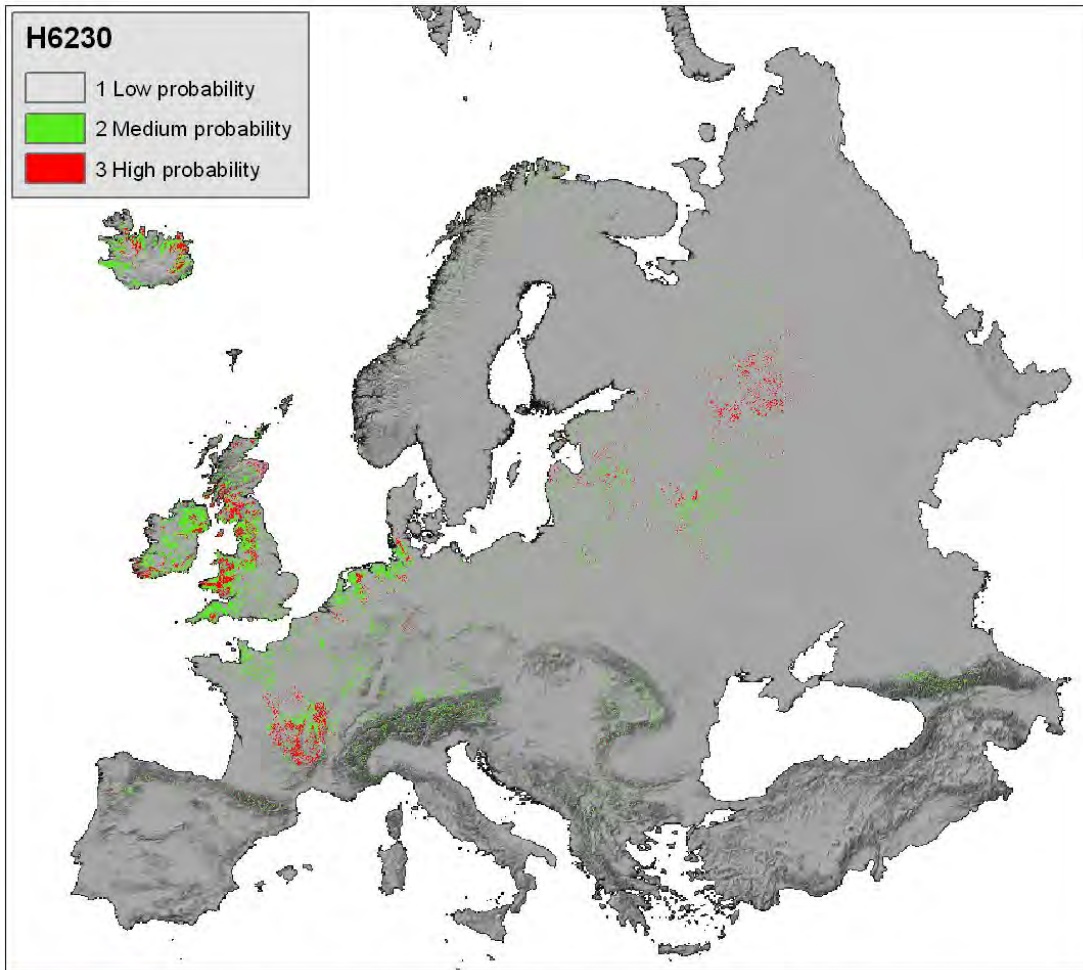


Photo 11 H6230 Species rich Nardus grassland on silicious substrate in the mountain area of Jauerling, Austria (Photo Thomas Wrбка).



Photo 12 H6230 Species rich Nardus grassland on silicious substrate in the mountain area of Yspertal, Austria (Photo Thomas Wrбка)

**RESULT H6230 SPECIES-RICH NARDUS GRASSLANDS ON SILICEOUS SUBSTRATES
IN MOUNTAIN AREAS**



5.7. H6240. Sub-pannonic steppic grasslands

Annex I description

Sub-pannonic steppic grasslands	
Natura 2000 habitat type code	6240
Palaearctic habitat code (and Corine Biotopes)	34.315
Priority habitat:	Yes
Parent:	Semi-natural dry grasslands and scrubland facies (6200)
Description	
Steppic grasslands, dominated by tussock-grasses, chamaephytes and perennials of the alliance <i>Festucion vallesiaca</i> and related syntaxa. These xerotherme communities are developed on southern exposed slopes with AC-soils on rocky substrate and on clay-sandy sedimentation layers enriched with gravels. They are partially of natural, partially of anthropogenic origin.	
Plants	
<i>Festuca vallesiaca</i> , <i>Allium flavum</i> , <i>Gagea pusilla</i> , <i>Hesperis tristis</i> , <i>Iris pumila</i> , <i>Ranunculus illyricus</i> , <i>Teucrium chamaedrys</i> , <i>Medicago minima</i> , <i>Globularia cordifolia</i> , <i>Helianthemum canum</i> , <i>Poa badensis</i> , <i>Scorzonera austriaca</i> , <i>Potentilla arenaria</i> , <i>Seseli hippomarathrum</i> , <i>Alyssum alyssoides</i> , <i>Artemisia austriaca</i> , <i>Chrysopogon gryllus</i> , <i>Astragalus austriacus</i> , <i>A. excapus</i> , <i>A. onobrychis</i> , <i>Oxytropis pilosa</i> , <i>Daphne cneorum</i> , <i>Iris humilis</i> ssp. <i>arenaria</i> , <i>Carex humilis</i> , <i>Festuca rupicola</i> , <i>Stipa capillata</i> , <i>S.joannis</i> , <i>Botriochloa ischaemum</i> .	
Geographic distribution	
Austria (most important sites: south slopes of the Leitha mountains, Hainburger mountains, mountains of the Waschberg range).	
Austria (Alpine, Continental), Czech Republic (Continental, Pannonian) Germany (Atlantic, Continental), France (Alpine, Mediterranean), Hungary (Pannonian), Italy (Alpine, Continental), Slovakia (Alpine, Pannonian)	
http://eunis.eea.europa.eu/habitats-factsheet.jsp?idHabitat=10123	

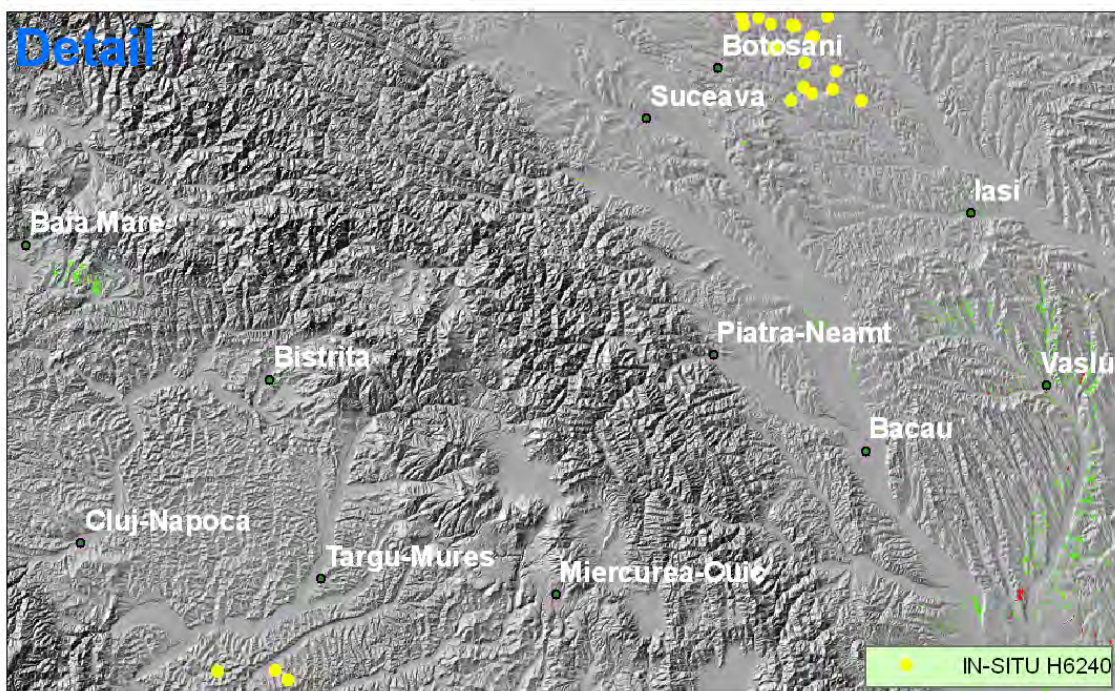
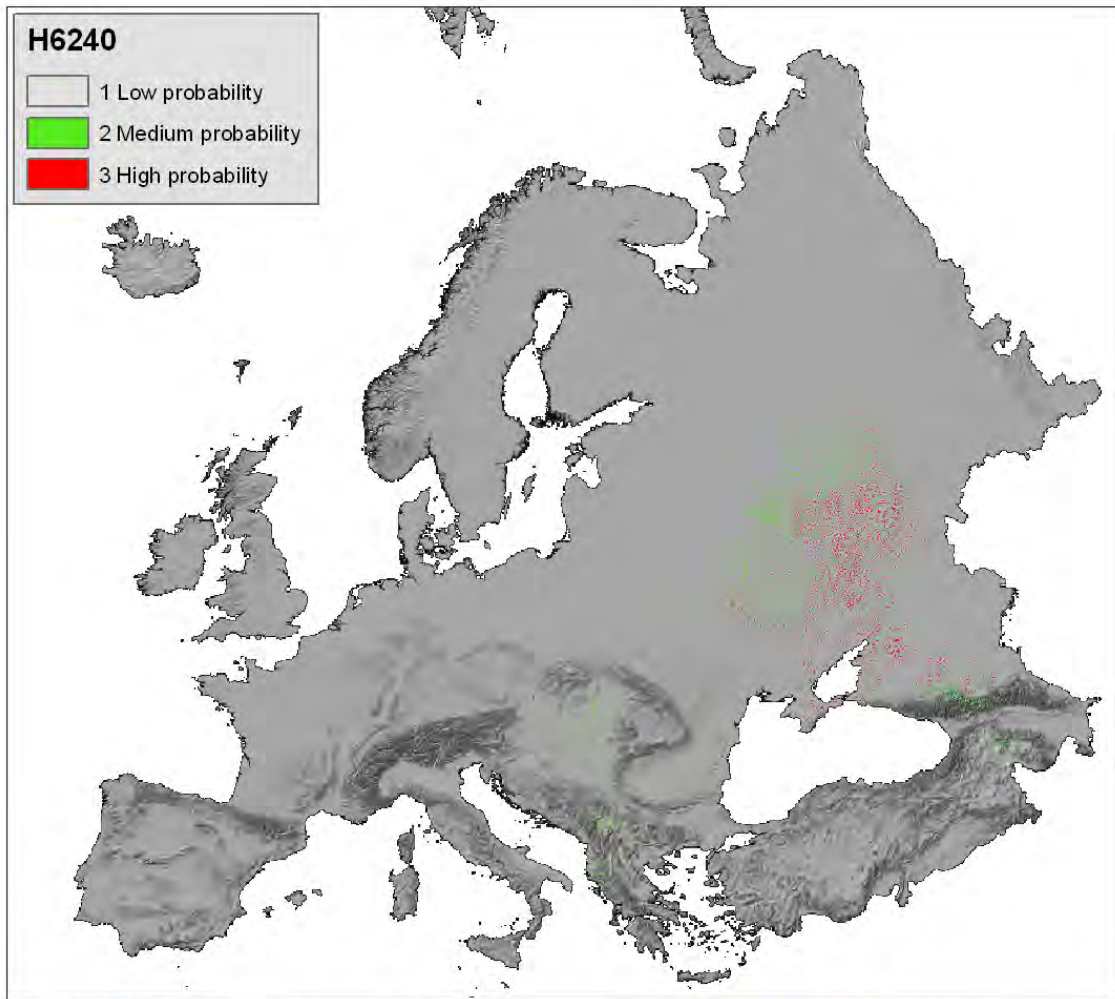
EBONE rules

CLC:	321 - Natural grasslands (incl. Pastures)
Annex I:	6240 - Sub-pannonic steppic grasslands
Mapping rules:	Pannonian and eastern Continental classes below 500 m clays / sands / gravels. South facing.
Indicator species:	<i>Alyssum alyssoides</i> , <i>Astragalus austriacus</i> , <i>Iris humilis</i> ssp. <i>Arenaria</i> , <i>Stipa capillata</i> .
GHC:	-CHE/LHE + xeric soils + variable soil structure + species + expert judgement
Field identification:	Straightforward because detailed description of a restricted vegetation type included.
Occurrence:	-probably in small fragmented patches
Direct threats:	Some are more or less climax others depend on grazing but probably mostly the former so limited threats except for fertilization.
Climate	Could expand under the likely drier conditions but adjacent land may be cultivated so expansion

ANNEX-1
Annex 1-EBONE Task 513 Report Mucher version-3

change:	unlikely.											
Succession:	Colonization: status: probably Ceaspitose hemicryptophytes / Leafy hemicryptophytes with a representation of Shrubby chamaephytes which may expand without any management but otherwise stable.											
Distribution (sites):	<i>aln</i>	<i>bor</i>	<i>nem</i>	<i>atn</i>	ALS	CON	<i>atc</i>	PAN	<i>lus</i>	<i>mdm</i>	<i>mdn</i>	<i>mds</i>
Distribution (Bunce):	<i>aln</i>	<i>bor</i>	<i>nem</i>	<i>atn</i>	<i>als</i>	CON	<i>atc</i>	PAN	<i>lus</i>	<i>mdm</i>	<i>mdn</i>	<i>mds</i>

RESULTS H6240 SUB-PANNONIC STEPPIC GRASSLANDS



5.8. H6250. Pannonic loess steppic grasslands

Annex I description

Pannonic loess steppic grasslands
Natura 2000 habitat type code 6250
Palaearctic habitat code (and Corine Biotopes) 34.91
Priority habitat: Yes
Parent: Semi-natural dry grasslands and scrubland facies (6200)
Description
Grassland communities rich in perennial grasses and herbs on loess deposits. Originally covering large areas, nowadays restricted to specific land forms like loess ridges formed by fluvial erosion and accumulation.
Plants
<i>Artemisia pontica, Astragalus vesicarius, A. austriacus, A. onobrychis, Crambe tataria, Nonea pulla, Salvia nemorosa, Ornithogalum pannonicum, Agropyron pectinatum, Phlomis tuberosa, Bromus inermis, Festuca rupicola, Falcaria vulgaris, Peucedanum alsaticum, Elymus hispidus, Chamaecytisus supinus, Achillea pannonica.</i>
Geographic distribution
Austria (Alpine), Austria (Continental), Czech Republic (Pannonian), Hungary (Pannonian), Slovakia (Pannonian)
http://eunis.eea.europa.eu/habitats-factsheet.jsp?idHabitat=10124

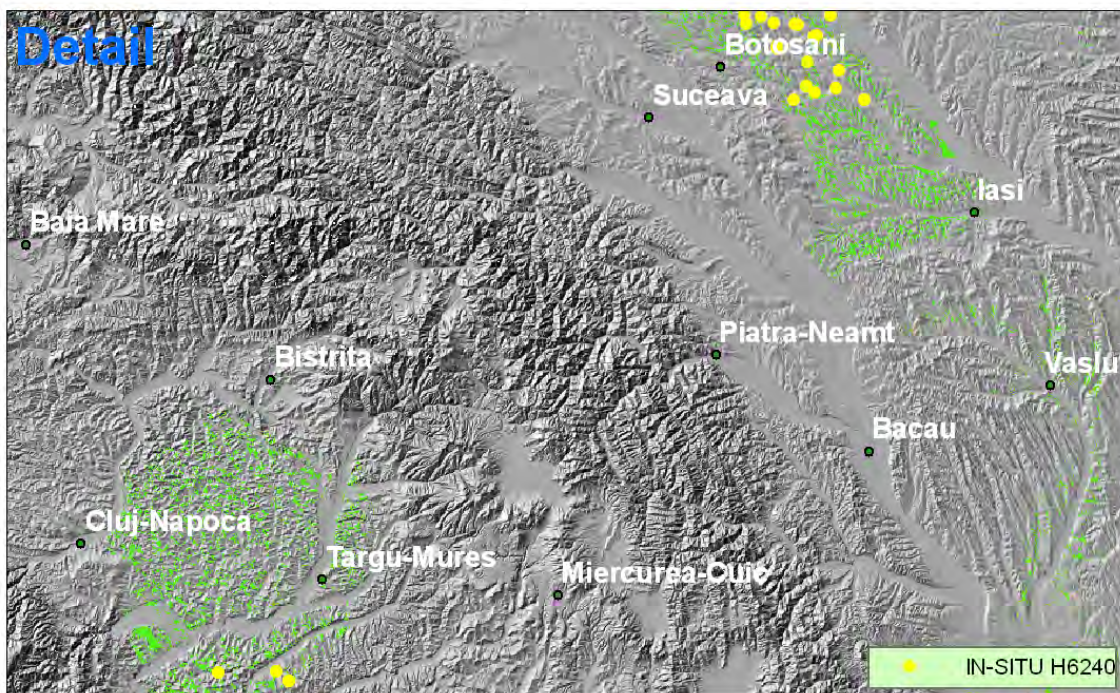
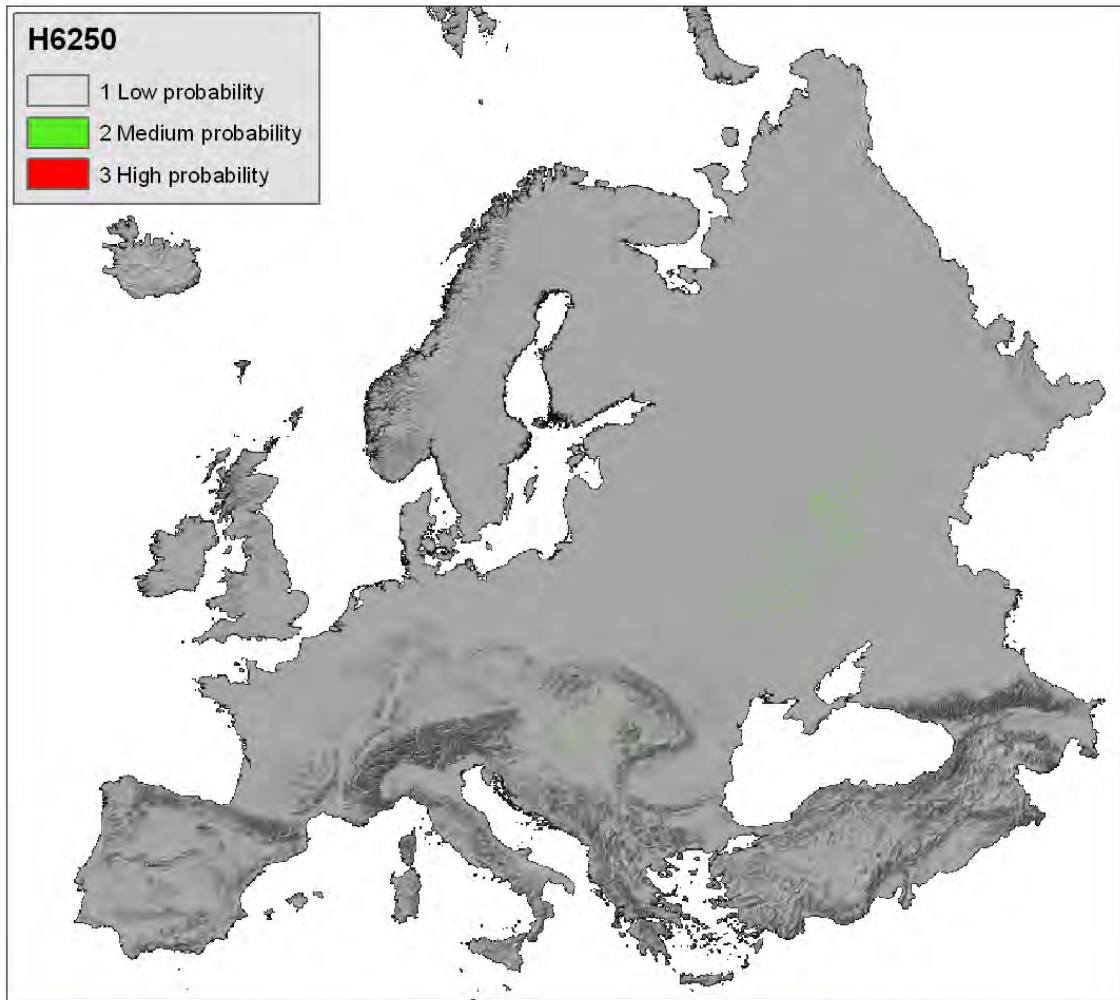
EBONE rules

CLC:	321 - Natural grasslands (incl. Pastures)											
Annex I:	6250 - Pannonic loess steppic grasslands											
Mapping rules:	Pannonian below 500 m. Loess soils.											
Indicator species:	Artemisia pontica, Ornithogalum pannonicum, Achillea pannonica.											
GHC:	-CHE/LHE + xeric loess soils + critical species + expert knowledge											
Field identification:	As 6240.											
Occurrence:	-Small fragmented units											
Direct threats:	Information on management needs to be checked.											
Climate change:	Could expand into other grasslands but likely to be slow because of surrounding cultivated land.											
Succession:	Colonisation: status Cespitose hemicryptophytes / Leafy hemicryptophytes may be susceptible to expansion of Shrubby chamaephytes and Low phanerophytes and eventually Mid phanerophytes but restricted by xeric conditions.											
Distribution (sites):	aln	bor	nem	atn	als	con	atc	PAN	lus	mdm	mdn	mds
Distribution (Bunce):	aln	bor	nem	atn	als	con	atc	PAN	lus	mdm	mdn	mds



Photo 13 H6250: Transcaucasian steppe landscape in hilly country east of Tbilisi near the David Gareji monastery/ Georgia (U. Bohn).

RESULT H6250 PANNONIC LOESS STEPPIC GRASSLANDS



5.9. H7110. Active raised bogs

Annex I Description

Active raised bogs
Natura 2000 habitat type code 7110
Palaearctic habitat code (and Corine Biotopes) 51.1
Priority Habitat: Yes
Parent: Sphagnum acid bogs (7100)
Description
Acid bogs, ombrotrophic, poor in mineral nutrients, sustained mainly by rainwater, with a water level generally higher than the surrounding water table, with perennial vegetation dominated by colourful Sphagna hummocks allowing for the growth of the bog (<i>Erico-Sphagnetalia magellanici</i> , <i>Scheuchzerietalia palustris</i> p., <i>Utricularietalia intermedio-minoris</i> p., <i>Caricetalia fuscae</i> p.). The term "active" must be taken to mean still supporting a significant area of vegetation that is normally peat forming, but bogs where active peat formation is temporarily at a standstill, such as after a fire or during a natural climatic cycle e.g., a period of drought, are also included.
Plants
Erico-Sphagnetalia magellanici- <i>Andromeda polifolia</i> , <i>Carex pauciflora</i> , <i>Cladonia</i> spp., <i>Drosera rotundifolia</i> , <i>Eriophorum vaginatum</i> , <i>Odontoschisma sphagni</i> , <i>Sphagnum magellanicum</i> , <i>S.imbricatum</i> , <i>S. fuscum</i> , <i>Vaccinium oxycoccos</i> ; in the Boreal region also <i>Betula nana</i> , <i>Chamaedaphne calyculata</i> , <i>Calluna vulgaris</i> , <i>Ledum palustre</i> and <i>Sphagnum angustifolium</i> . <i>Scheuchzerietalia palustris</i> p., <i>Utricularietalia intermedio-minoris</i> p., <i>Caricetalia fuscae</i> p.- <i>Carex fusca</i> , <i>C. limosa</i> , <i>Drosera anglica</i> , <i>D. intermedia</i> , <i>Eriophorum gracile</i> , <i>Rhynchospora alba</i> , <i>R. fusca</i> , <i>Scheuchzeria palustris</i> , <i>Utricularia intermedia</i> , <i>U. minor</i> , <i>U. ochroleuca</i> ; in the Boreal region also <i>Sphagnum balticum</i> and <i>S. majus</i> .
Geographic distribution
Austria, Belgium, Denmark, Finland, France, Germany, Italy, Ireland, Netherlands, Spain (Pyrenees and Cantabrian mountains), Sweden, United Kingdom.
EU27
http://eunis.eea.europa.eu/habitats-factsheet.jsp?tab=0&idHabitat=10142

EBONE rules

CLC:	412 - Peat bogs
Annex I:	7110 - Active raised bogs
Mapping rules:	Atlantic Central / Atlantic North / Boreal / Nemoral below 300m.
Indicator species:	<i>Andromeda polifolia</i> , <i>Vaccinium oxycoccos</i> , <i>Drosera anglica</i> , <i>Drosera intermedia</i> .
GHC:	Complexes of Cryptogames / Aquatic / Dwarf chamaephytes / Ceaspitose hemicryptophytes qualified with bog.
Field identification:	Difficult to separate from 7120 – Sphagnum dominated areas indicate quality habitat.

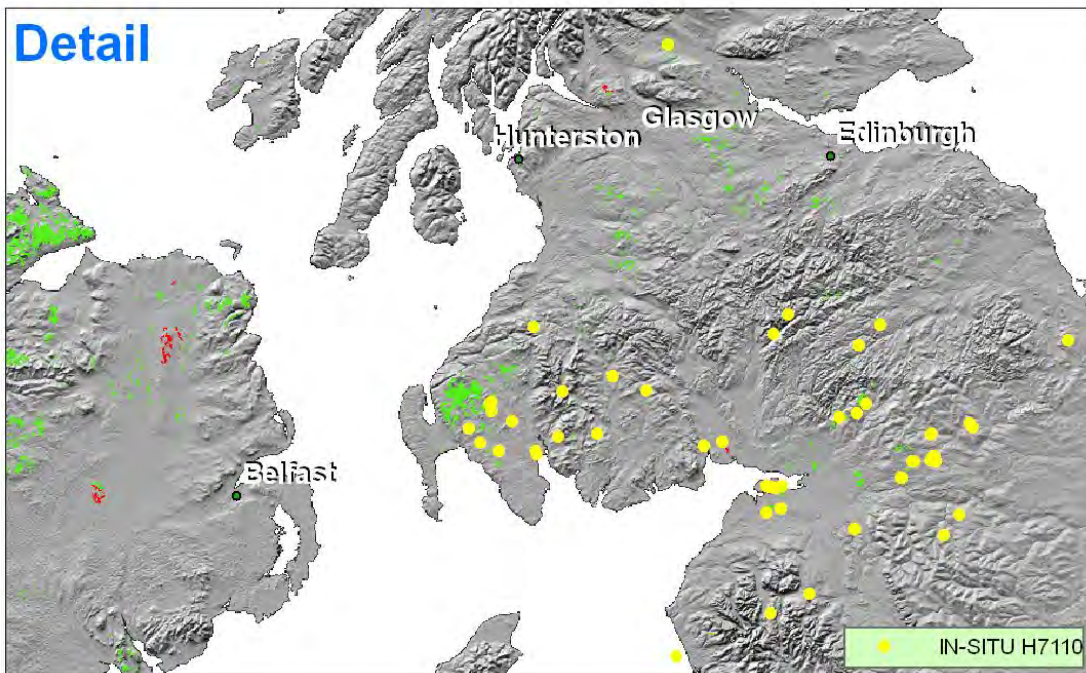
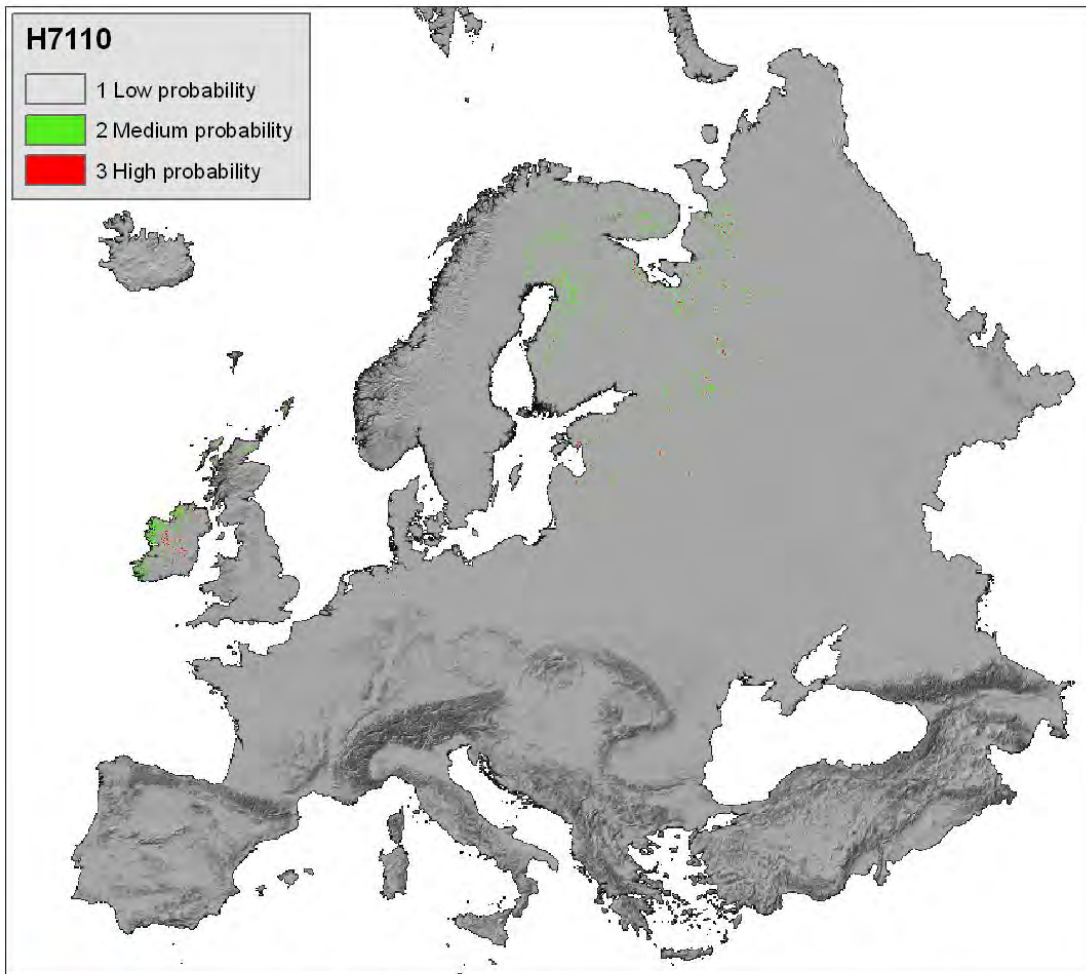
ANNEX-1
Annex 1-EBONE Task 513 Report Mucher version-3

Occurrence:	Usually in discrete units but in the Atlantic zones difficult to separate from other bogs.											
Direct threats:	Drainage, peat cutting.											
Climate change:	Increases the rate of drying out and colonization by scrub and loss of Sphagnum species.											
Succession:	Colonization by Low phanerophytes / Mid phanerophytes and eventually Tall phanerophytes. drying out and destruction of the bog surface. .											
Distribution (sites):	<i>aln</i>	BOR	NEM	ATN	ALS	CON	ATC	<i>pan</i>	LUS	MDM	<i>mdn</i>	<i>mds</i>
Distribution (Bunce):	<i>aln</i>	<i>bor</i>	<i>nem</i>	<i>atn</i>	<i>als</i>	<i>con</i>	<i>atc</i>	<i>pan</i>	<i>lus</i>	<i>mdm</i>	<i>mdn</i>	<i>mds</i>



Photo 14 Active raised bogs at Endla, Estonia (Photo Mucher).

RESULT H7110. ACTIVE RAISED BOGS



5.10. H7130 Blanket bogs (* if active bog)

Annex I Description

Blanket bogs (* if active bog)	
Natura 2000 habitat type code	7130
Palaearctic habitat code (and Corine Biotopes)	52.1 & 52.2
Priority Habitat:	Yes
Parent:	Sphagnum acid bogs (7100)
Description	
<p>Extensive bog communities or landscapes on flat or sloping ground with poor surface drainage, in oceanic climates with heavy rainfall, characteristic of western and northern Britain and Ireland. In spite of some lateral water flow, blanket bogs are mostly ombrotrophic. They often cover extensive areas with local topographic features supporting distinct communities [<i>Erico-Sphagnetalia magellanici</i>: <i>Pleurozio purpureae-Ericetum tetralicis</i>, <i>Vaccinio-Ericetum tetralicis</i> p.; <i>Scheuchzerietalia palustris</i> p., <i>Utricularietalia intermedio-minoris</i> p., <i>Caricetalia fuscae</i> p.]. Sphagna play an important role in all of them but the cyperaceous component is greater than in raised bogs. The term "active" must be taken to mean still supporting a significant area of vegetation that is normally peat forming.</p> <p>Sub-types in the British Isles 52.1 – HyperAtlantic blanket bogs of the western coastlands of Ireland, western Scotland and its islands, Cumbria, Northern Wales ; bogs locally dominated by sphagna (<i>Sphagnum auriculatum</i>, Interpretation Manual - EUR25 Page 74 <i>S. magellanicum</i>, <i>S. compactum</i>, <i>S. papillosum</i>, <i>S. nemoreum</i>, <i>S. rubellum</i>, <i>S. tenellum</i>, <i>S. subnitens</i>), or, particularly in parts of western Ireland, mucilaginous algal deposits (<i>Zygogonium</i>). 52.2 – Blanket bogs of high ground, hills and mountains in Scotland, Ireland, Western England and Wales.</p>	
Plants	
52.1- <i>Calluna vulgaris</i> , <i>Campylopus atrovirens</i> , <i>Carex panicea</i> , <i>Drosera rotundifolia</i> , <i>Erica tetralix</i> , <i>Eriophorum vaginatum</i> , <i>Molinia caerulea</i> , <i>Myrica gale</i> , <i>Narthecium ossifragum</i> , <i>Pedicularis sylvatica</i> , <i>Pinguicula lusitanica</i> , <i>Pleurozia purpurea</i> , <i>Polygala serpyllifolia</i> , <i>Potentilla erecta</i> , <i>Racomitrium languginosum</i> , <i>Rhynchospora alba</i> , <i>Schoenus nigricans</i> , <i>Scirpus cespitosus</i> , <i>Sphagnum pulchrum</i> , <i>S. strictum</i> , <i>S. compactum</i> , <i>S. auriculatum</i> . 52.2 - <i>Calluna vulgaris</i> , <i>Diplophyllum albicans</i> , <i>Drosera rotundifolia</i> , <i>Empetrum nigrum</i> , <i>Erica tetralix</i> , <i>Eriophorum vaginatum</i> , <i>Myrica gale</i> , <i>Narthecium ossifragum</i> , <i>Rubus chamaemorus</i> , <i>Scirpus cespitosus</i> , <i>Vaccinium myrtillus</i> .	
Geographic distribution	
Austria (Alpine), Estonia (Boreal), Spain (Atlantic), Spain (Mediterranean), France (Atlantic), Greece (Mediterranean), Ireland (Atlantic), Italy (Alpine), Italy (Continental), Portugal (Macaronesian), Sweden (Alpine), United Kingdom (Atlantic)	
http://eunis.eea.europa.eu/habitats-factsheet.jsp?idHabitat=10144	

EBONE rules

CLC:	412 - Peat bogs
Annex I:	7130 - Blanket bogs (* if active bog)
Mapping rules:	Atlantic Central / Atlantic North above 300m.

ANNEX-1
Annex 1-EBONE Task 513 Report Mucher version-3

Indicator species:	Drosera rotundifolia, Eriophorum vaginatum, Empetrum nigrum, Rubus chamaemorus.											
GHC:	Leafy hemicryptophytes, but usually with under 30% Low phanerophytes / Evergreen.											
Field identification:	Several key species enable identification notably Rubus chamaemorus and Eriophorum vaginatum.											
Occurrence:	Large units where present.											
Direct threats:	Overgrazing and conversion to agriculture; drainage.											
Climate change:	Will lead to drying out and colonization by grasses.											
Succession:	At low altitudes could be colonized by Low phanerophytes / Mid phanerophytes but only if climate change reduces the water saturation.											
Distribution (sites):	<i>aln</i>	<i>bor</i>	<i>nem</i>	ATN	<i>als</i>	<i>con</i>	ATC	<i>pan</i>	LUS	<i>mdm</i>	<i>mdn</i>	<i>mds</i>
Distribution (Bunce):	<i>aln</i>	<i>bor</i>	<i>nem</i>	<i>atn</i>	<i>als</i>	<i>con</i>	<i>atc</i>	<i>pan</i>	<i>lus</i>	<i>mdm</i>	<i>mdn</i>	<i>mds</i>



Photo 15 Lowland blanket bogs, Connemara, Ireland.

(source: http://144.41.253.33/lacope/gallery/gallery/albums/connemara/Lowland_blanket_bogs_and_lakes.jpg)

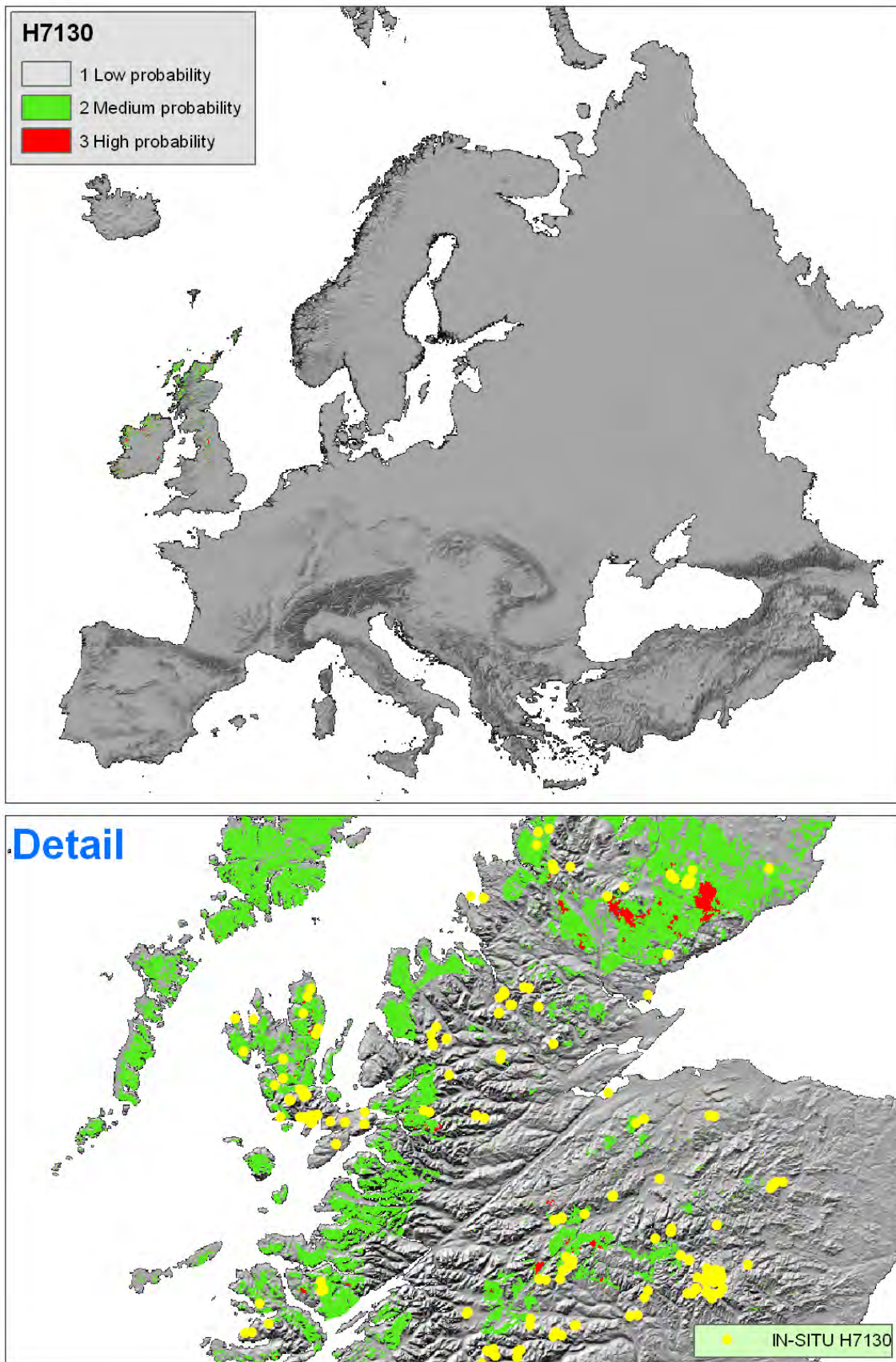


*Photo 16 H7130: Irish lowland blanket bog (S5) with *Molinia caerulea*, *Myrica gale*, *Schoenus nigricans* and *Calluna vulgaris*, Nephin Mountain behind with dry heath and scree; Owenboy, Co. Mayo/western Ireland (N. Lockhart).*



Photo 17 H7130: Extensive Irish blanket bogs of the lowlands, with numerous bog pools; Owenduff Valley, Co. Mayo/Ireland (J. Cross).

RESULTS H7130. BLANKET BOGS



5.11. H9150. Medio-European limestone beech forests of the Cephalanthero-Fagion

Annex I Description

Medio-European limestone beech forests of the Cephalanthero-Fagion	
Natura 2000 habitat type code	9150
Palaearctic habitat code (and Corine Biotopes)	41.16
Priority Habitat:	No
Parent:	Forestst of Temperate Europe (9100)
Description	
<p>Xero-thermophile <i>Fagus sylvatica</i> forests developed on calcareous, often superficial, soils, usually of steep slopes, of the medio-European and Atlantic domains of Western Europe and of central and northern Central Europe, with a generally abundant herb and shrub undergrowth, characterized by sedges (<i>Carex digitata</i>, <i>Carex flacca</i>, <i>Carex montana</i>, <i>Carex alba</i>), grasses (<i>Sesleria albicans</i>, <i>Brachypodium pinnatum</i>), orchids (<i>Cephalanthera</i> spp., <i>Neottia nidus-avis</i>, <i>Epipactis leptochila</i>, <i>Epipactis microphylla</i>) and thermophile species, transgressive of the <i>Quercetalia pubescentipetraeae</i>. The bush-layer includes several calcicolous species (<i>Ligustrum vulgare</i>, <i>Berberis vulgaris</i>) and <i>Buxus sempervirens</i> can dominate.</p> <p>Sub-types :</p> <ul style="list-style-type: none"> • 41.161 - Middle European dry-slope limestone beech forests Middle European sedge and orchid beech woods of slopes with reduced water availability. • 41.162 - North-western Iberian xerophile beech woods <i>Fagus sylvatica</i> forests of relatively low precipitation zones of the southern ranges of the Pais Vasco and of superficially dry calcareous soils of the Cordillera Cantabrica, with <i>Brachypodium pinnatum</i> ssp. <i>rupestre</i>, <i>Sesleria argentea</i> ssp. <i>hispanica</i>, <i>Carex brevicollis</i>, <i>Carex ornithopoda</i>, Interpretation Manual - EUR25 Page 98 <i>Carex sempervirens</i>, <i>Carex caudata</i>, <i>Cephalanthera damasonium</i>, <i>C. longifolia</i>, <i>Epipactis helleborine</i>, <i>Epipactis microphylla</i>, <i>Neottia nidus-avis</i>. 	
Plants	
<i>Fagus sylvatica</i> , <i>Carex digitata</i> , <i>C. flacca</i> , <i>C. montana</i> , <i>C. alba</i> , <i>Sesleria albicans</i> , <i>Brachypodium pinnatum</i> , <i>Cephalanthera</i> spp., <i>Neottia nidus-avis</i> , <i>Epipactis leptochila</i> , <i>Epipactis microphylla</i> , <i>Buxus sempervirens</i> .	
Geographic distribution	
EU27 (minus the Netherlands and Portugal)	
http://eunis.eea.europa.eu/habitats-factsheet.jsp?idHabitat=10189	

EBONE rules

CLC:	311 - Broad-leaved forest
Annex I:	9150 - Medio-European limestone beech forests of the Cephalanthero-Fagion
Mapping rules:	Atlant. Central all Alpine South / Continental 400-1200 + Calcareous soils + <i>Fagus</i> .
Indicator	<i>Fagus sylvatica</i> , <i>Carex digita</i> , <i>Cephalanthera</i> spp., <i>Neottia nidus-avis</i> .

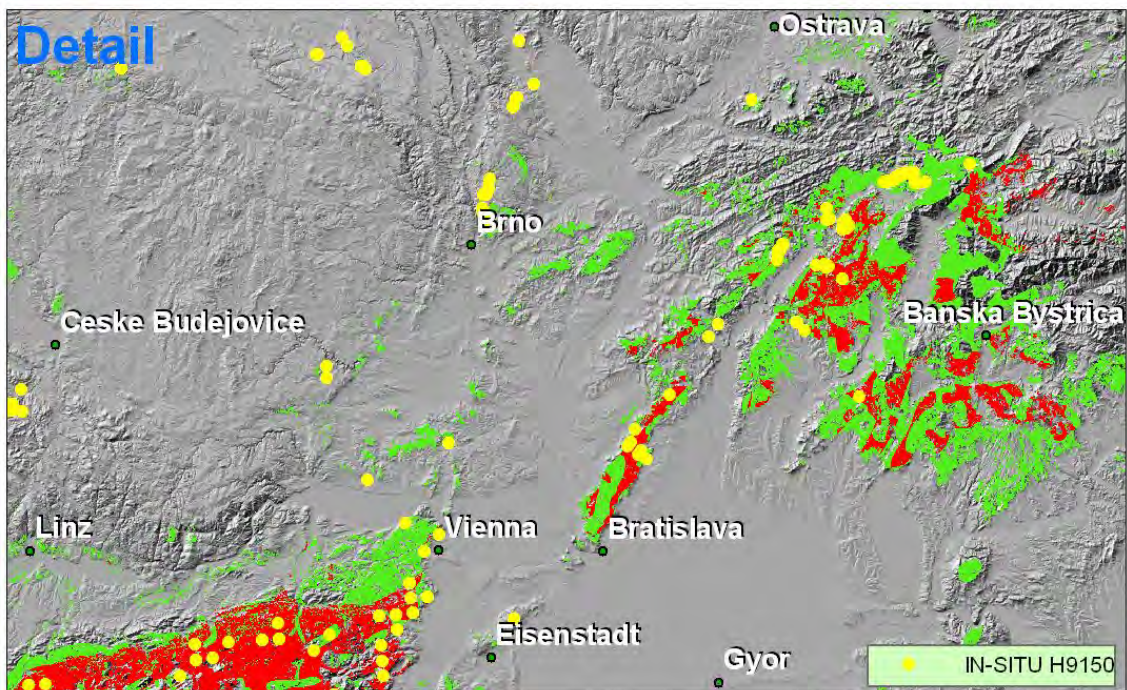
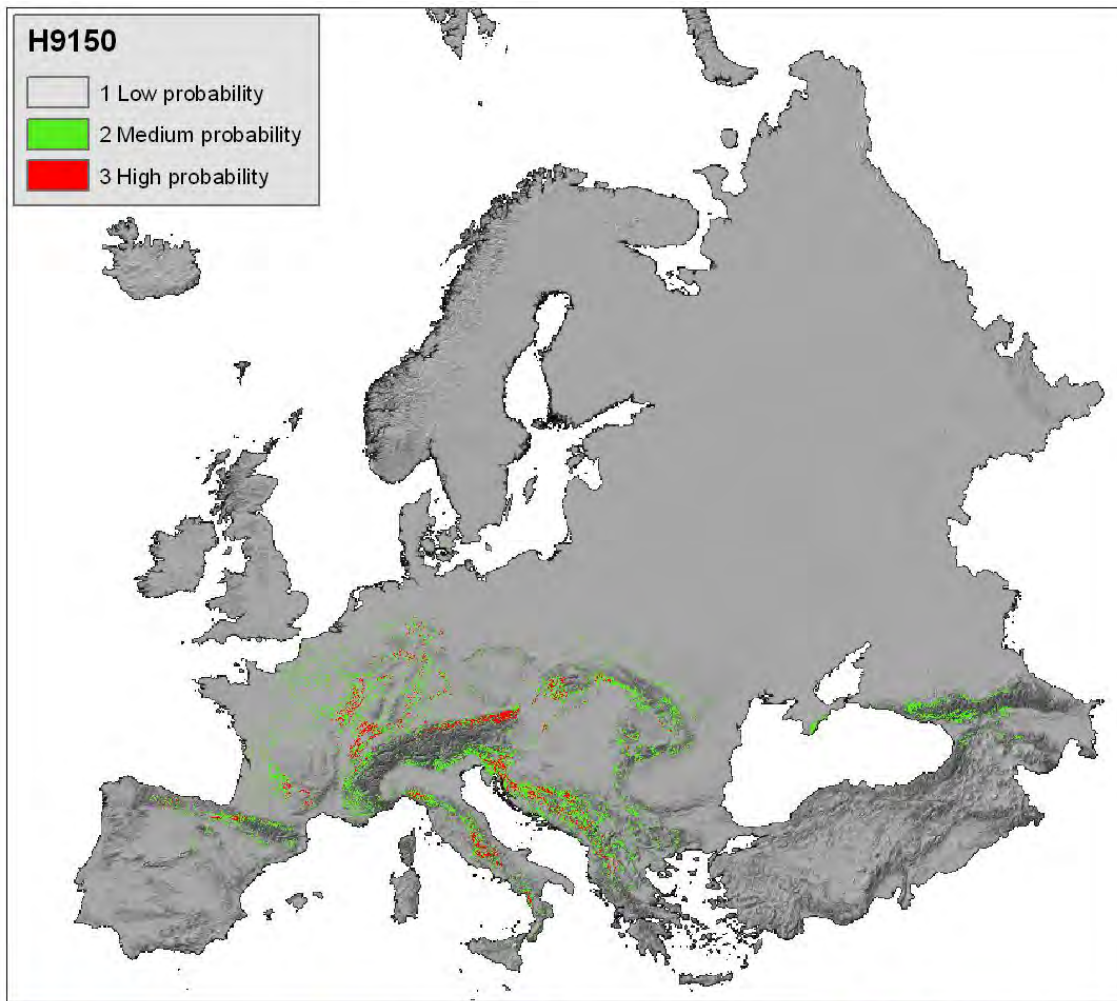
ANNEX-1
Annex 1-EBONE Task 513 Report Mucher version-3

species:												
GHC:	Forest phanerophytes / Winter deciduous + Fagus over 70% + shallow dry calcareous soils + steep slopes + ground flora species.											
Field identification:	A well defined category but grades into 9130.											
Occurrence:	Widespread in large patches but often replaced by Picea abies in the Alps.											
Direct threats:	Felling with deeper soils conversion to conifer.											
Climate change:	Thermophilic species will be favoured.											
Succession:	Climax.											
Distribution (sites):	<i>aln</i>	<i>bor</i>	<i>nem</i>	ATN	ALS	CON	ATC	PAN	LUS	MDM	MDN	<i>mds</i>
Distribution (Bunce):	<i>aln</i>	<i>bor</i>	<i>nem</i>	<i>atn</i>	ALS	<i>con</i>	ATC	PAN	<i>lus</i>	<i>mdm</i>	<i>mdn</i>	<i>mds</i>



Photo 18 Medio-European limestone beech forest on a slope above the Ticha orlice river, Ceskomoravska-mezibori hills, Eastern Bohemia, Czech Republic (photo Pavel Kovar).

RESULT H9150 MEDIO-EUROPEAN LIMESTONE BEECH FORESTS



5.12. H9410. Acidophilous *Picea* forests of the montane to alpine levels (*Vaccinio-Piceetea*)

Annex I description

Acidophilous <i>Picea</i> forests of the montane to alpine levels (<i>Vaccinio-Piceetea</i>)	
Natura 2000 habitat type code 9410	
Palearctic habitat code (and Corine Biotopes) 42.21 -> 42.23 (42.25)	
Priority Habitat: No	
Parent: Temperate Mountainous Coniferous Forests (9400)	
Description	
Sub-alpine and alpine conifer forests (dominated by <i>Picea abies</i> and <i>Picea orientalis</i>). Sub-types:	
<ul style="list-style-type: none"> • 42.21 - Alpine and Carpathian sub-alpine spruce forests. <i>Piceetum subalpinum</i>. <i>Picea abies</i> forests of the lower sub-alpine level, and of anomalous stations in the montane level, of the outer, intermediate and inner Alps; in the latter, they are often in continuity with the montane spruce forests of 42.22. The spruces are often stunted or columnar; they are accompanied by an undergrowth of decidedly sub-alpine affinities. <i>Picea abies</i> forests of the lower sub-alpine level of the Carpathians. • 42.22 - Inner range montane spruce forests. <i>Piceetum montanum</i>. <i>Picea abies</i> forests of the montane level of the inner Alps, characteristic of regions climatically unfavourable to both beech and fir. Analogous <i>Picea abies</i> forests of the montane and collinear levels of the inner basin of the Slovakian Carpathians subjected to a climate of high continentality. • 42.23 - Hercynian sub-alpine spruce forests Sub-alpine <i>Picea abies</i> forests of high Hercynian ranges 21. • 42.25 - Peri-Alpine spruce forests Spontaneous <i>Picea abies</i> formations occupying outlying altitudinal or edaphic enclaves within the range of more predominant vegetation types of the montane levels of the outer Alps, the Carpathians, the Dinarides, the Jura, the Hercynian ranges, the subalpine levels of the Jura, the western Hercynian ranges and the Dinarides 	
Plants	
<i>Picea abies</i> , <i>Vaccinium</i> spp.	
Geographic distribution	
Austria (Alpine, Continental), Czech Republic (Continental) Germany (Alpine, Continental), France (Alpine, Continental), Greece (Mediterranean), Italy (Alpine, Continental, Mediterranean), Poland (Alpine, Continental), Slovenia (Alpine), Slovakia (Alpine)	
Weblink: http://eunis.eea.europa.eu/habitats-factsheet.jsp?idHabitat=10228	

EBONE rules

CLC:	312 - Coniferous forest
Annex I:	9410 - Acidophilous <i>Picea</i> forests of the montane to alpine levels (<i>Vaccinio-Piceetea</i>)
Mapping rules:	Alpine South / Continental 800 m-1700 m ?. Mediterranean Mountains but north of Pyrenees only
Indicator species:	<i>Picea abies</i> , and rarely, <i>Picea orientalis</i> .
GHC:	- Forest phanerophytes/conifer over 70% + moist acid soils + key species
Field identification:	Well defined species patterns but depends whether converted <i>Fagus</i> /and/or plantation forests are included.
Occurrence:	Extensive forests often artificially pure spruce from forest practice. Also many converted <i>Fagus</i> forests.
Direct threats:	Felling
Climate change:	Could threaten spruce dominance by encouraging disease at lower altitudes

ANNEX-1
Annex 1-EBONE Task 513 Report Mucher version-3

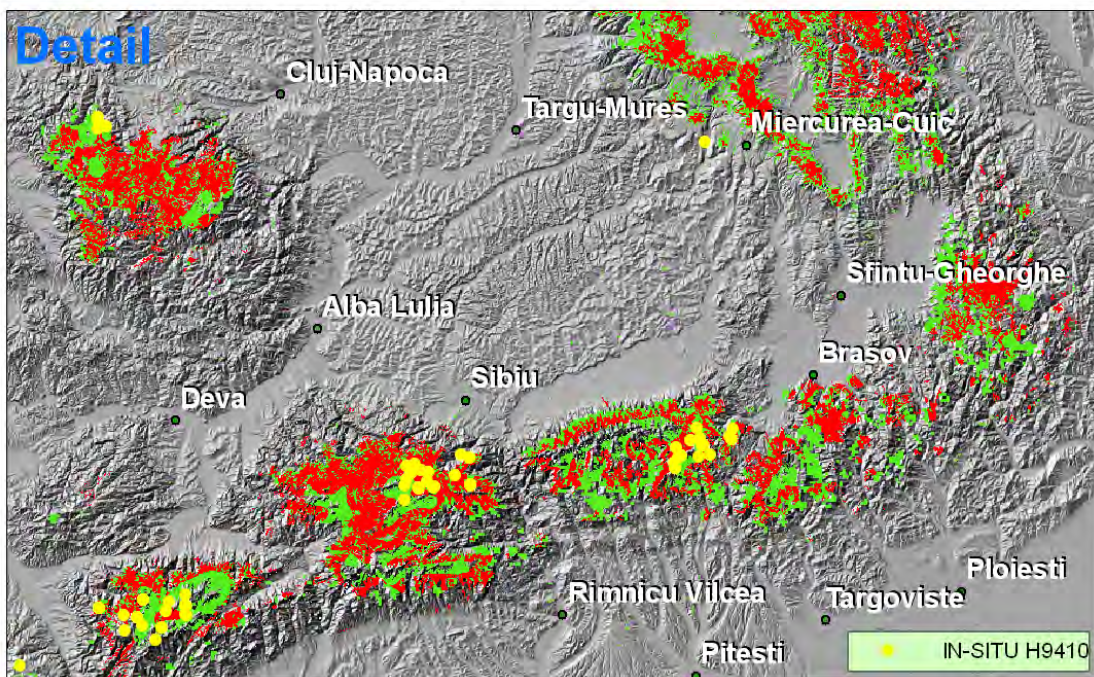
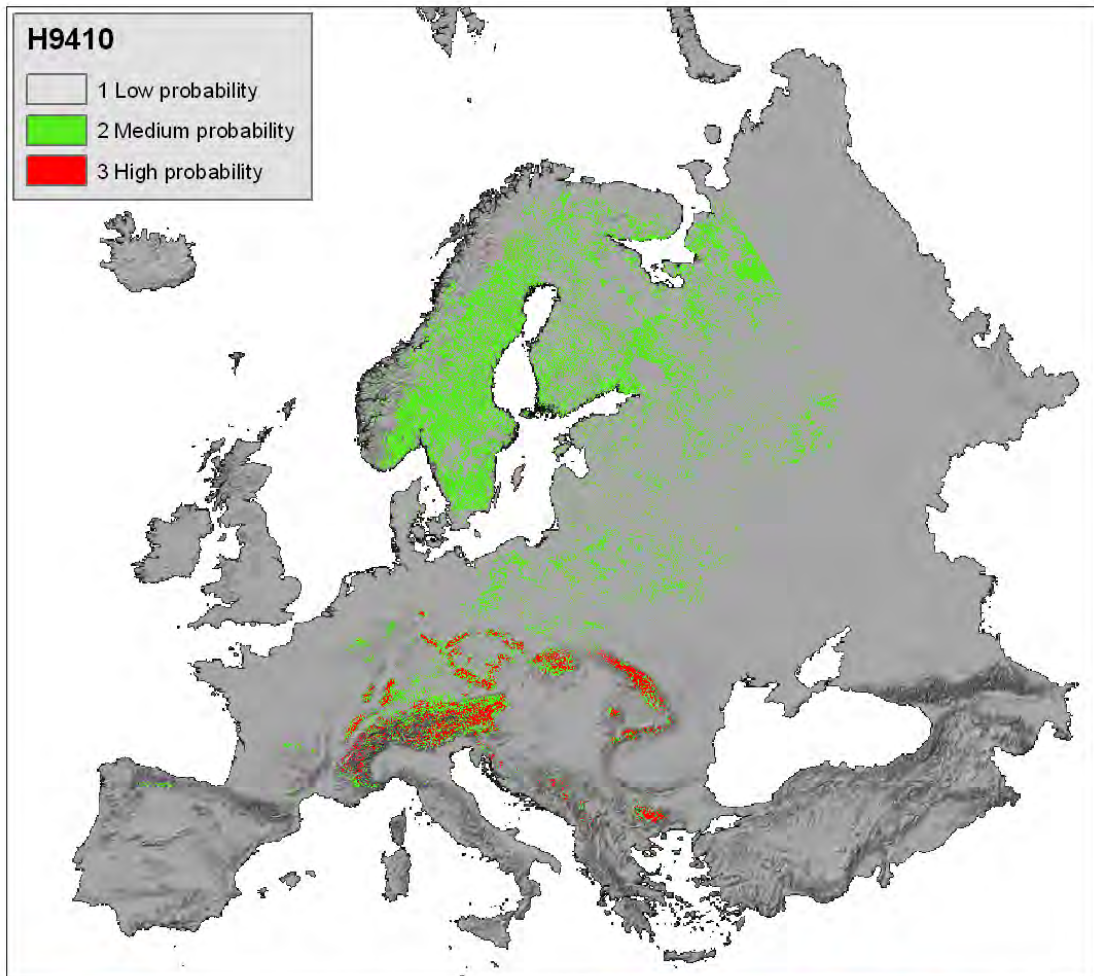
Succession:	Climax but structure will change with age											
Distribution (s):	<i>aln</i>	<i>bor</i>	<i>nem</i>	<i>atn</i>	ALS	CON	<i>atc</i>	<i>pan</i>	<i>lus</i>	MDM	<i>mdn</i>	<i>mds</i>
Distribution (B):	<i>aln</i>	<i>bor</i>	<i>nem</i>	<i>atn</i>	ALS	CON	<i>atc</i>	<i>pan</i>	<i>lus</i>	<i>mdm</i>	<i>mdn</i>	<i>mds</i>



Photo 19 Vysoké Tatry, Štrbské pleso, at 1400 m. Asociácia: *Vaccinio myrtilli-Piceetum*, zväz: *Piceion excelsae*, trieda: *Vaccinio-Piceetea* with *Vaccinium myrtillus* (Photo: Jaroslav Košťál, 14.6.2006)

Source: <http://www.sbs.sav.sk/atlas/admin/img/Vaccinio%20myrtilli-Picetum.JPG>

RESULT H9410 ACIDOPHILOUS PICEA FORESTS OF THE MONTANE TO ALPINE LEVELS



5.13. H9420. Alpine *Larix decidua* and/or *Pinus cembra* forests

Annex I Description

Alpine <i>Larix decidua</i> and/or <i>Pinus cembra</i> forests	
Natura 2000 habitat type code	9420
Palaearctic habitat code (and Corine Biotopes)	42.31 & 42.32
Priority Habitat:	No
Parent:	Temperate Mountainous Coniferous Forests (9400)
Description	
Forests of the sub-alpine and sometimes montane levels, dominated by <i>Larix decidua</i> or <i>Pinus cembra</i> ; the two species may form either pure or mixed stands, and may be associated with <i>Picea abies</i> or <i>Pinus uncinata</i> .	
Sub-types:	
<ul style="list-style-type: none"> • 42.31 - Eastern Alpine siliceous larch and arolla forests. <i>Larici-Cembretum</i>. Sub-alpine <i>Larix decidua</i>, <i>Pinus cembra</i>, or <i>Larix decidua</i>-<i>Pinus cembra</i> forests of the eastern and central Alps, mostly of the inner ranges, usually on siliceous substrates, with an often species-poor undergrowth comprising <i>Vaccinium myrtillus</i>, <i>Rhododendron ferrugineum</i>, <i>Calamagrostis villosa</i>, <i>Luzula albida</i>. • 42.32 - Eastern Alpine calcicolous larch and arolla forests. <i>Laricetum</i>, <i>Larici-Cembretum</i> <i>Rhododendretosum hirsute</i>. Sub-alpine and montane <i>Larix decidua</i>, <i>Larix decidua</i> - <i>Picea abies</i>, <i>Pinus cembra</i> or <i>Larix decidua</i>-<i>Pinus cembra</i> forests of the eastern and central Alps, mostly of the outer ranges, on calcareous substrates, with a usually species-rich undergrowth including <i>Erica herbacea</i>, <i>Polygala chamaebuxus</i>, <i>Rhododendron hirsutum</i> or <i>Pinus mugo</i>. • 42.35 - Carpathian larch and arolla forests Uncommon <i>Larix decidua</i> or <i>Pinus cembra</i> formations of the Carpathians, each occurring as a single dominant, together as codominants, or mixed with <i>Picea abies</i>. 	
Plants	
<i>Larix decidua</i> , <i>Pinus cembra</i> .	
Geographic distribution	
Austria (Alpine), Germany (Alpine), France (Alpine), Italy (Alpine) Poland (Alpine), Slovakia (Alpine).	
http://eunis.eea.europa.eu/habitats-factsheet.jsp?idHabitat=10229	

EBONE rules

CLC:	312 - Coniferous forest
Annex I:	9420 - Alpine <i>Larix decidua</i> and/or <i>Pinus cembra</i> forests
Mapping rules:	Alpine South 1000-1700 m?. Mediterranean mountains over 100m but north of Pyrenees only plus native distribution of <i>Larix</i> / <i>P.cembra</i> .
Indicator species:	<i>Larix decidua</i> , <i>Pinus cembra</i> , <i>Vaccinium myrtillus</i> .
GHC:	- Forest phanerophyte/Conifer over 70%/ + <i>Larix</i> or <i>P.cembra</i> but only native stands + moist acid soils + species indicators
Field identification:	Usually present as more or less pure stands so readily identifiable.
Occurrence:	Often present as altitudinal bands and relatively small patches. May be confused with deciduous forest in CLC and may be also below the minimum mappable unit.
Direct threats:	Felling and conversion to grazing land or spruce
Climate	Could exert pressure on tree health at lower altitudes but also increase altitude range

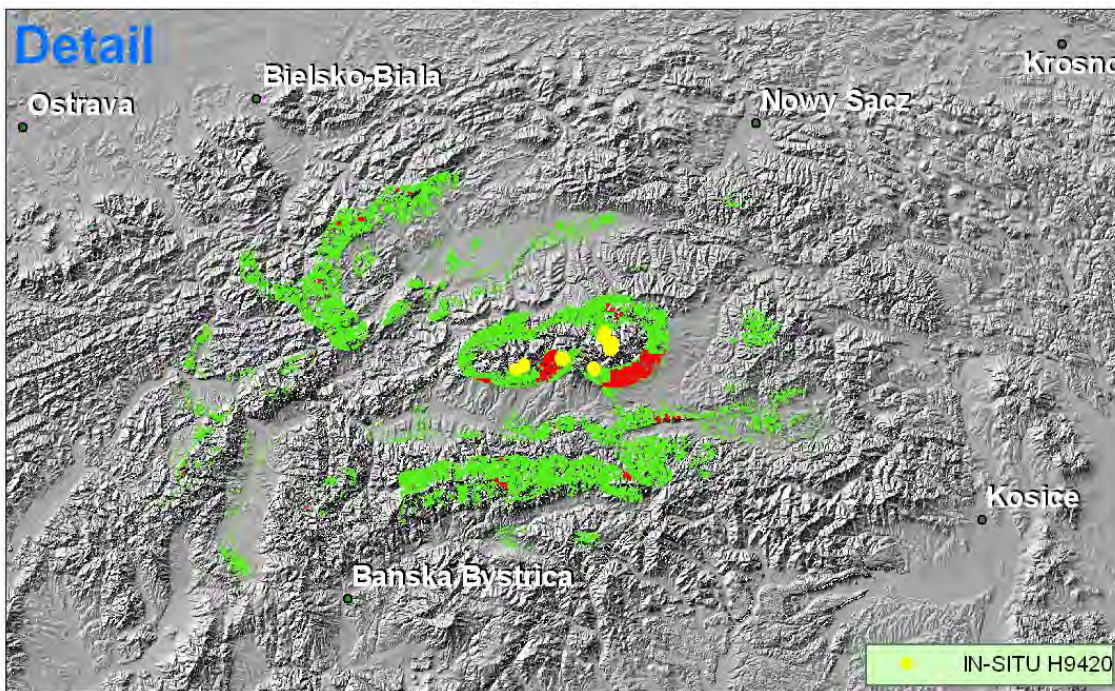
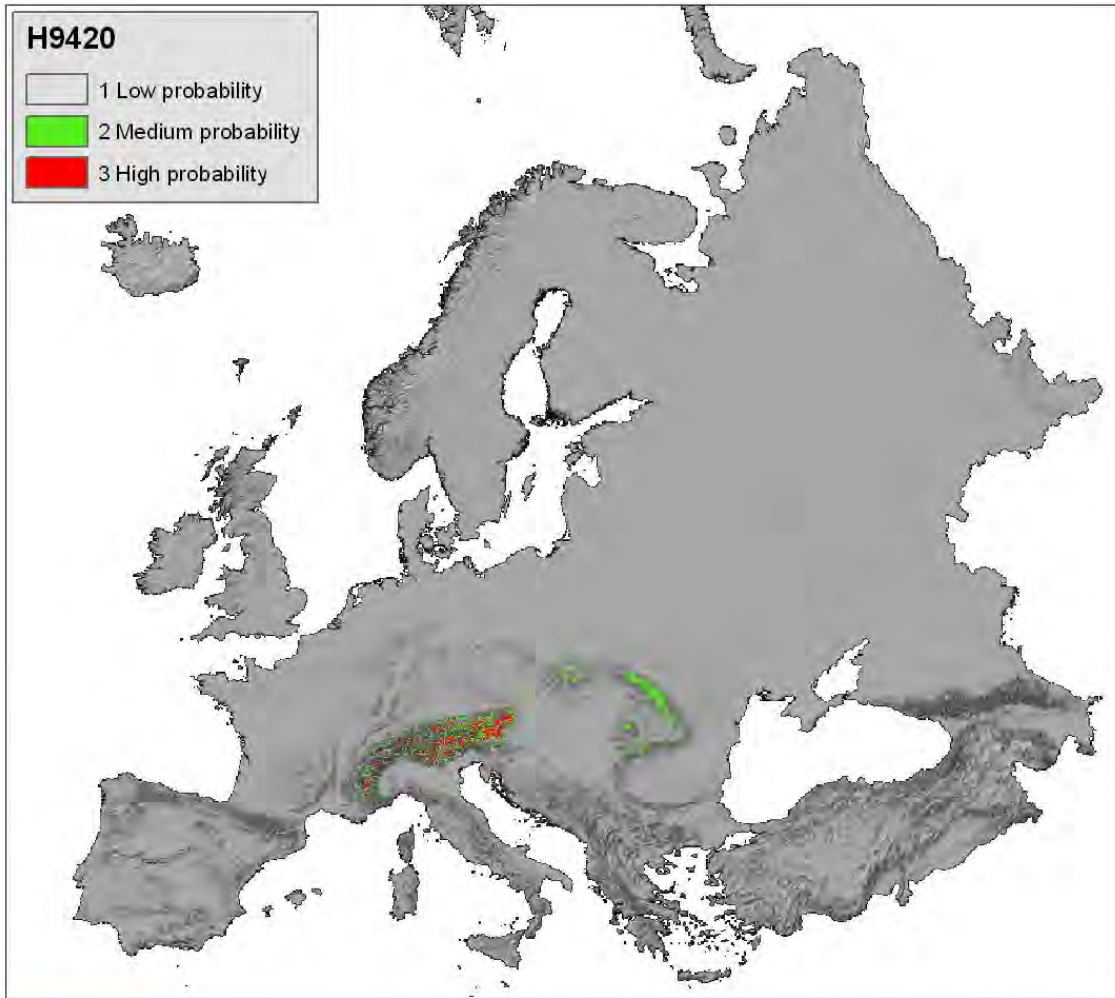
ANNEX-1
Annex 1-EBONE Task 513 Report Mucher version-3

change:												
Succession:	Probaly climax but proportions of species may change with age.											
Distribution (sites):	<i>aln</i>	<i>bor</i>	<i>nem</i>	<i>atn</i>	ALS	<i>con</i>	<i>atc</i>	<i>pan</i>	<i>lus</i>	MDM	<i>mdn</i>	<i>mds</i>
Distribution (Bunce):	<i>aln</i>	<i>bor</i>	<i>nem</i>	<i>atn</i>	ALS	<i>con</i>	<i>atc</i>	<i>pan</i>	<i>lus</i>	<i>mdm</i>	<i>mdn</i>	<i>mds</i>



Photo 20 9420: Subalpine arolla pine (Pinus cembra) forest in the Alps at the forestline in combination with dwarf shrub communities (C19); Oberhauser Zirbenwald, Deferegggen Valley, Eastern Tyrol/ Austria (K. Zukrigl).

RESULT H9420. ALPINE LARIX DECIDUA AND/OR PINUS CEMBRA FORESTS



5.14. H9510. Southern Apennine *Abies alba*

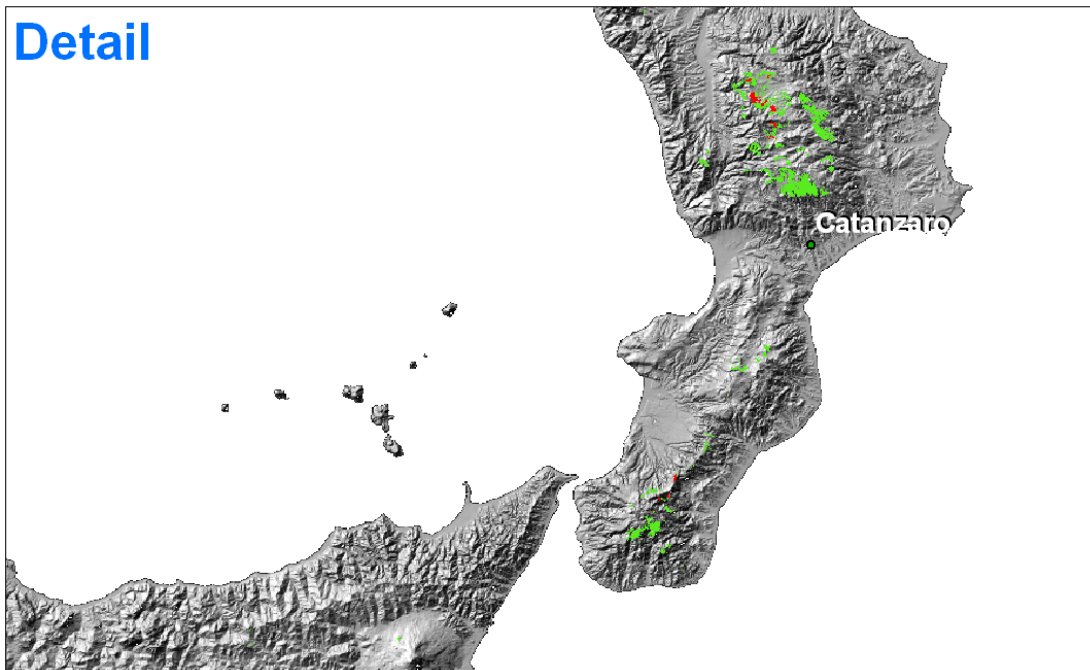
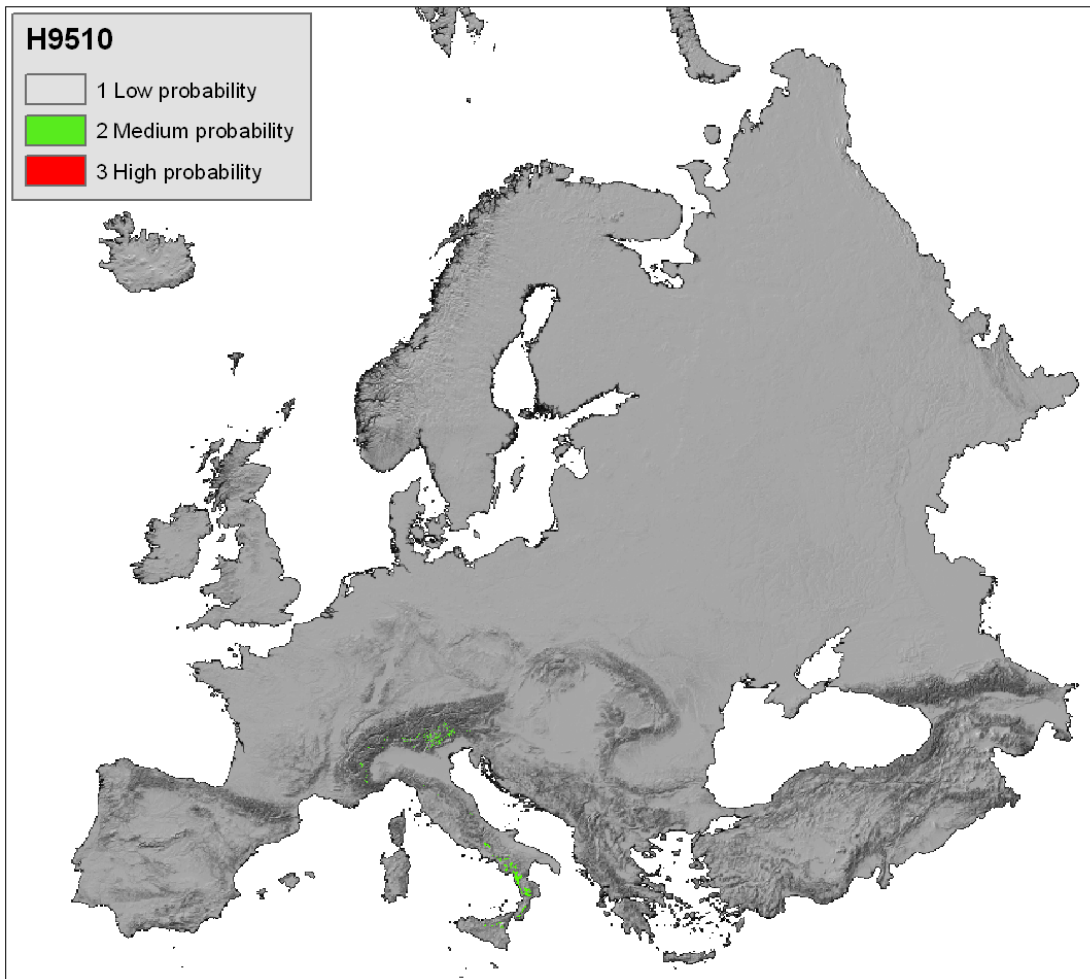
Annex I description

Southern Apennine <i>Abies alba</i>
Natura 2000 habitat type code 9510
Palaearctic habitat code (and Corine Biotopes)
Priority Habitat: Yes
Parent: Mediterranean and Macaronesian mountainous coniferous forests (9500)
Description
Relict <i>Abies alba</i> woods associated with the beech forests of the <i>Geranio versicolori-Fagion</i> .
Plants
<i>Abies alba</i> .
Geographic distribution
Southern Apennines (Molise, Basilicata, Calabria)
Italy (Alpine, Mediterranean)
http://eunis.eea.europa.eu/habitats-factsheet.jsp?idHabitat=10232

EBONE rules

CLC:	312 - Coniferous forest											
Annex I:	9510 - Southern Apennine <i>Abies alba</i>											
Mapping rules:	Mediterranean mountains southern Apennines only. Over 800m? <i>Abies alba</i> .											
Indicator species:	<i>Abies alba</i> .											
GHC:	- Forest phanerophytes/over70% conifer + <i>Abies alba</i> + further expert knowledge and indicators											
Field identification:	Dependant on one species therefore clear cut. But problem will be gradients with <i>Fagus</i> forests											
Occurrence:	No information.											
Direct threats:	Probably felling											
Climate change:	Could be threatened by increased summer drought											
Succession:	.likely to be climax											
Distribution (sites):	<i>aln</i>	<i>bor</i>	<i>nem</i>	<i>atn</i>	<i>als</i>	<i>con</i>	<i>atc</i>	<i>pan</i>	<i>lus</i>	<i>mdm</i>	MDN	<i>mds</i>
Distribution (Bunce):	<i>aln</i>	<i>bor</i>	<i>nem</i>	<i>atn</i>	<i>als</i>	<i>con</i>	<i>atc</i>	<i>pan</i>	<i>lus</i>	<i>mdm</i>	<i>mdn</i>	<i>mds</i>

RESULT H9510. SOUTHERN APENNINE ABIES ALBA



6. INTERCALIBRATION OF IN-SITU DATA WITH ENVIRONMENTAL DATA

6.1. *The decision tree experiment*

Decision trees are powerful tools for classification. However, how can we easily derive knowledge rules in an automated way from a certain number of environmental spatial data sets as an alternative method for spatial modelling of European habitats? Expert knowledge has been used in the former sections to build such rules. However, the construction of the decision rules might be time consuming, especially if you want to develop them for all Annex I habitat types. Moreover, the rules are in some cases arbitrary.

A different approach could be more appropriate, where in-situ data for specific habitats are used directly in combination with the available environmental data sets to determine the decision rules in a more automatic way. Finally, in order to identify the spatial distribution of the specific habitats across Europe, based on the available environmental data sets (including remotely sensed derived land cover information and other parameters).

In order to investigate this, a decision tree experiment was implemented for two Annex I habitats:

- Alpine and Boreal Heaths (H4060)
- Medio-European Limestone beech forests of the Cephalanthero-Fagion (H9150).

For each of these habitats, there were vegetation relevés (available as scattered sample points) over Austria, Czech Republic, Slovakia, Romania, see page 9-10. For H4060, there were even 435 sample points in Britain. To be exact, there were 1835 sample points for H4060 and 559 for H9150. All relevés were given a unique sample number. For each of these points the soil map was sampled, by means of a spatial join. Value extraction was used to sample 3 environmental layers, namely climate, altitude, and Corine land cover. Examples of environmental zones (climate) are: Atlantic North, Continental, Boreal and Arctic. The land cover and altitude rasters both had a cell size of 100 * 100 meters, but the raster representing the environmental zones had a cell size of 1000 * 1000 meters. Thus a dataset with 2394 (1835+559) records was acquired with over 128 attributes, mostly derived from the soil map.

Then a selection of the data was read into the software programme R – an environment for statistical computing and graphics. The following variables were selected as statistically significant data layers to fit a classification tree:

- Altitude (RASTERVALU)
- Biogeographic region (ECOREGION)
- Land cover class (LANDCOVER)
- Soil type acc. to the FAO85 classifications
- Available water capacity of the top soil
- Organic matter content of the top soil
- Dominant parent material (MAT1)
- Dominant surface textural class
- Depth class of an obstacle to roots (ROO)
- Dominant annual average soil water regime class of the soil profile.

Apart from the first variable, all the others are nominal variables (cf tables 5 and 6). All records were used for training. The variables actually used in the tree construction were: LANDCOVER, RASTERVALU, ECOREGION, MAT1 and ROO. With a misclassification error rate of only 0.02887, a reasonable result was obtained. It means that on the basis of values

ANNEX-1

Annex 1-EBONE Task 513 Report Mucher version-3

for the mentioned variables, one would predict correctly from which of the 2 habitats the sample was taken in approx. 97% of the cases.

The output is given in table 4 below. The figures in red refer to the habitat: 1 refers to H9150 and 2 refers to H4060. A picture of the tree was also obtained (figure 4).

Subsequently we used the digital soil map and the various input rasters to determine for which of the grid cells the values conform to the found classification tree – in other words: which grid cells could possibly host one of the two habitats used in this experiment. The preliminary results were encouraging.

Table 4 Experimental decision tree (cf tables 5 and 6 for code values).

```

node), split, n, deviance, yval, (yprob)
* denotes terminal node
1) root 2355 2581.000 2 ( 0.237367 0.762633 )
  2) as.factor(LANDCOVER): 2,3,8,12,18,20,21,23,25,29,41 598 621.000 1 ( 0.785953
    0.214047 )
    4) RASTERVALU < 1041 467 222.700 1 ( 0.935760 0.064240 )
      8) as.factor(ECOREGION): 6,8,11 390 53.500 1 ( 0.987179 0.012821 ) *
      9) as.factor(ECOREGION): 4,5 77 97.070 1 ( 0.675325 0.324675 )
        18) as.factor(MAT1): 1,4,8,21 58 42.720 1 ( 0.879310 0.120690 ) *
        19) as.factor(MAT1): 9,13,15,17,18,25,26,NA,NA 19 7.835 2 ( 0.052632
          0.947368 ) *
      5) RASTERVALU > 1041 131 147.900 2 ( 0.251908 0.748092 )
        10) as.factor(MAT1): 4,13 64 88.660 1 ( 0.515625 0.484375 ) *
        11) as.factor(MAT1): 8,15,16,18,21 67 0.000 2 ( 0.000000 1.000000 ) *
    3) as.factor(LANDCOVER): 24,26,27,31,32,34,36 1757 704.300 2 ( 0.050655
    0.949345 )
      6) as.factor(MAT1): 3,4,8,11,15,21,24,NA 334 360.700 2 ( 0.230539 0.769461 )
      12) RASTERVALU < 945 63 17.740 1 ( 0.968254 0.031746 ) *
      13) RASTERVALU > 945 271 121.600 2 ( 0.059041 0.940959 ) *
      7) as.factor(MAT1): 1,2,5,9,13,16,17,18,19,20,22,23,25,26,NA,NA 1423 138.500
2 ( 0.008433 0.991567 )
        14) as.factor(ROO): 2 137 81.360 2 ( 0.087591 0.912409 )
          28) RASTERVALU < 1355.5 12 13.500 1 ( 0.750000 0.250000 ) *
          29) RASTERVALU > 1355.5 125 28.310 2 ( 0.024000 0.976000 ) *
        15) as.factor(ROO): 0,1,3,4 1286 0.000 2 ( 0.000000 1.000000 ) *
  
```

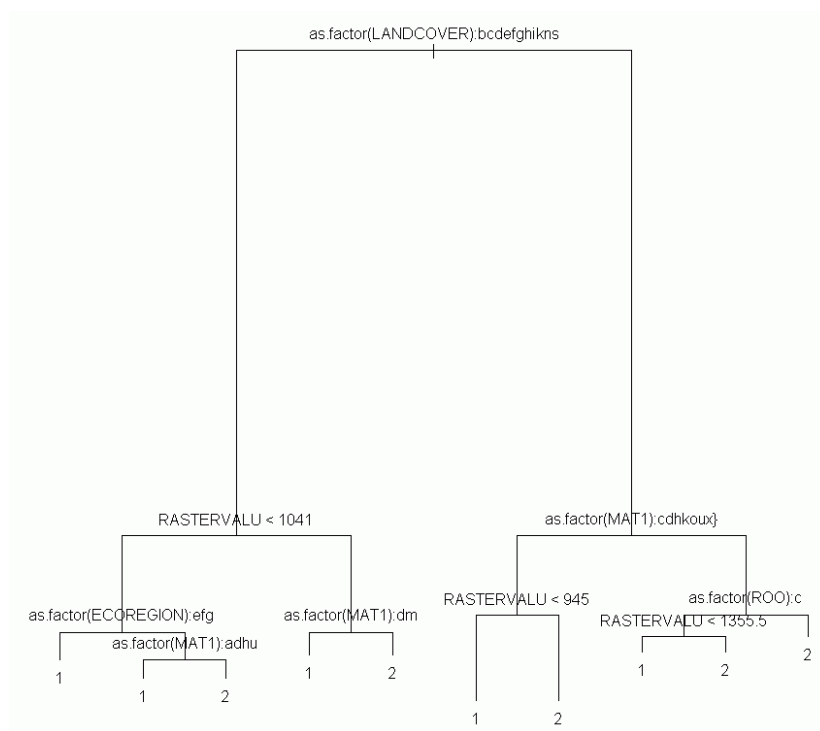


Figure 4 Diagram of the decision tree

Table 5 The legend of the CORINE land cover.

Class nr	Class description
1	continuous urban fabric
2	discontinuous urban fabric
3	industrial and commercial units
4	road and rail networks and associated land
5	port areas
6	airports
7	mineral extraction sites
8	dump sites
9	construction sites
10	green urban areas
11	port and leisure facilities
12	non-irrigated arable land
13	permanently irrigated land
14	rice fields
15	vineyards
16	fruit trees and berry plantation
17	olive groves
18	pastures
19	annual cops associated with permanent crops
20	complex cultivation patterns
21	land principally occupied by agriculture with significant natural vegetation
22	agro-forestry areas
23	broad-leaved forest
24	coniferous forest
25	mixed forest
26	natural grasslands
27	moors and heath lands
28	sclerophyllous vegetation
29	transitional woodland-scrub
30	beaches, sand, dunes
31	bare rocks
32	sparsely vegetated areas
33	burnt areas
34	glaciers and perpetual snow
35	inland marshes
36	peat bogs
37	salt marshes
38	salines
39	intertidal flats
40	water courses
41	water bodies
42	coastal lagoons
43	estuaries
44	sea and ocean

Table 6 The legend for the classification into environmental zones

Class nr	Class description
1	Alpine North
2	Boreal
3	Nemoral

ANNEX-1
Annex 1-EBONE Task 513 Report Mucher version-3

4	Atlantic North
5	Alpine South
6	Continental
7	Atlantic Central
8	Pannonian
9	Lusitanian
10	Anatolian
11	Mediterranean Mountains
12	Mediterranean North
13	Mediterranean South
14	Arctic
15	Steppic

The legend for the predominant mother material (MAT1) is:

Class nr	Class description
10	Undifferentiated alluvial deposits (or glacial deposits)
11	River alluvium
12	Estuarine/Marine alluvium
13	Glaciofluvial deposits
14	Glaciofluvial drift
15	Colluvium
20	Calcareous rocks
21	Limestone
22	Secondary chalk
23	Marl
24	Gypsum
25	Dolomite
30	Clayey materials
31	Old clayey sedimentary deposits
32	Alluvial or glaciofluvial clay
33	Residual clay from calcareous rocks
34	Claystone, mudstone
35	Calcareous clay
40	Sandy materials
41	Old sandy sedimentary deposits
42	Alluvial or glaciofluvial sands
43	Eolian sands
44	Coastal sands (Dune sands)
45	Sandstone
50	Loamy materials
51	Residual loam
52	Eolian loam
53	Siltstone
60	Detrital formations
61	Arkose
62	Breccia and Puddingstone
63	Flysch and Molasse
64	Ranas
70	Crystalline rocks and migmatites
71	Acid crystalline rocks (and migmatites)
72	Non acid crystalline rocks (and migmatites)
73	Crystalline metamorphic rocks
74	Schists
75	Other metamorphic rocks
80	Volcanic rocks
81	Acid volcanic rocks
82	Basic volcanic rocks
83	Volcanic slag
90	Other rocks
91	Organic materials

The legend for the rooting depth (ROO) is:

Class nr	Class description
0	No information
1	No obstacle to roots between 0 and 80 cm
2	Obstacle to roots between 60 and 80 cm depth
3	Obstacle to roots between 40 and 60 cm depth
4	Obstacle to roots between 20 and 40 cm depth
5	Obstacle to roots between 0 and 80 cm depth

The decision rules from the above tree were then applied to the whole European grid. First classifications were carried out for all the branch nodes, after which classifications were done for the terminal nodes or leaf nodes. The result of the latter steps is shown in figure 5 below. The leaf nodes pertaining to the beech forest habitat (9150) are shown in lilac colors and those pertaining to the heath habitat (4060) in green colors.

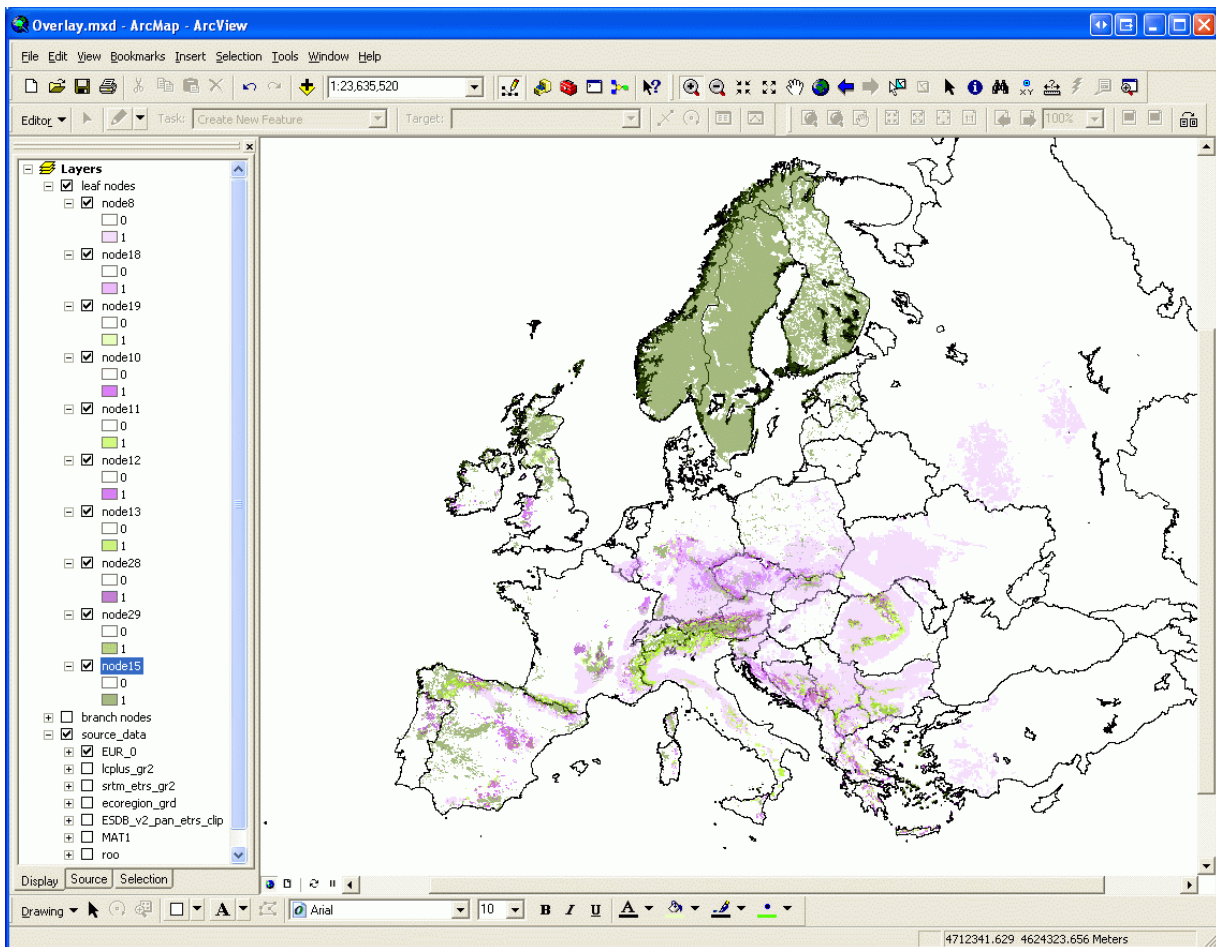


Figure 5 Result of the decision tree classification experiment

When compared with maps earlier obtained, see page 19 for H4060 and page 60 for H9150, the predicted habitats are much too large. It is obvious that the in-situ data have to be selected more carefully, especially in relation to the scale of the environmental data sets. It is obviously strange that areas with land covers such as “discontinuous urban fabric” and “industrial and commercial units” are indicated as potential host areas for the two selected habitats. This was based upon only 18 vegetation relevés, and hence were wrongly selected.

There is also a need to be more critical also about the biogeographic regions. This variable is important only in one part of the tree and at that point only 5 different biogeographic regions

are considered out of the 7 which occur in the data. In the whole of Europe up to 16 different biogeographic regions occur. In other words: the tree is based upon samples from more or less the same latitude in Europe where only few of the possible biogeographic regions occur, but it was applied to the whole of Europe.

The conclusion is that it only makes sense to use decision trees for classifying when representative samples are included. And that sometimes it might be necessary to prune a decision tree before it is applied.

7. EO TIME-SERIES ANALYSIS TO IDENTIFY HABITATS

7.1. Introduction

As the objective here is to enhance the spatial distribution of European habitats based on their phenology. For this reason NDVI-time series have been analysed that could be processed for the whole of Europe. There is a demand for a high temporal resolution together with a spectral resolution that allows the calculation of the Normalized Difference Vegetation Index (NDVI). The best suitable sensor, concerning a high temporal resolution and adequate spectral and spatial resolution, is MERIS (300m) or MODIS (250m). Since the latter is easy and freely downloadable, we used MODIS satellite data for our purpose. MODIS has a daily revisit time with a spatial resolution of 250 meter.

MODIS satellite data

The analysis is based upon multi-annual time series of MODIS images. MODIS has the highest resolution (250 m) of freely available remote sensing images with a daily revisit time. MODIS has an additional advantage, since it also provides composite images from the 16-days-maximum-NDVI product (MOD13Q1). More precisely, this MODIS product is the NDVI 16-Day L3 Global 250m. We used the version 5 MODIS product. Version-5 MODIS / Terra NDVI products have “Validated Stage 2”, meaning that accuracy has been assessed over a widely distributed set of locations and time periods via several ground-truth and validation efforts. Although there may be later improved versions, these data are ready for use in scientific publications. The 16-days-maximum-NDVI composite images have the advantage to exclude cloud affected data. Only when all 16 days in a composite are cloudy, the image is cloud affected. Unfortunately this is a regular occurrence in The Netherlands, so screening is necessary to filter out the cloud affected data. Additionally, the 16-day composites use a mask to filter out the large surfaces of open water, like sea and lakes. This mask is known to be inconsistent, which makes the results near the shoreline (within 15 km) unreliable. In spite of the shortcomings of the composite images, the 16-days-maximum-NDVI product also saves a large amount of time in pre-processing and provides annually 23 images which is sufficient to be used in time series analyses. Therefore the NDVI composite product has been downloaded and used during this research.

HANTS algorithm

The seasonal cycle of the NDVI can be approximated by a limited number of frequency components derived from a Fourier analyses. This principle is implemented in the HANTS algorithm (Harmonic Analysis of NDVI Time-Series) (Roerink et al., 2000) which employs an iterative routine to filter out poor NDVI estimates due to cloud cover or other disturbances from the NDVI cycle. In the current analyses only the zero (mean), first (annual cycle) and second (half-yearly cycle) frequency components of the Fourier analysis were used to describe the NDVI cycle.

The HANTS algorithm was originally developed by Wout Verhoef from NLR (Netherlands Space Laboratory) in the Netherlands. The idea behind the algorithm was to have a fast method for smoothing and reconstructing NDVI time-series at continental scales. For various purposes it was desirable to have a version of HANTS which was easy to use but with similar functionality. This has led to the implementation of HANTS using the remote sensing software package IDL-ENVI.

The basic concept behind the algorithm is that the vegetation development as indicated by the NDVI has a strong seasonal effect in most parts of the world (apart from the tropics) which can be described using a series of low frequency sine functions with different phases, frequencies and amplitudes. Cloud cover and other disturbing effects are usually more or less randomly occurring “spikes” in the NDVI time-series and can be considered as high frequency “noise”. The working of the HANTS algorithm is therefore based on a Fourier analysis.

In contrast to the standard fast Fourier transform (FFT), the HANTS algorithm works in an iterative manner (see next figure). The algorithm starts in the upper left block with the raw NDVI time series. These are used as input in the FFT and the relevant frequencies (usually mean, annual and half-year signal) are selected from the fourier spectrum. The inverse FFT (iFFT) then transforms the spectrum back into a filtered NDVI time-series. Next, a comparison is made between the filtered NDVI time-series and the original NDVI time-series. The difference is calculated between the filtered and the original NDVI time-series. Any points in the original NDVI time-series that are below a user-defined threshold are considered ‘cloudy’ and are replaced with the value of the filtered NDVI time-series. However, by replacing values in the NDVI time-series the average of the entire profile changes (becomes larger). Therefore a next iteration is needed and again the NDVI time-series is searched for possible cloud contaminated NDVI observations. This process continues until no new points are being found.

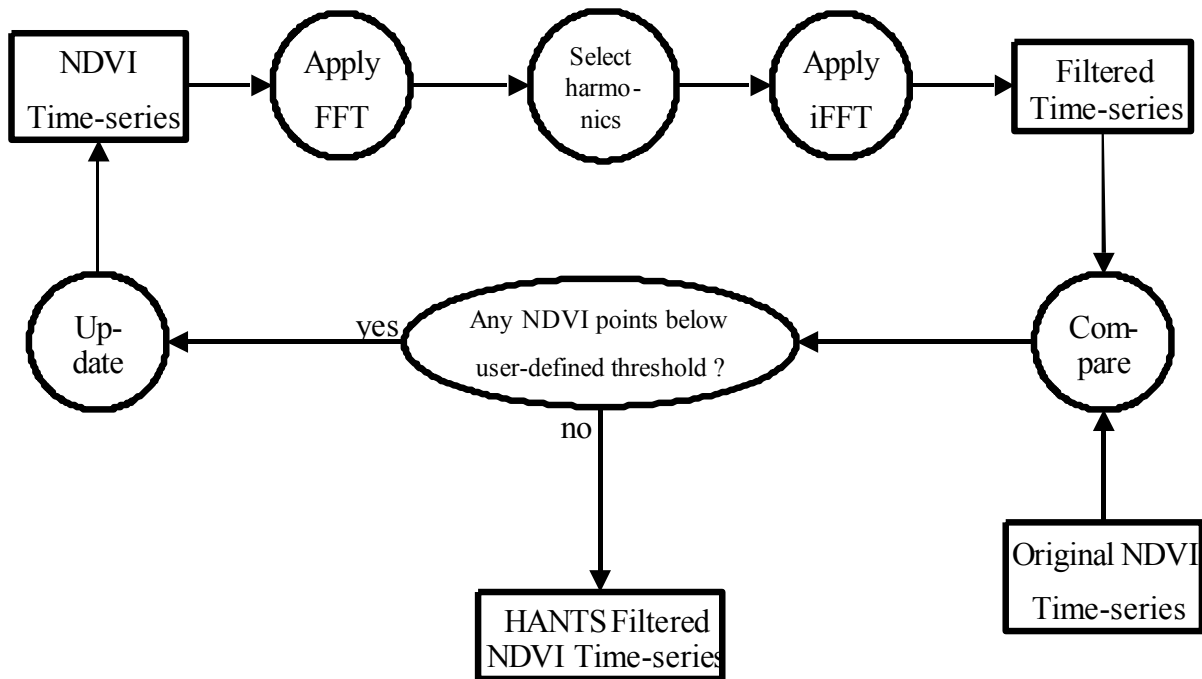


Figure 6 Iterative workflow of the HANTS algorithm. See text for explanation of the algorithm and acronyms.

The use of time series analysis on remote sensing images offers great opportunities for year-to-year monitoring of the earth surface. However, two serious drawbacks have to be dealt with, namely (i) time series analysis on remote sensing data produces huge amounts of data that needs to be processed and analysed and (ii) the presence of erroneous data, like cloud affected or missing pixels. The selected HANTS (Harmonic ANalysis of Time Series) algorithm (Roerink et al., 2000) deals with the latter mentioned drawbacks pretty well, and has three major benefits (Roerink & Danes, 2010):

- *Large data reduction.* The method allows reducing the amount of data by a factor of at least 5 without loss of information. In the example in the Figure 7 the individual NDVI values from 36 decades (10 day periods) are reduced into 5 HANTS components (3 amplitude and 2 phase values).
- *Exclusion of deviant data exclusion.* The method is able to exclude cloud affected and missing pixels in the analysis
- *Vegetation dynamics.* Objective and quantitative characterisation of plant phenology. The time series of NDVI remote sensing images are described by the Fourier components (amplitude and phase)

Because of its benefits, HANTS has been used successfully in various applications, such as cloud screening, removal and replacement (Roerink et al., 2000), land cover classification (Zhang et al., 2008), plant phenology characterisation (White et al., 2009) and climate variability assessment (Roerink et al., 2003).

HANTS is a least squared curve fitting procedure, based on harmonic components (cosine-functions), and considers only the most significant frequencies expected to be present in the time profiles. In an iterative process, input data values that have a large positive or negative deviation from the current estimated curve are excluded from the procedure. This process is repeated until the maximum error is acceptable or the number of remaining values becomes too small. The entire curve fitting procedure is controlled by 5 parameters, which have to be set at the beginning of each HANTS run:

- Number Of Frequencies (NOF). A curve is described by mean of its average (frequency zero) and a number of cosine functions with different frequencies. By this control parameter the user defines how many cosine functions are used and what the frequency (time period) of each cosine function is. This results in $2 \times \text{NOF} - 1$ output parameters (an amplitude and phase value for each frequency), where NOF includes a frequency zero (time series average), which has no phase.
- High/Low Suppression Flag (SF). This flag indicates whether high or low values (outliers) should be rejected during curve fitting.
- Invalid Data Rejection Threshold (IDRT). In some cases one might know that digital numbers below or above a certain threshold should be considered invalid.
- Fit Error Tolerance (FET). During curve fitting the absolute difference in the Hi/Lo direction of the remaining (i.e. not rejected) data values with respect to the current curve is determined after each iteration. The iteration stops when the difference of all remaining values becomes smaller than the FET. The FET value should not be set too low, as otherwise the fit might be based on too few values, which gives unreliable results.
- Degree of OverDeterminedness (DOD). The number of valid observations must always be greater than or equal to the number of parameters that describe the curve ($2 \times \text{NOF} - 1$). In order to get a more reliable fit the user can decide to use more data values than the necessary minimum. The minimum number of extra data values, which have to be used in the ultimate fit, is given by the DOD value.

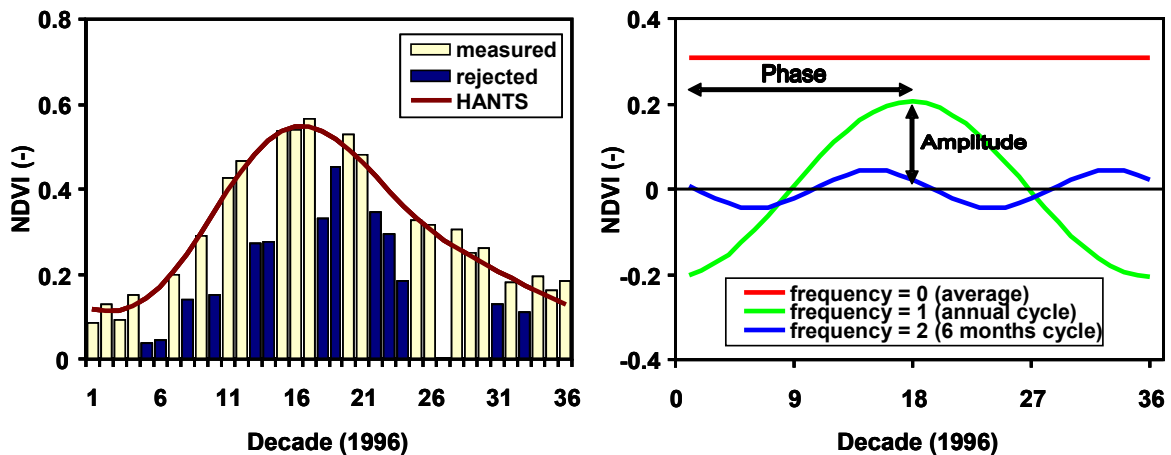


Figure 7 Visualisation of the HANTS algorithm (after Roerink et al., 2000).

The basic principle how HANTS works is visualised in Figure 7, where an original and HANTS reconstructed NDVI time series for a pixel of arable farming in Northern France are shown. The number of frequencies used by HANTS was set at 3: the average NDVI (frequency = 0), the yearly amplitude (frequency = 1) and the amplitude of 6 months (frequency = 2). The iteration stopped when 14 out of the 36 original NDVI values were rejected, i.e. classified as cloud affected data points. In this case, the remaining 22 values are allowed to have a maximum negative deviation from the curve of 0.05 NDVI units (=FET). The right graphs in Figure 7 shows the harmonic components of the 3 different frequencies, from which the cloud-free profile is reconstructed. Frequency zero (straight line) is represented only by amplitude and no off-set, while the other remaining frequencies (cosine functions) are defined by an amplitude and a phase value.

Example HANTS Results

HANTS has been applied now on the MODIS 16-day maximum NDVI composites for the years 2001 & 2006. The curve fitting process is controlled by 5 control parameters, which have to be set at the beginning of each HANTS run (Roerink and Danes, 2010). In the framework of this study the control parameters are set at:

- NOF = 3, where ;
 - Frequency 0: NDVI average
 - Frequency 1: Phase and amplitude of the annual cosine function
 - Frequency 2: Phase and amplitude of the six monthly cosine function
- SF = Low; which means only low values (outliers) should be rejected during curve fitting, as they correspond to cloud affected data.
- IDRT = 0; as missing data in the original NDVI composites have a value 0.
- FET = 0.05; as the NDVI values ranges from 0 to 1, a FET of 0.05 means that 5% deviation from the fitted curve is tolerated.
- DOD = 8; the maximum number of data points that may be rejected is 10 out of 23 available values.

Since this HANTS operation includes three frequencies, the output will consist out of five images:

Image 1. The amplitude of frequency 0, which is the average NDVI value, or the average amount of vegetation over a year (frequency 0 has no phase as it is a constant value over the year, i.e. has no starting point)

Image 2. The amplitude of frequency 1, which reflects the seasonal vegetation difference between summer and winter

- Image 3. The phase of frequency 1, which describes when exactly the peak vegetation takes place.
- Image 4. The amplitude of frequency 2, which is the amplitude of the 6 months cosine function. As in most cases vegetation dynamics have only one growing season during a year, the six months amplitude has no physical meaning like the annual amplitude, but is necessary for a smooth curve fitting procedure.
- Image 5. The phase of frequency 2 which is phase of the 6 months cosine function; like the amplitude of the six months cosine function its physical meaning is limited, but is necessary for a smooth curve fitting procedure.

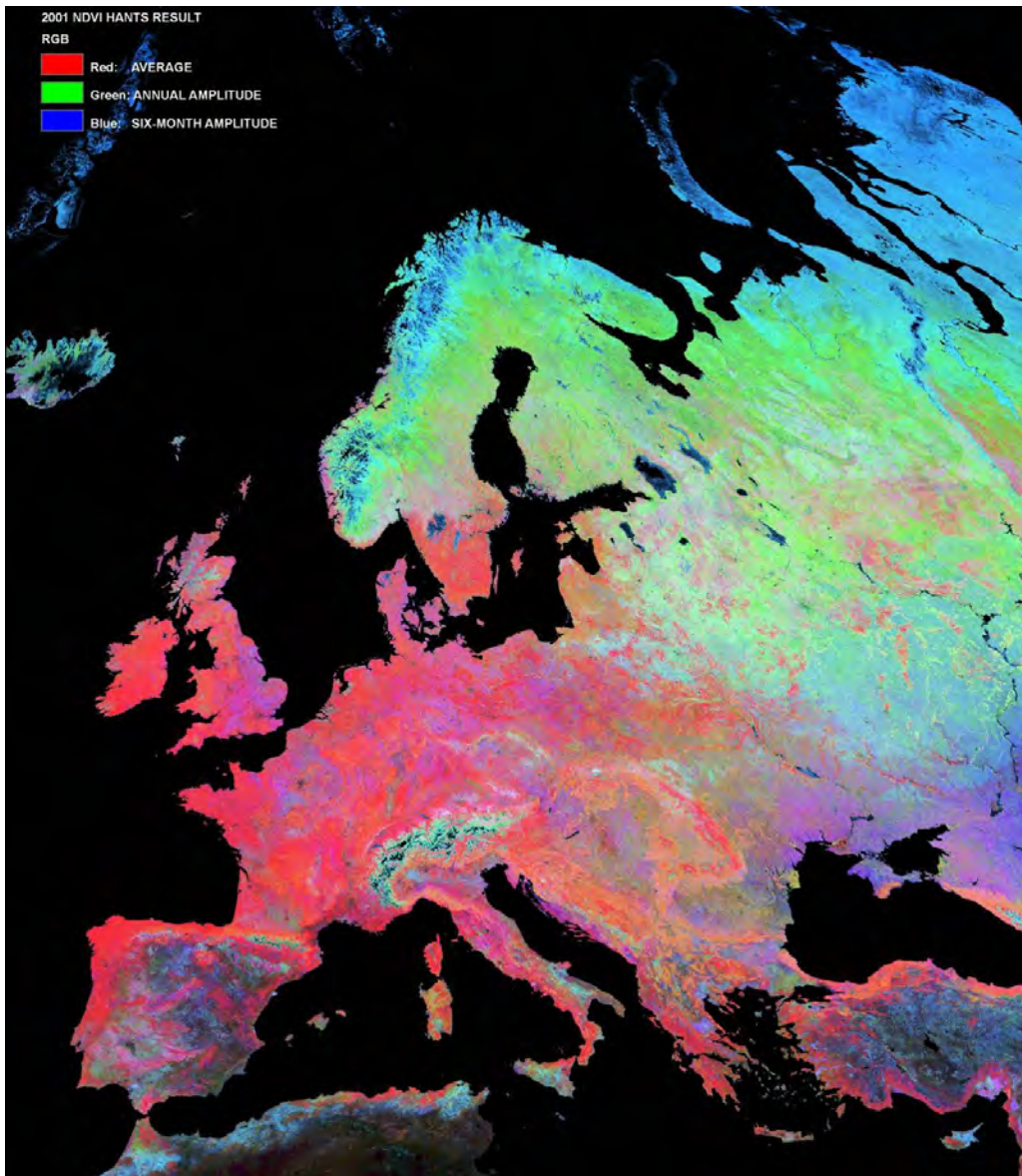


Figure 8 False colour European composite image of the HANTS results of the year 2001, where red colour indicates the NDVI average, green colour indicates the amplitude of annual frequency, and the blue colour indicates the amplitude of the six months frequency contacts: matthijs.danes@wur.nl or gerbert.roerink@wur.nl

7.2. Classifications

Many land cover classes have a typical phenological cycle, as shown in the figure below. This is only partly true for habitat classes that are moreover most of the time extremely fragmented in their spatial distribution over Europe. The first classification experiments using MODIS time series at a 1km spatial resolution failed completely. In other words, these data are too coarse to spatially identify different habitats as described in the former sections.

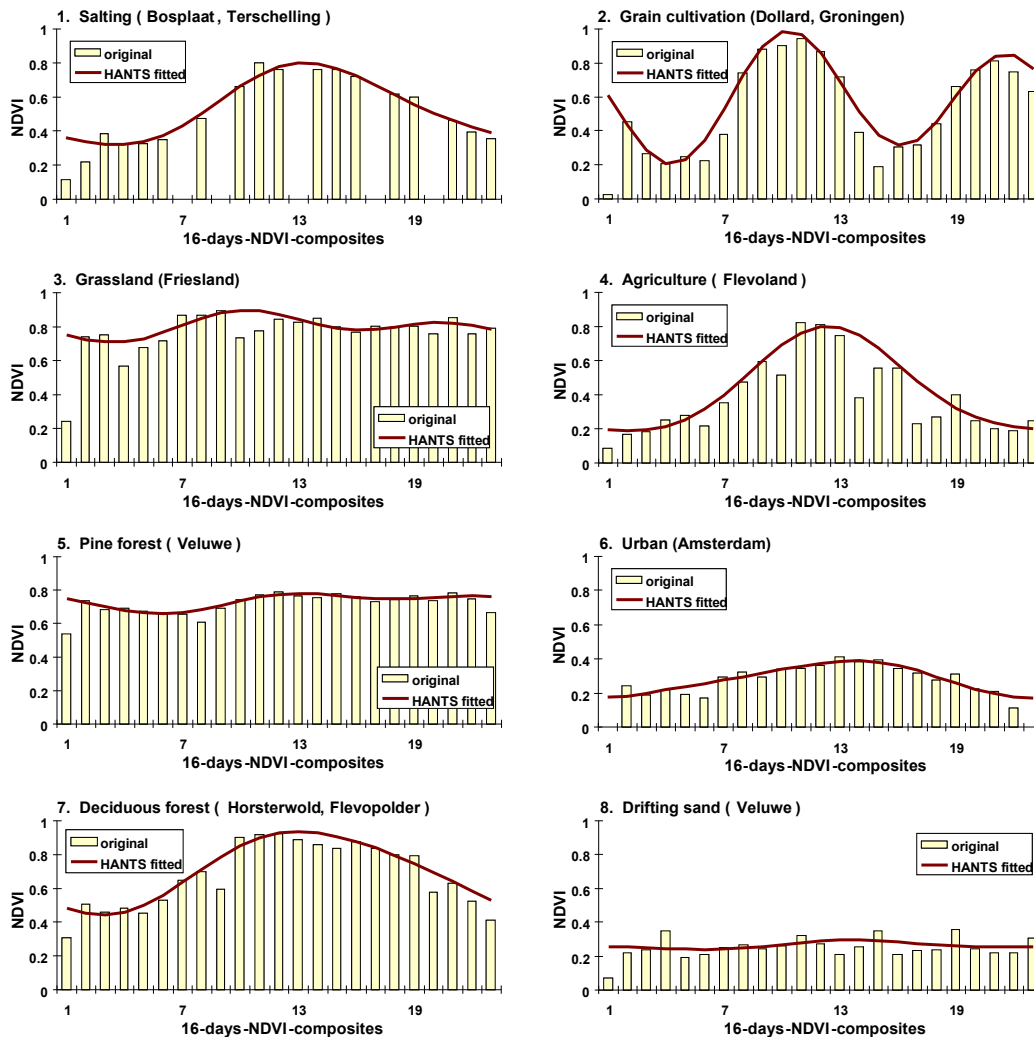


Figure 9 Yearly profiles of original NDVI values and the HANTS fitted curve of typical land cover types in the Netherlands.

The time-series analysis experiment performed here is based on MODIS 250 meter NDVI time series and aimed to explore the value of the HANTS results in helping to better define areas in which specific Natura 2000 habitats may occur.

7.3. Material

The material used in these experiments are 1) HANTS results based on MODIS 250m 16 days-maximum-NDVI time series for the year 2006; 2) Environmental zones (EnZ) (Metzger et al., 2005); 3) CORINE Land Cover 2006; 4) habitat information and 5) Natura2000 database.

Ad.1. The MODIS 250m 16 days-maximum-NDVI time series for the year 2006 were processed by the HANTS algorithm i.e a time series analysis of vegetation development by fourier analysis (Roerink et al., 2000). The fitting process was controlled by 5 control parameters (see section 7.4). The amplitude and phase of the vegetation development is described by a cosines function. The amplitude and phase are recalculated into xy-coordinates which were used for the classification.

Ad.2. The experiment focussed on the Alpine South (ALS) and Continental (CON) Environmental zones as for these zones sufficient in situ habitat measurements were available.

Ad.3. The CORINE Land Cover (CLC 2006) dataset was used as ancillary data to define suitable training sets for the classification of the different habitats selected.

Ad.4. In-situ data (vegetation releves) from countries (see section 3), results from habitat distribution modelling (section 5 and Mucher et al., 2009) were used to select training sets for classifying a specific habitat on the HANTS results. The classification focussed on H4060 '*Alpine and Boreal heaths*' and H9150 '*Medio-European limestone beech forest of the Cephalathero-Fagion*'.

Ad.5. The Natura2000 database was used in the assessment of the classification results.

7.4. Methodology

Classifications were made separately for each environmental zone as the vegetation development between zones is very different due to biophysical conditions. The HANTS results were classified with the Maximum Likelihood parametric rule based on a signature file. The signature file contained two groups of training sets: i) general land cover signatures and ii) specific signatures related to the selected habitats. For the specific habitat-training sites the in situ data (vegetation releves) were used in combination with the probability maps resulting from the habitat distribution modelling exercise (section 5) and the CORINE Land Cover database. The signatures were created by region growing in which seeding properties were adapted and more restricted for the specific habitat signatures (e.g. spectral euclidean distance was smaller/ narrow band width). Signatures for the habitats were compared and outliers were removed. The habitat classification was repeated several times with different number of training sets for a specific habitat. Finally, the ultimate classification was based on a limited number of signatures for that specific habitat (preferably the signature should be a pure endmember, but this is difficult to realise at a spatial resolution of 250 by 250 meters). Mainly training sites were used for areas that have a high probability that the specific habitat is present, located on the site where an in-situ measurement indicated the presence of the habitat and a 'logical' land cover type in the CORINE database.

7.5. Results

The distribution of the habitats H4060 and H9150 were classified on basis of the HANTS results for the Alpine South and Continental Environmental zone. Figure 11 and 12 show the results for the Alpine South environmental zone for H4060 and H9150. Comparing the classification results with the results from the habitat distribution modelling (probabilities) the habitat is more widely distributed and the presence of H9150 is largely overestimated. The contrary is the case for H4060. See also section 7.5.4. 'Assessment of results'.

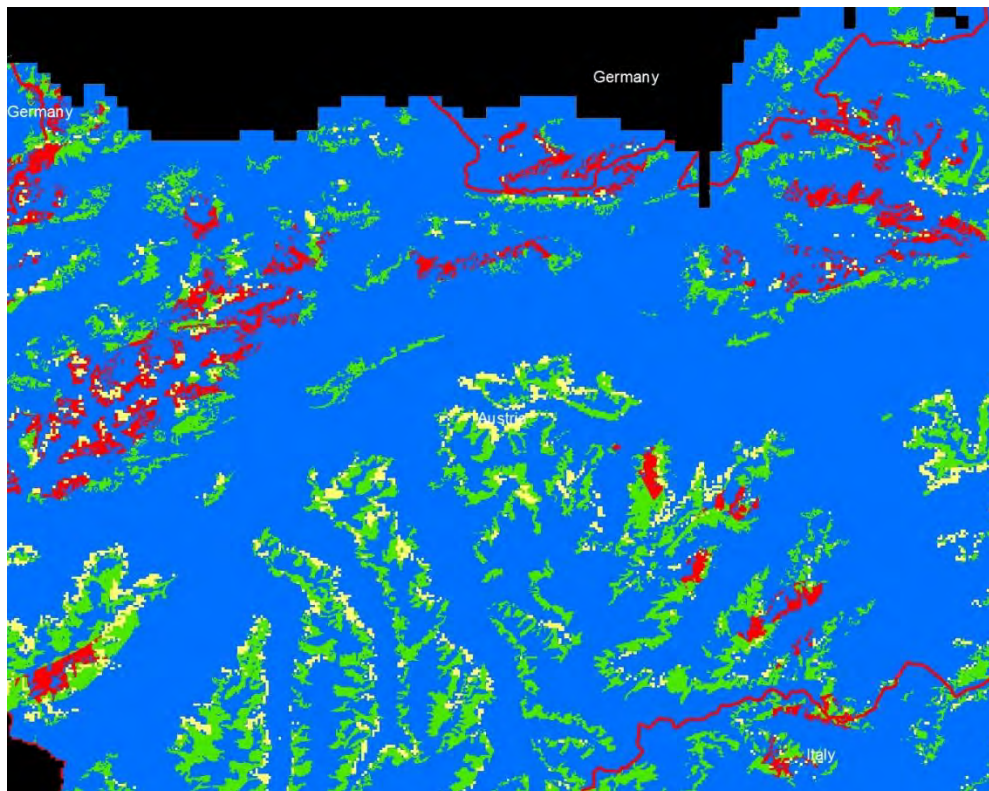


Figure 11 The Alpine environmental zone (blue) with in red (high) and green (low) probabilities that H4060 is present in this part of Austria. The yellow colour indicates the result of the HANTS classification. The classification result shows a limited presence of H4060 mainly distributed over areas with high and low probabilities.

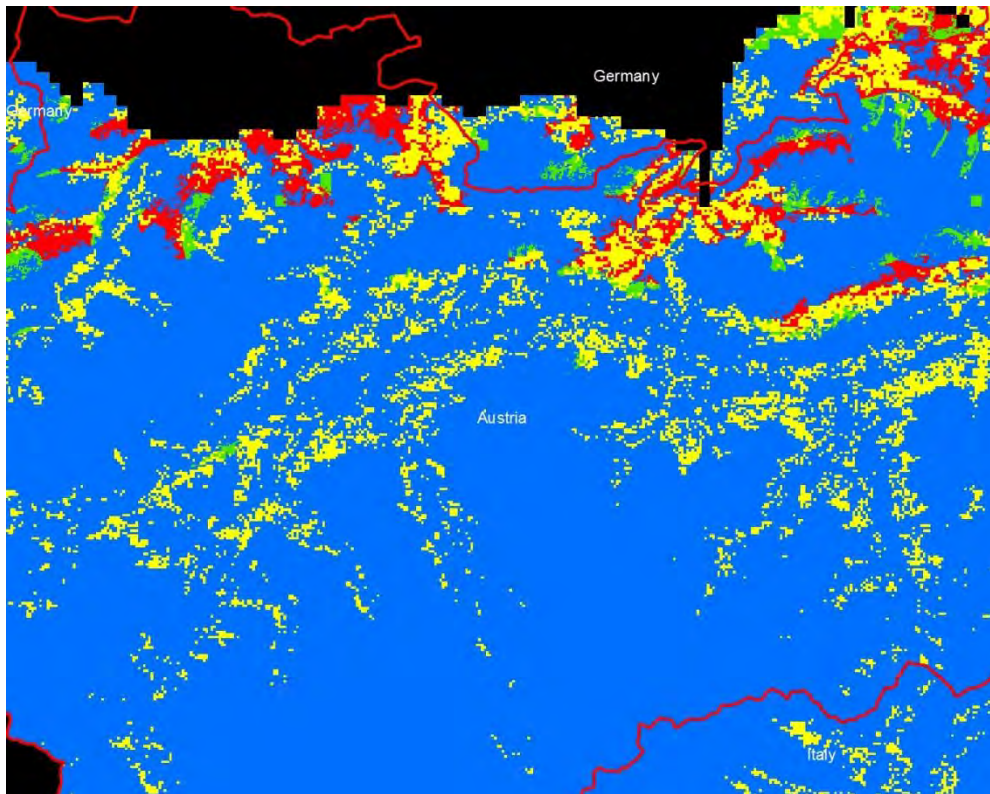


Figure 12 The Alpine environmental zone (blue) with in red (high) and green (low) probabilities that H9150 is present in this part of Austria. The yellow colour indicates the result of the HANTS classification. The classification result shows an overestimation of H9150 that is distributed all over the environmental zone. The distribution is not restricted to areas with high and low probabilities.

The results for the Continental zone are limited to the H9150 habitat, since there were no in situ H4060 habitat data available. The distribution of H9150 in the Continental zone shows an similar/intermediate position as in the Alpine south environmental zone: a large overestimation of H9150 and a scattered distribution all over the environmental zone (see Figure 13). The overestimation for H9150 in both environmental zones is, when comparing with CLC, partly due to the classification of mixed and coniferous forest as H9150.

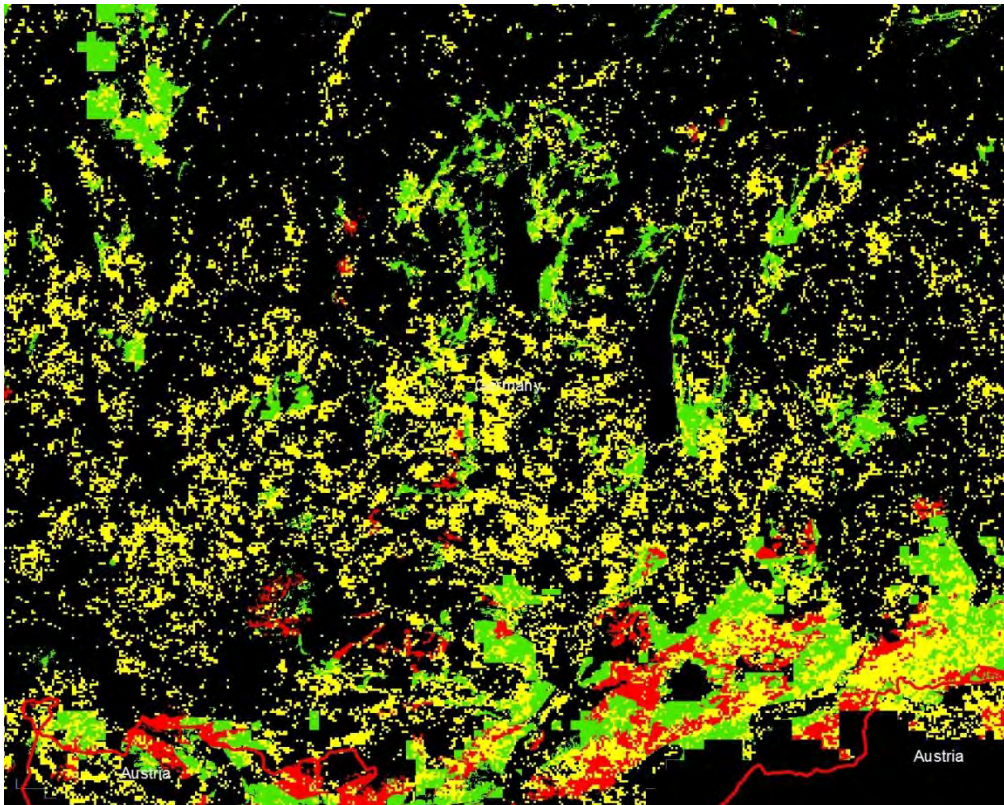


Figure 13 The Continental environmental zone (black) with in red (high) and green (low) the probabilities that H9150 is present in this part of Germany. The yellow colour indicates the result of the HANTS classification. The classification result shows an overestimation of H9150 that is distributed all over the environmental zone. The distribution is not restricted to areas with high and low probabilities.

7.6. Assessment of results

Table 7 indicates the number of pixels (as percentage of the total number of pixels) that agree between the different probability classes and the classification results.

For all three combinations (H4060-environmental zone ALS, H9150-environmental zone ALS and H9150-environmental zone CON) only small proportions of pixels are classified as H4060/H9150 and having low or high probability distributions. This is to be expected as the majority of pixels fall within the classes having no probability or within the classes not having that specific habitat. The table presents a possible overestimation of pixels classified as H9150 as the number of pixels falling in the probability class 0 is higher than the total number of pixels classified as not having that specific habitat (e.g. 86.0% versus 81.0% for the H9150/ALS combination). For H4060 this comparison may conclude that there is an underestimation of pixels classified as H4060 (93.0% versus 99.3%).

In case of the H4060/ALS combination a relatively high percentage of “correctly” classified pixels of 92.8% (92.5 + 0.2 + 0.1%) compared to the other two combinations with 75.4% (71.2 + 3.3 + 0.9%) and 86.3% (85.6 + 0.5 + 0.2%) can be found. The H4060 classification agrees better with the probability mapping of the habitat distribution modelling results than for the other two combinations.

ANNEX-1
Annex 1-EBONE Task 513 Report Mucher version-3

Table 7 A cross table of probability versus the classification results for the combinations H4060/ALS, H9150/ ALS and H9150/CON (areas as percentages of total number of pixels). Classification values 0 and 1 mean that the area is not classified respectively is classified having that specific habitat. Probability values 0, 2 and 3 mean that the specific habitat is probably not, with low respectively high probability present in the area based on the modelling in chapter 5.

H4060/ALS	Probability				Total
		0	2	3	
Classification	0	92.5%	5.7%	1.1%	99.3%
	1	0.5%	0.2%	0.1%	0.7%
		93.0%	5.9%	1.1%	100.0%

H9150/ALS	Probability				Total
		0	2	3	
Classification	0	71.2%	8.3%	1.5%	81.0%
	1	14.8%	3.3%	0.9%	19.0%
		86.0%	11.6%	2.4%	100.0%

H9150/CON	Probability				Total
		0	2	3	
Classification	0	85.6%	4.1%	1.2%	90.9%
	1	8.4%	0.5%	0.2%	9.1%
		94.0%	4.7%	1.4%	100.0%

Table 8 Number of Natura2000 sites with specific habitat for the specific habitat-environmental zone combinations that contain MODIS pixels classified as having that specific habitat. The Natura2000 sites are grouped according to the amount of pixels falling within the Natura2000 site.

Habitat	EnZ	Total sites with specific habitat	Number of site within EnZ	Number of pixel counts			Total
				1-5	5-25	>25	
4060	Als	157	91	13	13	3	29
9150	Als	47	10	2	1	-	3
9150	Con	47	9	1	1	7	9

Of the 91 Natura2000 sites with H4060 falling in the environmental zone ALS, 29 sites match the H4060 classification (see Table 8). Only 3 sites contain more than 25 MODIS pixels classified as having H4060. The H9150/CON combination shows that all 9 Natura2000 sites with H9150 have also pixels classified as H9150. The majority of these sites even contain more than 25 pixels with that specific habitat. One important remark to be made is that the number of pixels classified as having a specific habitat that fall within a Natura2000 site depends on the area of the Natura2000 site. So it is difficult to make conclusions based on

ANNEX-1

Annex 1-EBONE Task 513 Report Mucher version-3

the number of pixels falling within a site without weighting for the surface areas of the Natura2000 sites.

Table 9 All Natura2000 sites for a specific habitat-environmental zone combination and the number of sites that contain MODIS pixels classified as having that specific habitat. The Natura2000 sites are grouped according to the amount of pixels falling within the Natura2000 site.

Habitat/EnZ	Number of sites within EnZ	Number of pixel counts			Total
		1-5	5-25	>25	
H4060/ALS	1367	72	60	27	159
H9150/ALS	1367	222	283	531	1036
H9150/CON	6375	1623	1291	1084	3998

The majority of all Natura2000 sites within the ALS and CON environmental zones contain pixels that are classified as having H9150 MODIS pixels (see Table 9). This suggest an overestimation of the H9150 classification in both environmental zones.

Table 10 Error matrices between Natura2000 sites and the classification of HANTS phenology product. The number of Natura2000 polygons with or without MODIS pixels classified for a specific habitat/Environmental Zone combination (H4060/ALS, H9150/ALS and H9150/CON).

H4060/ALS		Natura2000 (N2K)		Total
		present	not present	
classification RS	present	29	130	159
	not present	62	1146	1208
	Total	91	1276	1367

H9150/ALS		Natura2000 (N2K)		Total
		present	not present	
classification RS	present	3	1033	1036
	not present	7	324	331
	Total	10	1357	1367

H9150/CON		Natura2000 (N2K)		Total
		present	not present	
classification RS	present	9	3989	3998
	not present	0	2377	2377
	Total	9	6366	6375

In Table 10 pivot tables are presented between the Natura2000 database and the remote sensing classification results for each habitat/environmental zone combination. The number of Natura2000 polygons with a specific habitat that has a match with pixels classified as having that specific habitat, but also the polygons without that specific habitat and not containing pixels classified as having that habitat are an indication of the quality of the classification. So the summation of the number of Natura2000 polygons on the axis present/present and not present/not present as percentage of the total number of polygons in

that specific Environmental Zone are an indication of the quality of the classification. The H4060/ALS classification with 86% showed up as best, while the H9150/ALS and H9150/CON classifications with 23.9% and 37.4% have relatively low levels of agreement between the reference data (Natura2000 sites) and the classification results.

7.7. Discussion

The assessment of the classification results suggests an overestimation of the H9150 habitats in both environmental zones. An underestimation is present in the case of H4060, although there are indications that this classification is better than in the case of the H9150 classifications. However, the classification of habitats on basis of satellite imagery needs improvement. The main limitation is the lack of more detailed (higher resolution) HANTS vegetation phenology product, next to the fact that many habitats do not have a unique phenology. The present spatial resolution of the times series analysis was 250 meter based on the MODIS satellite imagery, while most of the Natura 2000 habitats are still very fragmented at this scale. So for most habitats it will be impossible to find good training samples. Therefore, the resolution/scale of habitat observations and the classification results should be more in line with each other to make them comparable. Remote sensing imagery with higher spatial and/or spectral resolution would improve the possibilities of habitat classification with remote sensing. Next to the fragmented character of the habitats, also the agreement between temporal profiles of for example different forest habitats shows the limitations of the classification methodology.

The quality of the classification results differ between habitats and between environmental zones. Generic classification parameters valid for all kinds of habitat-environmental zones combinations will be an utopia. Habitats differ in reflectance from each other and differ between environmental zones as the biophysical conditions and the phenology development is different. As a consequence the classification of habitats is partly subjective as it depends on the selection and delimitation of training sites.

8. REFERENCES

- Büttner, G., Feranec, J., Jaffrain, G., Mari, L., Maucha, G. & Soukup, T. 2004. The CORINE Land Cover 2000 Project. in R. Reuter, (Editor). EARSeL eProceedings, 3, (3). EARSeL0, Paris, pp. 331-346.
- Bossard, M., Feranec, J., and O'ahel', J. 2000. CORINE land cover technical guide – Addendum 2000. Technical report, 40. European Environment Agency, Copenhagen. <http://terrestrial.eionet.eea.int>.
- Bunce, R.G.H.; Bogers, M.M.B.; Roche, P.; Walczak, M.; Geijzendorffer, I.R.; Jongman, R.H.G., 2011. Manual for habitat and vegetation surveillance and monitoring : temperate, mediterranean and desert biomes, Wageningen : Alterra, 2011 (Alterra-report 2154).
- CEC, 1994. CORINE land cover. Technical guide. Office for Official Publications of European Communities, Luxembourg.
- European Commission, 2007. Interpretation manual of European Habitats – EUR27. Published by the European Commission, DG Environment, Nature and biodiversity.
- Evans, D., 2006. "The habitats of the European union habitats directive." Proceedings of the Royal Irish Academy - Section B, Biol. Environ. 106 (3): 167-173.
- Hennekens, S.M. and , J.H.J., 2001. TURBOVEG, a comprehensive data base management system for vegetation data. Journal of Vegetation Science, 12 (4), pp. 589-591.
- Metzger M.J., Bunce R.G.H, Jongman R.H.G, Múcher C.A. & Watkins J.W, 2005. A climatic stratification of the environment of Europe. Global Ecology and Biogeography 14: 549-563.
- Múcher, C.A., S.M. Hennekens, R.G.H. Bunce and J.H.J. Schaminée, 2004. Mapping European Habitats to support the design and implementation of a Pan-European Ecological Network. The PEENHAB project. Alterra report 952, Wageningen.
- Múcher, C.A., Hennekens, S.M., Bunce, R.G.H., Schaminée, J.H.J., Schaepman, M.E., 2009. Modelling the spatial distribution of Natura 2000 habitats across Europe. Landscape Urban Plan. 92 (2), 148-159. doi:10.1016/j.landurbplan.2009.04.003.
- Múcher, C.A., 2009. Geo-spatial modelling and monitoring of European landscapes and habitats using remote sensing and field surveys. PhD thesis Wageningen University, Wageningen, The Netherlands, ISBN 978-90-8585-453-1, 269 pp.
- Opdam, P., Verboom, J., Pouwels, R., 2003. Landscape cohesion: an index for the conservation potential of landscapes for biodiversity. Landscape Ecol. 18, 113–126.
- Opdam, P., Steingröver, E., van Rooij, S., 2006. Ecological networks: a spatial concept for multi-actor planning of sustainable landscapes. Landscape Urban Plan. 75 (3–4), 322–332.
- Rodwell, J.S., Schamineé, J.H.J., Mucina, L., Pignati, S., Dring, J., Moss, D., 2002. The Diversity of European Vegetation. An overview of phytosociological alliances and their

relationships to EUNIS habitats. EC-LNV Report nr. 2002/054. Wageningen, the Netherlands, 168 p.

Roerink, G.J., Menenti, M. and Verhoef, W., 2000. Reconstructing cloudfree NDVI composites using Fourier analysis of time series. *International Journal of Remote Sensing*, 21(9): 1911-1917.

Roerink, G.J., Menenti M., Soepboer W., Su Z. (2003), Assessment of climate impact on vegetation dynamics by using remote sensing, *Physics and Chemistry of the Earth*, Vol. 28, pp. 103-109;

Roerink, G.J.; Danes, M.H.G.I. (2010) General surveillance of genetically modified crops : possibilities of GIS and remote sensing

Schaminée, J.H., Hennekens, S.M., Ozinga, W.A., 2007. Use of the ecological information system SynBioSys for the analysis of large datasets. *J. Veg. Sci.* 18, 463-470.

Schaminée, J. H. J., Janssen, J. A. M., Hennekens, S. M., Ozinga, W. A. (2011): Large vegetation databases and information systems: New instruments for ecological research, nature conservation, and policy making, *Plant Biosystems - An International Journal Dealing with all Aspects of Plant Biology*, 145:sup1, 85-90

White, M.A., de Beurs, K.M., Didan, K., Inouye, D.W., Richardson, A.D., Jensen, O.P., O'Keefe, J., Zhang, G., Nemani, R.R., van Leeuwen, W.J.D., Brown, J.F., de Wit, A., Schaepman, M., Lin, X., Dettinger, M., Bailey, A.S., Kimball, J., Schwartz, M.D., Baldocchi, D.D., Lee, J.T., Lauenroth, W.K. (2009), *Intercomparison, interpretation, and assessment of spring phenology in North America estimated from remote sensing for 1982-2006*, *Global Change Biology*, Vol. 15, pp. 2335-2359;

Zhang, X., Sun, R., Zhang, B., Tong, Q. (2008), Land cover classification of the North China Plain using MODIS_EVI time series, *ISPRS Journal of Photogrammetry and Remote Sensing*, Vol. 63, pp. 476-484;

Annex I Criteria used to classify the SynBioSys vegetation releves into the relevant Annex I habitat types for the various countries for which in-situ data were obtained.

Vegetation type	Britain	Netherlands	Belgium (Flanders)
Basic grassland	Comm. U1 - U21	vegetation class 15	--
Acid grasslands	Comm. CG1 - CG14	vegetation alliance 19AA	ph <= 4.4
4070 Pinus mugo	--	--	--
6150 Siliceous alpine and boreal grasslands	Comm. U7,U8,U9	--	--
6170 Alpine and subalpine calcareous grasslands	presence of Dryas octopetala	--	--
9410 Acidophilous Picea forests of the montane to alpine levels (Vaccinio-Piceetea)	--	--	--
9150 Medio-European limestone beech forests of the Cephalanthero-Fagion	--	--	--
6240 Sub-pannonic steppic grasslands	--	--	--
6250 Pannonic loess steppic grasslands	--	--	--
9510 Southern Apennine Abies alba	--	--	--
4060 Alpine and boreal heath	Comm. H16, H17, H19, H20, H21, H22	--	--
7110 Active raised bogs	Comm. M18, M20	Selection on Annex I 7110	--
7130 Blanket bog	Comm. M17, M18, M19, M20	--	--
6210 Semi-natural dry grasslands and scrubland facies on calcareous substrates (Festuco-Brometalia)	Brachypodium pinnatum >10% cover or Bromus erectus >10% cover	Selection on Annex I 6210	--
9420 Alpine Larix decidua and/or Pinus cembra forest	--	--	--
6230 Species-rich Nardus grasslands	Comm. U5, U7 AND one of the next 4 species: Gentiana pneumonanthe, Carex panicea, Carex ericetorum, Antennaria dioica	Selection on Annex I 6230	--

Vegetation type	Austria	Tjechia	Slovakia
Basic grassland		predefined	Vegetation class 06 and 10
Acid grasslands	field ACIDSOIL' = "X"	predefined	Vegetation class 13
4070 Pinus mugo	preselected	Pinus mugo > 75% cover	Pinus mugo > 75% cover
6150 Siliceous alpine and boreal grasslands	Juncus trifidus > 5% cover or Carex bigelowii > 5% cover	--	Juncus trifidus > 5% cover or Carex bigelowii > 5% cover
6170 Alpine and subalpine calcareous grasslands	Dryas octopetala	--	Dryas octopetala and vegetation class 06
9410 Acidophilous Picea forests of the montane to alpine levels (Vaccinio-Piceetea)	--??	preselected	preselected
9150 Medio-European limestone beech forests of the Cephalanthero-Fagion	preselected	preselected	Syntaxon 27BD10
6240 Sub-pannonic steppic grasslands	Stipa pennata > 10% cover	preselected	preselected
6250 Pannonic loess steppic grasslands	--	preselected	--
9510 Southern Apennine Abies alba	--	--	--
4060 Alpine and boreal heath	Arctostaphylos alpinus >20% cover or Rhododendron ferruginum >20% cover or Rhododendron hirsutum >20% cover	preselected	preselected
7110 Active raised bogs	Andromeda polifolia	Andromeda polifolia	Andromeda polifolia
7130 Blanket bog	--	--	--

ANNEX-1

Annex 1-EBONE Task 513 Report Mucher version-3

6210 Semi-natural dry grasslands and scrubland facies on calcareous substrates (Festuco-Brometalia) 9420 Alpine Larix decidua and/or Pinus cembra forest	Brachypodium pinnatum >10% cover or Bromus erectus >10% cover ??	Brachypodium pinnatum >10% cover or Bromus erectus >10% cover --	Brachypodium pinnatum >10% cover or Bromus erectus >10% cover preselected
6230 Species-rich Nardus grasslands	Nardus stricta > 5% cover AND one of the next 4 species: Gentiana pneumonanthe, Carex panicea, Carex ericetorum, Antennaria dioica	Nardus stricta > 5% cover AND one of the next 4 species: Gentiana pneumonanthe, Carex panicea, Carex ericetorum, Antennaria dioica	Nardus stricta > 5% cover AND one of the next 4 species: Gentiana pneumonanthe, Carex panicea, Carex ericetorum, Antennaria dioica
Vegetation type	Switzerland	Bulgaria	Romania
Basic grassland	pH > = 7.0	field BASICROCK='limestone'	??
Acid grasslands	ph <= 4.4 and Nardus >= 25% cover	field BASICROCK='silicate'	??
4070 Pinus mugo	--	--	Pinus mugo > 75% cover
6150 Siliceous alpine and boreal grasslands	Juncus trifidus > 5% cover	--	Juncus trifidus > 5% cover
6170 Alpine and subalpine calcareous grasslands	Dryas octopetala and pH >= 7.0	--	Dryas octopetala > 5% cover
9410 Acidophilous Picea forests of the montane to alpine levels (Vaccinio-Piceetea)	--	--	Picea abies > 50% cover
9150 Medio-European limestone beech forests of the Cephalanthero-Fagion	--	--	Fagus sylvatica > 50% cover + Cephalanthera rubra preselected
6240 Sub-pannonic steppic grasslands	--	--	--
6250 Pannonic loess steppic grasslands	--	--	--
9510 Southern Apennine Abies alba	--	--	--
4060 Alpine and boreal heath	--	--	--
7110 Active raised bogs	--	--	--
7130 Blanket bog	--	--	--
6210 Semi-natural dry grasslands and scrubland facies on calcareous substrates (Festuco-Brometalia) 9420 Alpine Larix decidua and/or Pinus cembra forest	Brachypodium pinnatum >10% cover or Bromus erectus >10% cover --	--	Pinus cembra > 20 cover or Larix decidua >20% cover
6230 Species-rich Nardus grasslands	Nardus stricta > 5% cover AND one of the next 4 species: Gentiana pneumonanthe, Carex panicea, Carex ericetorum, Antennaria dioica	--	Nardus stricta > 5% cover AND one of the next 4 species: Gentiana pneumonanthe, Carex panicea, Carex ericetorum, Antennaria dioica

Annex-2

EBONE



European Biodiversity Observation Network: Design of a plan for an integrated biodiversity observing system in space and time

D5.1.2c: A regionally adaptive EO Approach for determining GHC with focus on using LiDAR for landscapes in the Netherlands

Ver 3.0

Document date: 2010-11-01

Document Ref.: EBONE-D5.1.2c-3.0

Use of LiDAR to map and monitor habitats



Authors: C.A. Múcher, L. Roupioz, H. Kramer and A. Griffioen

EC-FPV Contract Ref: ENV-CT-2008-212322

D5.1.2c: A regionally adaptive EO Approach for determining GHC with focus on using LiDAR for landscapes in the Netherlands

Use of LiDAR to map and monitor habitats

Authors: C.A. Múcher, L. Roupioz, H. Kramer and A. Griffioen

Alterra, Wageningen University and Research Centre

Reviewed by France Gerard (CEH) in October 2010



Content

1. Introduction	6
1.1 Background	6
1.2. Objectives.....	8
1.3 Contents of the report.....	9
2. State of the art on LiDAR	10
2.1. What is airborne LiDAR ?	10
2.2. Discrete return	11
2.3. Full waveform	11
2.4. Application of LiDAR system in environmental sciences	11
2.5. Difference between discrete-return and full waveform in ecological applications.....	13
2.6. Limitations	14
2.7. Conclusions	14
2.8. Future developments	15
3. Study area & materials	16
3.1. Study area.....	16
3.2. Materials.....	18
3.2.1. LiDAR.....	18
3.2.2 Aerial photographs	21
3.2.3 Fieldwork	21
3.3. LiDAR software	21
3.3.1. Fusion software	21
3.3.2. Commercial software packages.....	24
4. Methodology & Results	25
4.1. Methodology of habitat recording.....	25
4.2. Height measurements LiDAR	28
4.4. Preliminary results.....	31
4.5. Segmentation and classification for an entire 1km ² sample.....	32
4.6. Validation	38
Discussion	45
5. Conclusions	46
6. References	47

Figures

Figure 1 Relations between different land and biodiversity observation levels.	7
Figure 2 Number of hits per year for the search “LiDAR AND vegetation” in scopus (www.scopus.com).	10
Figure 3 Location of the study area Chaam in the Southern part of the Netherlands. The aerial photograph below shows the study area in detail with the objects of interest.	16
Figure 4 Location of the objects of interest in the study area. Below you find a snapshot of all objects of interest.	17
Figure 5 Photo of the tree nursery in the village of Chaam The tree nursery is located with a box in figure 4 in the southern part of the study area.	18
Figure 6 A schematic figure of an aircraft equipped with a LiDAR instrument that collects elevation information in so called data clouds with XYZ measurements.	19
Figure 7 Planning schema AHN-2. Status at July 2009.	20
Figure 8 Snapshot of Fusion with a 3D view which shows the LiDAR points draped over by an aerial	22
Figure 9 Example of outputs from FUSION	23
Figure 10 Height and width measurements on a single tree in LiDAR point data. The low Z values are displayed in blue, shifting into green, yellow, orange and finally to red for relatively high values.	28
Figure 11 Visual comparison of a single tree (object 1) as seen in the field (left) and 3D view by LiDAR measurements. Red pole indicates the height measurement of the object in the field. Green dots are the LiDAR measurements.	29
Figure 12 Visual comparison of a hedge and tree (object 23) as seen in the field (left) and 3D view by LiDAR measurements. Red pole indicates the height measurement of the object in the field. Brown dots are the LiDAR measurements.	29
Figure 13 Visual comparison of a fringe of reed (object 5) as seen in the field (left) and 3D view by LiDAR measurements. Red pole indicates the height measurement of the object in the field. Brown dots are the LiDAR measurements.	30
Figure 14 An example a different layers calculated by FUSION software for the LiDAR data and layers derived from the false-colour aerial photographs that are integrated by a decision tree classifier to identify the individual plant life forms at a pixel level.	31
Figure 15 Visual comparison of the aerial photograph and the identified plant life forms at the pixel level. Major problem is still to identify the proper mapping units used for the General Habitat Categories.	32
Figure 16 NDVI index mask (left) and Top10 vector mask (right)	33
Figure 17 Canopy height mode (left) and pixel based classification output (right)	33
Figure 18 Visualization of the habitat mapping units created during the segmentation. The number identifying the polygons are used in table 4.	34
Figure 19 Visual comparison of semi-automated (yellow) and field based manual (blue) delineation of the habitat patches.	38
Figure 20 Identification of the habitat mapping units defined during the field work.	39
Figure 21 Validation graphs for Leafy hemicryptophytes (LHE) and Caespitose hemicryptophytes (CHE) and details concerning an outstanding value.	44
Figure 22 Validation graphs for Mid phanerophytes (MPH) and details concerning an outstanding value.	45

Tables

Table 1 LiDAR processing software..... 24

Table 2 Life forms for recording General Habitat Categories (GHCs), based on life forms as defined by Raunkiaer (1934). Adapated from Bunce et al., 2008..... 26

Table 3 Field measurement on vegetation objects in the study area of Chaam in February 2010..... 30

Table 4 Percentage of each general habitat category by habitat mapping units 35

Table 5 Comparison between semi-automated and field based plant life forms identification inside each habitat mapping unit..... 40

1. Introduction

1.1 Background

This study has been implemented within the framework of the EU- FP7 project EBONE “European Biodiversity Observation Network: a project to design and test a biodiversity observing system, integrated in time and space” (Grant Agreement no: 212322). The key challenge is to develop a biodiversity observation system that is transmissible, cost effective and provides added value to the currently independent data sources of in situ data and EO. The key activities will involve the integration between EO with field measurements in a consistent and repeatable manner. Measuring and reliable reporting of trends and changes in biodiversity requires that data and indicators are collected and analysed in a standard and comparable way. This is valid for a national park, but also for larger areas such as the European Union. However, at present, all responsible authorities (over 100 national and regional agencies) have different approaches. Worldwide the problem is even greater because in different continents species and ecosystems differ. Therefore there is a need to develop a coherent system for data collection that can be used for assessments at the European and global scales. EBONE will deliver a European contribution to the development of a global biodiversity observation system that is spatially and topically prioritized. In the GEOSS (Global Earth Observation System of Systems) 10 year implementation plan (GEO, 2005) it is stated that GEOSS will unify many of the disparate biodiversity observing systems and create a platform to integrate biodiversity data with other types of information. Harmonisation of observations, real- or near real-time monitoring integration of information from in situ and space based observations will be advocated. GEO BON, the Group on Earth Observations Biodiversity Observation Network, is the biodiversity arm of the GEOSS. The GEO BON working group (http://www.earthobservations.org/geobon_a.shtml) was initiated since the Earth’s biosphere is such a complex system that a comprehensive monitoring network for simultaneously tracking individual species and populations and monitoring trends in forests and other ecosystems has never been built and requires expertise from a wide amalgam of scientists, not working only in the field of biology and climate research, but also in the field of Earth Observation (EO). To present a full picture of what is happening to biological diversity, this monitoring network would also need to integrate masses of biological information with data and forecasts on climate change, pollution and other threats to biodiversity. The lack of comprehensive information about the world’s biological resources continues to undermine the efforts of policymakers and managers to set priorities, elaborate strategies and assess the effectiveness of their actions. Fortunately, new EO technologies are improving the collection and analysis of biodiversity information. These increasingly sophisticated monitoring systems, which consist of satellite, air, land and ocean-based instruments, are being interlinked through the Group on Earth Observations (GEO) to form a Global Earth Observation System of Systems (GEOSS). EBONE is a partnership of sixteen universities and research institutes in Europe, Israel and South Africa.

Background in methodological aspects of the EBONE project date back to the BIOHAB project. The Biohab project showed that the way forward was to measure habitat diversity as a proxy for biodiversity on the basis of plant life forms but also including information on environmental variation in humidity and trophic levels using a stratified random sampling system. Based on these lifeforms a total of 130 General Habitat Categories (GHCs) were defined, which is still being extended in the current project. The same categories can be applied to areal, linear and point features to assist recording and subsequent interpretation at the landscape level. The distribution and change of landscape ecological parameters, such

as connectivity and fragmentation, can then be derived and their significance interpreted. The accompanied monitoring system should consist of a baseline monitoring system combined with selected sites for intensive sampling in conservation sites (Natura 2000) and sites for long term intensive ecological monitoring and research (LTER) on the cause-effect relationships at the site level.

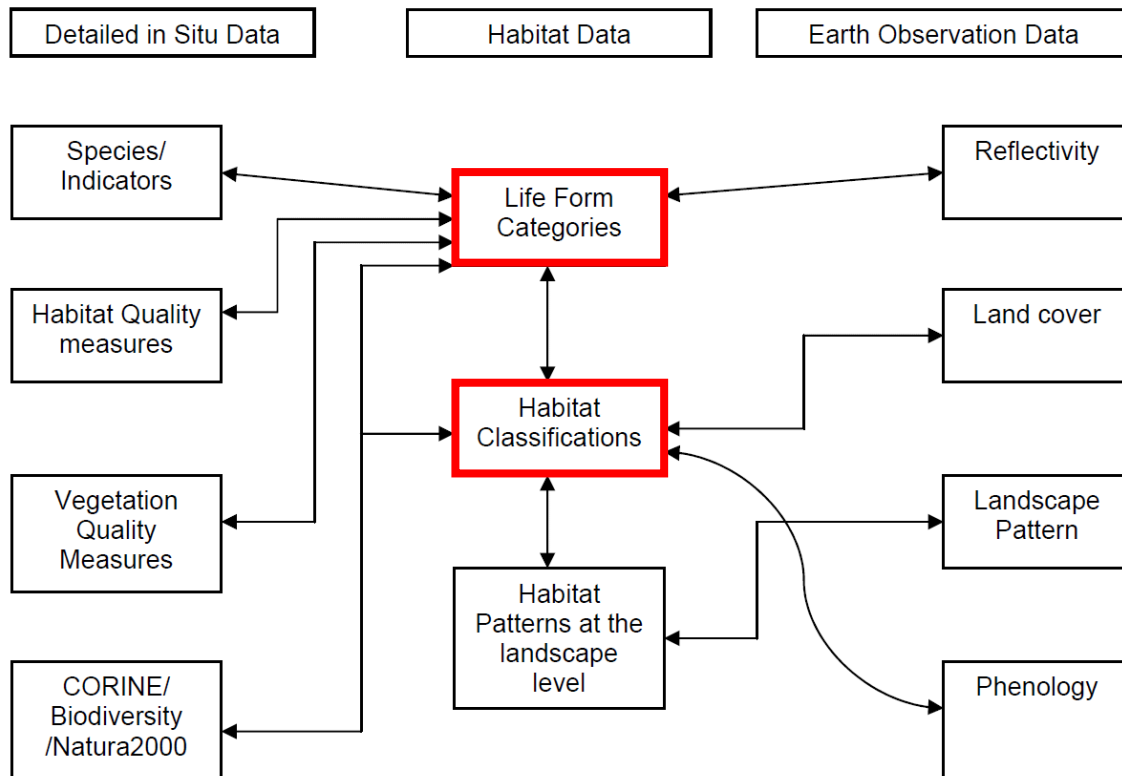


Figure 1 Relations between different land and biodiversity observation levels.

More information of the BIOHAB/EBONE methodology on habitat recording is given in Chapter 4.

1.2. Objectives

The objective of this study is: **to what extent can we use LiDAR data to map and monitor plant life forms and General Habitat Categories according to BioHab/EBONE (Bunce et al. 2008) methodology ?**

The study for the Netherlands is implemented for a test site near Chaam, in the Southern part of the Netherlands in the Province Noord-Brabant, for which we obtained test data from FUGRO (largely responsible for AHN-2), see also Chapter 3.

The objective is an integral part of WP5 'Inter-calibration of EO data with in situ observation' of the EBONE project. WP 5 will involve the processing of remotely sensed images and their integration with habitat data linked to biodiversity indicators. Different EO efforts have aimed at characterising either the compositional, structural or functional aspect of the landscape using a wide range of approaches. WP5 will pursue these options in line with the overall objective of developing and testing the biodiversity observation system. More precisely, this study is part of Task 5.1.2: Regionally/local specific and independent EO approaches (existing projects and programmes, novel developments) for determining GHCs. For the Netherlands there is a good reason to focus on the use of LiDAR data since the Netherlands was covered for the first time in 2003 from wall to wall, with 1 height measurement per square meter, namely for the construction of a detailed and accurate national elevation model. However, for the construction of this elevation model the influence of the vegetation was removed. In that sense vegetation was considered as noise and the potentials for vegetation research in the Netherlands, still had to be discovered. In the meantime a second version is becoming available in the next years (2011/2012) with a even higher precision. The intention is to cover the Netherlands completely every 5 years and is largely financed by subscription of waterboards that need this information for their water management. Errors in height measurements can have dramatic consequences for the assessment of flooding risks.

Alterra is not the only partner that is interested in the use of LiDAR. In Sweden there is already a longer tradition in the use of LiDAR, but especially related to their forests that have a wide extent and represent a large economic value. Sveriges Lantbruksuniversitet (SLU) runs two of the major environmental monitoring programmes in Sweden, the Swedish National Forest Inventory and NILS (National Inventory of Landscapes in Sweden). SLU will investigate the added value of LiDAR for habitat monitoring based on their experiences within their national programmes. Moreover, they plan to cover entire Sweden in the coming next ten years with LiDAR data. Other partners that will investigate the role that LiDAR data can play in their country for habitat monitoring are the Estonian University of Life Sciences (EMU) and Israel Nature and Parks Authority (INPA). The later is an Israeli government corporation associated with the Israel Ministry of Environment. Its role is to preserve and develop nature reserves and parks, protect wild plants, wild animals and other natural assets, safeguard the quality of the environment in open areas, maintain the aesthetic quality of Israel's landscapes, and provide visitor services in parks and nature reserves in Israel. Moreover, INPA was the first partner within EBONE that showed their preliminary results with LiDAR for habitat mapping according to the above mentioned methodology. However, their assessment was hampered by the availability of reliable field measurements on the vegetation objects.

1.3 Contents of the report

Chapter one is an introductory chapter and introduces the background of this study and highlights why we want to investigate the use of LiDAR data for habitat mapping and monitoring, with a special emphasis on plant life forms. Chapter 2 discusses the state of art on the application of LiDAR in vegetation research. It summarizes a short literature review. It also shows that the number of applications of LiDAR data is strongly increasing within the scientific community. Chapter 3 describes the study area of Chaam, the LiDAR data used for this area, and the software tools that were available for the analysis of the LiDAR data. Chapter 4 describes the methodology and results of the study. It start with the used methodology for habitat mapping, and continues with the assessment of height measurements with LiDAR to identify the various plant life forms, and ends with the possibilities of semi-automatic classification of vegetation objects based on the combination of LiDAR and false-colour infrared aerial photographs. Chapter 5 presents the major conclusions and contains also a short discussion. Chapter 6 gives the references.

2. State of the art on LiDAR

2.1. What is airborne LiDAR ?

The use of airborne laser scanning dates back to the 70s. In 1980s, high performance airborne Light Detection And Ranging (LiDAR) systems were generated supported by the advent of Global Positioning Systems (Akay et al. 2008). However, their commercial development is traced back to the mid-1990s only. From the perspective of ecological research, LiDAR can be therefore considered as a relatively new technology (Carson et al. 2004). Figure 2 presents the number of hits per year scored in scopus¹ for the search “LiDAR AND vegetation” between 2000 and 2009. This figure shows a obvious increase of publications during the past decade translating the increase of scientific interest linked to this topic.

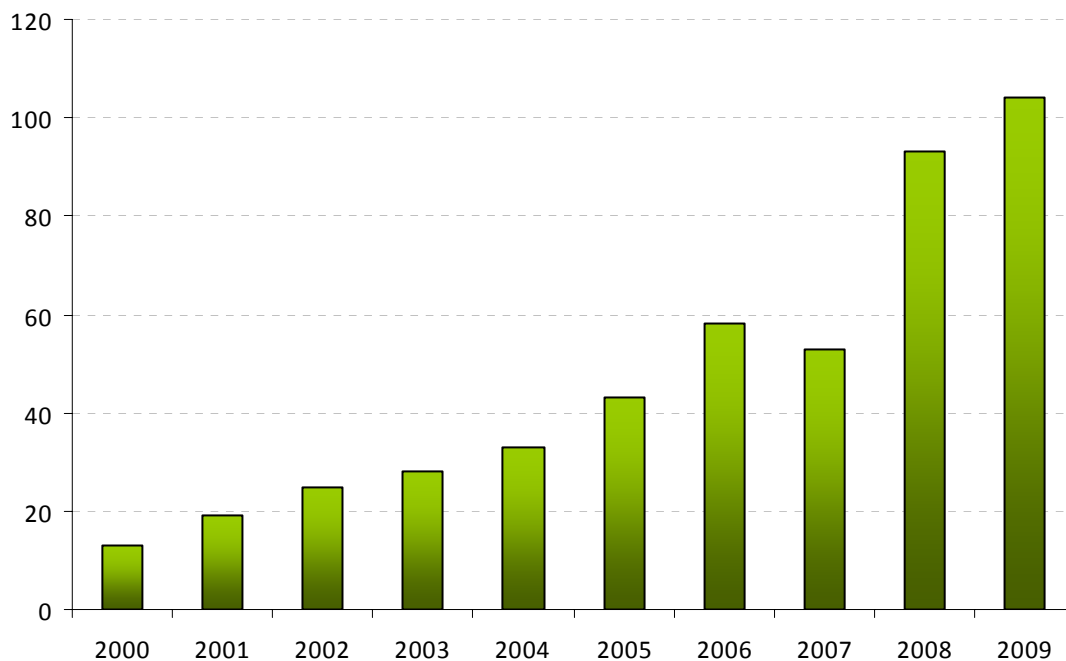


Figure 2 Number of hits per year for the search “LiDAR AND vegetation” in scopus (www.scopus.com).

Airborne LiDAR is an active remote sensing technique that measures the properties of emitted scattered light to determine the 3D coordinates (x, y, z) and other properties of a distant target (St-Onge 2005; Mallet et al. 2009). To do so, the LiDAR instrument transmits light pulses out to a target and calculates the distance based on light which is reflected/scattered from the target back to the instrument. The time for light pulses to return back to the LiDAR sensor is used to calculate the distance to the target (Akay et al. 2008). LiDAR provides thus geometric data but also radiometric data, such as signal intensity, amplitude, and pulse angle (Hall et al. 2005; Evans et al. 2006). The laser measurements are combined with the aircraft’s position and altitude data - measured by a differential global positioning system (GPS) and an inertial navigation unit (INU) - identifying the position and elevation of each collected point (Wehr et al. 1999). The “xy” accuracy of the pulse center is typically 0.1–0.5 m, depending on the flying height. The accuracy in “z” is usually better than 0.2 m. Values range from 0.2 m to 1.0 m for flying heights of 1–5 km (Korpela et al. 2009).

¹ www.scopus.com

Considering those characteristics, airborne LiDAR offers the possibility to collect high horizontal and vertical resolution data, over larger spatial extents than could not be obtained by field survey (Bradbury et al. 2005). Thus, LiDAR, in contrast to optical remote sensing techniques, can be expected to bridge the gap in structural information at the landscape scale (Graf et al. 2009).

The vertical distribution of surfaces can be recorded by either 'full waveform' or 'discrete return' devices which correspond respectively to large footprint, continuous-return LiDAR, or small-footprint, discrete-return LiDAR. They differ from each other with respect to the number of returns recorded for each emitted laser pulse and the footprint characteristics (Lim et al. 2003). The footprint can be defined as the circular sampling illuminated area on the ground which increases in size with distance from the sensor.

2.2. Discrete return

Discrete return LiDAR are small-footprint systems that record one or several returns from laser pulses over small areas (Bergen et al. 2008). It typically allows for one (first or last), two (first and last), or a few returns to be recorded for each pulse during a flight (Lim et al. 2003), being then categorized as single or multiple-return systems. The distance and sometimes the intensity of each peak are recorded by this type of system (Wehr et al. 1999). Discrete point return systems typically operate at a very high spatial resolution, with the laser illuminating a very small spot (footprint is between 0.2 to 0.9 m), and record up to six points per laser pulse (Mallet et al. 2009).

2.3. Full waveform

Full waveform LiDAR are large-footprint systems that record the complete waveform of the backscattered energy over relatively large areas. Those systems sense and digitize the time-varying intensity of the returned energy from each laser pulse, providing a record of the height distribution of the surfaces illuminated by the laser pulse over a large footprint diameter varying from 5 m to 70 m (Dubayah et al. 2000). Because each emitted laser pulse is aimed toward a different footprint location, aggregating the pulse-return signal records produces a 3D map of surface structure (Vierling et al. 2008). Full waveform LiDAR systems only exist as commercial systems since 2004 (Mallet et al. 2009).

Over the past decade, LiDAR data have been increasingly used in ecological sciences, among other domains. In this study, we will focus on its applications in forestry, habitat monitoring and vegetation mapping. In this literature review, airborne LiDAR systems are presented but it is also important to mention that those systems can also be mounted on ground-based or spaceborne platforms.

2.4. Application of LiDAR system in environmental sciences

LiDAR was originally introduced to generate more accurate digital elevation models (DEMs) (Evans et al. 2006) but has recently become an effective tool for natural resources applications (Akay et al. 2008). The laser light emitted is reflected back to the sensor as it intercepts objects in its path, including vegetation elements and the ground (Dubayah et al. 2000). In the process of creating a DEM, only reflections from the ground level are used, and reflections from vegetation are considered redundant. Recent studies with LiDAR data have explored the possibilities to use these redundant vegetation reflections as a new source of geospatial data that can provide fine-grained information about the 3-D physical structure of terrestrial and aquatic ecosystems (Geerling et al. 2007). This result can then be applied in forestry, ecological (habitat) mapping and vegetation monitoring (Hyde et al. 2005).

Forestry/Vegetation structure

Vegetation vertical structure is defined as the bottom to top configuration of aboveground vegetation including for example, canopy cover, tree and canopy height, vegetation layers, and biomass or volume (Bergen et al. 2008). LiDAR remote sensing being capable of providing both horizontal and vertical information at high spatial resolutions and vertical accuracies, allows then forest attributes to be directly or indirectly retrieved from LiDAR data (Dubayah et al. 2000; Akay et al. 2008).

Both discrete-return and full waveform devices have been used worldwide for characterizing forest structure (Lefsky et al. 2002; Lim et al. 2003). These technologies have successfully been used to retrieve tree height (Jan 2005; Wang et al. 2008; Rosette et al. 2009), above ground biomass and timber volumes (Means et al. 2000; Lefsky et al. 2002; Zimble et al. 2003; Patenaude et al. 2004; Zhao et al. 2009) and tree properties (Roberts et al. 2005; Heurich et al. 2008) across various ecosystems such as temperate (Anderson et al. 2006) or tropical forest (Drake et al. 2002). The combination of airborne LiDAR data with other optical remote sensing data also shows promising results for the estimation of forest structural characteristics (Coops et al. 2004), often better than when LiDAR data were used alone (Hudak et al. 2002; Wulder et al. 2003). In some cases the intensity recorded by the LiDAR sensors is also used to measure tree metrics and vegetation structure (Lovell et al. 2003; Hall et al. 2005; Evans et al. 2006; Weishampel et al. 2007).

Those studies have demonstrated the ability of LiDAR techniques to measure vegetation height, and cover as well as more complex attributes of canopy structure. From those measurements, further analysis can be done related to the vegetation attributes and function.

Habitat and vegetation monitoring

Vegetation attributes and structure information generated from airborne LiDAR data have also applications beyond forestry and are of a great help for ecological functions understanding. Indeed those canopy metrics and structural data have been proven to be strong predictors of species richness for woodland birds in several studies (Vierling et al. 2008; Mason et al. 2003; Hill et al. 2005), even in difficult terrain (Hyde et al. 2005). Furthermore, the correlation between LiDAR-derived estimates of vegetation structure important to birds have been demonstrated in areas ranging from grasslands to forests (Bradbury et al. 2005; Hinsley et al. 2006). LiDAR have been also demonstrated to be able to identify differently structured habitat units and to quantify variation in vegetation structure within those units (Bradbury et al. 2005). LiDAR can also provide indication about territories and breeding success of several types of birds species (Bergen et al. 2008). Graf et al. (2009) concluded their study on the great potential offered by LiDAR for effective habitat monitoring and management of endangered species. In Korpela et al. (2009) the result obtained using LiDAR for the mire habitat classification accuracy were considered as surpassing earlier results with optical data. Some studies also highlighted that the result of habitat analysis obtained with LiDAR may be enhanced when used in combination with spectral data (Bergen et al. 2007; Clawges et al. 2008; Hyde et al. 2006).

In view of those results, LiDAR remote sensing shows considerable efficacy for habitat mapping/characterization and wildlife management in fine detail across broad areas. It may replace many labor-intensive, field-based measurements, and can characterize habitat in novel ways (Vierling et al. 2008)

Considering monitoring applications, the repeatable and high absolute "xyz" accuracy is advantageous since changes can be detected at submeter scales and the same

measurement units can be monitored over time (Korpela et al. 2009). In that sense, LiDAR constitutes an efficient tool for short and long term monitoring of changes in surface structure and vegetation. For example, Wieshampel et al. (2007) used LiDAR measurements to monitor vegetation recovery after several disturbances.

Vegetation mapping/classification

Studies conducted in order to map vegetation using LiDAR showed that discrimination of some vegetation types was possible based on vegetation height and density (Geerling et al. 2007; Geerling et al. 2009). Vegetation types that are similar in structure or with a relatively low vegetation structure are difficult to separate, but discrimination between bushes and trees is high. LiDAR appeared to succeed well in characterizing tree species with the canopy height as the strongest explanatory variables in the vegetation classification (Korpela et al. 2009; Geerling et al. 2007).

The integration of spectral information coming from optical remote sensing data and canopy height data generated from LiDAR into the classification has been demonstrated to produce an ecologically meaningful thematic product for a complex woodland environment (Hill et al. 2005).

In most of the ecological studies based on LiDAR techniques, the intensity/amplitude is rarely used as it must be calibrated and corrected first (Mallet et al. 2009), even if it appears as a potential important factor for feature extraction or land cover classification. Antonarakis et al. (2008) demonstrate that the combination of intensity and elevation data from LiDAR point clouds can be enough to classify multiple land types using object-based classification method. Other studies using intensity values were conducted and their results imply that the intensity of the laser return signal can be used for classification purposes (Lim et al. 2003; Brennan et al. 2006; Korpela et al. 2009).

2.5. Difference between discrete-return and full waveform in ecological applications

As presented previously, numerous studies confirmed discrete-return and full waveform LiDAR's capacity to measure stand metrics and demonstrate that they can be an effective tool to remotely quantify vegetation structural attributes important to habitat mapping, monitoring and classification.

Concerning discrete-return or full waveform LiDAR, the choice of one LiDAR system over the other should be made considering the objective of the study. A discrete-return instrument may be useful in representing canopy heights, but may not be able to detect subcanopy vegetation unless returns are available from laser pulses that penetrate through canopy gaps. A discrete-return LiDAR instrument, even one producing multiple returns, may be unable to detect understory vegetation in a closed canopy forest (Clawges et al. 2008). For vegetated environments, full waveform provides better description of the vertical structure of the vegetation (Lefsky et al. 2002). Then, for research where capturing the true vertical profile of the canopy is a critical measure, it is better to use full waveform LiDAR (Lim et al. 2003), especially for studies related to biodiversity and habitat (Bergen et al. 2008).

Small-footprint systems may not be optimal for forestry also due to the risk of missing tree tops. Large-footprint systems appears better for getting canopy height because the large footprint does not miss tree tops. It should be noted, however, that data from large-footprint systems are not generally suited to detection and measurement of individual trees and therefore, can not give a direct determination of relative stem density (Dubayah et al. 2000).

Even if full waveform return appears are the best LiDAR data source for ecological studied, most of the studies carried out until now and presented in this literature review are mainly based on discrete return laser scanners and have presented reliable estimates of canopy height and structural data, as well as satisfying results concerning habitat and land cover mapping.

2.6. Limitations

LiDAR is an accurate technology concerning vegetation analysis and mapping. However some important specifications and limitations should be quoted. First of all, the performance of LiDAR based method is directly affected by the resolution of the data (Akay et al. 2008). Secondly, the laser wavelength used by the system largely determines the interaction with various surface types, thus dictates how the 3D structure of potential elements is recorded by the sensor (Vierling et al. 2008). Thirdly, the recorded values distributions in vegetation canopies can also be influenced by the size of the footprint.

Concerning intensity value measurements, they are also influenced by the previously quoted parameters but also strongly influenced by differences in the surface moisture. This should be considered when interpreting the results as well as the fact that the site fertility may affect specific tree species intensity characteristics (Korpela et al. 2009). Moreover, the intensity of discret-return LiDAR is not affected only by the target backscatter reflectance but also by several characteristics linked to the sensor and its relation to the target (e.g the intentional and random power variation of the transmitted pulse, the electronic noise in the receiver, the surface geometry...) (Wehr et al. 1999). The structural diversity of the forests, such as the mixture of tree species and the presence of deadwood, can also be a factor influencing the measurements (Heurich et al. 2008).

The accuracy of LiDAR measurements is highly dependent on terrain slope, surface roughness, and land cover. Thus an accurate estimation of the CHM requires a good-quality DEM (Jan 2005; Antonarakis et al. 2008). In that respect, topographic slope can cause the LiDAR ground return to spread, leading to inaccurate ground determination, and consequently, canopy heights. (Hyde et al. 2005).

Even with calibrated data, retrieval of the reflectance of objects smaller than the footprint remains difficult. This constitutes a challenge for the use of LiDAR in vegetation classification and explains why the integration of other optical remote sensing sources is sought in many cases (Antonarakis et al. 2008)

2.7. Conclusions

Because airborne LiDAR captures high-resolution vertical and horizontal spatial data, it shows great potential for integration with ecological research (Lefsky et al. 2002). In contrast with other optical remote sensing techniques offering only a continuous coverage, it directly measures the physical attributes of vegetation canopy structure, highly correlated with the basic ecological functions of interest to scientists. Moreover, LiDAR is less affected by shadows and occlusions, as well as less dependent on weather conditions (St-Onge 2005; Korpela et al. 2009).

Concerning ecological research, LiDAR has proved to be an accurate and cost-effective way to rapidly obtain 3D data of objects over large scale areas (Patenaude et al. 2004). This explains why LiDAR is replacing passive remote sensing in many tasks, although data analysis still remain a challenge regardless of the method by which the 3D points were collected (Korpela et al. 2009). It is also important to keep in mind, as quoted in several

studies, that results obtained using LiDAR may be enhanced when used in combination with spectral data.

In literature, airborne LiDAR systems are presented as a promising technology for the vegetation structure analysis. Lefsky (2002) even describe LiDAR as *“an emerging remote sensing technology that directly measures the three-dimensional distribution of plants canopies, can accurately estimate vegetation structural attributes and should be of particular interest to forest, landscape, and global ecologist”*.

2.8. Future developments

As explained previously, each LiDAR return is stored as a x,y,z coordinates and often tagged with auxiliary variables such as the intensity, scan-angle... So far, most of the LiDAR researches have focused on the use of LiDAR coordinates information while only few studies partially investigated the utility of LiDAR auxiliary variables. The results of the latter were satisfactory and thus show opportunities to explore for further development and application of airborne LiDAR techniques. In some cases the use full-waveform laser scanners should also be considered as potential contribution to improve the estimations (Heurich et al. 2008).

Most of the study quoted in this review stressed that the results obtained with airborne LiDAR are often improved when used in combination with other remote sensing products. Another possibility is the integration of airborne LiDAR data and terrestrial LiDAR data as shown in the study of Chasmer et al. (2005) which examines the ability of airborne and terrestrial LiDAR to map canopy structure. While canopy structure analysis using airborne LiDAR systems have been widely used, especially for forestry purposes, the combination of terrestrial and airborne LiDAR is rather unexplored and appears has a promising techniques for vegetation analysis and mapping.

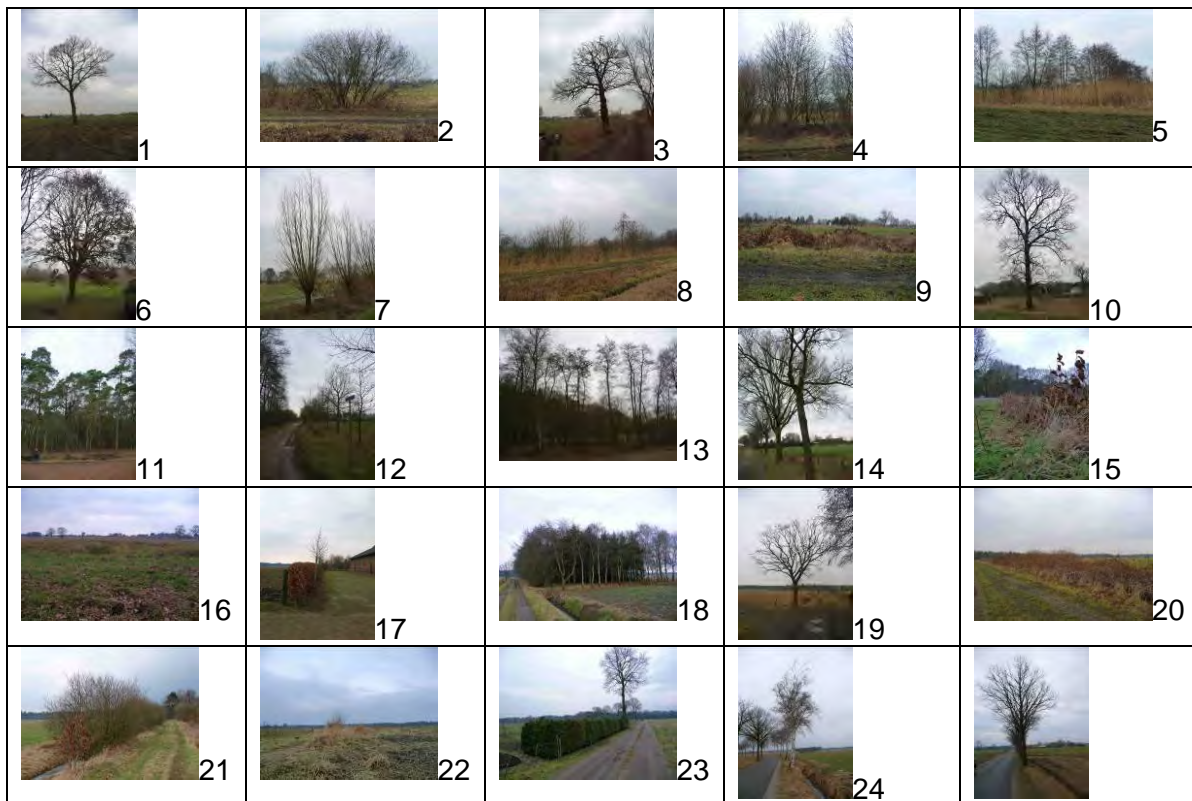
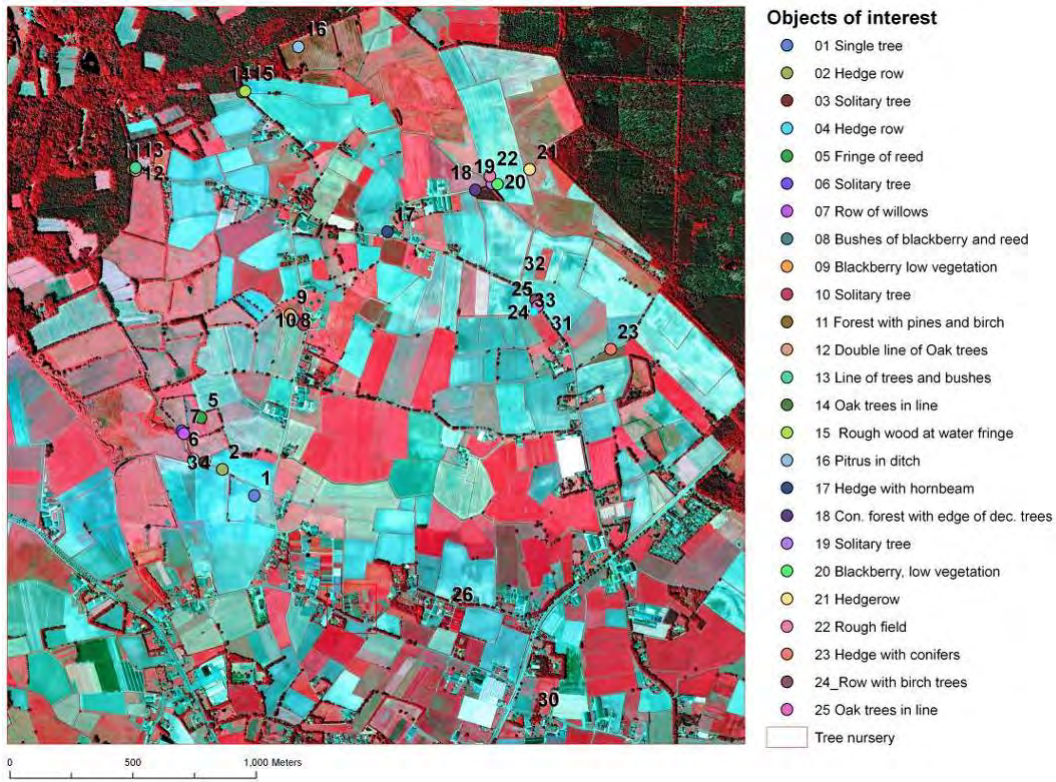


Figure 4 Location of the objects of interest in the study area. Below you find a snapshot of all objects of interest.



Figure 5 Photo of the tree nursery in the village of Chaam The tree nursery is located with a box in figure 4 in the southern part of the study area.

3.2. Materials

3.2.1. LiDAR

LiDAR (Light Detection And Ranging) is a remote sensing system used to collect topographic data. A LiDAR uses a laser (emitter) to send a pulse of light to an object and a telescope (receiver) to measure the intensity scattered back (backscattered) to the LiDAR.

Aircraft permits the collection of topographic information over a strip ~ 300 meters in width from 600 meter altitude. Also helicopters are being used for the collection of LiDAR data. Most laser systems can record several returns for each pulse. Multiple returns occur when the laser beam is only partially blocked. Part of the laser energy is reflected back to the sensor The remaining laser energy continues downward. In principle you can have up to 5 returns per pulse, but more typically is 2-3 returns. By acquiring first- and last-pulse data simultaneously, it is possible to measure both tree heights and the topography of the ground. Normally, you have 1 -10 measurements per m² or 10,000 – 100,000 measurements per ha. Most systems record the amount of energy reflected by target objects, such as intensity. Data delivered as XYZ points in a “data cloud”.

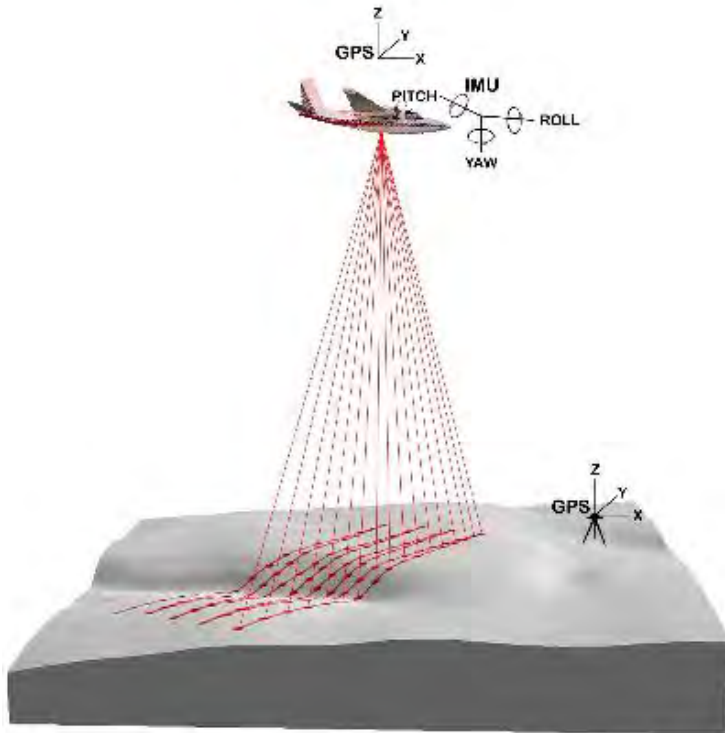


Figure 6 A schematic figure of an aircraft equipped with a LiDAR instrument that collects elevation information in so called data clouds with XYZ measurements.

The precision or accuracy of LiDAR data has improved increasingly. For example, for the Netherlands, that was covered completely in 2003 for the first time for the construction of a precise national elevation model (AHN-1) had a precision of 15 centimeters with 1 measurement per square meter. The second version of national elevation model (AHN-2) is planned now for 2012 and will have a precision of approximately 5 centimeters with 10 measurements per m^2 . An update is being planned every 5 years, mainly by subscription by the 26 Dutch waterboards, that need this information urgently for their water management. The Ministry of Waterworks pays approximately 50% of all costs (waterboards the other half).

Some of the LiDAR Myths are summarized by Fugro ([/www.fugroearthdata.com](http://www.fugroearthdata.com)) as:

- **Myth 1:** More points are always better. Point spacing (the distance between points) and point density (the coverage of points within a given area) are critical considerations for any LiDAR mapping project. Factors that determine optimum point spacing include desired vertical accuracy, terrain, land cover, and the ultimate data application. For many applications, a lower point density is sufficient and can save time and costs by reducing acquisition time and data processing as well as potential data storage and handling difficulties.
- **Myth 2:** LiDAR can see through foliage. LiDAR does not “see through foliage.” However, some LiDAR points do reach the ground through openings in the tree canopy. As the LiDAR point density increases, so does the probability of obtaining returns from the ground.
- **Myth 3:** LiDAR replaces traditional mapping techniques. LiDAR is a complement to, not a replacement for, traditional aerial mapping methodologies. For most uses, LiDAR intensity imagery is not a viable replacement for aerial photography, nor does LiDAR data provide an option for planimetric mapping.
- **Myth 4:** LiDAR is an all-weather system. The target must reflect the near infrared portion of the electro-magnetic light spectrum for LiDAR to work. Data collection can

occur beneath the clouds and in some haze, but because water absorbs most near infrared light, it will not operate correctly during fog, rain, or snow.

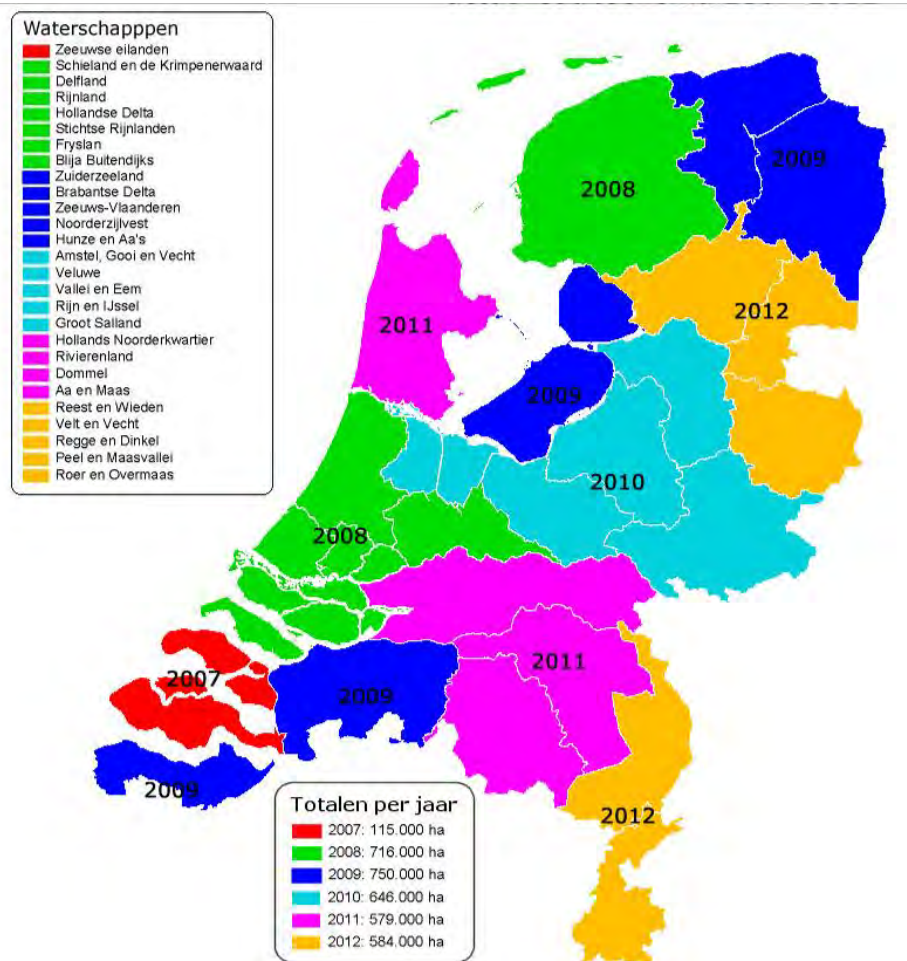


Figure 7 Planning schema AHN-2. Status at July 2009.

Fugro Aerial Mapping BV is one of the companies that collects LiDAR data in the framework of the AHN-2 project. Alterra obtained a test data set from Fugro for the study area Chaam in 2009. For this data set FUGRO used the FLI-MAP 400 system. This system is carried on board of a helicopter, integrated with high-resolution photo and video camera and a precise GPS system. The data was acquired during three days in 2009, March 13, 15 and 16, with a minimum point density of 10 points per m² at three different scan angles: forward 30°, nadir, backward 30°. Additional important characteristics are the options for a 150.000 Hz or 250.000 Hz scan using Multiple Pulse in Air (MPiA) technology, and direct in line-scan attachment of RGB colours to the laser measurements. The absolute accuracy for a single point can be guaranteed below 3 cm. An additional advantage is that data are delivered classified into ground points & non-ground points.

Prices AHN-2

A detailed overview of prices can be found at www.ahn.nl/bestellen/prijzen_ahn_2. Commercial prices are about 28 cent / ha). But for non-commercial the entire country (~ 35.0000 km²) can be obtained for €1500,- !!

3.2.2 Aerial photographs

The aerial photos were false colour images and were required on the 8th of May 2008 by Eurosense B.V. with a 25 centimeter resolution. See Figure 4 for the aerial photographs over the study area. The aerial photographs are available for the whole of the Netherlands and are updated about every 2 to 3 years.

3.2.3 Fieldwork

Field work was done by Arjan Griffioen in December 2009 and February 2010. Field work was hampered in by severe winter conditions and caused some delays. All photographs in figure 4 were taken on the 22nd of February 2010 when weather conditions were already slightly better. For objects with a height lower than 2.5 meter a measuring staff was used. For objects there were taller a laser distance meter was used. First the horizontal distance was measured, secondly the angle to the crown of e.g. tree was measured. The following formula was applied:

Height = distance * TAN(RADIANS(angle)) + height tripod

Of all interesting vegetation objects in the study area photographs were taken (Figure 4) and height and width measurements were made (see Table 3).

3.3. LiDAR software

3.3.1. Fusion software

FUSION/LDV is a free software developed by USDA (United States Department of Agriculture) Forest Service Pacific Northwest Research Station in collaboration with the University of Washington and distributed by the USDA Forest Service Remote Sensing Applications Center (RSAC). The software is built to help researchers understand, explore, and analyze LiDAR data (McGaughey, 2010). LiDAR data sets are generally large and require extensive preprocessing before these can be used in GIS or image processing software. Fusion handles simple tasks such as extracting a sample of LiDAR returns for an area of interest and allows to view the data interactively. The program is primarily a viewing tool for LiDAR data, but also providing basic analysis functions designed to explore and extract information from LiDAR data. As it was developed to support the Forest Service in obtaining forest resource information, most of the functionalities of FUSION are forestry and vegetation monitoring oriented.

The last version of the software, released in March 2010, consists of two main programs - FUSION and LDV (LiDAR data viewer) - and a collection of task-specific command line programs. The primary interface, provided by FUSION, consists of a graphical display window and a control window.

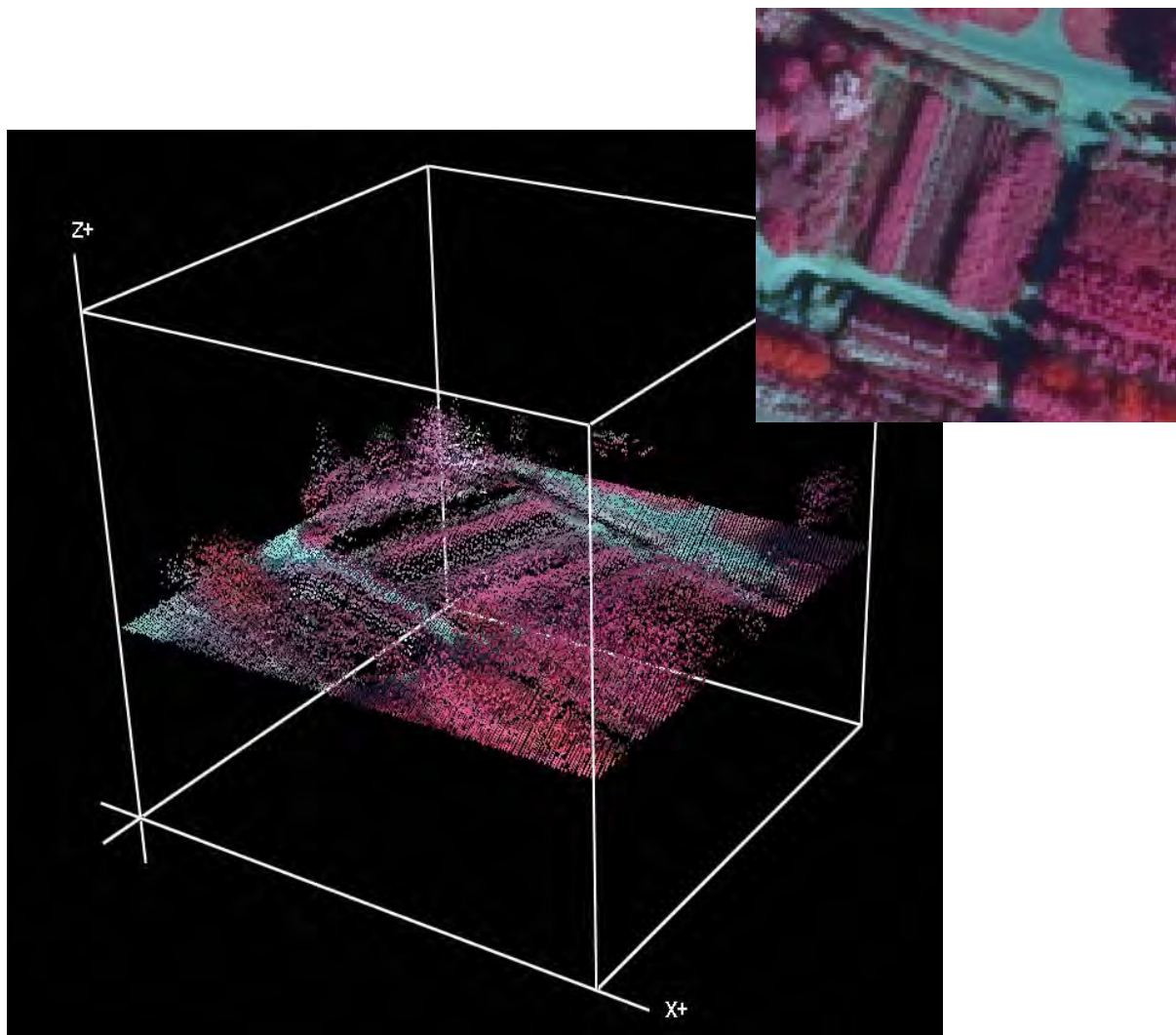


Figure 8 Snapshot of Fusion with a 3D view which shows the LiDAR points draped over by an aerial photograph. The area concerns a small part of the tree nursery in the Chaam area.

The FUSION display shows all project data using a 2D display typical of geographic information systems. It supports a variety of data types and formats including shapefiles, raster images, digital terrain models, canopy surface models, and LiDAR return data. LDV provides the 3D visualization environment for the examination and measurement of spatially-explicit data subsets. Command line programs provide specific analysis and data processing capabilities designed to make FUSION suitable for processing large LiDAR acquisitions (McGaughey, 2010). Fusion is based on non proprietary algorithms and methods that allow for user adjustments and the processes that are used are documented in publicly available literature.

FUSION software has already been used in several studies. In Moskal et al. (2009), FUSION was used as a data preparation tool and to normalize the vegetation heights above a constant ground elevation. Quality assurance and quality control procedures on airborne LiDAR acquired for a nation-wide carbon inventory of planted forests were performed using some of the functionalities of FUSION (Stephens et al., 2008). The FUSION software was used to assess data, to determine first return density, to produce an intensity image of the area covered by the datasets, and to create a ground surface model. Finally, in Wezyk et al.

(2008), FUSION was used to calculate canopy metrics in order to describe selected canopy layer parameters of Scots pine stands.

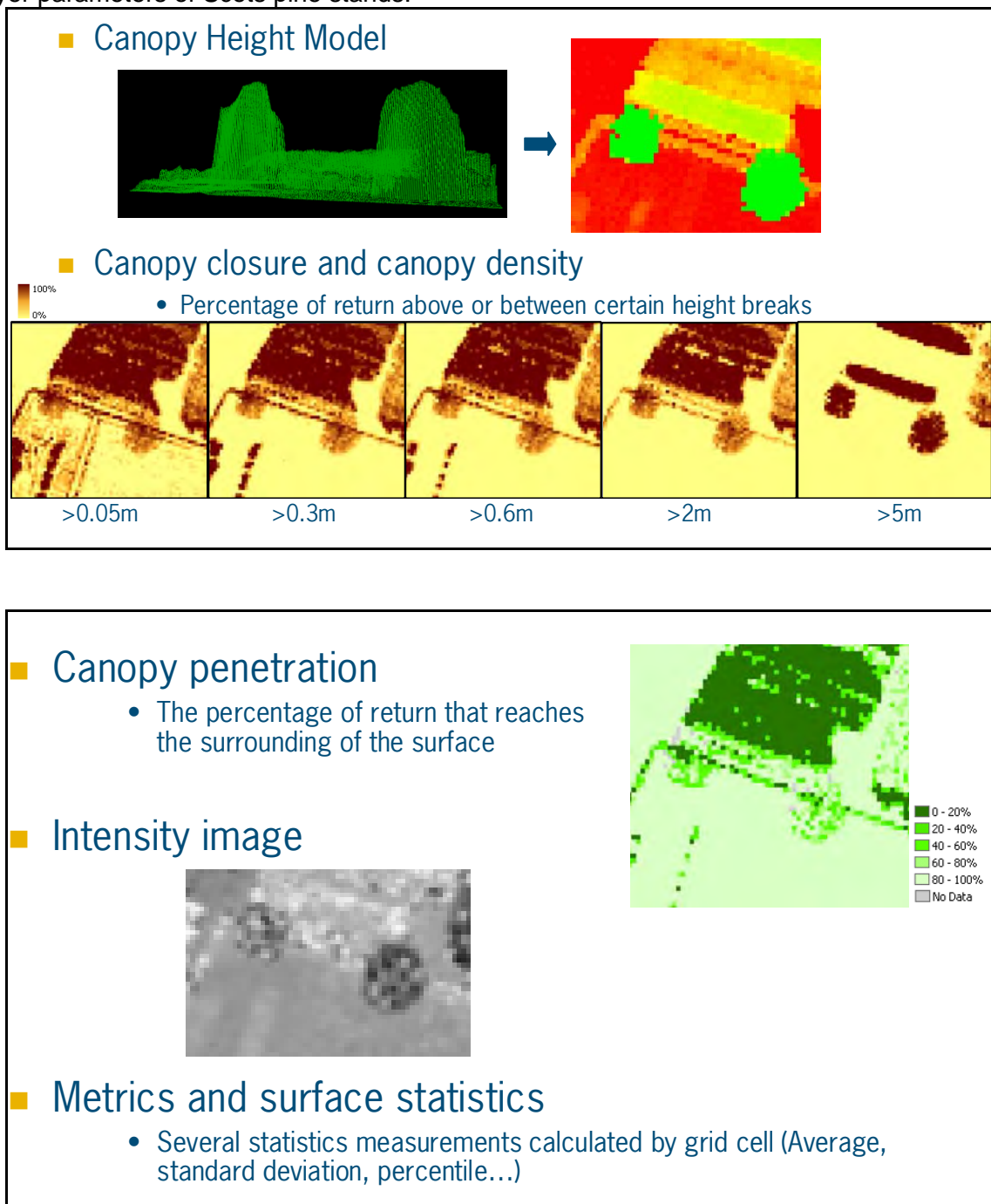


Figure 9 Example of outputs from FUSION

3.3.2. Commercial software packages

Many commercial software packages that can handle LiDAR data are available. The main functionality offered by these software packages is the processing of the LiDAR point data to produce an accurate terrain elevation model. Table 1 lists several of these packages.

Table 1 LiDAR processing software.

Software	Company	Website
MARS	Merrick	http://merrick.com/index.php/services/mars-software
LP360	QCoherent	http://qcoherent.com/
SCOP++	Inpho	http://www.inpho.de
Quick Terrain modeler	Applied imagery	http://www.appliedimagery.com/
VG4D product suite	Virtual geomatics	http://www.virtualgeomatics.com/resources.html

Software that also aims at the classification of features like buildings and trees is the LiDAR Analyst software made by Visual Learning Systems Inc. (website http://www.featureanalyst.com/lidar_analyst.htm). This software contains workflows for the automated extraction of buildings, single trees and forests from LiDAR point cloud data.

There is also a development in more 'traditional' software that is used for image processing or geographic analysis like ArcGIS from ESRI, Ecognition from Definiens and Imagine from Erdas. All these companies are developing modules and functionality to make the processing of LiDAR point cloud data possible. The benefit of this development is that it can be used in cooperation with the already available tools for the processing of geographic data and therefore the user can benefit from existing expertise.

4. Methodology & Results

4.1. Methodology of habitat recording

When recording habitats and biodiversity at the landscape level, the difficulty has always been in reconciling the observed complexity of points, lines and patches with recognisable categories that can be consistently and repeatedly recorded in the field and then converted into national and regional estimates. It is therefore necessary to link the detailed records to a strategic framework, as described by Sheail and Bunce (2003). Monitoring and surveillance also have to be integrated spatially and temporally with other data sources. Monitoring European habitats requires definitions that can be applied consistently in the field across Europe (Brandt et al., 2002). Habitats are defined as: "An element of the land surface that can be consistently defined spatially in the field in order to define the principal environments in which organisms live" (Bunce et al., 2005). Existing European habitat classifications have been based on species, geographical location, vegetation classes and environmental factors (e.g., the EUNIS system, Davies and Moss, 2002). Whilst these classifications have been successfully applied to produce general descriptions of the occurrence of classes in protected areas, they are not appropriate for monitoring, because definitions of many of the terms used; e.g., montane and sub-Mediterranean; are not provided. The present recording procedure therefore adopted plant life forms, as described by Raunkiaer (1934) as the basis of the habitat categories. It is widely recognized (e.g., Woodward and Rochefort, 1991) that, at a continental level, biomes need to be defined in terms of the physiognomy and life forms of the dominant species, because individual species are too limited to encompass widely dispersed geographical locations. Ecological behaviour of species can also vary within their distribution and vicarious species further preclude the use of individual species. A given species may also show plasticity, because of environmental and local factors such as grazing, so the overall height of the whole unit is used as a measure of its status at a given time. Further advantages of using life forms are that they provide direct links between in-situ data and dynamic global vegetation models (e.g., Sitch et al., 2003), but also with the patterns present on satellite images because of their relationship with vegetation structure. Plant life forms (Raunkiaer, 1934) are defined on the basis of the location of buds in the adverse season and separate grassland, shrub and forest species which can be used to develop rules for habitats that can be applied consistently in the field. Within the shrub and forest categories a further breakdown is made according to the way the leaves of the plants are retained in the adverse growth season. Raunkiaer demonstrated that the life form spectra in different regions were correlated with the main environmental gradient from the equator to the arctic: they are therefore widely used in global change modeling as indicators for projecting vegetation change (e.g., Sitch et al., 2003).

Table 2 Life forms for recording General Habitat Categories (GHCs), based on life forms as defined by Raunkiaer (1934). Adapted from Bunce et al., 2008.

Herbaceous	HER	
1. Submerged hydrophytes	SHY	Plants that grow beneath the water. This category includes marine species and floating species which over-winter below the surface.
2. Emergent hydrophytes	EHY	Plants that grow in aquatic conditions with the main plant above water.
3. Helophytes	HEL	Plants that plants that grow in waterlogged conditions.
4. Leafy hemi-cryptophytes	LHE	Broad leaved herbaceous species, sometimes termed forbs.
5. Caespitose hemi-cryptophytes	CHE	Perennial monocotyledonous grasses and sedges.
6. Therophytes	THE	Annual plants that survive the unfavorable season as seeds.
7. Succulent chamaephytes	SUC	Plants with succulent leaves.
8. Geophytes	GEO	Plants with buds below the soil surface.
9. Cryptogams	CRY	Non-saxicolous bryophytes and lichens, including aquatic bryophytes,
10. Herbaceous chamaephytes	HCH	Plants with non-succulent leaves and non-shrubby form.
Shrubs and trees		TRS
11. Dwarf chamaephytes	DCH	Dwarf shrubs: below 0.05 m
12. Shrubby chamaephytes	SCH	Under shrubs: 0.05-0.3 m
13. Low phanerophytes	LPH	Low shrubs buds: 0.30-0.6 m.
14. Mid phanerophytes	MPH	Mid shrubs buds: 0.6-2.0 m
15. Tall phanerophytes	TPH	Tall shrubs buds: 2.0-5.0 m
16. Forest phanerophytes	FPH	Trees: over 5.0 m
Leaf retention divisions		
Winter deciduous	DEC	
Evergreen	EVR	
Coniferous	CON	
Non-leafy evergreen	NLE	
Summer deciduous and/or spiny cushion	SPI	

Some explanatory notes in relation to these plant life forms are given below.

Submerged hydrophytes (waterplants) - SHY

Gramineae and Cyperaceae are included here if they are growing in aquatic conditions (see environmental qualifiers for definitions). Otherwise they are in Caespitose hemicryptophytes.

Emergent hydrophytes (waterplants) - EHY

Helophytes (marsh plants) - HEL

Gramineae and Cyperaceae are included here if they are growing in waterlogged conditions (see environmental qualifiers for definitions). Otherwise they are in Caespitose hemicryptophytes.

Leafy hemicryptophytes; leafy, rosette and biennial (tall broad leaved herbaceous species, sometimes termed forbs) - LHE

This group includes biennial species as they play a similar role in vegetation. These categories include not only the tall herb vegetation traditionally registered in the category, but also ruderal (weed) vegetation and also clearing vegetation.

Caespitose Hemicryptophytes - caespitose most gramineae and cyperaceae (grasses and sedges, herbs with buds at soil level) - CHE

Therophytes - THE

They are the life forms which are adapted to survive unsuitable periods (e.g. summer drought periods or cold winters) in seed form. In northern situations there are often found on distinctive soils or rocky surfaces, but usually in small patches below the minimum mappable unit. They are also characteristic of highly disturbed situations.

Geophytes- bulbs, root tubers, stem tubers or corms - GEO

Buds below soil surface. Vernal woodland geophytes are excluded, as they perennate this way to flower before canopy closure. Geophytes are widespread especially in the Mediterranean, characteristic of very dry summers and are locally dominant. Many species never achieve the 30% cover and are minor elements of the vegetation. Gramineae, Cyperaceae and Juncaceae are excluded from this class, as explained in the introduction.

Herbaceous chamaephytes including both succulent and cushion forms that have their buds above the ground surface - HCH

Characteristic of severe environments – succulents are included here because they occur in small patches, although they could be included as a separate class if deserts are to be included subsequently. *Carpobrotus edulis* and *Opuntia* are two exceptions but do not justify a separate life form category.

Cryptogams (bryophytes & lichens) - CRY

There are present usually with a high % of rock. Remember that areas over 70% rock is recorded as “sparsely vegetated”, usually in extreme environments although occasionally high cover also occur on degraded lowlands on sandy soils

Dwarf ligneous chamaephytes (have buds above the ground below 0.05m) - DCH

Some of these plants are called espaliers (Spaliersträucher), e.g. *Dryas octopetala*. Others are espalier forms of ligneous chamaephytes, e.g. *Betula nana*, others dwarf forms of chamaephytes due to extreme environments, e.g. *Vaccinium myrtillus*.

Forest phanerophytes (>5m) - FPH

These habitats are dominated by trees over 5m with > 30% cover. These are the forest species of Europe. The forest categories have been determined on the basis of their structure and adaptation to the environment. All pure categories are over 70% and the mixtures determined as all combinations with between 30-70% of either category.

Further details and examples of the species in the 16 life forms are given in Bunce et al. (2005, 2008). Since plant lifeforms are strongly related to vegetation structure, and have strict height definitions, it provides a good opportunity for integration with LiDAR sensors that measure heights of objects with a high spatial resolution (provides x, y and z co-ordinates). See also next paragraph on the objectives of this study and chapter 2 that provides an overview of the application of LiDAR in vegetation science.

4.2. Height measurements LiDAR

The VG4D viewer from the VG4D product suite was used to carry out the measurements on the objects in the LiDAR data. For this, a profile view of the object of interest was created and the object width and height was measured on screen using the interactive distance measure tool in the profile view window.

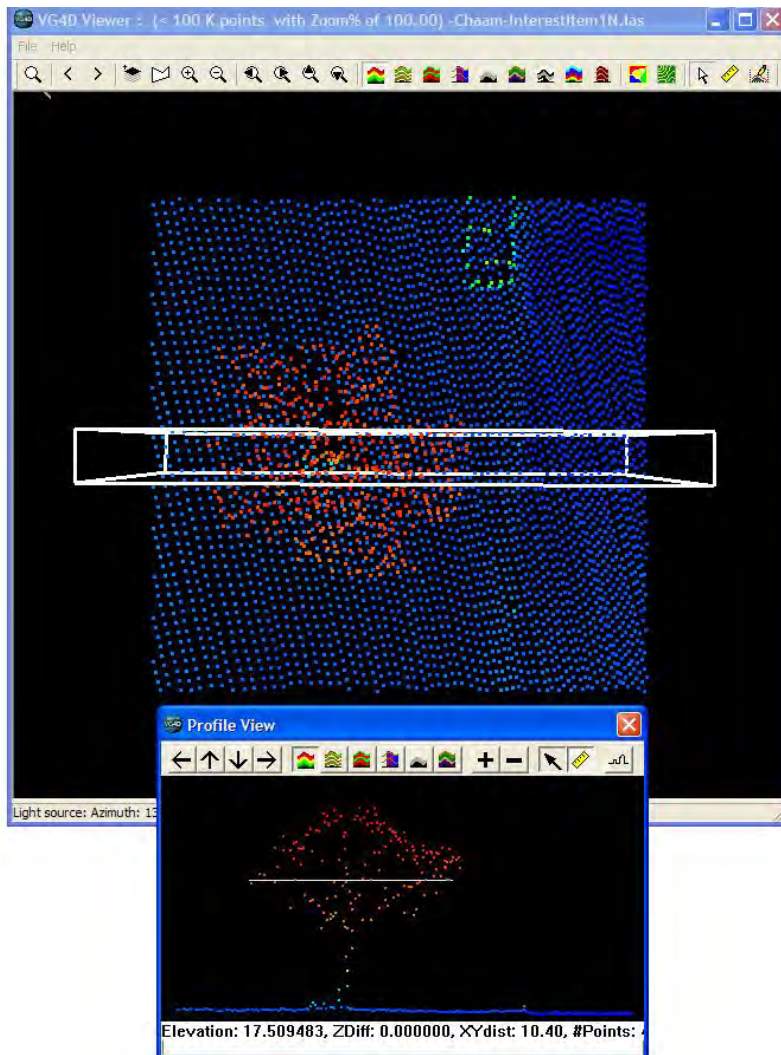


Figure 10 Height and width measurements on a single tree in LiDAR point data. The low Z values are displayed in blue, shifting into green, yellow, orange and finally to red for relatively high values.

Figure 10 gives an example of the measurement of a single tree object. In both views, the LiDAR points are displayed using a colour scheme that represents the height (Z-value), points. The low Z values are displayed in blue, shifting into green, yellow, orange and finally to red for relatively high values. In the top view the tree crown is displayed by red dots and the shape of the tree crown is easy to recognize. In the profile (bottom) view both the stem and the tree crown can be recognized. One observation that can be made from both views is that the exact width and height is not easy to determine. A best approximation was made by measuring several extreme points and using the average value.

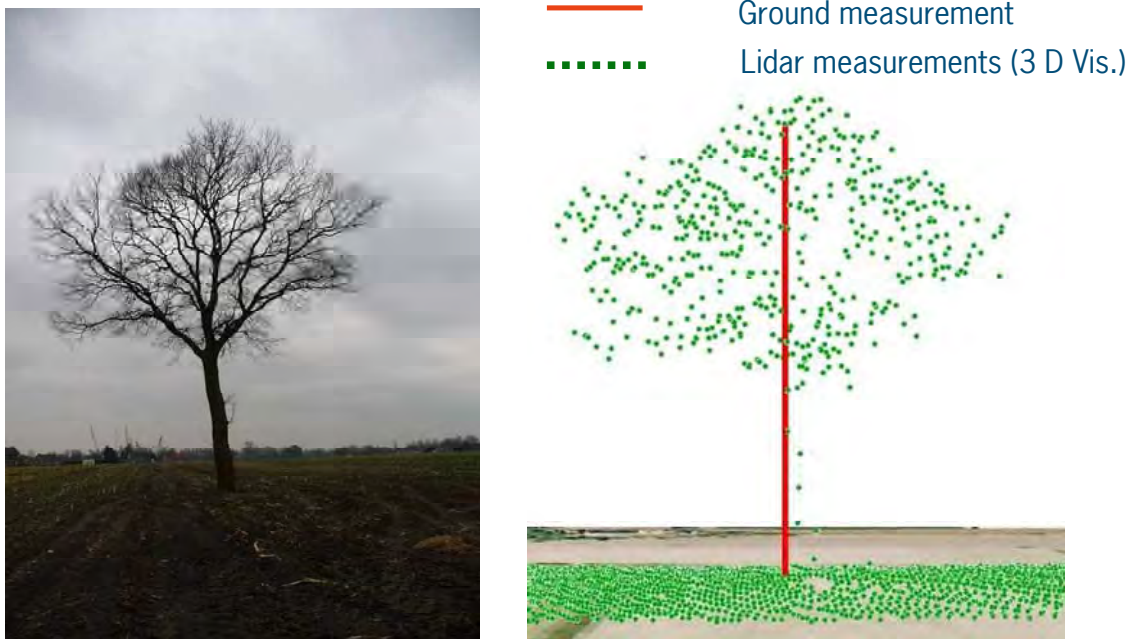


Figure 11 Visual comparison of a single tree (object 1) as seen in the field (left) and 3D view by LiDAR measurements. Red pole indicates the height measurement of the object in the field. Green dots are the LiDAR measurements.

Compound objects like a hedgerow or a line of trees vary a lot in both width and height due to the differences in width and height of the single objects that are part of the compound object. Height and width of a compound object is estimated by averaging both minimum and maximum values. Table 3 shows the measurements for all selected objects.

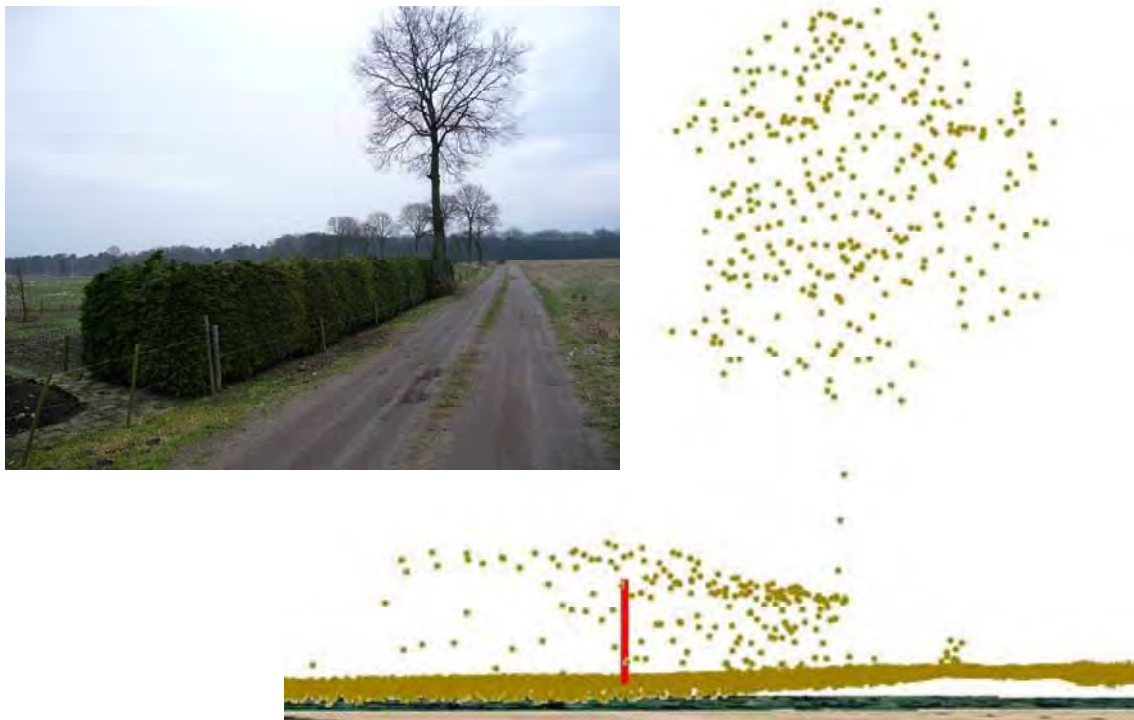


Figure 12 Visual comparison of a hedge and tree (object 23) as seen in the field (left) and 3D view by LiDAR measurements. Red pole indicates the height measurement of the object in the field. Brown dots are the LiDAR measurements.

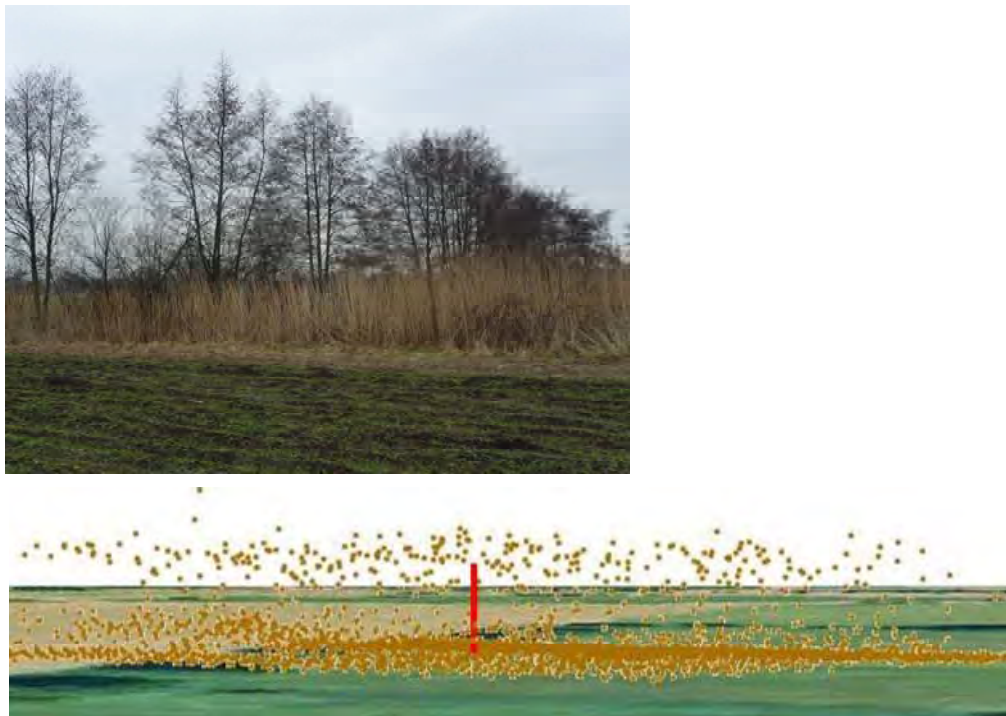


Figure 13 Visual comparison of a fringe of reed (object 5) as seen in the field (left) and 3D view by LiDAR measurements. Red pole indicates the height measurement of the object in the field. Brown dots are the LiDAR measurements.

Table 3 Field measurement on vegetation objects in the study area of Chaam in February 2010.

Object of interest	LiDAR		Fieldwork	
	Height	Width	Height	Width
Single tree	11.9	9.8	11.71	8
Hedge row with bush	4.4	2.5 - 5.3	5.20	2.5
Single tree	11.3		11.54	6
Hedge row	7 - 7.8	6.8 - 7.8	8.56	5
Fringe of reed	2.9	3.6 - 5	2.20	4
Solitary tree	11.1	7.8	12.53	8
Row of willows	6.7 - 7	2.0 - 3	9.34	2
Blackberry and reed	1.3 - 5	4.0 - 7	5.20	4
Blackberry, low vegetation	0.25	-	0.75	4
Single tree	17.2	9.0 - 12	19.53	10
Forest with pines and birch	16.4 - 20		17.45 -	
Double line of Oak trees	8.5 - 8.9	4.7 - 6.4	9.57	5
Line of trees and bushes	15.9	7.0 - 8	15.89	10
Oak trees in line	14.0 - 16	8	16.00	8
Rough wood at water fringe	0.6	0.6 - 2.5	0.75	2
Pitrus in ditch	ruis		0.75	7
Hedge with hornbeam	1.2	0.3 - 0.5	1.10	35
Con. Forest with edge of dec.	10.5		11.10	36
Solitary tree	10.25	8.5 - 10.8	11.28	5
Blackberry, low vegetation	1.2	3.5 - 4	1.70	4
Hedgerow	3.6 - 4.2	4.1 - 5	4.45	4
Rough field	0	-	1.00 -	
Hedge with conifers	1.6	0.6	1.50	0
Row with birch trees	10.6	4.2	11.75	3
Oak trees in line	11.4	5 - 8	12.82	6

If we take the maximum height from the LiDAR data we can calculate the regression statistics with the field measurements. The regression analysis shows a good correlation between the field measurements and the LiDAR measurements, with an adjusted R square of 0.95 (n = 24). For the width of objects there is more variance and is also more difficult to measure in the field, especially if objects are larger. For the regression analysis we took the average width measured by LiDAR against the field measurements. The result is an adjusted R square of 0.89 (n = 19), which still can be considered as good. This small study shows that measurements made by LiDAR are quite accurate, even if data are acquired in early spring when no leaves are present. The only vegetation that did not give any return from the LiDAR data was a field with Pitrus (*Juncus effesus*). It is not clear yet why the Pitrus does not give any return, while a reed fringe (object 5) consisting of *Phragmites communis* gives consistent measurements.

4.4. Preliminary results

Preliminary results as shown in Figure 14, using a decision tree classifier based on information derived from the false-colour aerial photographs and LIDAR data using the FUSION software, show reasonable results, but also shows that object recognition of habitat patches according to the BioHab/Ebone methodology needs an additional approach since the decision tree is implemented on a pixel-basis. were integrated. Integration of aerial photograph and LiDAR images is partly hampered by relief displacement in the aerial photographs at a detailed spatial level. More research is needed to explore all new possibilities with eCognition to be able to perform a good segmentation with LiDAR data (section 4.5). Moreover, the ground data were not always labelled correctly by Fugro for all LiDAR points. Dense and very low buxus trees (30 cm height) were labelled as ground level. It was decided to explore more the FUSION software to calculate a new canopy height model and to calculate derived characteristics (height, density, etc.) at the pixel level. A decision tree (in our case using spatial modeller in ArcGIS) can then provide a good classifier to identify the individual plant life forms at the pixel level. The use of aerial photographs as an additional source of information is essential, especially to discriminate vegetation from non-vegetated areas.

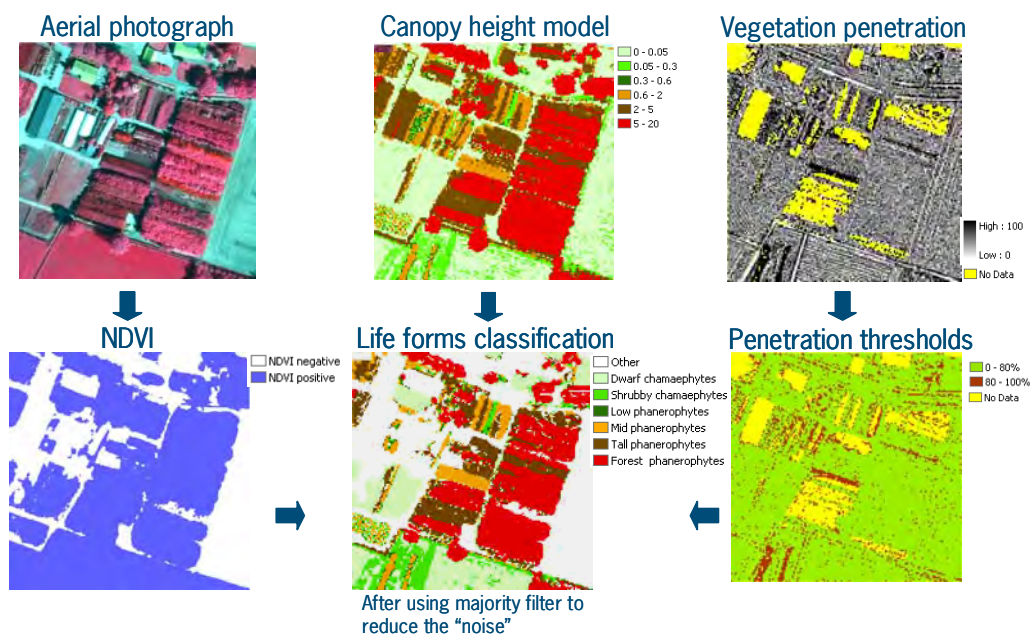


Figure 14 An example a different layers calculated by FUSION software for the LiDAR data and layers derived from the false-colour aerial photographs that are integrated by a decision tree classifier to identify the individual plant life forms at a pixel level.

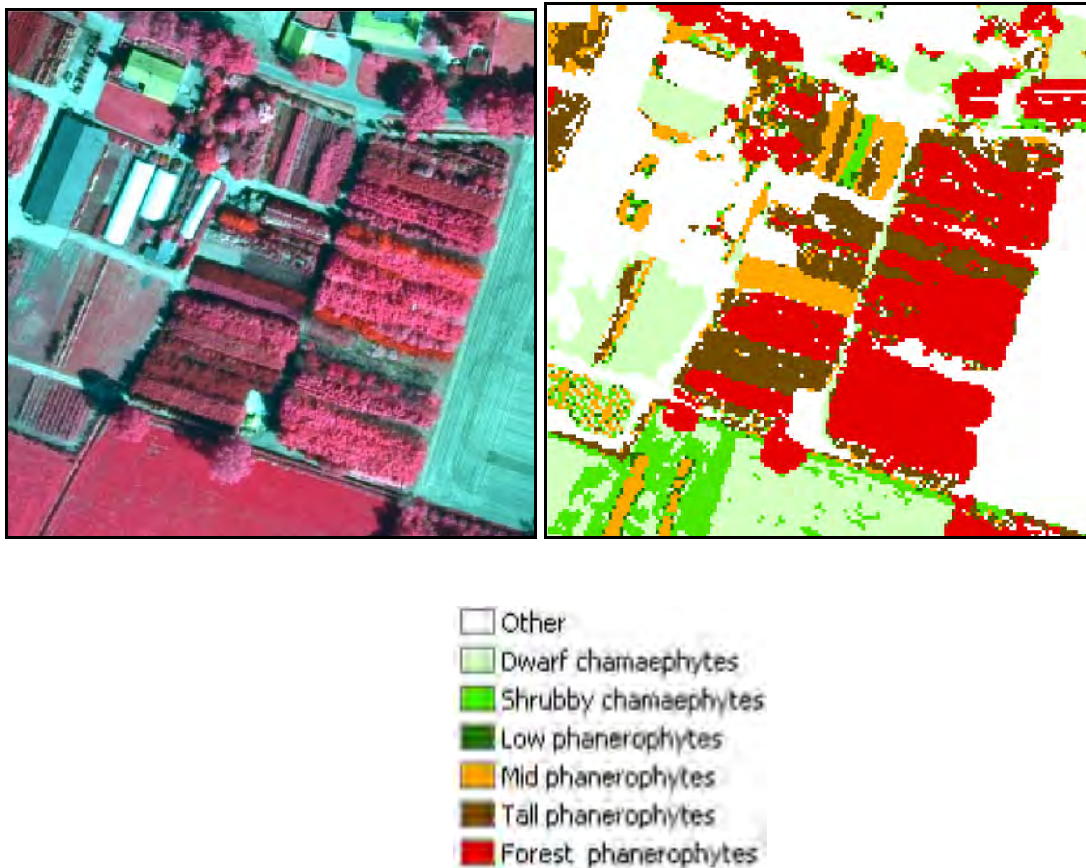


Figure 15 Visual comparison of the aerial photograph and the identified plant life forms at the pixel level. Major problem is still to identify the proper mapping units used for the General Habitat Categories.

Figure 14 and 15 show that the preliminary results from the decision tree classifier are quite satisfactory by integration of LiDAR data with false-colour aerial photographs. In fact, the above given example is a tree nursery and this area should be classified as urban (URB) according to the BIOHAB/EBONE methodology. By integration with topographic maps urban areas can be removed (see section 4.5). Moreover, the composition of individual plant life forms is determined normally for every habitat mapping unit with a minimum area of 400 m². The identification of the proper habitat mapping units using semi-automatic procedures is now seen as a major challenge that needs more research.

4.5. Segmentation and classification for an entire 1km² sample

Following the promising results obtained using a decision tree classifier to identify plant life form at pixel level, more research has been performed now to develop a semi-automated procedure for the detection of the proper mapping units used for the General Habitat Categories (GHC). To do so, the pixel-based classification method presented above was applied on a larger study area (1x1km) and used as starting point for the habitat mapping unit identification.

Pixel-based classification

As explained in the previous example, a NDVI index computed from the aerial photographs is used to discriminate vegetated and artificial areas. This selection is completed integrating the Dutch topographic map (Top10 vector) to remove urban or crop elements. Concerning the

latter, not all the crops are filtered out. Some types of crops, like vineyards, are considered as relevant habitat categories.



Figure 16 NDVI index mask (left) and Top10 vector mask (right)

From the LiDAR data, a canopy height model is computed at 2m grid cell size. The NDVI mask, Top10 vector mask and the canopy height model are then integrated (mosaic). The classification rules are applied on the mosaic in order to produce 9 categories on a pixel basis :

1. No vegetation (from the NDVI information)
2. Crop field (from the top10 data)
3. Other (from the top10 data)
4. Tree nursery (from the top10 data)
5. Canopy height between 0 and 10cm (from the canopy height model)
6. Canopy height between 10 and 60cm (from the canopy height model)
7. Canopy height between 60cm and 2m (from the canopy height model)
8. Canopy height between 2 and 5 m (from the canopy height model)
9. Canopy height higher than 5m (from the canopy height model)

The tree classification output was smoothed using a majority filter with a kernel window of 3 by 3 pixels.



Figure 17 Canopy height mode (left) and pixel based classification output (right)

Segmentation to identify habitat patches

The pixel-based plant life form classification (smoothed result) can be used as the point of departure to identify the habitat patches using segmentation techniques. To do so, a multi-resolution segmentation and a spectral difference segmentation has been carried out using eCognition software of Definiens.

First the multi-resolution segmentation is run using a scale factor of 15. The shape criteria is set really low (0.05) whereas the compactness criteria is relatively high (0.7). Then the spectral difference segmentation is carried out in two steps. First, the segmentation is applied to all the objects created during the multi-resolution segmentation using a maximum spectral difference set as 0.17. Then a second spectral difference based segmentation is performed only for the objects presenting a average value superior to 2.5 (see the value attributed to the pixel according to the classification described above) using a maximum spectral difference value of 0.5. The composition of the individual plant life forms is determined for every habitat patch with a minimum area of 400 m². In order to meet to this requirement, a “cleaning” is done to dissolve all objects presenting an area smaller than this limit. A filtering is also performed based on the ratio width/length of the object to remove the small and long objects that can be generated by border effect. The width/length ratio used is set as superior or equal to 7. The produced objects are exported as shapefile (figure 18) and some zonal statistics are computed in order to give the percentage of each general habitat category present in each polygon as presented in table 4.

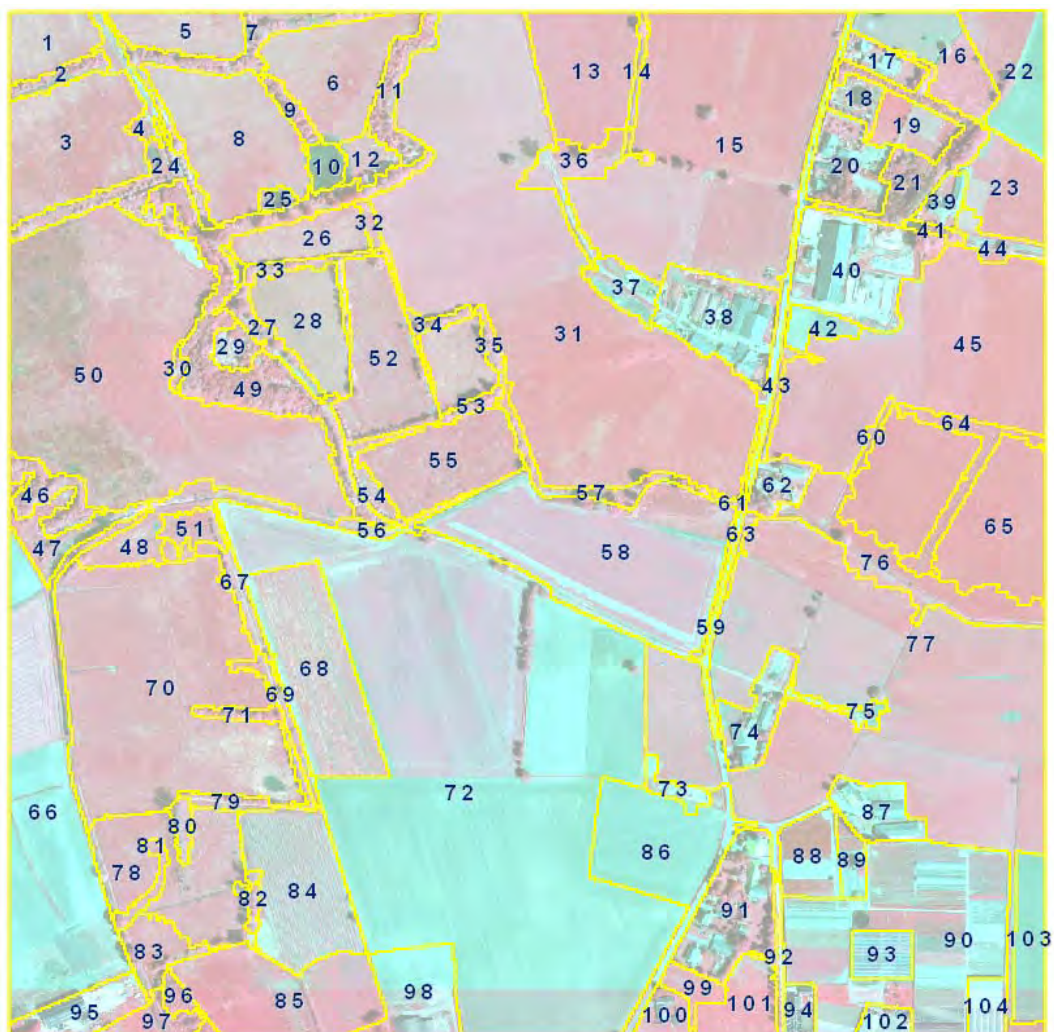


Figure 18 Visualization of the habitat mapping units created during the segmentation. The number identifying the polygons are used in table 4.

Table 4 provides the composition of plant life forms for each habitat patch (see polygons in Figure 18). The plant life forms used in this classification are:

- Plant life form lower than 10cm (< 10cm)
- Leafy hemicryptophytes and Caespitose hemicryptophytes (LHE /CHE)
- Mid phanerophytes (MPH)
- Tall phanerophytes (TPH)
- Forest phanerophytes (FPH)

The last column in table 4 indicates the corresponding Top10 vector class. "No vegetation" indicates it is a semi-natural areas according to the Top10 vector and that the NDVI index indicated that no vegetation was detected at this location.

Table 4 Percentage of each general habitat category by habitat mapping units

Object ID	< 10cm	LHE/CHE	MPH	TPH	FPH	Top10 class/NDVI
1	93.50	4.64	0.68	1.10	0.08	Grassland
2	15.10	15.59	16.83	41.09	11.39	Forest
3	79.90	19.08	0.66	0.30	0.06	Grassland
4	46.22	24.64	13.67	13.67	1.80	Grassland
5	92.95	3.36	0.57	1.48	1.64	Grassland
6	88.71	8.02	1.15	1.26	0.86	Grassland
7	15.25	11.05	15.03	24.61	34.05	Forest
8	95.59	3.22	0.25	0.74	0.19	Grassland
9	6.94	5.68	6.31	11.99	69.09	Forest
10	60.70	20.05	13.82	4.61	0.81	No vegetation
11	2.88	6.73	10.15	47.33	32.91	Forest
12	51.08	24.46	9.27	8.68	6.51	Grassland
13	97.60	1.80	0.00	0.04	0.56	Grassland
14	12.93	52.72	14.29	0.68	19.39	Grassland
15	92.68	4.39	0.51	0.39	2.04	Grassland
16	68.38	18.79	4.00	4.00	4.82	Grassland
17	17.35	6.02	11.33	35.93	29.38	Other
18	22.41	26.14	22.41	15.98	13.07	Grassland + No vegetation
19	91.96	1.36	1.47	2.72	2.49	Grassland
20	20.03	5.86	15.80	22.34	35.97	Other
21	4.25	1.30	2.24	3.54	88.66	Forest
22	83.95	9.80	1.85	0.60	3.80	Crops
23	92.12	5.19	1.04	1.59	0.06	Grassland
24	11.16	21.17	17.71	25.92	24.05	Forest + Grassland
25	19.32	30.11	23.30	18.18	9.09	Grassland + No vegetation
26	93.02	1.92	0.32	1.12	3.61	Grassland
27	11.04	5.60	8.48	17.92	56.96	Forest
28	96.92	0.55	0.50	0.61	1.41	Grassland
29	3.35	31.44	17.78	36.60	10.82	Forest
30	13.11	45.08	16.39	23.77	1.64	Forest
31	96.44	2.40	0.19	0.20	0.77	Grassland
32	17.28	70.99	6.79	0.62	4.32	Grassland

33	15.12	1.58	3.84	8.35	71.11	Grassland
34	15.67	11.00	12.33	16.33	44.67	Grassland
35	9.90	6.25	1.56	5.21	77.08	Grassland
36	58.33	23.53	3.59	0.40	14.16	Grassland
37	42.88	44.33	12.50	0.29	0.00	Grassland + No vegetation
38	19.23	15.44	20.03	31.32	13.98	Other
39	27.55	7.87	16.44	36.81	11.34	Other
40	23.35	17.60	21.14	18.44	19.47	Other
41	16.89	10.14	0.68	0.00	72.30	Other
42	77.70	17.08	2.04	2.12	1.06	Other
43	24.62	51.92	23.08	0.00	0.38	Grassland
44	50.19	37.07	4.63	1.54	6.56	Grassland + No vegetation
45	96.00	3.63	0.23	0.01	0.13	Grassland
46	1.65	5.41	6.82	18.21	67.92	Grassland + Other
47	9.69	55.34	18.38	10.59	5.99	Grassland + Other
48	52.56	35.88	7.87	3.70	0.00	Grassland
49	5.85	4.81	3.24	18.61	67.49	Forest
50	92.18	6.72	0.28	0.40	0.42	Grassland
51	91.70	6.28	2.02	0.00	0.00	Grassland
52	28.97	52.07	1.86	5.90	11.19	Crops
53	13.30	3.94	0.99	2.46	79.31	Grassland
54	16.74	24.90	18.62	17.36	22.38	Grassland
55	89.59	9.62	0.43	0.12	0.24	Grassland
56	43.61	49.18	5.57	1.31	0.33	Grassland
57	9.03	32.15	16.28	10.26	32.28	Grassland
58	86.59	9.48	0.58	0.50	2.85	Crops
59	70.57	28.37	1.06	0.00	0.00	No vegetation
60	21.43	73.81	4.76	0.00	0.00	Grassland
61	18.36	60.33	18.69	0.00	2.62	No vegetation
62	16.31	12.80	11.89	27.29	31.71	Other
63	30.88	59.56	9.56	0.00	0.00	Grassland
64	17.70	76.92	5.28	0.10	0.00	Grassland
65	97.89	1.39	0.71	0.00	0.00	Grassland
66	66.53	27.51	4.72	0.90	0.35	Crops
67	22.29	37.25	18.17	20.61	1.68	Grassland
68	44.94	29.40	24.55	0.62	0.49	Crops (Vineyard)
69	34.55	37.05	9.09	13.64	5.68	Grassland
70	85.50	13.47	0.26	0.40	0.37	Grassland
71	14.22	11.93	2.52	27.75	43.58	Grassland
72	87.38	10.64	1.09	0.28	0.62	Crops
73	78.74	12.57	7.19	1.50	0.00	No vegetation
74	39.23	13.05	9.12	22.79	15.82	Other
75	70.96	16.54	8.09	1.10	3.31	No vegetation
76	48.97	43.29	4.60	1.03	2.11	Grassland
77	90.20	7.01	1.18	0.44	1.17	Grassland
78	68.00	23.06	3.11	0.94	4.90	Grassland

79	25.69	38.19	2.08	9.72	24.31	Grassland
80	6.07	4.05	0.40	0.00	89.47	Grassland
81	8.04	15.73	41.61	16.78	17.83	Grassland
82	7.11	4.06	2.03	2.03	84.77	Grassland
83	24.57	31.11	23.65	6.89	13.78	Grassland
84	30.55	44.66	23.43	0.56	0.80	Crops (Vineyard)
85	77.40	7.76	3.51	3.75	7.58	Crops
86	88.69	7.58	2.43	0.49	0.81	No vegetation
87	26.46	9.12	9.42	39.94	15.06	Other
88	81.73	6.62	7.33	3.00	1.32	Crops
89	82.29	4.32	4.97	0.65	7.78	Grassland + No vegetation
90	68.35	14.30	9.13	7.64	0.58	Tree nursery
91	20.86	8.11	6.76	27.10	37.16	Other
92	15.24	23.49	1.59	7.30	52.38	Other
93	0.00	0.00	0.00	100.00	0.00	Other
94	31.58	9.70	34.07	12.47	12.19	Other
95	46.12	13.23	10.21	8.03	22.40	Other
96	3.27	1.09	0.73	2.91	92.00	Forest
97	54.37	25.86	9.32	4.75	5.70	Grassland + Forest
98	59.86	20.59	4.62	8.14	6.78	Other
99	79.02	10.26	1.86	7.46	1.40	Grassland
100	59.27	3.02	4.09	29.53	4.09	Other
101	98.70	0.75	0.37	0.09	0.09	Grassland
102	43.03	0.62	4.95	17.34	34.06	Other
103	86.02	13.89	0.00	0.00	0.08	Crops
104	0.40	3.41	4.02	92.17	0.00	Other

4.6. Validation

In order to validate the classification results for each habitat type a comparison was made with data obtained from the field according to the BIOHAB/EBONE methodology. The habitat mapping in the field was performed by Bob Bunce and Sander Múcher on the 20th of June 2010 according to the EBONE habitat mapping protocols.

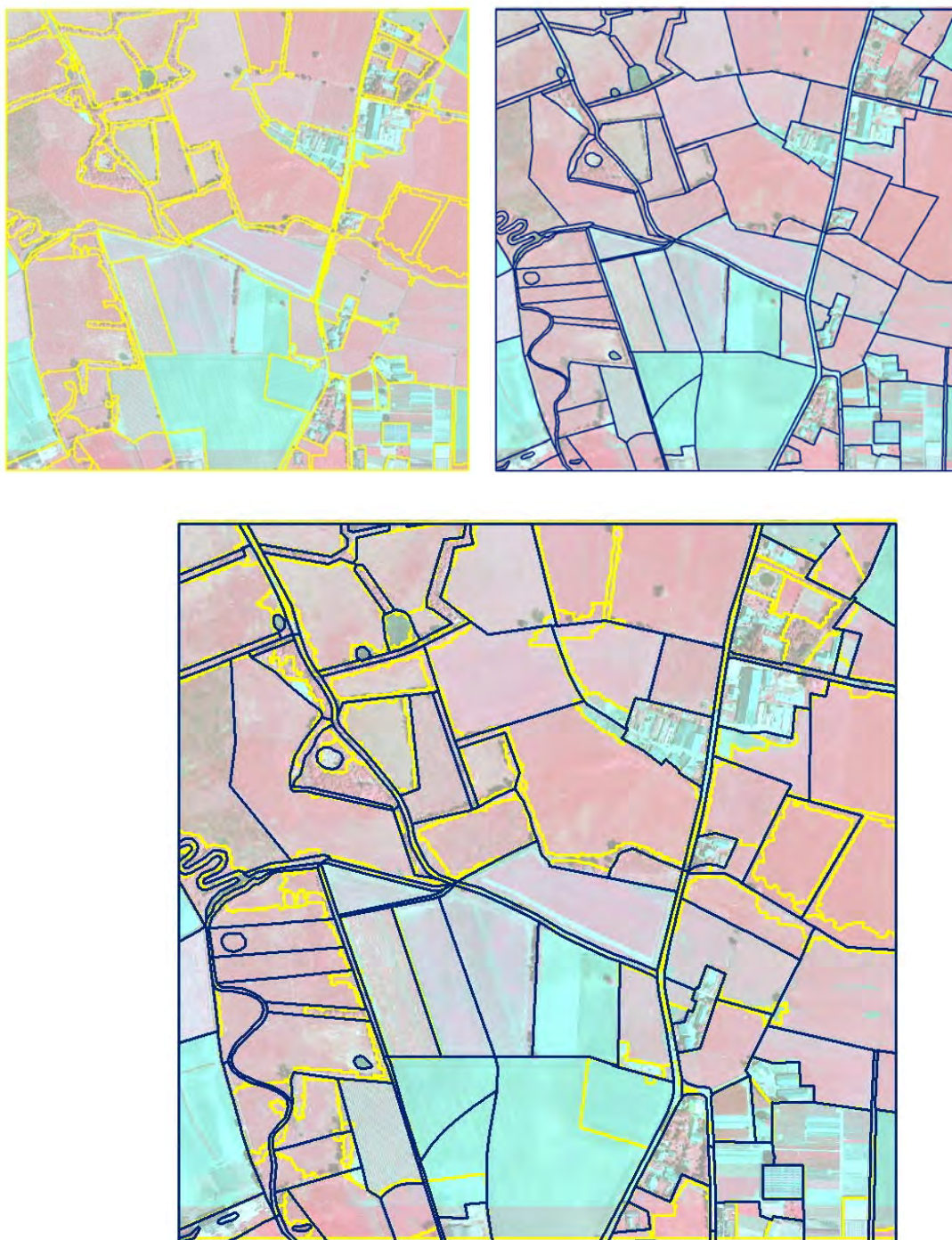


Figure 19 Visual comparison of semi-automated (yellow) and field based manual (blue) delineation of the habitat patches.

When comparing the results in figure 19, the segmentation results of habitat patches are quite good when compared to the field based interpretation of habitat patches.

The next validation step was to compare the composition of plant life forms for habitat patch (field based versus classification result). Table 5 shows the composition of the habitat patch (as identified in the field) versus the composition in plant life forms based on the semi-automatic classification.

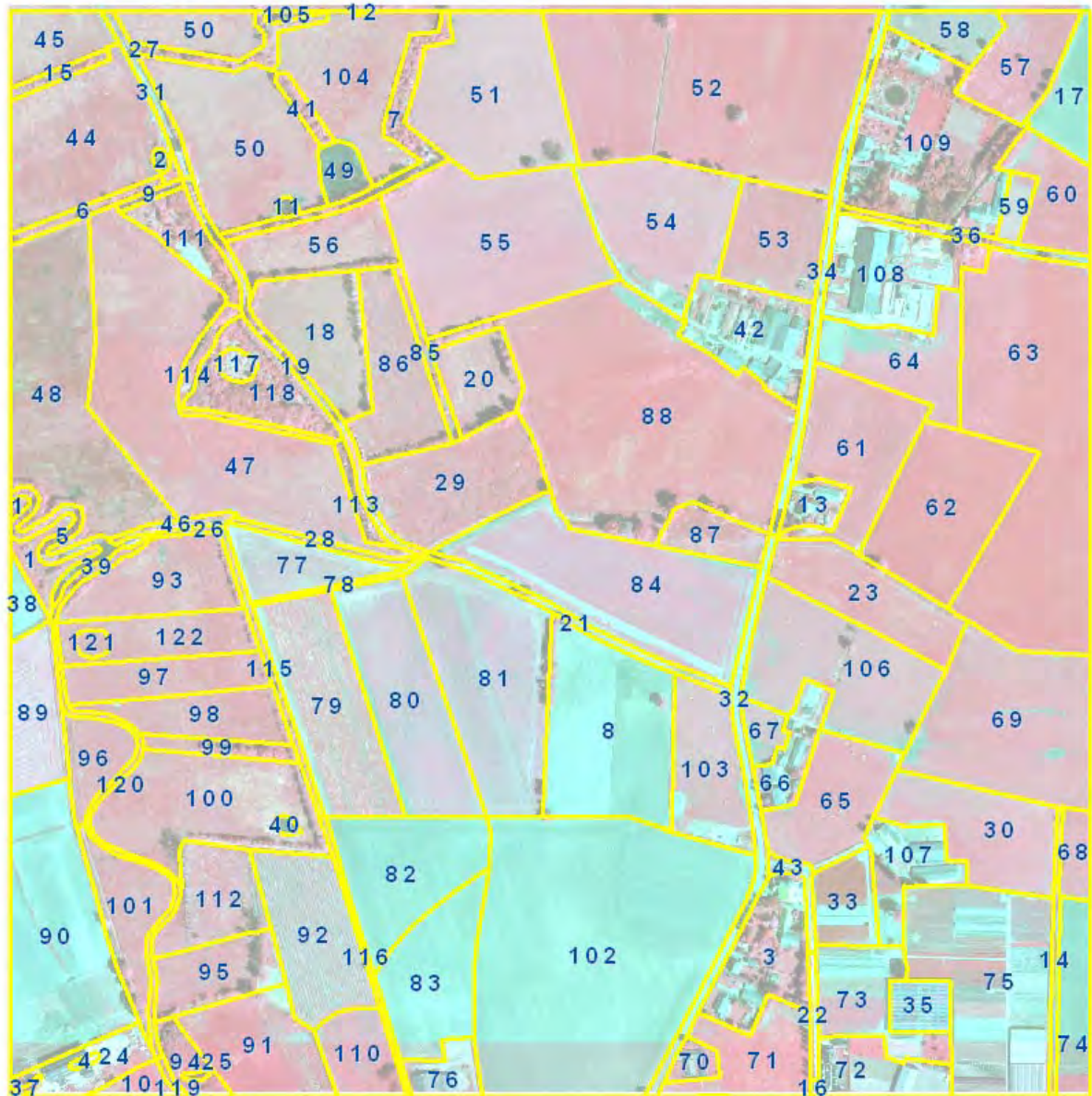


Figure 20 Identification of the habitat mapping units defined during the field work.

Table 5 Comparison between semi-automated and field based plant life forms identification inside each habitat mapping unit

ID	FIELDWORK RESULTS											SEMI-AUTOMATED CLASSIFICATION RESULTS										
	GHC	LF1	%	LF2	%	LF3	%	LF4	%	LF5	%	LHE/CHE	MPH	TPH	FPH	Crop	Aqua	< 10cm	LHE/CHE	MPH	TPH	FPH
1	LHE/CHE	CHE	60	LHE	30	EHY	10					100						11.86	65.05	7.49	8.58	7.02
2			0															3.17	25.40	47.62	23.81	0.00
3	ART		0															20.99	8.26	6.95	27.63	36.16
4			0															8.16	8.16	8.16	0.00	75.51
5	FPH/DEC	FPH	0												100			4.36	19.82	23.25	21.40	31.18
6			0															2.05	12.31	32.05	34.87	18.72
7			0															1.67	5.44	6.28	38.66	47.95
8	CRO	CRO	100												100			85.67	12.03	1.20	0.06	1.05
9			0															6.50	4.07	5.69	41.46	42.28
10	CHE	CHE	70									70						79.25	8.68	7.17	3.40	1.51
11	FPH	FPH	50	AQUA	30	SHY	20					20		50		30		2.94	25.00	42.65	26.47	2.94
12			0															0.00	0.00	23.08	15.38	61.54
13	ART		0															18.25	13.16	13.86	31.05	23.68
14			0															64.36	31.03	4.10	0.00	0.51
15			0															4.74	10.22	16.06	52.55	16.42
16			0															20.00	70.00	0.00	0.00	10.00
17	CRO	CRO	100												100			83.21	10.77	1.26	0.54	4.22
18	CHE/LHE	CHE	60	LHE	40							100						82.79	0.75	1.12	2.83	12.51
19			0															16.53	7.12	3.86	14.23	58.26
20	CHE	CHE	50									50						80.26	3.41	1.67	2.03	12.63
21			0															36.95	31.70	11.03	4.55	15.76
22			0															15.17	20.85	1.42	5.21	57.35
23	CHE	CHE	100									100						83.83	13.18	1.66	0.36	0.97
24	ART		0															47.99	14.16	10.74	9.04	18.07
25			0															7.32	26.83	17.07	26.83	21.95
26	CHE	CHE	80	FPH	20							80		20				10.39	83.12	6.49	0.00	0.00
27			0															1.83	9.32	9.98	30.12	48.75
28	CHE	CHE	60	LHE	30	AQUA	10					90				10		49.82	49.11	1.07	0.00	0.00
29	CHE	CHE	70	LHE	30							100						74.52	13.35	3.49	2.18	6.46
30	LHE	CHE	100									100						89.84	6.17	2.28	0.46	1.25
31			0															23.74	12.53	10.55	35.60	17.58

ID	FIELDWORK RESULTS												SEMI-AUTOMATED CLASSIFICATION RESULTS									
	GHC	LF1	%	LF2	%	LF3	%	LF4	%	LF5	%	LHE/CHE	MPH	TPH	FPH	Crop	Aqua	< 10cm	LHE/CHE	MPH	TPH	FPH
32			0															57.33	37.73	4.20	0.08	0.66
33	CRO		0															82.14	6.90	6.45	3.18	1.33
34			0															47.39	40.93	5.79	2.90	2.99
35	CHE	CHE	0	THE								100						0.00	0.00	0.00	100.00	0.00
36			0															21.53	18.22	2.69	0.41	57.14
37			0															9.38	9.38	0.00	0.00	81.25
38	CRO	CRO	100													100		70.02	14.99	8.35	6.39	0.25
39	CHE	CHE	80	FPH	20							80			20			14.67	60.00	20.00	3.11	2.22
40			0															29.87	70.13	0.00	0.00	0.00
41			0															0.40	1.98	1.98	10.71	84.92
42			0															19.35	15.26	20.23	31.22	13.94
43			0															46.79	14.72	12.08	10.94	15.47
44	CHE	CHE	70									70						75.09	20.94	2.13	1.62	0.22
45	CHE/LHE	CHE	60	LHE	40							100						90.95	5.39	2.82	0.83	0.00
46			0															17.57	43.10	18.41	12.97	7.95
47	CHE	CHE	70									70						90.03	8.59	0.40	0.31	0.67
48	CHE	CHE	80	LHE	20							100						90.50	2.18	0.16	0.96	6.20
49	CHE	CHE	100									100						51.16	19.57	13.76	7.95	7.56
50	SPA		0															86.85	5.56	2.15	2.39	3.06
51	CHE	CHE	70	LHE	30							100						92.22	3.13	0.78	1.13	2.75
52	CHE	CHE	100									100						92.08	4.62	0.64	0.05	2.61
53	CHE	CHE	70	LHE	30							100						92.29	4.02	0.76	1.56	1.37
54	LHE	CHE	100									100						82.19	12.29	2.90	0.30	2.31
55	LHE	CHE	100									100						93.33	1.92	0.47	0.42	3.87
56	CHE	CHE	70	LHE	30							100						66.14	8.81	3.93	3.09	18.03
57	CHE	CHE	70	LHE	30							100						70.89	13.62	4.52	2.37	8.59
58	CHE	CHE	0	THE														68.94	18.21	1.23	4.25	7.37
59	CHE	CHE	0	THE														79.73	10.68	1.92	7.40	0.27
60	CHE	CHE	100									100						83.86	7.62	1.22	0.00	7.30
61	CHE	CHE	100									100						85.82	8.85	2.45	0.39	2.49
62	CHE	CHE	100									100						76.41	20.85	1.94	0.03	0.78
63	CHE	CHE	100									100						87.72	10.65	1.17	0.14	0.33

ID	FIELDWORK RESULTS												SEMI-AUTOMATED CLASSIFICATION RESULTS									
	GHC	LF1	%	LF2	%	LF3	%	LF4	%	LF5	%	LHE/CHE	MPH	TPH	FPH	Crop	Aqua	< 10cm	LHE/CHE	MPH	TPH	FPH
64	CHE	CHE	100									100						81.43	13.99	4.09	0.36	0.13
65	CHE	CHE	70	LHE	30							100						91.92	5.28	0.49	0.66	1.65
66	ART		0															34.93	12.67	9.91	25.23	17.26
67	CHE	CHE	70	LHE	30							100						81.56	14.89	2.44	0.67	0.44
68	CRO	CRO	100													100		84.41	12.61	0.70	0.00	2.28
69	CRO	CRO	100													100		86.02	11.21	1.05	0.52	1.20
70	ART		0															45.69	2.30	5.46	40.23	6.32
71	CHE	CHE	100									100						87.77	4.23	0.90	2.54	4.57
72	ART		0															48.75	15.03	14.36	8.93	12.94
73	CRO		0															68.33	10.26	17.73	2.90	0.78
74			0															86.33	13.51	0.00	0.00	0.15
75	CRO		0															62.07	13.42	6.35	17.56	0.60
76	ART		0															37.12	26.08	8.48	19.36	8.96
77	LHE	LHE	60	SPA	30	CHE	10					70				30		71.66	16.96	7.83	3.54	0.00
78	LHE/CHE	LHE	50	CHE	50							100						76.07	23.93	0.00	0.00	0.00
79	WOC	WOC	100	CHE	90							70	30					43.97	29.44	24.82	0.98	0.79
80	WOC	WOC	100	THE	70	SPA	30					40	30			30		78.46	20.04	1.42	0.03	0.05
81	CRO	CRO	100													100		91.84	6.74	0.54	0.21	0.67
82	CHE	CHE	100									100						78.78	20.28	0.85	0.03	0.06
83			0															84.21	13.79	1.20	0.29	0.51
84	LHE	CHE	100									100						91.45	7.28	0.29	0.44	0.54
85	CHE	CHE	100									100						5.19	34.70	10.66	25.96	23.50
86	THE	THE	100									100						32.92	55.48	0.64	2.30	8.66
87	CHE	CHE	100									100						81.61	9.57	0.65	0.11	8.06
88	LHE	CHE	100									100						86.88	5.40	1.49	1.00	5.24
89	LHE	CHE	100									100						89.35	6.77	3.12	0.77	0.00
90	CRO	CRO	100									100						62.87	32.15	4.25	0.42	0.32
91	CHE	CHE	90	LHE	10							100						75.64	5.93	5.67	4.15	8.61
92	WOC	WOC	100	CHE	90							70	30					29.94	43.77	25.57	0.38	0.34
93	LHE	LHE	60	SPA	30	CHE	10					70				30		67.20	21.14	6.72	4.94	0.00
94	TPH	THP	40	FPH	20	AQUA	20	LHE	10	CHE	10	20		40	20	20		20.75	17.01	5.42	2.99	53.83
95	CHE	CHE	70									70						48.21	23.83	11.08	3.51	13.36

ID	FIELDWORK RESULTS												SEMI-AUTOMATED CLASSIFICATION RESULTS									
	GHC	LF1	%	LF2	%	LF3	%	LF4	%	LF5	%	LHE/CHE	MPH	TPH	FPH	Crop	Aqua	< 10cm	LHE/CHE	MPH	TPH	FPH
96	CHE	CHE	70									70						77.20	21.74	0.96	0.00	0.10
97	LHE	LHE	90	CHE	10							100						87.16	11.83	0.19	0.75	0.06
98	CHE	CHE	70									70						86.45	11.26	0.42	1.69	0.18
99	CHE	CHE	90	LHE	10							100						47.94	16.88	2.33	15.44	17.41
100	CHE	CHE	70									70						78.49	13.33	0.41	2.61	5.15
101	CHE	CHE	70									70						55.43	24.74	6.74	2.74	10.34
102	CRO	CRO	100													100		96.10	3.43	0.16	0.00	0.31
103	LHE	CHE	100									100						90.14	6.16	2.76	0.95	0.00
104	CHE	CHE	70	LHE	30							100						85.18	9.20	3.03	1.53	1.06
105			0															35.71	11.22	15.31	18.37	19.39
106	CHE	CHE	70	LHE	30							100						92.79	4.55	0.90	0.22	1.55
107	ART		0															44.33	7.83	7.76	27.40	12.69
108	ART		0															23.52	14.95	19.90	19.51	22.12
109	ART/THE	ART	50	TRE	50	GRA	20					20			50			29.23	6.12	10.30	16.73	37.63
110	CHE	CHE	90	LHE	10							100						78.35	9.80	0.26	3.32	8.27
111			0															9.66	24.24	3.60	13.26	49.24
112	CHE	CHE	70									70						52.53	24.74	4.68	1.20	16.86
113	FPH/DEC	FPH/DEC	40	CHE	30	LHE	30					60			40			13.62	18.27	6.64	32.89	28.57
114			0															12.21	18.31	7.90	25.13	36.45
115	CHE	FPH	10	FPH	20	CHE	60	LHE	10			70			30			36.22	44.67	7.33	8.44	3.33
116	CHE	CHE	80	FPH	20							80			20			20.51	61.90	9.52	1.10	6.96
117	LHE	LHE	100									100						6.73	50.48	23.08	13.46	6.25
118	FPH/DEC		100		80										100			0.23	3.00	3.34	29.40	64.05
119	CHE	CHE	100									100						23.21	64.29	12.50	0.00	0.00
120	CHE	AQUA	30	CHE	50	LHE	20					70				30		58.17	28.24	10.84	2.44	0.31
121	AQUA	AQUA	60	SPA	20										20	60		99.41	0.59	0.00	0.00	0.00
122	CHE	CHE	70									70						85.11	12.28	0.89	1.72	0.00

Figure 21 shows that most of the percentages of Leafy hemicryptophytes (LHE) and Caespitose hemicryptophytes (CHE) obtained using the semi-automated procedure are less than 20% different from the field observations (in between the red lines).

The point circled in blue in the graph presents a large difference between the field measured value (100%) and the semi-automated predicted value (40%) for the combined class LHE/CHE. When looking at the specific habitat patch, it appears that some trees are present in the unit (from a vertical projection) that were not noticed in the field (classified as 100% LHE/CHE). So in fact, the percentages obtained from the semi-automatic classification seem to be more realistic, than the percentages obtained in the field (due to the missing of the vertical projection of the tree crowns). The table in figure 21 presents the classified or predicted (white) and observed (green) percentage of the different life forms for this particular unit.

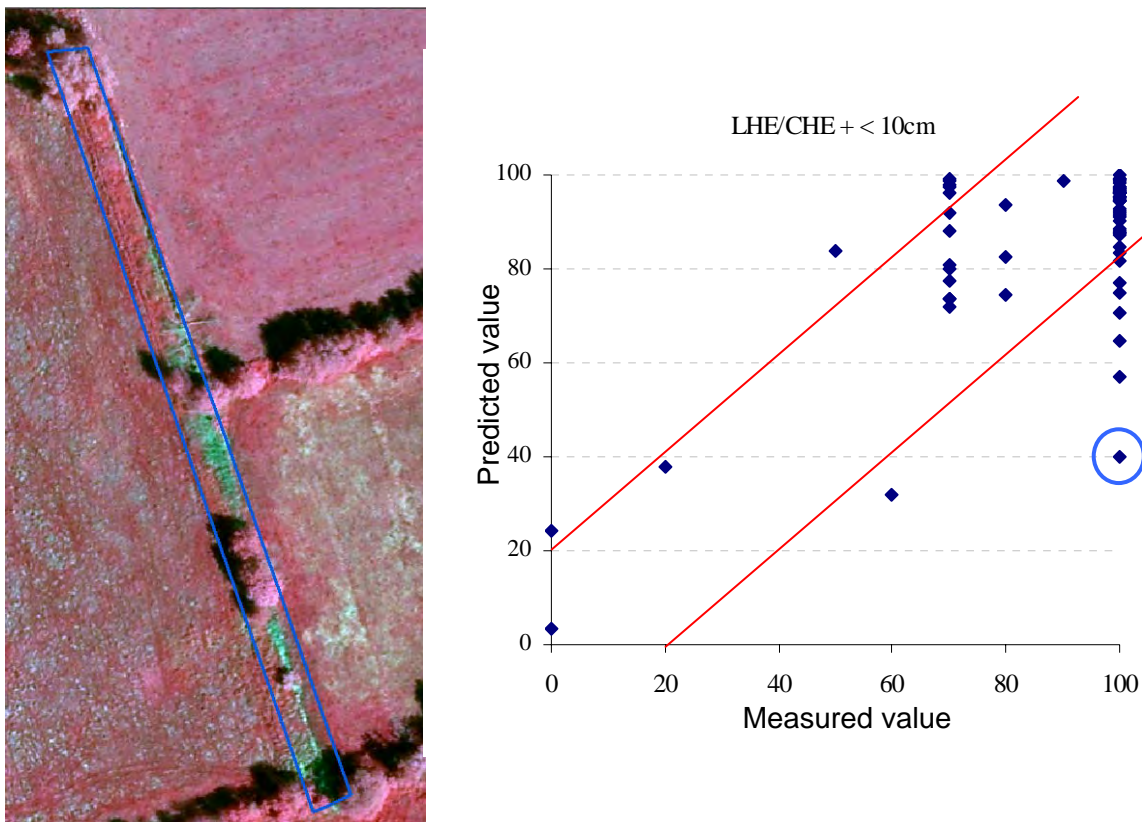


Figure 21 Validation graphs for Leafy hemicryptophytes (LHE) and Caespitose hemicryptophytes (CHE) and details concerning an outstanding value.

Figure 22 shows that most of the percentages of Mid phanerophytes (MPH) obtained using the semi-automated procedure are less than 10% different from the field observations.

The point circled in yellow in the graph presents a larger difference between the field measured value (0%) and the semi-automated predicted value (24%) than the other points. The aerial photographs shows that the specific habitat patch is highly heterogeneous explaining the difference between predicted and measured value. Also here it seems that mistakes were made in the field to estimate the percentages of the different life forms. The

patch is quite large and the interpretation in the field was that this patch concerned only Forest (FPH). The table in figure 22 presents the classified or predicted (white) and observed (green) percentage of the different life forms for this particular unit.

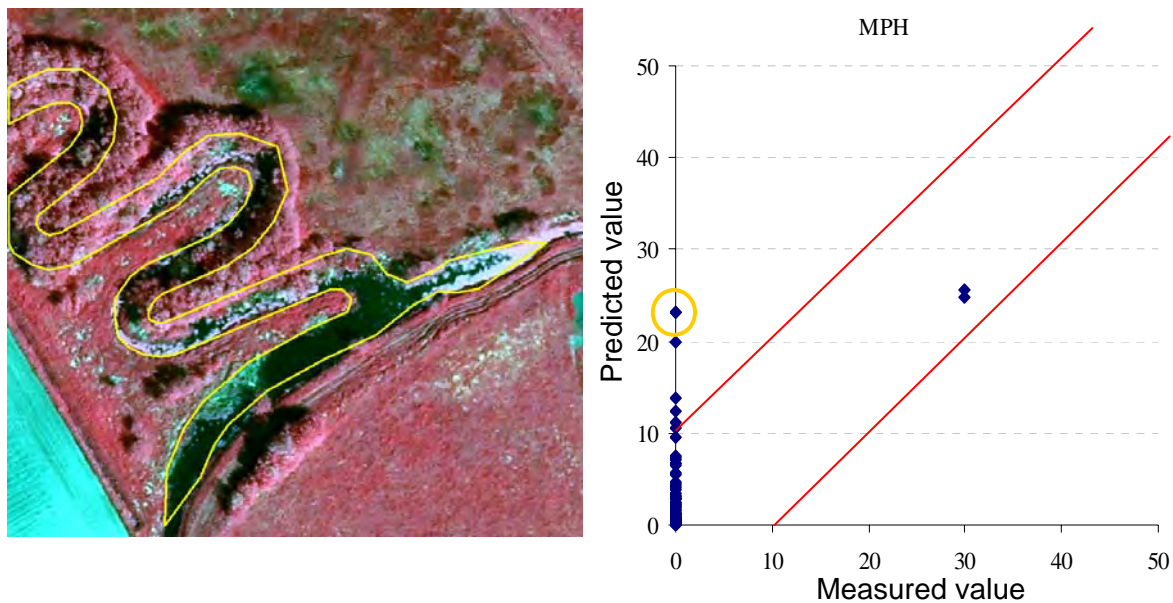


Figure 22 Validation graphs for Mid phanerophytes (MPH) and details concerning an outstanding value.

Discussion

To improve the semi-automatic identification of habitat patches, it would be interesting to exploit more the use of NDVI. In this study, NDVI is only used to differentiate vegetated and non-vegetated surfaces. As mentioned previously, the quality of the DEM (what is the ground layer) used to compute the canopy height model is also important and can have a large influence on the classification result. It would be also interesting to test the sensitivity of the general habitat classification result in relation to the pixel size and the methodology used to produce the canopy height model. Further, it would be interesting to analyze the influence of the result of the pixel based classification used as input for the segmentation on the object delineation.

Notice also that in this study, the three input datasets - aerial photographs, topographic maps and LiDAR data - used for the pixel based classification originate from different years. Furthermore, the LiDAR data have been collected in early spring which is not the most suitable period for the general habitat identification aimed in this study. The roads should be also masked using the Top10 vector data to exclude it from the classification of the general habitat categories.

5. Conclusions

LiDAR provides accurate height measurements on shrubs and trees. Even in early spring when the objects of interest still did not have any leaves. Early spring is the standard time for LiDAR measurements over the entire area of the Netherlands (primary interest is the update of the Dutch elevation model). Regression analysis between field measurements and LiDAR measurements of the height of various plant life forms showed an adjusted R square of 0.95. Unfortunately, not the whole range of plant life forms could be measured with LiDAR. Since the latest generation of LiDAR measurements have an accuracy of approximately 2 to 3 centimeters, it is assumed that cryptogams and dwarf chamaephytes (below 5 cm) are difficult to measure with LiDAR. In general, it has been demonstrated in this study that good characterization of 3d-vegetation objects is possible with LiDAR. But surprisingly, there were also problems with the identification of some specific vegetation types, such as fields with *Juncus effusus* (caespitosa hemicriptophytes). This vegetation type does not reflect any LiDAR measurements and is therefore invisible for LiDAR. Occasional data gaps occurred through "shadow effects", but the use of different scan angles solves this problem. Combination of LiDAR with false-colour aerial photographs, both available for the whole of the Netherlands, provides a power tool with e.g. FUSION software and decision tree classifiers for the identification of plant life forms. Additional combination with topographic maps was needed to mask out urban environments for which the BIOHAB/EBONE does not distinguish plant life forms. Major challenge was to identify the proper habitat patches based on segmentation of the classification result, in order to translate the composition of the plant life forms within the patch to a General Habitat Category (GHC). Comparison with a full field survey of the general habitat categories was essential. Segmentation and classification results are quite satisfactory based on the combined use of LiDAR, topographic maps and aerial photographs using segmentation as well as decision tree classifiers (using spatial modeller in ArcGis). It has been proofed, that in some cases estimates based on a semi-automatic classification are better than the estimates made in the field. Moreover, semi-automatic classification could save costs in the end. Major concern stays, that not all plant life forms can be identified on basis of remotely sensed information, in the first place due to the fact that acquisitions were made in early spring when most vegetation is still not present. A last remark is that the Centre of Geo-Information will obtain a ground LiDAR sensor later this year which makes the assessment of airborne LiDAR even more complete. Combination of LiDAR (height) measurements in combination with more species specific hyperspectral measurements are the way forward to identify General Habitat Categories from space.

6. References

Bibliography

- Akay, A. E., H. Oğuz, et al. (2008). "Using LiDAR technology in forestry activities." Environmental Monitoring and Assessment: 1-9.
- Anderson, J., M. E. Martin, et al. (2006). "The use of waveform LiDAR to measure northern temperate mixed conifer and deciduous forest structure in New Hampshire." Remote Sensing of Environment **105**(3): 248-261.
- Antonarakis, A. S., K. S. Richards, et al. (2008). "Object-based land cover classification using airborne LiDAR." Remote Sensing of Environment **112**(6): 2988-2998.
- Bergen, K. M., A. M. Gilboy, et al. (2007). "Multi-dimensional vegetation structure in modeling avian habitat." Ecological Informatics **2**(1): 9-22.
- Bergen, K. M., S. J. Goetz, et al. (2008). "Remote sensing of vegetation 3-D structure for biodiversity and habitat: Review and implications for LiDAR and radar spaceborne missions." Journal of geophysical research **114**(G00E06).
- Bradbury, R. B., R. A. Hill, et al. (2005). "Modelling relationships between birds and vegetation structure using airborne LiDAR data: A review with case studies from agricultural and woodland environments." Ibis **147**(3): 443-452.
- Brennan, R. and T. L. Webster (2006). "Object-oriented land cover classification of LiDAR-derived surfaces." Canadian Journal of Remote Sensing **32**(2): 162-172.
- Carson, W. W., H. E. Andersen, et al. (2004). LiDAR applications in forestry – An overview, Denver, Colorado.
- Chasmer, L., C. Hopkinson, et al. (2005). Integration of airborne and terrestrial LiDAR for assessing structural components of conifer trees. Proceedings of the 26th Canadian Symposium on Remote Sensing.
- Clawges, R., K. Vierling, et al. (2008). "The use of airborne LiDAR to assess avian species diversity, density, and occurrence in a pine/aspen forest." Remote Sensing of Environment **112**(5): 2064-2073.
- Coops, N. C., M. A. Wulder, et al. (2004). "Comparison of forest attributes extracted from fine spatial resolution multispectral and LiDAR data." Canadian Journal of Remote Sensing **30**(6): 855-866.
- Drake, J. B., R. O. Dubayah, et al. (2002). "Estimation of tropical forest structural characteristics, using large-footprint LiDAR." Remote Sensing of Environment **79**(2-3): 305-319.
- Dubayah, R. O. and J. B. Drake (2000). "LiDAR Remote Sensing for Forestry." Journal of Forestry **98**(6): 44-52.
- Evans, D. L., S. D. Roberts, et al. (2006). "LiDAR - A new tool for forest measurements?" Forestry Chronicle **82**(2): 211-218.

- Geerling, G. W., M. Labrador-Garcia, et al. (2007). "Classification of floodplain vegetation by data fusion of spectral (CASI) and LiDAR data." International Journal of Remote Sensing **28**(19): 4263-4284.
- Geerling, G. W., M. J. Vreeken-Buijs, et al. (2009). "Mapping river floodplain ecotopes by segmentation of spectral (CASI) and structural (LiDAR) remote sensing data." River Research and Applications **25**(7): 795-813.
- Graf, R. F., L. Mathys, et al. (2009). "Habitat assessment for forest dwelling species using LiDAR remote sensing: Capercaillie in the Alps." Forest Ecology and Management **257**(1): 160-167.
- Hall, S. A., I. C. Burke, et al. (2005). "Estimating stand structure using discrete-return LiDAR: An example from low density, fire prone ponderosa pine forests." Forest Ecology and Management **208**(1-3): 189-209.
- Heurich, M. and F. Thoma (2008). "Estimation of forestry stand parameters using laser scanning data in temperate, structurally rich natural European beech (*Fagus sylvatica*) and Norway spruce (*Picea abies*) forests." Forestry **81**(5): 645-661.
- Hill, R. A. and A. G. Thomson (2005). "Mapping woodland species composition and structure using airborne spectral and LiDAR data." International Journal of Remote Sensing **26**(17): 3763-3779.
- Hinsley, S. A., R. A. Hill, et al. (2006). "The application of LiDAR in woodland bird ecology: Climate, canopy structure, and habitat quality." Photogrammetric Engineering and Remote Sensing **72**(12): 1399-1406.
- Hudak, A. T., M. A. Lefsky, et al. (2002). "Integration of LiDAR and Landsat ETM+ data for estimating and mapping forest canopy height." Remote Sensing of Environment **82**(2-3): 397-416.
- Hyde, P., R. Dubayah, et al. (2005). "Mapping forest structure for wildlife habitat analysis using waveform LiDAR: Validation of montane ecosystems." Remote Sensing of Environment **96**(3-4): 427-437.
- Hyde, P., R. Dubayah, et al. (2006). "Mapping forest structure for wildlife habitat analysis using multi-sensor (LiDAR, SAR/InSAR, ETM+, Quickbird) synergy." Remote Sensing of Environment **102**(1-2): 63-73.
- Jan, J. F. (2005). "Comparison of forest canopy height derived using LiDAR data and aerial photos." Taiwan Journal of Forest Science **20**(1): 13-27.
- Korpela, I., M. Koskinen, et al. (2009). "Airborne small-footprint discrete-return LiDAR data in the assessment of boreal mire surface patterns, vegetation, and habitats." Forest Ecology and Management **258**(7): 1549-1566.
- Lefsky, M. A., W. B. Cohen, et al. (2002). "LiDAR remote sensing of above-ground biomass in three biomes." Global Ecology and Biogeography **11**(5): 393-399.
- Lefsky, M. A., W. B. Cohen, et al. (2002). "LiDAR remote sensing for ecosystem studies." BioScience **52**(1): 19-30.
- Lim, K., P. Treitz, et al. (2003). "LiDAR remote sensing of forest structure." Progress in Physical Geography **27**(1): 88-106.

- Lovell, J. L., D. L. B. Jupp, et al. (2003). "Using airborne and ground-based ranging LiDAR to measure canopy structure in Australian forests." Canadian Journal of Remote Sensing **29**(5): 607-622.
- Mallet, C. and F. Bretar (2009). "Full-waveform topographic LiDAR: State-of-the-art." ISPRS Journal of Photogrammetry and Remote Sensing **64**(1): 1-16.
- Mason, D. C., G. Q. A. Anderson, et al. (2003). "Measurement of habitat predictor variables for organism-habitat models using remote sensing and image segmentation." International Journal of Remote Sensing **24**(12): 2515-2532.
- Means, J. E., S. A. Acker, et al. (2000). "Predicting forest stand characteristics with airborne scanning LiDAR." Photogrammetric Engineering and Remote Sensing **66**(11): 1367-1371.
- Patenaude, G., R. A. Hill, et al. (2004). "Quantifying forest above ground carbon content using LiDAR remote sensing." Remote Sensing of Environment **93**(3): 368-380.
- Roberts, S. D., T. J. Dean, et al. (2005). "Estimating individual tree leaf area in loblolly pine plantations using LiDAR-derived measurements of height and crown dimensions." Forest Ecology and Management **213**(1-3): 54-70.
- Rosette, J. A., P. R. J. North, et al. (2009). "A comparison of biophysical parameter retrieval for forestry using airborne and satellite LiDAR." International Journal of Remote Sensing **30**(19): 5229-5237.
- St-Onge, B. (2005). LiDAR remote sensing: Overview of technology and applications. Proceedings of the 26th Canadian Symposium on Remote Sensing.
- Vierling, K. T., L. A. Vierling, et al. (2008). "LiDAR: Shedding new light on habitat characterization and modeling." Frontiers in Ecology and the Environment **6**(2): 90-98.
- Wang, C. and N. F. Glenn (2008). "A linear regression method for tree canopy height estimation using airborne LiDAR data." Canadian Journal of Remote Sensing **34**(SUPPL. 2): S217-S227.
- Wehr, A. and U. Lohr (1999). "Airborne laser scanning - An introduction and overview." ISPRS Journal of Photogrammetry and Remote Sensing **54**(2-3): 68-82.
- Weishampel, J. F., J. B. Drake, et al. (2007). "Forest canopy recovery from the 1938 hurricane and subsequent salvage damage measured with airborne LiDAR." Remote Sensing of Environment **109**(2): 142-153.
- Wulder, M. A., P. Norman, et al. (2003). "Special Issue: LiDAR remote sensing of forest structure and terrain." Numéro spécial: La télédétection LiDAR de la structure de la forêt et du terrain **29**(5): ii-iii.
- Zhao, K., S. Popescu, et al. (2009). "LiDAR remote sensing of forest biomass: A scale-invariant estimation approach using airborne lasers." Remote Sensing of Environment **113**(1): 182-196.
- Zimble, D. A., D. L. Evans, et al. (2003). "Characterizing vertical forest structure using small-footprint airborne LiDAR." Remote Sensing of Environment **87**(2-3): 171-182.

Annex-3



Classification of EBONE General Habitat Categories in a Swedish forest area by using LiDAR in combination with SPOT satellite data

Karin Nordkvist, Ann-Helen Granholm, Johan Holmgren, Mats Nilsson, Håkan Olsson
Section of forest remote sensing
Department of forest resource management
Swedish University of Agricultural Sciences (SLU)
Umeå Sweden

e-mail: karin.nordkvist@srh.slu.se

Version 1.0, May 18, 2011

Intermediate delivery to EBONE Task 5.1.2. Regionally/local specific and independent EO approaches

Abstract

We have investigated to which degree a combination of optical satellite data and LiDAR data can improve classification accuracy of the General Habitat Categories (GHC) used by the FP7 project European Biodiversity Observation Network (EBONE), compared to using satellite data alone. The study was carried out in Remningstorp, a forest dominated area in southern Sweden. The remote sensing data used for the study were (i) a SPOT 5 image from August 2009 and (ii) LiDAR data (26 points/m²) from September 2008. Ground truth samples were collected by interpretation of color infrared digital air photos from September 2009. Maximum likelihood and Random Forests classifications were made with satellite data and with a combination of satellite and LiDAR data. The classification scheme consisted of six forest classes, arable land and pasture land. The use of LiDAR data improved over-all accuracy with 6% for maximum likelihood classification and 7% for Random Forests. The highest over-all accuracy was obtained with Random Forests, but on the expense of the smaller classes.

Introduction

Automated satellite image classification is an established method for producing large area land cover maps. Examples of operational projects are the classification of the forest classes in the Swedish national version of the CORINE land cover data base, (Hagner and Reese, 2007); a state-wide land cover mapping of Wisconsin (Reese et al. 2002); LCMGB (Fuller et al. 1994); and MODIS Land Cover (Friedl et al. 2002), just to mention a few. The accuracy obtained for such products, based on 2-dimensional optical data only, is however limited. LiDAR data has proved useful in mapping of certain vegetation types such as mires (Genc et al. 2004, Korpela et al. 2009). Several studies also have shown the benefits of combining LiDAR data with different kinds of imagery for example for estimations of forest variables (Hudak et al. 2002, Hill and Thomson 2005, Hyde et al. 2006, Holmgren et al. 2008, Erdody and Moskal 2010, Ke et al. 2010), and vegetation or habitat mapping in rangeland and coastal zones (Lee and Shan 2003, Bork and Su 2007, Chust et al. 2008).

From the beginning of 2009, the Swedish National Land Survey (NLS) has been collecting laser scanner data for the whole country. Although the main purpose is the production of a new national digital elevation model (DEM), the nation-wide coverage of laser data could also be a resource for future vegetation mapping. SPOT images are freely available from the SACCESS data base, which is updated yearly with a dataset covering the entire country during the vegetation period (http://saccess.lantmateriet.se/map_viewer?map=29&maplevelindex=0).

The aim of this study is to contribute to an initial understanding of the degree to which the addition of LiDAR data can improve GHC classification accuracies achieved using optical satellite (airborne) data alone¹. The assessment was carried out for a forest dominated test area in southern Sweden.

An earlier version of the work was presented as a poster at the International Conference in Landscape Ecology 2010 in Brno, Czech Republic and at the SilviLaser Conference 2010 in Freiburg, Germany (Nordkvist et al, 2010). Here the same datasets are used; the difference is the evaluation of the GHC classes as well as the test of the Random Forests algorithm.

Material and methods

Study area

The Remningstorp estate is located in southern Sweden (lat. 58° 30' N, long. 13° 40' E). It is mainly covered by managed, hemiboreal forests dominated by Scots pine (*Pinus Sylvestris*), Norway spruce (*Picea Abies*) and birch (*Betula* spp). Figure 1 shows an orthophoto and a SPOT 5 image of the 1.0 km × 1.5 km test site used in this study.

¹ The General Habitat Classification system is a habitat classification system where the vegetation is described using physiognomic characteristics some of which (i.e. canopy height thresholds) are particularly suitable for being estimated by LiDAR.

Remote sensing data

The optical satellite data used in this study was a SPOT 5 HRG XS scene from August 20, 2009. The pixel size is 10 m × 10 m for the green, red and near infrared bands, and 20 m × 20 m for the shortwave infrared band. The image was geo-rectified and co-registered to the Swedish grid system SWEREF 99, with an error of less than 0.5 pixels. LiDAR data was acquired for the test area on September 4, 2008, using a TopEye MkII system carried by a helicopter. The wavelength was 1024 nm, the flying altitude 250 m above ground and the average point density 26 m⁻². First and last returns were recorded for each pulse.

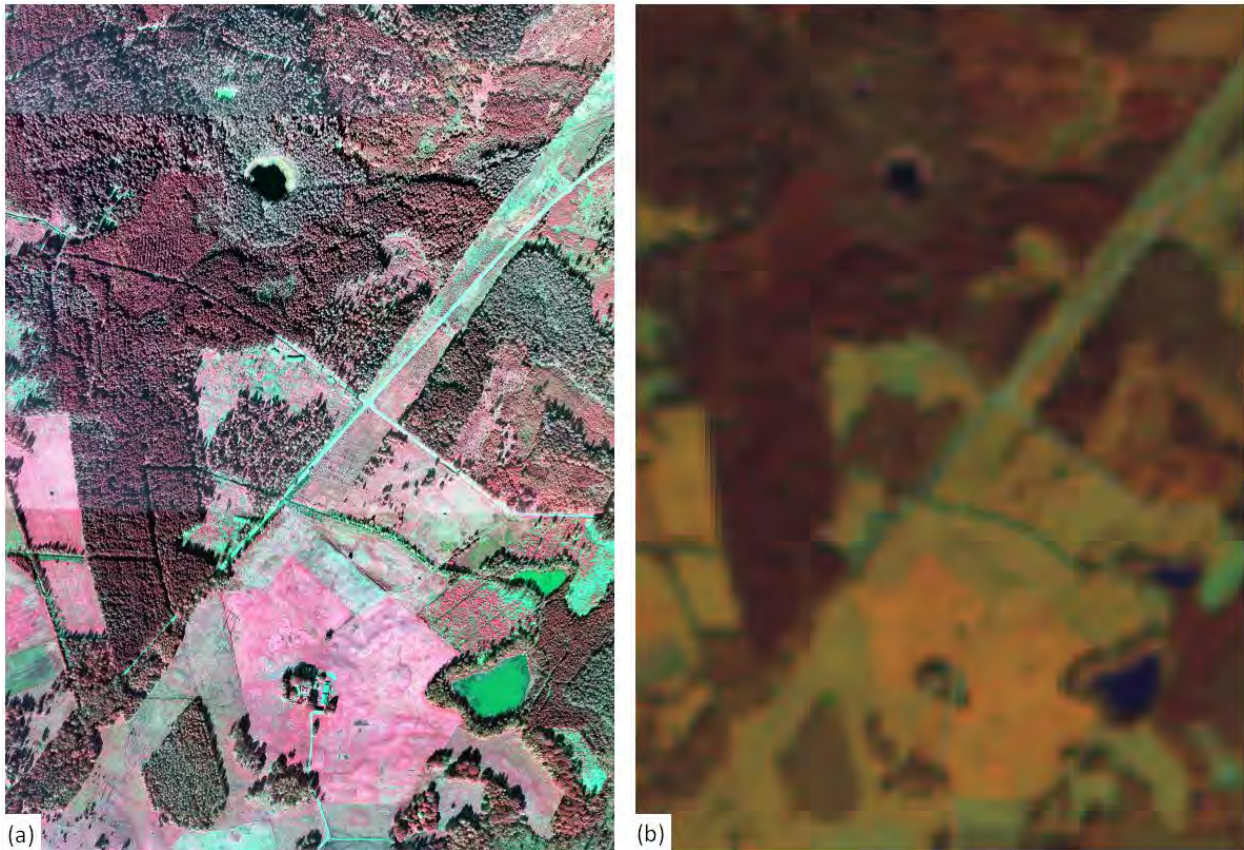


Figure 1. (a) Orthophoto and (b) SPOT 5 image of the test site at Remningstorp used in this study.

Vegetation reference data

The vegetation reference data ('ground truth') was collected through the interpretation of color infrared aerial photos. The photos were acquired by the national land survey at 1200 meters above average ground level in September 2009 using a Z/I DMC digital mapping camera. In total 999 circular sample plots with 10 meter radius were distributed on a regular 40m grid and photo interpreted in a digital photogrammetric work station. Plots falling within the forest, newly clear felled areas and agriculture masks according to the Swedish terrain map were used in the study. Plots that contained two or more classes were excluded, which left a set of 817 plots. The following data were registered per plot: mean basal area weighted tree height (m), tree species composition (percentage of canopy cover), diffuse canopy cover (percentage) and EBONE General Habitat Categories (GHC),

Classification of EBONE General Habitat Categories in a Swedish forest area by using LiDAR in combination with SPOT satellite data

(<http://www.ebone.wur.nl/UK/Project+information+and+products/General+Habitat+Categories/>). The GHC structure has three levels and an optional fourth level of Life Form qualifiers. The first level consists of six supercategories, and the higher levels are derived from definitions. A combination of two habitats can also be used as a GHC. Figure 2 shows the GHCs used in this study. Two classification schemes based on the GHC-classes are used (table 1). They are essentially the same, the only difference being that the agriculture class in scheme 1 is the combination of arable land and pasture land from scheme 2.

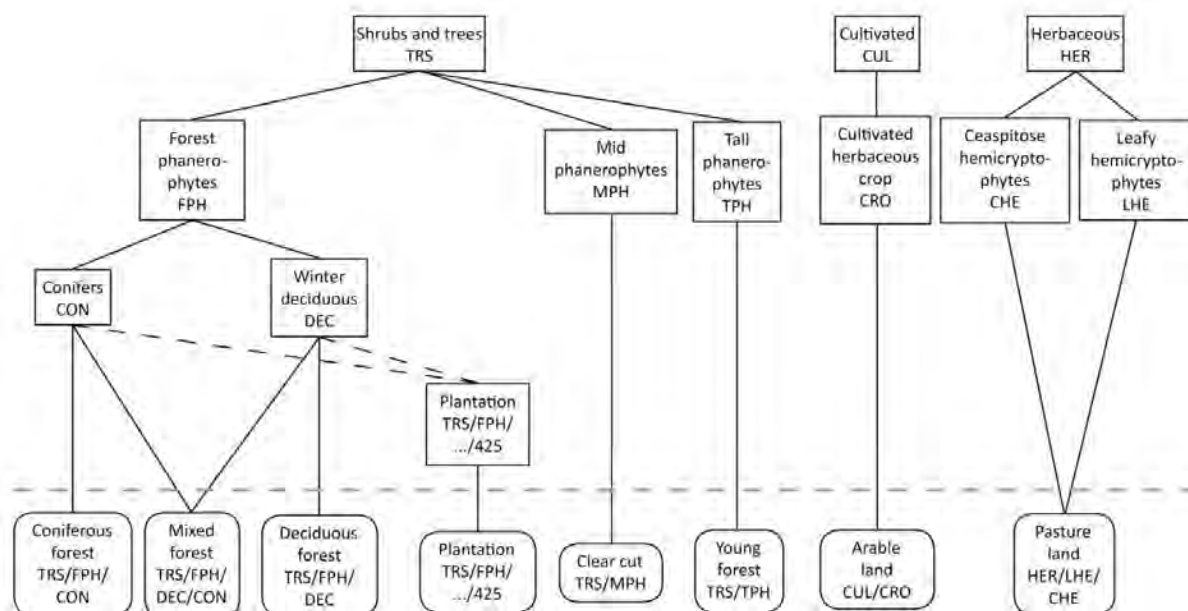


Figure 2. The boxes below the dashed line shows the GHC classes used in this study.

Processing of remote sensing data

Height distributions of laser returns were used to create a raster covering the entire study area. First, the laser returns were classified as ground or vegetation returns using a progressive triangular irregular network densification (TIN) method (Axelsson 1999, 2000) implemented in the TerraScan software (Soininen 2004). A digital elevation model (DEM) was estimated by linear TIN interpolation with the laser returns classified as ground hits. The height value (dz) of a laser return was computed as the difference between the z -value of the laser return and the z -value of the DEM. A height threshold of 10% of the maximum laser height and ≥ 1.0 m was applied in order to separate canopy returns from returns of ground, stones, and low vegetation. Several variables were extracted from laser data within each raster cell, based on the dz distribution of laser returns above the height threshold, and used to calculate raster cell values, one band for each derived variable. The variables were 10th percentile (h_{10}), 20th percentile (h_{20}),..., 100th percentile (h_{100}), and 95th percentile (h_{95}). A vegetation-ratio (V_r) was calculated as the ratio between number of laser returns above the height threshold and total number of returns.

ANNEX-3

Classification of EBONE General Habitat Categories in a Swedish forest area by using LiDAR in combination with SPOT satellite data

Table 1. Class definitions for classification schemes 1 and 2

GHC Class	Explanation	Canopy cover (%)	Tree height (m)	Species composition (%)		N° of plots scheme 1	N° of plots scheme 2
				Coniferous	Deciduous		
TRS/MPH	Clear cut*	0-100	<2	0-100	0-100	83	83
TRS/TPH	Young 2-5 m	0-100	2-5	0-100	0-100	20	20
TRS/FPH	Plantation > 5 m	0-100	>5	0-100	0-100	59	59
TRS/FPH/CON	Coniferous	≥30	>5	≥70	<30	318	318
TRS/FPH/DEC	Deciduous	≥30	>5	<30	≥70	93	93
TRS/FPH/DEC/CON	Mixed	≥30	>5	<70	<70	42	42
CUL/CRO	Arable land	<30	Any	0-100	0-100	-	28
HER/LHE/CHE	Pasture land	<30	Any	0-100	0-100	-	174
CUL/CRO +	Arable and	<30	Any	0-100	0-100	202	-
HER/LHE/CHE	pasture land						

*The plot should show traces of felling, e.g. stumps, machine tracks and debris.

The LiDAR grid cells coincided with the pixels in the SPOT scenes, and each circular ground truth sample plot was centered over four adjacent pixels (figure 3). A training data set was generated by extracting the mean value of these four pixels or grid cells, which corresponds to a resampling of the data to 20 m × 20 m pixels.

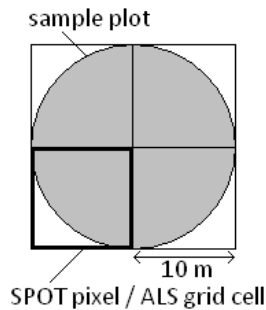


Figure 3. Schematic sketch of a circular sample plot (shaded), centered over four SPOT pixels/LiDAR grid cells.

Two classification methods were tested: maximum likelihood (ML) and Random Forests (RF) (Breiman, 2001). The Minitab 15 statistical software was used for the ML classification, and accuracies were estimated by leave-one-out cross validation. Random Forests was run using the R statistical software version 2.12.0 (<http://www.r-project.org/>). With the RF method, an unbiased estimate of the test set error can be made internally, the so called out-of-bag (OOB) error estimate. For both methods, a first classification was made using the four SPOT bands. Then different combinations of height percentiles and/or vegetation ratio from the LiDAR data were used as additional “bands” with the ML method. A test with ML classification in two steps was also made. In the first step the plots were classified into two height classes, which were then treated separately and classified according to the schemes. RF classification was done using all available height percentiles and the vegetation ratio together with the satellite data. The number of trees used in each RF classification was 1000, and the

ANNEX-3

Classification of EBONE General Habitat Categories in a Swedish forest area by using LiDAR in combination with SPOT satellite data

number of variables tested at each split was 2 when only the SPOT bands were used and 5 when the LiDAR data were added.

Results

Over-all accuracies for the different classifications are shown in tables 2 and 3, together with producer’s accuracies for each class. When satellite and LiDAR data are used together, the over-all accuracy is improved with approximately 6% (ML) and 7% (RF) compared to using SPOT data only. This holds for both classification schemes. For scheme 1, ML classification using SPOT data gave an over-all accuracy of 71.1%. When the height percentile 60 (h60) and the vegetation ratio (Vr) from the LiDAR data were added, the accuracy increased to 77.0%. Random Forests gave over-all accuracies of 77.2 % and 84.1 % for SPOT and SPOT+LiDAR, respectively. The same pattern was observed for scheme 2, but with a few percent lower accuracies: 67.8% and 73.7% with the ML method, and 75.5 % and 82.4 % with RF. The biggest improvement when adding laser data was less confusion between deciduous forest and plantations > 5 m, and between deciduous forest and young forest 2-5 m. Classification in two steps did not improve the result. The RF method gave higher over-all accuracies than ML, and very high accuracies for the largest classes: coniferous > 15 m and pasture land. This is, however, on the expense of the smaller classes, especially mixed and young forest. Attempts with weighting the classes only gave a small improvement (results not shown).

Table 2. Producers and overall accuracies for scheme 1, obtained from leave one-out cross validation for the ML classifier and Out-of-bag estimates in the case of Random Forest (RF)

Method	ML	ML	RF	RF
Bands†	S1-S4 (%)	S1- S4,h60,Vr	S1-S4	S1-S4, all LiDAR
Clear cut	65.1	69.9	67.5	80.7
Young 2-5 m	40.0	55.0	10.0	30.0
Plantation > 5 m	62.7	79.7	61.0	84.7
Coniferous > 5 m	84.9	83.0	94.3	95.3
Deciduous > 5 m	45.2	64.5	60.2	74.2
Mixed > 5 m	38.1	33.3	11.9	9.52
Arable and pasture land	76.2	86.6	87.1	93.1
Over-all	71.1	77.0	77.2	84.1

† S1-S4 are the four SPOT bands, h60 is the LiDAR height percentile 60, Vr is the vegetation ratio and all LiDAR means all available LiDAR features as described in the text.

Table 3. Producers and overall accuracies for scheme 2, obtained from leave one-out cross validation for the ML classifier and Out-of-bag estimates in the case of Random Forest (RF)

Method	ML	ML	RF	RF
Bands	S1-S4	S1-S4,h70	S1-S4	S1-S4, all LiDAR
Clear cut	55.4	73.5	72.3	81.9
Young 2-5 m	40.0	50.0	10.0	30.0
Plantation > 5 m	62.7	83.1	61.0	86.4
Coniferous > 5 m	84.9	83.0	93.7	95.0
Deciduous > 5 m	45.2	65.6	58.1	75.3
Mixed > 5 m	38.1	40.5	16.7	11.9
Arable land	71.4	78.6	46.4	57.1
Pasture land	66.1	67.8	84.5	89.1

Classification of EBONE General Habitat Categories in a Swedish forest area by using LiDAR in combination with SPOT satellite data

Over-all	67.8	73.7	75.5	82.4
----------	------	------	------	------

† S1-S4 are the four SPOT bands, h70 is the LiDAR height percentile 70, and all LiDAR means all available LiDAR features as described in the text.

Discussion

The main objective of this study was to investigate how and to which degree a vegetation classification using optical satellite data can be improved by integrating LiDAR data. It was found that the laser features giving the greatest improvement were h60 and h70, probably because they are more strongly correlated with the mean height than for example h100, which is sensitive to single emergent trees which are taller than the mean. The advantage of LiDAR data can be seen in the case of young forest, which often contains lots of birch before the pre-commercial thinning has been done. Several plots from this class were mistakenly classified as deciduous forest when only satellite data was used. When h60 or h70 was added, the young forest class with its low mean height was more easily separated from the taller deciduous class. In the previous study by Nordkvist et al. (2010), a slightly different classification scheme was used which divided the coniferous forest into two height classes: 5-15 m and > 15 m. The use of LiDAR data improved the accuracies from 51.3% to 74.3% and from 83.8% to 89.3% for these classes, mostly due to reduced confusion between the two of them. This results indicates that the three dimensional information in LiDAR data gives new possibilities to use height classes.

Among the error sources can be mentioned the aerial photo interpretation, since it is based on subjective estimations and the performance of the interpreter is likely to vary. This will affect the quality of the training data, and thus the classification. In an attempt to improve the accuracy in the estimation of canopy cover, the interpreter used a calibration software (Gallegos 2005). The maximum likelihood classification assumes normally distributed training data for each class, which is not always the case in our data set. The distance between sample plots is small, which may lead to auto-correlation in the training data set.

Further studies will be performed using data from the national LiDAR dataset (approx. 0.5 pulses/m²) to evaluate the potential of this method for forest mapping on a national scale. Mire classes, that were to rare in the Remningstorp test site, will then be included. One way to improve separation of the mixed forest class could be to use two satellite scenes over the same area, acquired under leaf on and leaf off conditions, respectively.

Acknowledgements

This study is part of the EU FP7 Project European Biodiversity Observation Network (EBONE). It is based on material financed by the Swedish National Space Board and the EMMA research programme financed by the Swedish Environmental Protection Agency. The Swedish National Land Survey contributed with the air photos.

References

- Bork, E. W. and Su, J. G. 2007. Integrating LiDAR data and multispectral imagery for enhanced classification of rangeland vegetation: A meta analysis. *Remote Sensing of Environment*, 111:11-24.
- Breiman, L. 2001. Random Forests. *Machine Learning*, 45:5-32.
- Chust, G., Galparsoro, I., Borja, A., Franco, J., and Uriarte, A. 2008. Coastal and estuarine habitat mapping, using LiDAR height and intensity and multi-spectral imagery. *Estuarine Coastal and Shelf Science*, 78:633-643.
- Engberg, A. 2005. Produktspecifikation av svenska CORINE Marktäckedata. Lantmäteriet Gävle

Classification of EBONE General Habitat Categories in a Swedish forest area by using LiDAR in combination with SPOT satellite data

-
- Erdody, T. L. and Moskal, L. M. 2010. Fusion of LiDAR and imagery for estimating forest canopy fuels. *Remote Sensing of Environment*, 114:725-737.
- Friedl, M.A., McIver, D.K., Hodges, J.C.F., Zhang, X.Y., Muchoney, D., Strahler, A.H., Woodcock, C.E., Gopal, S., Schneider, A., Cooper, A., Baccini, A., Gao, F., and Schaaf, C. 2002. Global land cover mapping from MODIS: algorithms and early results. *Remote Sensing of Environment*, 83:287-302.
- Fuller, R.M., Groom, G.B., and Jones, A.R. 1994. The Land Cover Map of Great Britain: an automated classification of Landsat Thematic Mapper data. *Photogrammetric Engineering and Remote Sensing*, 60:553-562.
- Genc, L., Dewitt, B., and Smith, S. 2004. Determination of wetland vegetation height with LiDAR. *Turkish Journal of Agriculture and Forestry*, 28:63-71.
- Hagner, O., Reese, H. 2007. A method for calibrated maximum likelihood classification of forest types. *Remote Sensing of Environment*, 110:438-444.
- Hill, R. A., and Thomson, A. G. 2005. Mapping woodland species composition and structure using airborne spectral and LiDAR data. *International Journal of Remote Sensing*, 26:3763-3779.
- Holmgren, J., Persson, A., and Soderman, U. 2008. Species identification of individual trees by combining high resolution LiDAR data with multi-spectral images. *International Journal of Remote Sensing*, 29:1537-1552.
- Hudak, A. T., Lefsky, M. A., Cohen, W. B., and Berterretche, M. 2002. Integration of LiDAR and Landsat ETM plus data for estimating and mapping forest canopy height. *Remote Sensing of Environment*, 82:397-416.
- Hyde, P., Dubayah, R., Walker, W., Blair, J. B., Hofton, M., and Hunsaker, C. 2006. Mapping forest structure for wildlife habitat analysis using multi-sensor (LiDAR, SAR/InSAR, ETM plus, Quickbird) synergy. *Remote Sensing of Environment*, 102:63-73.
- Ke, Y., H., Quackenbush, L. J., and Im, J. 2010. Synergistic use of QuickBird multispectral imagery and LiDAR data for object-based forest species classification. *Remote Sensing of Environment*, 114:1141-1154.
- Korpela, I., Koskinen, M., Vasander, H., Holopainen, M., and Minkinen, K. 2009. Airborne small-footprint discrete-return LiDAR data in the assessment of boreal mire surface patterns, vegetation, and habitats. *Forest Ecology and Management*, 258:1549-1566.
- Lee D. S. and Shan, J. 2003. Combining LiDAR elevation data and IKONOS multispectral imagery for coastal classification mapping. *Marine Geodesy*, 26:117-127.
- Granhlm, A., Nilsson, M., and Holmgren, J. 2010. Combining optical satellite data and airborne laser scanner data for vegetation classification. *SilviLaser*, September 14-17 2010, Freiburg, Germany.
- Reese, H. M., Lillesand, T. M., Nagel, D. E., Stewart, J. S., Goldmann, R. A., Simmons, T. E., Chipman, J. W., and Tessar, P. A. 2002. Statewide land cover derived from multiseasonal Landsat TM data – A retrospective of the WISCLAND project. *Remote Sensing of Environment*, 82:224-237.

Annex-4



Studying the vertical accuracy of LiDAR data in different vegetation types and using LiDAR data with combination of aerial images to classify EBONE General Habitats Categories in Estonia

Ants Vain, Janar Raet, Kalev Sepp, Tambet Kikas
Department of Landscape Management and Nature Conservation
Institute of Agricultural and Environmental Sciences
Estonian University of Life Sciences (EULS)
Tartu Estonia

e-mail: ants.vain@emu.ee

ANNEX - 4

Studying the vertical accuracy of LiDAR data in different vegetation types and using LiDAR data with combination of aerial images to classify EBONE General Habitats Categories in Estonia

Abstract

LiDAR technology is an important development in the field of remote sensing for delivering high detailed and accurate digital elevation models (DEM). As a result nationwide coverage is expected to be increasingly common across Europe. The purpose of the work presented was to find out if LiDAR can help improve the identification of GHC and whether different flight specifications such as altitude could affect the effectiveness of LiDAR in this role. More specifically we looked at how the penetration level of LiDAR affects the vertical accuracy of the DEM and subsequently derived height estimates. LiDAR data provides a bulk of points that can be used to form a 3D model of the environment. Different types of vegetation have different effects on the penetration rate of the laser beam. Asphalt road, crop fields, natural hayfields and different forest types were used in this study to see how well the laser beam can penetrate to ground level in different conditions. The lower dense vegetation had a considerable effect on the Z (height) component of LiDAR points. The vertical accuracy of the DEM derived from the 2400 m (flight altitude) national wide ALS (Airborne Laser Scanning) data and the 1300 m special flight data were similar. 2400 m data has lower point resolution, therefore less points under canopy.

Also, the possibility to use LiDAR data in combination with aerial images and RGB values assigned to individual LiDAR points were studied. The combination of LiDAR and aerial image gave a better overview of the studied area and made linear objects visible, and therefore more easily recognizable.

ANNEX - 4

Studying the vertical accuracy of LiDAR data in different vegetation types and using LiDAR data with combination of aerial images to classify EBONE General Habitats Categories in Estonia

1. Airborne Laser Scanning in Estonia

The first ALS project in Estonia was carried out in 2004 when an Optech scanner was used to measure roads in North and North-East part of Estonia. In 2008 the Estonian Land Board (ELB) bought an airplane and Leica ALS50-II scanner. This started a new project of which its goal was to produce an elevation model for all of Estonia. The main task was to use this elevation model to correct aerial images. But ALS data can be used for other purposes as well (forestry, mapping flooded areas, mining etc).

1.1. ALS50-II scanner

The Leica ALS50-II scanner is a time-of-flight (TOF) based scanner. It means that it uses the time measurements between output and input laser pulse to calculate the distance from sensor to the object. The ALS50-II scanner can operate on altitudes from 200 m to 6000 m. The maximum scan rate is 90 Hz (scan lines per second), maximum pulse rate is 150 kHz (pulses per second). The ALS50-II scanner has an option to use multiple pulses in the air (MPiA). It means that the laser can shoot out the next pulse even though the previous pulse has not been returned yet. MPiA starts to operate at the altitude of 1200 m and it gives the users much more returns per square meter. The number of returns per pulse that the ALS50-II scanner can record is 4 (first, second, third and last) and the number of intensities is 3 (first, second, third). Maximum scan angle is 75° and it can record up to 300 GB of data.



Fig. 2. ALS50-II scanner setup.

The ALS50-II scanner has also an extra feature that previous versions did not have. It is called *Automatic Gain Control (AGC)*. Its main purpose is to reduce ringing effect and therefore increase the number of points detected. But AGC has also an effect on intensity values and

ANNEX - 4

Studying the vertical accuracy of LiDAR data in different vegetation types and using LiDAR data with combination of aerial images to classify EBONE General Habitats Categories in Estonia

therefore should be corrected (Vain et al., 2010 and Korpela et al., 2010). This makes the use of intensity data a little bit complex, especially around water object where intensity could deviate a lot due to the AGC effect (Vain et al., 2010).

1.2. National wide ALS measurements in Estonia

The Estonian Land Board (ELB) is equipped with an ADS40 digital camera and an ALS50-II laser scanner that are mounted on a Cessna Grand Caravan 208B airplane. This combination of aerial camera and laser scanner provides aerial images simultaneously with laser points.



Fig. 3. Aerial camera ADS40 and ALS50-II scanner mounted on airplane.

The purpose of ALS measurements for ELB is to get digital elevation model for all of Estonia which can be used to correct aerial images. The main altitude is 2400 m above ground level that gives a 0.45 pts/m^2 density and maximum point distance of 2.6 m. The laser footprint size on the ground is 54 cm and the accuracy of the height component is estimated by ELB to be from 0.07 to 0.12 cm.

ANNEX - 4

Studying the vertical accuracy of LiDAR data in different vegetation types and using LiDAR data with combination of aerial images to classify EBONE General Habitats Categories in Estonia

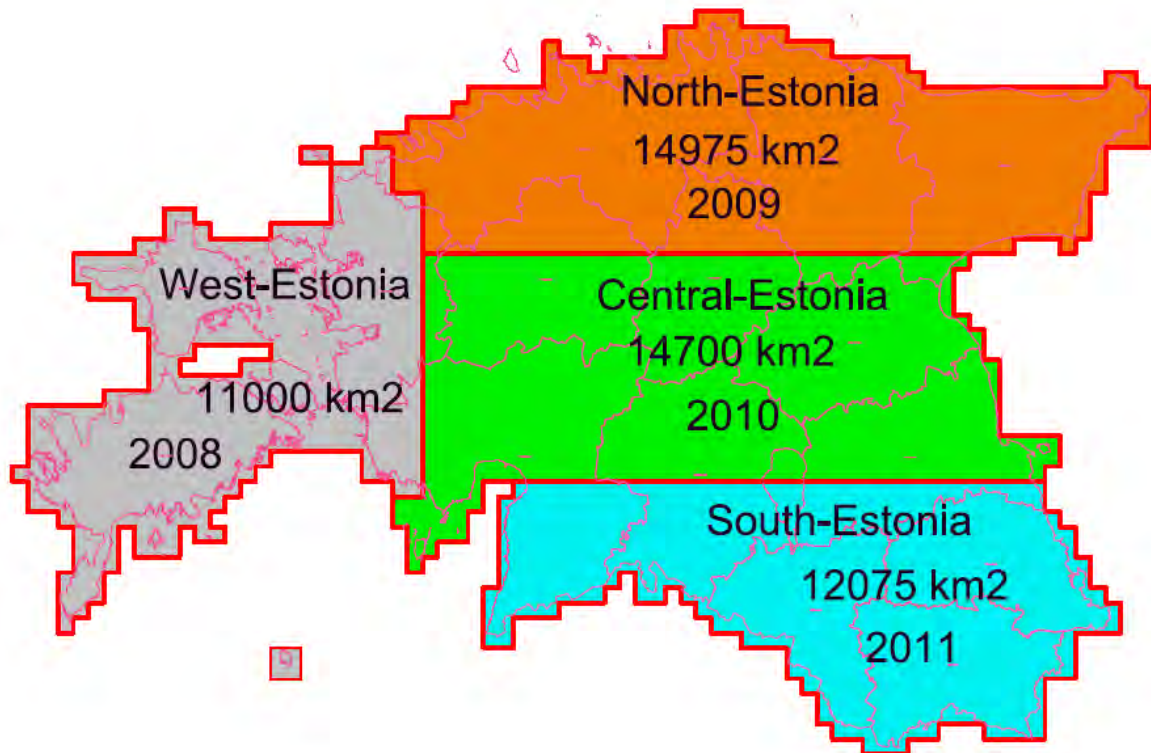


Fig. 4. Coverage of ALS measurements in Estonia by ELB.

Most of Estonia is or will be covered with ALS data acquired at 2400m altitude by the autumn 2011. The city of Tallinn and the city of Pärnu are covered with 1500 m altitude data. For agricultural and forestry purposes a 3800 m altitude was used in South-Estonia.

The data can be bought from ELB in ASCII format. 2400 m and 3800 m flights are classified into 3 classes:

- 1) Unclassified;
- 2) Ground;
- 3) Noise.

The 1500 m flights for cities are classified into 4 classes:

- 1) Unclassified;
- 2) Ground;
- 3) Buildings;
- 4) Noise.

Unclassified points are those that are above the ground (e.g. vegetation). The ASCII format contains 6 columns:

- 1) Class (e.g. ground);
- 2) X;
- 3) Y;
- 4) Z;
- 5) Intensity;
- 6) Echo type.

ANNEX - 4

Studying the vertical accuracy of LiDAR data in different vegetation types and using LiDAR data with combination of aerial images to classify EBONE General Habitats Categories in Estonia

The intensity value is recorded in 8-bit range (0 to 255) and describes the backscattering properties of the observed object. Echo type describes the return type (ALS50-II can record up to 4 returns from one pulse):

- Only – only return from one pulse;
- First – first return from one pulse (usually a tree top);
- Intermediate – any intermediate return, but not the first or last return from one pulse (higher grass or middle points from the trees);
- Last – last return of the pulse (ground or e.g. grass).

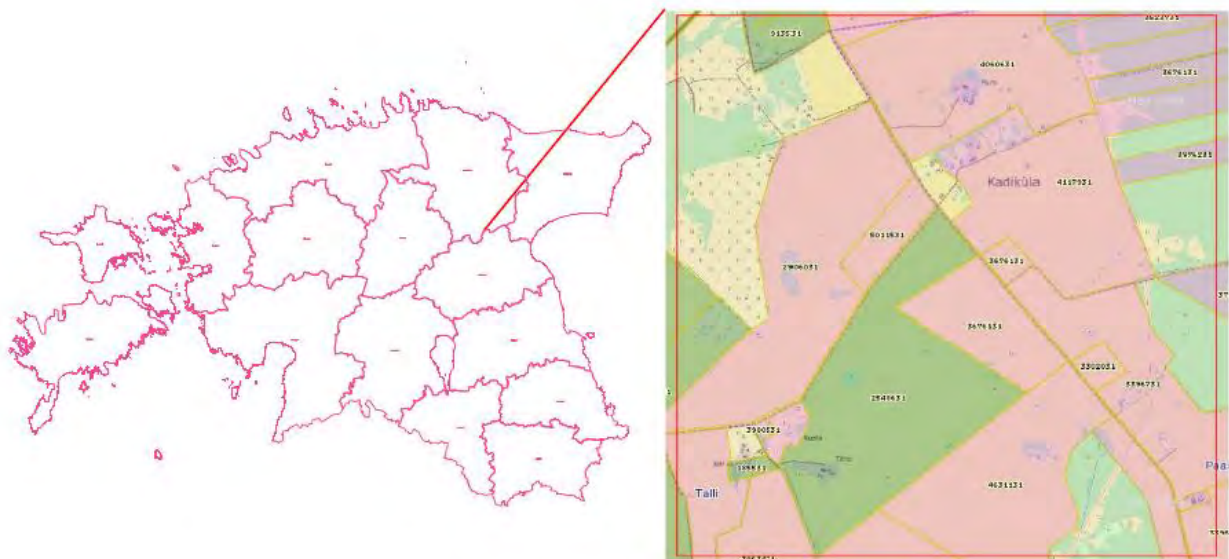
2. Study aims

The purpose of our bit of work was to study the vertical accuracy of laser points over different type of vegetation. Trees and especially lower vegetation has an influence on the vertical accuracy of laser points. Therefore, different vegetation types were chosen for this comparison. These different vegetation plots were measured with RTK GPS and total station and there results were compared with laser points from ALS. The results from this study give us a rough estimation of what kind of vertical accuracy we can expect from different vegetation types.

The second part of this study was to test different methods for extracting GHC types from laser data. Using echo information and height data the automatic area classification was established (see Fig. 16 and Fig. 16). This kind of approach is good for extracting forested areas from crop fields and classifies these forests according to the tree heights.

3. Test flight in Emumäe

A special flight was ordered from ELB over the test area in Emumäe, Central-Estonia (see Fig. 5).



ANNEX - 4

Studying the vertical accuracy of LiDAR data in different vegetation types and using LiDAR data with combination of aerial images to classify EBONE General Habitats Categories in Estonia

Fig. 5. Test area in Emumäe, Central-Estonia. The area is 2x2 km.

The test area is 2x2 km in dimension and has mainly agricultural coverage. In the north-west part of the area, there is a forest of mixed tree species (mainly leafy trees).

The ALS measurements were acquired in August 2010 with the ALS50-II scanner. The flying altitude was 1300 m (because the MPiA system starts to operate at 1200 m it gave us more points per square meter), the field of view was 40 degrees, the pulse repetition frequency 150 kHz, scan rate was 45 Hz and the average point density was 5-6 pts/m². The total number of flightlines was 6, three of them in north-south direction and three in west-east direction. This gives double the point density compared to three parallel flightlines. The flightlines are shown in Fig. 6.

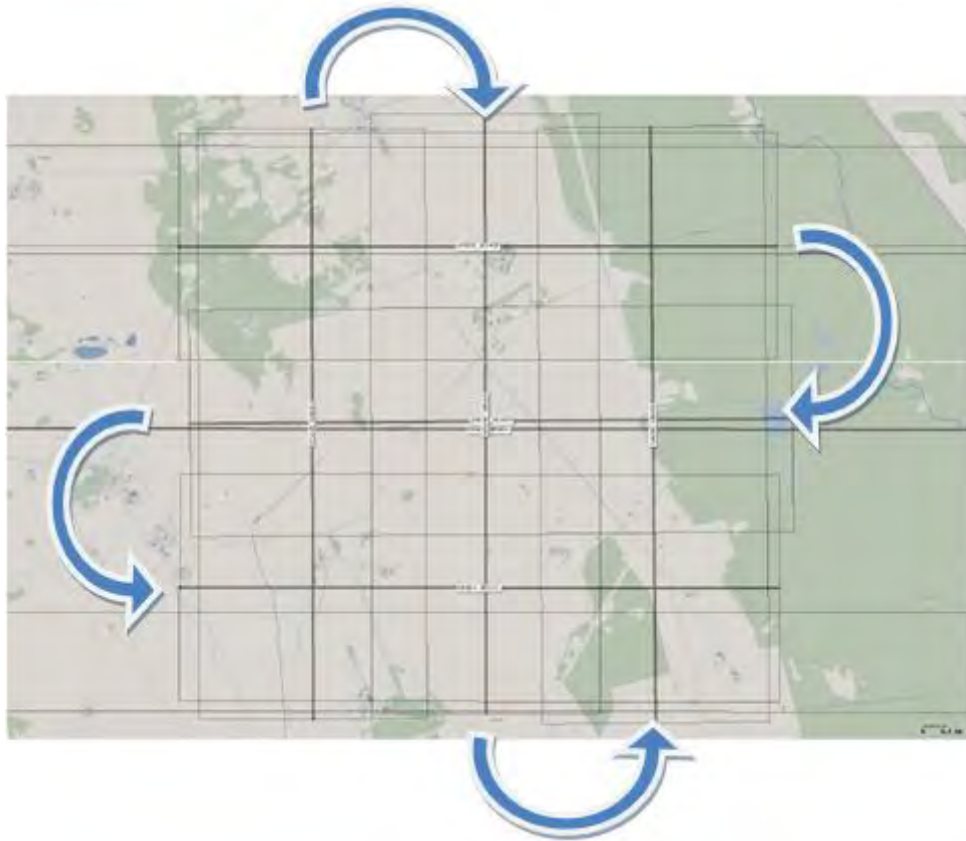


Fig. 6. Flightlines in the Emumäe test area: 3 flightlines in north-south direction and three in west-east direction.

The second set of ALS data that was used was sourced from the nationwide 2400m ALS ELB acquisitions of summer 2010.

4. Field work

The field work involved two activities:

ANNEX - 4

Studying the vertical accuracy of LiDAR data in different vegetation types and using LiDAR data with combination of aerial images to classify EBONE General Habitats Categories in Estonia

1. A field survey to characterise the habitats present within the 2kmx2km area. This was done during the summer of 2010 and following the “Handbook for Surveillance and Monitoring of Habitats, Vegetation and Selected Species“ (Bunce et al., 2010). The results are shown on Fig. 7.
2. The collection of surface height measurements for different types of vegetation (forest, grass) and for different surfaces (asphalt, cut or uncut grass). In total 9 small areas were chosen and measured with a total station and RTK (*Real Time Kinematic*) GPS (*Global Positioning System*). The chosen areas are shown in Fig. 8. The “Uncut CRO 1” and “Uncut CRO 2” are areas where crop has not yet been cut and has a height of about 70-80 cm. The “Cut CRO 1” and “Cut CRO 2” are areas where crop has already been cut and the laser can reach the ground. “Asphalt road” is a 100 m section of asphalt road. “Forest 1” is an area where the taller vegetation is not very dense but the understorey vegetation is very dense. “Forest 2” has a dense layer of tall vegetation but almost no understorey vegetation. “Slope” is a temporary road area in a natural hay area where the grass is short and the tilt of the road is about 20%. “Natural hay” represents an area where there has not been any agricultural activity for a long time and the height of the grass is about 50-60 cm.



ANNEX - 4

Studying the vertical accuracy of LiDAR data in different vegetation types and using LiDAR data with combination of aerial images to classify EBONE General Habitats Categories in Estonia

Fig. 6. GHC as recorded during the fieldwork on the Emumäe test area in summer 2010.

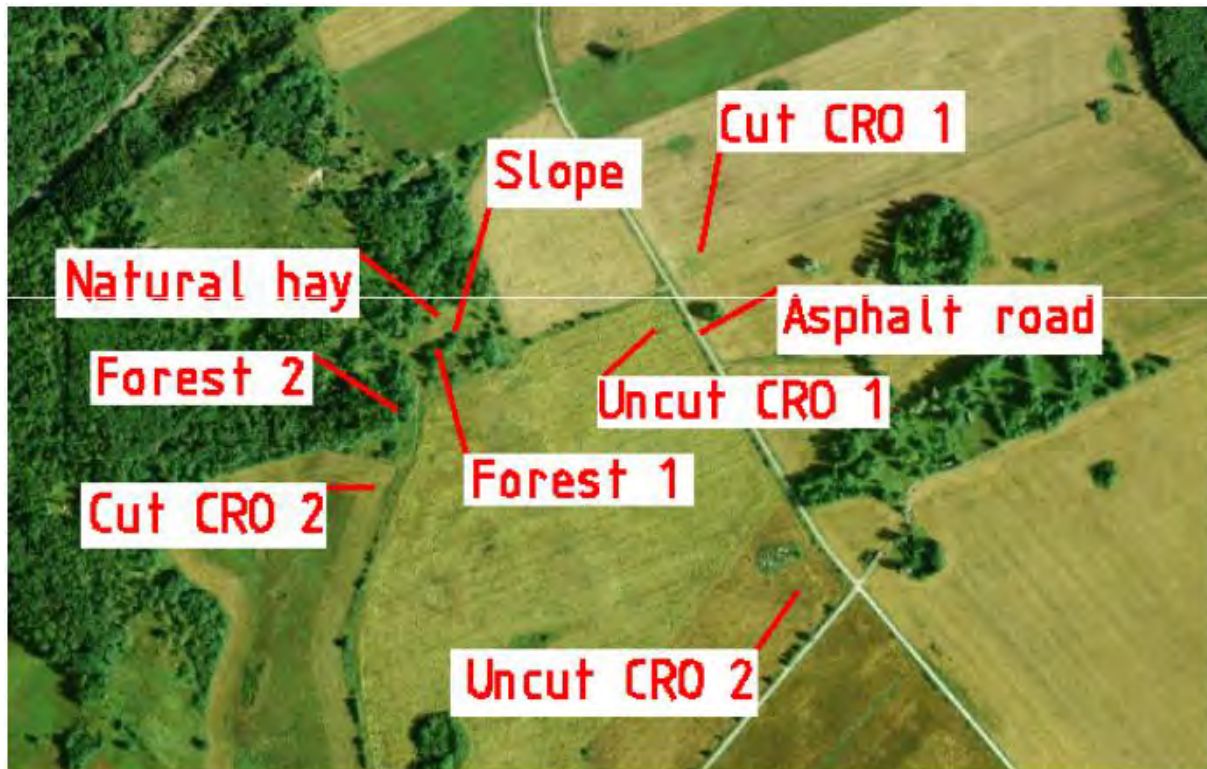


Fig. 8. The location of the 9 different areas within the test area of Emumäe where the surface height measurement were taken.

5. In-situ –LiDAR comparison

The field measurement points were compared to the ALS points (1300 m and 2400 m) for all the 9 different areas. This comparison shows us how well the laser can penetrate through different type of vegetation. The results for 1300 m data are in Fig. 9 and for 2400 m data in Fig. 10.

ANNEX - 4

Studying the vertical accuracy of LiDAR data in different vegetation types and using LiDAR data with combination of aerial images to classify EBONE General Habitats Categories in Estonia

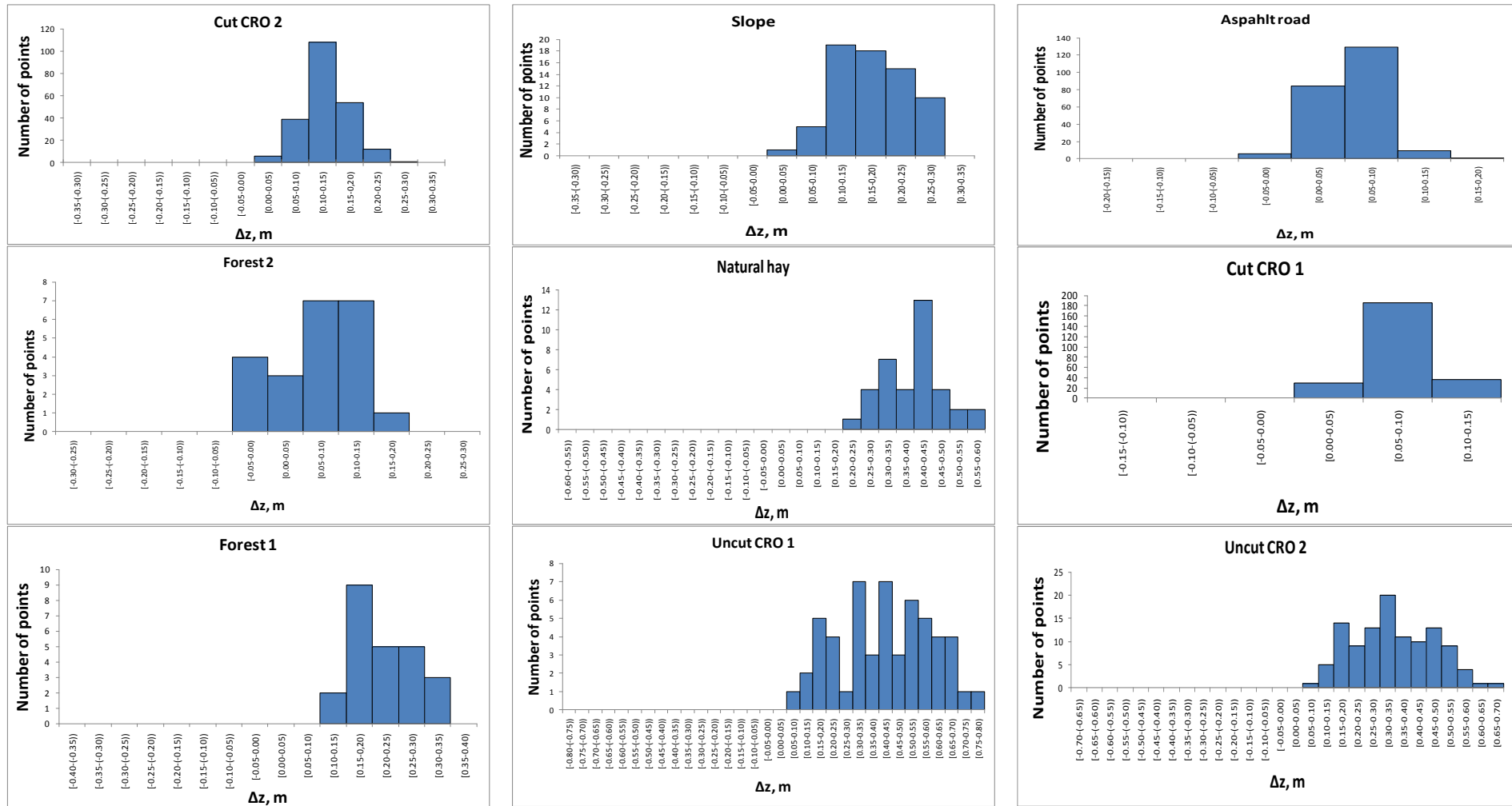
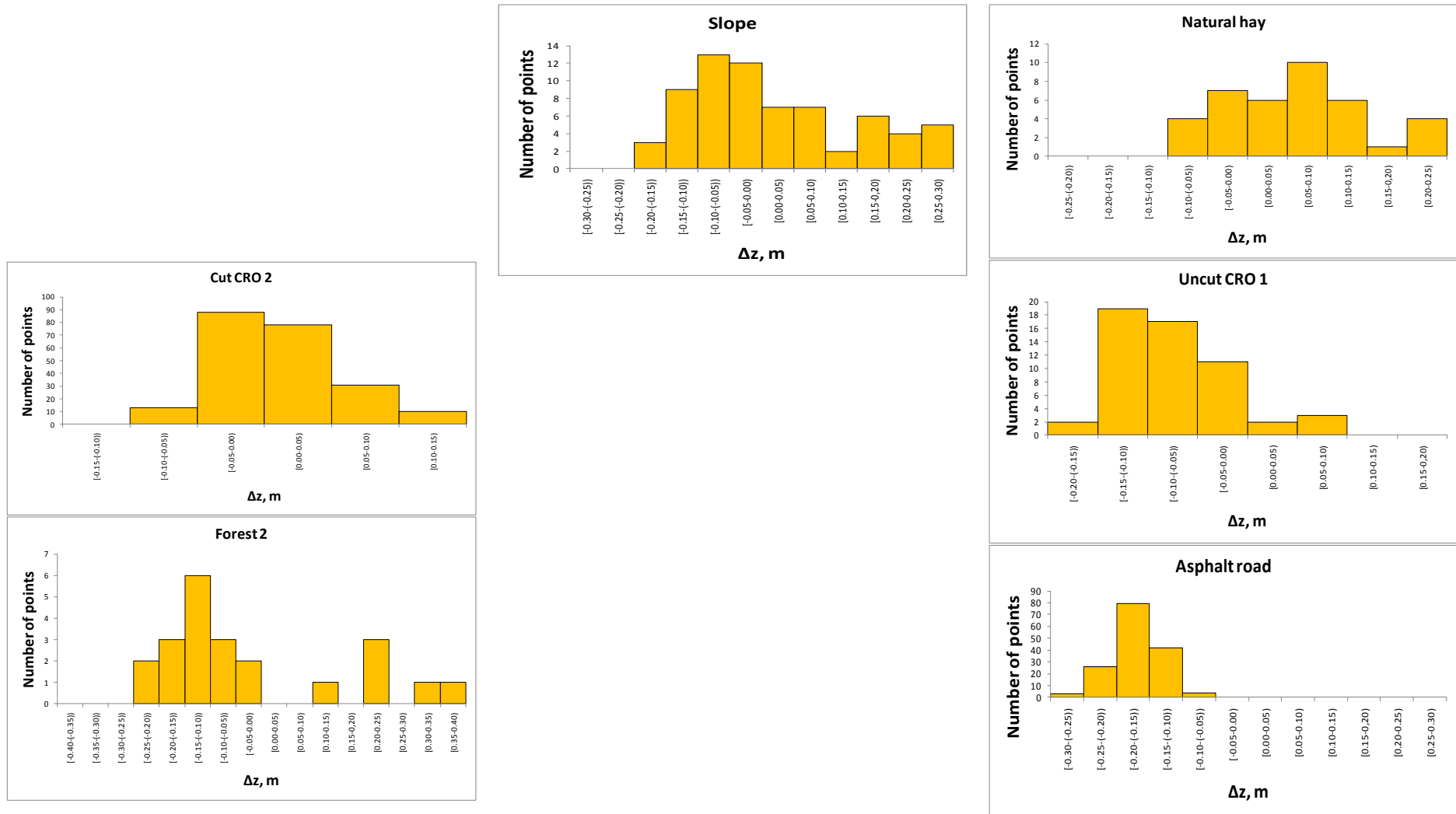


Fig. 9. Vertical differences of 1300m laser points from field measurements.

ANNEX - 4

Studying the vertical accuracy of LiDAR data in different vegetation types and using LiDAR data with combination of aerial images to classify EBONE General Habitats Categories in Estonia



ANNEX - 4

Studying the vertical accuracy of LiDAR data in different vegetation types and using LiDAR data with combination of aerial images to classify EBONE General Habitats Categories in Estonia

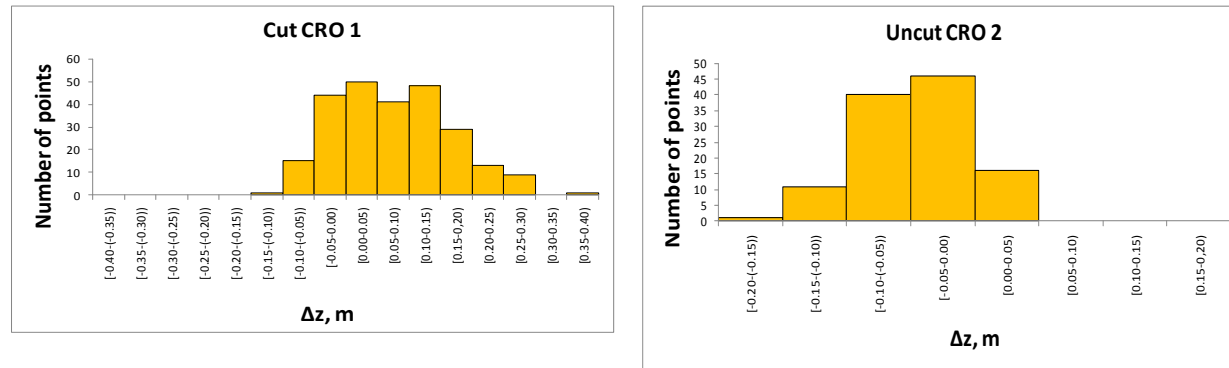


Fig. 10. Vertical differences of 2400m laser points from field measurements.

ANNEX - 4

Studying the vertical accuracy of LiDAR data in different vegetation types and using LiDAR data with combination of aerial images to classify EBONE General Habitats Categories in Estonia

From the results in Fig. 10 we can see that there were no laser points from 2400 m in “Forest 1” area because the density of lower vegetation in that area was high. The “Cut CRO 1” and “Cut CRO 2” are quite close to the field measurement data. Most of the laser points are up to 15 cm higher. The “Uncut CRO 1” and “Uncut CRO 2” show the same results which is caused by the fact that the ELB data from the Emumäe test area was gathered in June which means that the crop was still quite low. The “Forest 2” area shows that the distribution of laser points beneath the forest canopy can be very different due to the density of vegetation. Therefore the accuracy and penetration of the laser point can vary quite much. The “Slope” pit was measured to see if there is a difference in height component with the tilted ground. Most of the laser points are within +/- 10 cm which can be considered as a good result from 2400 m altitude. In theory there should be a difference in Z value from the areas with rough topography (Baltsavas, 1999). Put in practice it cancels out with the modelling of the surface because then average values are calculated. The “Natural hay” pit shows that the 90% of the laser points are within -10 to +15 cm, which can be explained also with the flight time (June 2010). The “Asphalt road” distribution is quite close to normal distribution which is expected since asphalt is a stable target and has been used well as a calibration target for ALS intensity (Vain et al., 2009; Coren and Strezai, 2006).

The “Cut CRO 1” and “Cut CRO 2” from 1300 m altitude showed similar results. They both are close to normal distribution; “Cut CRO 1” has a smaller error (10 cm) and “Cut CRO 2” a little bit larger (up to 25 cm). The “Uncut CRO 1” and “Uncut CRO 2” produced results that were expected. The crop was about 70 cm in height and as we can see from Fig. 9 and Fig. 10 then the distribution of errors are not close to normal distribution and can vary from 5 cm up to 85 cm. This is quite expected because the laser points cannot penetrate through rough vegetation. The “Forest 1” pit has laser points from 1300 m that have reached through the vegetation but they are 20-40 cm higher than field measurements which is caused by the dense lower vegetation. But the comparison of 1300 m and 2400 m data for “Forest 2” pit shows that the probability of laser to penetrate through the higher and lower vegetation is higher with lower flying altitude due to the fact that there is less atmosphere between the laser and object, therefore less energy losses and more chance to get stronger response back to the detector (see more detailed information about the physical background of ALS systems in Wagner, 2010). The “Slope” showed quite similar results to 2400 m data, but the distribution of errors is closer to normal distribution. The “Natural hay” shows that the laser points are 30-40 cm higher than the ground and we can see that it is more than with 2400 m data which can be also explained with the flight time and the growth of vegetation. The “Asphalt road” is very well distributed and showed good results (almost 95% are within 10 cm).

5.1. RGB and intensity images

The possibility to use intensity data that is recorded simultaneously with position information (X, Y and Z) and the combination of RGB and LiDAR data was also tested to see whether it helps to speed up the classification procedure.

The intensity describes the backscattering properties of the target (Kaasalainen et al., 2005) and therefore is an additional information source about the object. The intensity image is usually used as a background data and it helps to understand the studied area better (see Fig. 11).

ANNEX - 4

Studying the vertical accuracy of LiDAR data in different vegetation types and using LiDAR data with combination of aerial images to classify EBONE General Habitats Categories in Estonia

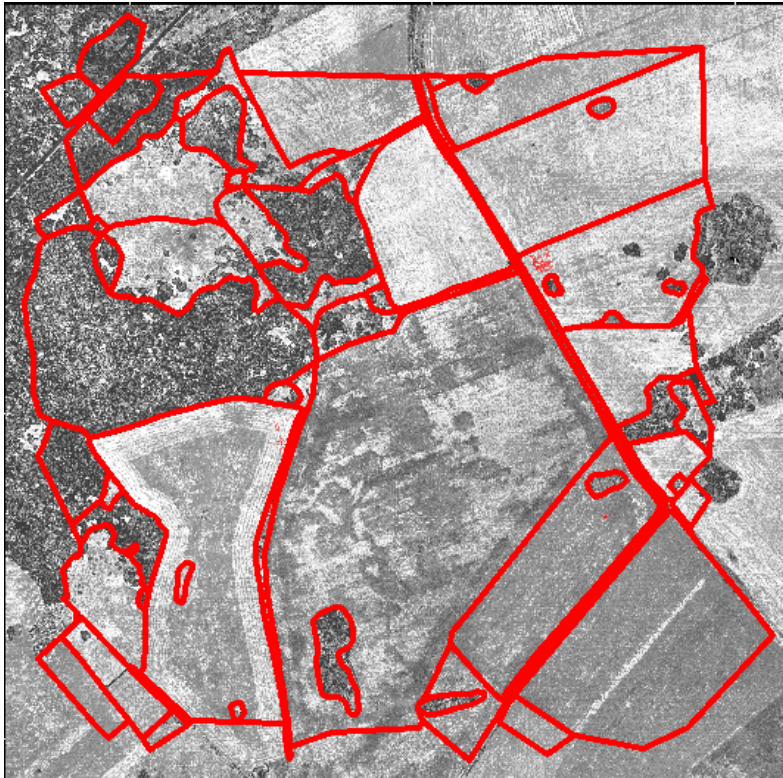


Fig. 11. The intensity image used as a background for field measurement results.

The negative side of the intensity image is that it is monochromatic and therefore all objects are not visible. The other option is to assign RGB values from areal images to individual laser points (see Fig. 12). This makes the laser data similar to aerial image, but we do not need stereo equipment to see it in “3D”.

ANNEX - 4

Studying the vertical accuracy of LiDAR data in different vegetation types and using LiDAR data with combination of aerial images to classify EBONE General Habitats Categories in Estonia



Fig. 12. RGB values from aerial image has been assigned to individual laser points.

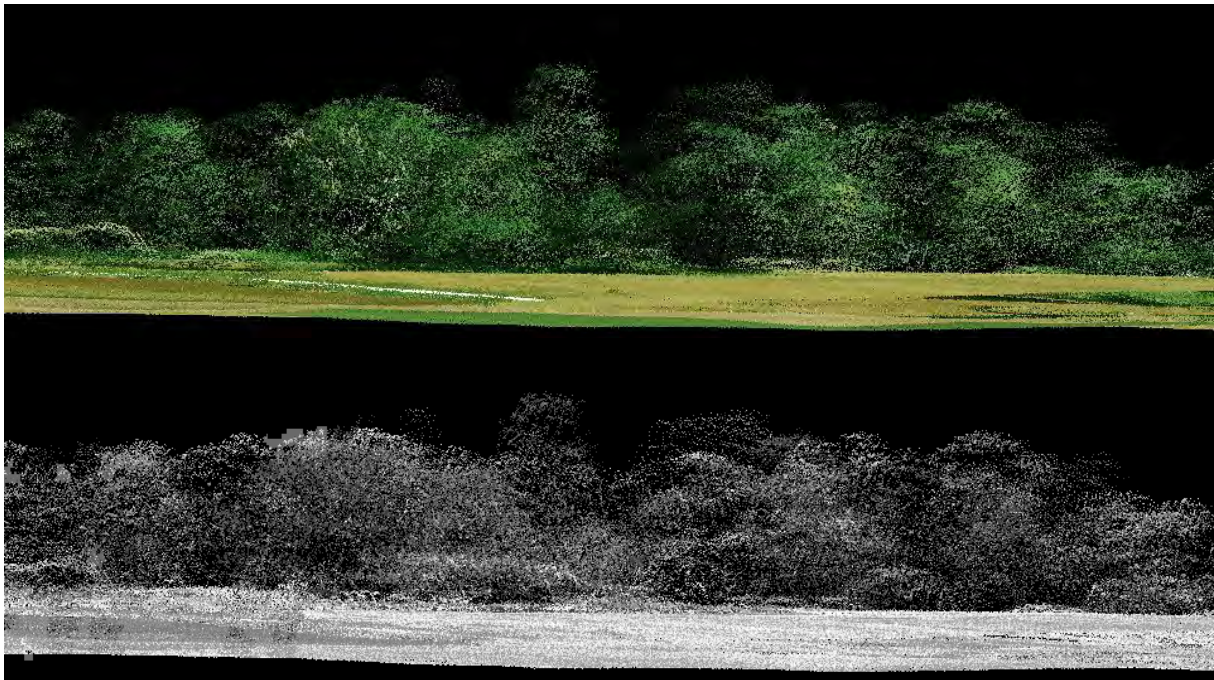


Fig. 13. Profile of the same area. RGB values have been used on the top image and intensity data on the bottom.

As we can see from Fig. 12 and Fig. 13 the RGB values have giving the laser data much more information about the objects, especially linear object (see Fig. 13 where the road in white colour is visible on the RGB image).

ANNEX - 4

Studying the vertical accuracy of LiDAR data in different vegetation types and using LiDAR data with combination of aerial images to classify EBONE General Habitats Categories in Estonia

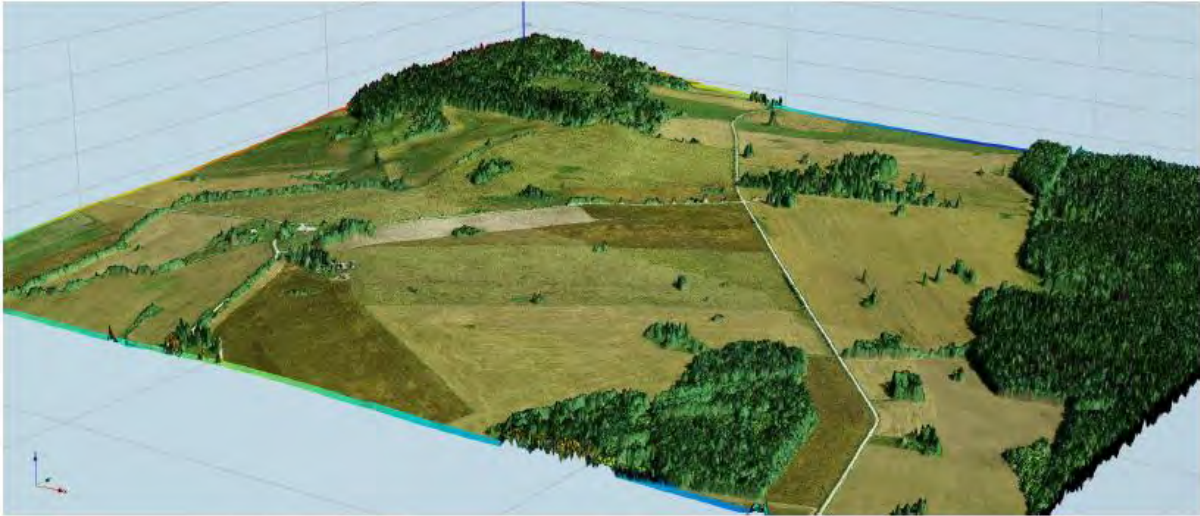


Fig. 14. 3D image of the combination of aerial image and LiDAR data.

The combination of aerial image and LiDAR data is useful for mapping and detecting individual small object (see Fig. 14). Also linear object are very well visible and the understanding of the environment is much better than using just aerial image or just LiDAR data.

5.2. Elements extracted from LiDAR data

Forest

Using the echo data we can extract data points that represent the forest areas. Since the forest areas have several echoes from single pulse we can use that information and select only these areas that have several echoes.

ANNEX - 4

Studying the vertical accuracy of LiDAR data in different vegetation types and using LiDAR data with combination of aerial images to classify EBONE General Habitats Categories in Estonia

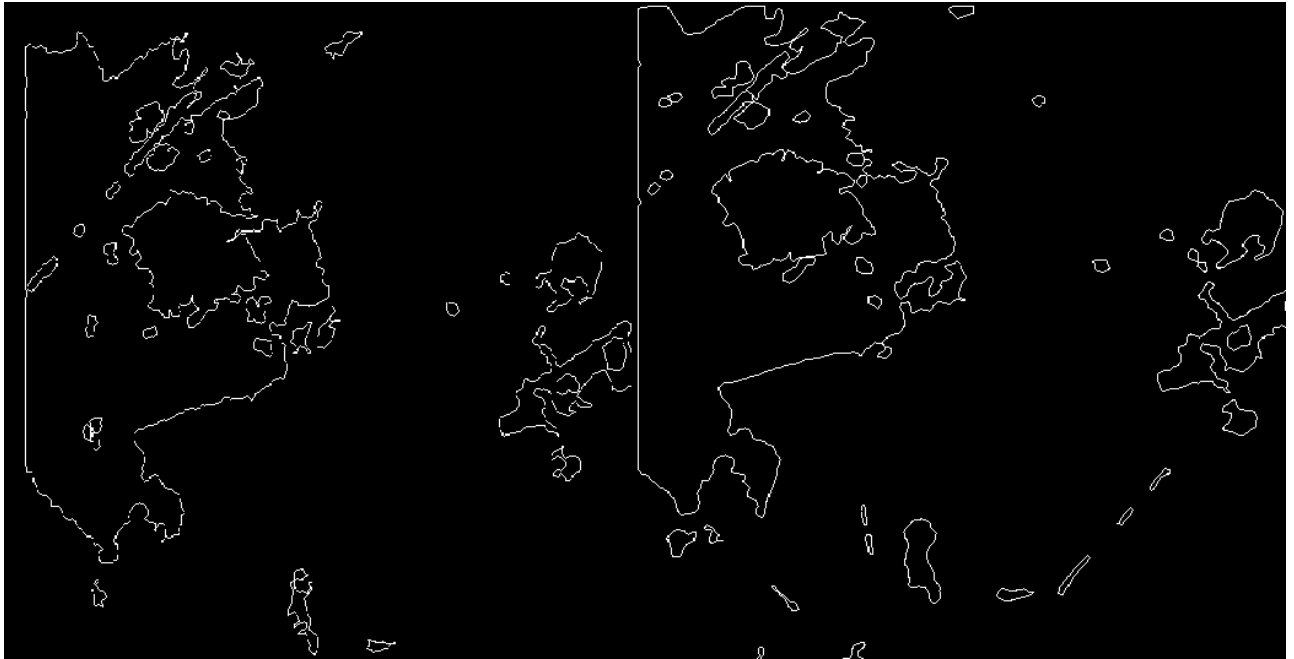


Fig. 15. Left: 2400 m echo data used to isolate forest areas. Right: 1300 m echo data used to isolate forest areas.

As we can see from Fig. 15 then data points that are from the forest areas can be isolated using echo information. The 1300 m data is more representative to the actual situation and give more detailed information about the studied area. The minimum size of the area was 400 m² and the minimum gap between data points was 10 m. Comparing the result to the filed measurements we can see that the level of detail is much higher and some areas are even left out because they did not fit to the minimum size requirements (see Fig. 16). And we can also notice that the areas extracted from 1300 m data have formed 3 different areas (south-east part of the picture) instead of one as it was done during the field measurements. Notice that these areas are missing from 2400 m image.

ANNEX - 4

Studying the vertical accuracy of LiDAR data in different vegetation types and using LiDAR data with combination of aerial images to classify EBONE General Habitats Categories in Estonia



Fig. 16. White line represents the areas automatically drawn from LiDAR data and red lines are the areas from field measurements.

The same solution can be used for mapping individual elements (single trees e.g.) that are within 100 m² and 400 m².

Using the echo information we can also see the height distribution of the vegetation. For that we simply classify points from ground level according to the height from ground. As we can see from Fig. 17 the points are with different colours according to the distance from ground level. The ground level itself is coloured white; vegetation up to 2 m from ground is light blue, 2-5 meters dark blue, 5-15 meters light green and 15-40 meters is red. These categories are taken from the “Handbook for Surveillance and Monitoring of Habitats, Vegetation and Selected Species“ (Bunce et al., 2010) but they can be changed according to the needs.

ANNEX - 4

Studying the vertical accuracy of LiDAR data in different vegetation types and using LiDAR data with combination of aerial images to classify EBONE General Habitats Categories in Estonia

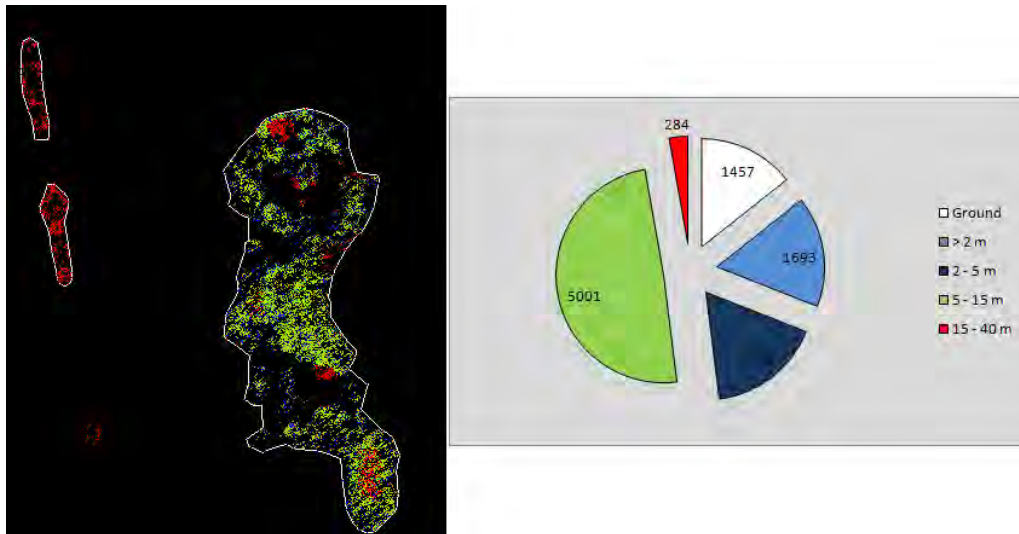


Fig. 17. Area classified according to the height from ground. The right sector diagram shows the distribution of points. Almost 50% of the points are 5-15 m from ground.

Roads

Using the intensity and RGB information that is stored for every point, we can extract the roads. A first step is to take sample measurements from the roads. The deviation of the intensity values were from 50 to 70 units and the RGB (or HSV – Hue Saturation and Value) numbers were: $H= 60\pm 25$; $S= 15$ to 30 ; and $V= 75$ to 95 . Since the road has only one echo coming back to the sensor, the first step is to select data point with “Only” echo. Second step is to use intensity values (50-70) to remove unwanted points (field crops etc) and the third step is to use HSV numbers to do the final selection. The result is shown on Fig. 18.

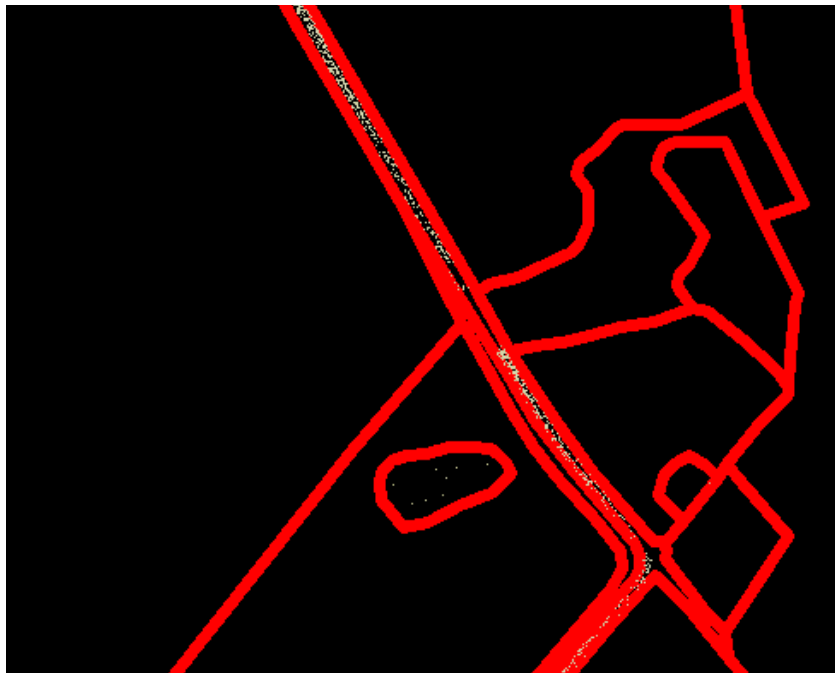


Fig. 18. Extracted LiDAR points from 1300 m data that represent road. The intensity, echo and HSV information was used.

ANNEX - 4

Studying the vertical accuracy of LiDAR data in different vegetation types and using LiDAR data with combination of aerial images to classify EBONE General Habitats Categories in Estonia

As we can see from Fig. 18 then the points inside the small area (stones) near the road have also the same characteristics as the road data points. Using RGB or HSV values can be difficult because the aerial images are taken in different periods throughout the Europe and therefore HSV values e.g. for asphalt road can differ quite a lot.

Conclusions

We have investigated the vertical accuracy and penetration rate of LiDAR data in different vegetation types. We used two LiDAR data sets: 2400 m and 1300 m flight data. The results showed that the penetration rate is higher with 1300 m data, which was expected due to the fact that the laser light attenuates less with lower flying altitude. This makes the incoming energy level higher and therefore more points can be detected. The vertical accuracy of laser points on asphalt road was estimated to be within 10 cm with both altitudes. This shows that the vertical accuracy is pretty much the same with 2400 m and 1300 m. The effect of vegetation on penetration rate was also noticed. Uncut crop and lower vegetation beneath the trees had an impact on the overall accuracy of laser point. The laser could not penetrate through the dense lower vegetation and also trees reduced the number of points that reach the ground level. The national wide LiDAR data in Estonia (2400 m) can be used for environmental monitoring but the vertical layers are not described in such detail as it would be with 1300 m data.

We also tested the possibility to use LiDAR data with combination of aerial images and RGB values that was assigned to LiDAR points from aerial images. The use of aerial images and LiDAR data together will increase the recognition of linear object more easily and makes the mapping of smaller areas much simpler than just to use either aerial image or just LiDAR data.

The use of echo information is useful for mapping forest areas and classifying them according to the height.

The future work would be study the possibility to use LiDAR and aerial images to automatically detect natural habitats boundaries (as can be seen from Fig. 16). LiDAR data would also allow us to map layers for different habitats.

Acknowledgements

This study is part of the EU FP7 Project European Biodiversity Observation Network (EBONE). The aerial images and ALS data was provided by Estonian Land Board.

References

- Baltsavias, E. P. 1999. Airborne laser scanning: basic relations and formulas. *ISPRS Journal of Photogrammetry & Remote Sensing*, 54: 199-214
- Bunce, R. G. H., Roche, P., Bogers, M. M. B., Walczak, M., de Blust, G., Geijzendorffer, I. P., van den Borre, J. 2010. Handbook for Surveillance and Monitoring of Habitats, Vegetation and Selected Species. *Alterra-EBONE Handbook*, 102 p
- Coren, F., Sterzai, P. 2006. Radiometric correction in laser. *International Journal of Remote Sensing*, 27(15-16): 3097-17

ANNEX - 4

Studying the vertical accuracy of LiDAR data in different vegetation types and using LiDAR data with combination of aerial images to classify EBONE General Habitats Categories in Estonia

- Kaasalainen, S., Ahokas, E., Hyyppä, J. & Suomalainen, J. (2005). Study of surface brightness from backscattered laser intensity: calibration of laser data. *IEEE Geoscience and Remote Sensing Letters*, Vol. 2, No. 3, pp. 255-259
- Korpela, I.S., Ørka, H. O., Hyyppä, J., Heikkinen, V., Tokola, T. 2010. Range and AGC normalization in airborne discrete-return LiDAR intensity data for forest canopies. *ISPRS Journal of Photogrammetry and Remote Sensing*, 65: 369-379
- Vain, A., Kaasalaine, S., Pyysalo, U., Krooks, A. & Litkey, P. (2009). Use of naturally available reference targets to calibrate airborne laser scanning intensity data. *Sensors*, Vol. 9, pp. 2780-2796
- Vain, A., Yu, X., Kaasalainen, S. & Hyyppä, J. (2010). Correcting airborne laser scanning intensity data for automatic gain control effect. *IEEE Geoscience and Remote Sensing Letters*, Vol. 7, No. 3, pp. 511-514
- Wagner, W. 2010. Radiometric calibration of small-footprint full-waveform airborne laser scanner measurements: Basic physical concepts, *ISPRS Journal of Photogrammetry and Remote Sensing*, 65(6): 505-513

Annex-5

EBONE



European Biodiversity Observation Network:

Design of a plan for an integrated biodiversity observing system
in space and time

ID5.8: A regional adaptive approach

Hyperspectral imagery to map General Habitat Categories and relation of classification success with site complexity

Ver 3.0

Document date: 2011-04-21

A contribution to Document Ref.: EBONE-D5.5-2.0

Authors:

Wouter Hantson, Sander Mûcher , Lammert Kooistra

ID5.8: A regional adaptive approach

Hyperspectral imagery to map General Habitat Categories and relation of classification success with site complexity

Authors:

Wouter Hantson, Sander Múcher , Lammert Kooistra



ANNEX-5

**Hyperspectral imagery to map General Habitat Categories and relation of classification success
with site complexity**

**Hyperspectral imagery to map General Habitat Categories and relation of classification success
with site complexity**

Table of contents

1 INTRODUCTION	6
1.1 CONTEXT	6
1.2 PROBLEM DEFINITION.....	6
1.3 RESEARCH OBJECTIVES	7
2 LITERATURE REVIEW	9
2.1 GHC HANDBOOK.....	9
2.2 FROM REFLECTANCE TO LIFE FORMS	9
2.2.1 Remote Sensing	9
2.2.2 Classification algorithms	10
2.3 SITE COMPLEXITY	12
2.3.1 Biological complexity	12
2.3.2 Spectral complexity.....	13
2.3.3 Landscape complexity	14
3 MATERIALS AND METHODS	15
3.1 STUDY SITES	15
3.1.1 Haaksbergerveen	16
3.1.2 Korenburgerveen	16
3.1.3 Millingerwaard.....	17
3.1.4 Wageningen floodplain	17
3.1.5 Natura 2000 habitat types.....	18
3.2 DATA	20
3.2.1 Aerial Photographs	20
3.2.2 HyMap – Imaging spectroscopy data	20
3.3 GHC MAPS	20
3.4 CLASSIFICATION	21
3.4.1 SAM classification algorithm.....	21
3.4.2 SAM endmember selection.....	21
3.4.3 SAM validation data	22
3.5 MAPPING SUCCESS.....	22
GHC-classification	22
3.6 SITE COMPLEXITY INDICATORS	22
3.6.1 Biological complexity	22
3.6.2 Spectral complexity.....	23
3.6.3 Landscape complexity	23
4 RESULTS	26
4.1 HAAKSBERGERVEEN	26
4.1.1 GHC map of Haaksbergerveen	26
4.1.2 SAM classification.....	27
4.1.3 Mapping success	28
4.1.4 GHC mapping success	28
4.2 KORENBURGERVEEN	32
4.2.1 GHC map of Korenburgerveen	32
4.2.3 SAM validation	33
4.2.4 GHC classification	34
4.2.5 GHC map of Millingerwaard.....	34
4.2.6 SAM classification.....	35
4.2.7 Mapping success	36
4.2.8 GHC classification success	37
4.3 WAGENINGEN FLOODPLAIN	38
4.3.1 GHC map of Wageningen floodplain	38
4.3.2 SAM classification.....	39

ANNEX-5

Hyperspectral imagery to map General Habitat Categories and relation of classification success with site complexity

4.4	OVERVIEW OF THE SITE COMPLEXITY	42
4.4.1	Biological Complexity.....	42
4.4.2	Spectral Complexity.....	42
4.4.3	Landscape complexity	43
	THE RELATION BETWEEN MAPPING SUCCESS AND SITE COMPLEXITY	43
4.4.4	Mapping success	43
4.4.5	The relation between Biological Complexity and Mapping Success	44
4.4.6	The relation between Spectral Complexity and Mapping Success	45
4.4.7	The relation between Landscape Complexity and Mapping Success	47
5	DISCUSSION.....	49
5.1	GHC MAPPING	49
5.2	SAM CLASSIFICATIONS	49
5.3	GHC CLASSIFICATION SUCCESS	50
5.4	SITE COMPLEXITY COMPARED TO CLASSIFICATION SUCCESS	50
6	REFERENCES	53

1 Introduction

1.1 Context

As a contracting party to the United Nations (UN) Convention on Biological Diversity (CBD), the European Union (EU) wanted to stop the decline of biodiversity in Europe by 2010 via restoring and conserving habitats and natural ecosystems (UNEP, 2002). One policy instrument to stop the decline in biodiversity is through the realization of the Natura 2000-network, the EU network of sites designated under the Birds Directive (1979) and the Habitat Directive (1992) (EC 2002). To assess and evaluate the conservation status of the designated habitat types, policy makers and nature reserve managers increasingly require hard figures that give details on the state of habitats as well as the definition of historical trends to evaluate international conventions and commitments (Bunce et al. 2008). Due to many concepts and definitions of habitats there is a wide range of regional, national and European habitat classifications, and so there are no consistent figures on habitats in Europe (Mücher et al. 2009). Monitoring biodiversity at large scales, using traditional (ground-based) surveying techniques are logistically difficult and/or financially prohibitive (Duro et al. 2007). A remote sensing based assessment of vegetation patterns could be a cost effective method to map and monitor the development of biodiversity. Imaging spectroscopy is especially interesting for vegetation mapping. The spectral information provided by hyperspectral sensors allows up to species-level detection (Clark et al. 2005; Underwood et al. 2007; Andrew and Ustin 2008) and like Gao (1999), Thenkabail et al. (2003) and Lucas and Carter (2008) argued, a fine spectral resolution may be more important than a greater spatial resolution in characterization vegetation to obtain a good mapping success.

1.2 Problem definition

Consistent monitoring and analysis of biodiversity, which is the total sum of all biotic variation (Purvis and Hector 2000), of European ecosystems requires a general methodology that is applicable over Europe. The recently developed GHC (General Habitat Mapping) method, which is validated for surveillance and monitoring of European Habitats (Bunce 2005; Bunce et al. 2008), has been used as a basis for habitat mapping. Bunce et al. (2005) defined habitat as: 'An element of the land surface that can be consistently defined spatially in the field in order to define the principle environments in which organisms live'. This is related to the definition of the Habitat Directive (EC 2002): 'Terrestrial or aquatic areas distinguished by geographic, abiotic and biotic features, whether entirely natural or semi-natural'. Individual species are too specific to encompass all Europe's variation so GHCs are based on Raunkiaer's classification of plant life forms (Raunkiaer 1934). Combinations of plant life forms are used to define 160 General Habitat Categories (GHCs). These GHCs are recorded in the field, and at the same time the use of plant life forms might provide direct links with the patterns present on satellite images due to their relationship with vegetation structure (Bunce et al. 2008; Mücher, 2009). So remote sensing could potentially be used for the creation of GHC maps for ecosystems.

Remote sensing derived vegetation maps are usually the result of non-continuous vegetation mapping with sharp boundaries around the classified patches which do not necessarily follow the concrete local discontinuities (Schmidtlein et al. 2007). The image classification has reduced the ecotones, zones of transition between adjacent ecological systems (Gosz 1993), to simple lines between internally homogeneous areas. This way of mapping has often been

Hyperspectral imagery to map General Habitat Categories and relation of classification success with site complexity

criticized (Zonneveld 1974; Kent et al. 1997; Schmidlein et al. 2007). Fortin et al. (2000) mentioned that shifts in the location of ecotones may indicate environmental and/or climate change, because species may be at the limits of their tolerance in these transitional zones. The use of continuous vegetation maps represents abrupt transition as well as gradual transitions between vegetation types (Schmidlein et al. 2007). Following the GHC mapping methodology, habitats consists of a mixture of one or more plant life forms. The GHCs are based on different life form combinations and can be computed by assuming that the reflectance of a habitat is the result of a mixture of the reflectances of the 'end-members' (i.e. lifeforms) present in the habitat. The end-member training pixels must be representative of pure life forms.

In this study we evaluate how well hyperspectral imagery is able to map GHCs. The selection of representative spectral end-members using GHC field observations will be difficult as the GHCs already represent mixed vegetation which could be expressed as a polygon containing a mixture of pure life form pixels or a mixture of pixels each representing a mixture of pure life forms, or a combination of both. At the other hand hyperspectral imagery is particularly suited for an end-member based classification as the many narrow spectral bands increase the likelihood of finding features in the spectral signature which are unique to the end-members of interest.

1.3 Research objectives

The objective of this research is to investigate and define the relationship between site complexity and mapping success of classified hyperspectral remote sensing images for different ecosystems (peatland and riparian). The research is subdivided in the following parts:

1. Apply the GHC methodology for habitat mapping in the field for 4 different sites that are characterized by two different ecosystems in the Netherlands: peat bogs (2 sites) and floodplains (2 sites).
2. Classification of Hymap-images for the 4 study areas with a well-selected classification algorithm, to derive GHC's like they are defined in the GHC methodology.
3. Validate the Hymap classifications with field data and the GHC maps derived from the fieldwork, compare the mapping success in the different GHC's and ecosystems.
4. Examine different (combinations of) analysis tools to determine the different aspects of site complexity and bring them into practice for the 4 study areas (and 2 ecosystems).
5. Investigate the relationship between the site complexity and the mapping success.

The **hypothesis** is that an increase in complexity tends to an decrease in mapping success.

Based on the research objective, the following research questions are derived:

- I. Which remote sensing based classification algorithm applicable to Hymap data can deliver Life Forms as output, and can it be transposed to GHC's?
- II. What are the differences in mapping success, after validating the GHC's classification results with the field-based GHC maps, for the different ecosystems and what are the specific differences?

ANNEX-5

Hyperspectral imagery to map General Habitat Categories and relation of classification success with site complexity

- III. How can you define site complexity using species, spectral, landscape and/or structural diversity measures?
- IV. What are the differences in site complexity for the different ecosystems and what are the site-specific differences?
- V. What's the relationship between site complexity and mapping success in the different ecosystems?

2 Literature review

Before the start of the study, several decisions had to be made concerning two of the five research questions proposed in chapter one. This was based on a literature study in advance. The first decision concerned the question, "Which classification algorithms are applicable to HyMap that can deliver Life Forms as output, and can it be transposed to GHC's?". It must deliver a useful and well performing algorithm to carry out the classification of the HyMap images. And the second decision concerned: "How can you define site complexity using species, spectral, landscape and/or structural diversity measures?". It must be a definition of site complexity and a set up to analyse it but first an introduction to the Raunkiaert Life Forms and the GHC methodology.

2.1 GHC handbook

Based on the GHC Handbook 'Handbook for Surveillance and Monitoring of European Habitats' by Bunce et al. (2005) we give hereafter a short description of the GHC mapping methodology. The overall goal of the GHC methodology was to set up a methodology designed for collecting information on European habitats in order to obtain statistically robust estimates of their extent and associated changes in biodiversity. GHCs are thus a consistent methodology for field recording and monitoring of habitats.

In this methodology the term habitat refers to: "An element of land that can be consistently defined spatially in the field in order to define the principal environments in which organisms live." This division is done by using predetermined General Habitat Categories (GHC's) for recording point-, linear- and areal habitat elements. The Raunkiaer classification of plant Life Forms (LF) is the basis for these GHC's. Raunkiaert divided plant species on the location of the plants growth point during seasons with adverse conditions e.g. winter or dry seasons.

The use of plant life forms enables the recording of habitats with comparable structures within contrasting bio-geographical zones that have similar habitat structures. Based on the hypothesis that habitat structure is related to the environment and thus it will correspond to phytosociological classes at high level. For the European region 130 GHC's are derived from 16 Life Forms. The variation within a GHC is additional expressed by environmental, management and global qualifiers.

2.2 From Reflectance to Life Forms

2.2.1 Remote Sensing

Remote sensing (RS), the science and art of obtaining information about an object, area, or phenomenon through the analysis of data acquired by a device that is not in contact with the object, area, or phenomenon under investigation (Lillesand et al., 2008), is suggested for the monitoring of vegetation in combination with GHCs. This implies that we need to go from reflectance (captured through remoter sensing images) to life forms. The electromagnetic radiation from the sun is reflected by the earth's surface and an optical remote sensing devices captures the radiation reflected in the direction of the sensor. The atmosphere, the reflecting surface and the height of the sun are the main factors that influence this captured radiation. The atmospheric effect on the received signal is a combination of scattering and absorption. Scattering is the unpredictable diffusion of radiation in the atmosphere and absorption results in the effective loss of energy to atmospheric constituents in specific

Hyperspectral imagery to map General Habitat Categories and relation of classification success with site complexity

wavelength bands. The wavelength ranges without absorption are the so-called 'atmospheric windows', which are used in RS (Lillesand et al., 2008).

Radiation from the sun passed the atmosphere, is reflected by the earth's surface, passed again (a part of) the atmosphere and is finally captured by the sensor. Reflectance, which is the interaction between radiation and surface (radiative transfer), is surface dependent and makes thus optical remote sensing possible. A graph of the spectral reflectance of an object in function of the wavelength is called a spectral reflectance curve (Lillesand et al., 2008). This will be used for the classification and can be derived from the image itself, an spectral library or from field measured spectra.

It's obvious that the height of the sun influences the radiative transfer and the reflectance in the direction of the sensor, and thus the 'properties' of the object that reflected the radiation. The lower the sun the more influence shade will have on the reflectance image.

Radiative transfer in vegetation comprises reflectance, transmission, absorption and emission, intrinsically related to the vegetation (biophysical and biochemical) properties which cause variation in absorbance and transmittance across wavelength via multiple scattering processes throughout the canopy and background (Verrelst, 2010). Specific biochemical vegetation properties like the higher absorption in blue and red (chlorophyll absorption bands) and the high reflectance of the leaves in the green part of the spectrum can be seen in the reflectance curve, while other are more structural vegetation properties like vegetation cover. The information in the spectral reflectance curve is thus only information from properties that have an impact on the reflectance of the radiation (Chen et al., 2000). The more spectral bands, the more specific absorption features can be seen and thus distinguished. For example for the research presented in this study, HyMap images with 126 spectral bands will be used

The HyMap (Hyperspectral Mapper) sensor is an airborne hyperspectral sensor. The HyMap images are acquired with 126 spectral bands from the visible till the infrared (covering the spectral range from 450 nm till 2480 nm) and a spatial resolution of 5 m. These hyperspectral images make it possible to detect most absorption features in the vegetation spectrum (Ustin et al. 2004). To deal with this hyperspectral data a specific classifier is needed.

2.2.2 Classification algorithms

There are several classifiers like the Spectral Angle Mapper (SAM), Spectral Mixture Analysis (SMA) or a modified version Multiple Endmember Spectral Mixture Analysis (MESMA) who can take advantage of hyperspectral images, but it's also possible to apply one of the traditional classification methods like Maximum Likelihood (ML). These methods differentiate from each other on the way they deal with the training data to assign a pixel to a 'class' or 'classes'.

These classifiers have been commonly used for vegetation and/or land cover mapping:

- I. SAM: Lass et al. 2002; Silvestri et al 2003; Hestir et al. 2007,
- II. SMA: Rosso et al. 2005; Hestir et al. 2007, and
- III. MESMA: Okin et al. 2001; Rosso et al. 2005; Schaepman-Strub et al. 2009.

Maximum Likelihood

The ML classifier differentiates from the SAM and SMA classifiers by the use of a training set instead of an endmember to categorise a class. This training sets are a collection of statistics that describe the spectral response pattern of each class to be classified in the image. The

Hyperspectral imagery to map General Habitat Categories and relation of classification success with site complexity

ML quantitatively uses both the mean and covariance matrix, that summarize the spectral response of each class, to determine the class with the highest statistically probability for a single pixel in the image (Lillesand et al. 2008).

Spectral Angle Mapper

The SAM classifier (Kruse et al. 1993) uses, as motioned before, endmembers of the various classes to assign each single pixel to a certain class. These endmembers represents the pure spectral signatures of the classes. Each endmember and pixel can be considered as a vector in a multidimensional space (dimensions are equal to the number of spectral bands). To compare an image spectra with an endmember, the vectors, which have a common origin, are defined and the spectral angle between the two is calculated.

This spectral angle (θ) is the error metric for the spectral similarity. By comparing different endmembers, the endmember who delivers the lowest spectral angle is considered to match (if this spectral angle is under a defined threshold). The advantage of this spectral angle is that SAM isn't sensitive for differences in overall illumination due to the presence of a mix of sunlight and shadows, the albedo, which is measured by the length of the vector of the modelled spectrum (Lillesand et al. 2008).

Length of a spectrum vector (L_ρ):

$$L_\rho = \sqrt{\sum_{\lambda=1}^M \rho^2_\lambda}$$

Spectral angle (θ):

$$\theta = \cos^{-1} \left(\frac{\sum_{\lambda=1}^M \rho_\lambda \rho'_\lambda}{L_\rho L_{\rho'}} \right)$$

Spectral Mixture Analysis

SMA assumes that a value of a given pixel is the result of a linear combination of one or more endmembers (Adams et al. 1986, Smith et al. 1990). These spectral mixed pixels are compared to a set of endmembers ('pure' reference spectra). During the unmixing, SMA estimates the fit of selected endmembers to the pixel in order to estimate it's composition (Rosso et al. 2005). The amount of used endmembers is limited, since including large amounts of endmembers while there are few represented in the pixel leads to additional errors (Roberts et al. 1998).

MESMA, based on SMA, allows an almost unlimited number of endmembers. It evaluates the best fit for each pixel using a root mean square error (RMSE) error metric, thus avoiding over fitting due to too many endmembers (Roberts et al. 1998).

$$RMSE = \sqrt{\frac{\sum_{\lambda=1}^M (\varepsilon_\lambda)^2}{M}}$$

The SAM algorithm is less sensitive to the overall albedo than the MESMA algorithm.

In choosing a spectral algorithm, the advantages and disadvantages of the model must be evaluated but also the endmember selection is critical. Endmember selection is crucial and

Hyperspectral imagery to map General Habitat Categories and relation of classification success with site complexity

algorithm dependent, like Foody (2009) mentioned: a training site that could be used to derive a highly accurate classification from one classifier may yield a considerably lower accuracy if used with another classifier. Some candidate endmembers can be easily selected, other only appear as mixed spectra, but the training sample should provide a representative and unbiased description of the classes (Foody and Mathur 2006). Different approaches to obtain endmembers are possible: endmembers from a spectral library, field-based and image based endmember extraction.

2.3 Site complexity

The information in the spectral reflectance curve used for the classification only represents the properties of the feature of interest (i.e. GHC; lifeform) that have an impact on the reflectance of the incoming radiation (Chen et al., 2000). When the spectral detectability of a habitat is assessed the environmental context of the study area is often only briefly mentioned, even though this aspect is important to understand how the neighbouring habitats' spectral properties influence its detectability so that inferences about the suitability of a habitat for EO mapping are not confounded by discrepancies in the mapping success (Andrew and Ustin, 2008). Andrew and Ustin (2008) mention that the mapping success is influenced by the site complexity. Quantifying site complexity from independent information would give a better understanding of the origin of the classification errors that occur when remote sensing is used and would lead to an improved determination of the suitability of a habitat for being mapped using remote sensing.

Warren Weaver (1948) defined 'complexity' as 'the degree of difficulty to predict properties'. So the more complex, the more difficult it is to predict the properties of a site. This indeed refers to our hypothesis. 'Complex' also refers to a lot of interacting components, Merriam-Webster (<http://www.merriam-webster.com/dictionary/complex>) called it the sum of factors/components characterizing a condition. So, by determining the 'condition' or separating the different 'properties' of a site we can define the complexity of this site. Here we subdivide 'site complexity', like previously done by Andrew and Ustin (2008), into

- i. Biological complexity, i.e., the number and relative distribution of species, life forms, habitat types or other measures of relevance to the interpretation of the remote sensing information for the site;
- ii. Spectral complexity, i.e., the richness and diversity of the spectral signature for the site, assuming that such spectral diversity reflects the diversity of habitat properties;
- iii. Landscape complexity, i.e., the richness and diversity of landscape patterns and other structures of the site.

2.3.1 Biological complexity

Biological complexity can be assessed by a measure of **Species Richness**. In this case this measure is limited to the total number of abundant plant species, since plants, unlike animals, will have relevance for the reflectance properties of the site. Plant species data can be easily extracted from vegetation relevés collected from a site. In a vegetation relevé all species and their coverage are recorded.

However, Species Richness does not take the evenness, the relative abundance of different species in an area, into account. More complex species diversity indices do this:

- **The Simpson's diversity index** (Smith and Wilson 1996):

**Hyperspectral imagery to map General Habitat Categories and relation of classification success
with site complexity**

$$\sum \frac{ni(ni-1)}{N(N-1)}$$

N_i = the number of individuals of species i which are counted

N = the number of all individuals counted

The Simpson's diversity index varies between 0 and 1, representing the probability that two randomly selected individuals belong to the same species. A value of 1 represents 100% probability of selecting the same species, so there will be no diversity.

- **The Shannon diversity index** (Kalacska et al. 2007):

$$H = -\sum p_i \ln p_i$$

p_i = fraction of individuals belonging to the i -th species

A Shannon diversity index result of zero means there is just one species occurring in the site, thus a low diversity. The higher the value of the indices, the higher the diversity, i.e. more evenly distributed species.

These measures of richness and diversity can also be applied to other representations of a site's biological complexity, such as the GHCs life forms of the vegetation.

2.3.2 Spectral complexity

Spectral complexity is dealing with the spectral signature directly derived from the remote sensing images and is based on the Spectral Variation Hypothesis (SVH) (Palmer et al. 2000, 2002): habitat heterogeneity may be estimated from spectral heterogeneity. Palmer et al. (2000, 2002) used single waveband panchromatic images with a 1m resolution and concluded that the relationship is scale-dependent and increases with the size of the window of analyses. Rocchini et al. (2004), who used images with 4 bands and a spatial resolution of 4m, found also a significant relationship for smaller scales. The HyMap-images, with their 126 bands and 5m spatial resolution, will probably deliver a significant relationship for even smaller scales. The SVH approach deals with continuous data, without loss of information due to classifying into discrete classes (Palmer et al. 2002). Oldeland et al. (2010) used hyperspectral images, but he investigated the relationship of richness and abundance-based diversity measures with spectral variability. Schmidteitn and Sassin (2004) are critical of this hypothesis and showed that homogeneous reflectance did not necessarily indicate a homogeneous plant species composition, but heterogeneous reflectance was always a sign of heterogeneous (floristic) composition. The species richness relationship defined by Carlson et al. (2007) is based on the spatial variation of the reflectance derivative spectra at 530, 720, 1201, and 1523nm. These bands are chosen because they predict woody species richness with a high precision. This is the reason why Andrew and Ustin (2008) called it the 'spectral richness index'; their datasets were very different from those used to parameterise the species richness.

Hyperspectral imagery to map General Habitat Categories and relation of classification success with site complexity

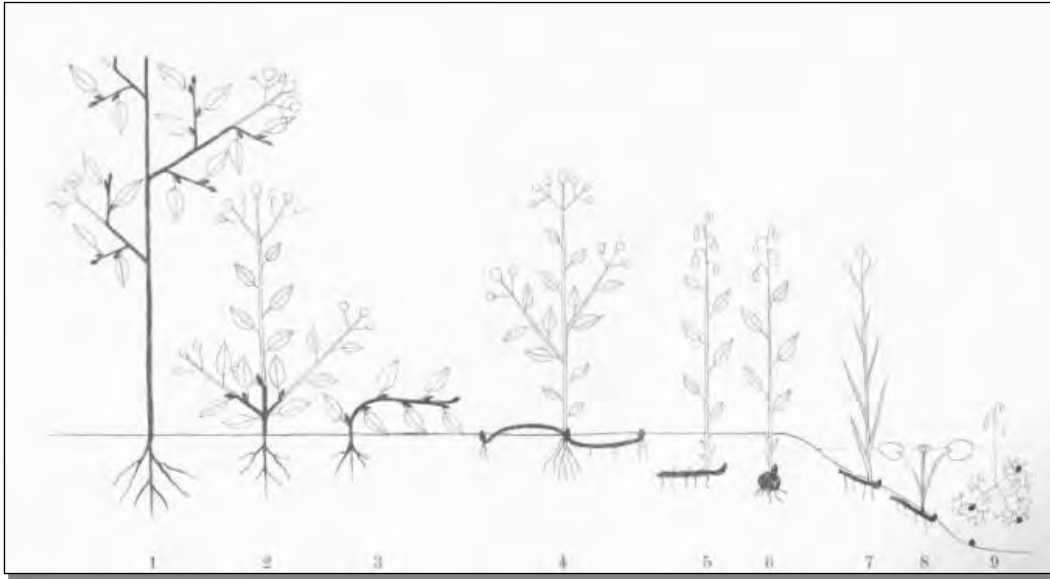


Figure 1 Raunkiaer's life forms. http://en.wikipedia.org/wiki/Raunkiaer%27s_plant_life-form (2010).

The spectral variance (Andrew and Ustin 2008) is another approach, based on the Minimum Noise Fraction (MNF) transformation of the images. MNF is a statistical data reduction technique that performs a series of two principal component analyses to isolate noise and reduce the dimensionality of the dataset (Green et al. 1988). The spectral variance is estimated by the total variation covered by the first three MNF bands. This can also be covered by a Principal Component Analysis (PCA).

2.3.3 Landscape complexity

A study site's landscape complexity may be represented by various landscape metrics. Honnay et al. (2003) noticed that the composition and structure of a landscape mosaic influence biotic processes and hence species richness. This relationship between landscape structure and plant diversity has been extensively studied, see Uuemaa et al. (2009) for an overview. Interesting relationships are the Shannon's diversity index with a riparian woody plant species index ($r=-0.78$) (Burtyon and Samuelson, 2008); edge density and species richness ($r=0.56$), number of patches and species richness ($r=0.61$) (Moser et al. 2002). Andrew and Ustin (2008) also represented landscape heterogeneity with landscape-level metrics. Patch size, shape and evenness were defined. There is also some criticism of the use of landscape indices, noticing that some of the landscape indices are complex or have a nonlinear formulation and should be avoided in correlation analysis, their complex structure results in unpredictable responses to changing pattern, scale or classification (O'Neill et al., 1988; Li and Wu 2004). The use of landscape indices is made easier by the program FRAGSTATS, developed to quantify landscape structure. FRAGSTATS makes a distinction between patch, class, and landscape metrics; calculating the metrics respectively for each patch, each class and the entire patch mosaic. The program offers a comprehensive choice of landscape metrics (McGarigal and Marks 1995, Mc Carigal 1994), but as noted by O'Neill et al. (1988) and Li and Wu (2004) a proper selection in terms of scale and purpose is crucial. Cashman (2008) identified consistent combinations of methods that universally describe the major attributes of landscape structure with a focus on 'objective' structure metrics, which are constant among studies

3 Materials and methods

The mapping success assessment will focus on the remote sensed life form classification, but also on the ability to determine GHCs based on these classified life forms. Site complexity will be described in terms of the biological, spectral, and landscape complexity. This analysis will be done for two different ecosystems: Peat bogs and Floodplains, each represented by two study sites.

3.1 Study sites

The 4 study sites, for which Hymap data is available (see section 2.2.2), are all located in the central / eastern part of The Netherlands (fig. 2). They cover the two habitat types:

- 2 sites in Peat bogs: Haaksbergerveen and Korenbergerveen.
- 2 sites in Floodplains: Millingerwaard and Wageningen floodplain.



Figure 2: Location of the study sites in the Netherlands (Google Earth, 2010).

Hyperspectral imagery to map General Habitat Categories and relation of classification success with site complexity

3.1.1 Haaksbergerveen

Haaksbergerveen is located to the south-east of the city Haaksbergen, near the German border. It's 500 ha degraded raised bog are managed by Staatsbosbeheer. On the German side the area continues in the Ammeloër Venn (70 ha).



Figure 3: Haaksbergerveen. a) *Spagnum* species covered by *Erica tetralix*; *Phragmites australis* and *Juncus effuses* are developing, at the back there's more *Molinia caerulea* and *Betula*. b) *Molinia caerulea* forming perennial, and *Betula* sprouting.

The Haaksbergerveen is the southern part of the Natura 2000 area 'Buurserzand en Haaksbergerveen' and is a relict of one of the last raised bog areas in the Netherlands. Due to peat cutting, water drainage and an enrichment of the soil the reserve is degraded. During the last decades a network of dams was constructed in order to restore the water table, which is necessary to allow the bog vegetation to recover. The management objectives are to secure a sustainable abiotic system to create the most optimal conditions for the restoration of a vivid bog area, and to ensure an open moor landscape to reduce the evaporation of the system (Natura, 2009).

3.1.2 Korenburgerveen

Korenburgerveen is located north-west of Winterswijk, most of the area (509 ha) is owned and managed by Natuurmonumenten.



Figure 4: Korenburgerveen. A) *Molinia caerulea* mixed with *Myrica gale*. B) A smaller wet part with *Potentilla palustris*, *Typha latifolia*, *Nuphar lutea* and *Salix*.

The Korenburgerveen is a raised bog area and is incorporated as a Natura 2000 site. Due to the input of highly nutritious ground and surface water and the ground water exploitation the

Hyperspectral imagery to map General Habitat Categories and relation of classification success with site complexity

reserve has been degraded. There is a central raised bog area surrounded by (wet) peat forests. In the south of the area, the raised bog gradually evolves into a stream bed with wet grassland (Junco-Molinion) and swamps.

The management objectives are to restore the peat by restoring the alkaline groundwater table, which is necessary to allow the raised bog vegetation to recover.

3.1.3 Millingerwaard

The Millingerwaard (400 ha) is located south of the Waal, in the neighbourhood of Millingen a/d Rijn and Kekerdom.



Figure 5: Millingerwaard. Pictures are taken during winter 2010.

The floodplain Millingerwaard is a part of the Gelderse Poort nature reserve. The area has gradually been improving since 1990 when arable land and production grassland were converted into nature. Amongst other measures, the fences between the parcels were removed and a low density of cattle for natural grazing was introduced (Kooistra et al. 2005). This resulted in a heterogeneous landscape with river dunes, softwood forest and vegetation in different stages of succession. Also an old clay pit is present in the centre of the study area.

3.1.4 Wageningen floodplain

The floodplain is located south of the city Wageningen, at both sides of the river Rhine.



Figure 6: Wageningen floodplain. Pictures are taken during winter 2010.

**Hyperspectral imagery to map General Habitat Categories and relation of classification success
with site complexity**

The Wageningen floodplain is a part of the Natura 2000 area 'Uiterwaarden Neder-Rijn'. Before the natural reconstruction of the floodplain, due to huge flooding problems in the nineties, the area had an agricultural formation. Now the floodplain is converted into extensive semi-natural grazing land. This has resulted in a wide range of vegetation types from grassland over shrubs to wet forest. The northern part of the study area is covered by housing, forest and the Arboretum on the Westerberg

3.1.5 Natura 2000 habitat types

Annex 1 of the Habitat directive (EC 2002) lists the natural (and semi-natural) habitats of community interest whose conservation require the designation of special conservation areas. Table 1 gives an overview of these special protected natural habitat types for the Natura 2000 sites covering the study sites. Also the EU code listed in the Habitat Directive and a short version of the definition given by the habitat directive (EC 2002) are shown in table 1.

ANNEX-5

Hyperspectral imagery to map General Habitat Categories and relation of classification success with site complexity

Table 1: Overview of the Natura 2000 habitat types per study site.

Natura 2000 habitats		Haaksbergerveen	Korenburgerveen	Wageningen	Milingerwaard
Coastal sand dunes and inland dunes	2				
Inland dunes, old and decalcified	23				
Dry sands heaths	2310	v			
Freshwater habitats	3				
Standing water	31				
Oligotrophic to mesotrophic waters	3130	v			
Natural eutrophic lakes	3150				v
Running water	32				
Rivers with muddy banks	3270			v	v
Temperate heath and scrub	4				
Northern Atlantic wet heaths	4010A	v	v		
Scelerophyllous scrub	5				
Juniperus communis formations on heaths or calcareous grasslands	5130	v			
Natural and semi-natural grassland formations	6				
Natural grasslands	61				
Xeric sand calcareous grasslands	6120				v
Semi-natural tall-herb humid meadows	64				
Molina meadows on calcareous, peaty or clayey-silt-laden soils	6410		v		
Hydrophilous tall herb fringe communities of plains	6430A&C				v
Mesophile grasslands	65				
Lowland hay meadows	6510A			v	v
Raised bogs, mires, and fens	7				
Sphagnum acid bogs	71				
Active raised bogs	7110A	v	v		
Degraded raised bogs still capable of natural regeneration	7120	v	v		
Calcareous fens	72				
Calcareous fens	7210		v		
Forests	9				
Forests of boreal Europe	91				
Bog woodland	91D0	v	v		
Alluvial forests	91E0A				v
Alluvial forests	91E0C		v		
Riparian mixed forests along the great rivers	91F0			v	v

Hyperspectral imagery to map General Habitat Categories and relation of classification success with site complexity

3.2 Data

3.2.1 Aerial Photographs

The aerial photographs used in this study were acquired in 2008. They have a spatial resolution of 25cm and are in the Red Green Blue (RGB) colour model. They served as input for the construction of the preliminary GHCs maps for the study sites Haaksbergerveen and Korenbergerveen.

3.2.2 HyMap – Imaging spectroscopy data

The airborne HyMap data of the Millingerwaard floodplain were acquired on the 28th of July 2004 and that of Wageningen on the 2nd of August 2004. They were atmospherically corrected with the modules PARGE and ATCOR4 to obtain geo-coded top-of-canopy reflectance data and geometrically corrected to the UTM-projection (zone 31 N, geodetic datum WGS84). For more information about the HyMap acquisition: Kooistra et al. (2005); Clevers (2005). The Haaksbergerveen and Korenbergerveen airborne HyMap data were acquired on 24th of July 2008 by DLR (Deutsches Zentrum für Luft- und Raumfahrt). The data are ortho-rectified radiance data performed with ORTHO (zone 32 N, geodetic datum WGS84). The atmospheric correction is performed with the ATCOR4 model.

3.3 GHC maps

The preliminary GHCs maps, based on visual interpretation of the aerial photographs, were used as a first guide in the field. These boundaries were checked and if necessary adapted. Then the percentage cover of each life form was estimated, from a vertical perspective, in the field. The determination of GHCs was based on two percentage rules, >70% for single GHCs, and 40-60% for GHCs that were a combination of two life forms. Also all life forms with a cover >10% and single species present over 30% were recorded. The standard mapping area was one square kilometre. The result of the fieldwork survey was a map with polygons showing the different GHCs present in the one square kilometre. Usually, also data about line and point observations and environmental, management and global qualifiers were collected but these have not been included in this analysis. As this study focuses on the vegetation part of the study areas, the GHCs Urban and Crops were not subdivided into life forms. The vegetation GHCs and their life forms are shown in table 2. The subdivision of the shrubs and trees GHCs is based on the vegetation height, also given in table 2.

Hyperspectral imagery to map General Habitat Categories and relation of classification success with site complexity

Table 2: The vegetated GHCs and their life forms.

General Habitat Category		Life Form		Hight
Sparsly vegetated	SPV	Aquatic	AQU	
		Terrestrial	TER	
Vegetated herbacious	HER	Submergerd hydrophytes	SHY	
		Emergent hydrophytes	EHY	
		Helophytes	HEL	
		Leafy hemicryptophytes	LHE	
		Caespitose hemicryptophytes	CHE	
		Therophytes	THE	
		Geophytes	GEO	
		Herbaceous chamaephytes	HCH	
		Cryptogams	CRY	
Shrubs and trees	TRS	Shrubby chamaephytes	SCH	0.05-0.30m
		Low phanerophytes	LPH	0.3-0.6m
		Mid phanerophytes	MPH	0.6-0.2m
		Tall phanerophytes	TPH	2-5m
		Forest phanerophytes	FPH	>5m

3.4 Classification

3.4.1 SAM classification algorithm

The SAM classification algorithm (Dennison et al., , 2004) was selected for use on the hyperspectral HyMap images because it deals with the whole spectral information delivered by the HyMap data and is not affected by the albedo. The SAM algorithm is included in the IDL-ENVI software version 4.5. The maximum spectral angle used was the default 0.1 radians. The same threshold value was used for all the classes. Problems using this approach were expected for areas consisting of pixels with a high complexity in their spectra, like water bodies and clear soil. They appear mostly as mixed pixels, making it impossible to collect homogeneous spectra. The Normalised Difference Vegetation Index (NDVI) is based on the near-infrared and red spectral bands and designed to determine green vegetation, making it possible to discriminate and mask out non-vegetated areas before the SAM classification is carried out.

3.4.2 SAM endmember selection

Aerial photographs in combination with a vegetation map overlay are used to select the endmembers without fieldwork. Potential endmembers were selected where its occurrence is homogeneous in the aerial photograph. Some endmembers were easily selected, but were not. Foody and Mathur (2006) noticed that the training sample should provide a representative and unbiased description of the classes. The selection of mixed endmembers is thus not representative. Plant life forms which only occur in mixed pixels were excluded from the classification. The number of life forms for which endmember spectra were extracted differs thus from site to site.

Hyperspectral imagery to map General Habitat Categories and relation of classification success with site complexity

3.4.3 SAM validation data

The approach for the collection of validation data was identical to the endmember selection, but strictly separated. Endmembers were not used for validation and vice versa. So, the aerial photographs are used in combination with a vegetation map overlay to select the validation data without fieldwork. Validation pixels were selected where its occurrence is homogeneous in the aerial photograph.

3.5 Mapping success

Mapping success is a general term used for the life form classification accuracy and the ability to determine GHCs with the life form classification result. The life form classification accuracy indicates the ability to determine the different life forms with the classification algorithm whereas the GHCs classification accuracy determines the ability to identify the correct GHC category with the classification result. Another distinction is the scale of the accuracy assessments, the SAM classification accuracy applies to a site whereas the GHC accuracy assessment may apply to single patches or the complete site. The classification accuracy for the SAM classification of the HyMap images was assessed by calculating an error matrix and the kappa-statistic per classified image.

GHC-classification

The GHCs classification accuracy indicates the ability to identify the GHCs (or major life forms) obtained during the field work with the classification result obtained from the HyMap data. The classified maps were overlaid with the representative GHCs map and the percentage cover of each life form in each polygon was calculated. Because the GHC maps used as an overlay are already a simplification and generalisation of the ground truth the relative occurrence of the life forms in the patches was compared with the life form percentages. This means that only the relative proportion was taken into account, and not the exact spatial location of the life forms. To make the life forms mapping success comparable with the SAM mapping success, the same validation pixel to life form ratio was used. The accuracy assessment was represented by:

- Error matrix
- Kappa coefficient

3.6 Site complexity indicators

3.6.1 Biological complexity

The species lists from the SynBioSys database (www.synbiosys.alterra.nl/natura2000/googlemapslvd.aspx) do not provide the abundance data of a certain species. However there are different field samples available that were recorded in the field for the different study sites. This information was taken into account to calculate the diversity indices.

The biological complexity will be covered by:

- Species Richness
- Simpson diversity index
- Shannon diversity index
- Total number of life forms

Hyperspectral imagery to map General Habitat Categories and relation of classification success with site complexity

- Total cover of GHC's with mixed life forms

3.6.2 Spectral complexity

The spectral complexity will be covered by:

- Spectral richness
- Explained variance by the first 3 Principal Components bands
- Total Principal Components bands to cover $\geq 99.9\%$ of the variation in the data

3.6.3 Landscape complexity

The selected landscape metrics, available in Fragstats and described by McGarigal and Marks (1995), to encompass the landscape complexity per study site are:

- Number of patches (NP): The total number of patches in the study site. $NP \geq 1$, if NP equals 1 then there is only one patch in the site.
- Patch Density (PD): The total number of patches divided by the total area, expressed in patches per 100 hectare.
- Total Edge (TE): The sum of the lengths in meters of all edge segments in the study site.
- Edge Density (ED): The total edge in meters, but relative to the area size converted to 100 hectares. This is thus the edge length (in meters) per unit area (100 hectares).
- Area Mean: The sum of all patch areas of a study site divided by the total number of patches of that site. The average patch mean per site.
- Area Standard Deviation: The standard deviation of the average patch area, a measure of variation in a study site.
- Shape Mean: Mean of the patch perimeter divided by the minimum perimeter for each patch. $Shape \geq 1$, a shape of one indicates a maximum compact shape like a square, and increased with an increased irregularity.
- Shape Standard Deviation: The standard deviation of the average shape mean, a measure of variation in shape irregularity in a study site.
- Shannon's Diversity Index (SHDI): The positive value of the sum of the proportional abundance of each patch type multiplied by that proportion. $SHDI \geq 0$ and if SHDI equals zero then there is only one patch, so there isn't diversity. The value increases with an increase of patch types and/or the proportional distribution of area among the patch types become more equitable. The index is somewhat more sensitive to rare patch types than the Simpson's diversity index.
- Shannon's Evenness Index (SHEI): The positive value of the observed Shannon's Diversity Index divided by the maximum SHDI for that number of patch types. $0 \leq SHEI \leq 1$, SHEI equal zero when the landscape contains only one patch and thus no diversity and if the distribution of area among the different patch types are dominated by one patch type. SHEI equals one when the distribution of the area among the patches is perfectly even, so the proportional abundances are the same.

Hyperspectral imagery to map General Habitat Categories and relation of classification success with site complexity

- Simpson's Diversity Index (SIDI): Represents the probability that any two pixels selected at random would be different patch types. $0 \leq SIDI \leq 1$, SIDI equal zero when the landscape contains only one patch and thus no diversity and SIDI equals one as the number of different patch types increases and the proportional distribution of area among patch types become more equitable.
- Modified Simpson's Diversity Index (MSIDI): Transforms the Simpson's diversity index to a general diversity index. $MSIDI \geq 0$, MSIDI equal zero when the landscape contains only one patch and thus no diversity and increases as the number of different patch types increases and the proportional distribution of area among the different patch types become more equitable.
- Simpson's Evenness Index (SIEI): The positive value of the observed Simpson's Diversity Index divided by the maximum SIDI for that number of patch types. $0 \leq SIEI \leq 1$, SIEI equals zero when the landscape contains only one patch and thus no diversity and if the distribution of area among the different patch types become increasingly uneven. SIEI equals one when the distribution of the area among the patches is perfectly even, so the proportional abundances are the same. An even distribution of area among patch types results in a maximum evenness.
- Modified Simpson's Evenness Index (MSIEI): The observed MSIDI divided by the maximum MSIDI for that number of patch types. $0 \leq MSIEI \leq 1$, MSIEI equal zero when the landscape contains only one patch and thus no diversity and as the distribution of the area among the different patch types become increasingly uneven, so dominated by one type. The MSIEI equals one when the distribution among the patch types is perfectly even and have thus the same proportional abundances. An even distribution of area among patch types results in maximum evenness, so evenness is the complement of dominance.

ANNEX-5

**Hyperspectral imagery to map General Habitat Categories and relation of classification success
with site complexity**

**Hyperspectral imagery to map General Habitat Categories and relation of classification success
with site complexity**

4 Results

4.1 Haaksbergerveen

4.1.1 GHC map of Haaksbergerveen

The preliminary GHCs map was based on the RGB aerial photographs of 2008 (fig 7a) and existing vegetation maps. The validation of this map was made in the field during October 2009. Due to the high fragmentation and the occurrence of dikes most of the area was accessible. Some parts were too wet and thus impossible to visit. These parts were checked by the use of a binocular or in a small number of cases not checked.

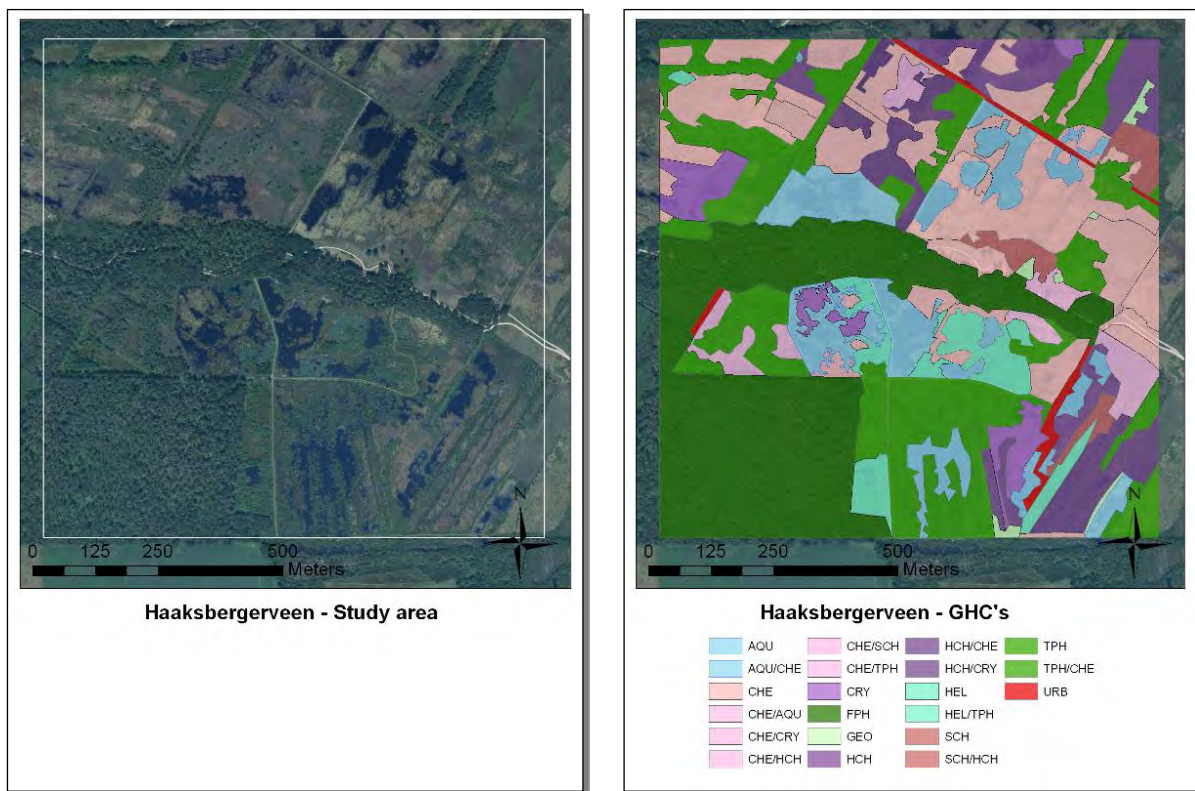


Figure 7: Haaksbergerveen (a) Aerial photograph with the study area delineated; (b): Identified GHCs.

There are 135 polygons divided over 10 single and 12 mixed GHCs. The classes with the highest number of patches are CHE, TPH and AQU covering in total 48.2% of the study area. FPH, CHE and TPH have fewer patches but occupy the most area (63.9%) (table 3). The 12 mixed classes jointly add up to 23 patches and represent 16% of the study area. In the south-west there is the only 'homogeneous' FPH patch, covering 23.2% of the total area (fig. 12b). The rest of the site is more fragmented.

Hyperspectral imagery to map General Habitat Categories and relation of classification success with site complexity

Table 3: Life form distribution of the Haaksbergerveen study site, showing the number of patches (n) and their representative area cover (%).

GHC	n	%	GHC	n	%
AQU	22	7,5	GEO	6	0,6
AQU/CHE	3	2,7	HCH	6	5,1
CHE	34	20,1	HCH/CHE	2	2,6
CHE/AQU	1	0,5	HCH/CRY	4	2,3
CHE/CRY	1	0,3	HEL	7	2,8
CHE/CRY/HCH	2	0,1	HEL/TPH	1	1,6
CHE/HCH	1	0,5	SCH	1	0,5
CHE/SCH	1	0,3	SCH/HCH	2	1,6
CHE/TPH	2	1,9	TPH	25	19,3
CRY	5	3,3	TPH/CHE	3	2,0
FPH	1	23,2	URB	5	1,2

4.1.2 SAM classification

The SAM classification of the Haaksbergerveen HyMap image is shown in figure 8a. The GHC URB is beyond the scope of this study and is excluded from the classification. SCH only appears in mixed GHCs and is excluded because it was impossible to select a pure endmember. Based on knowledge from the field, the other endmembers (fig.8b) were selected on the aerial photographs (fig.7a).

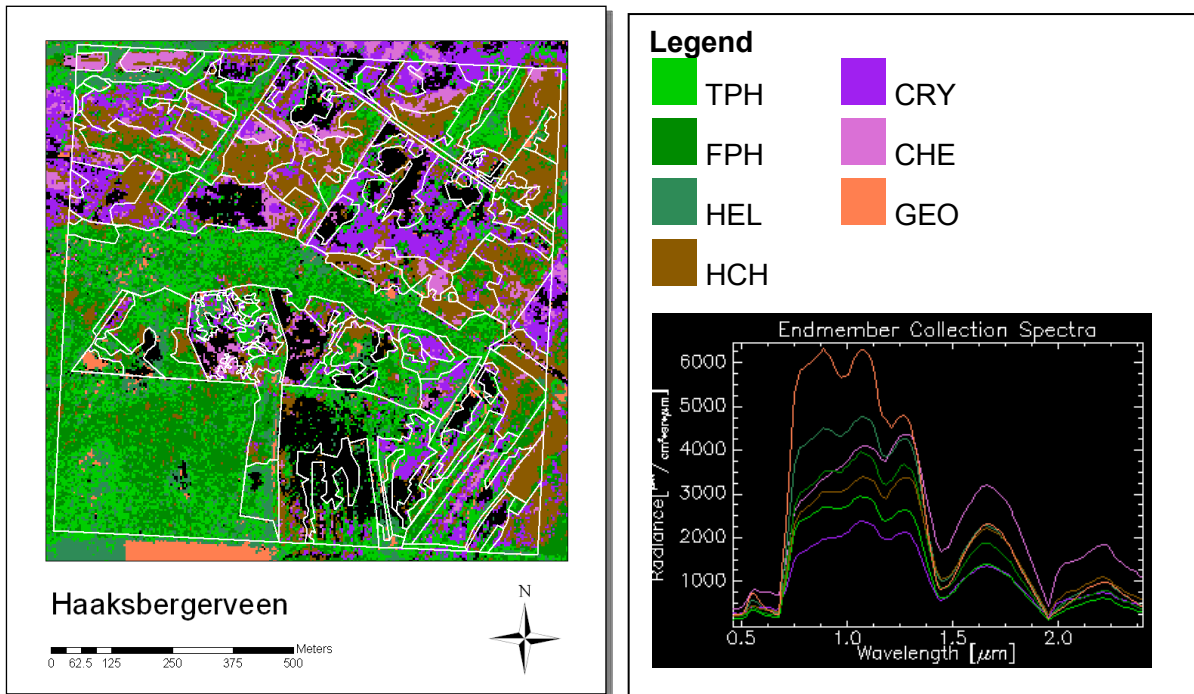


Figure 8: (a) The SAM classification of the Haaksbergerveen HyMap with the GHC maps as an overlay and (b) The endmembers used for the SAM classification.

The most striking shown by figure 8a are the classes almost entirely covered with the black 'not classified' dots. These correspond well with the occurrence of 'open' water in the area.

ANNEX-5

Hyperspectral imagery to map General Habitat Categories and relation of classification success with site complexity

The homogeneous FTP patch visible in figure 7b appears in the classification (fig.8a) as a mixture of categories, whereas other classes fit well with the GHC overlay.

4.1.3 Mapping success

There were 53 validation points selected on the aerial photograph, which results in 53 control pixels for the calculation of the error matrix.

Table 4: Confusion matrix of the SAM classification for the HyMap image of Haaksbergerveen.

Class	Ground Truth		(Percent)					Total
	CHE	HEL	CRY	FPH	TPH	HCH	GEO	
Unclassified	6	0	0	0	11	9	0	6
CHE	56	0	0	0	0	9	0	19
HEL	0	60	0	0	0	9	0	8
CRY	6	0	100	0	0	0	0	9
FPH	0	0	0	80	11	0	0	9
TPH	6	20	0	0	78	0	0	17
HCH	25	20	0	0	0	73	0	25
GEO	0	0	0	20	0	0	100	6
Total	100	100	100	100	100	100	100	100
Class	Prod. Acc. (Percent)		User Acc. (Percent)		Prod. Acc. (Pixels)		User Acc. (Pixels)	
CHE	56		90		9/16		9/10	
HEL	60		75		3/5		3/4	
CRY	100		80		4/4		4/5	
FPH	80		80		4/5		4/5	
TPH	78		78		7/9		7/9	
HCH	73		62		8/11		2/13	
GEO	100		67		2/2		2/3	

The overall mapping success is high: 71.15% and a Kappa coefficient of 0.65. From table 4 we see that especially GEO and CRY score well with 100% producers accuracy, whereas CHE (56%) and HEL (60%) scores low. The 'confusion' takes place with HCH and TPH, with low users accuracy.

4.1.4 GHC mapping success

The overall GHC-classification (table 5) is comparable with the Producers accuracy from the SAM classification (table 4) despite the fact that the overall success of the SAM classification is higher. The R^2 of the linear regression is 0,52 (fig.9) if the result of the GEO-life form, with no correct classification, isn't taken into account (if so R^2 is 0,05).

ANNEX-5

Hyperspectral imagery to map General Habitat Categories and relation of classification success with site complexity

Table 5: GHC mapping success for the combination SAM LF classification of Haaksbergerveen.

Haaksbergerveen								
	Life Form	CHE	HEL	CRY	FPH	TPH	HCH	GEO
Small	n	12	3	4	0	7	3	5
	Correct	1	1	2	0	1	3	0
	%	8	33	50	0	14	100	0
Middle	n	20	2	7	0	9	11	0
	Correct	2	0	7	0	1	6	0
	%	10	0	100	0	11	55	0
Large	n	27	3	6	1	16	10	0
	Correct	5	1	5	1	6	7	0
	%	19	33	83	100	38	70	0
Total	n	59	8	17	1	32	24	5
	Correct	8	2	14	1	8	16	0
	%	14	25	82	100	25	67	0

Comparing the mapping success in relation to the relative size of the patches, the large patches have in general a better classification than the overall mean and smallest patches. Figure 9 indicates in the direction of a linear relation between the SAM mapping success and the GHCs mapping success, but the accuracy for CHE, HEL, TPH and GEO is very low, even for the largest patches. None of the 5 GEO patches are correctly classified. Most of the GEO-patches are classified as HCH with a small central GEO-area (fig.8a). For the HEL life form, only one out of four is correct classified and there is a strong mixture with FPH/TPH (fig 8a). TPH in its turn is generally classified as FPH, and CHE is in general classified as CRY, HCH, and FPH in smaller patches.

Hyperspectral imagery to map General Habitat Categories and relation of classification success with site complexity

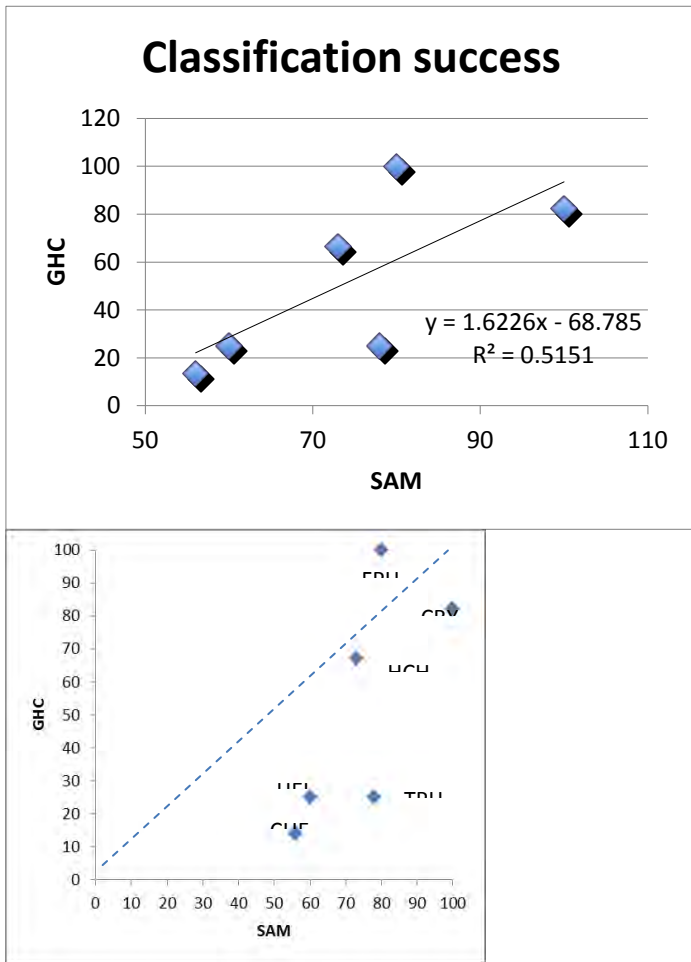


Figure 9: The relation between SAM- and GHC mapping success for Haaksbergerveen.

ANNEX-5

Hyperspectral imagery to map General Habitat Categories and relation of classification success with site complexity

Table 6: *GHC mapping success with combined life forms for Haaksbergerveen*

Haaksbergerveen			
	Life Form	CHE/CRY/HCH	FPH/TPH
Small	n	15	7
	Correct	8	7
	%	53	100
Middle	n	38	9
	Correct	34	8
	%	89	89
Large	n	26	16
	Correct	23	10
	%	88	63
Total	n	79	32
	Correct	65	25
	%	82	78

This indicates a strong confusion between comparable classes. The life forms which are frequently confused are aggregated in table 6. The combination of FPH and TPH give a mapping success of 78%, combining CHE, HCH, and CRY delivers a mapping success of 82%.

4.2 Korenburgerveen

4.2.1 GHC map of Korenburgerveen

The preliminary GHCs map was obtained from the aerial photographs of 2008 (fig. 10a). The validation of the GHC map was done in the field during October in 2009. Most of the area was accessible to control the preliminary borders, but some parts were too wet and/or just impossible to visit. These borders were checked by the use of a binocular or in a small number of cases not checked. The study area is delineated in figure 10a, the final GHCs map is shown in figure 10b.

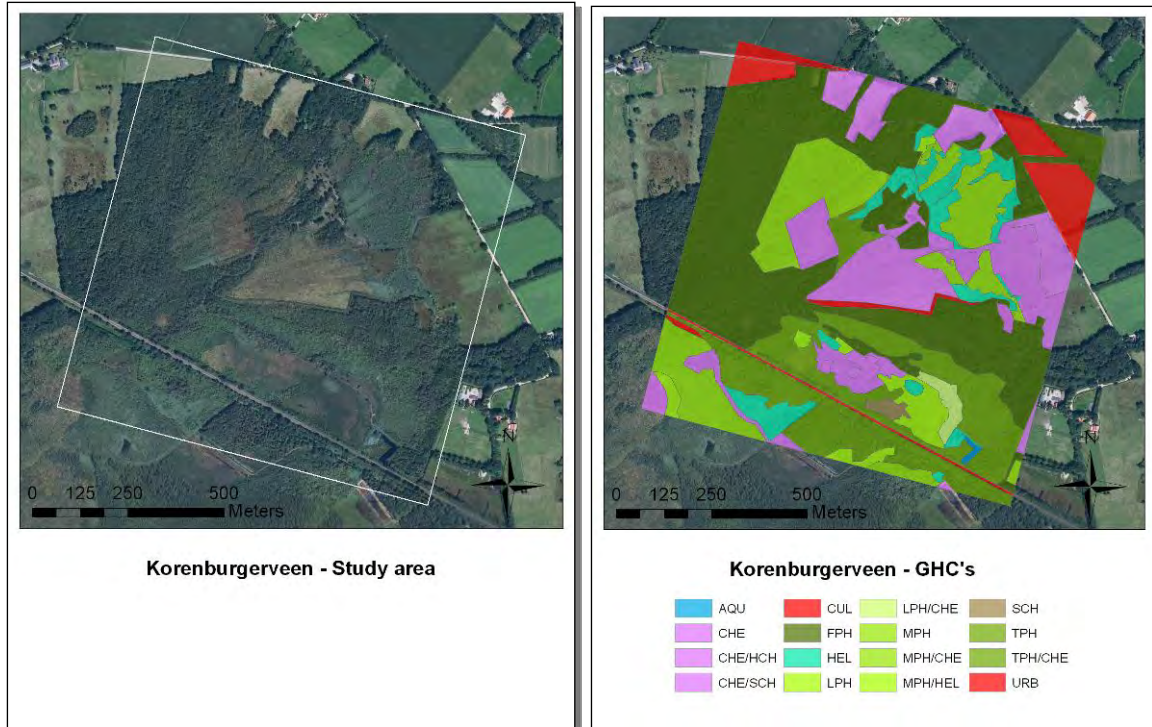


Figure 10: Korenburgerveen a) Aerial photograph with the delineated study area; b) Identified GHCs.

Table 7: Life form distribution of the Korenburgerveen study site, showing the number of patches (n) and their representative area cover (%).

GHC	n	%	GHC	n	%
AQU	1	0,1	LPH/CHE	1	0,8
CHE	13	12,7	MPH	6	8,0
CHE/CRY/HCH	1	4,3	MPH/CHE	2	4,1
CHE/HCH	3	1,1	MPH/HEL	1	0,1
CHE/SCH	1	0,6	SCH	1	0,4
CUL	5	5,3	TPH	12	14,5
FPH	10	33,9	TPH/CHE	1	2,3
HEL	16	5,6	URB	4	1,4
LPH	5	2,9			

The most frequent GHC patches are HEL, CHE, TPH and FPH. HEL accounts for most patches but covers just 6% of the area whereas CHE covers 17%, and TPH and FPH

respectively 15% and 34% (Table 7). The dominant life form is Phanerophytes, varying from low shrubs (LPH) to tall forest trees (FPH), and covers 60% of the area. Seven out of seventeen habitat classes have mixed life forms. However they cover just 13%. There is only a small patch of open water (AQU, 0.1%).

4.2.2 SAM classification

The classification of the Korenburgerveen HyMap image is done with the SAM classifier. The classification result is overlaid with the GHC field based polygon map (figure 11a). The GHCs URB and CUL are beyond the scope of this study and are excluded from the classification. Also the life forms that only appear in mixed GHCs (CRY, HCH, and SCH), AQU, and HEL are excluded because it was impossible to select pure endmembers. The other endmembers (fig.11b) were selected using the aerial photograph (fig.10), combined with knowledge from the field.

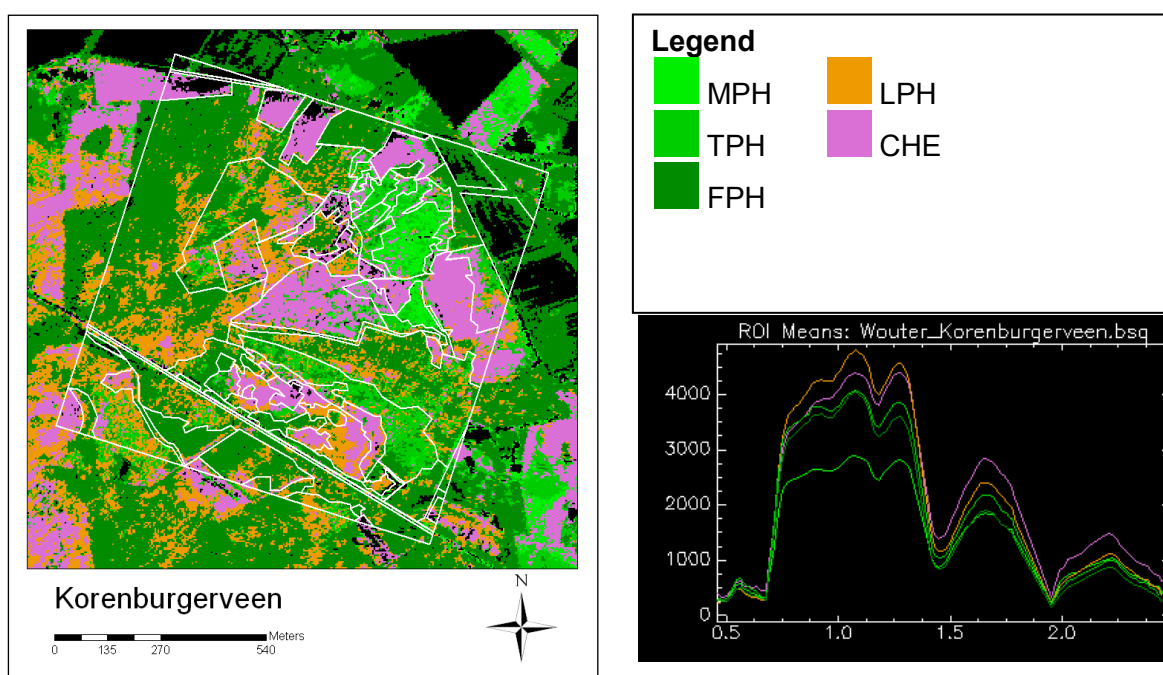


Figure 11: (a) The SAM classification of the Korenburgerveen HyMap overlaid with the GHC field maps and (b) its endmembers used.

As shown in figure 11a, some classified categories, such as CHE, match up well with the GHC outlines acquired from the field. The GHC-boundaries delineate (relatively) well the CHE classification. Other GHCs tend to show a more mixed/speckled classification like the FPH. Especially LPH tends to appear in FPH GHC patches (compare with fig.10b). Figure 11b shows the endmembers of FPH and LPH popping up amongst CHE and TPH. The black dots are 'not classified', due to a lack of endmembers for the cultivated species, water bodies and rare mixed life forms.

4.2.3 SAM validation

36 validation points were selected on the aerial photograph, and used for the calculation of the confusion matrix.

Table 8: Confusion matrix of the SAM classification for the HyMap image of Korenburgerveen.

Class	Ground Truth					Total
	MPH	CHE	LPH	TPH	FPH	
Unclassified	0	0	0	0	0	0
MPH	20	0	0	0	0	3
CHE	0	100	0	0	0	25
LPH	0	0	83	0	0	14
TPH	40	0	0	50	0	14
FPH	40	0	17	50	100	44
Total	100	100	100	100	100	100

Class	Prod. Acc. (Percent)	User Acc. (Percent)	Prod. Acc. (Pixels)	User Acc. (Pixels)
MPH	20	100	1/5	1/1
CHE	100	100	9/9	9/9
LPH	83	100	5/6	5/5
TPH	50	60	3/6	3/5
FPH	100	63	10/10	10/16

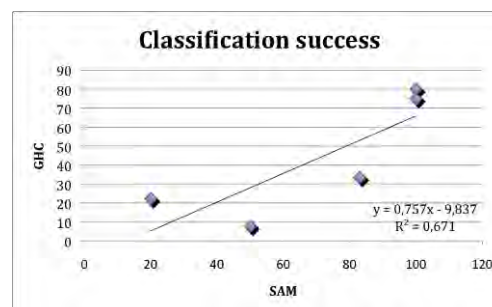
The overall mapping success is 77,78% with a Kappa coefficient of 0,71. Especially CHE and FPH score well with 100% producers accuracy, whereas MPH and TPH score low with 20 and 50% (table 8). The 'confusion' occurs mostly with FPH. Half of the TPH and 40% of the MPH training pixels are classified as FPH; as well 40% of MPH and 17% of LPH is classified as TPH. This is also represented in the low users accuracy (table 8) for TPH and FPH.

4.2.4 GHC classification

The total GHC-classification (table 9) is comparable with the Producers accuracy (table 8) from the SAM classification but overall the classification success of SAM is higher. The R^2 of the linear regression is 0,67 (fig.12), suggesting an positive relation (note that the number of observations is very limited).

Table 9: GHC mapping success of Korenburgerveen.

Korenburgerveen						
Area	Life Form	MPH	CHE	LPH	TPH	FPH
Small	n	3	6	2	1	3
	Correct	0	4	0	0	3
	%	0	67	0	0	100
Middle	n	2	10	2	6	1
	Correct	0	9	0	0	0
	%	0	90	0	0	0
Large	n	4	12	2	6	6
	Correct	2	8	2	1	5
	%	50	67	100	17	83
Total	n	9	28	6	13	10
	Correct	2	21	2	1	8
	%	22	75	33	8	80

**Figure 12:** Relation between SAM- and GHC mapping success for Korenburgerveen.

Comparing the mapping success in relation to the size of the patches, the large patches achieve a higher accuracy than the overall classification. The small- and middle-sized patches generally show lower classification successes.

4.2.5 GHC map of Millingerwaard

The GHC map of Millingerwaard (fig. 13) was already presented in the the internshop report of Ana Ruiz: 'Monitoring habitats by remote sensing data'. The fieldwork was realized during July and August 2006.

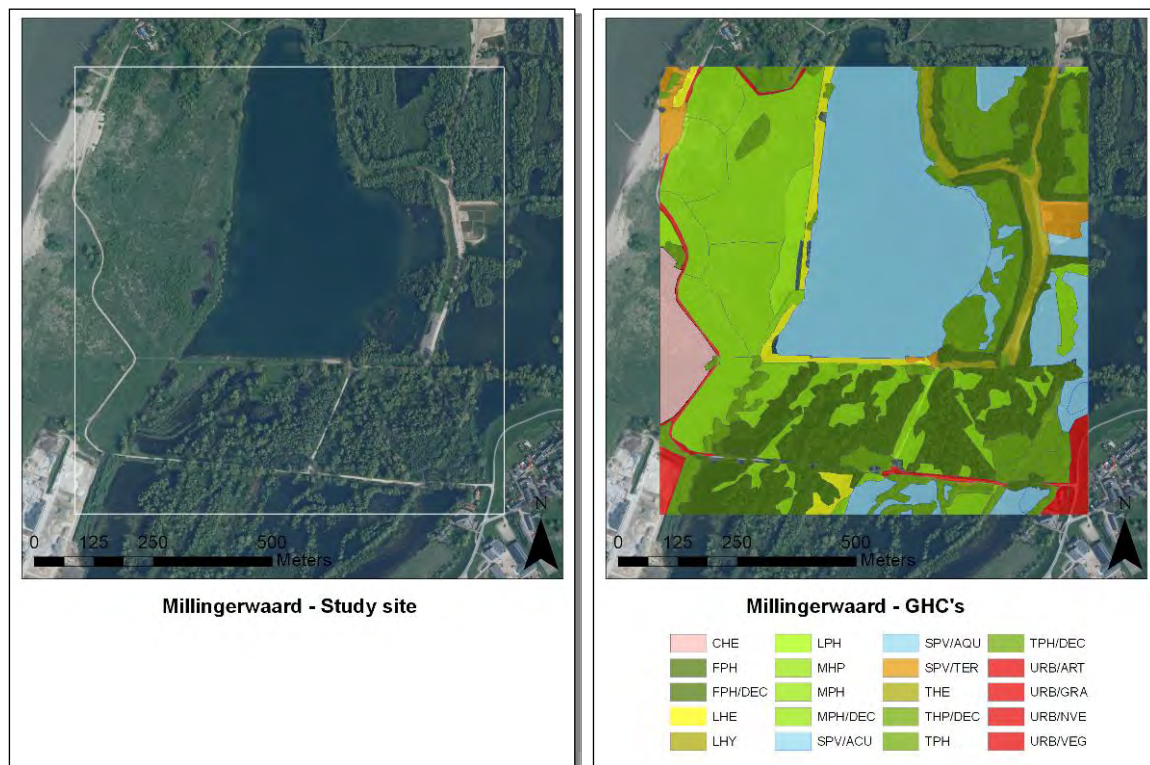


Figure 13: Millingerwaard (a): Aerial photograph with the delineated study area; (b): Identified GHCs.

Table 10: Life form distribution of the Millingerwaard study site, showing the number of patches (n) and their representative area cover (%).

Millingerwaard		
GHC	n	%
CHE	1	2,7
FPH	4	20,5
LHE	3	4,9
LPH	2	1,7
MHP	15	23,8
SPV/AQU	5	27,1
SPV/TER	3	1,7
THE	1	0,2
TPH	11	14,4
URB/ART	1	1,0
URB/GRA	1	1,1
URB/NVE	1	0,6
URB/VEG	1	0,2

Table 10 shows that the 49 polygons are divided over 14 GHC classes (10 classes if the URB classes are merged). The classes with the highest number of patches are MPH and TPH while AQU, MPH and FPH occupy the most area. Most of the classes are based on the differences between the phanerophytes.

4.2.6 SAM classification

The classification of the Millingerwaard HyMap image is done with the SAM classifier. The GHC category URB is beyond the scope of this study and is excluded from the classification. CHE, CRY, THE, LPH, EHY and HCH only appear in mixed GHCs and

were excluded because it was impossible to select pure endmembers. The other endmembers were selected on the aerial photographs, with knowledge from the field.

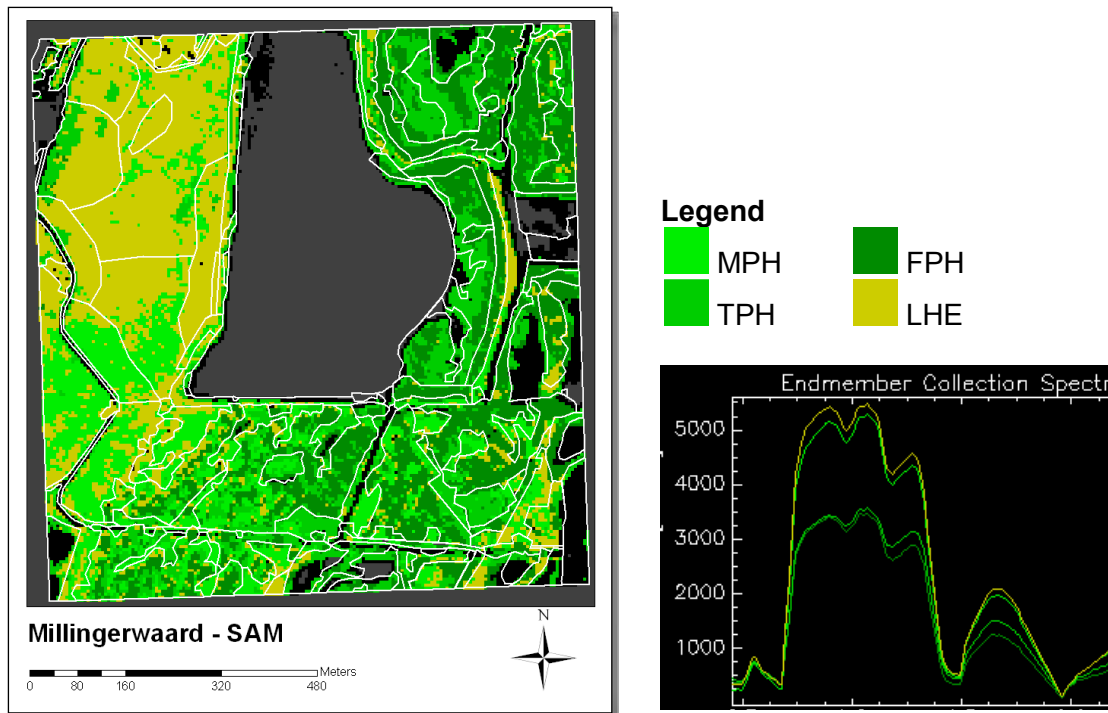


Figure 14: (a) The SAM classification of the Millingerwaard HyMap with the GHC maps as an overlay and (b) the endmembers used for the classification.

The spectra of the endmembers (fig.14b) show two separated endmember-classes: FPH/TPH (lower two) and MPH/LHE (upper two), with closely related spectra. For FPH/MPH the SAM classification follows relatively well the GHCs (eastern part of fig.14a), whereas for MPH/LHE it does not do a good job (western part of fig.14a). The central grey spot is the clay pit, masked out with an NDVI-mask. Compared with figure 13a, most of the other black spots are also water or bare soil.

4.2.7 Mapping success

There were 40 points selected on the aerial photograph, which results in 40 control pixels for the calculation of the confusion matrix.

Table 11: Confusion matrix of the SAM classification for the HyMap image of the Millingerwaard.

Class	Ground Truth (Percent)				Total
	FPH	TPH	MPH	LHE	
Unclassified	0	9	0	9	3
FPH	100	27	11	0	40
TPH	0	55	0	13	18
MPH	0	0	67	13	18
LPH	0	9	22	75	23
Total	100	100	100	100	100

Class	Prod. Acc.	Users Accr.	Prod. Acc.	Users Accr.
	(Percent)	(Percent)	(Pixels)	(Pixels)
FPH	100	75	12/12	12/16
TPH	55	86	6/11	6/7
MPH	67	86	6/9	6/7
LHE	75	67	6/8	6/9

The overall mapping success is high: 75,00% and a Kappa coefficient of 0,67. From table 11 we see that only FPH scores 100% producers accuracy, and that there is a lot of confusion between MPH, TPH and FPH. Here again we can notice the two classes, distinguished by the spectrum in figure 14b. MPH and LHE have their largest confusion in between. For TPH the confusion happens with FPH, but not the other way around.

4.2.8 GHC classification success

The overall GHC-classification success (table 12) is comparable with the producers accuracy from the SAM classification (table 11) despite the fact that the overall success of the SAM classification is bit higher. The R^2 of the linear regression is 0,93 (fig.15) indicating a relationship between the mapping success of the SAM classification and the determination of the GHCs.

Table 12: Mapping success for the determination of GHCs for the Millingerwaard.

Millingerwaard					
	Life Form	TPH	MPH	FPH	LHE
Small	n	3	8	0	4
	Correct	0	4	0	2
	%	0	50	0	50
Middle	n	2	8	0	6
	Correct	2	3	0	5
	%	100	38	0	83
Large	n	4	8	4	7
	Correct	2	5	4	6
	%	50	63	100	86
Total	n	9	24	4	17
	Correct	4	12	4	13
	%	44	50	100	76

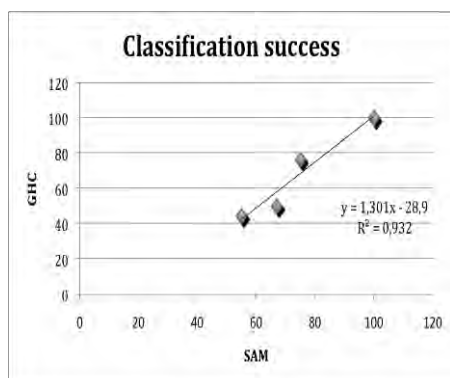


Figure 15: Relation between SAM- and GHC- mapping success for the Millingerwaard.

Comparing the mapping success in relation to the size of the patches (table 12), the large patches have a relatively better classification than the overall classification. The accuracy for TPH and MPH is low, even for the largest patches because most of the patches with an MPH or TPH life form are classified as FPH. Another remarkable effect is the difference in proportion between the GHC and SAM map of the combination MPH-LHE. Due to the elimination of the CHE, CRY, THE, LPH, EHY and HCH classes in the SAM classification these classes are excluded from this validation.

4.3 Wageningen Floodplain

4.3.1 GHC map of Wageningen floodplain

The GHC map of the Wageningen Floodplain was already presented in the Internship report of Ana Ruiz: 'Monitoring habitats by remote sensing data'. The fieldwork was realized during July and August 2006.

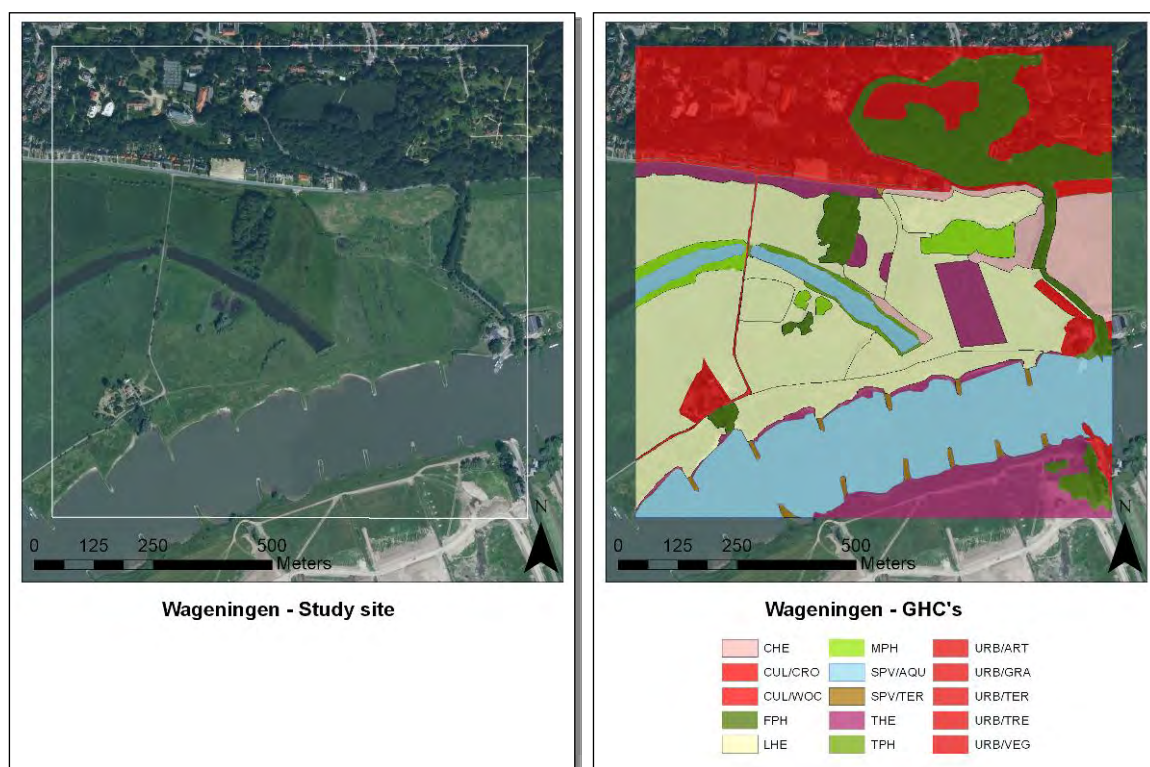


Figure 16: Wageningen (a): Aerial photograph with the delineated study area; (b): Identified GHCs.

Table 13: Wageningen, total number of patches (*n*) and their % area cover.

Wageningen		
GHC	N	%
CHE	3	4,2
CUL/CRO	1	0,4
CUL/WOC	1	0,2
FPH	8	9,8
LHE	9	32,8
MPH	5	2,1
SPV/AQU	2	18,1
SPV/TER	2	0,5
THE	6	9,6
TPH	1	0,5
URB/ART	4	1,4
URB/GRA	1	3,6
URB/TER	1	14,0
URB/TRE	1	1,5
URB/VEG	1	1,7

Table 13 shows that there are 46 polygons delineated during the GHC mapping, divided over 15 GHC classes. The classes with the highest number of patches are FPH and LHE, and together with AQU they occupy most of the area.

4.3.2 SAM classification

The classification of the Wageningen Floodplain HyMap image is done with the SAM classifier. The GHC category URB is beyond the scope of this study and is excluded from the classification. It was not possible to select MPH and TPH endmembers. The other endmembers were selected on the aerial photographs, with the knowledge from the field.

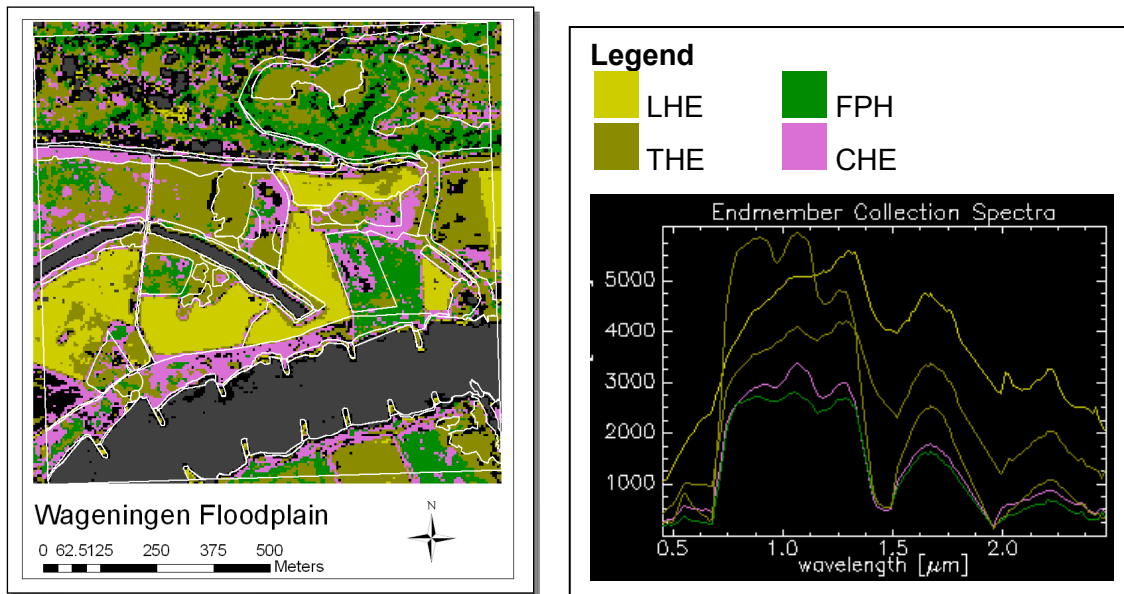


Figure 17: (a) The SAM classification result of the Wageningen floodplain overlaid with the GHC field maps (b): The endmembers used for the classification.

Although the endmembers are well separated from each other (fig.17b), the classification appears to be speckled (fig.17a). The endmember spectrum (fig. 17b) of LHE does not display the typical spectral features of vegetation which is clearly visible in the other spectra.

4.3.3 Mapping Success

There were 36 points selected on the aerial photograph, which results in 36 control pixels for the calculation of the confusion matrix.

Table 14: Confusion matrix of the SAM classification for the HyMap image of the Wageningen floodplain.

Class	Ground Truth (Percent)					Total
	CUL/THE	CHE	FPH	LHE	THE	
Unclassified	0	14	0	0	0	3
CUL/THE	100	14	0	8	20	14
CHE	0	71	0	17	40	25
FPH	0	0	70	8	0	22
LHE	0	0	0	58	0	19
THE	0	0	30	8	40	17
Total	100	100	100	100	100	100

Class	Prod. Acc. (Percent)	User Acc. (Percent)	Prod. Acc. (Pixels)	User Acc. (Pixels)
CUL/THE	100	40	2/2	2/5
CHE	71	56	5/7	5/9
FPH	70	88	7/10	7/8
LHE	58	100	7/12	7/7
THE	40	33	2/5	2/6

The overall mapping success is 64,00% and a Kappa coefficient of 0,55. Especially CUL scores well with 100% producers accuracy, whereas THE scores low (table 14). The 'confusion' happens with both CUL and THE, with low users accuracy.

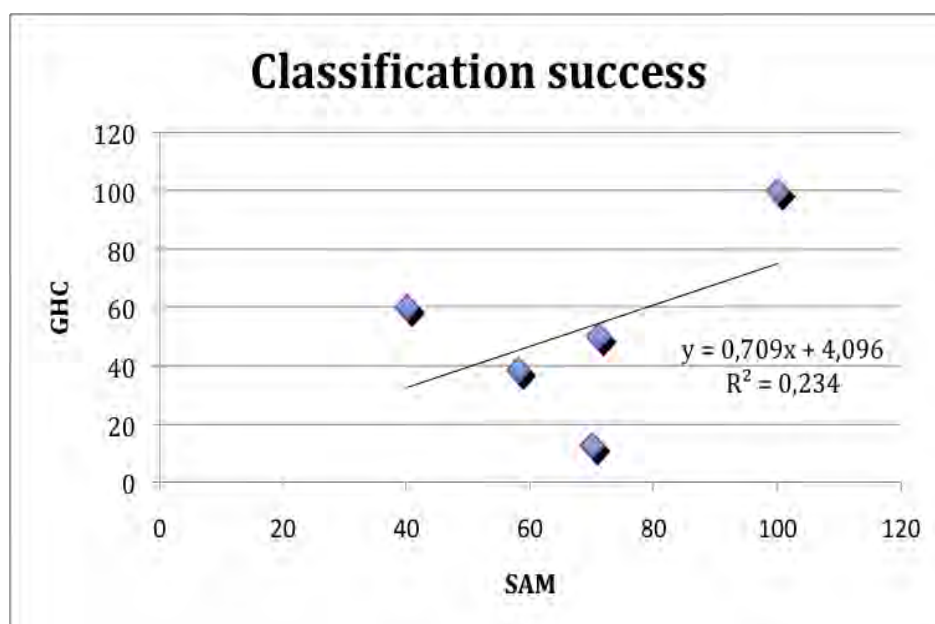
4.3.4 GHC classification success

The overall GHC-classification (table 15) is comparable with the producers accuracy from the SAM classification (table 14) despite the fact that the overall success of the SAM classification is higher. Figure 18 shows a linear regression (R^2 of 0,23).

Comparing the mapping success in relation to the size of the patches in table 15, the large patches have a better classification success. Especially the small patches have a very low classification success, only two patches are classified correct. The accuracy to determine FPH- and LHE-patches is also low. The mapping success of LHE is even low for the largest patches, LHE only appears in patches with mixed life forms. For FPH none of the small and middle patches are correctly classified, most of them are classified as THE. Due to the elimination of the MPH- and TPH-classes in the SAM classification these classes are excluded from this validation.

Table 15: Mapping success for the determination of GHCs for the Wageningen floodplain.

Wageningen floodplain						
	Life Form	CUL (THE)	CHE	FPH	LHE	THE
Small	n	1	1	5	4	2
	Correct	1	0	0	0	1
	%	100	0	0	0	50
Middle	n	0	4	2	2	3
	Correct	0	2	0	1	0
	%	0	50	0	50	0
Large	n	0	7	1	7	5
	Correct	0	4	1	4	5
	%	0	57	100	57	100
Total	n	1	12	8	13	10
	Correct	1	6	1	5	6
	%	100	50	13	38	60

**Figure 18:** Relation between SAM- and GHC- mapping success for the Wageningen floodplain

4.4 Overview of the site complexity

4.4.1 Biological Complexity

Table 16 gives the biological diversity measures calculated for the different study sites which are grouped according to habitat.

Table 16: Overview of the Biological complexity indicators.

Biological Complexity	Floodplains		Peat bogs	
	Wageningen	Millingerwaard	Korenburgerveen	Haaksbergerveen
Plant Species	103	109	43	45
Shannon	4,45	4,57	2,94	3,3
Simpson	0,00913	0,00636	0,03280	0,02496
LF-diversity	7	10	9	10
Mixed LF(%)	36,9	56,3	13,3	14,3

For 4 of the 5 diversity measures a clustering according to habitat can be observed. Wageningen-Millingerwaard have a comparable number of species occurrence, a higher species diversity, so a higher Shannon diversity index and a lower Simpson's diversity index, and a higher coverage with mixed Life Forms. Only the life form diversity does not follow this trend. This indicates that floodplains have a higher biological complexity than peat bog areas.

There are also within-habitat differences: the differences between Wageningen and Millingerwaard are very small but the general trend is that the Millingerwaard has a higher biological complexity than the Wageningen floodplain. The differences for peatland are also very small, indicating that Haaksbergen has a higher biological diversity than Korenburgerveen.

These biological complexity indicators show that Millingerwaard and Wageningen, as representations of the floodplains, tend to have a higher biological complexity than Korenburgerveen and Haaksbergerveen (peat bogs) and that the within-habitat differences are very small.

4.4.2 Spectral Complexity

An overview of the spectral complexity indicators is given in table 17, separated for the different study sites and habitats.

Table 17: Overview of the Spectral complexity indicators.

Spectral Complexity	Floodplains		Peat bogs	
	Wageningen	Millingerwaard	Korenburgerveen	Haaksbergerveen
Spectral richness	9,54	7,18	15,24	8,65
Spectral richness SD	3,34	1,58	2,63	1.00
1 PC variance	82,03	94,12	81,87	89,32
2 PC variance	97,27	99,55	85,67	97,37
3 PC variance	98,66	99,75	97,28	98,24
number of bands for 99,9% variance	9	5	15	13

The spectral richness of Korenburgerveen is much higher than the three other areas. This trend is also present in the relatively low explained variance for the first two principle components. Korenburgerveen has the overall highest spectral complexity.

The inside-habitat differences for floodplains show a clear pattern, Wageningen has a higher spectral complexity than Millingerwaard. For the peatland areas Korenburgerveen has a higher spectral complexity. The difference is greater between the peatland areas than between the floodplain areas.

4.4.3 Landscape complexity

An overview of the calculated landscape complexity indicators, is given in table 18.

Table 18: Overview of the Landscape complexity indicators.

Landscape Complexity Indicator	Floodplains		Peat bogs	
	Wageningen	Millingerwaard	Korenburgerveen	Haaksbergerveen
NP	75	88	71	106
PD	70,4	96,5	47,3	105,5
TE	20740	26320	30810	33880
ED	194,6	288,7	205,3	337,1
Area Mean	1,329	0,961	2,114	0,943
SD	4,538	2,690	5,831	2,488
Shape Mean	1,7926	2,009	2,010	1,957
SD	0,852	0,858	1,084	0,775
SHDI	1,779	1,881	2,060	2,307
SIDI	0,799	0,807	0,812	0,855
MSIDI	1,602	1,646	1,672	1,931
SHEI	0,773	0,733	0,713	0,747
SIEI	0,887	0,874	0,860	0,896
MSIEI	0,696	0,642	0,578	0,625

The pattern from table 18 is that the Wageningen-Korenburgerveen (W&K) and Millingerwaard-Haaksbergerveen (M&H) cluster together for the landscape complexity indicators. W&K has a lower patch and edge density and a tendency for larger area means, but also for higher standard deviations on that mean. For the more complex landscape metrics like the Shannon and Simpsons indices, this pattern is not clear. The differences between the peat bog areas are most of the time larger than those of the floodplains, indicating a higher within-habitat complexity. The within-habitat differences show that Millingerwaard has a higher landscape complexity than Wageningen and Haaksbergerveen tends to have the highest landscape complexity for the peatland areas.

The relation between mapping success and site complexity

4.4.4 Mapping success

An overview of the mapping success for the different habitats and study sites is given in table 19.

Table 19: Mapping Success.

	Floodplains		Peat bogs	
	Wageningen	Millingerwaard	Korenburgerveen	Haaksbergerveen
SAM Classification (%)	64,0	75,0	77,8	71,2
Kappa	0,55	0,67	0,71	0,65
GHC Classification (%)	39,9	64,7	50,9	40,4

Wageningen has the lowest classification success for the SAM and the GHC classification (table 19). Although Haaksbergerveen shows a good SAM mapping, the recognition of the life forms is low in comparison to the Millingerwaard and Korenburgerveen. They have a comparable SAM classification but the Millingerwaard has a better GHC classification. On average peat bogs show a higher classification success, but the values of Millingerwaard and Korenburgerveen are almost similar. The differences within the habitats are clear, Millingerwaard for the floodplains and Korenburgerveen for the peat bog areas have the best mapping success. In the next sections the Kappa coefficient is used to represent the SAM Mapping Success.

4.4.5 The relation between Biological Complexity and Mapping Success

There is a negative relation between the kappa coefficient and the species richness (fig.19a), indicating that a higher species richness tends to result in a lower mapping success. The same pattern appears for the diversity indices (fig.19bc), a high diversity, represented by a high Shannon and a low Simpson index value, leads to a lower mapping success. For the percentage cover of mixed life forms, no pattern is observed (fig 19d, $R^2=0.08$).

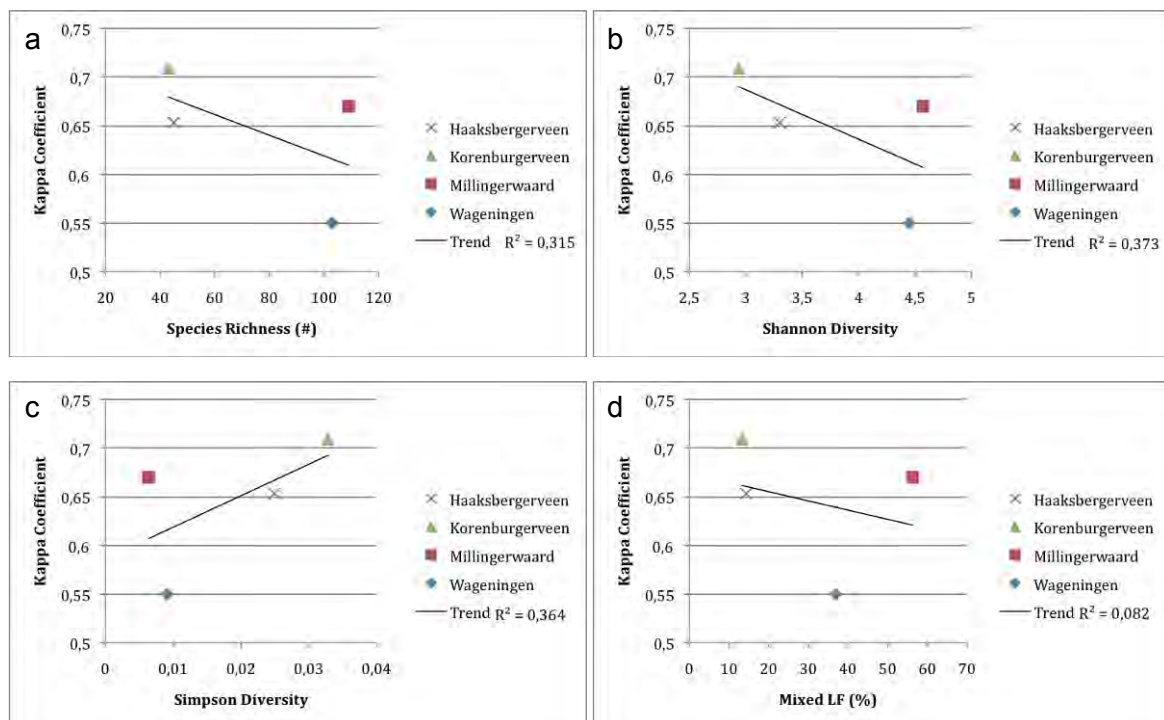


Figure 19: Mapping success, represented by the kappa coefficient, versus the indicators for the Biological Complexity. a) species richness, b) Shannon diversity, c) Simpsons diversity, and d) Mixed life forms(%).

A contradictory observation is seen in figure 20, the relation between the number of life forms in a study area and the mapping success, suggesting that the more life forms present in the area, the better is the classification. Wageningen, with the lowest mapping success, shows the most distinct values (fig 19 and 20).

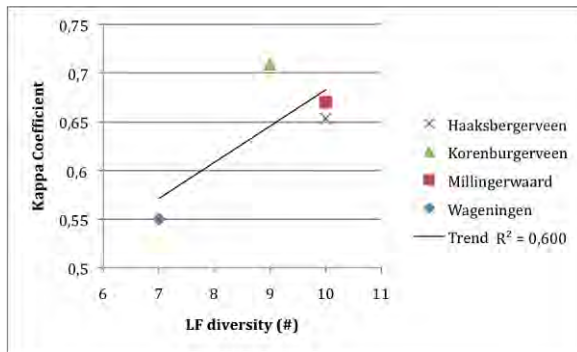


Figure 20: Mapping success, represented by the kappa coefficient, versus Life Form diversity.

4.4.6 The relation between Spectral Complexity and Mapping Success

The spectral complexity was covered by the spectral richness, the explained variance by the first 3 PC bands and the total PC bands to cover at least 99.9% of the variation. Only the spectral richness will be related to the mapping success, the two others are more descriptive.

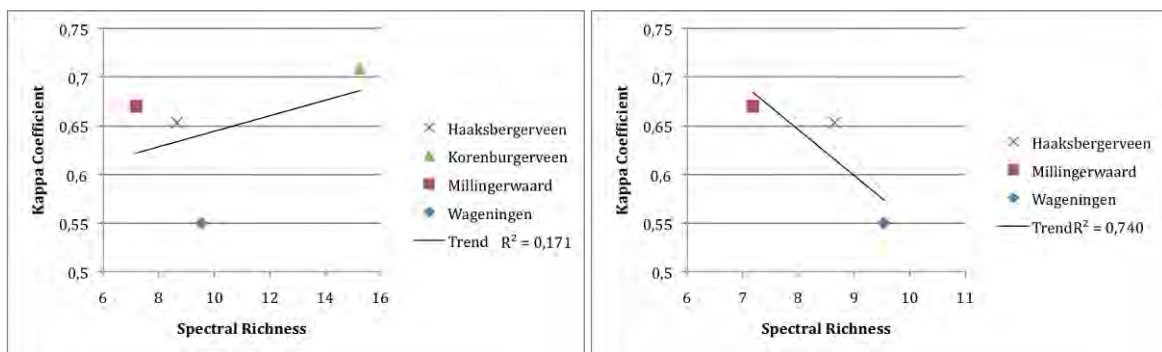


Figure 21: Mapping success, represented by the kappa coefficient, versus spectral richness. Left, With Korenburgerveen area, R^2 of 0.17; right, Without Korenburgerveen area, R^2 of 0.74.

The graph in figure 21a indicates a (weak) positive relationship between the spectral richness and the mapping success. The point with the highest spectral richness can be seen as an outlier. Due to the appearance of cloud shade in the image and visible residuals in the corrected spectroscopy data Korenburgerveen is left out. Further research is needed to determine the exact cause of this high value. The result in figure 22b is a stronger but negative relationship between spectral richness and the kappa coefficient, suggesting that a high spectral richness leads to a lower mapping success.

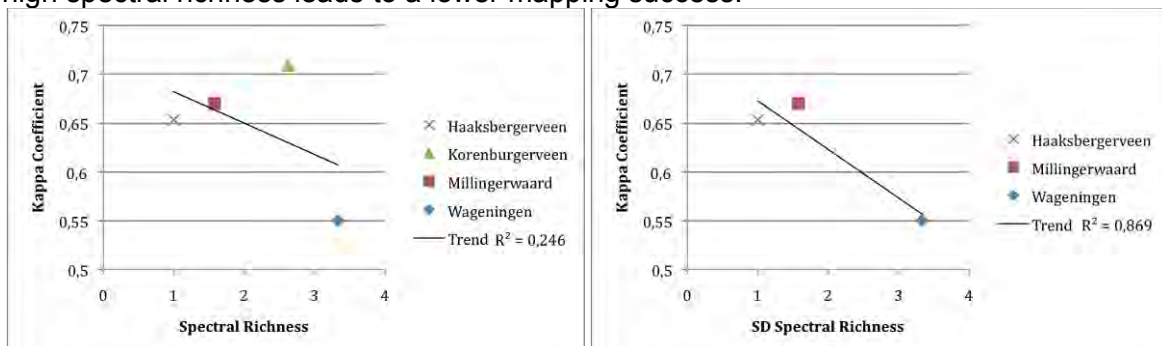


Figure 22: Mapping success, represented by the kappa coefficient, versus the standard deviation of the spectral richness. Left, With Korenburgerveen area, R^2 of 0.25; right, Without Korenburgerveen area, R^2 of 0.87.

The graph in figure 22a indicates a negative relationship between the SD Spectral richness and the mapping success. The result in figure 22b without the Korenburgerveen shows a stronger negative relationship, suggesting that a high SD spectral richness lead to a lower mapping success.

4.4.7 The relation between Landscape Complexity and Mapping Success

There is a positive relationship observed between the area mean, the shape mean, and the edge density in relation with the mapping success represented by the kappa statistic (fig. 23, a, c, e). This indicates contradictory relations: A larger area mean seems to give a better classification, indicating a better mapping success for larger mean patches of less complexity (area mean). However, also more complex landscape patterns seem to improve the classification (shape mean and total edge). The standard deviations of the area mean and shape mean (fig. 24 b, c) follow the same pattern, indicating that a higher standard deviation leads to a better mapping success.

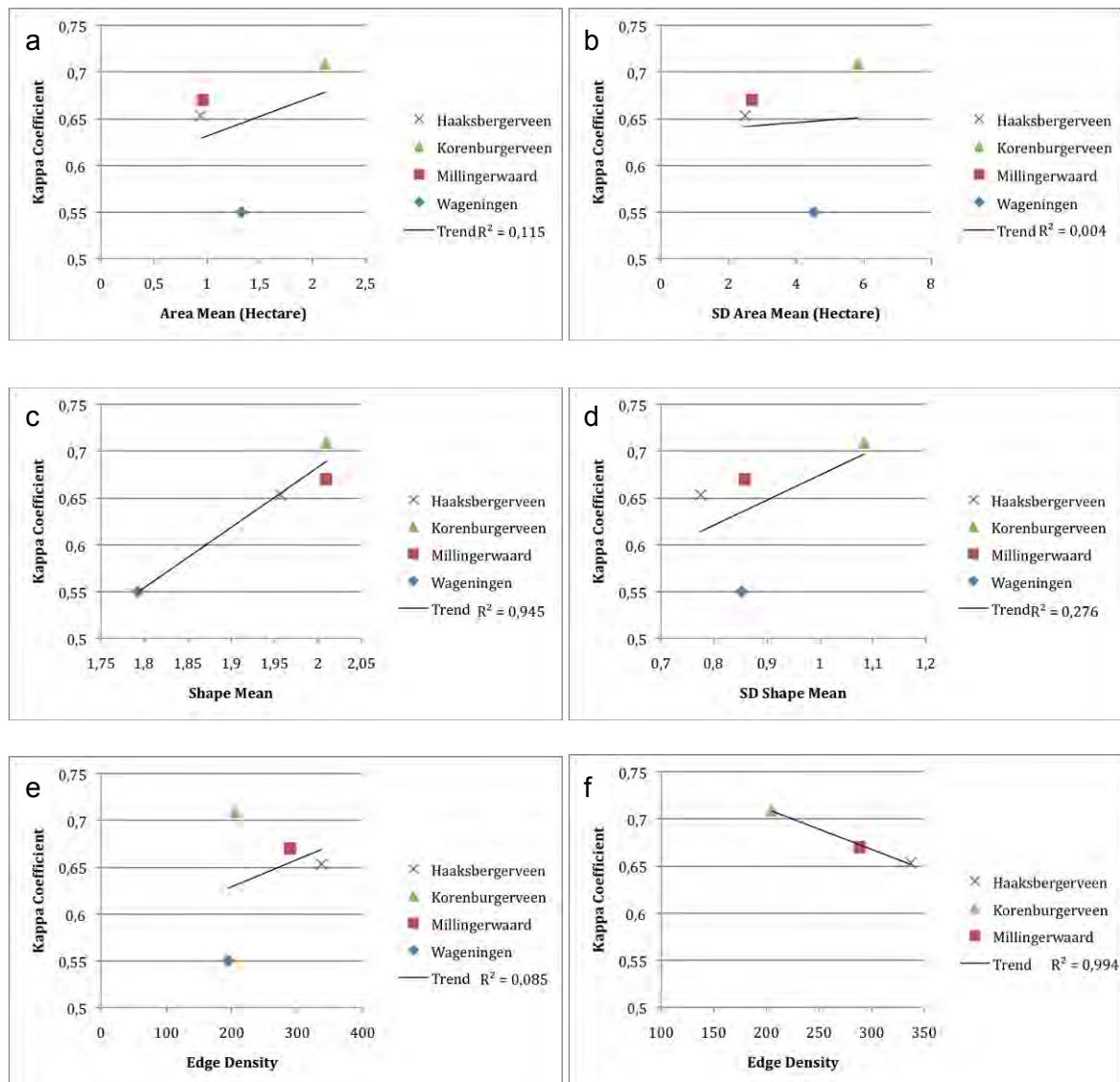


Figure 23: Mapping success, represented by the kappa coefficient, versus the Landscape Complexity indicators: **a)** Area Mean, R^2 of 0,12; **b)** SD Area Mean, R^2 of 0; **c)** Shape mean, R^2 of 0,94; **d)** SD Shape Mean, R^2 of 0,28; **e)** Shape Mean, R^2 of 0,09; **f)** Edge Density, without Wageningen, R^2 of 0,99.

Figure 23 also clearly indicates that the floodplain of Wageningen has an exceptional behaviour in relation to the other study sites (fig 23, a-e). Figure 23f shows a strong pattern ($R^2=0.99$) without Wageningen, indicating that a high edge density causes a lower mapping success. This is contradictory to fig 23e with Wageningen included. The evenness indices in relation to the mapping success suggest strong negative relationships (fig. 24, b, d, f): the Simpson's evenness index (SIEI, $R^2=0.39$), the modified Simpson's evenness index (MSIEI,

$R^2=0.89$) and the Shannon's evenness index (SHEI, $R^2=0.94$). This relationship indicates that the higher the evenness is, so the more even the distribution of the area, the lower the mapping success. A positive but very weak relationship is observed between the diversity indices and mapping success (fig. 24, a, c, e). The floodplain of Wageningen shows again a different behaviour in relation to the other study sites (fig 24, a, c, d, e).

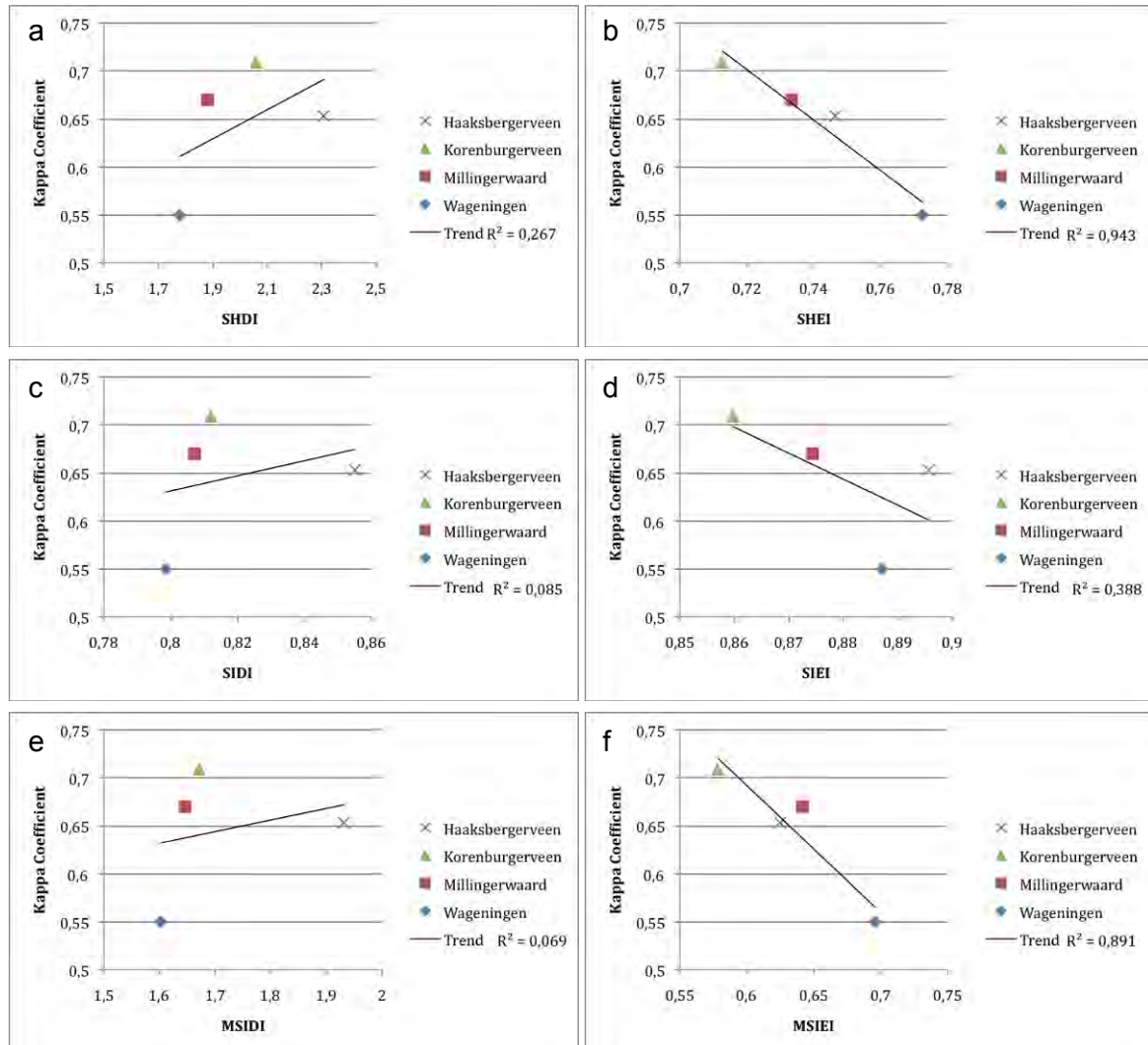


Figure 24: Mapping success, represented by the kappa coefficient, versus the Landscape Complexity indicators: **a)** Shannon Diversity index, R^2 of 0.27; **b)** Shannon Evenness Index, R^2 of 0.94; **c)** Simpson Diversity Index, R^2 of 0.09; **d)** Simpson Evenness Index, R^2 of 0.39; **e)** Modified Simpson Diversity Index, R^2 of 0.08; **f)** Modified Simpson Evenness Index, R^2 of 0.89.

5 Discussion

5.1 *GHC mapping*

The GHC classification methodology was successfully applied to four sites, covering two different ecosystems in the Netherlands. The results are representative habitat maps of these areas. Although two different observers made the field-based habitat maps at different a time. This can influence the results because the delineation is based on assumptions you make while interpreting the aerial photographs and the situation in the field. The suggestion from the handbook (Bunce et al. 2005) for an intensive training before the application of the GHC methodology will improve the success and comparability of the results. Analysis shows that the dominant life forms (70-100% cover) are overestimated in the field, whereas a secondary life forms are slightly underestimated by the SAM classification This indicates that 100% life form cover often is an overestimation whereas the life forms with a small coverage are often underestimated. The Millingerwaard shows also an over and underestimation problem. There were many under and overestimations by comparing the GHCs cover percentages with the SAM result. There may also be something wrong with the SAM classification, or the estimation of cover percentage is difficult in the case of Phanerophytes in lower vegetation: How to define the exact vertical cover of trees in a grassland? A last remark on the GHC methodology: In the determination of the GHC categories, Phanerophytes are overruling the other life forms by definition whereas for the evaluation of the habitat these percentages could be an indicator of the ecological status of the area. This is especially the case in peatland where the occurrence of Phanerophytes like birch could be an indicator for degradation.

5.2 *SAM classifications*

All areas were classified using the SAM classifier for the hyperspectral HyMap data. Although the overall mapping success is high, from 64 till 78% (table 19), there are huge differences in classification accuracy between the classified life forms. A common 'error' in the SAM classification is that one phanerophyte class with a high producers accuracy but a low users accuracy tends to overrule another phanerophyte class with the low producers and high users accuracy. This can be observed by comparing table 4&5, 7&8, and 11&12. This is probably because the HYMAP data cannot differentiate height classes if they are dominated by the same species. This was clearly observed in the Haaksbergerveen study area where the life forms TPH and FPH probably were represented by a 'species' endmember. The occurrence of the endmember species can be related to a representative life form but can also occur (under different site conditions) as another life form, e.g. under ideal conditions oak or birch occur as FPH, but younger trees or trees under stress can also occur as MPH or TPH. The SAM classifier is able to detect phanerophytes, probably on a species-level, but for the determination of the height aspect another technique is needed, like LiDAR is needed. Difficulties were encountered with the selection of representative endmembers for water bodies and bare soil, due to a high spectral variability. Here the theory of Underwood et al. (2007) is applicable: finer spatial resolution may reduce the classification accuracy by increasing within-class variability. Even with an NDVI-mask it was not possible to mask out all the water bodies For several life forms it wasn't possible to select a representative endmember based on the aerial photographs and so they were not used in the classification. Also the selection of reference pixels should be spatially randomly selected, proportional to the covered area to obtain a better and comparable mapping success

5.3 GHC classification success

Constructing GHC maps with the SAM classification data tends to yield a lower mapping success than that of the SAM classifier, from 40% till 65%. The observed linear relationship between GHC mapping success and the SAM mapping success (R^2 from 0.23 to 0.93) indicates that the identification of GHCs from the SAM classification strongly depends on SAM mapping success. This is logical, the better the SAM classification, the better is the input for classifying GHCs.

The use of hyperspectral imagery could be quite powerful if life forms are spectrally distinct and the within life form spectral range (variability) does not overlap between life forms. To achieve a GHC map you will need to (depending on the spatial resolution of the imagery) either impose parcel outlines or unmix the imagery. For the distinction of the height based life forms you will need to use lidar. The SAM classifier performance will depend on the quality of the training set it was given and the spectral separability of the life forms at that point in time. Better classification results could be obtained with the SAM classifier in combination with Lidar data that give information on the height of the vegetation. Also the pure pixel-approach of the SAM classifier is completely different from the patch-approach of the GHC methodology. Therefore a patch-based classifier or segmentation techniques could be a better solution.

5.4 Site complexity compared to Classification Success

Biological complexity

The regression analyses showed weak relationships between the parameters of the biological complexity and the classification success indicating that a high biological complexity (represented by a higher species richness, a higher Shannon diversity, a lower Simpson diversity, and a higher cover with Mixed life forms) decreased the mapping accuracy. However, Andrew and Ustin (2008) found that the mapping success (of a specific species) was inversely related to the species richness of the site. In this study the best classification result was obtained in the area with the lowest species diversity. Also the Shannon and the Simpsons indices showed this relation and the lowest classification result was obtained in the area with almost the most species. The strongest positive relation ($R^2=0.60$; fig. 20) was found between the number of life forms in an area and the mapping success. This is indicating the opposite!

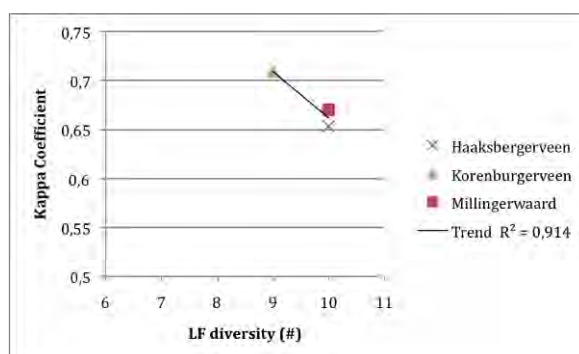


Figure 25: Mapping success, represented by the kappa coefficient, versus Life Form diversity without Wageningen.

The three sites without the Wageningen site showed a negative trend ($R^2=0.91$; fig. 25), indicating that higher life form diversity leads to lower mapping success. The effect on this

relationship of one study site can be very large if there are only four sites. The analysis could be substantially improved by using more study sites (but would take much more efforts).

Spectral Complexity

The spectral richness is highest for the Korenburgerveen with the best classification result, followed by the Wageningen Floodplain with the lowest classification success. The explained variances of the first three Principle Components show the same trend. Figure 22a gives a weak indication of a positive relationship. However, the high spectral complexity value for the Korenburgerveen area is remarkable, because there was a lot of cloud shade in the image (fig. 27a). This may have influenced the spectral complexity.

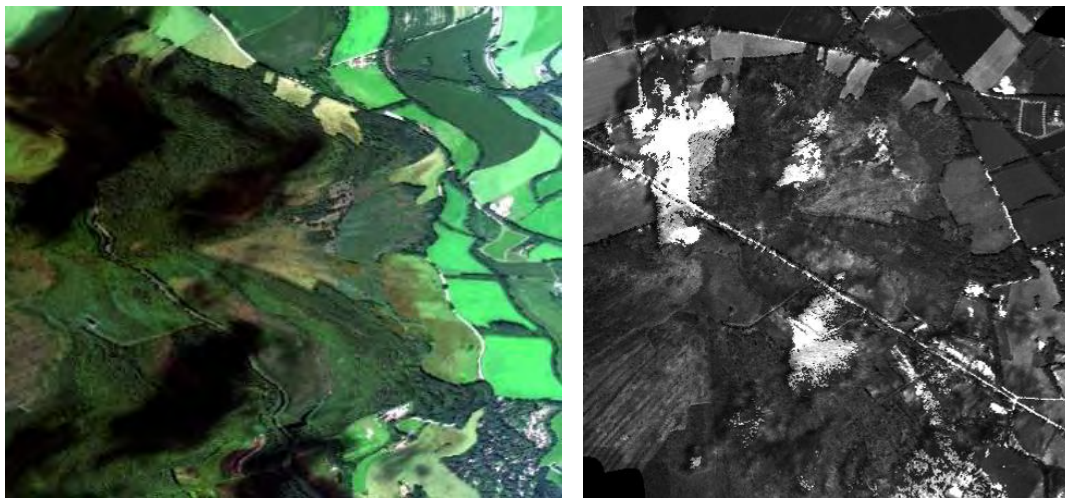


Figure 26: (a) Cloud shade and (b) the residuals of the cloud shade in the HyMap data of Korenburgerveen.

The image of the Korenburgerveen area (fig. 26) shows that a lot of the area is covered with cloud shade. After atmospheric correction some residuals are still visible and will probably influencing the spectral complexity. If we compare the relationship without the Korenburgerveen area (fig. 23b), the spectral complexity shows a negative relationship indicating that higher spectral complexity leads to lower mapping success. The occurrence of the high spectral complexity value for the Korenburgerveen needs further study. Spectral complexity calculations with the cloud shade masked out could give more insight into the spectral complexity of the Korenburgerveen HyMap data.

Landscape complexity

Evenness, indicating the variation between patches, seems to be the landscape complexity parameter with the most explanatory power in relation to the mapping success (fig. 24, b, d, e). A high evenness suggests a low mapping success. This can be the case, as high mapping success was mostly obtained within the largest patches. The four areas have almost the same number of patches, so a high evenness leads to a large difference between the patches and a higher amount of large patches. The area mean also indicated higher mapping success for an increased area mean (fig. 24), so the larger the mean areas the better the classification. The shape mean and the total edge, two straightforward measures of shape complexity, show a positive relationship with the mapping success (fig. 24). This indicates that higher landscape complexity results in better mapping success. This unexpected relationship for the shape mean is due to the areas in this study having in

general the same (high) amount of patches. A look at figure 24e of the total edge shows that the linear relationship without Wageningen is more representative for the trend in the data ($R^2=0.99$; fig. 24f), indicating that a higher edge complexity leads to a lower mapping success. The Shannon and Simpson's diversity indices are indicating that a higher landscape diversity leads to a better mapping success.

Site complexity compared to Mapping Success, overall discussion

Based on this study, the general pattern is that with an increase in Biological Complexity the mapping success will decrease. This supports the conclusions of Andrew and Ustin (2008). They also found an inverse relationship between the Spectral Complexity and mapping success, but to rely on the result for this study the effect of cloud shade in the image of Korenburgerveen must be first investigated. The landscape complexity indices showed mostly the dependence of the classifier for large patches, indicating that sites with most small patches will have the worst classification result. Some complexity indicators disagree with our hypothesis, like the landscape diversity indices. Also Andrew and Ustin (2008) could not find a direct logical relationship at landscape scale but most of their indices were indicating that increased complexity reduces the mapping success. There are still several uncertainties like the really low mapping success of the Wageningen floodplain and the effect of cloud shade in the data of Korenburgerveen. This can have a large effect on the observed patterns based on only four study sites.

6 References

Adams, J. B., Smith, M. O., and Johnson, P. E., 1986. Spectral mixture modeling – a new analysis of rock and soil types at the Viking lander-1 site. *Journal of geophysical research* 91 (B8): 8098-8112.

Andrew, M. E. and Ustin, S.L., 2008. The role of environmental context in mapping invasive plants with hyperspectral image data. *Remote Sensing of Environment* 112(12): 4301-4317.

Blaschke, T., 2010. Object based image analysis for remote sensing. *ISPRS Journal of Photogrammetry and Remote Sensing* 65 (1): 2-12.

Bunce, R., Groom, G., Jongman, R., and Padoa-Schioppa, E., 2005. *Handbook for surveillance and monitoring of European Habitats*. Wageningen, Alterra.

Bunce, R., Metzger, M., Jongman, R., Brandt, J., De Blust, G., Elena-Rossello, R., Groom, G., Halada, L., Hofer, G., Howard, D., Kovar, P., Múcher, C., Padoa-Schioppa, E., Paelinx, D., Palo, A., Perez-Soba, M., Ramos, I., Roche, P., Skanes, H., and Wrbka, T., 2008. A standardized procedure for surveillance and monitoring European habitats and provision of spatial data. *Landscape Ecology* 23(1): 11-25.

Burton, M. and Samuelson, L. J., 2008. Influence of urbanization on riparian forest diversity and structure in the Georgia Piedmont, US. *Plant Ecology* 195 (1): 99-115.

Carlson, K., Asner, G., Hughes, R., Ostertag, R., and Martin, R., 2007. Hyperspectral Remote Sensing of Canopy Biodiversity in Hawaiian Lowland Rainforests. *Ecosystems* 10(4): 536-549.

Chen, J. M., Li, X., Nilson, T., and Strahler, A., 2000. Recent advances in geometrical optical modelling and its applications. *Remote Sensing Reviews*, 18, 227-262.

Clark, M., Roberts, D., and Clark, D., 2005. Hyperspectral discrimination of tropical rain forest tree species at leaf to crown scales. *Remote Sensing of Environment* 96(3-4): 375-398.

Clevers, J.G.P.W., 2005. HyEco'04: An airborne imaging spectroscopy campaign at Wageningen, the Netherlands. CGI Report 2005-01, Wageningen UR.

Congalton, R., 1991. A Review of Assessing the Accuracy of Classifications of Remotely Sensed Data. *Remote Sensing of Environment* 37(1): 35-46.

Dennison, P., Halligan, K., and Roberts, D., 2004. A comparison of error metrics and constraints for multiple endmember spectral mixture analysis and spectral angle mapper. *Remote Sensing of Environment* 93(3): 359-367.

Duro, D., Coops, N., Wulder, M., and Hant, T., 2007. Development of a large area biodiversity monitoring system driven by remote sensing. *Progress in Physical Geography* 31(3): 235-260.

EC, 2002. <http://ec.europa.eu/environment/nature/info/pubs/docs/nat2000/2002> on 1/09/2009.

Foody, G. M. and Mathur, A., 2006. The use of small training sets containing mixed pixels for accurate hard image classification: Training on mixed spectral responses for classification by a SVM. *Remote Sensing of Environment* 103 (2): 179-189.

Fortin, M., Olson, R., Ferson, S., Iverson, L., Hunsaker, C., Edwards, G., Levine, D., Butera, K., and Klemas, V., 2000. Issues related to the detection of boundaries. *Landscape Ecology* 15(5): 453-466.

Gao, J., 1999. A comparative study on spatial and spectral resolutions of satellite data in mapping mangrove forests. *International Journal of Remote Sensing* 20(14): 2823-2833.

Gosz, J.R., 1993. "Ecotone Hierarchies. *Ecological Applications* 3(3): 370-376.

Green, A. A., Berman, M., Switzer, P., and Craig, M. D., 1988. A transformation for ordering multispectral data in terms of image quality with implications for noise removal. *Geoscience and Remote Sensing* 26 (1): 65-74.

Harbin, Li. and Wu, J., 2004. Use and misuse of landscape indices. *Landscape Ecology* 19: 389-399.

Hestir, E. L., Greenberg, J. A., and Ustin, S. L., 2007. Retrieval of water quality parameters in a highly turbid estuary from hyperspectral remote sensing imagery. American Geophysical Union, Fall meeting 2007.

Honnay, O., Piessens, K., Van Landuyt, W., Hermy, M., and Gulinck, H., 2003. Satellite based land use and landscape complexity indices as predictors for regional plant species diversity. *Landscape and Urban Planning* 63 (4): 241-250.

Johansen, K., Arroyo, L. A., Armston, J., Phinn, S., Witte, C., 2001. Mapping riparian condition indicators in a sub-tropical savanna environment from discrete return LiDAR data using object-based image analysis. *Ecological Indicators* 10:796-807.

Kalacska, M., Sanchez-Azofeifa, G., Rivard, B., Caelli, T., White, H., and Calvo-Alvarado, J., 2007. Ecological fingerprinting of ecosystem succession: Estimating secondary tropical dry forest structure and diversity using imaging spectroscopy. *Remote Sensing of Environment* 108(1): 82-96.

Kent, M., Gill, W., Weaver, R., and Armitage, R., 1997. Landscape and plant community boundaries in biogeography. *Progress in Physical Geography* 21(3): 315-353.

Kooistra, L., Wamelink, W., Schaepman-Strub, G., Schaepman, M., Van Dobben, H., Aduaka, U., and Batelaan, O., 2005. HyEco'04: an airborne imaging spectroscopy campaign in the floodplain Millingerwaard, the Netherlands. CGI Report 2005-07, Wageningen UR.

Kruse, F. A., Lefkoff, A. B., Boardman, J. W., Heidebrecht, K. B., Shapiro, A. T., Barloon, P. J., and Goetz, A. F. H., 1993. The spectral image processing system (SIPS)- interactive visualization and analysis of imaging spectrometer data. *Remote Sensing of Environment* 44 (2-3): 145-163.

Lillesand, T., Kiefer, R., and Chipman, J., 2008. *Remote sensing and image interpretation*. New York: John Wiley and Sons, Inc.

Lass, L. W., Thill, D. C., Shafii, B. and Prather, T. S., 2002. Detecting spotted knapweed with hyperspectral remote sensing technology. *Weed Technology* 16: 426-432.

Lucas, K., and Carter, G., 2008. The use of hyperspectral remote sensing to assess vascular plant species richness on Horn Island, Mississippi. *Remote Sensing of Environment* 112(10): 3908-3915.

McGarigal, K. and Marks, B., 1995. FRAGSTATS: spatial pattern analysis program for quantifying landscape structure. General Technical Report - US Department of Agriculture, Forest Service.

Moser, D., Zechmeister, H. G., Plutzer, C., Sauberer, N., Wrbska, T., and Grabherr, G., 2002. Landscape patch shape complexity as an effective measure for plant species richness in rural landscapes. *Landscape Ecology* 17 (7): 657-669.

Mücher, C.A, Hennekens, S., Bunce, R., Schaminee, J., and Schaepman, M., 2009. Modelling the spatial distribution of Natura 2000 habitats across Europe. *Landscape and Urban Planning* 92(2): 148-159.

Mücher, C.A., 2009. Geo-spatial modelling and monitoring of European landscapes and habitats using remote sensing and field surveys. PhD thesis Wageningen University, Wageningen, The Netherlands, ISBN 978-90-8585-453-1, 269 pp.

O'Neill, R. V., Krummel J. R., Gardner R. H., Sugihara, G., Jackson, B., DeAngelis, D. L., Milne B. T., Turner M. G., Zygmunt B., Christensen, S. W., Dale, V. H., and Graham, R. L. (1988). Indices of landscape pattern. *Landscape Ecology* 1: 153-162.

Okin, G. S., Roberts, D. A., Murray, B., and Okin, W. J., 2001. Practical limits on hyperspectral vegetation discrimination in arid and semiarid environments. *Remote Sensing of Environment* 77: 212-225.

Oldeland, J., Wesuls, D., Rocchini, D., Schmith, M., and Jürgens, N., 2010. Does using species abundance data improve estimates of species diversity from remotely sensed spectral heterogeneity? *Ecological Indicators* 10: 390-396.

Palmer, M. W., Wohlgemuth, T., Earls, P., Arévalo, J. R., and Thompson, S. D., 2000. Opportunities for long-term ecological research at the Tallgrass Prairie Reserve, Oklahoma. Cooperation in long term ecological research in central and eastern Europe, Proceedings of the ILTER Regional Workshop 22-25 June 1999, Budapest, Hungary.

Palmer, M. W., Earls, P. G., Hoagland, B. W., White, P. S., and Wohlgemuth, T., 2002. Quantitative tools for perfecting species list. *Envirometrics* 13: 121-137.

Purvis, A., and Hector, A., 2000. Getting the measure of biodiversity. *Nature* 405(6783): 212-219.

Raunkiaer, C., 1934. *The Life Forms of Plants and Statistical Plant Geography*.

Rosso, P. H., Ustin, S. L., and Hastings, A., 2005. Mapping marshland vegetation of San Francisco Bay, California, using hyperspectral data. *International Journal of Remote Sensing* 26 (23): 5169-5191.

Rueda, C., Greenberg, J., and Ustin, S., 2005. "StarSpan: A Tool for Fast Selective Pixel Extraction from Remotely Sensed Data." Davis, CA: Center for Spatial Technologies and Remote Sensing.

Schaepman-Strub, G., Limpens, J., Menken, M., Bartholomeus, H. M., and Schaepman, M.E., 2009. Towards spatial assessment of carbon sequestration in peatlands: spectroscopy

based estimation of fractional cover of three plant functional types. *Biogeoscience* 6: 275-284.

Schmidtlein, S., Zimmerman, P., Schupferling, R., and Weiss, C., 2007. Mapping the floristic continuum: Ordination space position estimated from imaging spectroscopy. *Journal of Vegetation Science* 18(1): 131-140.

Schmidtlein, S., and Sassin, J., 2004. Mapping of continuous floristic gradients in grasslands using hyperspectral imagery. *Remote Sensing of Environment* 92: 126-138.

Silvestri, S., Marani, M., and Marani, A., 2003. Hyperspectral remote sensing of salt marsh vegetation, morphology and soil topography. *Physics and Chemistry of the Earth* 28: 15-25.

Smith, B., and Wilson, J., 1996. A consumer's guide to evenness indices. *Oikos* 76(1): 70-82.

Smith, M. O., Ustin, S. L., Adams, J. B., and Gillespie, A. R., 1990. Vegetation in deserts: A regional measure of abundance from multispectral images. *Remote Sensing of Environment* (31): 1-26.

Thenkabail, P., Hall, J., Lin, T., Ashton, M., Harris, D., and Enclona, E., 2003. Detecting floristic structure and pattern across topographic and moisture gradients in a mixed species Central African forest using IKONOS and Landsat-7 ETM+ images. *International Journal of Applied Earth Observation and Geobservation* 4(3): 255-270.

Townsend, P. A., 2000. A quantitative fuzzy approach to assess mapped vegetation classifications for ecological applications. *Remote Sensing of Environment* 72(3): 253-267.

Underwood, E., Ustin, S., and Ramirez, C., 2007. A comparison of spatial and spectral image resolution for mapping invasive plants in coastal California. *Environmental Management* 39(1): 63-83.

Unep, 2002. Report of the sixth meeting of the conference of the parties to the convention on biological diversity. <http://www.cbd.int/decision/cop/?id=7200> on 1/09/2009.

Ustin, S. L., Roberts, D. A., Gamon, J. A., Asner, G. P. and Green, R. O., 2004. Using imaging spectroscopy to study ecosystem processes and properties. *BioScience* 54: 523-534.

Uuemaa, E., Antrop, M., Roosaare, J., Marja, R., and Mander, Ü., 2009. Landscape metrics and indices: An overview of their use in landscape research. *Living Reviews in Landscape Research* 3: 1.

Verrelst, J., 2010. Space-borne spectrodirectional estimation of forest properties. PhD Thesis, Wageningen University, Wageningen.

Warren, W., 1948. Science and Complexity. *American Scientist* 36:536.

Zonneveld, I., 1974. On abstract and concrete boundaries, arranging and classification. *Tatsachen und Probleme der Grenzen in der Vegetation. Bericht über das Internationale Symposium der Internationalen Vereinigung für Vegetationskunde in Rinteln 8.-11. April 1968: 17-43*

Annex-6

Mapping of life form based general habitat categories (GHC) using medium spatial resolution multispectral images



Mait Lang
Tambet Kikas
Janar Raet
Kalev Sepp
Valdo Kuusemets

Estonian University of Life Sciences



Tartu 2011

Table of Contents

Introduction.....	2
Material and methods.....	3
Test site.....	3
Field data.....	4
Satellite image.....	4
Data processing and image classification.....	5
Results and discussion.....	8
Summary and conclusions.....	14
References.....	15
Appendix 1. Field maps	17
Appendix 2. Maximum likelihood classification in EE04.....	19
Appendix 3. Example of classification validation cross tabulation.....	20

Introduction

Radiative transfer in vegetation is influenced by the arrangement, structure, functioning of plants and their optical properties. Incident radiation is absorbed, transmitted and reflected in the vegetation. The amount of energy that is reflected towards a sensor can be recorded and stored as an image. The images are characterised by their spatial, radiometric and spectral resolution. Many scanners are able to aim at different angles to the object or area of interest. The recorded signal is also influenced by atmospheric and illumination conditions and sensor characteristics.

The spectral signature of an object or an area represents the recorded radiance (or reflectance or reflectance factor) at different wavelengths (channels) and can be assumed to be characteristic to this object. It can also be assumed that objects with different properties have separable signatures. However, different objects can have similar spectral signatures and objects with similar properties with regard to our focus (e.g land cover types) can have different spectral signatures. In general, the spectral signature of a pixel over a vegetated landscape is a function of viewing and illumination geometry, canopy structure, tissue optics, landscape structure and soil optics (Asner, 2004). In a similar way angular and temporal signatures for an object can be defined.

The spectral signature of a image pixel is proportionally dependent on spectral signatures of the objects within this pixel and the respective areas of the objects in view direction. In medium spatial resolution images one pixel (10-30 meters) over the vegetation consists of four basic components: illuminated canopy, shaded canopy, illuminated ground and shaded ground (Kasischke *et al.* 2004). If the pixel is located in a homogeneous surrounding then neighbourhood influence can be neglected. Alternatively, contrasting neighbourhood influences the pixel through multiple scattering in the land-atmosphere system (Liang, 2004). Atmosphere between the sensor and target has a pronounced influence in certain wavelength ranges on the spectral signature and so called atmospheric correction procedure is usually needed prior to analysing and using relationships between objects of interest and their spectral signatures (Liang, 2004). The temporal signature of a pixel is influenced by many components from which the main are the actual changes occurring in the area, atmosphere, illumination and view geometry, mapping and binning the observed raw signals (including geometric correction) into raster image and scanner degradation.

There are numerous studies on estimating vegetation and in general ecosystem characteristics using spectral signatures from remotely sensed images. General habitat categories are the units used to

describe biodiversity over wide range of ecosystems (Bunce *et al.*, 2011). Based on the life forms (Bunce *et al.*, 2011 referring to Raunkiaer, 1934), the general habitat categories (GHC) are expected to be different in their vegetation structure and functioning. Hence, it could be assumed that GHC-s differ also by their spectral signatures in the extent that makes it possible to use spectral image data to map GHC-s over large areas. Changes in the optical properties of vegetation during the growing season can be informative for distinguishing otherwise spectrally similar GHC-s (Clerici and Weissteiner, 2010; Levin *et al.*, 2011)

In practical fieldwork the Minimum Mappable Element (MME) for an areal GHC element is 400m² with minimum dimensions of 5 x 80m or 20 x 20m (Bunce *et al.*, 2011). This corresponds roughly to the pixel size of medium spatial resolution satellite images. Hence, it is not realistic to distinguish the MME-size general habitat area unless it is significantly different by its spectral characteristics from the surroundings. The true content of a pixel in geo-referenced consecutive images is never the same, since imaging platforms (planes, satellites) are not fixed but moving. This also makes it difficult to remotely detect changes of the pixel size areas, adds noise for larger areas in multi date change detection and complicates direct assignment of GHC class codes using raw digital number combinations from spectral channels and multi temporal images. However, the number of detailed field survey areas is usually limited because of time, cost and labour restrictions and therefore such medium resolution satellite images, each of which extends over 60 to 185 kilometre's depending on scanner, can be still useful to extend the local ground surveillance information over larger areas (*e.g.* landscapes). Even more, the small number of detailed field sites does not allow to draw statistically significant conclusions for the whole area of interest. The sample-only based design does not work because of the small sample size. On the other hand, multispectral images do allow the application of so called model based sampling design, provided that the spectral signatures and the properties of objects of interest are well correlated.

In this study atmospherically corrected Landsat-7 ETM+ image (SLC-off mode) and field measurements from European Biodiversity Observation Network (EBONE, 2011) monitoring areas in Estonia were used to test the applicability of medium resolution multi-spectral data to map general habitat categories. The spectral content of image was studied with unsupervised iterative self organizing clustering (ISOCCLUS). Maximum likelihood classification (MAXLIKE) technique was used to extend the information from field measurements to outside the EBONE 1x1 km² monitoring squares. The main aim was to extrapolate the information in EBONE field sites over a larger area.

Material and methods

Test site

Estonia is a small country (total area 45 227 km²) located in the North-East of Europe. The climate and weather are mainly determined by the Gulf stream and air masses from the Atlantic ocean (west) and continental air from Russia (Figure 1). Depending on the prevailing air mass the weather can be mild and wet or dry with rather high summer or low winter temperatures. The rate of annual precipitation is higher than evaporation and 20-25% of the land suffers from swamping (Vallner, 1998; Valk, 2005).

The topography of Estonia is generally flat, with a maximum elevation of 318 m above mean sea level. According to the National Forest Inventory (NFI) data more than half (51,5%) of Estonia is forest land, on third is arable land (30,3%) and 5,3 % are wetlands (Pärt, *et al.*, 2008). However, estimates of the percentage of forest land at the beginning of the last century in Estonia is 18.3%

(Etverk, 2003). Since 1958 the forest area of Estonia has almost doubled (from 12 711 km² to 21 133 km²) and the growing stock volume has more than tripled (from 131.18 * 10⁶m³ to 453.04 * 10⁶ m³) (Pärt *et al.* 2008). The causes of this increase are the conversion of agricultural lands into forest after World War II when the soviet system introduced collective farming and increased final felling ages of the stands (Etverk, 2003). After the collapse of the Soviet Union in 1990 about 300 000 hectares of agricultural land was abandoned.

Forests are characteristic to the hemiboreal zone. Forest growth conditions have a wide range dependent on soil type, local relief and water regime. The forest site types range from dry alvars, poor dry or wet sandy or gley soils to the fertile typical brown soils and fertile brown lessive soils. Phytoproductivity (dry mass per hectare in year) of the forest ecosystems reaches up to 15 Mg ha⁻¹y⁻¹ (Kõlli and Lemetti, 1999). Main forest forming species in Estonia are Scots pine (*Pinus sylvestris*), Norway spruce (*Picea abies*), Silver birch (*Betula pendula*), grey alder (*Alnus incana*), black alder (*Alnus glutinosa*) and aspen (*Populus tremula*).

Field data

Eight EBONE 1x1 km² monitoring squares in North-East Estonia (Figure 2) were mapped in the July 2010 (Appendix 1). Each monitoring square is identified by the code EE and a number starting from one. Around each EBONE field monitoring site a 3 by 3 grid of one square kilometre size squares was created in mapping software. These squares are further referred as surrounding squares.



Figure 1: Location of the EBONE field monitoring areas used in this study.

Satellite image

Landsat-7 ETM+ image acquired in 29.06.2010 (WRS-2 path=187, row=19) was downloaded from USGS archive. The image has missing data stripes due to scene line corrector failure (SLC-off mode, Figure 2). Atmosphere was clear and only a marginal amount of cumulus clouds were found in the image. Raster was re-projected from UTM into Estonian basic map coordinate system. MODIS image with close acquisition time was checked for any visible trends in transparency and it was concluded that the air mass was with similar properties over all the ETM+ image. Atmospheric correction was done with a modified 6S code that included two layer homogeneous canopy

reflectance model (Andres Kuusk, Tartu Observatory, personal communication). Aerosol size distribution data, spectral refraction index, aerosol optical thickness and amounts of absorbing gasses measured at Tõravere AERONET station (58° 15' 55" N, 26° 27' 58" E) were used.

Data processing and image classification

Image processing was done using IDRISI Taiga. Cloud and cloud shadow mask was digitized manually. The image fields of single channels are slightly shifted and a pixel near the missing data stripe can have a usable value in visible and NIR channels, but zero value in the short-wave infrared channels. Therefore, additional common mask to exclude all pixels with missing data in any of the six channels was created.

The spectral variability of the ETM+ image (Figure 2) was studied using unsupervised iterative self organising clustering (ISOCLUST). The number of classes was set to 41 including one class for background (missing data). The unsupervised classification produced several spectral classes for open water due to lakes having water with different spectral properties (see Figure 1 and Figure 2). These were merged into a single class. From the classified ISOCLUST image the pixel groups (segments) with an area larger than one hectare were extracted for further interpretation and analysis.

To extend the habitat/cover knowledge obtained from field monitoring squares, maximum likelihood classification (MAXLIKE) of ETM+ image was used. First, minimum limit of one hectare was imposed on the size of mapped GHC polygons to select training areas. This rule excluded almost all urban (URB) superclass GHC areas. Next, possible mixed pixels along the borders of adjacent areas were excluded from the training areas. Finally, only those training areas, which after the mixed pixel exclusion had more than five data pixels remaining, were kept for further use. In total 120 of such training areas were identified from the eight field monitoring sites.

In the first classification test, eight separate classifications were produced each of which using as input training areas from a single EBONE field site (EE01 to EE08). Each training area (GHC polygon) was used as an individual class assuming that similar individual objects do exist in near vicinity. Common GHC codes were assigned after classification. IDRISI Taiga MAXLIKE offers the option to set the minimum likelihood threshold to classify a pixel. If the maximum likelihood of a pixel is less than the critical (minimum) level then the pixel is left unclassified. This can be, to some extent, used to identify objects for which there are no training areas. Following minimum likelihood levels were used for each monitoring square: 0.00 (classify all) and 0.05.

In the second classification test all 120 training areas (Table 1) from the eight monitoring squares were used inclusively. Additional minimum likelihood threshold levels (0.10, 0.15, 0.50) were tested.

The classification accuracy assessment is usually done by evaluating how well the predicted cover classes match up (thematically and spatially) with a validation dataset. The percentage of correctly classified pixels and kappa index of agreement derived from a correspondence matrix are the most commonly used accuracy statistics. Both were calculated keeping in mind that the standard version of kappa index might not be the most informative (Pontius, 2000). Usually validation sites and training sites are expected to be independent, however on this occasion, splitting up the eight field sites into a separate calibration and validation set was not an option because of the small sample size and the distance (in average 20 kilometres and maximum 65 kilometres) between EBONE field sites. Nordkvist *et al.* (2010) used the leave-one-out for accuracy assessment, which gives also the estimate of local variability over the image. This option was also not used in this study because it requires spatially systematically distributed samples. Instead the accuracy assessment was done using all the training areas as the validation areas. Using this approach would invariably produce

elevated accuracy results (compared to a classical validation procedure), but also provide an indication of the internal homogeneity of the training areas. Since the aim of the tests was to extrapolate the knowledge about landscape information to near vicinity around each central square the minimum likelihood threshold and its influence to the classification results was considered to be the most informative.

Table 1: Number of individual distinct spectral signatures per general habitat category that were used in maximum likelihood classification.

General habitat category	Number of signatures / training areas
AQU	1
ART	1
CHE	17
CHE/LHE	14
CHE/MPH/DEC	1
CRO	25
FPH/CON	10
FPH/DEC	17
GRA	4
GRA/ART	1
LHE	7
LHE/CHE	16
NON	1
SPA	1
TPH/DEC	4



Figure 2: False color composite (bands 1,2,3) of the Landsat-7 ETM+ image from 29.06.2010, (courtesy of USGS). Empty stripes resulting from SLC failure are visible. Red squares mark the EBONE 1x1 km² field sites.

Results and discussion

Unsupervised classification produces the result where the content and labels for each class has to be determined after the procedure using existing maps and data. Pixels are grouped according to spectral similarity and the real world objects that the class represents can vary by their structural properties. Levin *et al.* (2011) used also self organizing clustering (ENVI isodata) starting with 50 classes which were interpreted and joined finally into 10 GHC categories. Considering that medium spatial resolution satellite images (pixel size about 15-30 m) contain many mixed pixels, it can be informative to separate the similar adjacent pixels belonging to the groups of some size. In this study the minimum group size was set to one hectare. This allows the separation of homogeneous areas according to the spectral information (Figure 3) which can be further used as training data. On the other hand, separating areas where the number of classes per unit area is high can be informative for detecting locations with high diversity in the spatial scale of the image. We can apply moving window filter to the image where pixel values represent area of pixel groups and calculate mode of group size. By selecting a mode value which is appropriate for the particular spatial resolution of the image (on the 30 metre pixel ETM+ image one hectare) spectrally variable areas can be delineated (Figure 4).

The unsupervised classification results can be used also to study the spectral variability within and around the EBONE monitoring squares (Figure 5, Appendix 1). It revealed, particularly for crop areas (CRO), significant spectral variability which indicated that a structure based GHC class can contain spectrally different areas. For example, the large LHE type area (*Trifolium sp. L.*, dominated grassland) in the square EE03 (Appendix 1) is composed of pixels belonging to four clusters. The same phenomena can be found in other squares. The drawback with the unsupervised classification is its inherent dependence on the image spectral properties and variability. If in the next image spectral variability is different (caused by seasonal or weather conditions) the content of classes changes and this makes it difficult to do change analysis.

In supervised classification the relationship between the spectral data and a class in interest is established prior to the procedure using training areas. Among many methods the maximum likelihood has been shown to produce reliable results (Nordkvist *et al.*, 2010; Levin *et al.*, 2011). Supervised classification can be used to extrapolate the knowledge from a field monitoring area over the larger surrounding (Figure 6c). Since one square kilometre size area might not be representative, additional rule can be applied to classify only those pixels which have the likelihood to a training area equal or more than a certain threshold (Figure 6d). When applied, the rule can exclude a significant amount of pixels from being classified (Appendix 2). This does not exclude the possibility of classifying a pixel correctly by a chance.

If the 1km field monitoring sites are close enough to be considered in the same vegetation and growth conditions then data all of them can be used as training areas together. Spectral signature for a class would then be created using several training areas which represent typical examples. However, instead of creating an average signature over several training sites with the same GHC (typical examples), each individual area shall be treated as a class first and then classification output must be relabelled. This corresponds to the idea of having similar individual landscape objects in the surrounding of the central monitoring square. The risk of classification error usually increases with distance from the training area and therefore the a priori probability maps can be useful for reducing appearance of classes on improbable locations (e.g. urban class in a wetland, or sparsely vegetated class in urban areas).

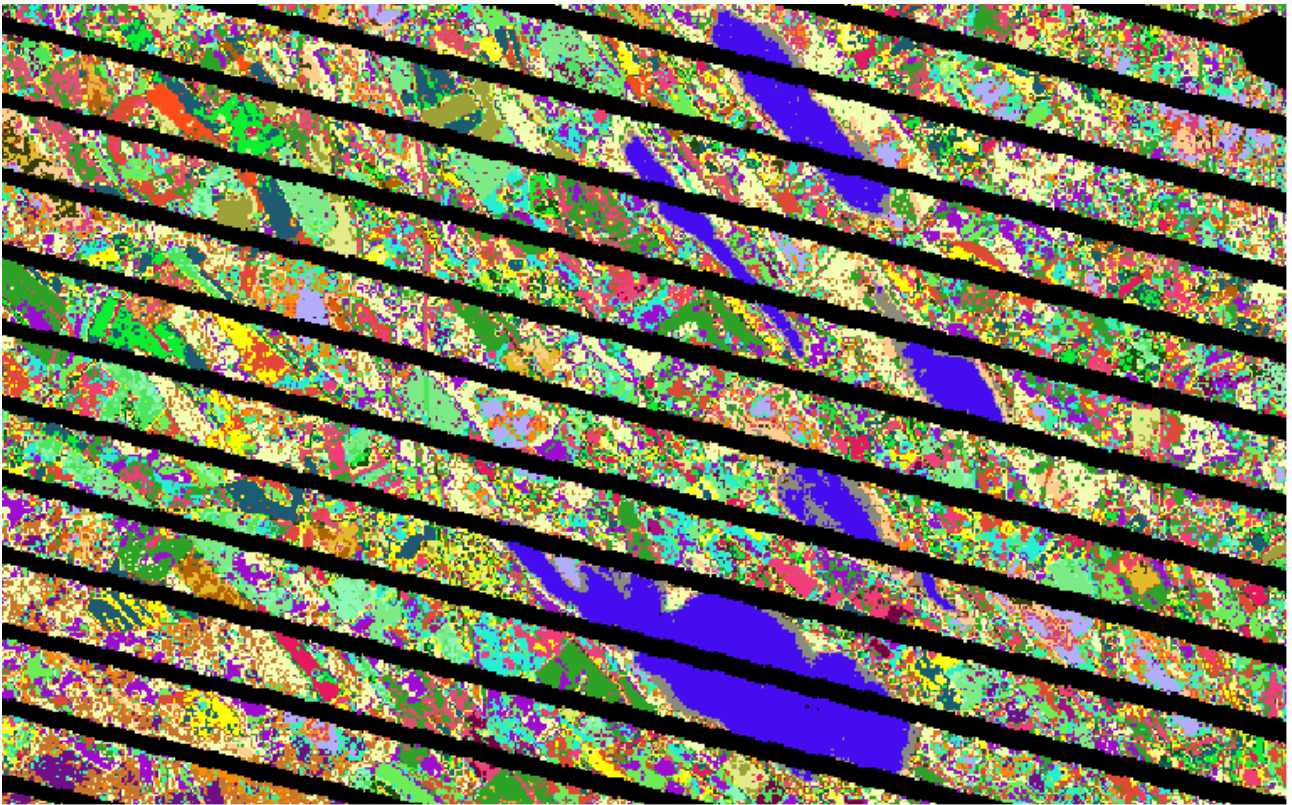
By combining minimum likelihood threshold applied supervised classification results and unsupervised classification results as overlays allows to identify locations for which well defined training areas were not found. The minimum likelihood threshold 0.05 causes a compact area to be excluded from the use-all-training-areas based classification (Figure 6e) from the North-West

surrounding square and from the South-West surrounding square (Figure 6f) of EE04 (locations are marked with red circle). The areas probably belong to a single class each, since unsupervised classification (Figure 6b) indicates homogeneous areas in these locations. Similar comparison on the only EE04 training areas based classification (Figure 6c, 6d) reveals that the straightforward extrapolation of the GHC class information from central square may not be always applicable, since usually in the unclassified areas spectrally homogeneous area exists according to the unsupervised classification (Figure 6b). For these areas respective higher level GHC class signature does probably not exist in field data.

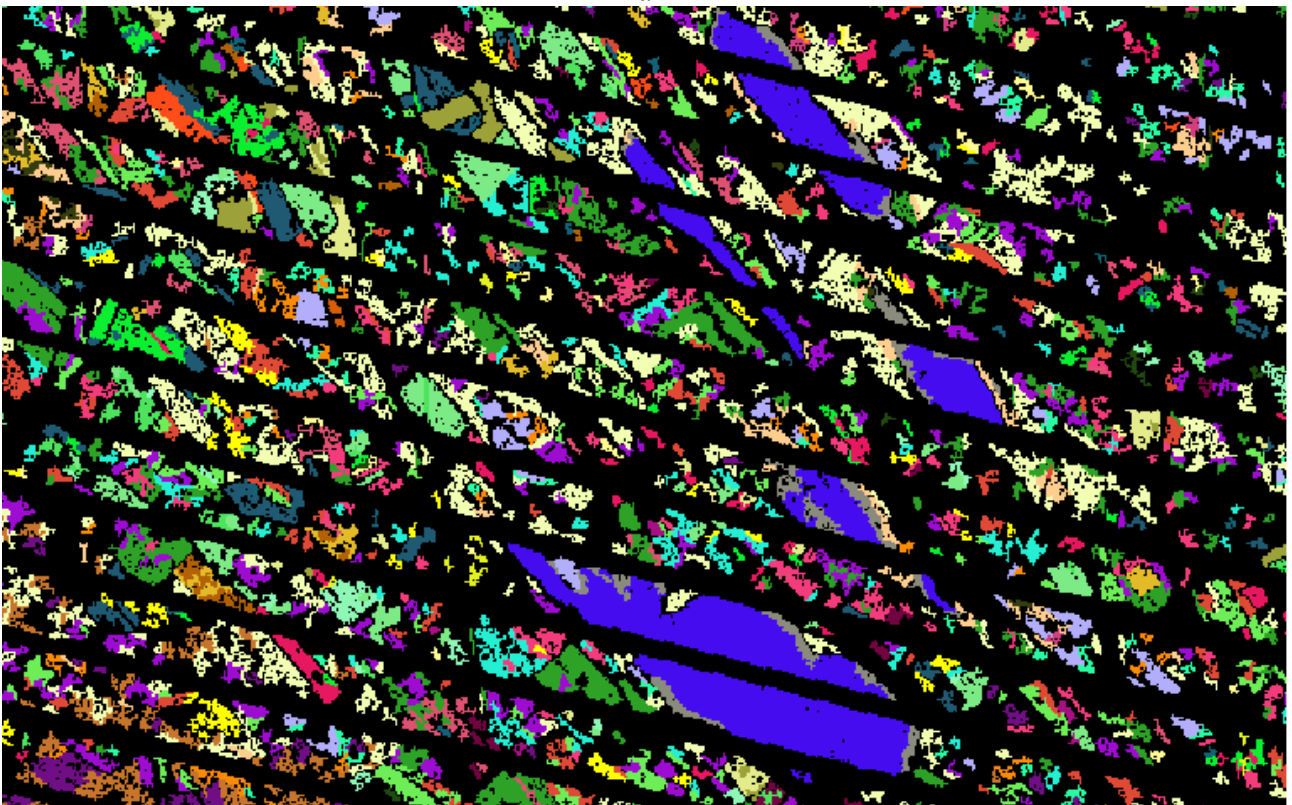
On the other hand, similar spectral signatures can be found on different GHC classes (Figure 7) according to Euclidean distance measure in spectral space (hclust procedure with complete link method in R, www.r-project.org). If we represent spectral signatures as a tree leaves then similar spectral signatures would belong to the same shoot of the tree. If those signatures belong to a GHC from the same super-group then the classified pixels could be joined into more general GHC category. If those signatures do belong to different GHC super-groups (Bunce, *et al.*, 2011) then respective pixels that were classified according to those signatures shall be treated separately, since they can represent a mixture of two classes. Topographic or soil maps can be used as a priori knowledge to separate spectrally similar but in reality different GHC areas to increase classification accuracy.

In maximum likelihood classification procedure several factors influence the result. Percentage of correctly classified pixels (GHC classes) varied from 75% in EE03 to almost 100% in EE05 (Figure 8a). Minimum likelihood threshold excluded 5...15% of pixels from classification in use-individual-square-signatures test. As a result the percentage of correctly classified pixels increased in all monitoring squares. The kappa index of agreement and percentage of correctly classified behaved similarly in this dataset (Figure 8a). The share of correctly classified pixels in use-all-signatures did not exceed 80,4% (Figure 8b). This seems somewhat low considering that the same areas were used for signature development and for validation of the classification. However, the explanation is 1) the within polygon spectral variability of GHC polygons and 2) spectral similarity of the GHC classes that were separated according to structural differences in the field. Leafy hemicryptophyte (LHE) and Caespitose hemicryptophyte (CHE) classes are spectrally similar and are frequently mutually misclassified (Table 2, in Appendix 3).

Because of internal spectral variability of training areas the classification accuracy in use-all-training areas test decreased, since there was more chance to find the most likely but possibly wrong signature for a single pixel in a mapped GHC area. Minimum likelihood threshold had a more pronounced influence on the result and at threshold=0.05 already more than 20% of pixels were left unclassified (Figure 8b). At the same time, by changing the minimum likelihood threshold from 0.00 to 0.05 improved classification accuracy about 10% according to the share of correctly classified pixels. Increasing the threshold *i.e.* including only the most similar pixels did not increase the kappa index of agreement or percentage of correctly classified significantly compared to the minimum likelihood threshold=0.05. The reason for somewhat contradicting results from use-single-square and use-all-training areas in classification with respect to the share of unclassified pixels is not clear and can be related to the maximum likelihood estimation dependence on the number of input signatures in IDRISI MAXLIKE procedure.



a



b

Figure 3: Window over Vooremaa landscape protection area of the ISOCLUST classification of Landsat-7 ETM+ SLC off image using 41 classes. In upper image (a) all pixels are retained and in lower image (b) only those adjacent pixels that belong to a group bigger than one hectare are retained. The size of the largest lake (blue colour) Saadjärv is 708 ha. Gray pixels along the coast belong to areas covered with *Phragmites australis* or shallow areas in lakes.

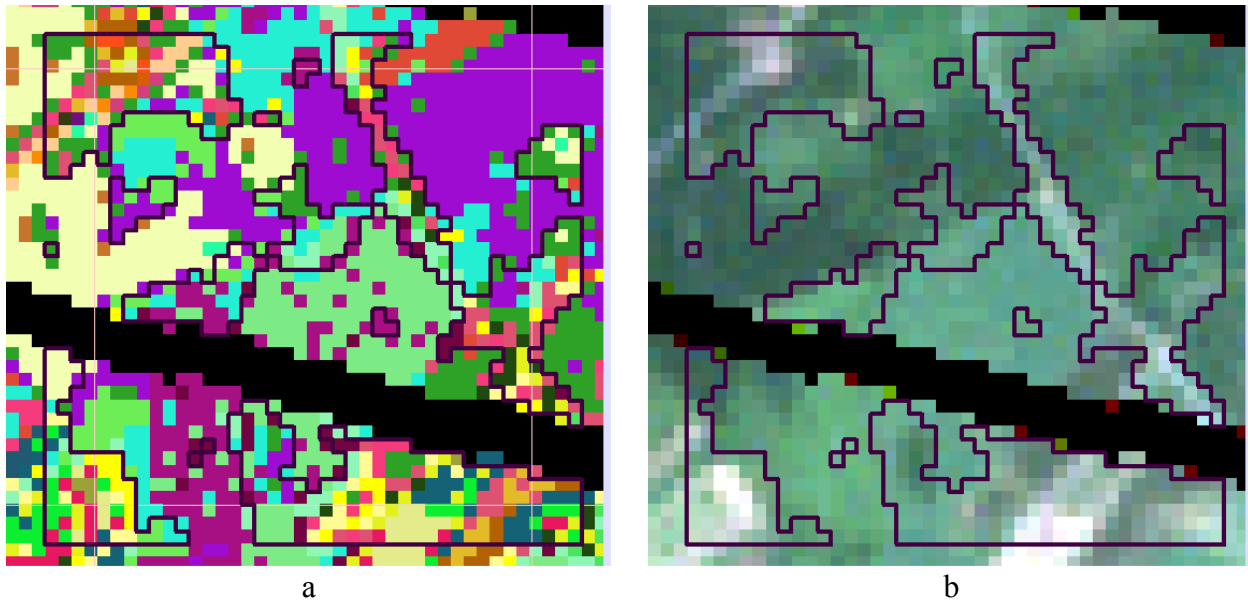


Figure 4: a) Spectrally variable areas delineated in EBONE field monitoring site EE04 based on ISOCLUST classification . b) Window from color composite image overlaid with the detected spectrally variable area borders is shown for comparison. Separated are the locations where the mode value of size of pixel groups in the ISOCLUST classification image under 3x3 pixel moving window was less than 12 pixels (roughly one hectare).

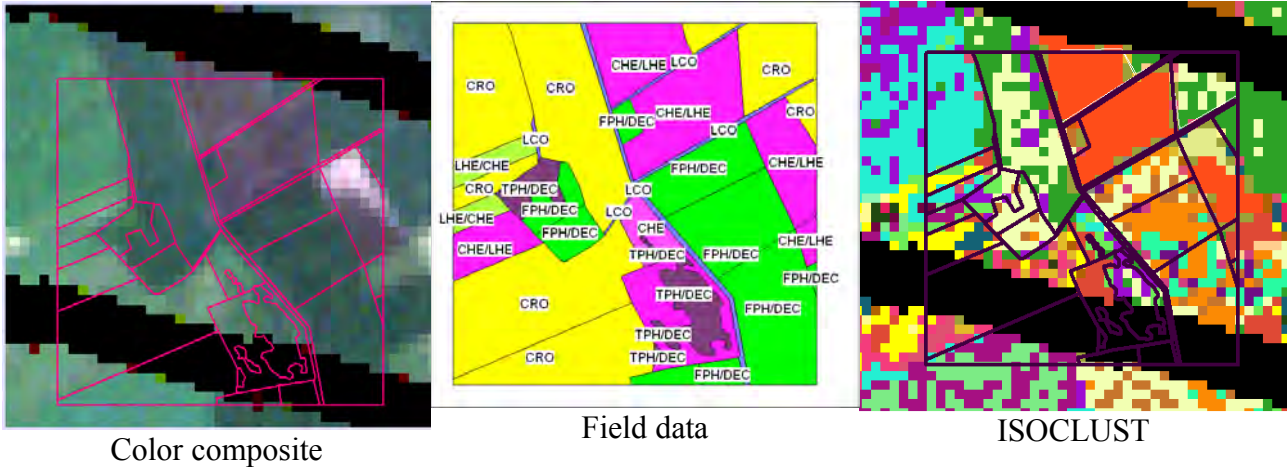


Figure 5: Window from color composite image, field measurements and unsupervised ISOCLUST classification result over EBONE field monitoring site EE01 in Estonia. The number of classes in ISOCLUST procedure was limited to 41.

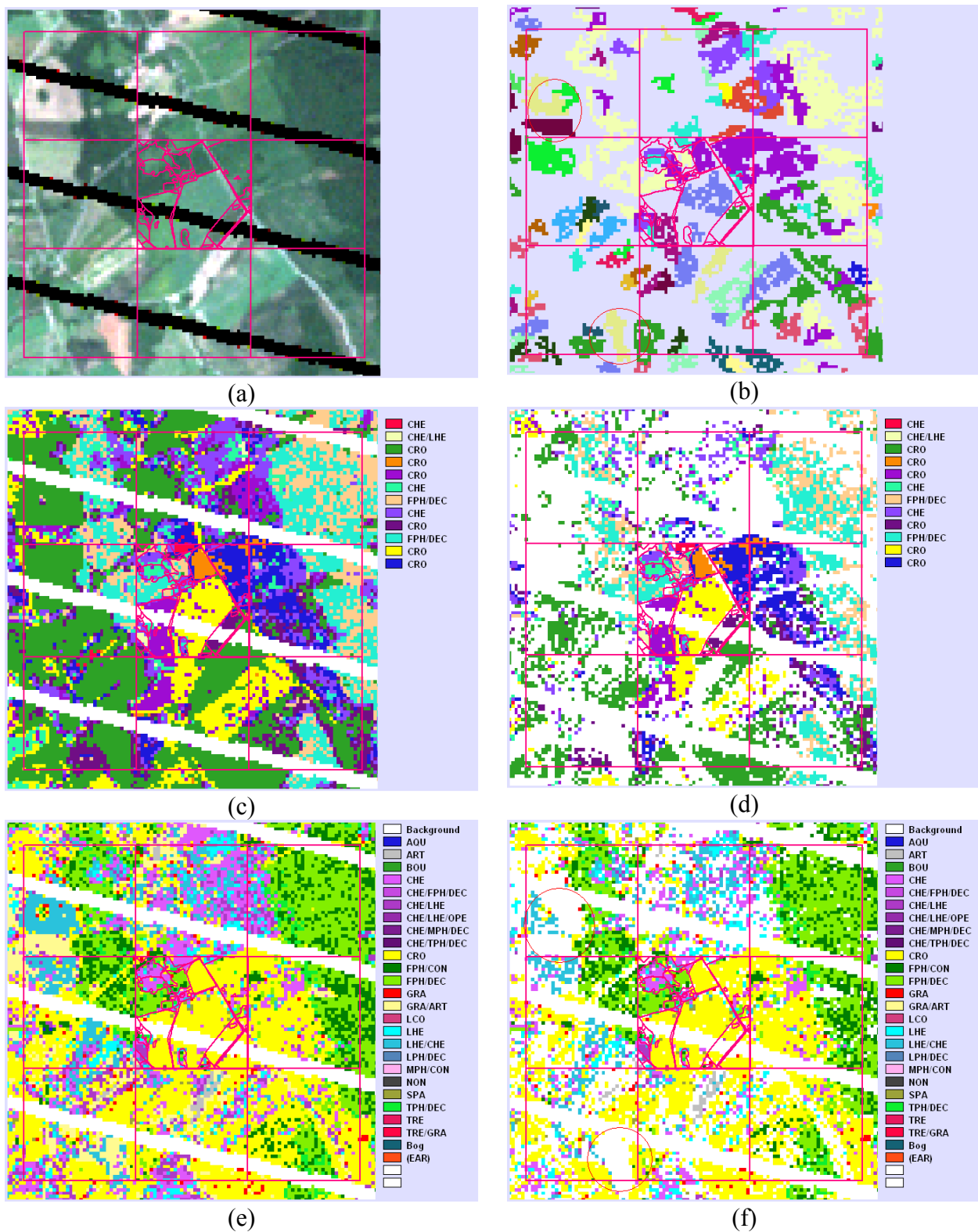
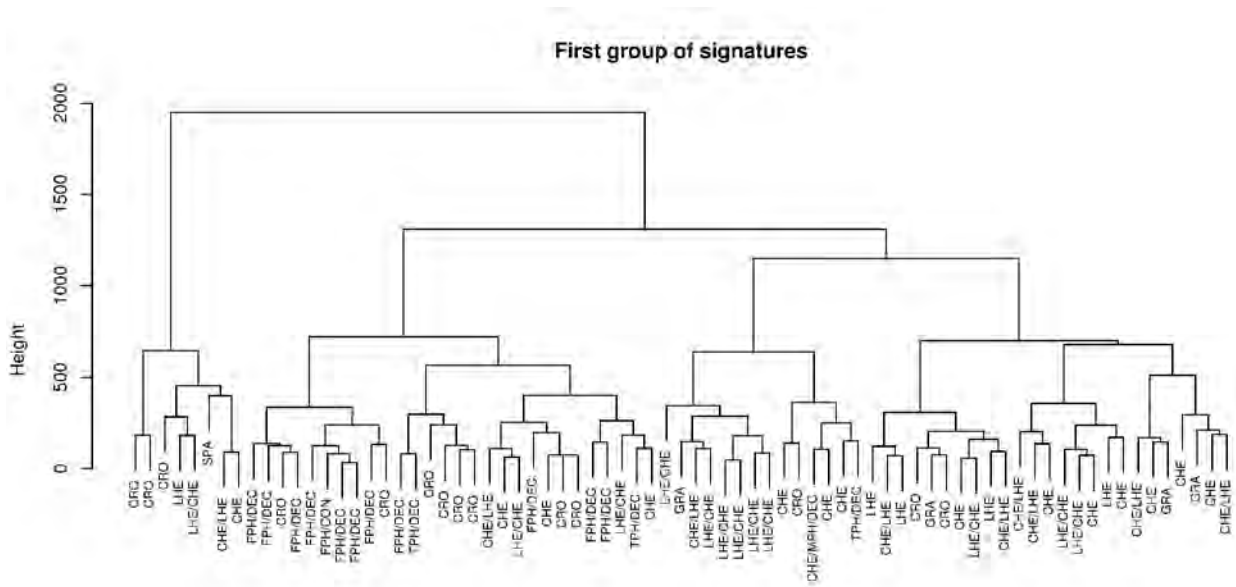
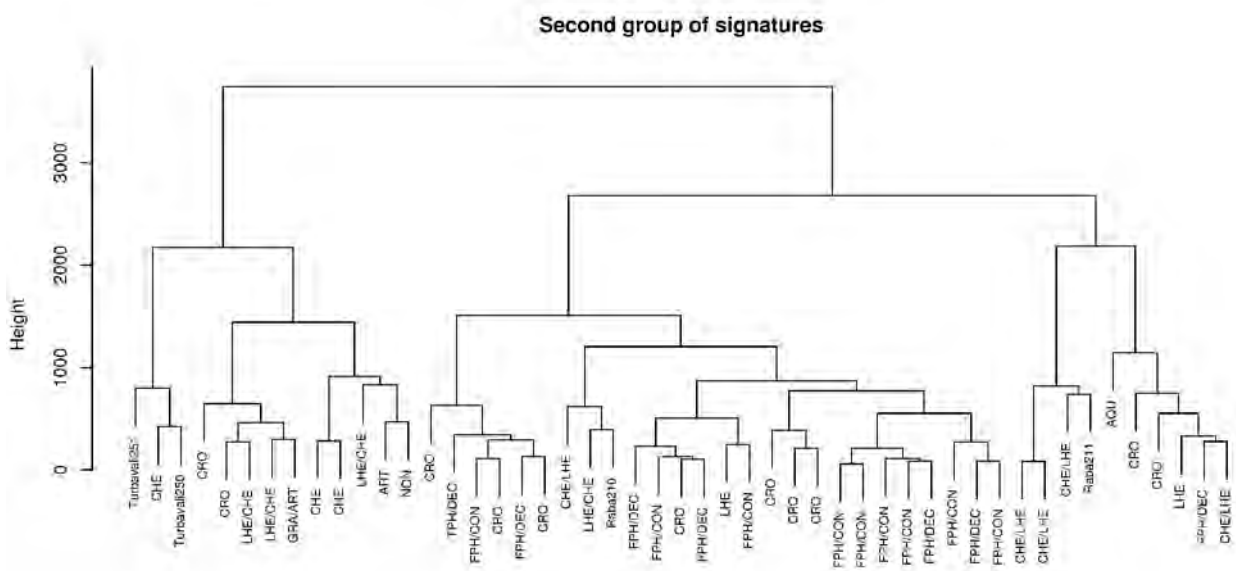


Figure 6: Supervised classification in EBONE monitoring square EE04. Central square and eight surrounding squares are shown. (a) is false colour colour composite; (b) shows the ISOCLUST areas larger than one hectare in size; (c) is the result using training sites from EE04 as individual classes; (d) is the same as (c) except that only those pixels which fulfilled the 0.05 minimum likelihood threshold were classified; (e) training data from all eight monitoring squares were used similar to (c) but the resultant individual classes were joined into common GHC class; (f) is the same as (e) but with 0.05 minimum likelihood threshold.



(a)



(b)

Figure 7: Similarity tree of training areas created with complete linkage clustering method. The tree is split into three large groups (branches) at height of 4000 for better readability. The group of additionally added large lake water signatures is not shown here (there was only one small shallow lake in monitor square EE03).

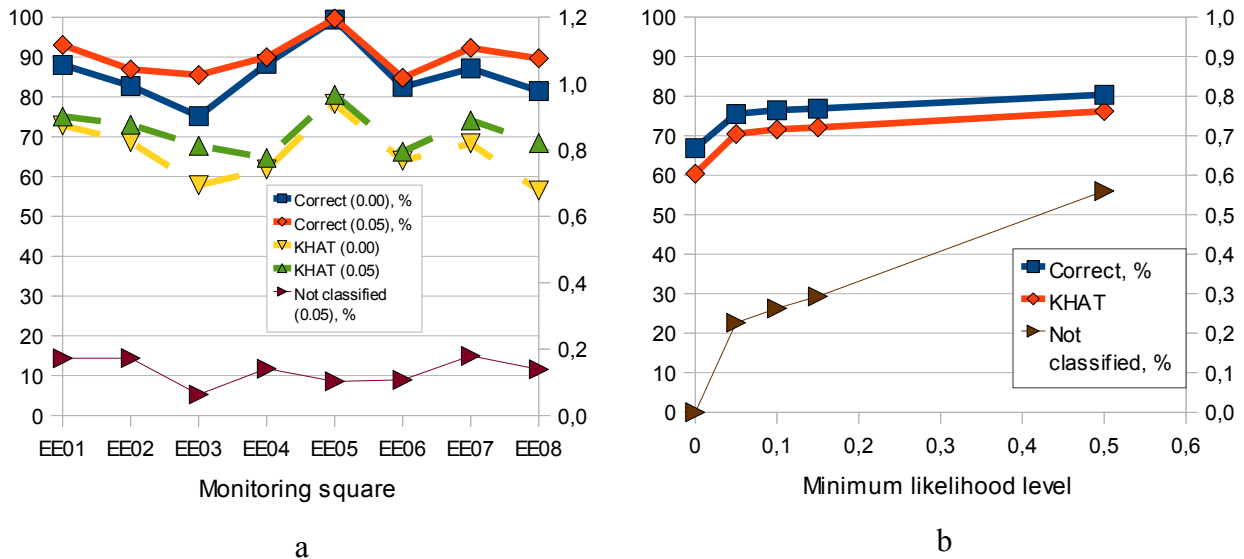


Figure 8: Descriptive statistics for maximum likelihood classification. Percentage of correctly classified pixels and kappa index of agreement (KHAT) depending on the minimum likelihood threshold are presented. The figures characterize the variability within field mapped GHC areas in monitoring squares. a) Each individual square as training area and validation area. b) All monitoring squares used as training areas and validation areas.

Summary and conclusions

In this study we show that Landsat-7 ETM+ images acquired in SLC-off mode since March, 2003, can be used to extend detailed information from limited field monitoring sites of the European Biodiversity Observation Network. An atmospherically corrected image from 28. June, 2010 was classified using iterative self organizing clustering and maximum likelihood method.

- Unsupervised image classification was useful to examine the spectral variation in the image, within field mapped GHC areas and to locate those areas for which the supervised classifier did not have a like training area in the monitoring square.
- Supervised maximum likelihood can be used to extrapolate knowledge from EBONE field monitoring squares to wider area by using each delineated GHC area as an individual class training site. However, in medium spatial resolution multi spectral images the pixel count requirement for signature development excludes small GHC areas which can be important for some aspects of biodiversity. Single central monitoring square can be non-representative for surrounding squares.
- By using training areas from several monitoring squares there is more chance for a pixel to be classified in a wrong class because the GHC areas are internally spectrally non-homogeneous. On the other hand, objects from different classes (e.g. CHE, LHE and CRO) can have similar spectral signatures.
- Minimum likelihood threshold in maximum likelihood classifier was useful to some extent to distinguish the pixels that caused classification error. Minimum likelihood threshold=0.05 resulted in 5...15% of unclassified pixels in use-single-square test and 20% of unclassified pixels in use-all-training areas test.

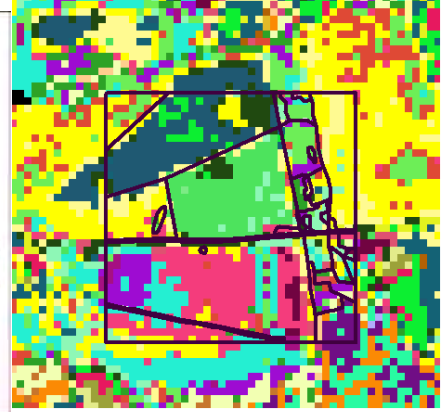
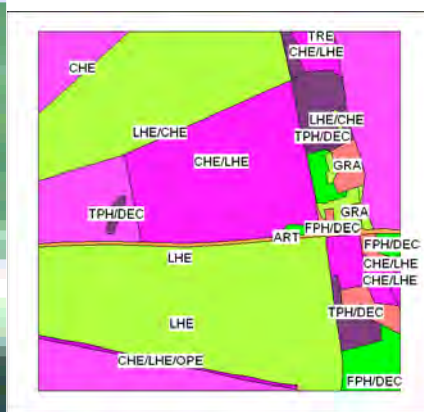
References

- Asner, P.G, 2004. Biophysical Remote sensing signatures of arid and semiarid ecosystems. In Ustin, S.L. (ed.). Remote Sensing for natural resource management and environmental monitoring. Manual of remote sensing. John Wiley & Sons, Inc, 53-110.
- Bunce, R.G.H., Bogers, M.M. B., Roche, P., Walczak, M., Geijzendorffer, I.R., Jongman, R.H.G. 2011. Manual for Habitat and Vegetation Surveillance and Monitoring: Temperate, Mediterranean and Desert Biomes. First edition. Wageningen, Alterra, Alterra report 2154. 106 pp.; 15 fig.; 14 tab.; 35 ref.
- Clerici, N., Weissteiner, C. 2010. Pilot investigation of phenology information for forest classification using SPOT VGT NDVI time series. 408-410. In: Operational tools in forestry using remote sensing techniques. (Eds.) Miranda, D., Suárez, J., Crecente, R.). Libería Troll. ISBN 978-84-693-5600-5.
- EBONE, 2011. European Biodiversity Observation Network. Web page <http://www.ebone.wur.nl/UK/Project+information+and+products/>.
- Etverk, I. 2003. 20th Century in Estonian Forests. Estonian Society of Foresters. ISBN 9985-78-653-X.
- Kasischke, E.S., Goetz, S., Hansen, M.C., Ozdogan, M., Rogan, J., Ustin, S.L., Woodcock, C.E. 2004. Temperate and boreal forests. In Ustin, S.L. (ed.). Remote Sensing for natural resource management and environmental monitoring. Manual of remote sensing. John Wiley & Sons, Inc, 235–238.
- Kõlli, R., Lemetti, I. 1999. Estonian soils (Eesti muldade lühiiseloostus. 1. Normaalsed mineraalmullad). Eesti Põllumajandusülikool. Tartu.
- Levin, N., Harari-Kremer, R, Carmel, Y. 2011. Remote sensing of Israel's natural habitats. Report delivered to Israel's Nature and Parks Authority, March 31st, 2011. 102 pp.
- Liang, S. 2004. Quantitative remote sensing of land surfaces. 534 pp. John Wiley & Sons, Inc. Hoboken, New Jersey.
- Nordkvist, K., Granholm A., Holmgren J., Nilsson, M., Olsson, H. 2010. Classification of EBONE General Habitat Categories in a Swedish forest area by using LiDAR in combination with SPOT satellite data. Draft version 2010.11.26. Section of forest remote sensing. Department of forest resource management, Swedish University of Agricultural Sciences, Umeå, Sweden. Manuscript, 10 pp.
- Pontius, R.G., 2000. Quantification Error versus Location Error in Comparison of Categorical Maps. In Photogrammetric Engineering and Remote Sensing, 66(8), 1011-1016
- Pärt, E., Adermann, V., Lepiku, P., 2008. Yearbook Forest 2007. Metsakaitse- ja Metsauuenduskeskus. pp 217. Available online <http://www.keskkonnainfo.ee/main/index.php/en/publications/publication>.
- Raunkiaer, C., 1934. The life forms of plants and statistical plant geography, being the collected papers of C. Raunkiaer. Clarendon, Oxford.
- Valk, U., 2005. Estonian bogs. (Eesti rabad. Ökoogilis-metsanduslik uurimus). Eesti Põllumajandusülikool. OÜ Halo Kirjastus. 314pp.
- Vallner, L, 1998. Assessment of the climate change impact on groundwater. In: Country case study on climate change impacts and adaptation assessments in the Republic of Estonia. Eds. Tarand, A., and Kallaste, T. Stockholm Environmental Institute Tallinn Centre. Tallinn ISBN: 9985-9114-3-1.

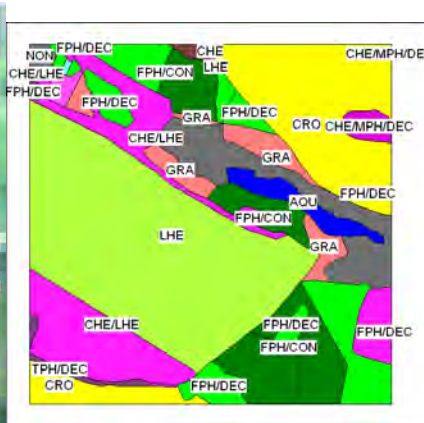
pp 83-85.

Appendix 1. Field maps

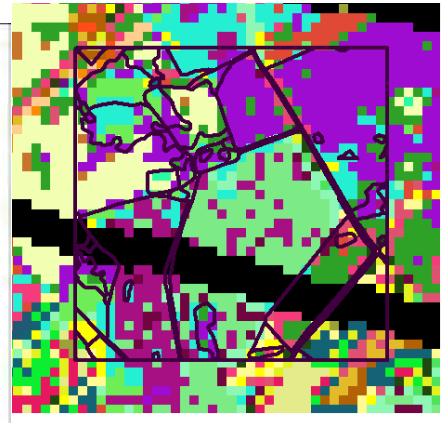
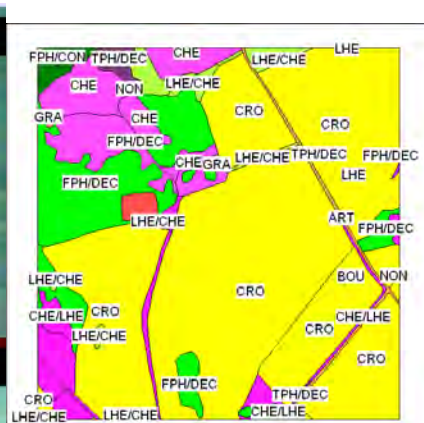
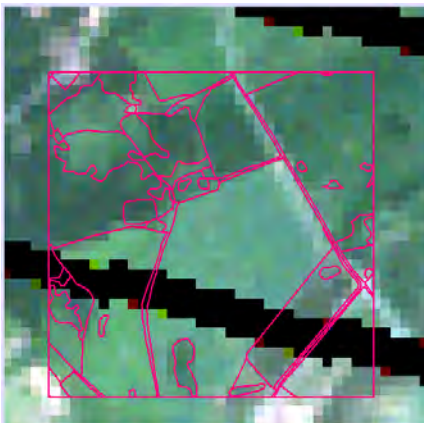
Landsat ETM+ image 29. June 2010 (Courtesy of USGS) as false colour composite, GHC classes from 2010 field measurements on EBONE 1x1 kilometre squares (EE02 to EE08) in Estonia and ISOCLUST classification (41 classes).



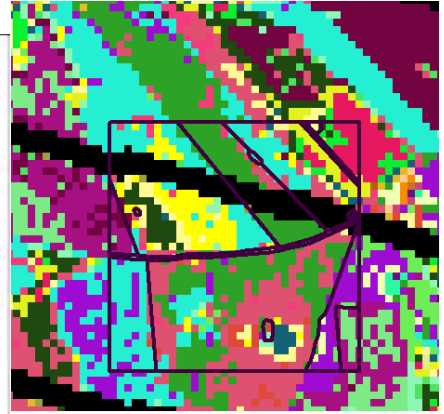
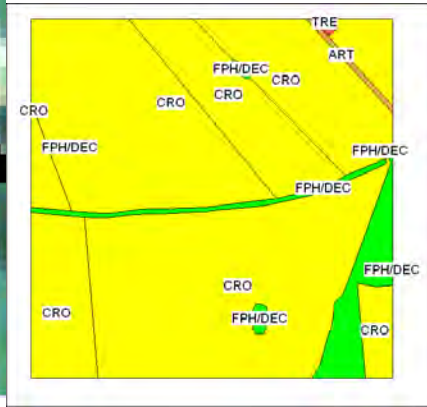
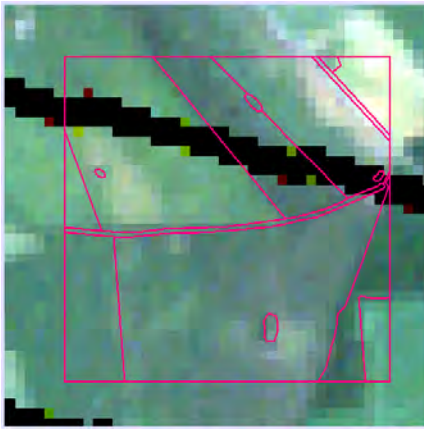
EE02



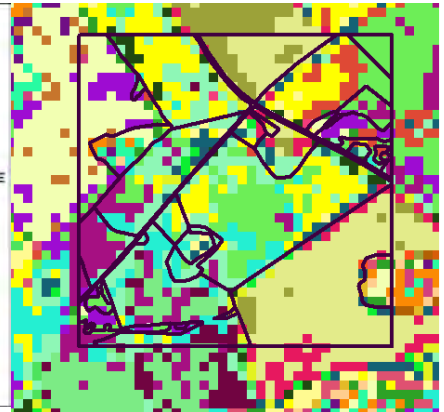
EE03



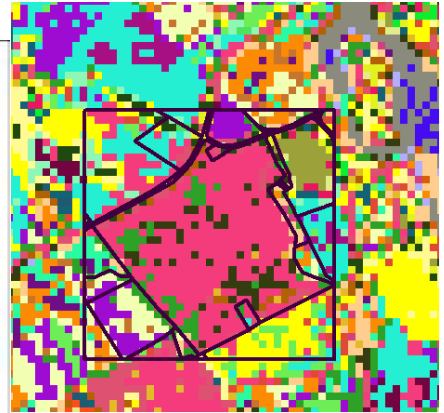
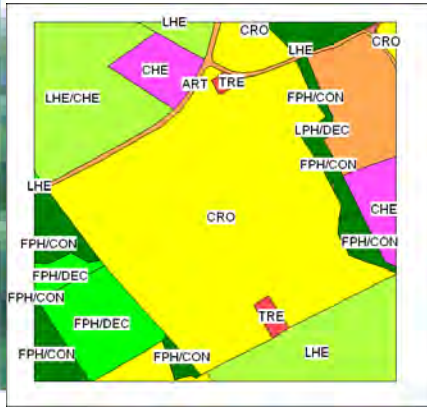
EE04



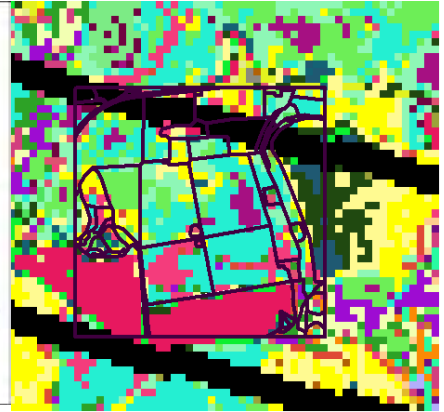
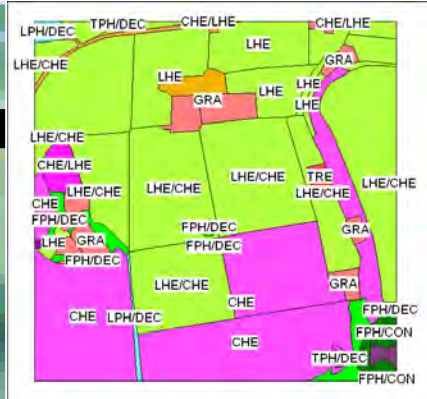
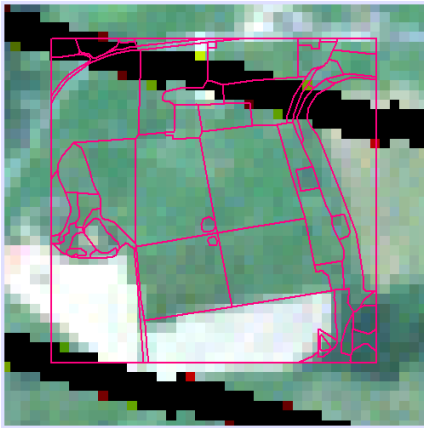
EE05



EE06



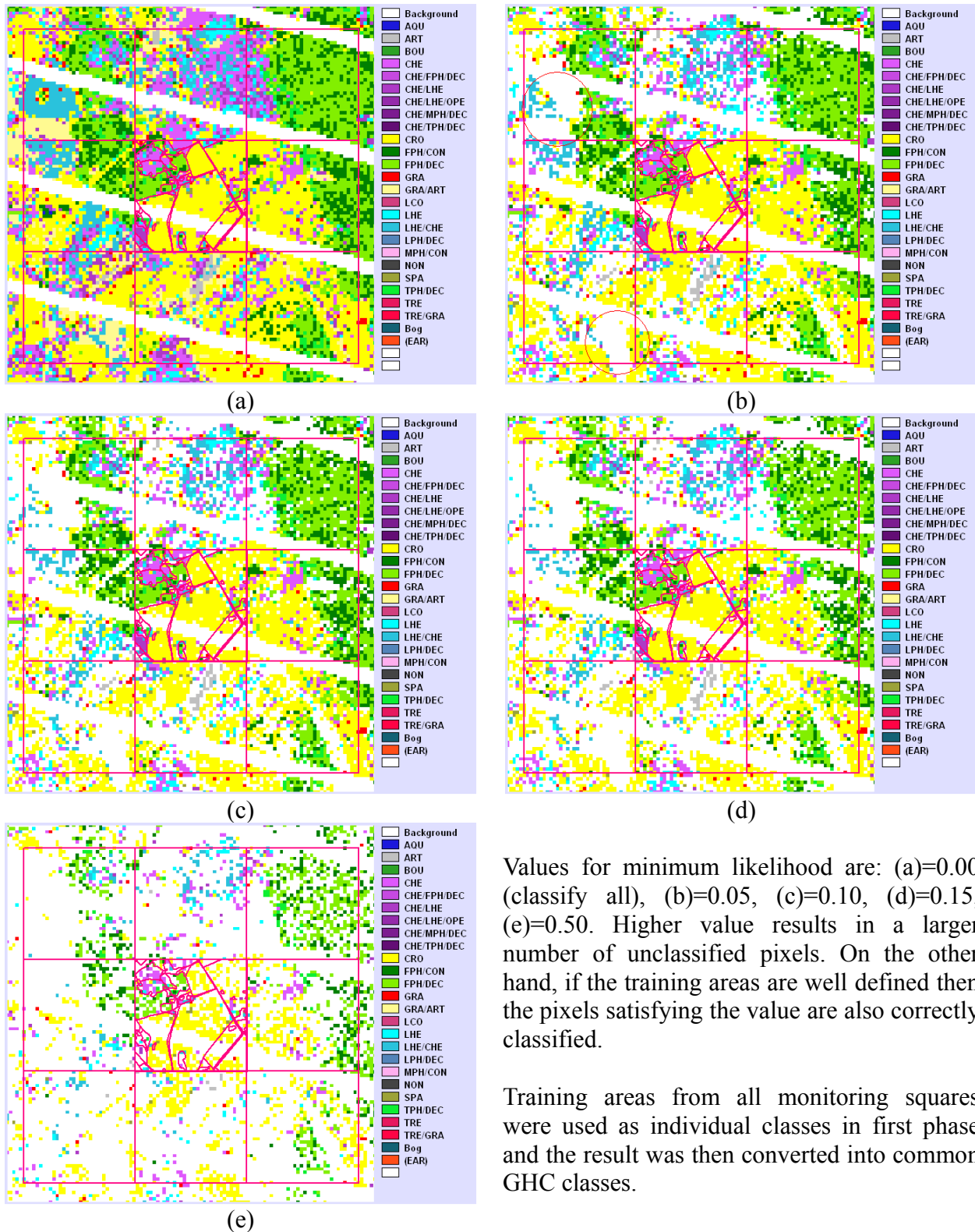
EE07



EE08

Appendix 2. Maximum likelihood classification in EE04

The influence on the minimum likelihood threshold value to the maximum likelihood classification procedure in EBONE monitoring square EE04. Legend represents all of the GHC codes found in field measurement data.



Values for minimum likelihood are: (a)=0.00 (classify all), (b)=0.05, (c)=0.10, (d)=0.15, (e)=0.50. Higher value results in a larger number of unclassified pixels. On the other hand, if the training areas are well defined then the pixels satisfying the value are also correctly classified.

Training areas from all monitoring squares were used as individual classes in first phase and the result was then converted into common GHC classes.

Appendix 3. Example of classification validation cross tabulation

Table 2: Validation cross tabulation of maximum likelihood classification in use-all-signatures test. Signatures were created for those training field polygons which had at least five pixels left after masking out border pixels. Exceptionally variable NON class signature from monitoring site EE03 was not used. Minimum likelihood threshold in classification was set to 0.

Validation		Classification													
		1	2	3	4	5	6	7	8	9	10	11	12	13	14
AQU	1	16	0	0	0	0	1	4	0	0	0	1	0	0	0
ART	2	0	41	2	5	0	14	1	0	0	4	3	5	0	0
CHE	3	0	3	661	39	0	22	4	12	5	24	33	64	0	8
CHE/LHE	4	0	2	77	521	0	38	7	11	6	15	25	30	0	17
CHE/MPH/DEC	5	0	0	1	0	6	3	0	0	0	0	0	1	0	0
CRO	6	0	0	174	98	0	1827	37	155	9	131	72	46	20	13
FPH/CON	7	2	1	3	3	0	15	165	65	0	3	0	1	0	4
FPH/DEC	8	0	0	37	8	0	46	108	477	2	5	3	6	1	45
GRA	9	0	3	18	13	0	15	0	0	26	10	1	14	1	1
GRA/ART	10	0	0	3	3	0	4	0	0	0	16	1	4	0	0
LHE	11	0	0	89	83	0	58	7	2	3	7	532	59	4	5
LHE/CHE	12	0	2	317	52	0	31	0	2	0	36	49	798	1	4
SPA	13	0	0	9	1	0	17	0	0	0	8	4	3	68	0
TPH/DEC	14	0	0	4	1	0	5	6	14	0	3	4	2	0	49

Annex-7

EBONE



European Biodiversity Observation Network:

Design of a plan for an integrated biodiversity observing system
in space and time

**A contribution to ID5.8: A regional adaptive
approach**

**Mapping of General Habitat Categories for Almeria
using high resolution multispectral imagery**

Authors:

Sander Mûcher

Table of contents

1 INTRODUCTION	3
2 STUDY AREA AND MATERIALS	5
STUDY AREA	5
MATERIALS	7
3 METHOD AND RESULTS	16
UNSUPERVISED CLASSIFICATION	19
RESOLUTION MERGE	20
HYMAP	23
3 CONCLUSIONS	26
4 REFERENCES	28
ANNEXES	29

1 Introduction

The spectral characterization of different habitats is related to the properties of the vegetation or the soil susceptible of being remotely received by the sensor, processed and send back to the ground station (Lillesand and Kiefer, 2000). A condition for a characterization from a spectral signal is the signature separability from different habitats. The different properties of the vegetation determining the reflectance are a matter of importance, and it still offers significant difficulties due to the multiple factors involved. Firstly, consider the leaf reflectance, phenological state, shape and water content. Then, other factors of consideration are the morphology of the plant (height, canopy structure, percentage of land cover). A third group of factors are those susceptible of being derived from the geographic location of the plant: slope, orientation, association with certain communities, geometric characteristics of certain plantations, etc (Chuvienco, 1995). The method of habitat mapping by means of signature classification has been applied throughout the last decades (Evans, 1994; Recio, 1998; Salvador and Pons, 1998; Eerens *et al.*, 1999). (Mücher *et al.*, 2000), showed that often poor accuracy was obtained with heterogeneous land cover from the Mediterranean region. To enable the mapping of the vegetation it requires the use of aerial photography or the use of high resolution satellite imagery that can capture the spatial complexity of Mediterranean vegetation. Moreover the vegetation can quickly change over and during the growing season, especially in arid places like the Southern part of Spain where the natural growing season is very short. This requires that proper timing of acquisition and having a multi-temporal approach is of utmost importance. A complication is that aerial photography in the Mediterranean is often out-of-date and not easily to obtain, while very high resolution satellite imagery like Worldview-II or QuickBird are mostly too expensive to use in an explorative study. Therefore there is an interest here to explore the use of high resolution satellite imagery that can be obtained freely from satellite archives through data portals, such as the ones from NASA and the USGS, e.g. <http://glovis.usgs.gov/>.

Our area of interest is Almeria in the South-west corner of Spain where fieldwork was done in the beginning of October 2009 (note already that this not the most optimal period, which is normally around the end of April). More specifically we did fieldwork in October 2009 in 4 small sites, namely: Cabo de Gata, Rodalquilar, Sorbas and Tabernas.

The field work for habitat recording was done according to the field protocols of the GHC Handbook 'Handbook for Surveillance and Monitoring of European Habitats' by Bunce *et al.*

(2005). Note that an update of the manual was published in 2011, amongst others based on the new experiences that were obtained during the fieldwork in 2009 in this semi-arid area. The overall goal of the GHC methodology was to set up a methodology designed for collecting information on European habitats in order to obtain statistically robust estimates of their extent and associated changes in biodiversity. GHCs are thus a consistent methodology for field recording and monitoring of habitats. The Raunkiaer classification of plant Life Forms (LF) is the basis for these GHC's. Raunkiaert divided plant species on the location of the plants growth point during seasons with adverse conditions e.g. winter or dry seasons. The use of plant life forms enables the recording of habitats with comparable structures within contrasting bio-geographical zones that have similar habitat structures. Based on the hypothesis that habitat structure is related to the environment and thus it will correspond to phytosociological classes at high level. For the European region 160 GHC's are now derived from 34 Life Forms. The variation within a GHC is additional expressed by environmental, management and global qualifiers.

During the duration of this project we got also access to HYMAP hyperspectral data for the Rodalquilar study area through Wim Bakker (ITC). The HYMAP data were included in this study since one of the conclusions from this report is that the spatial resolution of Landsat TM is too low to study the vegetation structure and GHCs in such complex areas.

2 Study Area and materials

Study area

Our primary study area is an area near Rodalquilar, situated in the Southwest of the Province Almeria, in the National Park Cabo de Gata. Almería is a province of the Autonomous Community of Andalucía, Spain. It is bordered by the provinces of Granada, Murcia, and the Mediterranean Sea. One of Europe's driest areas is found in Almería and is part of the Cabo de Gata-Níjar Natural Park. The semiarid landscape and climate that characterizes part of the province have made it an ideal setting for Western films, especially during the 1960s. Many interesting and unique species of animals native to the region are in the process of extinction. The most important economic activity is greenhouse farming. Millions of tons of vegetables are exported to other European countries and other parts of the world each year. Tourism is also a key sector of the economy, due to the sunny weather and attractive areas such as Roquetas de Mar, Aguadulce, Almerimar, Mojácar, Vera or Cabo de Gata (Wikipedia).



Figure 1 Southwest corner of the Province of Almeria, with the Natural Park Cabo de Gata, more or less situated between the Provincial capital Almeria and Carboneras.

The red drop with capital A indicates the study area Rodalquilar (source: Google Maps).ps).

The Natural Park Cabo de Gata-Níjar is covering 45,000 ha in the southeastern corner of Spain. Cabo de Gata-Níjar is Andalucía's largest coastal protected area, a wild and isolated landscape with some of Europe's most original geological features. The eponymous mountain range is Spain's largest volcanic rock formation with sharp peaks and crags in ochre-hues. It falls steeply to the sea creating jagged 100m-high cliffs, which are riven by gullies leading to hidden coves with white sandy beaches, some of the most beautiful in Andalucía. Offshore are numerous tiny rocky islands and, underwater, extensive coral reefs teeming with marine life (Williams). High temperatures (an annual average of 18°C) and the lowest rainfall in the Iberian peninsula (200mm annually on average) has created a large semi-desert area, with characteristic shrubby vegetation and dwarf fan palms. But the park also encompasses an outstanding variety of habitats, from coastal dunes, beaches, steep cliffs, salt pans, a substantial marine zone of 12,200ha, saltmarshes, inland arid steppe and dry river beds. Designated a Unesco Biosphere reserve in 1997, the park shelters an extraordinary wealth of wildlife, including many rare and endemic plants and endangered fauna.

Rodalquilar itself is a small village, surrounded by mines. The history of mining in the Cabo de Gata area goes back thousands of years. Copper, Alum, Lead, Silver and Zinc were just some of the minerals mined. However, it wasn't until the late 1800s that gold was discovered. Many small mines were opened up but it was 1925 before the first serious attempt was made. This was by the Rodalquilar Gold Mines Company. They used mercury to dissolve the gold as did a later company, the Exploitation of Rodalquilar Gold Mines. Both mines failed to make a profit and closed down (<http://www.faydon.com/Gold/Gold.html>). The study site is the The rocks in this area are dominated by quartz, alunite, jarosite, pyrophyllite, illite, kaolinite, hematite, and related minerals (Choe et al., 2008).

Materials

Aerial photographs

The true colour aerial photographs (3 bands) had a 1 meter spatial resolution and were from the year 2002. In other words, there were not very recent, and above all they did not have a very good quality. Nevertheless, they were already very useful to prepare the fieldwork.

The aerial photographs (APs) were provided by the University Polytechnica in Madrid as sid files and were already geometrically corrected.

The APs were delivered in the following national projection: PROJCS ["WGS_1984_UTM_Zone_30N",GEOGCS["GCS_WGS_1984",DATUM["D_WGS_1984",SPHEROID["WGS_1984",6378137.0,298.257223563]],PRIMEM["Greenwich",0.0],UNIT["Degree",0.0174532925199433]],PROJECTION["Transverse_Mercator"],PARAMETER["False_Easting",500000.0],PARAMETER["False_Northing",0.0],PARAMETER["Central_Meridian",-3.0],PARAMETER["Scale_Factor",0.9996],PARAMETER["Latitude_Of_Origin",0.0],UNIT["Meter",1.0]]

Ecognition

Once the location of the sample sites were obtained together with the aerial photographs, a preliminary segmentation was performed in eCognition. The following parameters settings were used in Ecognition:

- Layer weights: 1,1,1
- Scale factor: 100
- Shape factor: 0.1
- Compactness: 0.5

The shapefactor was set very low, since in fact the patches could have any shape. The compactness was set relatively high , since we did not want to obtain patches that were too large, which is not convenient for field mapping. The scale factor was set to 100 on a experimental basis. During field work the scale factor was encountered as too high, in other words the segments were still to detailed. Note also that shadowed parts have been segmented separately.

Rodalquilar

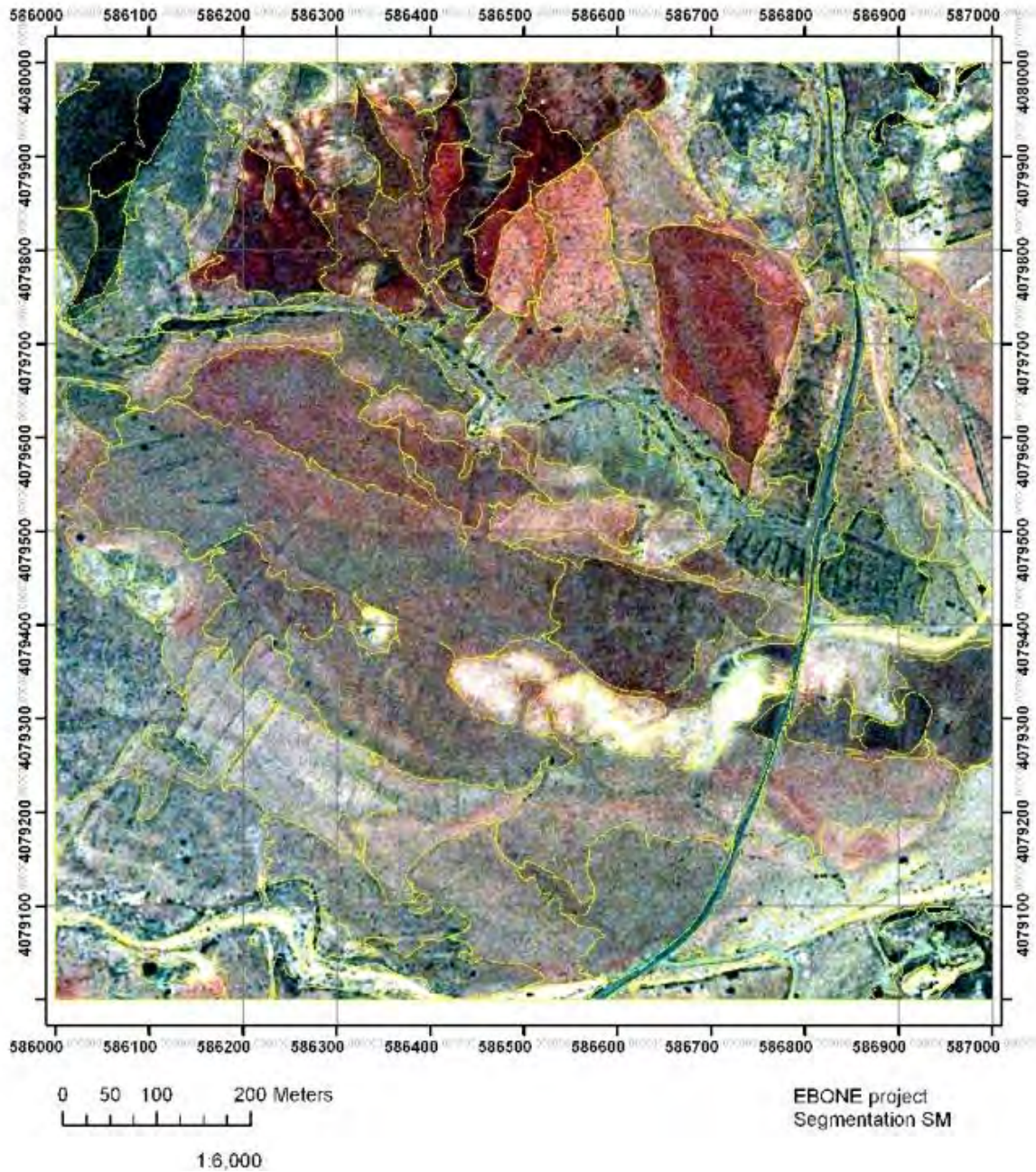


Figure 2 Segmented aerial photograph for the filed sample of 1 square kilometers of the site Rodalquilar.

Fieldwork

Fieldwork was done in the from the 30th of September 2009 till the 3rd of October 2010 in 4 small sites, namely: Aqua Amarga, Cabo de Gata, Rodalquilar, Sorbas and Tabernas. The fieldwork in Rodalquilar was done on the 30th of September 2009. Each time a GHC habitat map was produced for an area of 1 km² according the the field protocols of the handbook (Bunce et al, 2005).

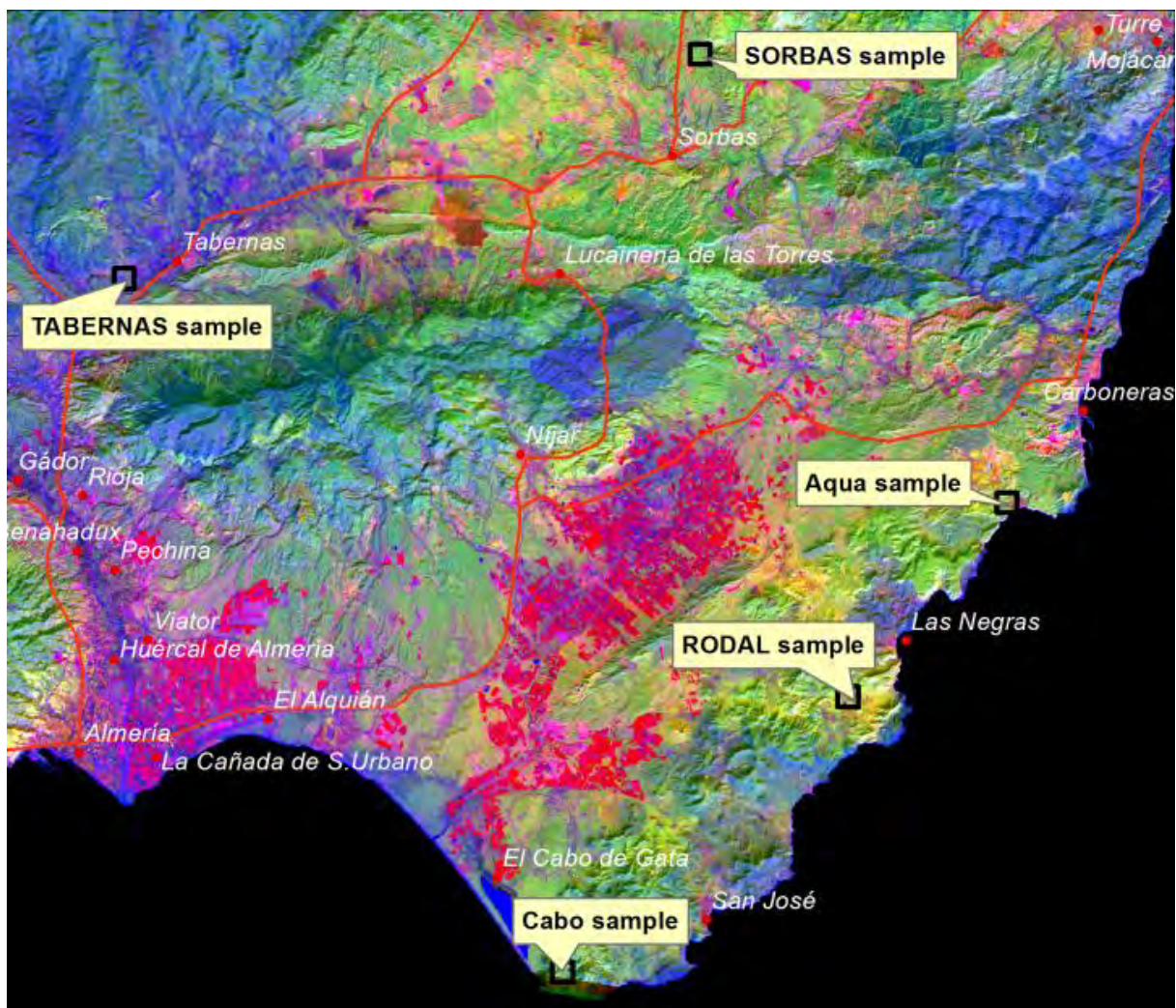


Figure 3 Location of the 1 km samples sites where habitat field recordings has been done in September and October 2009 according to the GHC field mapping protocols.

ANNEX-7

Mapping of General Habitat Categories for Almeria using high resolution multispectral imagery



*Photo 1 Rodalquilar study area is a semi-desert area. On the front is the characteristic dwarf palm, *Chamaerops humilis* (Mücher, 2009).*



Photo 2 Photograph taken from a hill overlooking the Rodalquilar study area (Mücher, 2009)



Photo 3. Hills of Sierra de Gata just outside the Rodalquilar km sample. (Mücher, 2009)

Landsat

The Landsat can be obtained freely from the USGS data portal GLOVIS (<http://glovis.usgs.gov/>). The USGS Global Visualization Viewer is a quick and easy online search and order tool for selected satellite and aerial data.

The Landsat 1, 2, and 3 satellites carried the Multispectral Scanner (MSS) sensor; the Landsat 4 and 5 satellites carry both the MSS and the Thematic Mapper (TM) sensors; and the Landsat 7 satellite carries the Enhanced Thematic Mapper Plus (ETM+) sensor. These sensors support the Landsat Project's mission to provide quality remote sensing data in support of research and applications activities. Landsat MSS, TM, and ETM+ data are provided in GeoTIFF for Level 1T (terrain corrected) products, or for either Level 1Gt (systematic terrain corrected) or Level 1G (systematic corrected) products, if Level 1T processing is not available. GeoTIFF defines a set of publicly available TIFF tags that

ANNEX-7

Mapping of General Habitat Categories for Almeria using high resolution multispectral imagery

describe cartographic and geodetic information associated with TIFF images. GeoTIFF is a format that enables referencing a raster image to a known geodetic model or map projection.

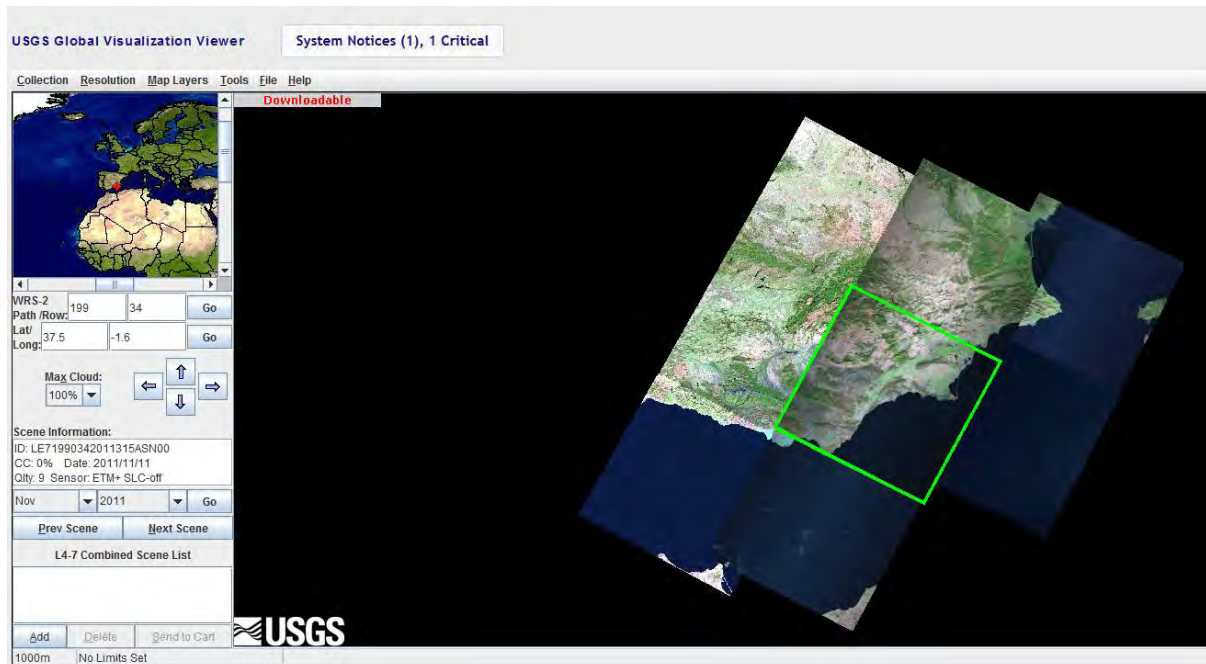


Figure 4 USGS Global Visualization viewer to enable selection and downloading satellite imagery.

In 1992, the US Congress authorized the procurement, launch and operation of a new Landsat satellite. This new system, Landsat 7, is now under construction and is scheduled for launch in April, 1999. It will be the latest in a series of earth observation satellites dating back to 1972. The twenty-two year record of data acquired by the Landsat satellites constitutes the longest continuous record of the earth's continental surfaces. Preservation of the existing record and continuation of the Landsat capability were identified in the law as critical to land surface monitoring and global change research (Source: <http://geo.arc.nasa.gov/sge/landsat/l7.html>).

Table 1

Band Number	Spectral Range(microns)	Ground Resolution(m)
1	.45 to .515	30
2	.525 to .605	30
3	.63 to .690	30
4	.75 to .90	30
5	1.55 to 1.75	30
6	10.40 to 12.5	60
7	2.09 to 2.35	30
Pan	.52 to .90	15
Swath width:	185 kilometers	

ANNEX-7

Mapping of General Habitat Categories for Almeria using high resolution multispectral imagery

Repeat coverage interval:	16 days (233 orbits)
Altitude:	705 kilometers
Quantization:	Best 8 of 9 bits
On-board data storage:	~375 Gb (solid state)
Inclination:	Sun-synchronous, 98.2 degrees
Equatorial crossing:	Descending node; 10:00am +/- 15 min.
Launch vehicle:	Delta II
Launch date:	April 1999

Landsat 5 TM scenes were downloaded for the following dates:

- 24 July 2009
- 12 October 2009
- 13 November 2009
- 24 May 2010
- 11 July 2010
- 27 July 2010

Since the vegetation in sem-arid areas have a very strong seasonal phenology, it's important to obtain time series for optimal identification of habitats.

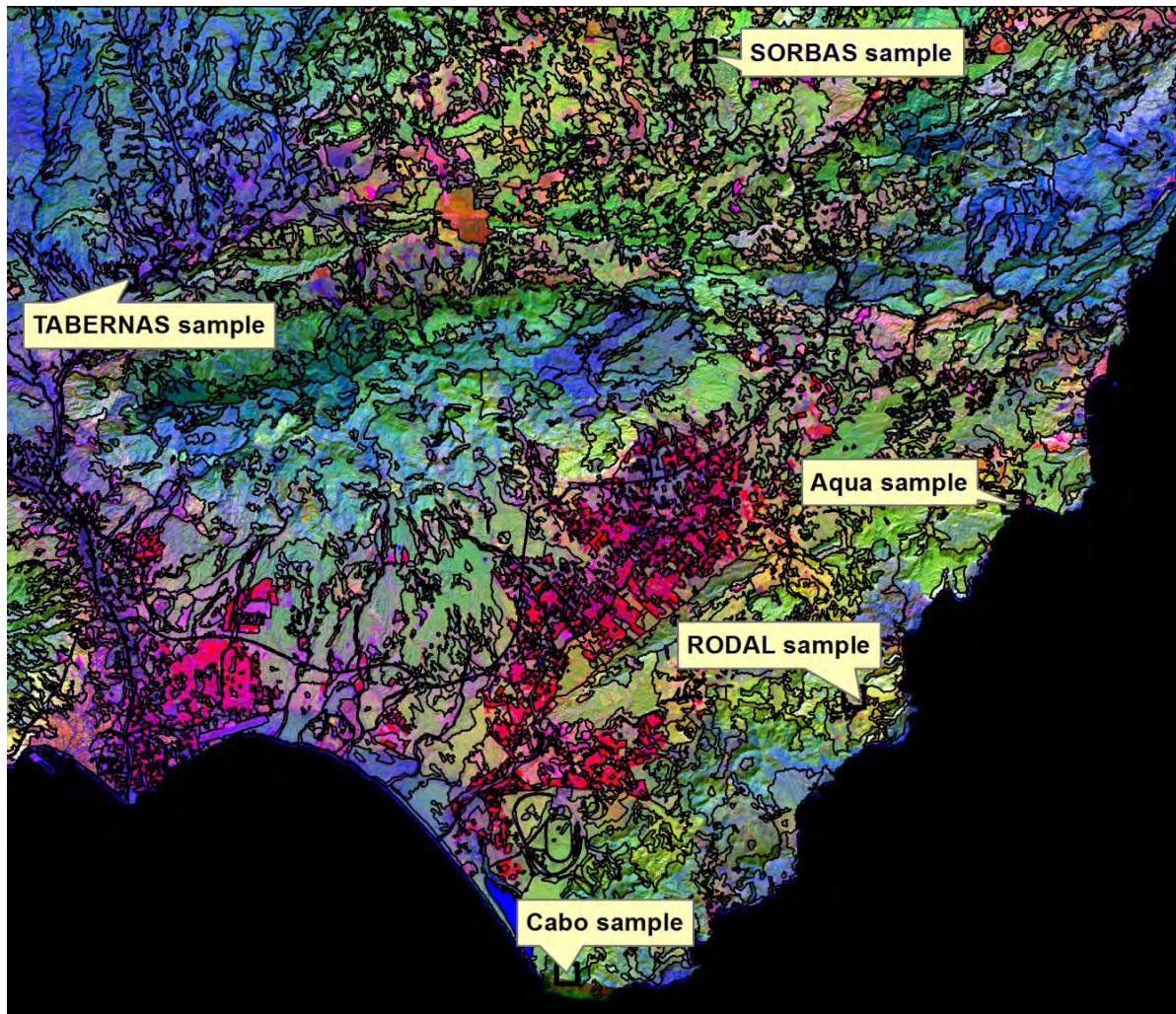


Figure 5 Combination of multi-temporal Landsat 5 TM scenes (R: 24 July 2009, G: 13 November 2009, B: 11 July 2010) that beautifully reflects the main land use types.

Mapping of General Habitat Categories for Almeria using high resolution multispectral imagery

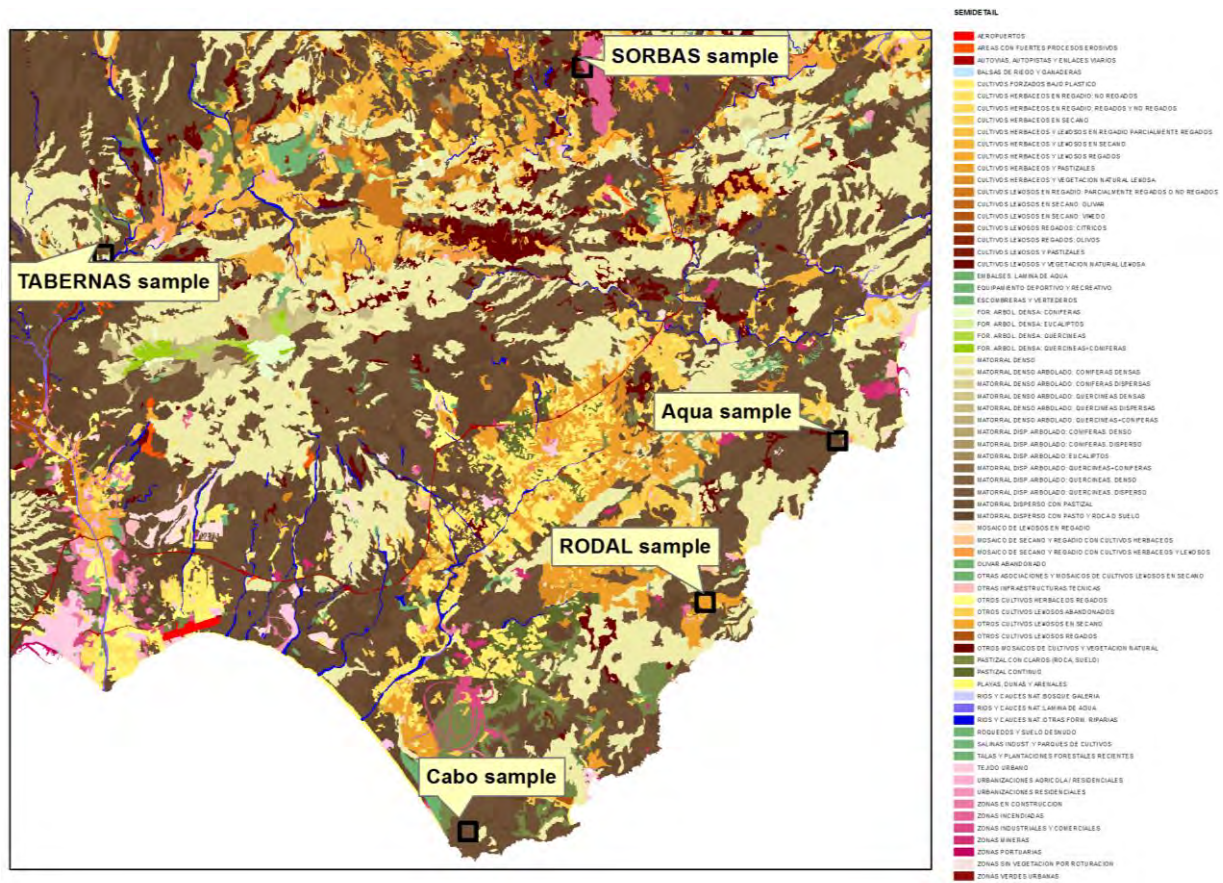


Figure 6 Land use of Almeria (Source: Junta de Andalucía) and reflects the visual interpretation of Landsat TM imagery as demonstrated in Figure 5.

The land use map of Andalusia has as original title “Mapa de Usos y Coberturas Vegetales de Andalucía”, and has a scale 1:50.000 and has been produced by the Junta de Andalucía. It is based on the visual interpretation of Landsat TM imagery (30 m) and IRS-PAN (5 m). (http://www.juntadeandalucia.es/medioambiente/red_ambiental/cartografia/usoscob/VisorRaster.html).

HYMAP

The HyMapH is an airborne imaging system developed by Integrated Spectronics, Sydney, Australia. It is normally placed on a fixed wing aircraft typically flown at an altitude of 2.5 km. The sensor collects reflected solar radiation in 126 bands covering the 0.45–2.5 mm wavelength range of the electromagnetic spectrum. The Rodalquilar HyMap scene was recorded on 11 July 2003 in 126 narrow bands, from 0.45 mm to 2.48 mm with 4m pixel size. The spectrometer of SWIR-1 (1.40–1.80 mm) did not work properly and so data from this part of the electromagnetic spectrum from the airborne imagery were not available. The

Mapping of General Habitat Categories for Almeria using high resolution multispectral imagery

Rodalquilar HyMap scene was geometrically and atmospherically corrected by the German Aerospace Center (DLR) using the software PARGE and ATCOR4 (Bedini et al., 2011).

3 Method and results

Field work was in September and October 2009, and resulted in habitat maps according to the the the field protocols of the handbook (Bunce et al, 2005). For the 1 square kilometer field sample of Rodalquilar the fielwork was done on the 30th of September 2009.

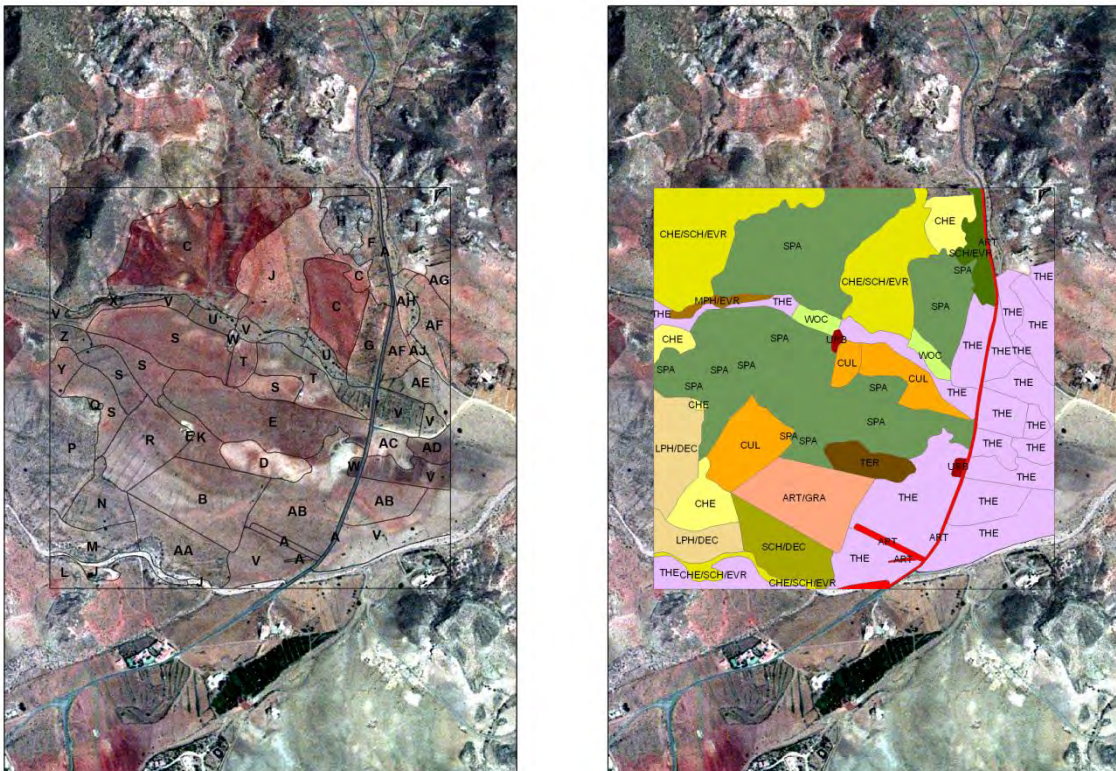


Figure 7 On the left, GHC habitat mapping with the boundaries of the habitat patches and alpha coe. The attributes can be found in the table below. On the right, the mapping result with the General Habitat Categories (GHCs).

Table 2 Example with part of the attributes for the GHC mapping units recorded during field work

ANNEX-7

Mapping of General Habitat Categories for Almeria using high resolution multispectral imagery

RODAL_ID	AREA	CODE	GHC	LF1	LF1%	SPECIES1	SP1%	LF2	LF2%	SPECIES2	SP2%	LF3	LF3%	SPECIES3	SP3%	
6	2124	A	ART	CHE	40	Lygeum spartum		20	THE	50	Stipa	10	0	0	Chamaerops humilis	5
21	7709	A	ART	CHE	40	Lygeum spartum		20	THE	50	Stipa	10	0	0	Chamaerops humilis	5
56	2898	A	ART	CHE	40	Lygeum spartum		20	THE	50	Stipa	10	0	0	Chamaerops humilis	5
61	451	A	ART	CHE	40	Lygeum spartum		20	THE	50	Stipa	10	0	0	Chamaerops humilis	5
54	29480	AA	SCH/DEC		0			0		0		0	0	0		0
43	45060	AB	THE		0			0		0		0	0	0		0
51	16713	AB	THE		0			0		0		0	0	0		0
44	7332	AC	THE		0			0		0		0	0	0		0
42	6462	AD	THE		0			0		0		0	0	0		0
32	12612	AE	THE		0			0		0		0	0	0		0
13	17055	AF	THE		0			0		0		0	0	0		0
15	8584	AF	THE		0			0		0		0	0	0		0
11	4653	AG	THE		0			0		0		0	0	0		0
12	6905	AH	THE		0			0		0		0	0	0		0
27	2229	AJ	THE		0			0		0		0	0	0		0
49	45219	B	ART/GRA		0			0		0		0	0	0		0
2	87847	C	SPA		0	Lygeum spartum	20			0	Stipa tenasissima	10	0	0	Lyceum	5
9	5077	C	SPA		0	Lygeum spartum	20			0	Stipa tenasissima	10	0	0	Lyceum	5
10	27198	C	SPA		0	Lygeum spartum	20			0	Stipa tenasissima	10	0	0	Lyceum	5
46	14311	D	TER	SCH	20	Thymus		20	LPH	10	Lyceum	5	0	0		0
34	54281	E	SPA	SCH	20	Thymus		20	LPH	10	Lyceum	5	0	0		0
45	356	E	SPA	SCH	20	Thymus		20	LPH	10	Lyceum	5	0	0		0
5	13180	F	SCH/EVR	SCH	20	Thymus		20	LPH	10	Lyceum	5	0	0		0



Figure 8 Multi-temporal Landsat TM scene (R: NIR of 24 July 2009, G: NIR of 13 November 2009, NIR of 24 May 2010) overlaid with GHC mapping units. The area demonstrated in the red box is an area of 3 by 3 km with the 1km sample site in the centre.

Unsupervised classification

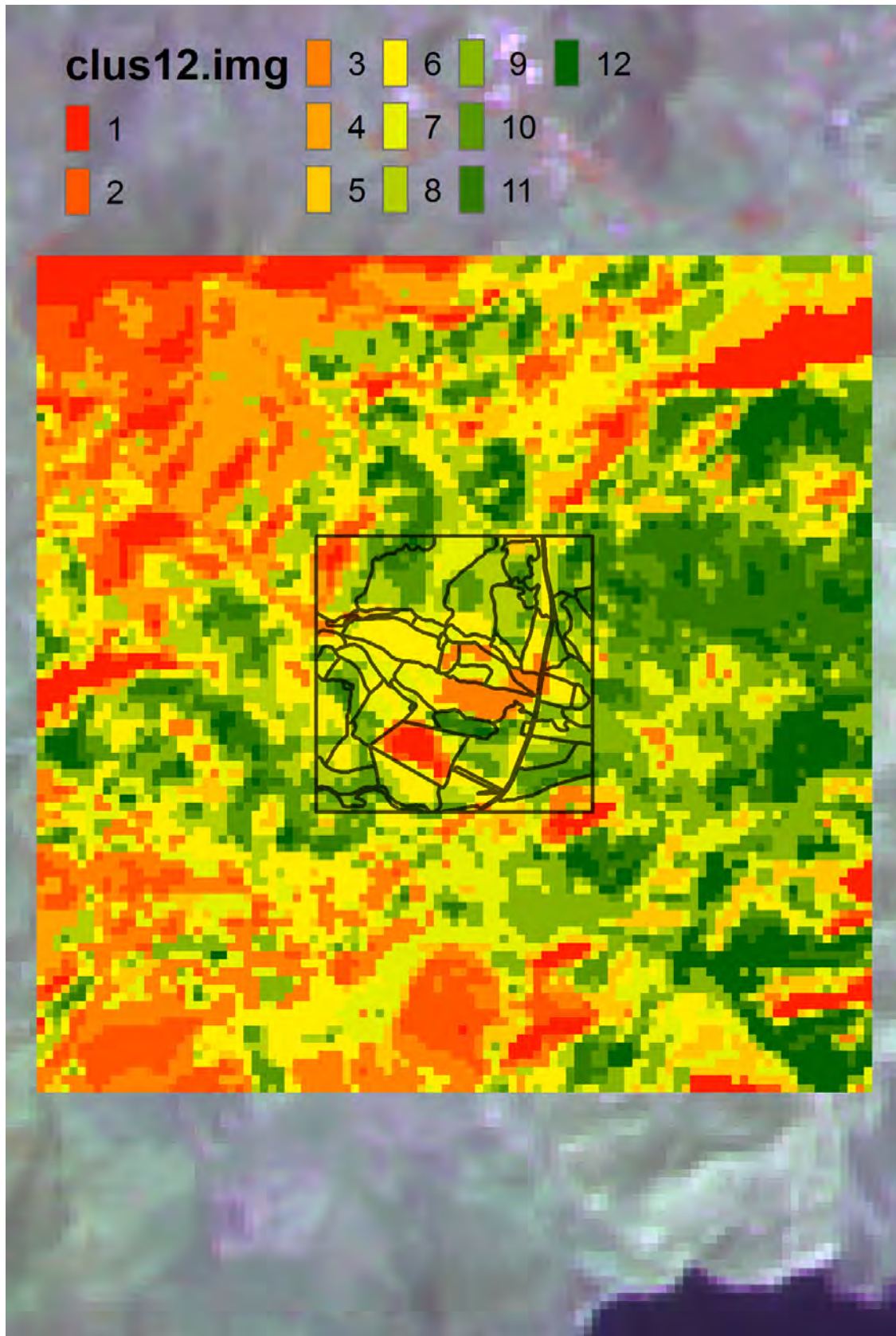


Figure 9 Unsupervised classification into 12 clusters using channels 3,4, and 5 of the multi-temporal Landsat TM scenes (24 July 2009, 13 November 2009, 24 May 2010)

An unsupervised classification was performed on the multi-temporal Landsat TM scenes ((24 July 2009, 13 November 2009, 24 May 2010) using the channels 3,4 and 5 into 12 clusters. Unfortunately, these clusters do not reflect well the General Habitat Categories. Nevertheless, all 12 spectral classes found in the area of 3 km by 3 km, were also found in the central square, indicating that the selection of the square was well representative for the area.

The only reason that the GHCs are not well represented by the spectral classes of the multi-temporal landsat TM scenes is probably the spatial resolution and that fact that each mapping unit exist out of very dispersed vegetation with much bare ground (amount of photosynthetic biomass is very low). Therefore some extra effort was spent on improving the spatial resolution of the Landsat TM imagery (30 m) with the aerial photographs (1m)

Resolution Merge

Software of ERDAS Imagine provides tools to fuse multi-spectral imagery with imagery of a high high spatial resolution. In other words, it helps to integrate integrate imagery of different spatial resolutions (pixel size). Since higher resolution imagery is generally single band (for example SPOT Panchromatic 10m data), while multispectral imagery generally has the lower resolutions (for example Landsat TM 30m), these techniques are often used to produce high resolution, multispectral imagery. This improves the interpretability of the data by having high resolution information which is also in color (source ERDAS). Resolution Merge offers three techniques: Multiplicative, Principal Components, and Brovey Transform. No to go into details of these different transformation, multiplicative and brovey gave slightly better results to integrate the APs with the Landsat TM imagery. Before the resolution merge was performed, a principal component (PC 5) was performed on the multi-temporal Landsat imagery (24 July 2009, 13 November 2009, 24 May 2010, 11 July 2010).

ANNEX-7

Mapping of General Habitat Categories for Almeria using high resolution multispectral imagery

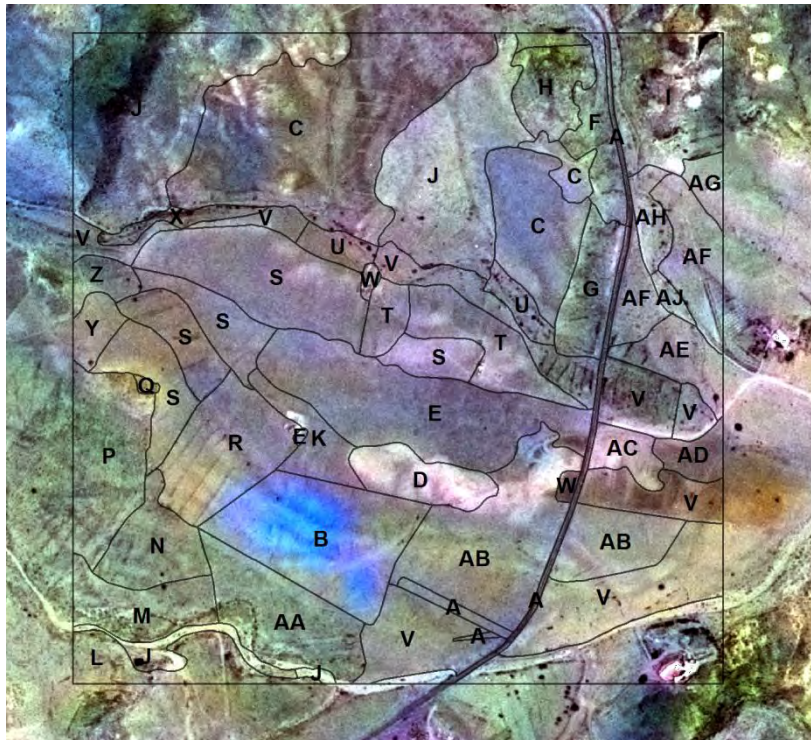
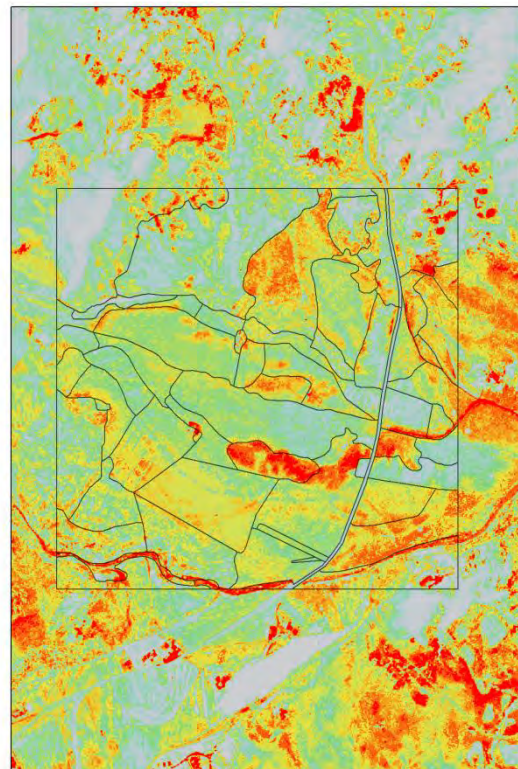
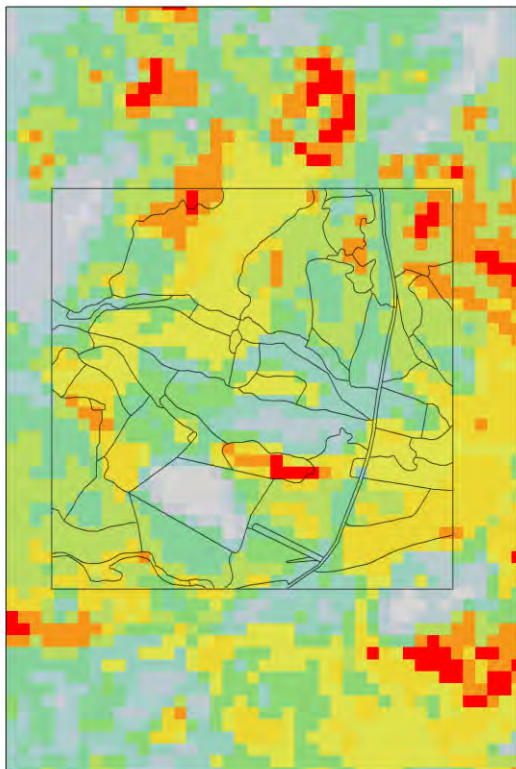


Figure 10 Result of the Brovey resolution merge of the available aerial photographs with Landsat TM imagery.



Mapping of General Habitat Categories for Almeria using high resolution multispectral imagery

Figure 11 On the left, result of an unsupervised classification on Landsat TM imagery. On the right, the result of an unsupervised classification of a Brovey resolution merge of the available aerial photographs with Landsat TM imagery.

From Figure 11 it become clear that a resolution merge is very helpful to improve the spatial resolution. Especially, the within field spatial variability becomes much clearer, next to the fact that linear features become much clearer. But not only the within field spatial variability of the vegetation becomes clear, it also shows that there is much differences between fields with the same GHC. For example all those field labeled as therophytes (THE) at the east side of the 1 km square sample, have quite some spatial difference in vegetation. Also the two fields marked with alpha code J (see Figure 7), have clear spectral differences. This makes it very difficult to come to a consistent classification of GHCs. For the author it is still not clear what hampers a good classification of this region, is it the complexity of the region, was the GHC field recording was done improperly due to improper timing of the field work, or is it the limitation of the imagery that does not reflect well the sparsely vegetated areas.

To support any conclusion it was decided in the last stage to have a closer look at the HYMAP hyperspectral imagery, although this image was recorded in July when the vegetation biomass is at its minimum.

HYMAP

An inverse MNF transform was performed in ENVI on the HyMap scene (4m spatial resolution) from 11 July 2003 for the Rodalquilar area, in order to minimize the noise.

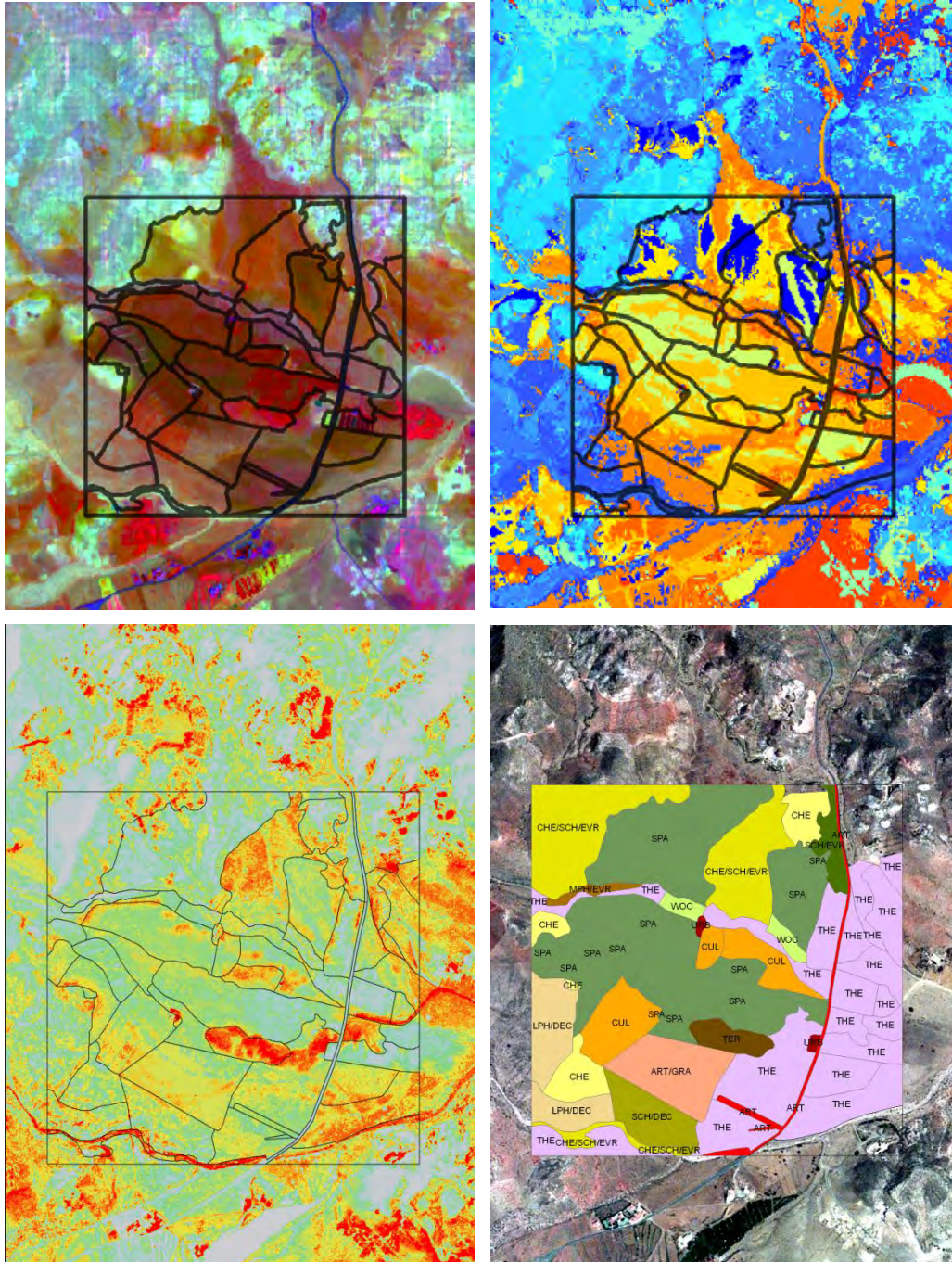


Figure 12 Above left, MNF output of the HYMAP image of 11 July 2003 with a 4 m spatial resolution. Above right, unsupervised classification of the MNF HYMAP image into 20 clusters. Below left, resolution merge of multi-temporal Landsat TM scenes and aerial photographs, to a 1 meter spatial resolution. Below right, GHC habitat map as a result of the fieldwork done on the 30th of September 2009.

Figure 13 Labeling of 20 clusters as an output of the unsupervised classification of the HYMAP image.

The output of the classified HYMAP image seems to be quite satisfactory although the image is from July 2003, and the fieldwork was done at the end of October 2009. This might explain amongst others why mapping units J do not belong to the same satellite derived classes. Since the recent TM imagery reflects the same difference, it is assumed that mistakes were made in the field or that the season for field recording was improper.

3 Conclusions

- The spectral characterization of different habitats is related to the spectral properties of the plant life forms and non-plant life forms.
- Landsat TM imagery is easy and freely accessible.
- Spectral information from Landsat TM imagery reflects well the land cover and often to the associated land use.
- Multi-temporal Landsat TM imagery helps a better identification of the land cover types, but is still hard to use for habitat mapping in semi-arid regions.
- Major limitation of the Landsat TM imagery in semi-arid regions, such as Almeria, seems to be its spatial resolution.
- Aerial photographs have a much higher resolution (often more detailed than 1 m) and greatly supports the preparation of the fieldwork.
- Segmentation of the aerial photographs into basic patches speeds up the field work, but the basic patches should be simple. The use of LPIS (Land Parcel Information System) could replace a basic segmentation, but is often not available.
- Preparation and elaboration of the field work into digitized and georeferenced products is often more time consuming than the fieldwork itself.
- Resolution merge of aerial photography and Landsat TM imagery counterbalances partly the low spectral resolution of the aerial photographs and the low spatial resolution of Landsat imagery. But still does not resemble the quality of the HYMAP hyperspectral imagery (which is clear for any RS expert)
- In this case, HYMAP provides the best GHC classification results.
- Extrapolation from the 1 km square to the surrounding area seems to be feasible using HYMAP satellite imagery (and to a lesser extent for Landsat TM imagery)
- Only a few of the spectral classes from the HYMAP image did not occur in the central sample square (Annex 9). These spectral classes (18,19 and 20) need targeted field visits.
- Supervised classifications of satellite imagery are only possible when targeted training samples have been collected in the field. This is especially valid in semi-arid regions where the contrast is also very high within and between mapping units.
- Unsupervised classification of multi-temporal satellite imagery (e.g. Landsat TM) into thematic spectral classes helps to prepare the GHC habitat mapping of larger areas.
- Good timing and preparation of the field work is essential. In semi-arid regions multi-temporal field visits seems to be essential for a good characterization of the habitats.

ANNEX-7

Mapping of General Habitat Categories for Almeria using high resolution multispectral imagery

- Classification of vegetation in semi-arid areas is more difficult than classification of vegetation in temperate regions.

4 References

Bedini, E., van der Meer, F., van Ruitenbeek, F., 2009: Use of HyMap imaging spectrometer data to map mineralogy in the Rodalquilar caldera, southeast Spain, *International Journal of Remote Sensing*, 30(2), 327-348.

Bunce, R.G.H., Groom, G.B., Jongman, R.H.G. and padoa-schioppa, E., 2005. Handbook for Surveillance and Monitoring of European Habitats. Alterra report. Alterra, WUR.

Chuvieco, E., 1995. Fundamentos de teledeteccion espacial. Madrid.

Choe, E., F. van der Meer, et al., 2008. Mapping of heavy metal pollution in stream sediments using combined geochemistry, field spectroscopy, and hyperspectral remote sensing: A case study of the Rodalquilar mining area, SE Spain." Remote Sensing of Environment 112(7): 3222-3233.

Eerens, H., Deronde, B., van Rensbergen, J. Badji, M. (1999). A new vegetation map of Central Africa. Update of the JRC-Trees map of 1992 with SPOT-VEGETATION imagery of 1998., VITO (Flemish Institute for Technological Research).

EP (2002). Decision No 1600/2002/EC of the European Parliament and of the Council of 22 July 2002 laying down the Sixth Community Environment Action Programme was published in OJ L 242 of 10/9/2002. 1600/2002/EC: 15.

Evans, D.L., 1994. Forest cover from Landsat Thematic Mapper data for use in the Catahoula Ranger District Geographic Information System. General Technical Report. F. Service. New Orleans, United States Department of Agriculture: 19.

Lillesand, T.M. and Kiefer, M.W., 2000. Remote sensing and image interpretation. New York.

Mücher, C.A., Heunks, C., Steinnocher, K.T. and Kressler, F.P., 2000. Land cover characterization and change detection for environmental monitoring of pan-Europe. *International Journal of Remote Sensing* 21(6-7): 1159-1181.

Recio, F., 1998. Clasificación de coberturas vegetales mediante la utilización combinada de imágenes NOAA/AVHRR y LANDSAT-TM. Aplicaciones prácticas en los Países Bajos y en la zona suroeste de la Comunidad de Madrid. E.T.S.I. Montes. Madrid, UPM: 470.

Roerink, G.J., Menenti, M. and Verhoef, W., 2000. Reconstructing cloudfree NDVI composites using Fourier analysis of time series." *International Journal of Remote Sensing* 21(9): 1911-1917.

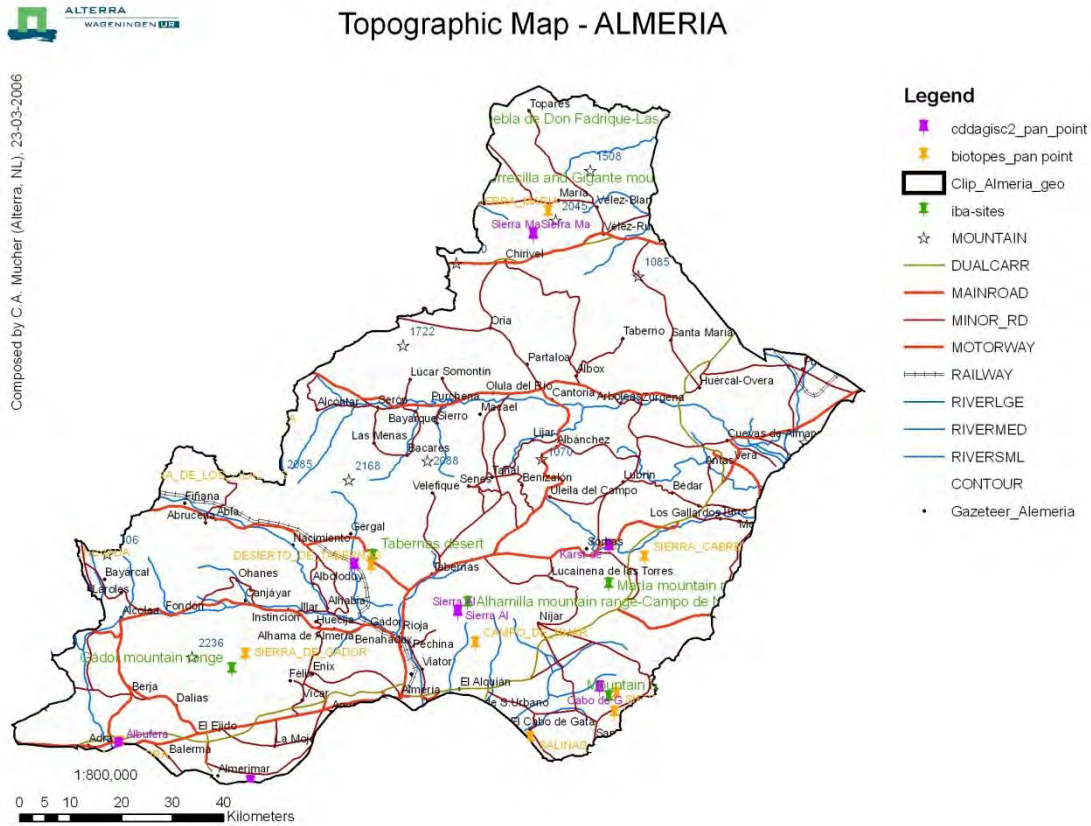
Salvador, R. and Pons, X., 1998. On the applicability of Landsat TM images to Mediterranean forest inventories." *Forest Ecology and Management* 104(1-3): 193-208.

SHOSHANY, M. (2000). "Satellite remote sensing of natural Mediterranean vegetation: A review within an ecological context." *Progress in Physical Geography* 24(2): 153-178.

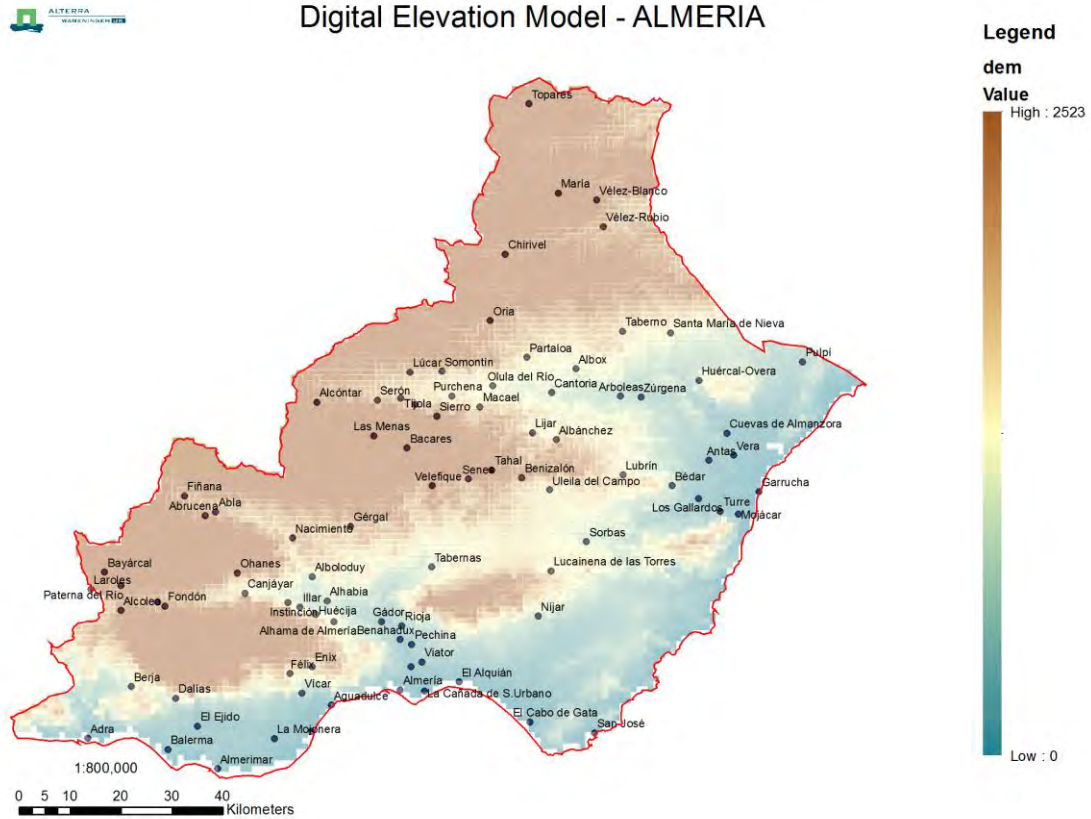
ANNEXES

Annex 1 Topography & DEM

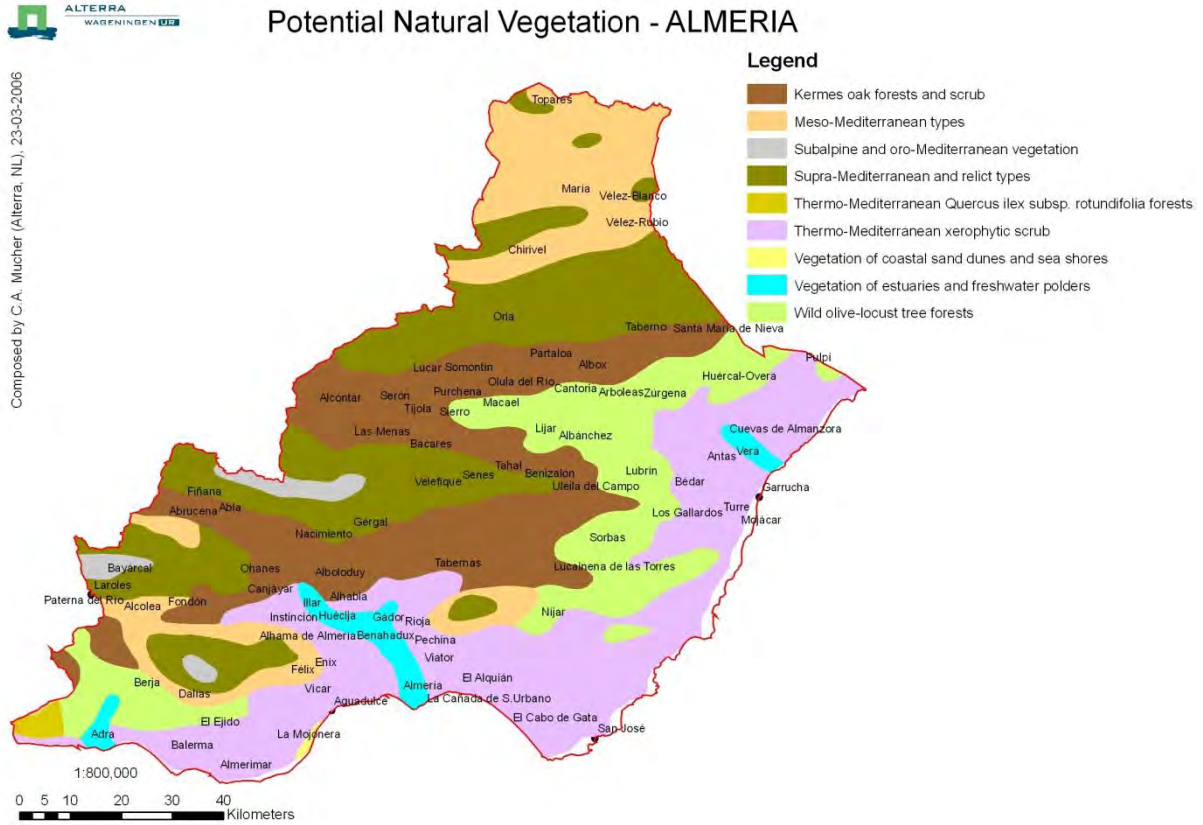
Topographic Map - ALMERIA



Digital Elevation Model - ALMERIA



Annex 2 PNV & Landscapes



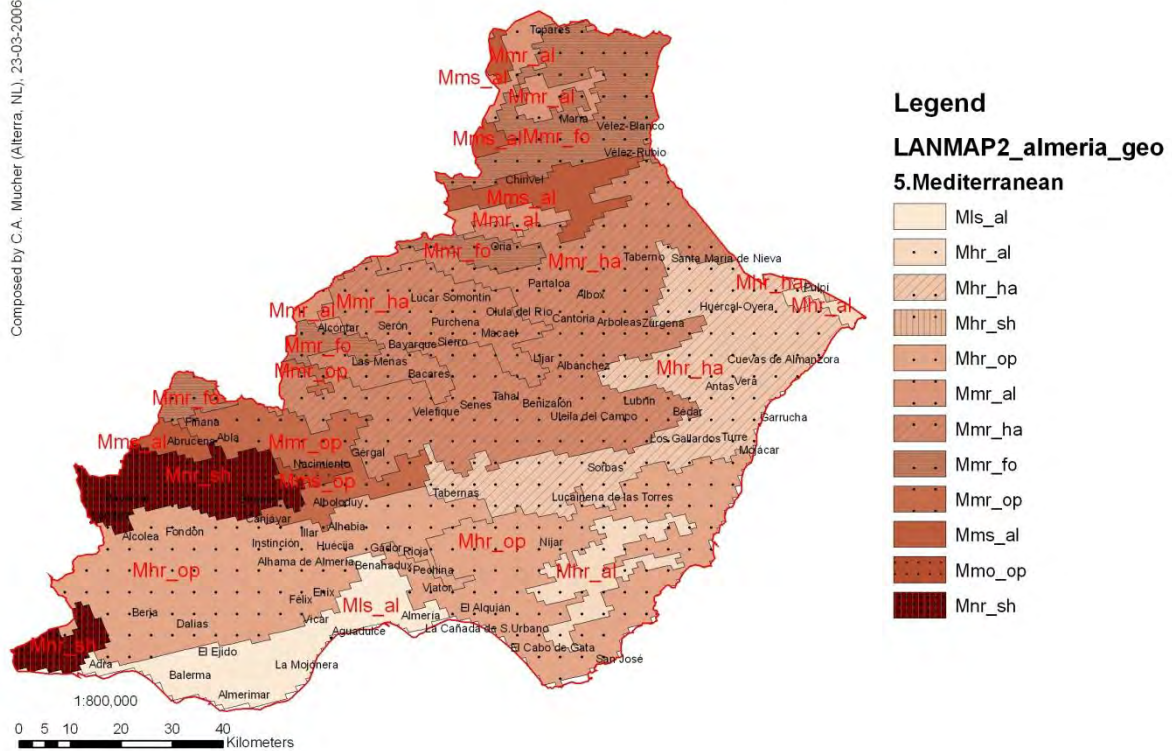
ANNEX-7

Mapping of General Habitat Categories for Almeria using high resolution multispectral imagery



Landscapes (LANMAP2) - ALMERIA

Composed by C.A. Mucher (Alterra, NL), 23-03-2006

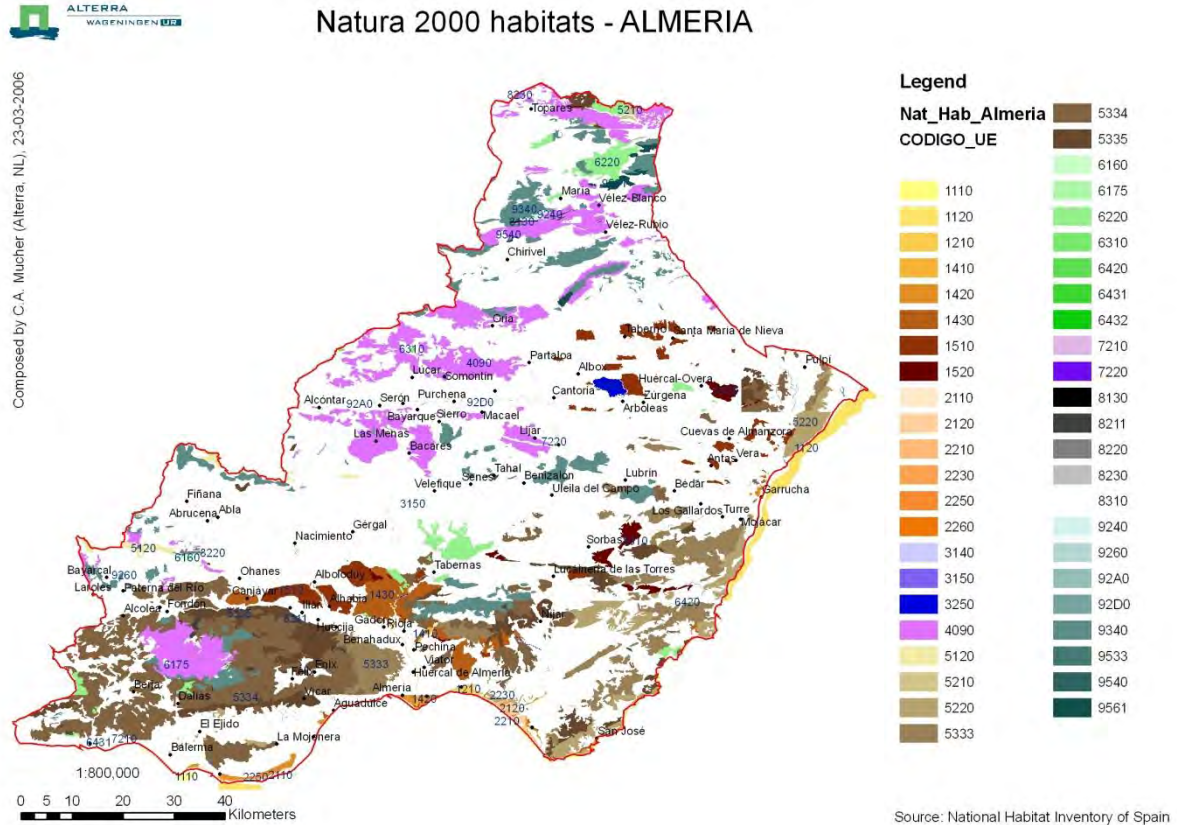


Annex 3 CORINE & National Forest Map

ANNEX-7

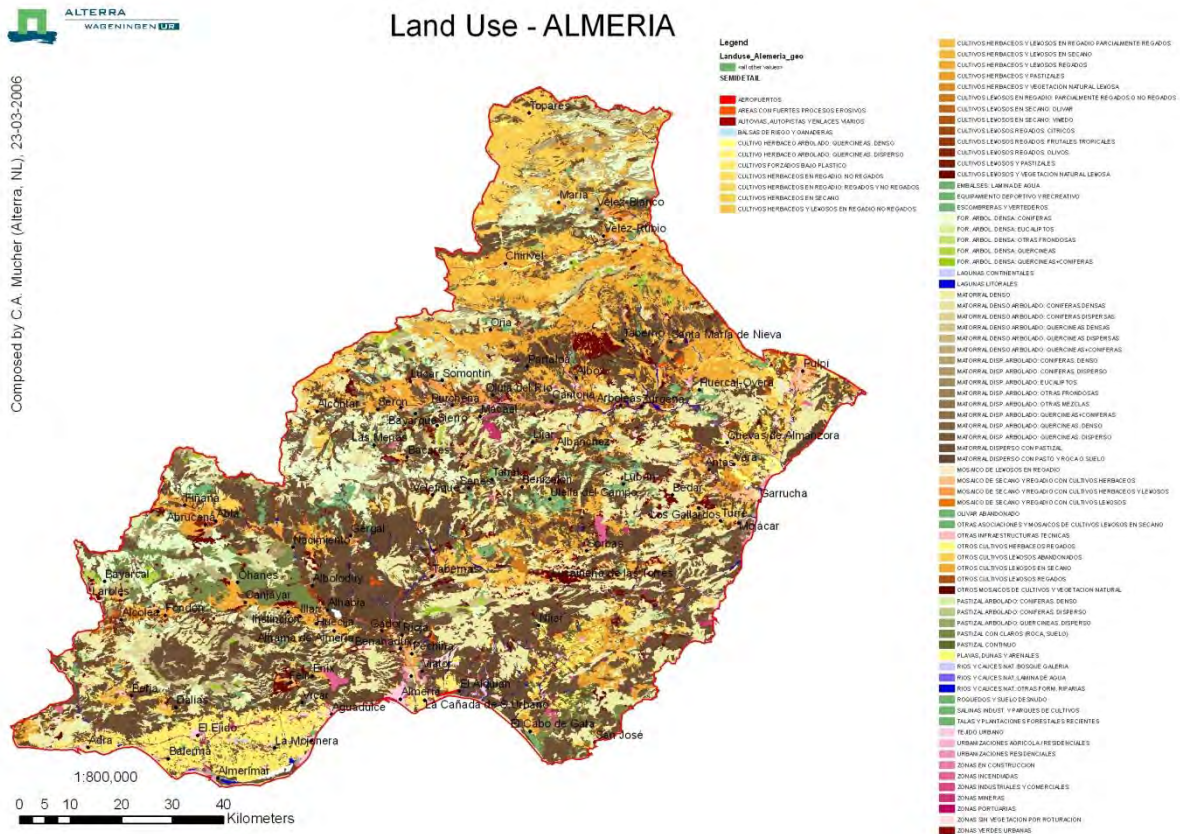
Mapping of General Habitat Categories for Almeria using high resolution multispectral imagery

Annex 4 Natura 2000 & land Use



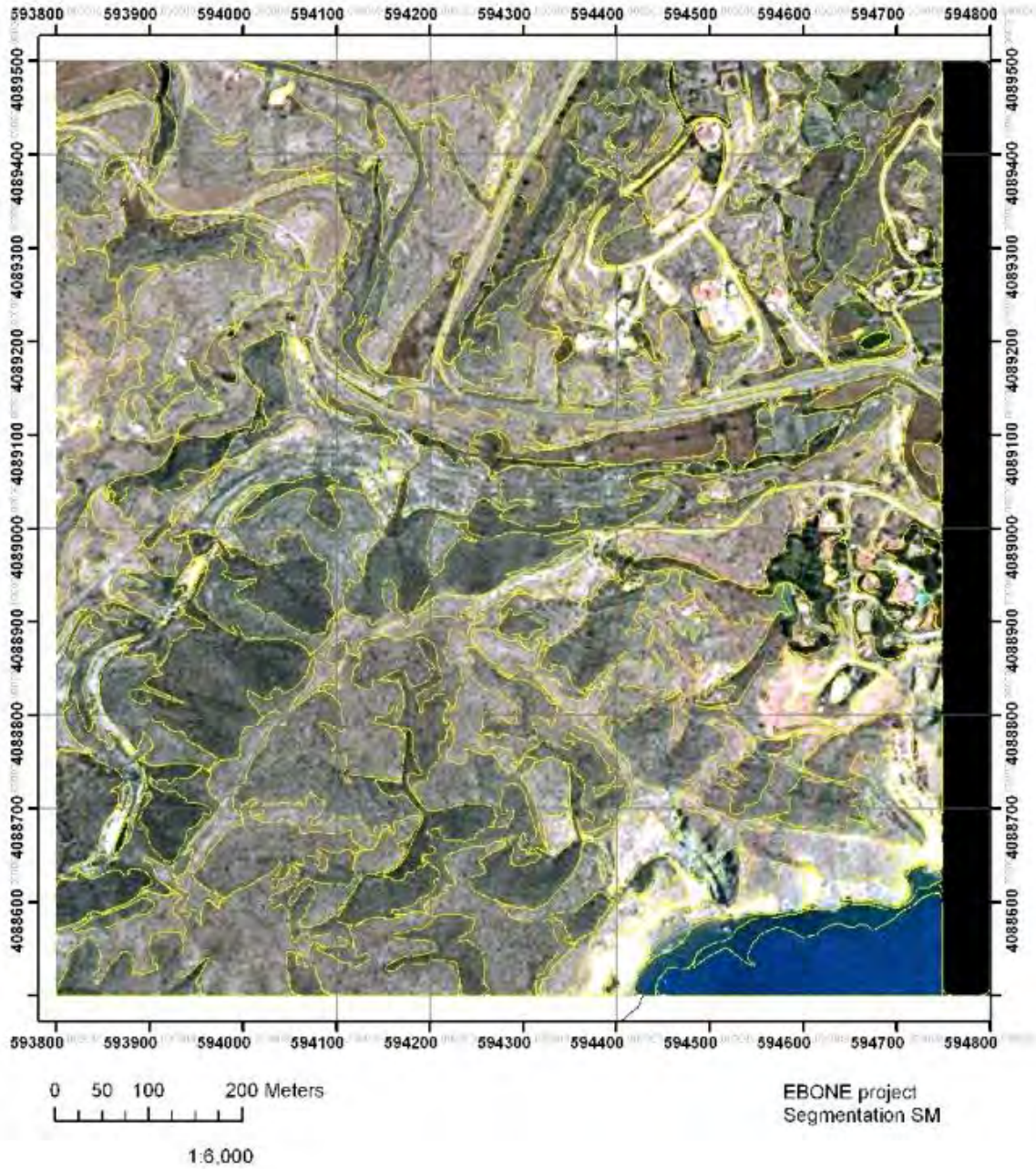
ANNEX-7

Mapping of General Habitat Categories for Almeria using high resolution multispectral imagery



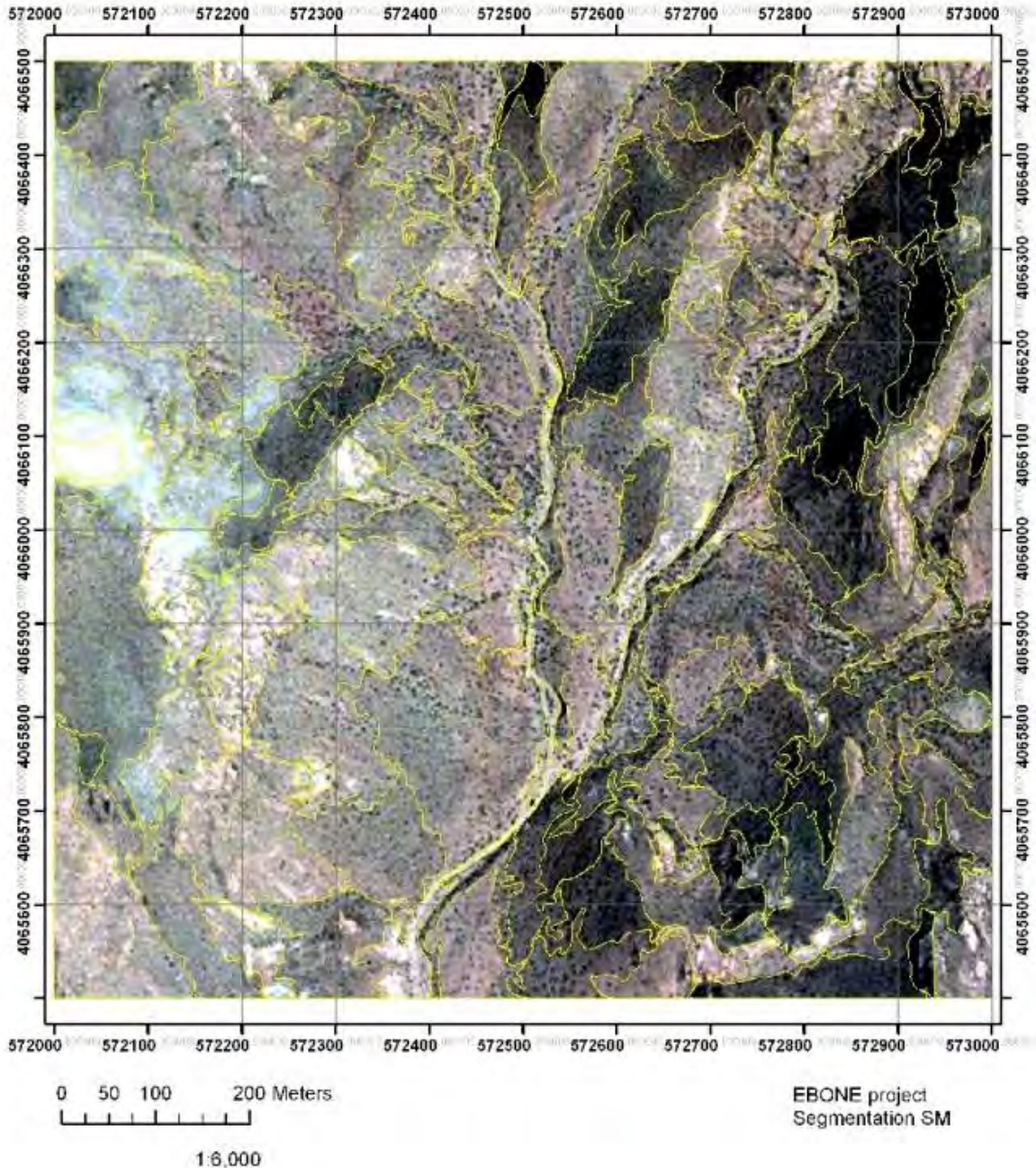
Annex 5 Segmented field sample Agua amarga

Agua amarga



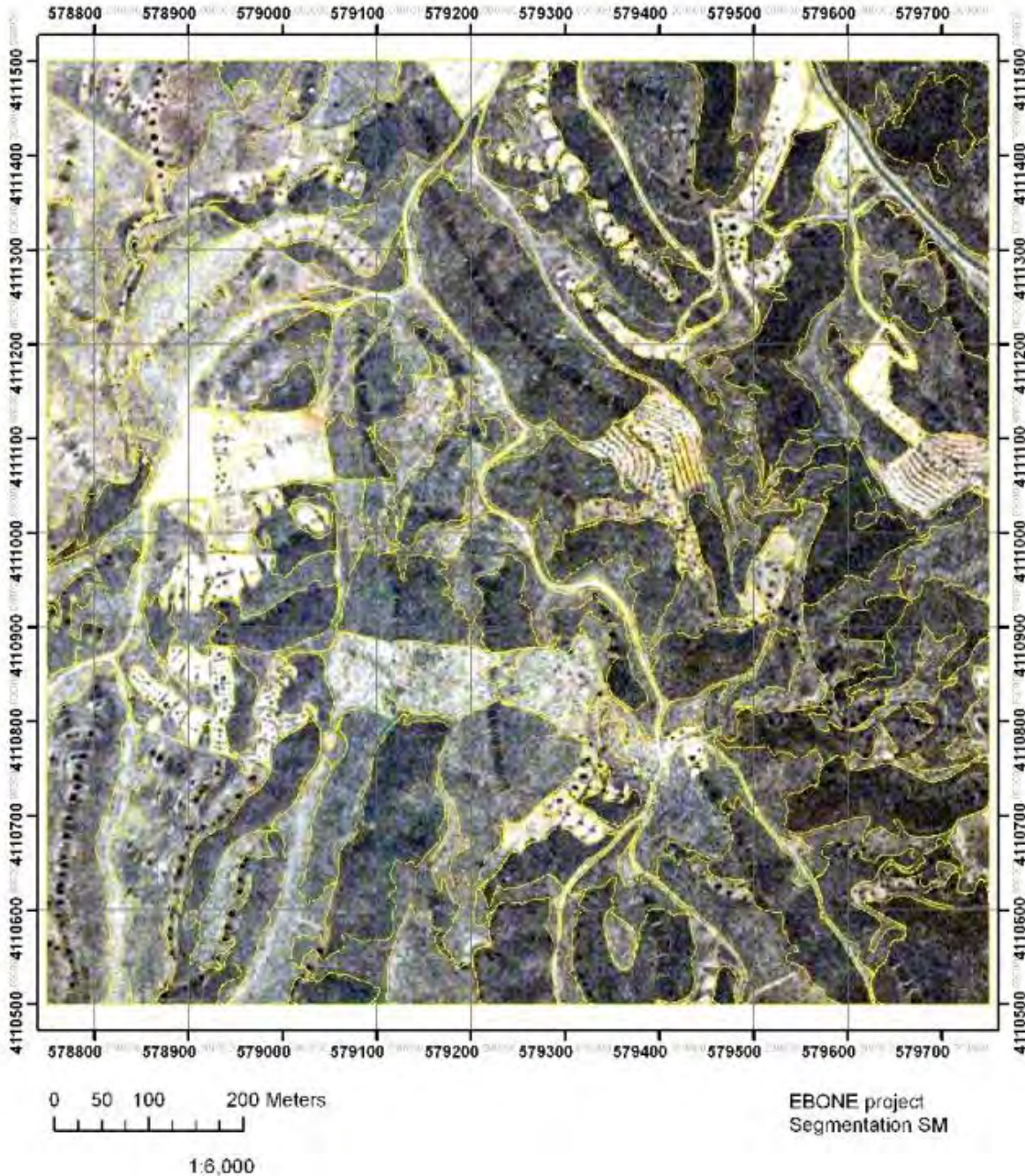
Annex 6 Segmented field sample Cabo de Gata

Cabo de Gata



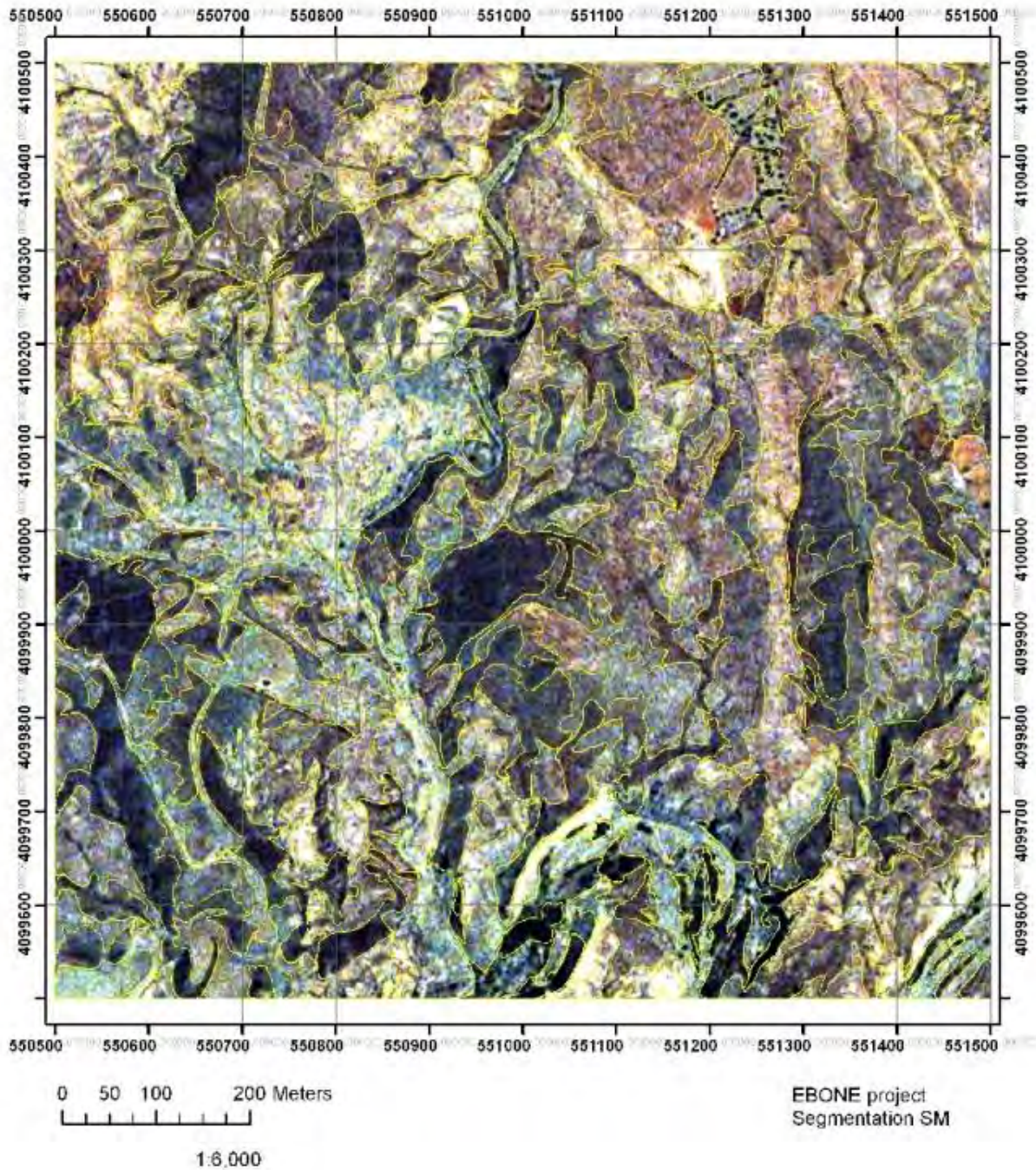
Annex 7 Segmented field sample Sorbas

Sorbas



Annex 8 Segmented field sample Tabernas

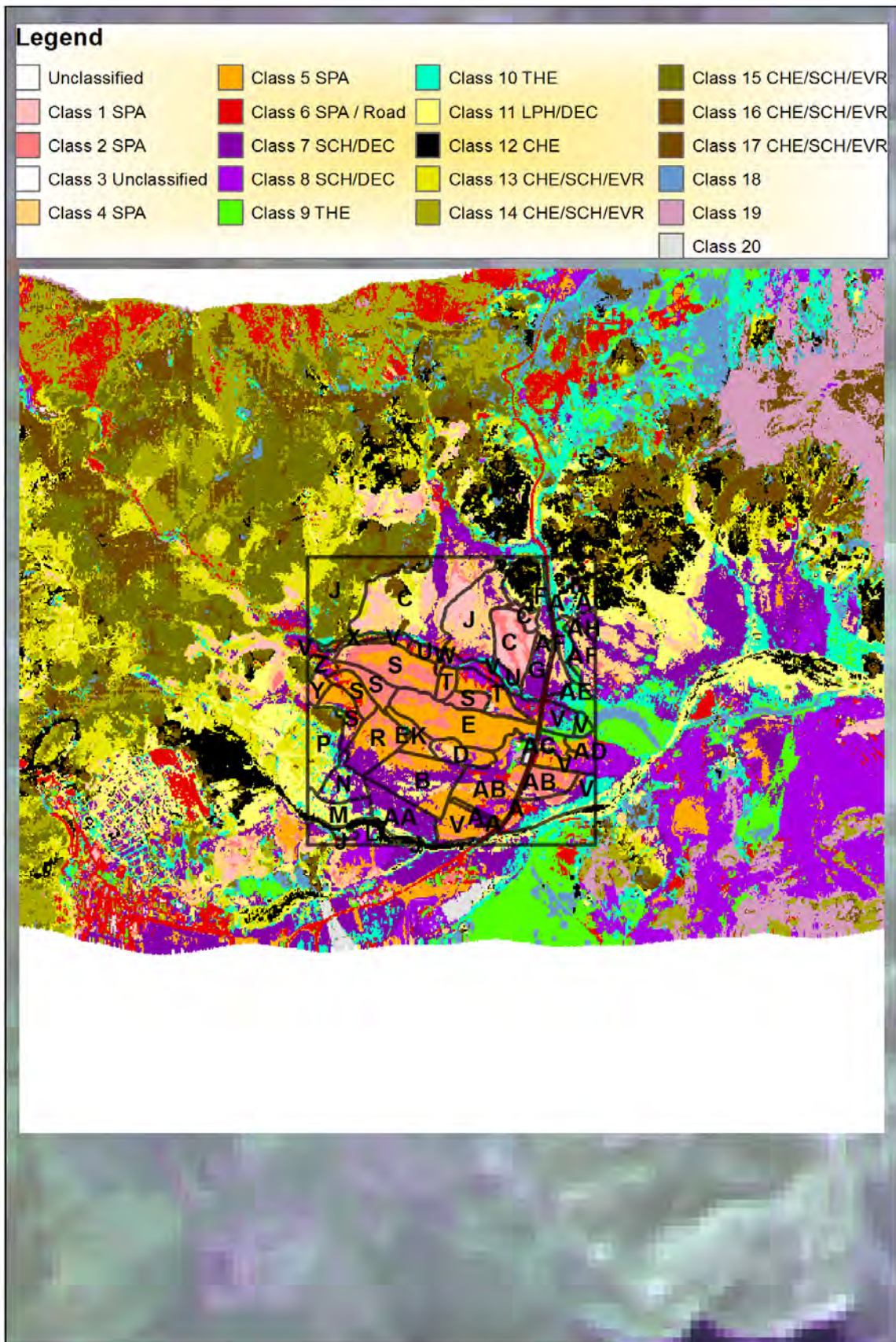
Tabernas



Annex 9 Classified HYMAP image

ANNEX-7

Mapping of General Habitat Categories for Almeria using high resolution multispectral imagery



Annex-8

Remote sensing of Israel's natural habitats

Noam Levin¹, Ruthie Harari-Kremer¹, Yohay Carmel²

¹ *Department of Geography, The Hebrew University of Jerusalem*

² *Faculty of Civil and Environmental Engineering, Technion - Israel Institute of Technology*

Report delivered to Israel's Nature and Parks Authority, March 31st, 2011

Table of Contents

1. Abstract	p. 3
2. Introduction	p. 6
3. Aims	p. 8
4. Methods	p. 8
5. Results – Landsat	p. 13
6. Results – QuickBird	p. 35
7. Results – MODIS	p. 76
8. Discussion	p. 97
9. Operational recommendations	p. 99
10. References	p. 100
11. Appendices	p. 11

1. Abstract

Background and aims: EBONE general habitat categories (GHC) have been suggested as a method for objectively mapping land cover categories, so that effective monitoring of biodiversity can be conducted. The aim of our study was to examine to what degree can available remote sensing methods separate and classify land cover categories as used within EBONE. In addition we aimed to determine the limitations of remotely sensed based classification with respect to the EBONE categories and the spatial and temporal heterogeneity characterizing Israel's Mediterranean and desert landscapes.

Methods: We used three passive sensors in the VIS-NIR-SWIR spectral regions, offering varying spatial, spectral and temporal resolutions: MODIS (250 m, every 16 days, 2000-2010), Landsat (30m, four seasons, early 2000s) and QuickBird (2.4m, spring and summer 2010, specially tasked for this study). All images underwent basic preprocessing steps prior to their analysis, which included geometric, radiometric, atmospheric and topographic corrections, depending on the imagery used. Our basic approach was to use phenology as the key to differentiate between vegetation and land cover types. Several mapping methods were applied, including supervised and unsupervised classification, spectral unmixing, time series analysis of significant trends and of abrupt changes. The GIS layers used for calibration and validation of the classification included land cover layers from Israel's Nature and Park Authority (including EBONE classification collected in three study sites: Ramat haNadiv, Lehavim Forest and Ein Avdat), forest stands from the Jewish National Fund, vegetation types from the Society for Protection of Nature in Israel, 1m orthophotos, as well as areas identified as belonging to specific land cover types.

Results: We will outline the main results for each sensor separately.

Landsat. Following a preliminary analysis it was found the topographic correction of shading effects was important for improving classification accuracy. Overall classification accuracies of the Landsat images were at the order of 90% (when using validation sites identified by us), but were lower in the Mediterranean sites when using the EBONE GHC field mapping validation sites (between 30% to 60%, after merging some of the EBONE classes). Among classes, trees (including maquis) were mapped well (accuracies between 60% to 90%), whereas the success in mapping the shrubs and herbaceous classes was lower within the supervised classification.

The results of the unsupervised classification were better when using the BAND-RATIOS than when using the RUGGED Landsat images as the source for the classification, with overall classification accuracies between 70%-90%. Mediterranean areas were reasonably classified, with the general distribution of perennial and herbaceous vegetation, agricultural areas and even the major urban areas showing quite well. However, desert areas were not differentiated, and were mostly classified as bare soil.

Spectral unmixing into the percent cover of perennial green vegetation, seasonal green vegetation and bare soil within a pixel was better when based on NDVI values. The resulting image clearly shows areas of maquis and of planted forests in Israel. In addition, this product presents the transition zones between the Mediterranean and desert areas, where the percent cover of seasonal green vegetation decreases gradually.

QuickBird. QuickBird imagery was used to spectrally unmix into the percent cover of perennial green vegetation, seasonal green vegetation and bare soil (as in the Landsat imagery). The improved spatial resolution of QuickBird allowed the mapping of sparse vegetation cover, undetected at the spatial resolution of Landsat.

Supervised classification of the QuickBird imagery was done using pixel-based approaches as well as using object-based image segmentation. The latter approach allows for an objective segmentation of the image into homogeneous areas. The spectra of coniferous trees of cypress (and to a lesser degree of pines) was shown to be different than that of maquis, enabling the separation of these vegetation classes (overall accuracy of 75% in Ramat haNadiv site).

MODIS. The NDVI time series of MODIS were denoised using Fourier transformation to remove erroneous data related to atmospheric attenuation. Statistically significant trends in vegetation cover were identified using the denoised NDVI time series, and were related to decrease in rainfall, recovery of vegetation from wildfires, and the development of built-up areas, to name just a few factors. In addition, the time and size of large fires can be mapped using raw MODIS time series (prior to noise removal).

A supervised classification based on a neural network classifier and a decision tree, was able to classify not only general land cover types, but also demonstrated that planted coniferous forests can be separated from maquis, based on their time series properties, mainly summer (minimum) NDVI values and the coefficient of variation (CV) values of NDVI, which are different (within rainfall zones) between maquis and coniferous trees (an overall accuracy of 77%).

Discussion: Overall remote sensing methods using operational passive sensors have been shown to enable the monitoring of gradual and abrupt changes in land cover and also enable mapping of broad types of Israel's land cover. The full breadth of EBONE classes was found to be too detailed to be replicated using passive remote sensing, and we therefore had to merge some EBONE classes prior to accuracy assessment so they better match with the remote sensing classifications. If vegetation height is an important consideration for land cover mapping, then LiDAR data should be acquired and used (out of the scope of our project). Using phenological data we have shown that perennial vegetation, seasonal vegetation and bare soil can be mapped at the sub-pixel level. Using detailed time series, monitoring of changes can be achieved, and the spatial distribution of seasonal vegetation can be mapped, being of special interest in

the transition zones and the desert, where rainfall is highly variable in space and in time. One of the challenges in mapping Mediterranean vegetation is that of separating between maquis and coniferous planted trees. We have shown that using either high spatial resolution or detailed time series, maquis and coniferous trees can indeed be separated, at accuracies > 70%.

While promising, we would like to note on the following limitations of remote sensing, as well as sources for errors in the classifications. While cloud cover over Israel is less than in Europe, full coverage cloud-free satellite images of Israel are not common, and therefore our analysis of Landsat imagery was confined to the early 2000s (in addition to acquisition problems of Landsat 7 since 2003). A critical issue when performing an accuracy assessment of classification results, is to have reliable reference data. Different data sets of collected by agencies in Israel provide a variety of land cover layers, using different classes and codes. While EBONE aims to create a uniform method for classification, it too has several limitations: (1) it is better suited for Mediterranean landscapes, leaving most of the desert areas classified as TER (bare soil); (2) being based on a polygonal characterization, within EBONE patches there is a lot of variability in vegetation cover; (3) EBONE classes are based on the highest vegetation type, even if it is not the dominant type in percent cover, whereas remote sensing methods are more affected by percent cover of area by a vegetation type, than by the height above ground.

Operational recommendations:

Following this work we recommend the following:

1. An annual tasking and acquisition of cloud-free images of all Israel thru a Landsat type sensor, around March and October, capturing maximum and minimum greenness.
2. An annual LiDAR coverage of Israel to be freely available for all government agencies, for monitoring of changes in vegetation height, coastal erosion (as well as urban uses).
3. Monitoring of large scale changes in vegetation cover in Israel using MODIS data, freely available for downloading.
4. To employ within the GIS unit of INPA a remote sensing technician, that will be able to conduct analysis of satellite imagery.
5. Within the LTER sites, add to the EBONE classification also detailed descriptions of percent cover of vegetation types (e.g., perennial, seasonal) within 100×100 m quadrats.
6. Object based image segmentation can be an objective method for defining homogeneous patches used in EBONE classification.

These recommendations can benefit not only INPA, but also other agencies managing Israel's open landscapes, such as the Ministry for Environmental Protection and the JNF.

2. Introduction

Israel's land cover and vegetation are the product of natural and human factors. Located between Europe, Asia and Africa, Israel's climate ranges from mesic Mediterranean in the north to extreme arid desert areas in the south. In addition, the long human history of domestication and agriculture in the Middle East, with varying levels of grazing, cutting and fire has left its mark on the vegetation characterizing Israel. Since the establishment of the State of Israel, human pressures of overgrazing and cutting have been reduced, and the Mediterranean maquis has been able to recover. Afforestation efforts have increased the area of coniferous planted forests in Israel, in some cases enabling the spreading to large forest fires. All this together with the growth in population density and urbanization, have led to highly fragmented landscape, with a heterogeneous mosaic of vegetation types at varying succession stages.

The specific objective of the BioHab framework for a European-wide monitoring of habitats, is "...to obtain statistically robust estimates of their extent and associated changes in biodiversity" (Bunce et al. 2005). The BioHab methodology is a system for consistent field recording of habitats and for subsequent monitoring. This is done by field recording of so-called General Habitat Categories (hereafter, GHC), and is based on the hypothesis that habitat structure is related to environmental factors. This is a practical, transmissible, and reproducible procedure for surveillance and monitoring habitats which can produce statistics integrated at the landscape level. BioHab mapping method is mainly based on the dominant growth forms, which are only noted down when having a cover higher than 10%. In addition this categorization is done from an aerial viewpoint; first the tall growth forms followed by the lower forms. The methodology is based on classical plant life forms, used in biogeography since the nineteenth century. The principal advantage of the GHCs is that they enable the primary decision on habitat category to be made in the field without the necessity of subsequent data analysis. Their primary disadvantage is the demanding resources of time, money, and human industry involved, restricting such mapping to relatively small areas. It was proposed that remote sensing and image analysis could be combined for automating mapping of GHCs, to complement mapping in situ, which could then be used for evaluation purposes. The major question here is how well could remote sensing products correspond to in situ BioHab vegetation mapping.

The spectral reflectance of electromagnetic radiation from vegetation is dependent upon several factors, among them are the geometry of the leaves, the morphological and physiological characteristics of the plant, the type of soil, the solar incidence angle and the climatic conditions (Barret and Curtis, 1992). The spectral range between 0.5-0.7 μm is characterized by absorption features caused by chlorophyll a and b pigments (Rast, 1991; Guyot et al., 1992). The spectral range between 0.7-1.35 μm is characterized by a high reflectance and low absorption, and is mainly influenced by the structure of the leaves. The spectral range between 1.35-2.5 μm is also influenced by the structure of the leaves, but also from the water content of the

leaves' tissue and its chemical composition. The above mentioned spectral characteristics of vegetation form the basis to many vegetation indices that serve as estimators for green vegetal biomass (Eastman, 2001). One of the first and most used indices is the Normalized Difference Vegetation Index (NDVI; Tucker, 1979; Kerr and Ostrovsky 2003):

$$\text{NDVI} = (\text{NIR} - \text{RED}) / (\text{NIR} + \text{RED})$$

Where NIR and RED stand for the near-infrared (NIR) and red bands of the sensor (bands 4 and 3 of Landsat).

Due to the limitations of field work monitoring, remote sensing has been suggested as a means for mapping and monitoring vegetation and land cover. Shoshany (2000) gave a review of remote sensing of natural Mediterranean vegetation and recommended a better synergy of methods and data sources between passive and active sensors, high and low spatial resolutions, multispectral, multitemporal and textural methods, as well as the use of ancillary data layers (such as topography, lithology and precipitation). Remote sensing estimations of vegetation cover using the VIS-NIR spectral range are considered difficult in arid and semi-arid regions where vegetation cover is sparse (lower than 25%-35%), due to the soil background reflectance (Tueller, 1987). Characteristic spectral reflectance curves of several desert habitats and of dominant desert vegetation were collected using a field spectrometer by Pinker and Karnieli (1995). The spectra collected includes key species common also to Israel's coastal dunes, e.g. *Ammophila arenaria*, *Artemisia monosperma* and *Retama raetam*. Separating Mediterranean vegetation species is a highly challenging task, and although some promising results have been shown using hyperspectral field measurements (Rud et al., 2006), due to lack of high signal-to-noise ratio operational hyperspectral sensors onboard satellites, this approach cannot, at the present, allow the classification of Mediterranean vegetation at a national scale. Using a single-date Landsat image within the northern Negev, Rozenstein and Karnieli (2011) demonstrated that a coarse land-use classification (6 classes) can be achieved, by combining remote sensing and ancillary land-use data. An alternative approach for pixel-based mapping of land cover is an object-based classification. Such an approach has been demonstrated by Mallinis et al. (2008) to delineate forest vegetation polygons in northern Greece, using a summer-time QuickBird image.

Another approach is to use multitemporal satellite imagery, to separate between vegetation types based on their phenology. Working on the Nizzana desert dunes, Schmidt and Karnieli (2000) and Karnieli (2003) found that the temporal analysis of natural vegetation in semi-arid environments should take

into account three components: annuals, perennials and biogenic crusts/lichens. Each of these vegetation components has a different phenological cycle. Biogenic crusts are very sensitive to moisture and turn green during the first rainy month. The annuals cover the ground only after a few intensive rainfall events, whereas the perennials are photosynthetically active throughout the year but show a higher spectral response toward the end of the rainy season. Shoshany and Svoray (2002) applied a multivariate adaptive unmixing technique to three Landsat images in the area between Bet-Guvrin and Lahav, to calculate the percent soil cover, herbaceous vegetation, dwarf-shrubs and shrubs. However, even working in a small area they had to partition the analysis in two sub-regions, due to climatic/biotic/lithologic transitions. Use of multitemporal Landsat imagery has been applied also by Fernandez et al. (2010) for mapping ecosystem functional types in Doñana (Spain), examining patterns in the normalized difference vegetation index (NDVI), surface temperature and albedo. Coarser spatial sensors such MODIS (0.25-1 km) or NOAA-AVHRR (1 km) have also been successfully used to map ecosystem functional types of vegetation based on NDVI time series (e.g., Alcaraz et al., 2006, for the Iberian Peninsula, or Duro et al., 2007 and Coops et al., 2008, for Canada).

3. Aims

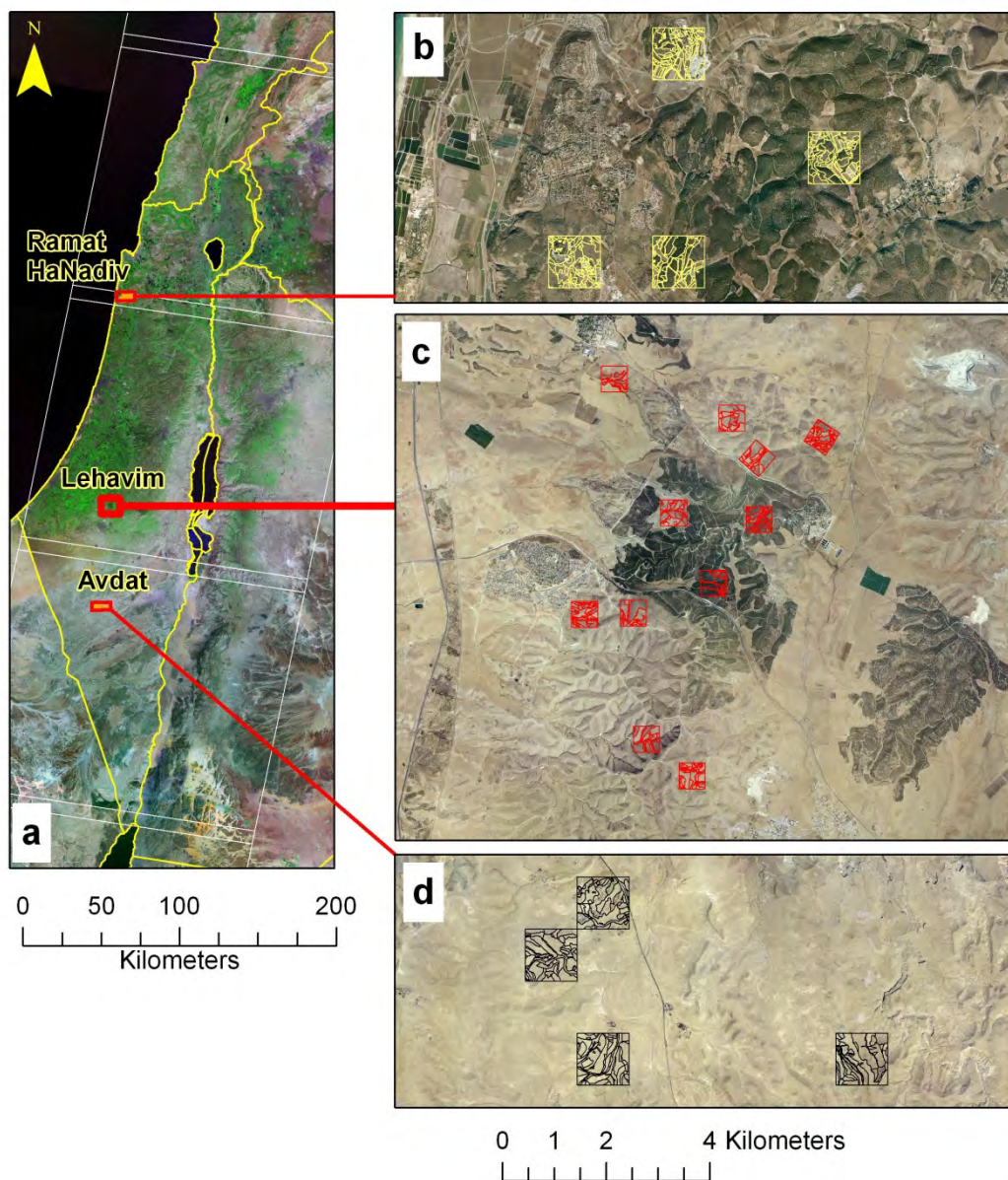
The aim of our work will be to examine several remote sensing methodologies for mapping EBONE land cover categories from space-borne sensors and to examine the relationship between the remotely sensed categories and in-situ habitat data. We will evaluate various sensors for this purpose, in order to develop a general methodology and specify sensors that offer good performance and yet are not prohibitively costly. In addition, we will examine what are the limitations of remotely sensed based classification with respect to the EBONE categories and the spatial heterogeneity characterizing Israel's Mediterranean and desert landscapes. Due to the short duration of the project, we aimed to demonstrate possible use of readily available images of passive multispectral sensors in the VIS-NIR-SWIR spectral regions.

4. Methods

a. Study area

Our study area covers the State of Israel and ranges from extreme desert in the south to Mediterranean areas in the north of the country. EBONE-wise field mapping of habitats has been conducted within three areas in Israel, Ramat HaNadiv in the north, Lehavim Forest in the transition zone, and En Avdat in the south (Figure 1). Additional calibration and validation GIS layers that we will use include the planted forest stands (Jewish National Fund), Vegetation associations (Amos Sabah, Israel's

Nature and Parks Authority), and average annual rainfall. A digital elevation model (John Hall and the Survey of Israel, at a spatial resolution of 25 m) will aid us in



performing some of the preprocessing of the Landsat imagery.

b. Classification scheme

Our classification scheme will aim at reflecting the primary EBONE classes. These include four height classes of woody vegetation: (1) FPH--Forest Phanerophytes, $FPH > 5m$. (2) TPH- Tall Phanerophytes, $5m > TPH > 2m$. (3) MPH- Mid Phanerophytes, $2m > MPH > 0.6m$. (4) LPH- Low Phanerophytes, $LPH < 0.6m$. Passive remote sensing may not be able to distinguish well between height categories (in contrast with LiDAR data) so merging of some of the classes may be needed. Our vegetation

Figure 1: Study area map.

a: Extent of Landsat scenes (in white) covering Israel;

b: Ramat HaNadiv field mapping sites; c: Lehavim; d: Avdat field mapping sites.

mapping will use both land cover classes, as well as quantitative mapping of vegetation properties (e.g., percent vegetation cover).

The minimum mapping unit defined within EBONE is 20×20m, roughly corresponding to the spatial resolution of Landsat TM (30×30m).

c. Remote sensing and specific sensors

Remote sensing of vegetation types has been long studied since the 1970s, using a wide array of sensors at various spatial, spectral and temporal resolutions (Duro et al., 2007). Our approach in mapping vegetation types will apply a variety of sensors at different scales, to examine upscaling and downscaling possibilities. High spatial heterogeneity at fine scales characterizes Mediterranean landscapes in general and those of Israel in particular. Thus, high spatial resolution (~ 2m) would be the obvious choice (Levin et al., 2007). However due to their restrictive costs, high spatial resolution images may not be available for mapping habitats at large spatial scales. Here we will evaluate the trade-off between high spatial resolution/ high performance on one hand and reasonable costs on the other hand. We will use high spatial resolution, as well as medium-spatial resolution sensors at the validation sites for which in-situ habitat data is available. At those sites we will calculate the spectral separability between the different GHCs, and then construct and evaluate habitat maps using various sensors. We will quantify habitat differentiation and classification accuracy (hereafter, performance) as a function of the spatial resolution. Compared with the Mediterranean areas, in the desert larger habitat may be delineated, which may allow the use of coarse spatial resolution sensors (~ 250m). Focusing on the natural habitats, we will use GIS Layers of Israel's built-up and agricultural areas (from the Survey of Israel) to exclude those areas from our analysis. Following atmospheric and topographic correction of all imagery (using ATCOR and ENVI), we will apply various classification techniques on the multi-temporal set..

Following is a short description of the different sensor. The Results for each sensor are described in a separate section within the work.

i. MODIS Time series

MODIS is a sensor on-board the TERRA and AQUA satellites of NASA. MODIS offers a ground reflectance product (MOD13Q1) that may be downloaded for free, at a spatial resolution of 250m, every 16 days (beginning February 2000). Using this type of data we will be able to study the phenology of vegetation in details, and to use that phenological information to characterize different habitat types. Such an approach has been recently developed for Canada, the Habitat Dynamic Index (Coops et al., 2008). This approach examines the cumulative annual greenness, the minimum level of perennial cover, and the degree of vegetation seasonality, to study and classify areas with different vegetation dynamics. Due to the coarse spatial resolution of MODIS and the high spatial heterogeneity in Israel's Mediterranean landscape, we expected that this approach will be more useful in the desert areas, however as will be

shown in the results, it also delivers good information in the Mediterranean areas. At this scale, we will also apply supervised classification techniques to demonstrate a nationwide mapping that can be done on a yearly basis. The phenological approach will be the basis for our mapping also with higher spatial resolution sensors, albeit they do not offer such high revisit times. We will carry out this analysis and others within Idrisi TAIGA GIS and remote sensing software (<http://www.clarklabs.org/>), which offers the Earth Trends Modeller, a geospatial software for the analysis of image time series.

ii. QuickBird/WorldView 2 imagery

Working at the field site level, we will analyze in details the sites of Ramat HaNadiv (540 mm/year), Lehavim Forest (300 mm/year) and En Avdat (100 mm/year). Within the project we tasked the acquisition of a spring image (March, when herbaceous vegetation is at its peak) and a summer image (when there's mainly perennial vegetation). Based on the phenological differences between herbaceous and perennial plants we expect to be able to differentiate between different vegetation units. Working at a spatial resolution of 2m allows the detection of fine details such as individual trees and large shrubs. We will then validate the accuracy of our classification using the in-situ habitat layer.

iii. 3.3 Medium spatial resolution imagery

Based on the classification procedures developed and tested above, we will use medium resolution imagery (30 m) to map Israel's natural habitats on a national scale. Whereas fine scale details (e.g., trees) cannot be at the spatial resolution of Landsat-like sensors, some trees can still be mapped using SPOT images of 10 m (Levin et al., 2009). At this scale we will also use a multi-temporal set of images, representing the winter, spring and summer seasons. Ideally SPOT images are best fit for this task, due to their higher spatial resolution (5, 10 and 20 m, depending on the spectral band). The drawback of SPOT imagery (in addition to their high cost; Table 1) is that more images will be required to cover the entire country (about 15 to cover Israel – i.e. more computation time and analysis required). Landsat images on the other offer full coverage of Israel in just three tiles (Figure 1). In addition, most Landsat images are now available for free from the USGS Earth Explorer website, making it an obvious source of data that should be examined.

d. Performance evaluation

Habitat maps based on the different sensors will be produced using the classification scheme described above. We will evaluate the accuracy of each product against two sources of independent information: (1) BIOHAB field mapping conducted last year in several locations in the country, (2) validation sites identified by us based on available GIS layers and a 1m orthophoto.

Table 1: Comparison of available sensors

Sensor	Spatial/spectral resolution	Coverage	Cost	Comments
MODIS	250m (B,R,NIR,SWIR1)	Entire country divided in four tiles. Available since 2000.	Free.	Low spatial resolution, every 16 days.
Landsat 5 (Landsat 7 has problems since 2003)	30m, 6 bands (B,G,R,NIR,SWIR1,SWIR2) 15m panchromatic – only in Landsat 7	Two scenes cover the entire Mediterranean area. Cloud-free images mostly prior to 2003.	Free from the USGS. 1500€ per scene from the European Station.	Full coverage, medium resolution, not recent
Aster	15m, 3 bands (G,R,NIR) 30m, 6 bands (SWIR)	Approximately Like SPOT	Cheap, 80\$ per scene	Medium resolution, some images available
SPOT	5m-10m-20m, 4 bands (G,R,NIR,SWIR1)	60x60 km.	5m: 5400€ 10m: 2700€ 20m: 1900€	high resolution, too expensive
QuickBird, WorldView 2	2m, 4 bands (B,G,R,NIR) by QuickBird, 8 bands in WorldView2 in the VIS-NIR The 0.5 m panchromatic band is not available for purchase over Israel's area.	Minimum area: ~90 km ² per tasked image, 25 km ² per archived image. Available since 2001.	20\$ per km ² for tasked image, 13\$ per km ² for archived image.	Fine resolution for validation sites alone.

5. Results - Landsat

5.1 Background

Landsat imagery (30 m) was used to map Israel's natural habitats on a national scale. We used a multi-temporal set of images, representing the winter, spring and summer seasons, to base our classification on the phenology of the vegetation. Ideally SPOT images are best fit for this task, due to their higher spatial resolution (5, 10 and 20 m, depending on the spectral band), as fine scale details (e.g., trees) can be mapped using SPOT images of 10 m (Levin et al., 2009). The drawback of SPOT imagery is that more images will be required to cover the entire country (about 15 to cover Israel – i.e. more computation time and analysis required). Landsat images on the other hand offer full coverage of Israel in just three tiles (Figure 1), and are now available for free from the USGS, making it an obvious source of data that should be examined.

Searching the USGS website for cloud-free Landsat imagery from different seasons at a relatively short time span (2-3 years), the Landsat images chosen for most of the analysis are given in Table 1. Four dates for each of the regions of Israel (North, Center, and South) were selected.

Table 1: List of Landsat images used for the project

	Winter – Nov, Dec, Jan, Feb	Spring - March, April, May	Summer - June, July, August	Late Summer - September and October
North (P174 R37)	2000/01/04	2002/03/24	2000/06/14	2002/10/18
Center (P174 R38)	2000/02/15	2002/03/08	2001/07/11	2003/09/11
South (P174 R39)	2003/01/06	2002/03/08	2001/07/27	2002/10/18

5.2 Preprocessing

Prior to the atmospheric correction, all the Landsat images were georeferenced to Israel Transverse Mercator coordinate system, using a 1m orthophoto as the reference image for collection of the ground points. At least 20 control points were used for each image, and the average RMS was about 0.2 pixels, using a second order polynomial transformation.

We corrected the satellite images for atmospheric scattering and absorption and for topographic effects of shading using the atmospheric/topographic correction of multispectral sensors for rugged terrain as applied in ATCOR 3 version 7.1 (© DLR 2010) (Richter, 1998), which is considered a reliable model for atmospheric corrections (Ben-Dor et al., 2005). We used a Digital Elevation Model (DEM) obtained from the Survey of Israel at a spatial resolution of 25 m (Hall et al. 1999) for calculating the slope, aspect, cosine of

the incident solar illumination and the sky view factor (i.e. the visible area of the sky as dependent upon the surrounding topography). Three types of preprocessed Landsat images were used and compared within this study:

- **RUGGED** - Topographic and atmospheric correction, using the DEM to calculate the expected shading effects. This approach is partly successful in eliminating the shading effects in moderate slopes, however in rugged areas overcorrection is expected (see Smith et al., 1980).
- **FLAT** - Flat atmospheric correction, i.e. without correcting for shading effects. This was done so as to avoid artifacts in the topographically corrected image, related to overcorrection, inaccuracies of the DEM, and georeferencing errors.
- **BAND RATIOS** - Band-ratios calculated on the flat atmospherically corrected image. Band ratio images enable to remove most of the shading effects contained within the original bands, without the use of external GIS layers such as a DEM. Although the resulting band ratio images are not in reflectance values and do not contain the information whether a pixel is bright or dark, they maintain the information about the shape of a spectra (the change in reflectance values between bands). The band ratios calculated were of the following form, and were calculated for each pair of bands, from the short to the long wavelengths:

$$\text{band ratio} = \frac{\text{band A} - \text{band B}}{\text{band A} + \text{band B}}$$

Following these preprocessing steps, we joined the four seasons to create three meta-files. The atmospherically corrected meta-files were comprised of 24 bands (4 seasons \times 6 bands) whereas the band-ratios meta-file was comprised of 20 bands (4 seasons \times 5 bands). The resulting metafiles were tested visually, comparing between the images, as well as by testing the classification accuracy on them (see below).

5.3 Vegetation mapping

Vegetation mapping can be performed to derive thematic maps of vegetation types (hard classification), or to derive maps of continuous variables such as vegetation (soft classification). For some approaches regions of interest (ROIs) whose vegetation type are known are first defined, whereas for in some approaches there is no need to define ROIs beforehand. We tested the following four approaches to map vegetation from the Landsat imagery, as shown in Table 2, and detailed below.

Table 2: the four approaches used to map vegetation from Landsat imagery

	Based on ROIs	Not based on ROIs
Hard classification (vegetation types)	1. Supervised	2. Unsupervised
Soft classification (% cover of perennial vegetation, seasonal vegetation and bare soil)	3. Spectral unmixing	4. NDVI derived vegetation cover

5.3.1 Supervised classification

5.3.1.1 Preliminary tests

We first compared the accuracy of a supervised classification in the northern Landsat scene of Israel with field data from Ramat Ha'Nadiv collected by INPA (Appendix 1), to test which of the preprocessed Landsat images (Flat, Rugged, Band ratios) was the most successful and would then be applied for the entire area of Israel. ROIs representing the different vegetation and land-cover categories were selected within each of the three Landsat scenes separately, using the interpreter knowledge as well as various GIS layers, for example: JNF and INPA layers (Stands_cov_Type_Dissolve and Eged_VegCov). ROI's as homogeneous as possible were selected to represent the different mapping categories. ROIs were selected not only in order to run the supervised classification but also in order to validate the accuracy of the classification maps. These ROIs were randomly divided into two groups. One group of ROIs was used for the calibration process of the supervised classification (calibrating ROIs, using all the EBONE GHC types), while the other group was used to validate the results of the classification (validating ROIs). An additional way to validate the results of the classification maps was by using ground truth field data that were collected by INPA in three areas: Ramat HaNadiv, Lehavim Area, and Avdat. Six supervised classification methods were used for each of the three metafiles: Maximum Likelihood, Minimum Distance, Paralleloid, Mahalanobis Distance, Spectral Angle Mapper and Spectral Information Divergence. The classification results and their accuracies were calculated and compared with field data from Ramat Ha'Nadiv and Avdat, collected by Margareta (Appendix 1 and 2). The best results (overall accuracy > 40% and kappa index > 0.4, within the Ramat ha Nadiv field sites) were achieved with maximum likelihood classifier over the atmospherically/topographically corrected images (rugged) as well as over the band-ratio images. Comparing different supervised classifiers over the Avdat field site, again the maximum likelihood classifier turned out to be the most successful (Appendix 2). Therefore we used the RUGGED and BAND-RATIOS sets of images for further analysis.

Two more supervised classification methods were tested for all three Landsat scenes: Support Vector Machine and Neural Network, in addition to the Maximum Likelihood. The classification results for all three Landsat scenes and their accuracies were calculated and compared with the validating ROI's and field data from Ramat Ha'Nadiv and Avdat, collected by Margareta (Appendix 3). The maximum likelihood was chosen as the method to run the supervised classification over the entire area of Israel.

An initial classification was conducted using the detailed ROIs. These ROIs include a various range of categories that were used in the initial step as a way to check our ability to classify the images using a detailed classification. Accuracy assessment calculations were used to validate the initial classification maps (Appendix 4). After analyzing the initial classification maps some of the categories were combined as a way to improve the accuracy of the classification maps (Table 3). These final categories were used to produce the final broader classification maps.

5.3.1.2 Accuracy Assessment

The accuracies of the final classification maps were calculated in two ways: (1) by comparing the results of the classification maps with the validating ROIs that were selected by the interpreter and (2) by comparing the results of the classification maps with field data polygons collected by INPA in three sites using the BIOHAB method (termed here as EBONE GHC): Ramat Ha'Nadiv, Lehavim and Avdat. Appendixes 4 through 7 show the results of these accuracies in different forms and analyses and an explanation of the accuracy assessment definitions.

Table 3: Summary of accuracy assessment of classification maps of the three Landsat scenes, prior to and after combining the ROI categories

		Accuracy Assessment with validating ROIs		Accuracy Assessment with INPA fieldwork data (EBONE GHC)	
		Overall Accuracy	Kappa Coefficient	Overall Accuracy	Kappa Coefficient
Prior to combining the ROI categories	North (P174 R37)	91.58%	0.89	Ramat Ha'Nadiv: 27.46%	Ramat Ha'Nadiv: 0.18
	Center (P174 R38)	87.72%	0.84	Ramat Ha'Nadiv: 36.92%	Ramat Ha'Nadiv: 0.20
				Lehavim: 49.16%	Lehavim: 0.33
South (P174 R39)	97.63%	0.96	Avdat: 95.31%	Avdat: 0	
After combining the ROI categories	North (P174 R37)	90.15%	0.84	Ramat Ha'Nadiv: 66.85%	Ramat Ha'Nadiv: 0.16
	Center (P174 R38)	91.34%	0.88	Ramat Ha'Nadiv: 58.07%	Ramat Ha'Nadiv: 0.08
				Lehavim: 40.27%	Lehavim: 0.18
South (P174 R39)	97.60%	0.94	Avdat: 94.69%	Avdat: 0.06	

Table 4: Categories used in the supervised classification:

Initial Categories	Final Categories
Bare Soil	Bare Soil
Bare Soil (Built up)	
Bare Soil – Sandy (Dunes)	Dunes
Herbaceous	Herbaceous
Herbaceous – Sandy	
Coniferous trees	Trees
Deciduous trees	
Evergreen trees	
Mixed Deciduous and Evergreen trees	
Deciduous shrubs	Shrubs
Evergreen shrubs	
Deciduous 'Sub' shrubs	
Sandy 'Sub' shrubs	
Water (Sea Water, Dead Sea Water, Water Bodies)	Water
Agriculture	Agriculture
Snow	Snow
Clouds	Clouds

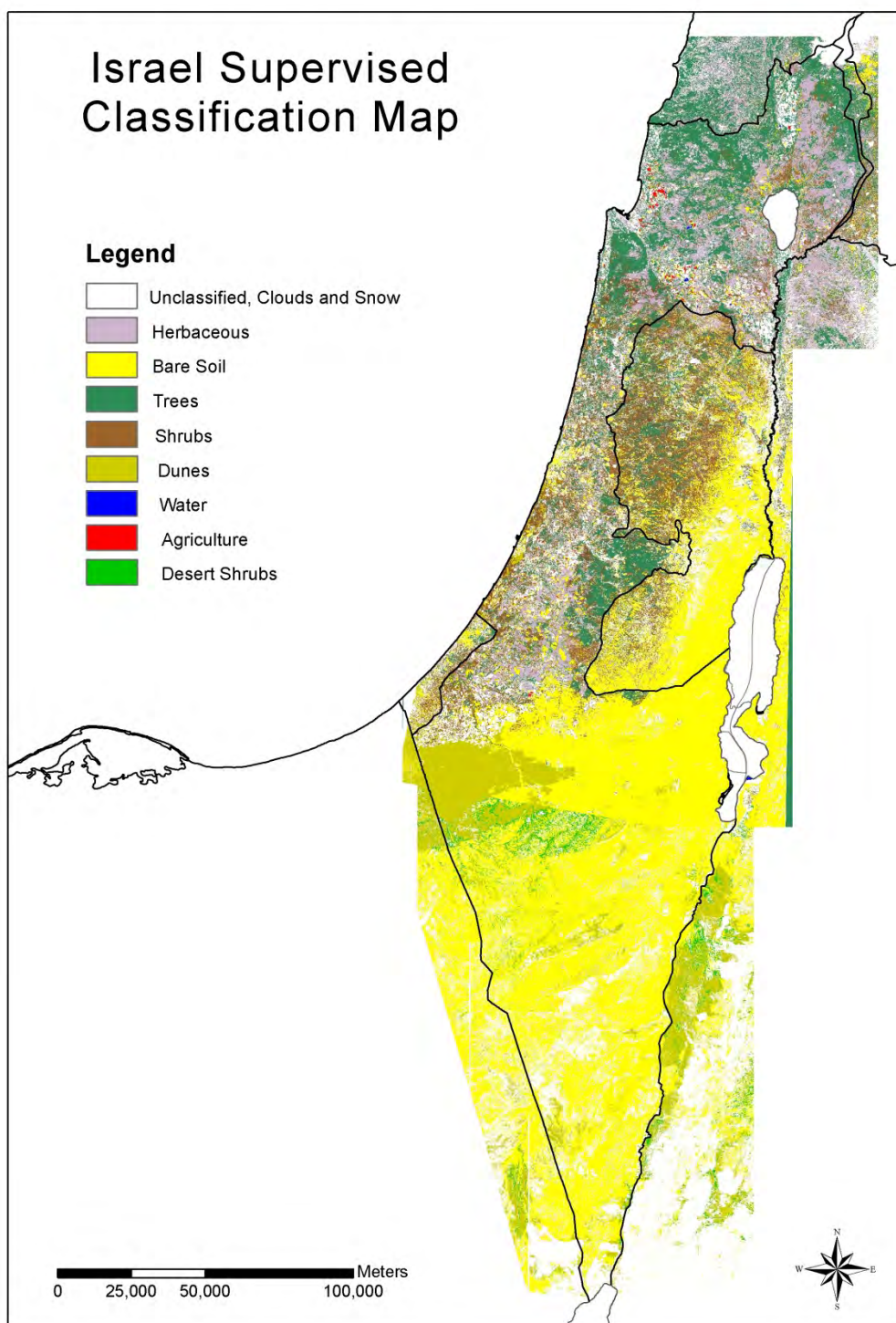


Figure 1: Supervised classification map of Israel, based on a maximum likelihood classifier applied on each Landsat scene separately.

Accuracy assessment of the supervised classification of overlapped areas

Comparing the classification results of overlapping areas was another method we used in order to check the classification accuracy of the images. We would expect to receive similar classification results. Yet, comparing the overlapped areas revealed differences in the classification.

Central and South Israel areas:

Within the overlap area of the central and southern Landsat scenes, the overall accuracy was 65.49%. Two main differences were noticed in the overlap areas: (1) The southern scene has areas classified as Desert Shrubs while the central scene shows no vegetated areas. (2) A bigger area of the southern scene is classified as dunes compared to the central scene.

Table 4: Percent accuracy of the category calculated using the total number of pixels in the overlap area between the southern and central scenes

Overall Accuracy: 65.49%

Kappa coefficient: .?

		Central scene				
		Dunes	Desert Shrubs	Bare Soil	Trees	Class Total
SOUTHERN scene	Dunes	29.55	0.05	15.12	0.00	44.71
	Desert Shrubs	2.50	0.02	16.35	0.00	18.86
	Bare Soil	0.49	0.00	35.93	0.00	36.41
	Trees	0.01	0.00	0.00	0.00	0.02
	Class Total	32.54	0.07	67.40	0.00	100.00

Looking at the list of images used and their dates show differences in the dates of the images used for the two regions. For spring time, images from the same date were used and images with very close dates were used for the summer. However, images of one year apart for late summer and 3 years apart for winter time were used. Ideally we would have used the same dates for images analyzed for the three geographical regions of Israel.

Central and Northern Israel areas:

Results of classification show an overall accuracy of 43.96% within the overlap area of the central and northern Landsat scenes. The classification of

the trees is relatively good but there were differences in the congruence between the other categories. The main difference between the overlapping areas is that the northern scene has an overestimation of herbaceous areas while in the central scene these areas are classified also as shrubs and as bare soil.

Table 5: Percent accuracy of the category calculated using the total number of pixels in the overlap area between the northern and central scenes

Overall accuracy: 43.96%

Kappa coefficient: ?

		Northern Scene					
		Herbaceous	Bare Soil	Trees	Shrubs	Agriculture	Row Total
Central Scene	Herbaceous	13.12	0.48	3.31	2.91	0.00	19.82
	Bare Soil	3.71	1.02	1.10	0.68	0.18	6.69
	Trees	7.90	0.48	23.56	2.33	0.05	34.33
	Shrubs	20.80	1.04	10.54	6.26	0.01	38.64
	Agriculture	0.15	0.01	0.31	0.05	0.00	0.51
	Class Total	45.67	3.02	38.83	12.22	0.24	100.00

Looking at the list of images used and their dates show adjacent dates for winter and spring images but differences in the dates of the images for summer and late summer - one year apart for summer and late summer images.

As we used reflectance values (radiometric correction) differences in the classification are not due to spectral differences but can be related to the fact that images used are from different dates (years and months) as well as from limitations in the data that can be collected from the images associated with the ROIs selected and the 30-meter spatial resolution of the Landsat images.

5.3.1.3 Results

NORTH Landsat scene:

Within the initial classification, prior to combining the vegetation categories, revealed some confusion in mapping correctly different categories of trees and shrubs (e.g., evergreen, deciduous, and coniferous; Appendix 4). Though the calculated overall accuracies are high, 91.58% (Table 3), problems can be visually seen when analyzing the classification results, especially when

analyzing the accuracy assessment with field data from Ramat Ha'Nadiv. For example: Evergreen trees identified in the fieldwork are misclassified as Coniferous, Deciduous or mixed trees; herbaceous are classified in the classification map not only as herbaceous but also as deciduous trees and coniferous

Final classification maps after combining the categories show a high improvement in the classification results, even though not in the overall accuracy, 90.15%. Trees can be correctly identified as well as shrubs. Yet, there is an overestimation of herbaceous area, especially in urban areas and agricultural fields.

Analyzing the final classification map with the field data reveals a problem with correctly classifying trees, shrubs and herbaceous.

The classification image shows unclassified areas that represent: agricultural fields, urban areas, shadows, snow, areas along the shore and other categories that were not defined as training sites (ROI's). Time permitting, it would have been better to select ROIs from these areas and re-run the classification.

CENTRAL Landsat scene:

Even though the calculated overall accuracies are high, 87.72% (Table 3), problems can be visually seen, as well as by analyzing the accuracy assessment table (Appendix 4). The initial classification results, prior to combining the categories, reveal confusions in classifying correctly the different types of trees and shrubs. For example herbaceous areas that are classified in the classification map as not only herbaceous but also as different categories of shrubs. Another example is mixture of trees that are mainly classified as evergreen trees.

Looking at the classification results when compared with field data from Ramat Ha'Nadiv shows a problem in mapping correctly herbaceous areas. These areas are misclassified as a various mixture categories of trees and mainly as deciduous trees. Evergreen Trees are classified not only as evergreen trees on the classification map but also as other types of trees. This shows the importance of combining the various categories of trees into one category.

Field data from Lehavim that was compared to the classification results show (1) a misclassification of herbaceous as mainly bare soils, and (2) a misclassification of shrubs also as bare soils.

Final classifications after combining the categories show a big improvement in the classification of trees, where 20% of the area is classified as trees

compared with 21% identified in the field. Yet, combining the categories reveals misclassification of herbaceous category as shrubs as well as shrubs areas as trees. This misclassification is also shown when looking at the analysis of the field data from Ramat Ha'Nadiv. Field data from Lehavim reveals misclassification of herbaceous areas as bare soils, trees and especially shrubs, a misclassification of shrubs as bare soils, but a good classification of trees.

There are various areas that were not classified and represent urban areas, agriculture, as well as shadows. Urban areas are classified as bare soil. Agricultural areas are classified as herbaceous and bare soil and in some areas they are unclassified. In addition, there is an overestimation of areas classified as bare soils, as well as an area of mixture between dunes and bare soils in the southern part of the region.

SOUTH Landsat scene:

Areas that were not classified represent areas of shadows as well as clouds that were present in one or more of the four Landsat TM images of the metafile image. Agriculture fields are also represented as unclassified as no ROIs were selected. More ROIs should be selected and used to classify the image in order to correctly classify these unclassified areas.

Looking at the initial classification, prior to combining the categories, the accuracy is very high, 97.63%. Yet, visually we see mixture between bare soil and dunes, as well as desert vegetation - shrubs that are not always correctly identified.

Final classification after combining the categories does not improve the accuracy results, 97.60%, but, it shows some problems of misclassification of trees with dunes and bare soils, as well as problems of mixture between dunes and bare soils.

The accuracy received for the classification maps of the three geographical regions is high, even though when analyzed there are various problems associated with the classification. The high accuracy results are related to the low amount of ROIs selected to validate the classification results as well as the way they were selected. These ROIs were selected in areas for which it was clear what they represent. These areas are the areas that represent "pure" categories and where no mixture exists. Yet, on the ground the pixels are not homogenous, as the selected ROIs tend to be, and most pixels represent mixtures of several categories. When running the accuracy assessment only the selected ROIs are involved. As they represent more homogeneous areas, the "pure" or homogenous pixels would be correctly classified while the

heterogeneous ones will not be tested in the accuracy assessment. Problems associated with them will not be recorded in the calculation of the Kappa and Overall accuracy numbers.

5.3.1.4 Discussion

Mapping the natural vegetation from Landsat images allowed us to produce vegetation maps of large areas at a broad spatial coverage. Even though the overall accuracies achieved were quite good, there are limitations with the data that can be collected and our ability to correctly separate between vegetation categories:

(1) Differentiating between various types of trees, e.g. evergreen vs. deciduous trees. These phenological changes can be detected when seasonal images from the same year are used. Therefore, requiring the use of a higher number of images from dates that allow the detection of the specific vegetation categories. For example, when mapping areas of deciduous trees it is important to select dates when the trees are with/without green leaves. This issue is complicated when working on large areas, where the same species may bloom or shed its leaves in different dates as a function of latitude/temperature/elevation. If an area is covered by deciduous trees and an image is acquired when they are without leaves, however the ground is covered by green herbaceous grasses, at the spatial resolution of Landsat the pixel will be interpreted as being with vegetation.

(2) The 30-meter spatial resolution of the TM Landsat images limits our ability to map areas with low vegetation cover. Most pixels represent heterogeneous areas of natural vegetation and unless the vegetation category covers a big area (of a pixel) and can be represented as a homogeneous area (covering more than one pixel) it is hard to map it, and therefore mapping the seasonal changes will be hard.

(3) Another problem is mapping a heterogeneous area that has, for example, both trees and herbaceous covering an area of the size of a pixel. Will this area be classified as trees or as herbaceous? This area can be classified as a mixture of the two categories or as a different category if spectrally the mixture of the two categories on the ground has a characteristic of a different category.

5.3.2 Unsupervised classification

Unsupervised classification was done using the Isodata algorithm within Envi 4.7, aiming for 50 classes. This was applied on both the band-ratios image and the topographically corrected reflectance imagery, within each Landsat scene separately.

Accuracy assessment was first conducted on the 50 raw classes using the validation ROIs collected for the supervised classification described above (15 classes in the north and centre, six in the south). Association between the unsupervised classes and the validation ROIs was performed automatically based on the class that corresponded with the maximum number of cells. Based on this approach, the percent accuracy achieved was above 70% (Table 2; detailed confusion matrices in Appendix 7).

Table 2: Accuracy assessment of the unsupervised classification, based on automatic association of the raw classes to validation ROIs, excluding water (in parentheses, the kappa index)

	Reflectance values	Band ratios
North	75% (0.61)	71% (0.56)
Centre	82% (0.76)	84% (0.77)
South	88% (0.80)	88% (0.80)

The resulting 50 classes were visually interpreted into the following 17 classes, based on orthophoto and Landsat imagery comparison: sea water, shallow water, perennial vegetation, sparse forest, sparse vegetation, herbaceous, bare soil, built-up area, small shrubs, bare dunes, agriculture, seasonal snow, sparse desert vegetation, dark bare soil, bright bare soil, seasonal desert vegetation and seasonally flooded. These 17 classes were then clumped into ten classes as shown in Figure U. Visually, it seems that the band ratios unsupervised product is better than the reflectance based one, as there is a larger distribution of agricultural areas (shown in pink), and as urban areas (shown in red) are mapped quite well. Although the accuracy assessment results are good, the unsupervised classification was not sensitive in desert areas that were mostly classified as bare soil, with very few areas classified as seasonally green vegetation.

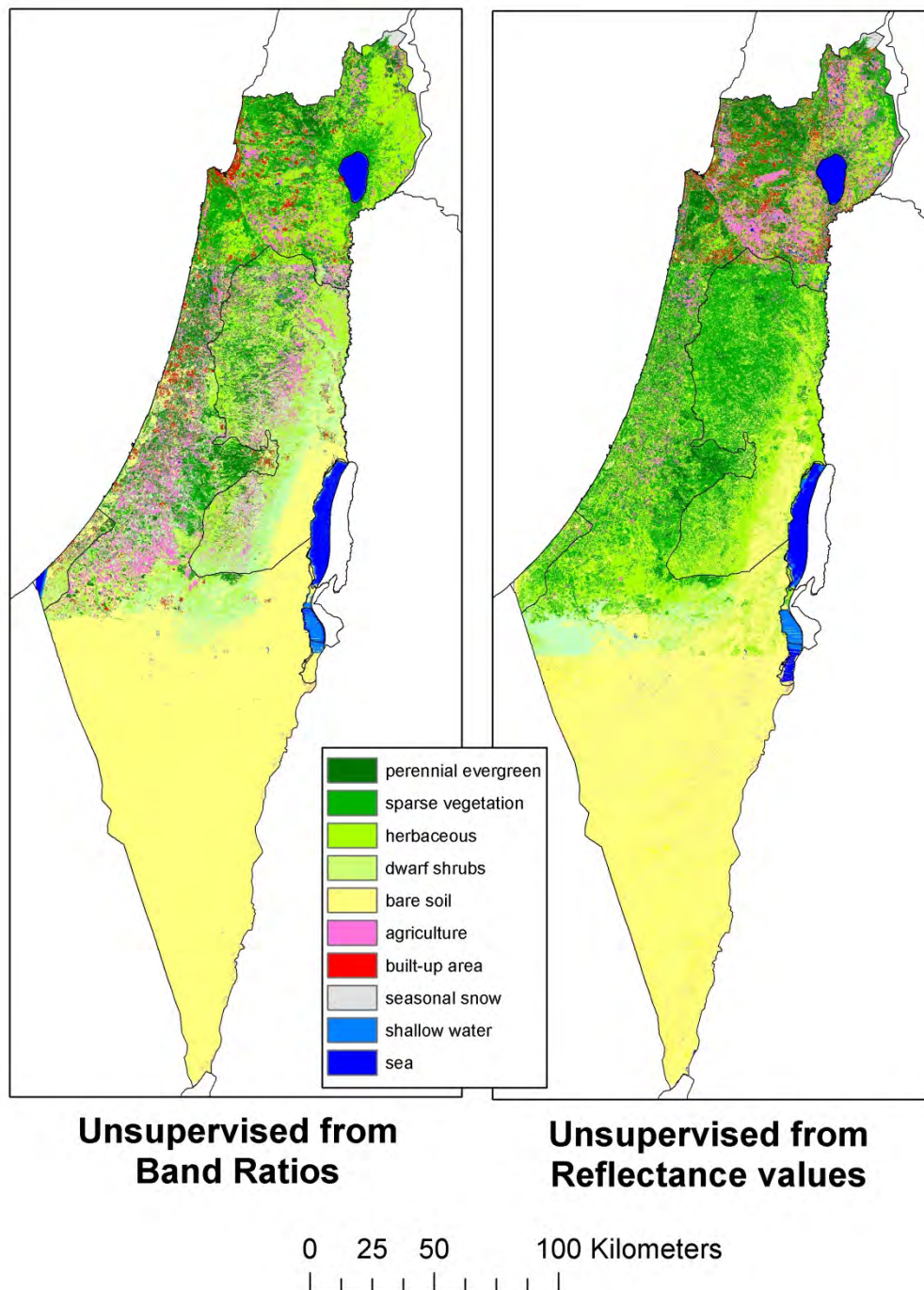


Figure U: Unsupervised classification of Landsat imagery. The classes shown are based on a visual interpretation and on joining the original unsupervised classes.

5.3.3 Mapping percent cover of seasonal and perennial vegetation

Following the approach suggested by Shoshany and Svoray (2002), we applied two methods to map the percent cover of three endmembers: perennial vegetation, seasonal green vegetation, and bare soil.

The first technique used was that of linear spectral unmixing. This was done based on 11-12 ROIs collected within each of the three Landsat scenes separately, that included areas of 100% vegetation cover, 100% bare soil (bright-dark), water and snow. Spectral unmixing was run on the five band ratios of the spring and fall Landsat images of each scene, representing maximum and minimum vegetation greenness. The Probability guided spectral unmixing available within Idrisi TAIGA was used to this end. The vegetation endmember images were then summed resulting in a spring percent vegetation image and a fall percent vegetation image. Based on these the maximum and minimum percent vegetation cover were calculated, and seasonal green vegetation was calculated as the difference between the maximum and the minimum green vegetation. Percent bare soil was calculated as $1 - \text{MaxVegetation}$.

Percent vegetation cover was also calculated based on Normalized Difference Vegetation Index (NDVI; Tucker, 1979) values, after the three scenes were mosaicked, for spring and for fall. Vegetation cover P_v was calculated based on scaled vegetation and NDVI (following Carlson and Ripley, 1997) as shown in the following equation, where VI stands for the value of a Vegetation Index in a certain pixel, VI_{baresoil} stands for the vegetation index value in an area with no vegetation, whereas $VI_{100\%}$ stands for the vegetation index value in area with maximum vegetation cover. Based on previously collected ROIs the following NDVI values were used to defined 0% vegetation and 100% vegetation: 0.15 and 0.63 for the spring image, and 0.27 and 0.57 for the fall image. The percent cover of perennial vegetation, seasonal green vegetation and bare soil was calculated as described above for the spectrally unmixed images (Figure %).

$$P_v = \frac{VI - VI_{\text{baresoil}}}{VI_{100\%} - VI_{\text{baresoil}}}$$

The resulting images can be used to derive vegetation classes defined by INPA (e.g., areas with > 90% perennial vegetation whose areas is > 10 ha can be defined as forest/maquis stands).

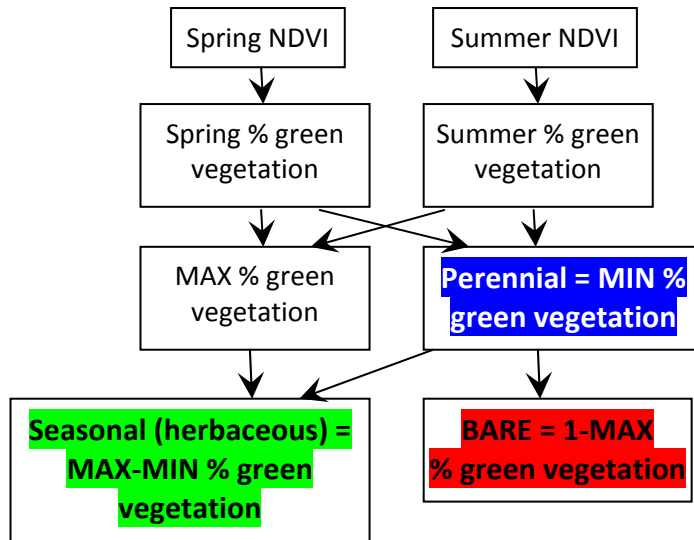
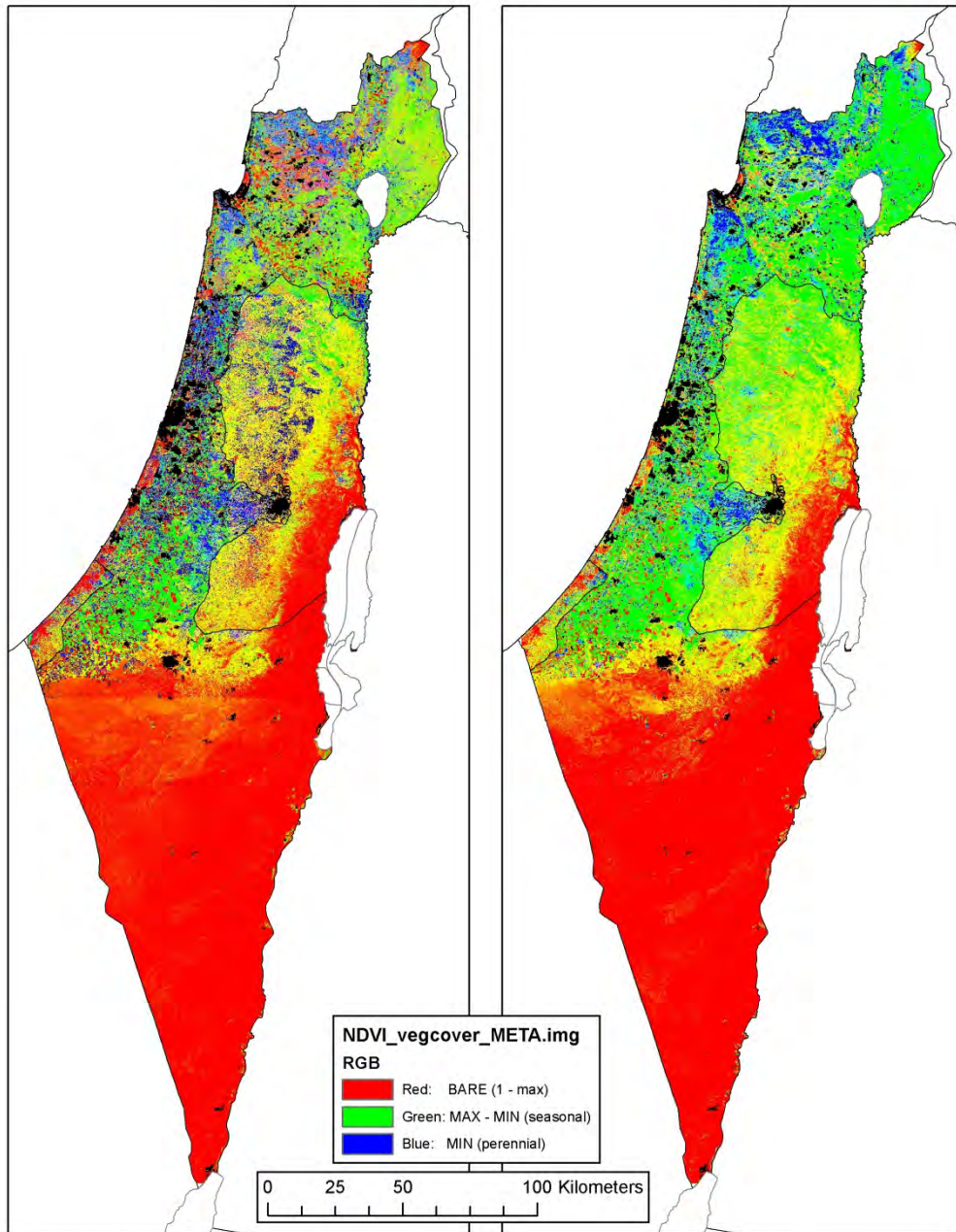


Figure %: Flowchart for calculating % cover of perennial vegetation, seasonal vegetation and bare soil.



**Linear unmixing
 vegetation cover
 (separate scenes)**

**NDVI derived
 vegetation cover
 (mosaicked scene)**

Figure A: Landsat based soft classification into % bare soil (in red), % seasonal green vegetation (in green), and % perennial vegetation (in blue).

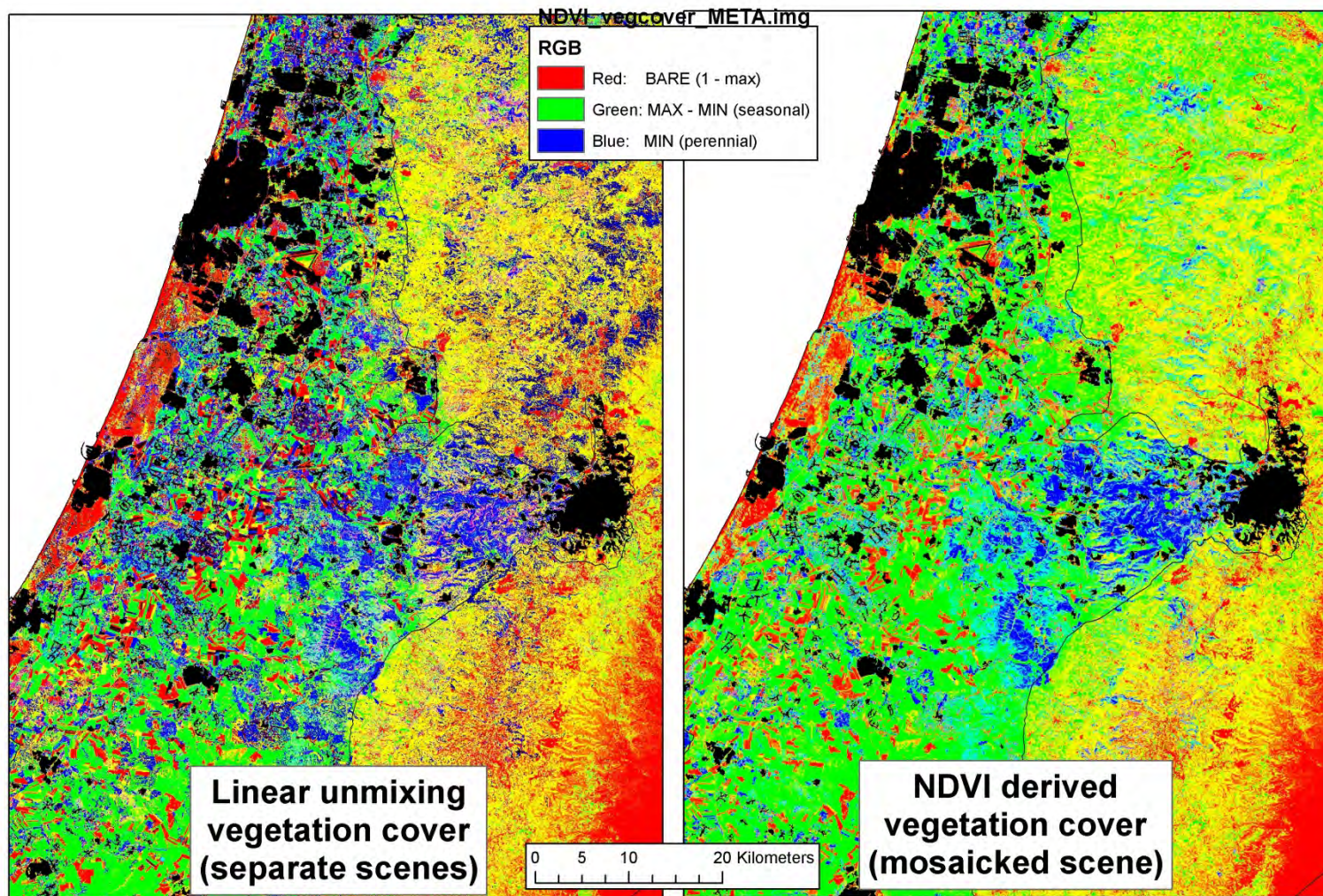


Figure B: Landsat based soft classification into % bare soil (in red), % seasonal green vegetation (in green), and % perennial vegetation (in blue).

As no field data was available from INPA to validate the percent cover of bare soil, seasonal green vegetation and perennial vegetation, the resulting maps were assessed visually, and statistically with respect to a similar spectral unmix analysis conducted using the QuickBird images (see in the QB section). Figures C, D and E compare the Landsat supervised classification and spectral/temporal unmixing results, with respect to EBONE classes and QuickBird imagery, within each of the field study sites of INPA, where EBONE GHC were mapped in the field.

Comparing the Landsat supervised classification to the EBONE GHCs, it is clear that the fine classification obtained in the field mapping, is not captured by the supervised classification that was applied on a national scale. On the other hand, the EBONE polygons are not homogeneous, and examining the Landsat percent cover maps, it can be seen that vegetation cover varies within the EBONE polygons. An additional problem with EBONE classes is apparent in the transition and arid field sites, where most of the area was classified as bare soil, while seasonal patterns of vegetation could be observed when using Landsat images from different seasons. Additional differences between EBONE GHCs and Landsat results could be attributed to the small size of some of the EBONE polygons, falling below what can be expected from the medium spatial resolution offered by Landsat.

Ramat ha Nadiv

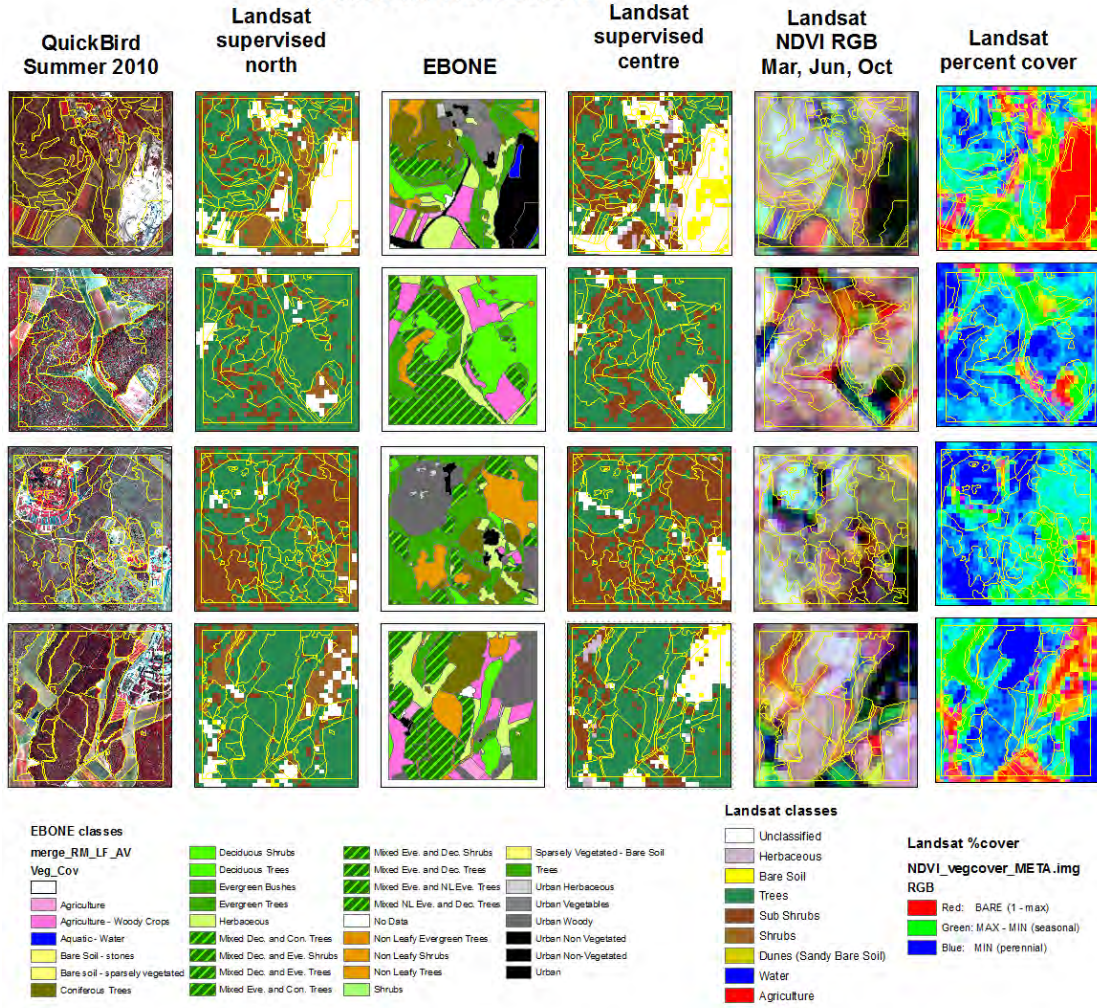


Figure C: Comparing the Landsat supervised classification and spectral/temporal unmixing results, with respect to EBONE classes and QuickBird imagery, within the Ramat ha Nadiv field site. Each row covers a field site of 1km². The QuickBird image (left column) is shown using a false color composite of bands 4, 3 and 2 (vegetation in red). The Landsat percent cover (right column) shows the relative percent cover within a pixel of bare soil (red), seasonal green vegetation (green) and perennial vegetation (blue). The Landsat NDVI RGB images (2nd column from the right) is a false color composite of NDVI values in the months of January (red), March (green) and July (blue); areas no vegetation appear in dark colors, while areas with perennial vegetation cover appear in white.

Lehavim Forest

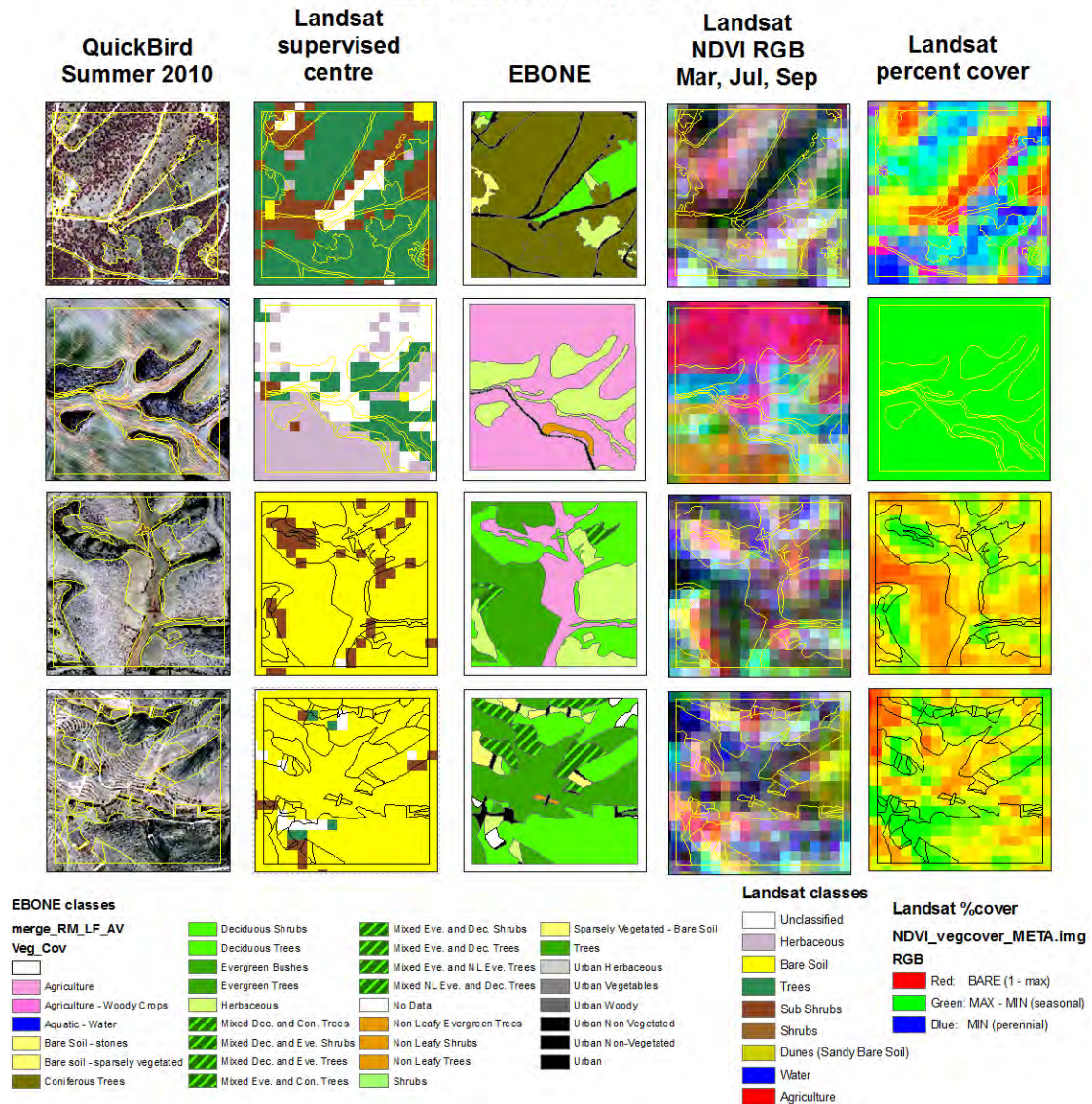


Figure D: Comparing the Landsat supervised classification and spectral/temporal unmixing results, with respect to EBONE classes and QuickBird imagery, within the Lehavim Forest field site. Each row covers a field site of 0.25km². The QuickBird image (left column) is shown using a false color composite of bands 4, 3 and 2 (vegetation in red). The Landsat percent cover (right column) shows the relative percent cover within a pixel of bare soil (red), seasonal green vegetation (green) and perennial vegetation (blue). The Landsat NDVI RGB images (2nd column from the right) is a false color composite of NDVI values in the months of January (red), March (green) and July (blue); areas no vegetation appear in dark colors.

Ein Avdat

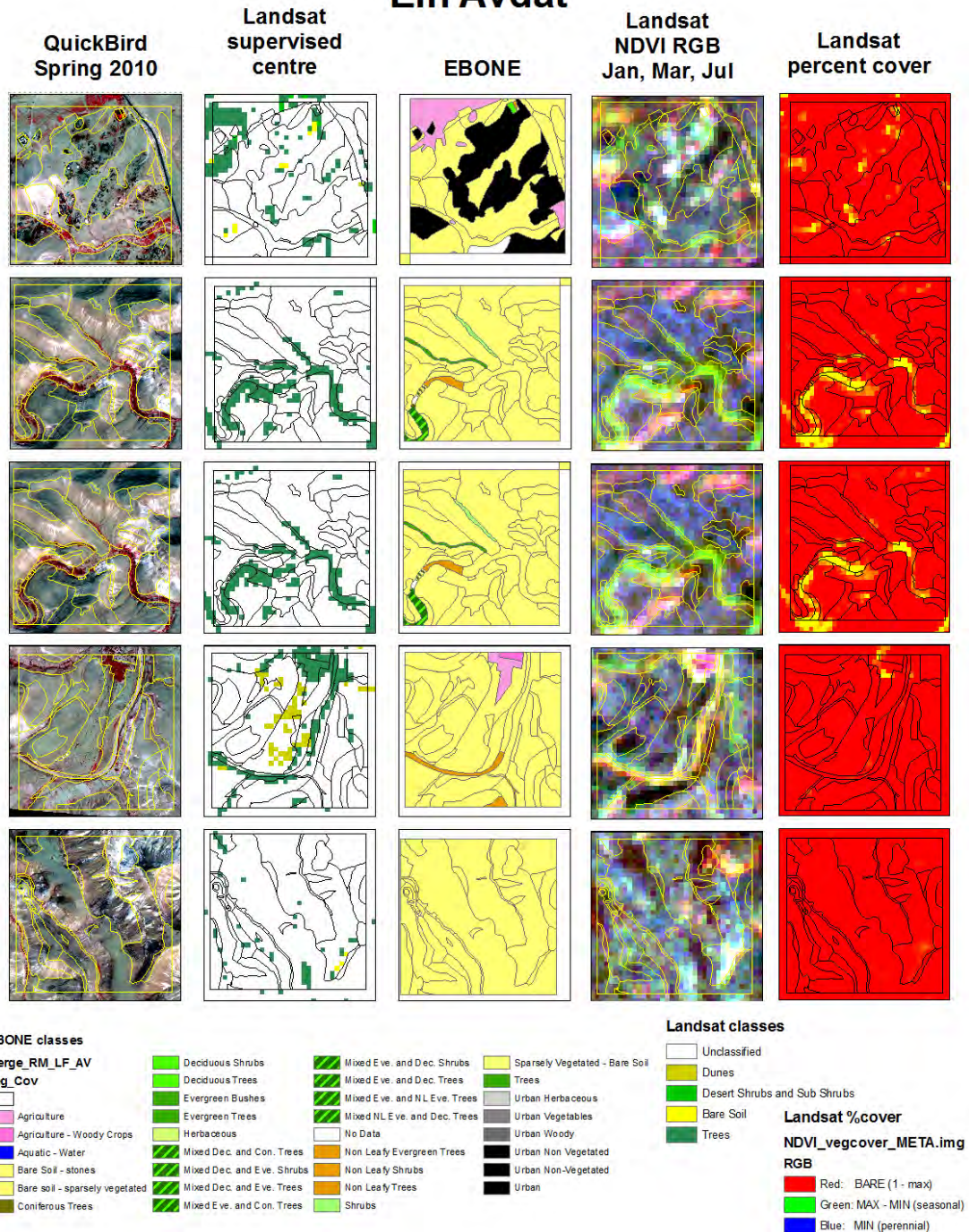


Figure E: Comparing the Landsat supervised classification and spectral/temporal unmixing results, with respect to EBONE classes and QuickBird imagery, within the Ein Avdat field site. Each row covers a field site of 1km². The QuickBird image (left column) is shown using a false color composite of bands 4, 3 and 2 (vegetation in red). The Landsat percent cover (right column) shows the relative percent cover within a pixel of bare soil (red), seasonal green vegetation (green) and perennial vegetation (blue). The Landsat NDVI RGB images (2nd column from the right) is a false color composite of NDVI values in the months of January (red), March (green) and July (blue); areas no vegetation appear in dark colors.

6. Results - QuickBird

6.1. Background

QuickBird imagery (2 m) was used to map Israel's natural habitats in three pilot areas. We used a 2-seasons set of images, representing the spring and summer seasons, to base our classification on the phenology of the vegetation. The drawback of QuickBird imagery is its cost as well as that a big number of images will be required to cover the entire country. It is therefore expected that this type of imagery will only serve for monitoring specific areas of interest.

QuickBird images tasked were acquired by Digital Globe Inc., for the seasons of spring and summer 2010. The images covered three pilot areas: Ramat Ha'Nadiv area, Lehavim Forest area and En Avdat area.

Table 1: List of QuickBird images used for the project in three pilot study areas

	Spring	Summer
Ramat Ha'Nadiv Area	20/4/2010	26/7/2010
Lehavim Forest Area	22/3/2010	18/7/2010
Avdat Area	5/4/2010	15/7/2010

6.2. Preprocessing

The images were atmospherically corrected using the flat atmospheric correction within ATCOR, and were then georeferenced to Israel Transverse Mercator (ITM) coordinate system in a two-stage process. First the spring images were referenced to the summer images, using more than 1,000 tie points automatically identified using the Förnster area-based image matching algorithm as applied in Envi 4.8. The images were then georeferenced to a 1m orthophoto using more than 100 tie points. The average RMS was about 10 m (due to relief displacement and off-nadir viewing of the satellite).

6.3. Methods

Vegetation mapping can be performed to derive thematic maps of vegetation types (hard classification), or to derive maps of continuous variables such as vegetation

(soft classification). For some approaches regions of interest (ROIs) whose vegetation type are known are first defined, whereas for in some approaches there is no need to define ROIs beforehand. We tested four approaches to map vegetation from the QuickBird imagery, as shown in Table 2.

Table 2: Four approaches used to map vegetation from QuickBird imagery

	Object-based	Pixel-based	
	Based on ROIs	Based on ROIs	Not based on ROIs
Hard classification (vegetation types)	Segmentation	Supervised	
Soft classification (% cover of perennial vegetation, seasonal vegetation and bare soil)			5. NDVI derived vegetation cover – woody vegetation density 6. NDVI derived vegetation cover – UnMixing

Each study area was analyzed separately. Mapping methods varied based on the vegetation categories and the field characteristics of the area.

Table 3: List of approaches used to map vegetation from QuickBird imagery for each of the pilot study areas

	Segmentation	Supervised Classification	UnMixing	Woody Vegetation Density
Ramat Ha'Nadiv area		√	√	√
Lehavim Forest area	√	√	√	
Avdat area			√	

6.3.1 Supervised Classification

The aim of this step was to check our ability to use supervised classification to distinguish between trees: pine and cypress and maquis.

Ramat Ha'Nadiv area

Two methods of supervised classification of the summer images were used: Maximum Likelihood and Support Vector Machine. Each method was used to create a classified image and a rule image. No probability threshold was applied at the initial stage.

We selected ROIs from the summer QuickBird image using GIS data from JNF, INPA and Hava Lahav surveys. We identified 'pure' and dense polygons that represent various vegetation categories: Maquis, Pine trees, Cypress trees, bare soil, clouds, shadow, and terrestrial water bodies. Differences between the summer spectra of pine trees, cypress trees and maquis were the following (figure 1): (1) the overall reflectance values of cypress tree were the lowest in all four bands; (2) the slope between the red and infra-red bands was highest for the maquis and lowest for the cypress trees. Using these ROIs initial classification and rule maps were produced. Based on the rule images we determined the probability threshold per category to generate a new classification image. Pixels that did not meet the threshold requirements were not assigned into a classification class.

The accuracy of the new classification images was then calculated by comparing the results of the classification maps with validating ROIS that were collected from GIS data layers received from JNF, INPA and Hava Lahav (SPNI) fieldwork in Ramat Ha'Nadiv. The three sources of layers were combined in ENVI based on their classification categories to produce three ROI categories: Maquis, Cypress, and Pine. The accuracy was calculated only for these categories.

As the GIS data collected in the field is of polygon type, patches of vegetation are mixtures of vegetation and bare soil. A polygon may be classified as pine trees but it may be a mixture of the pine trees with bare soil, herbaceous, and shrubs on the ground. Therefore, we have used the NDVI layer that was previously created as a 'filter' to identify "pure" woody vegetation areas. Only if a pixel was identified as woody vegetation on the NDVI derived image it was be assigned the ROI class.

This new class image showed a high presence of maquis. Therefore, we decided to randomly select 10,000 pixels of each category, to have an equal representation of the vegetation categories of interest. This final class image was used as the ground truth data when checking the accuracy of the supervised classification images.

Lehavim Forest area

In this study area we applied a different approach for image classification – an object-based classification, segmenting the image into homogeneous areas based on the spectral mean and variability of pixel values. Such approach has been shown to be of high value when classifying high spatial resolution images (Blaschke, 2010). As applied within Idrisi Taiga, the segmentation algorithm is based on the following four stages:

- (1) Applying a watershed based image segmentation process: a) derive a surface image based on the spatial variance of the input image bands; b) delineate watersheds from the surface image; and c) merge adjacent watersheds that meet stated standards to form image segments.
- (2) Select training image segments with the target classes to be used in the classification.
- (3) Apply a pixel based supervised classification on the image based on the previous training spectra.
- (4) Apply a majority rule classifier based on the majority class within an image segment.

The maximum likelihood supervised classification map of the Lehavim forest area was created during the Segmentation Analysis of the QuickBird summer image. In this analysis we used a different approach where a broader number of EBONE GHC categories were classified.

The training data used for the classification was produced during the segmentation analysis based on previous knowledge of the area and GIS layers.

6.3.2 Segmentation

The segmentation classification is a hard-classifier, and is an important step within the object-based remote sensing information retrieval process. In the segmentation process adjacent pixels are grouped into image segments according to their spectral similarity. These segments share a homogeneous spectral similarity.

We ran the segmentation in IDRISI software where the module SEGCLASS classifies imagery using a majority rule algorithm that is applied to image segments created by the module SEGMENTATION. Using the module SEGTRAIN training signatures are developed representing the classes within the imagery. These training signatures are identified by the interpreter the same way the Regions of Interest (ROI) are collected in ENVI for the supervised classification. The segmentation image created uses the segments identified on the image along with the training signatures in order to classify the image based on its textures.

For this project we created a segmentation image of the summer QuickBird image.

The accuracy of the segmentation image was then calculated by comparing the results of the classification map with field data collected following the EBONE GHC categories. The accuracy was calculated with only four categories: bare soil, herbaceous, shrubs, and forest trees.

As QuickBird images cannot detect changes in height of the vegetation there has been no attempt to differentiate low and high shrubs. Therefore, the accuracy of the segmentation image was calculated by comparing the classification results with ground truth data where low and high shrubs, identified in the field, were combined into one category of mixed shrubs.

6.3.3 UnMixing

6.3.3.1 Mapping bare soil, seasonal vegetation, and perennial vegetation

The aim of this analysis is to use the unmixing classification as a way to map percentage of coverage of bare soil, seasonal and perennial vegetation, per pixel.

NDVI images, for the spring and summer 2010 QuickBird images were produced. Based on these images NDVI thresholds representing 0% vegetation (i.e. bare soil) and 100% vegetation were defined. NDVI values between these two threshold values represent partial vegetation coverage within a pixel.

Different values of NDVI were applied as threshold values, as shown below (Table 4)

Table 4: List of NDVI values applied as threshold values to map bare soil, seasonal and perennial vegetation for each of the pilot study areas, on each QuickBird image

		Summer QuickBird image – NDVI value	Spring QuickBird image – NDVI value
Ramat Ha'Nadiv area	Bare soil	< 0.4	< 0.37
	Vegetation coverage	0.4 – 0.5	0.37 – 0.6
	Woody vegetation	> = 0.5	> = 0.6

Lehāvīm Forest area	Bare soil	< 0.4	< 0.3
	Vegetation coverage	0.4 – 0.55	0.3 – 0.55
	Woody vegetation	> = 0.55	> = 0.55
r i s o n Avdat area	Bare soil	< 0.17	< 0.15
	Vegetation coverage	0.17 – 0.5	0.15 – 0.55
	Woody vegetation	> = 0.5	> = 0.55

b

etween t

The vegetation coverage in the spring (peak greenness) and the summer (minimum greenness) will identify areas of perennial vegetation, seasonal vegetation, and bare soil:

Perennial vegetation → minimum % vegetation (woody vegetation)

Seasonal green vegetation → maximum - minimum % vegetation (herbaceous)

Bare soil (no vegetation) → 1 - maximum % vegetation

A meta file map was created where band 1 shows the percentage coverage of bare soil of the pixel, band 2 shows the percentage coverage of seasonal vegetation cover and band 3 shows the percentage coverage of perennial vegetation (shown as 432 in RGB). This final 3-bands metafile shows, per pixel, the percent coverage of bare soil, seasonal vegetation and perennial vegetation within a pixel.

Two accuracy assessments were tested:

(1) Comparison of UnMixing classification map with field data

Two types of analyses were produced:

(1) As an initial analysis the average percentage of vegetation coverage of bare soil, seasonal vegetation and perennial vegetation and its standard deviation was computed for each GHC category;

(2) The final analysis looks at the average percentage of bare soil, seasonal vegetation and perennial vegetation and its

standard deviation computed for four combined categories (herbaceous, shrub, high shrubs, and trees).

A metafile of the UnMixing classification results and EBONE field data was created. The data was exported to an ASCII file and a table where every row represent a pixel with its vegetation coverage (% coverage of bare soil, seasonal vegetation and perennial vegetation) and GHC category as defined in the field, was produced. As we were interested in analyzing the natural vegetation categories: bare soil, herbaceous, shrubs, high shrubs and trees, only pixels that belong to these GHC categories were analyzed.

We would expect the percentage of coverage of the three categories to vary within the EBONE GHC categories. High percentage of perennial vegetation for forest trees categories is expected and, on the contrary, high percentage coverage of seasonal vegetation for herbaceous categories.

(2) Comparison of UnMixing classification map of the QuickBird image with UnMixing classification map of the Landsat image

The aim of this analysis was to check the correlation between the results of the UnMixing classification of the Landsat TM with the results of the UnMixing classification of the QuickBird images. A high correlation between the results can indicate the effectiveness of using Landsat images that are cheaper to purchase and cover a longer historical dates, when it is important to map a big area.

Pixels values of the UnMixing classification maps produced for the Landsat TM and QuickBird images were exported to ASCII. A table with the pixels' values for each vegetation category: bare soil, seasonal, and perennial, for each of the two classification maps, was produced. The data was analyzed to check the correlation between the results of the classifications.

6.3.3.2 Mapping woody vegetation density

The aim of this step was to map the woody vegetation and calculate its density.

Woody vegetation density was calculated based on Normalized Difference Vegetation Index (NDVI; Tucker, 1979) values for the summer imagery. An NDVI image was produced and then used to determine the threshold value that represents the lowest NDVI value indicating the presence of woody vegetation. Any NDVI value higher than this threshold represents woody vegetation on the ground. A binary image was created where pixels with the

value of 1 represent woody vegetation and the value of 0 represent the other categories. A convolution filter was then run on the image. The convolution filters produced output images in which the value at a given pixel is a function of weighted average of the brightness of the surrounding pixels. In this analysis a circled convolution filter of 7x7 pixels was run. For each pixel a new value was calculated, based on its 48 neighbors, using the equation: (pixel value) / (max value) = woody vegetation density. The closer the neighboring pixels are, the higher their weight is. The new image is a map of the woody vegetation density.

The accuracy of the woody vegetation density map was tested by comparing the calculated average woody vegetation density and its standard deviation for each of the EBONE GHC categories: bare soil, herbaceous, shrubs, high bushes, and forest trees as collected by INPA in Ramat Ha'Nadiv area using the BIOHAB method (termed here as EBONE GHC). We would expect to have high woody vegetation density for polygons labeled as forest trees and lower values with polygons associated with bare soil and herbaceous for example.

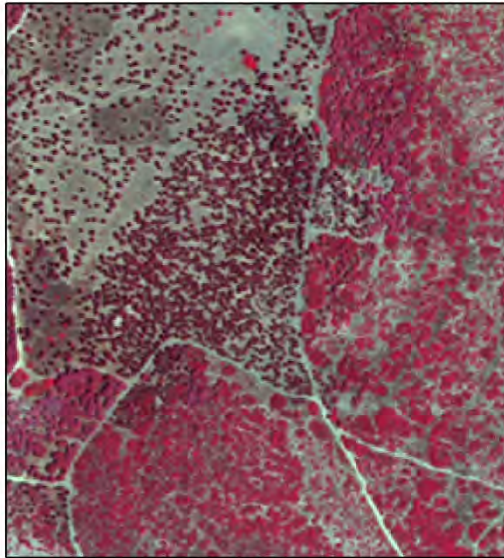
6.4. Results

6.4.1 Ramat Ha'Nadiv

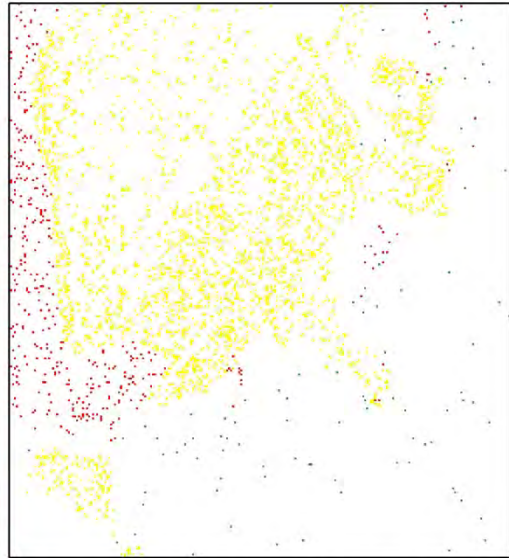
6.4.1.1. Maximum Likelihood Supervised Classification Method

As an initial step we have tried to correctly distinguish not only between Maquis and Forest but also between the two main tree species in the area: pine and cypress.

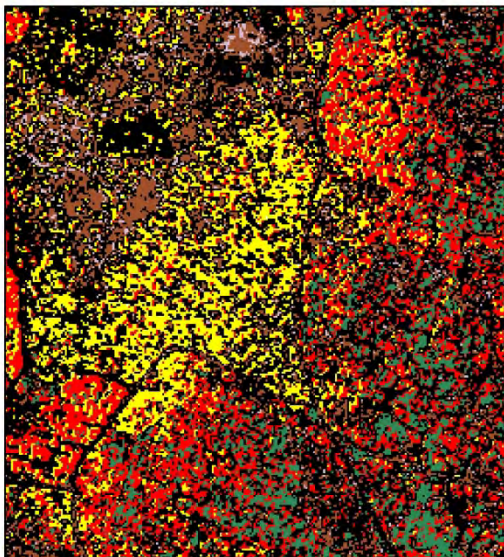
Figure 1: Example of the supervised classification map results in Ramat Ha'Nadiv area, using two classification methods.



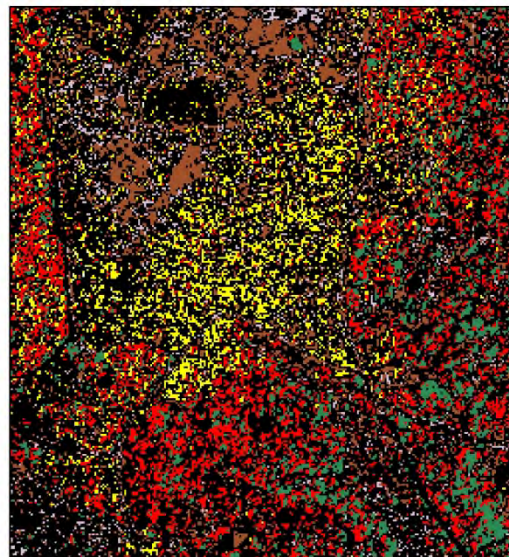
QuickBird image 26/7/2010
RGB: 4,3,2



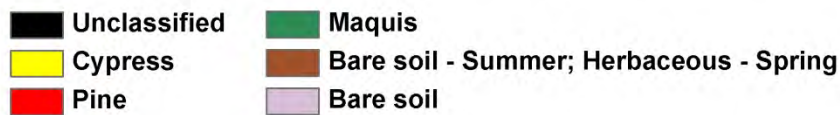
Example for the 10,000 pixels selected randomly per category (bare soil, seasonal and perennial vegetation)



Maximum likelihood supervised classification of the QuickBird image (26/7/2010)



Support vector machine supervised classification of the QuickBird image (26/7/2010)



The Maximum Likelihood supervised classification method gave an overall accuracy of 56% with a kappa value of 0.34, when trying to map the three categories: pine trees, cypress trees and maquis (Table 5). The individual accuracies show, as expected, a higher problem distinguishing between pine and cypress trees. For example, of the cypress trees identified in the field about 55% were classified as cypress trees and 32% as pine trees.

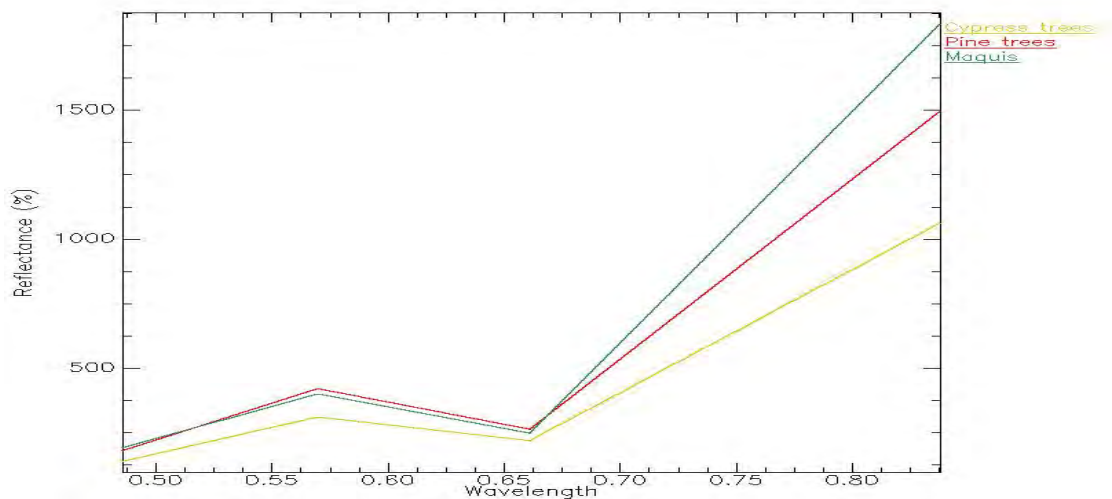
Table 5: Accuracy assessment of the maximum likelihood classification results in Ramat Ha'Nadiv area, looking at the total number of pixels

Overall Accuracy = 56%
 Kappa Coefficient = 0.34

		Ground Truth Data (GIS data layers)			
		Cypress	Pine	Maquis	Class Total
Classification image	Cypress	19.04	8.29	3.09	30.42
	Pine	11.13	17.99	9.56	38.68
	Maquis	4.73	7.20	18.98	30.91
	Class Total	34.89	33.48	31.63	100.00

Looking at the class total values we can see a good consistency between the total percentages of each vegetation category identified on the classification map compared to the ground truth data, for example: approximately 31% of the area was identified as Maquis both in the classification map and on the ground.

Figure 2: Spectral reflectance curves of Cypress, Pine and Maquis for the summer QuickBird image of Ramat Ha'Nadiv area



As by default the EBONE GHC categories do not differentiate between Pine and Cypress trees, and in addition the classification results show mixtures between pine and cypress trees, we produced a new map where the two tree categories were combined into one category of trees (Table 6).

Table 6: Accuracy assessment of the Maximum Likelihood classification results in Ramat Ha'Nadiv area, looking at the total number of pixels

Overall Accuracy = 75.42%
 Kappa Coefficient = 0.4283

		Ground Truth Data (GIS data layers)		
		Trees	Maquis	Class Total
Classification image	Trees	56.45	12.65	69.10
	Maquis	11.92	18.98	30.90
	Class Total	68.37	31.63	100.00

As can be expected combining the two categories improves the overall accuracy to 75% and the Kappa coefficient into 0.43.

6.4.1.2 Support Vector Machine Supervised Classification Method

Using the Support Vector Machine supervised classification method to map the three vegetation categories gave an overall accuracy of 52% with a kappa value of 0.27 (Table 7). The individual accuracies show problems in identifying correctly the vegetation categories, especially pine trees and maquis. For example, out of the pine trees identified on the field, about 42% were identified as pine trees and 40% as maquis on the classification map.

Looking at the class total values we can see a low representation of the cypress trees while the representation of the maquis is too big. For example: 39% of the area was identified on the ground as Maquis while on the classification maps 47% pixels were classified as Maquis.

Table 7: Accuracy assessment of Support Vector Machine Classification results in Ramat Ha'Nadiv area, looking at the total number of pixels

Overall Accuracy = 52%
 Kappa Coefficient = 0.27

		Ground Truth Data (GIS data layers)			
		Cypress	Pine	Maquis	Class Total

Classification image	Cypress	12.31	5.64	1.50	19.45
	Pine	8.48	13.82	11.37	33.67
	Maquis	7.40	13.23	26.25	46.88
	Class Total	28.19	32.69	39.12	100.00

As expected, when pine and cypress trees were combined our ability to correctly map trees vs. maquis was improved to an overall accuracy of 66.50% and a Kappa coefficient of 0.32 (Table 8).

Table 8: Accuracy assessment of Support Vector Machine Classification results in Ramat Ha'Nadiv area, looking at the total number of pixels

Overall Accuracy = 66.50%
Kappa Coefficient = 0.3207

		Ground Truth Data (GIS data layers)		
		Trees	Maquis	Class Total
Classification image	Trees	40.24	12.88	53.12
	Maquis	20.63	26.25	46.88
	Class Total	60.87	39.13	100.00

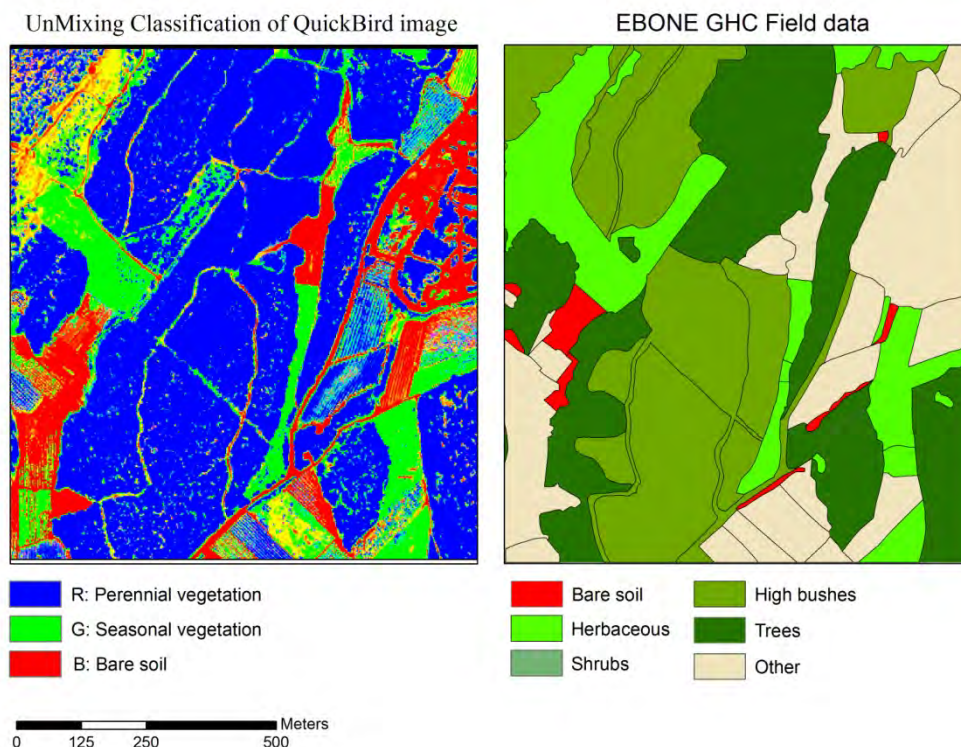
Results of both supervised classification methods show a good ability to correctly map trees (about 80% of the trees on the field are correctly identified), yet a lower ability to map maquis. Mixtures between maquis and forest trees categories can be due to various reasons that are discussed in detail at the discussion section.

In addition, the Maximum Likelihood classification method shows a higher accuracy, vs. the Support Vector Machine Classification method and should be used in this analysis.

6.4.1.3 UnMixing Classification Method – Mapping bare soil, seasonal vegetation, and perennial vegetation

6.4.1.3.1 Comparing results of the UnMixing classification of the QuickBird images with EBONE field data

Figure 3: Comparison of EBONE field data with UnMixing classification results in Ramat Ha'Nadiv area



(1) Initial analysis looking at each GHC natural vegetation category

Table 9: The average percentage of vegetation coverage and its standard deviation for GHC herbaceous polygons in Ramat Ha'Nadiv area

	GHC category	GHC codes	Number of pixels		QuickBird Bare Soil	QuickBird Seasonal	QuickBird Perennial
Herbaceous	Herbaceous	CHE/GTHE	6257	Average	0.32	0.60	0.09
				Std	0.28	0.30	0.25
	Herbaceous	GTHE	93627	Average	0.22	0.60	0.18
				Std	0.33	0.39	0.34
	Herbaceous	THE	2362	Average	0.45	0.48	0.07
				Std	0.29	0.28	0.23
	All Herbaceous categories		102246	Average	0.24	0.59	0.17
				Std	0.33	0.38	0.34

Figure 4: Representation of the percent coverage of bare soil, seasonal and perennial vegetation of EBONE GHC herbaceous categories in Ramat Ha'Nadiv

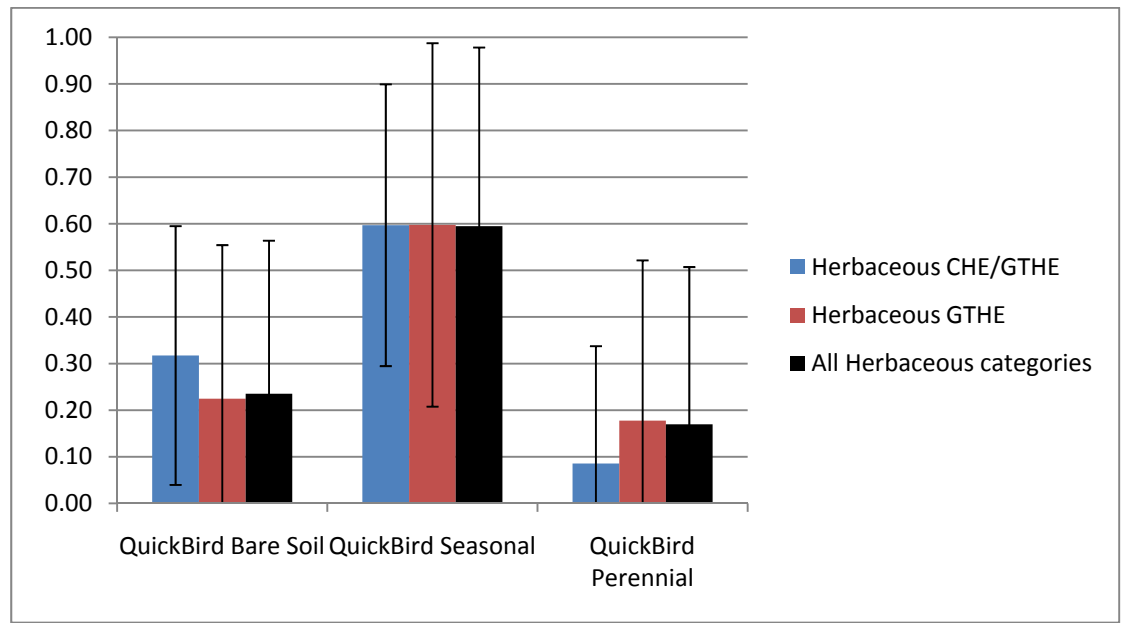


Table 10: The average percentage of vegetation coverage and its standard deviation for GHC shrubs polygons in Ramat Ha'Nadiv area

	GHC category	GHC codes	Number of pixels		QuickBird Bare Soil	QuickBird Seasonal	QuickBird Perennial
Shrubs	Mixed Eve. and Dec. Shrubs	LPH/EVR/SUM	1867	Average	0.33	0.34	0.33
				Std	0.25	0.23	0.35
	Dec. Shrubs	LPH/SUM	2657	Average	0.21	0.47	0.31
				Std	0.24	0.34	0.42
	Mixed Eve. and Dec. Shrubs	LSPH/EVR/SUM	3909	Average	0.32	0.42	0.26
				Std	0.32	0.32	0.39
	Deciduous Shrubs	LSPH/SUM	17637	Average	0.17	0.58	0.25
				Std	0.24	0.35	0.37
	All Mixed Shrubs		26070	Average	0.21	0.53	0.26
				Std	0.26	0.35	0.38

Figure 5: Percent coverage of bare soil, seasonal and perennial vegetation of EBONE GHC shrubs categories in Ramat Ha'Nadiv

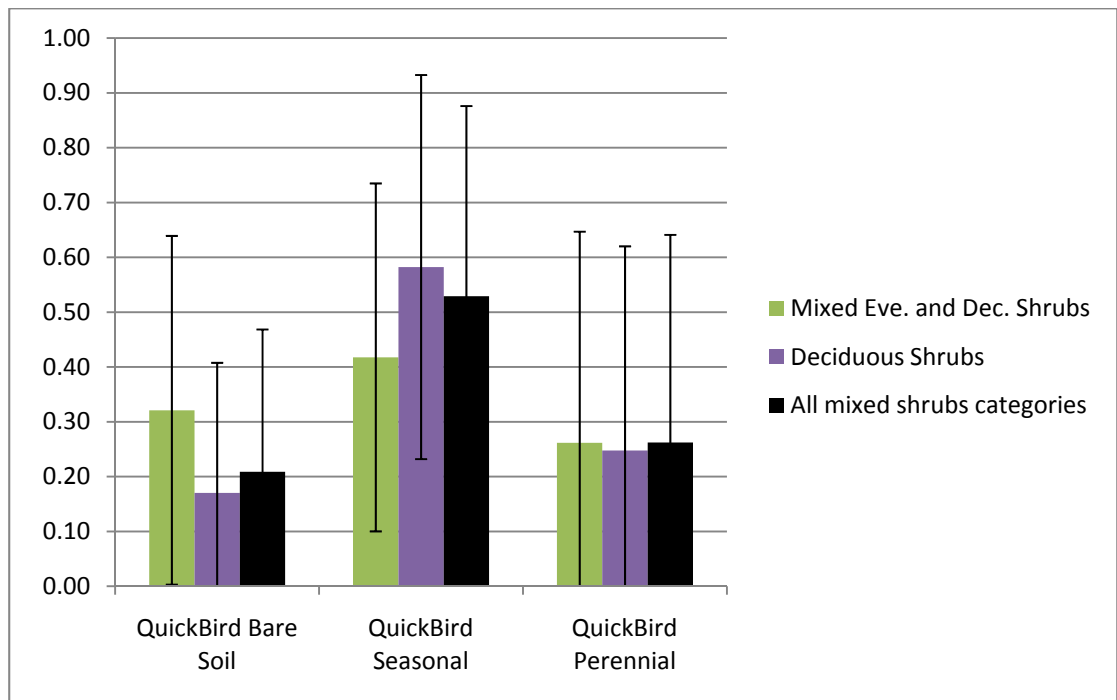


Table 11: The average percentage of vegetation coverage and its standard deviation for GHC bushes (high-height) polygons in Ramat Ha'Nadiv area

	GHC category	GHC codes	Number of pixels		QuickBird Bare Soil	QuickBird Seasonal	QuickBird Perennial
High Bushes	High Bushes	MPH/CAC	1068	Average	0.33	0.32	0.35
				Std	0.39	0.36	0.45
	Deciduous high bushes	MPH/DEC	478	Average	0.08	0.40	0.53
				Std	0.22	0.39	0.43
	Mixed Eve. and Dec. high Bushes	MPH/DEC/EVR	5387	Average	0.10	0.23	0.68
				Std	0.21	0.31	0.41
	Eve. high bushes	MPH/EVR	67279	Average	0.19	0.27	0.54
				Std	0.30	0.32	0.44
	Eve. high bushes	MPH/EVR/CAC	2694	Average	0.18	0.32	0.51
				Std	0.30	0.36	0.45
	Evergreen high bushes	MPH/EVR/FLE	614	Average	0.53	0.38	0.09

				Std	0.27	0.24	0.20
	Mixed Eve. and NL Eve. high bushes	MPH/EVR/NLE	127489	Average	0.08	0.15	0.76
				Std	0.21	0.27	0.37
	Non Leafy Evergreen high bushes	MPH/NLE	77519	Average	0.19	0.24	0.57
				Std	0.28	0.28	0.42
	All Mixed high bushes		282528	Average	0.14	0.21	0.65
				Std	0.26	0.29	0.42

Figure 6: Percent coverage of bare soil, seasonal and perennial vegetation of EBONE GHC high bushes categories in Ramat Ha'Nadiv

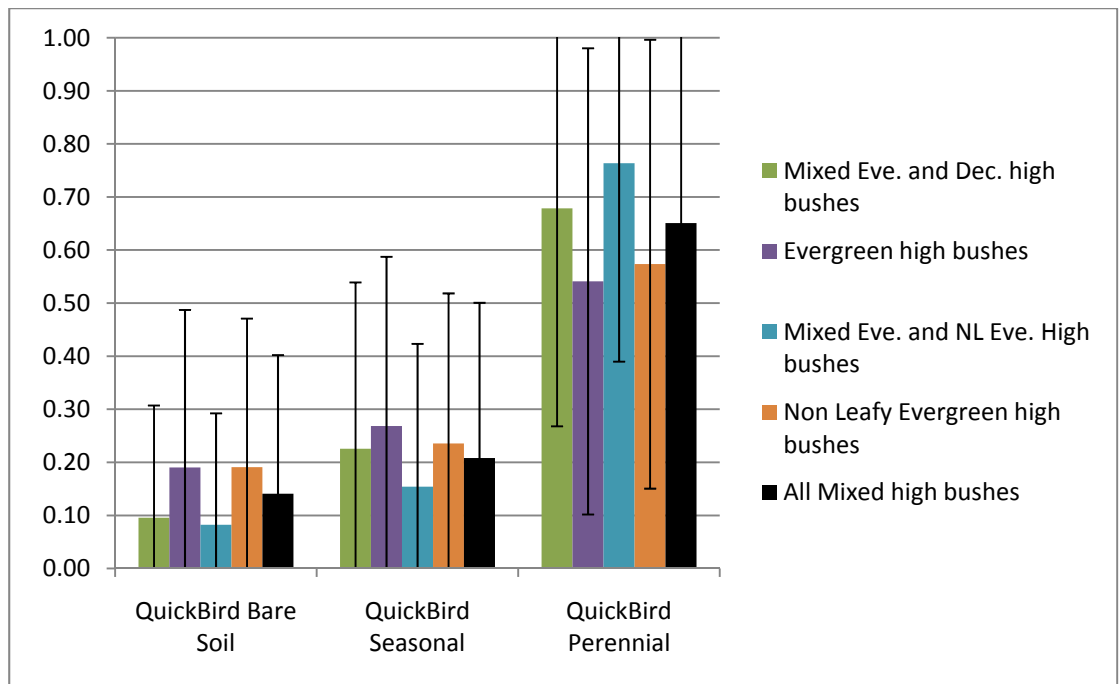
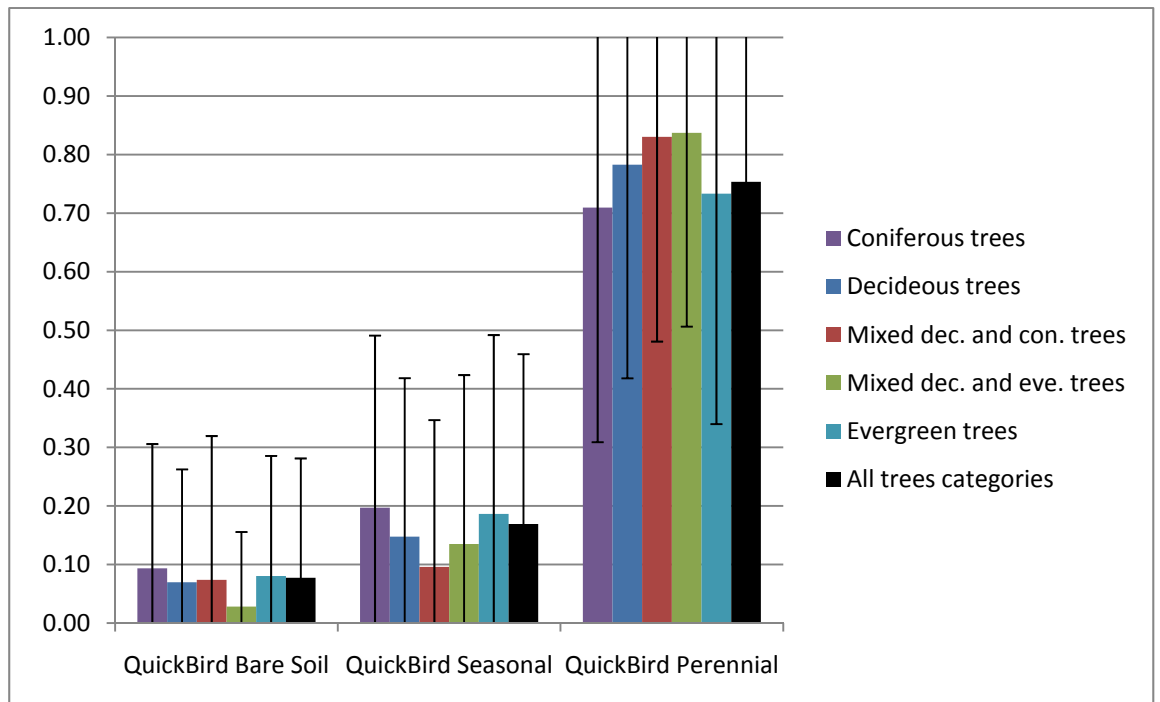


Table 12: The average percentage of vegetation coverage and its standard deviation for GHC trees polygons in Ramat Ha'Nadiv area

	GHC category	GHC code	Number of pixels		QuickBird Bare Soil	QuickBird Seasonal	QuickBird Perennial
Trees	Coniferous Trees	FTPH/CON	85860	Average	0.09	0.20	0.71
				Std	0.21	0.29	0.40
	Deciduous Trees	FTPH/DEC	89519	Average	0.07	0.15	0.78

				Std	0.19	0.27	0.36
	Mixed Dec. and Con. Trees	FTPH/DEC/CON	10879	Average	0.07	0.10	0.83
				Std	0.25	0.25	0.35
	Mixed Dec. and Eve. Trees	FTPH/DEC/EVR	32542	Average	0.03	0.13	0.84
				Std	0.13	0.29	0.33
	Evergreen Trees	FTPH/EVR	104385	Average	0.08	0.19	0.73
				Std	0.21	0.31	0.39
	Mixed Eve. and Con. Trees	FTPH/EVR/CON	4711	Average	0.20	0.09	0.71
				Std	0.37	0.19	0.42
	Non Leafy Evergreen Trees	FTPH/NLE	490	Average	0.15	0.28	0.56
				Std	0.32	0.37	0.44
	All Mixed Trees		328386	Average	0.08	0.17	0.75
				Std	0.20	0.29	0.38

Figure 7: Percent coverage of bare soil, seasonal and perennial vegetation of EBONE GHC trees categories in Ramat Ha'Nadiv



The results of this initial analysis show the problems in using the UnMixing classification, as done in this project, to classify accurately the detailed EBONE GHC categories. Additional study is needed to check this matter.

(2) Analysis looking at four combined GHC natural vegetation categories

Table 13: The average percentage of vegetation coverage and its standard deviation of the combined GHC categories polygons in Ramat Ha'Nadiv area

GHC category	Number of pixels		QuickBird Bare Soil	QuickBird Seasonal	QuickBird Perennial
Herbaceous	102246	Average	0.24	0.59	0.17
		Std	0.33	0.38	0.34
Trees	328386	Average	0.08	0.17	0.75
		Std	0.20	0.29	0.38
High bushes	282528	Average	0.14	0.21	0.65
		Std	0.26	0.29	0.42
Shrubs	26070	Average	0.21	0.53	0.26
		Std	0.26	0.35	0.38

Figure 8: Percent coverage of bare soil, seasonal and perennial vegetation of four combined EBONE GHC categories in Ramat Ha'Nadiv: herbaceous, shrubs, high bushes, and trees

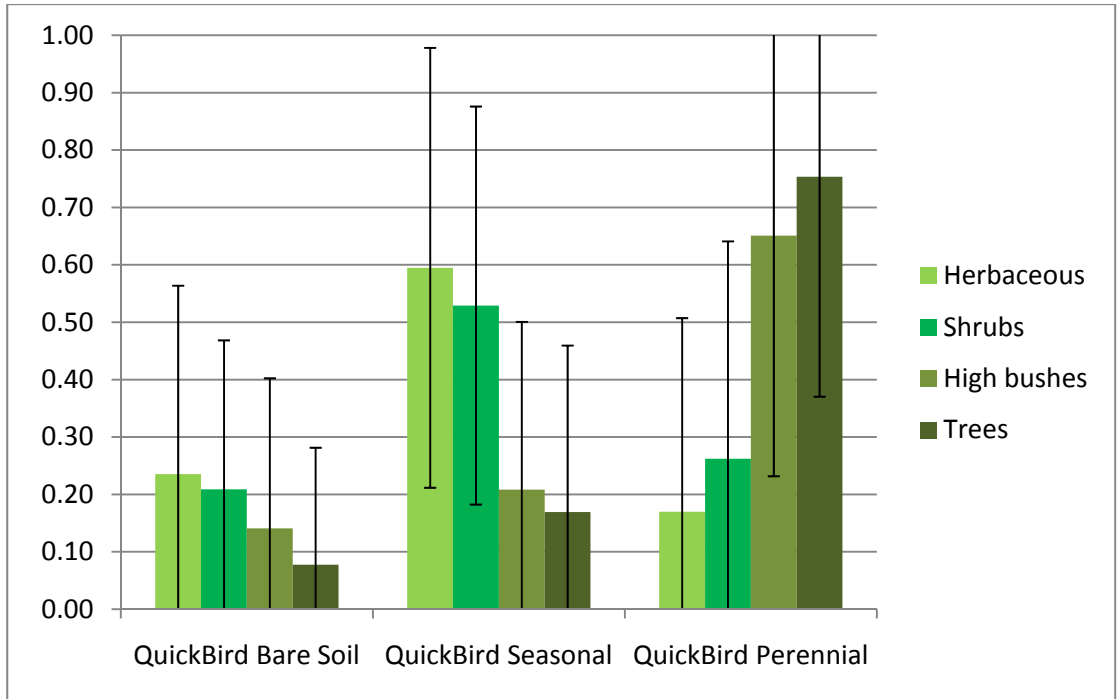


Figure 9: Representation of percent coverage of bare soil, seasonal and perennial vegetation for each of the four combined EBONE GHC categories in Ramat Ha'Nadiv: herbaceous, shrubs, high bushes, and trees

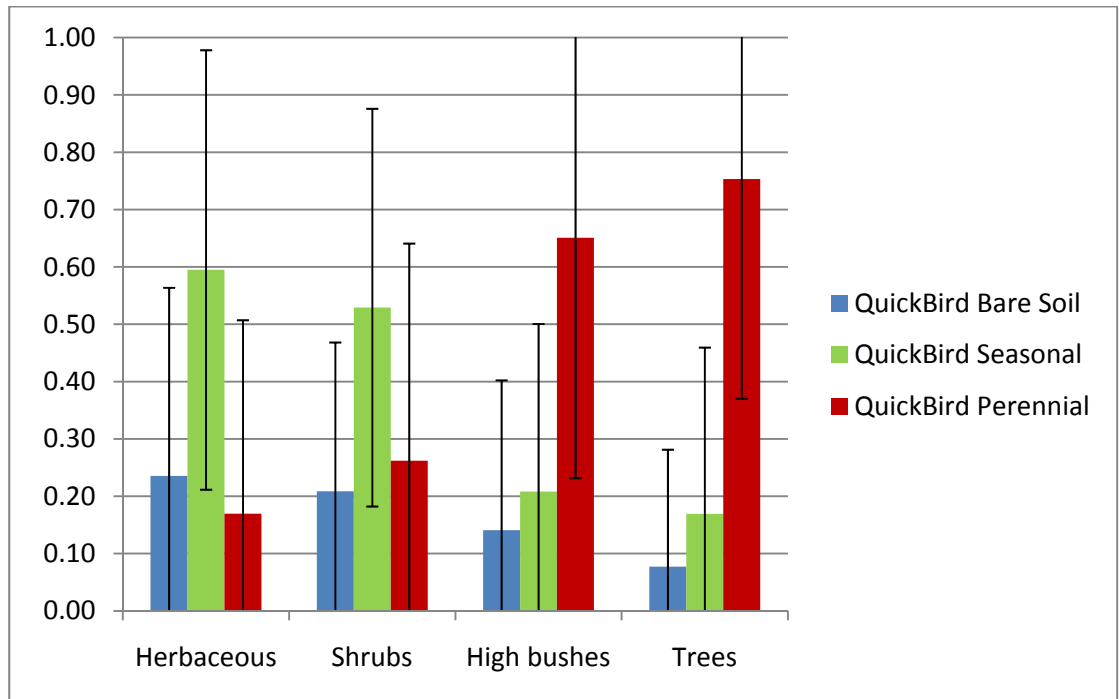


Table 14: Summary of the UnMixing classification results for Ramat Ha'Nadiv area:

	Bare soil coverage	Seasonal vegetation coverage	Perennial vegetation coverage
Herbaceous	low	high	low
Shrubs	low	high	low
High shrubs	lower	low	high
Trees	Very low	lower	Very high

Results of the UnMixing classification map of Ramat Ha'Nadiv show a good ability to map bare soil, seasonal and perennial vegetation, and associate them with the EBONE GHC categories, especially bare soil and trees categories (Table 14).

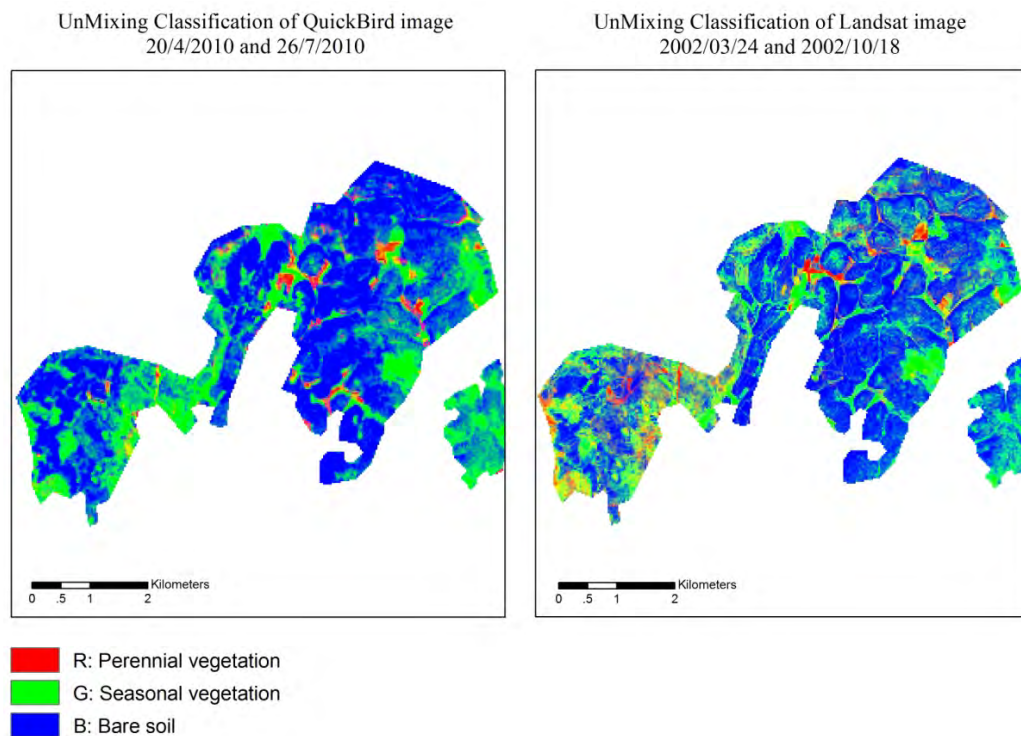
In this analysis, the UnMixing classification, by definition, is used in order to calculate, per pixel, the percent coverage of bare soil, seasonal vegetation (herbaceous) and perennial vegetation (woody vegetation). Looking at the results we can see that, as expected, pixels classified in the field as trees have, on average, a high percentage of perennial vegetation coverage and a lower percentage of seasonal vegetation and bare soil coverage. Pixels classified in the field as herbaceous show on the contrary a high percentage of seasonal vegetation coverage and a low percentage of bare soil and perennial coverage. Shrubs category (shrubs and high bushes) is a bit harder to classify using this method of classification. When looking at the shrub category without distinguishing between the two heights categories, it shows a higher coverage of perennial vegetation and lower percent of coverage of seasonal vegetation and bare soil. But, when differentiating between the two shrub categories, based on their height (as defined by EBONE GHC categories) we can see that lower height shrubs have higher seasonal vegetation coverage, like the herbaceous category, and on the contrary high bushes have a higher perennial coverage. This may introduce some errors when using this classification method as a way to distinguish shrubs from herbaceous as well as high bushes from forest trees.

When summarizing the results we can say that we can use the UnMixing classification as a reliable way to classify herbaceous and shrubs (low height) from high bushes and trees, yet more research is needed to improve our ability to accurately classify herbaceous from shrubs and high bushes from forest trees.

6.4.1.3.2 Comparing the results of the UnMixing classification of the QuickBird images with the results of the UnMixing classification of the Landsat TM

A high correlation between the results can indicate the effectiveness of using Landsat images that are cheaper to purchase and cover a longer historical dates, when it is important to map a big area.

Figure 10: Example for UnMixing classification results of QuickBird images vs. Landsat images in Ramat Ha'Nadiv area



For the comparison, four ROIs, representing mostly areas of natural vegetation and planted trees, were digitized on the QuickBird image. A table with the pixel values, for each vegetation category: bare soil, seasonal, and perennial, derived from the QuickBird and Landsat UnMixing classification maps was produced. The data was analyzed to check the correlation between the results of the classifications (Table 15).

Table 15: Results of the correlation analyses of results of the UnMixing classifications of Landsat and QuickBird data in Ramat Ha'Nadiv area

	Bare Soil	Seasonal	Perennial
--	-----------	----------	-----------

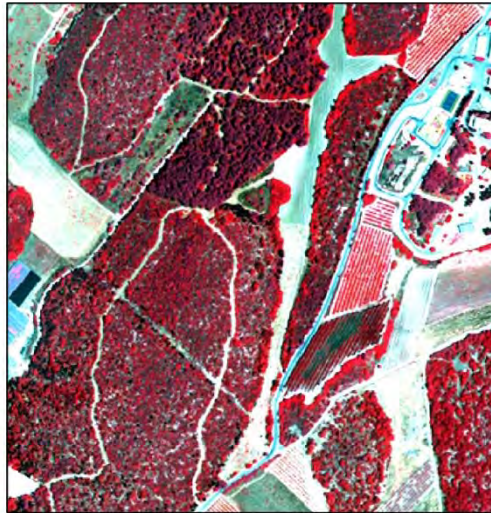
Correlation between Landsat and QuickBird data	0.74	0.53	0.75
---	------	------	------

Results of the correlation show the high correlation between the the UnMixing classification results of the two satellite images. The lower correlation of the seasonal vegetation classification does not necessarily show an error in the classification maps but can be due to various reasons that will be discussed in detail in the discussion section.

6.4.1.4 UnMixing Classification Method - Mapping Woody Vegetation Density

The woody vegetation density map was created based on the NDVI image of the summer QuickBird image, and its accuracy was tested by comparing the calculated average woody vegetation density and its standard deviation for each of the EBONE GHC categories: bare soil, herbaceous, shrubs, high bushes, and forest trees as collected by INPA in Ramat Ha'Nadiv.

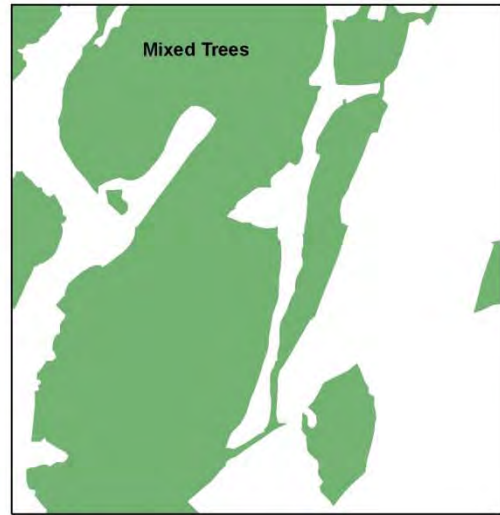
Figure 11: Example for the woody vegetation density results in Ramat Ha'Nadiv area – comparison of results of analysis of the QuickBird image with field data



QuickBird image 26/7/2010
 RGB: 4,3,2



Woody vegetation density, 0-100%
 White - high density



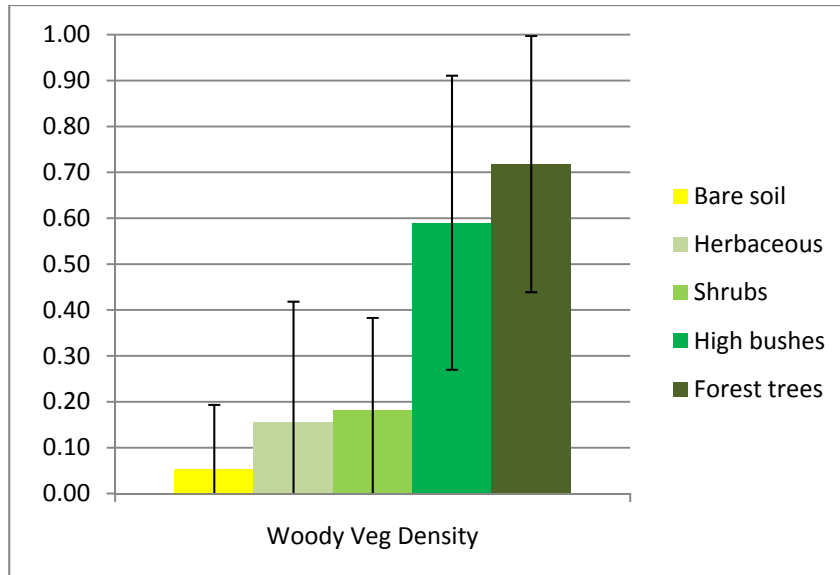
Map of Trees - green color
 based on EBONE GHC categories
 Field data collected by INPS

Table 16: The average woody vegetation density and its standard deviation for EBONE GHC categories: bare soil, herbaceous, shrubs, high bushes, and forest trees, in Ramat Ha'Nadiv area

EBONE GHC Category		Woody Vegetation Density	# pixels
Bare soil	Average	0.05	36184
	Std	0.14	
Herbaceous	Average	0.16	104797
	Std	0.26	
Shrubs	Average	0.18	26032
	Std	0.20	

High bushes	Average	0.59	286703
	Std	0.32	
Forest trees	Average	0.72	330698
	Std	0.28	

Figure 12: Woody vegetation density representation of combined EBONE GHC categories in Ramat Ha'Nadiv



When comparing the woody vegetation density map with the INPA field data we can see, on average that areas identified as trees and high bushes have high woody vegetation density value, while shrubs, herbaceous, and bare soil are associated with lower density values.

Possible reasons for errors in woody vegetation density values, calculated based on NDVI values will be discussed in detail in the discussion section.

Nevertheless, on average, the summer QuickBird NDVI map show a good ability to calculate the woody vegetation density.

6.4.2 Lehavim Forest

6.4.2.1 Maximum Likelihood Supervised Classification Method

A classification map of five EBONE GHC categories was created: bare soil, herbaceous, shrubs (maquis), forest trees, and agriculture (Figure 13). Its accuracy was calculated by comparing the classification results with field data (Table 18).

Table 17: Accuracy assessment of the Maximum Likelihood pixel-based classification results in Lehavim forest area, looking at the total number of pixels of all categories

Overall Accuracy = 55%
 Kappa Coefficient = 0.44

		EBONE GHC ground truth data					
		Agriculture	Bare soil	Forest trees	Herbaceous	Shrubs (Maquis)	Grand Total
Classification image	Agriculture	5.4	0.1	0.0	0.9	2.3	8.8
	Bare soil	0.1	1.0	0.4	2.6	2.3	6.4
	Forest trees	1.0	1.4	12.9	5.9	7.5	28.8
	Herbaceous	1.8	0.4	0.9	3.3	9.0	15.4
	Shrubs (maquis)	0.2	1.8	0.8	5.4	32.3	40.6
	Grand Total	8.6	4.7	15.2	18.1	53.4	100.0

Results reveal problems in classifying correctly the image, with higher mixture when classifying bare soil and herbaceous using this classification method. Most polygons that were associated, in the field, with one EBONE GHC category are on the ground heterogeneous polygons that have small patches of other vegetation categories. This can be clearly seen on Figure 13, when comparing the results of the supervised classification with field data. The field data show polygons represented by one specific category while the classification map reveals the mixture of patches of categories within these polygons.

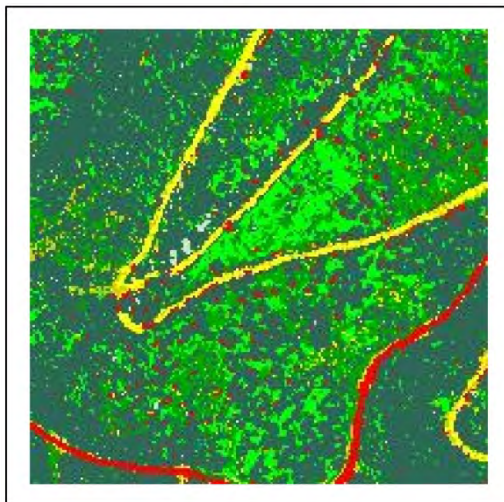
In addition to the observed mixture between the categories when classifying them using the supervised classification, we can also identify a problem when comparing the total % of coverage of each category between the classified image and the field data (Table 18). For example: there is an underestimation of the % coverage of shrubs on the classified map compared with field data, 40.6% vs. 53.4%. On the contrary there is an overestimation of the % coverage of forest trees on the classified map compared with field data, 28.8% vs. 15.2%.

There are various reasons that may contribute to these errors and they will be discussed in detail in the discussion section.

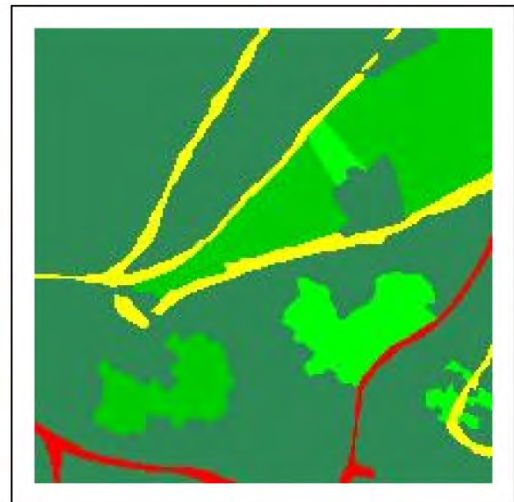
Figure 13: Example of the Maximum Likelihood supervised classification map in Lehavim forest area



QuickBird image 17/7/2010
RGB: 4,3,2



Maximum likelihood supervised classification of the QuickBird image (17/7/2010)



EBONE GHC field data (July 2010)

 Unclassified	 Herbaceous
 Forest	 Bare soil
 Shrubs	 Urban

6.4.2.2 Segmentation

Using the IDRISI software a segmentation image of the summer QuickBird image of Lehavim forest area was created (Figure 14).

Figure 14: Example of the Segmentation classification map in Lehavim forest area

Segmentation Classification of QuickBird image

EBONE GHC Field data

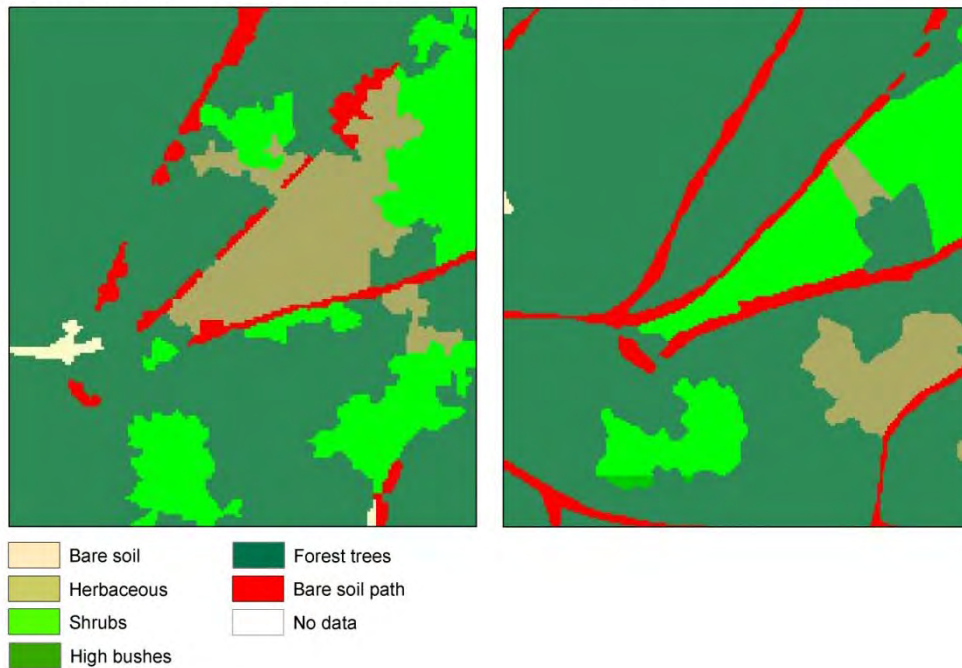


Table 18: Percent accuracy the segmentation classification results of Lehavim forest area compared with ground truth data (looking at the total number of pixels)

Overall Accuracy = 57.38%
 Kappa Coefficient = 0.32

		EBONE GHC Ground Truth Data				
Class		Herbaceous	Bare soil	Forest trees	Mixed Shrubs	Total
Classification image	Herbaceous	4.95	0.37	2.27	11.37	18.95
	Bare soil	0.71	0.00	0.22	0.97	1.90
	Forest trees	9.48	1.24	12.69	9.33	32.73
	Shrubs	5.11	0.71	0.85	39.75	46.42
	Total	20.24	2.32	16.02	61.41	100.00

Results show mixtures between the classified categories when classifying the QuickBird image using the segmentation method, e.g. areas of shrubs identified in the field that are classified as herbaceous in the classification map, herbaceous identified as forest trees, shrubs that are identified as forest trees on the classification map. In addition we can see again the inconsistency between the total % coverage of forest trees and shrubs identified in the field with their % coverage identified in the classification map.

Possible reasons for these errors will be discussed in detail in the discussion section.

6.4.2.3 UnMixing

4.2.3.1 Comparing the results of the UnMixing classification of the QuickBird images with EBONE field data

Figure 15: Example for UnMixing classification results of QuickBird images with EBONE field data in Lehavim forest area

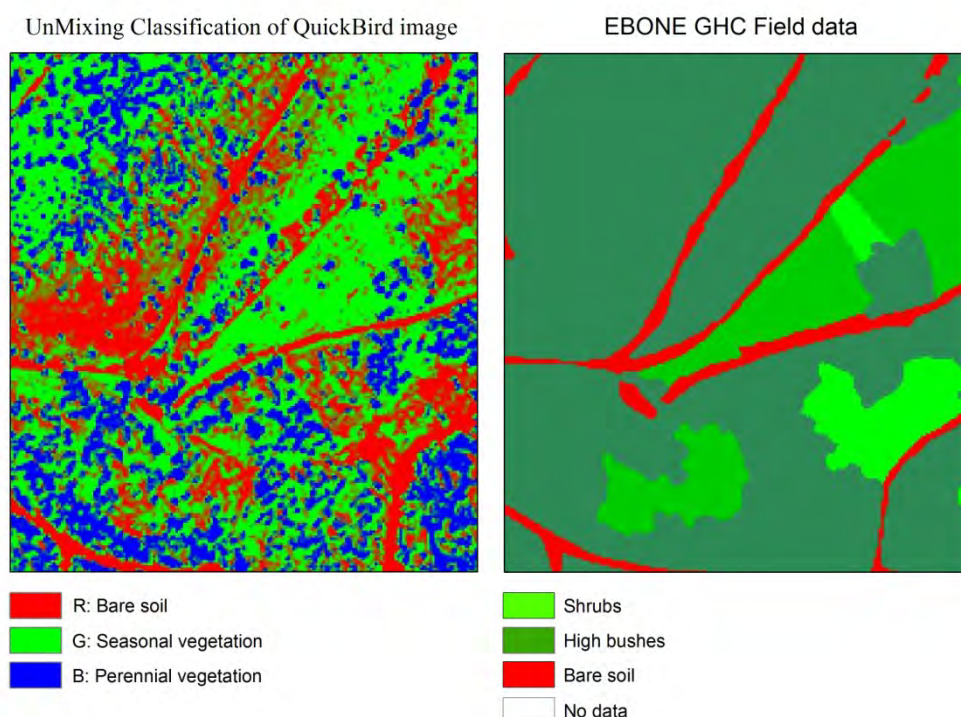


Table 19: The average percentage of vegetation coverage and its standard deviation of the combined GHC categories polygons in Lehavim forest area

EBONE GHC category	# pixels		Bare soil	Seasonal	Perennial
Urban - road	5783	Average	0.52	0.39	0.09
		Std	0.41	0.38	0.26
Urban	946	Average	0.77	0.18	0.05
		Std	0.38	0.33	0.20
Urban - bare soil	15327	Average	0.67	0.31	0.02
		Std	0.40	0.39	0.14
Herbaceous	124145	Average	0.29	0.71	0.00
		Std	0.34	0.35	0.06
Agriculture	57996	Average	0.28	0.72	0.00

		Std	0.26	0.26	0.01
Bare soil	16994	Average	0.20	0.80	0.00
		Std	0.30	0.31	0.06
Forest tree	305365	Average	0.15	0.37	0.48
		Std	0.29	0.39	0.45
Mixed Shrubs	364786	Average	0.48	0.51	0.00
		Std	0.38	0.38	0.06

Figure 16: Representation of percent coverage of bare soil, seasonal and perennial vegetation for each of the EBONE GHC categories in Lehavim forest area:

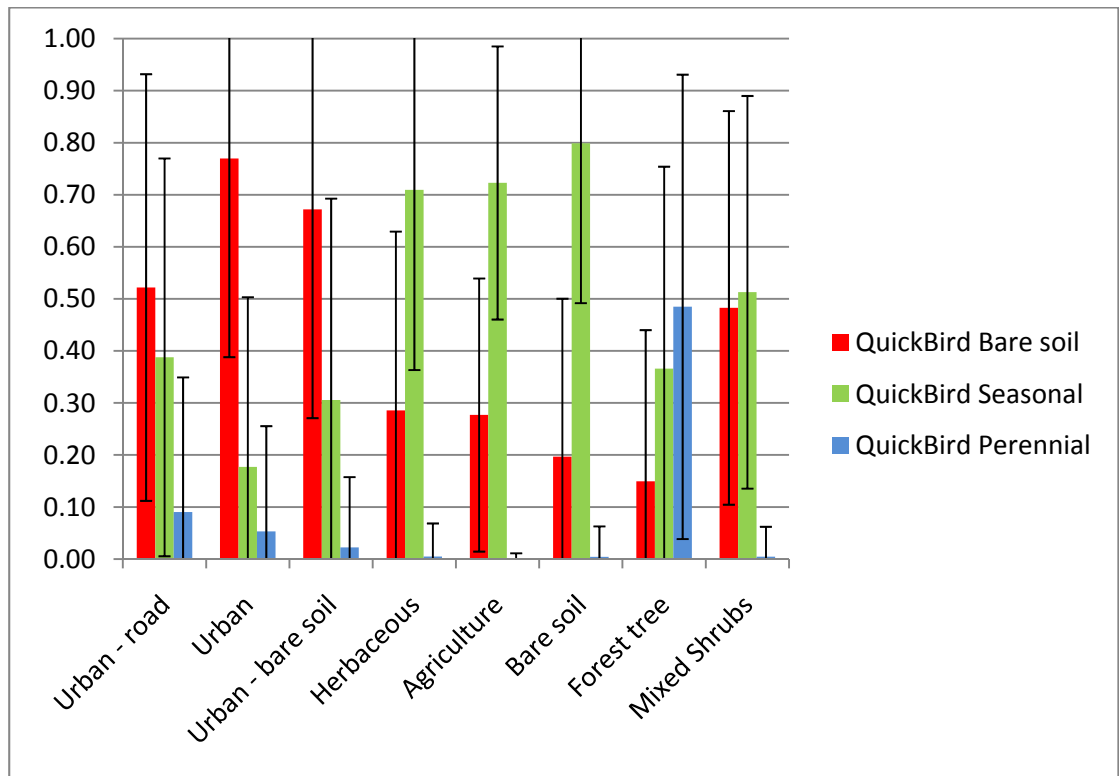


Figure 17: Representation of percent coverage of bare soil, seasonal and perennial vegetation for each of the four EBONE GHC categories: bare soil, herbaceous, mixed shrubs and forest trees, in Lehavim forest area:

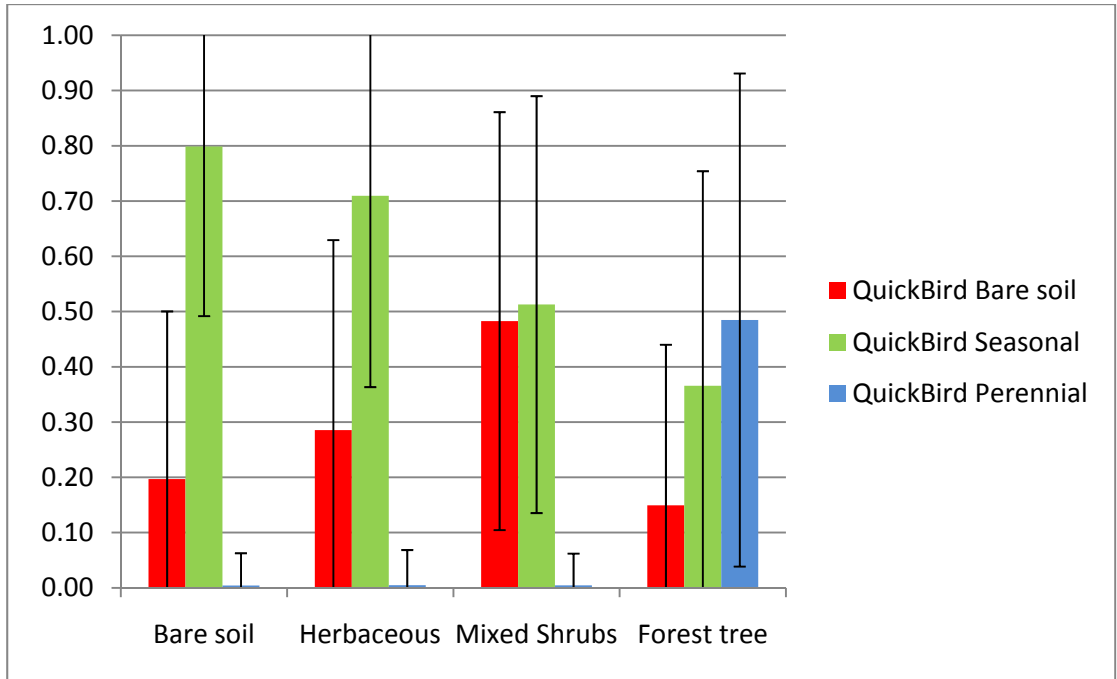


Figure 18: Percent coverage of bare soil, seasonal and perennial vegetation of three combined EBONE GHC categories: bare soil, herbaceous, shrubs and trees in Lehavim forest area:

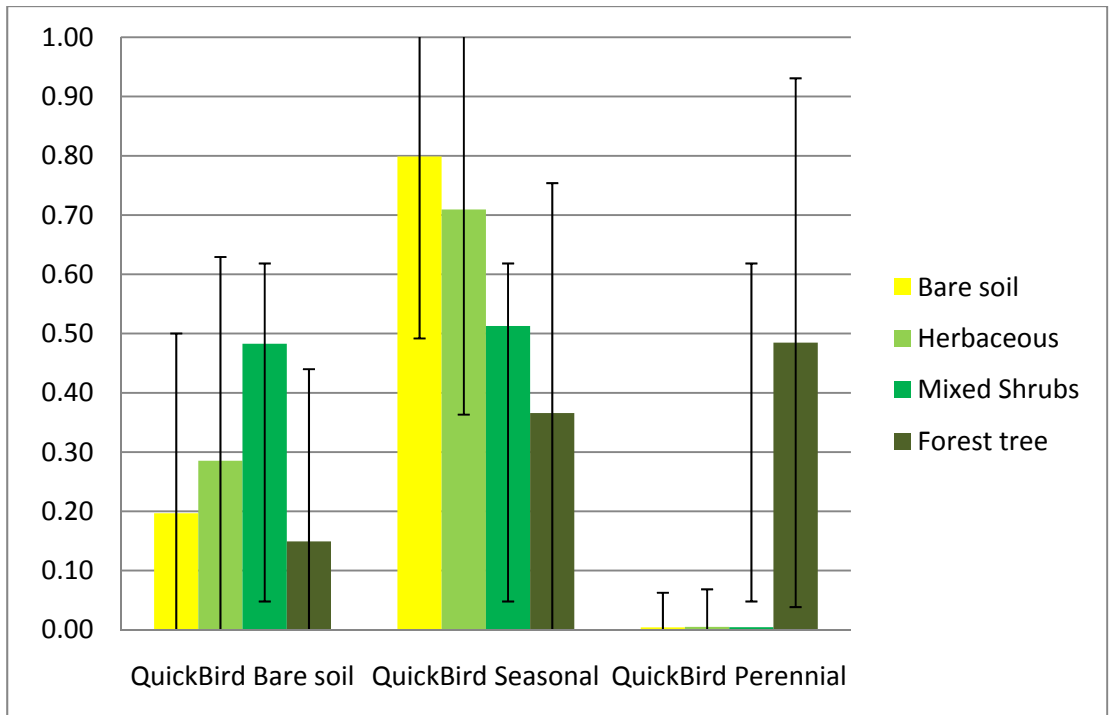


Table 20: Summary of the UnMixing classification results for Lehavim forest area:

	Bare soil coverage	Seasonal vegetation coverage	Perennial vegetation coverage
Bare soil	low	high	none
Herbaceous	low-medium	high	almost none
Shrubs	medium	medium	almost none
Trees	low	medium	high

Results of the UnMixing classification map show a good ability to map pixels based on their percent coverage of bare soil, seasonal and perennial vegetation per pixel and associate them with the combined EBONE GHC categories: shrubs (including high bushes) and trees. As bare soil and herbaceous categories show close results it is recommended to use seasonal changes in order to improve the accuracy of their mapping. The fact that there is a high association between percent coverage of seasonal vegetation with the presence of bare soil may indicate: 1. an error in the ground data due to the season of the fieldwork; and 2. a need to redefine the characteristics of the bare soil category and add more categories for bare soil, especially in arid areas.

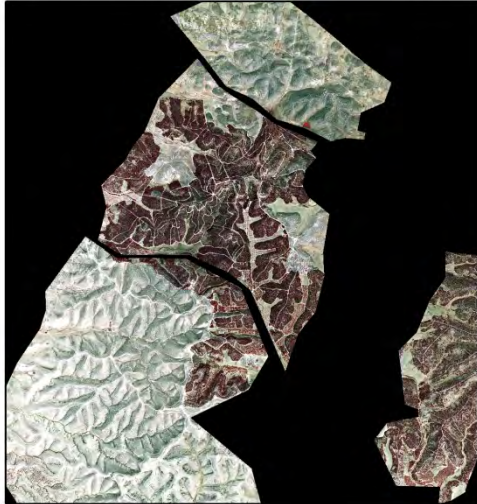
6.4.2.3.2 Comparing the results of the UnMixing classification of the QuickBird images with the results of the UnMixing classification of the Landsat TM

Table 21: Results of the correlation analyses of UnMixing classifications of the Landsat and QuickBird data in Lehavim forest area

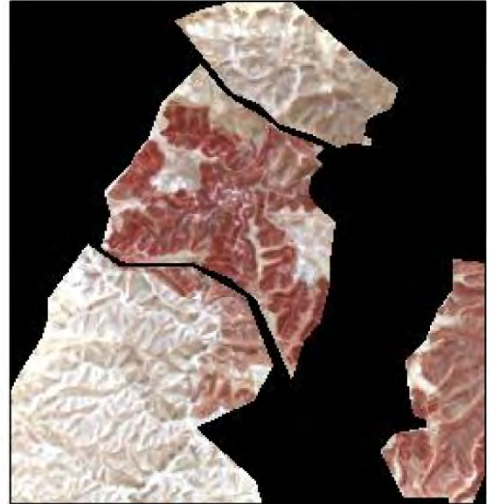
	Bare Soil	Seasonal vegetation	Perennial vegetation
Correlation between Landsat and QuickBird data	0.56	0.34	0.59

Figure 19: Example for UnMixing classification results of QuickBird images vs. Landsat images in Lehavim forest area

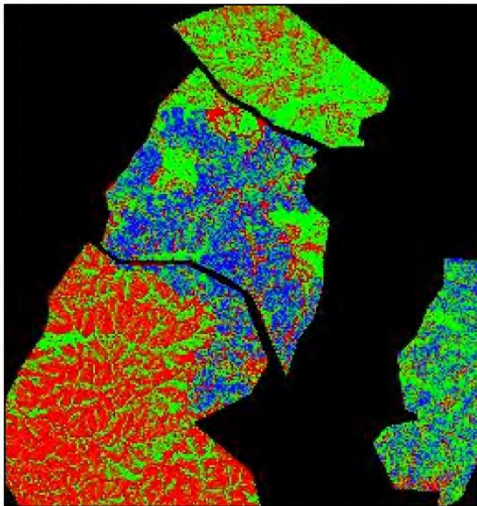
Subset of QuickBird image of Lehavim forest area: 18/7/2010



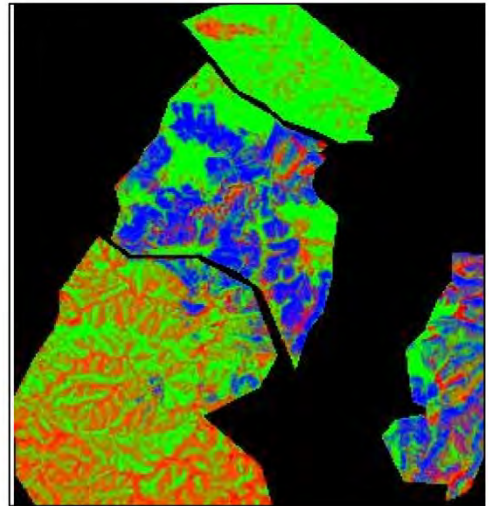
Subset of Landsat image of Lehavim forest area: 11/7/2002



UnMixing Classification of QuickBird image: 22/3/2010 and 18/7/2010



UnMixing Classification of Landsat image: 11/7/2001 and 8/3/2002



- R: Bare soil
- G: Seasonal vegetation
- B: Perennial vegetation

Results of the correlation show a lower correlation between the the UnMixing classification results of the QuickBird and Landsat images, compared with the correlation observed at Ramat Ha'Nadiv area. Yet, the lower corelation does

not necessarily show indicate an error in the classification, and can be due to various reasons that will be discussed in detail at the discussion section.

6.4.2 Avdat area

6.4.2.1 UnMixing

6.4.2.1.1 Comparing the results of the UnMixing classification of the QuickBird images with EBONE field data

Figure 20: Example for UnMixing classification results of QuickBird images with EBONE field data in Avdat area

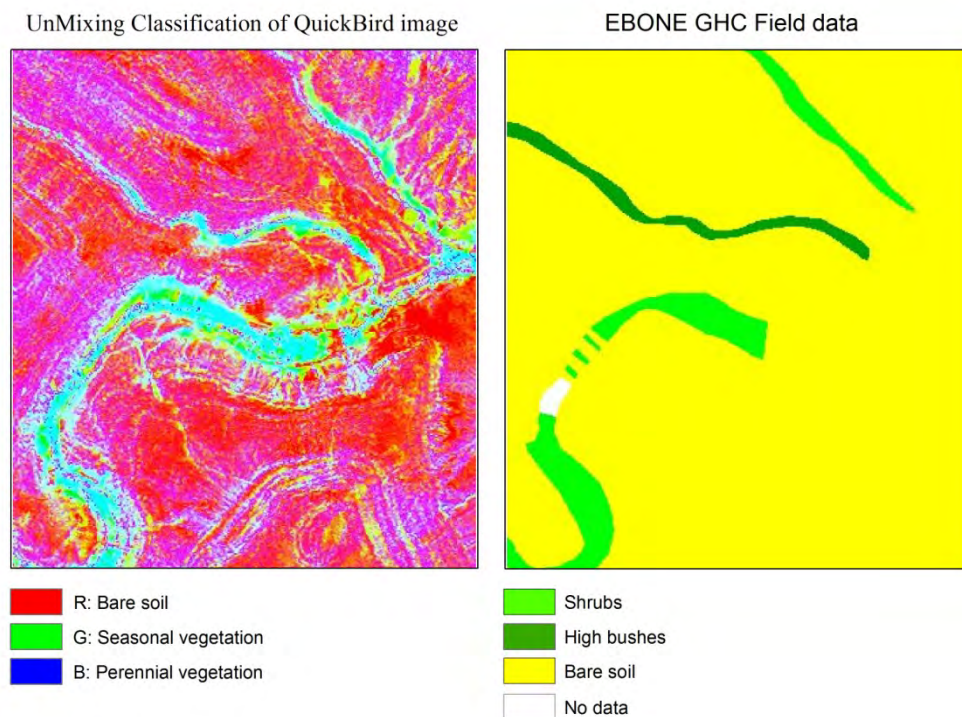


Table 22: The average percentage of vegetation coverage and its standard deviation of the combined GHC categories polygons in Lehavim forest area

EBONE GHC combined category	Number of pixels		QuickBird Bare Soil	QuickBird Seasonal	QuickBird Perennial
Bare Soil	945918	average	0.92	0.05	0.03
		std	0.12	0.09	0.05
Shrubs	12319	average	0.77	0.16	0.07
		std	0.20	0.17	0.07
High Bushes	4426	average	0.87	0.09	0.04
		std	0.16	0.14	0.05

Forest trees	841	average	0.12	0.27	0.61
		std	0.29	0.31	0.37
Agriculture - bare soil	31682	average	0.81	0.17	0.02
		std	0.25	0.23	0.06
Agriculture - woody crops	1910	average	0.80	0.10	0.10
		std	0.26	0.12	0.21
No data	4229	average	0.93	0.06	0.02
		std	0.13	0.10	0.05
Shrubs and Bushes	16745	average	0.80	0.14	0.06
		std	0.19	0.17	0.07

Figure 21: Representation of percent coverage of bare soil, seasonal and perennial vegetation for each of the five EBONE GHC categories: bare soil, shrubs, high bushes, and forest trees, in Avdat area

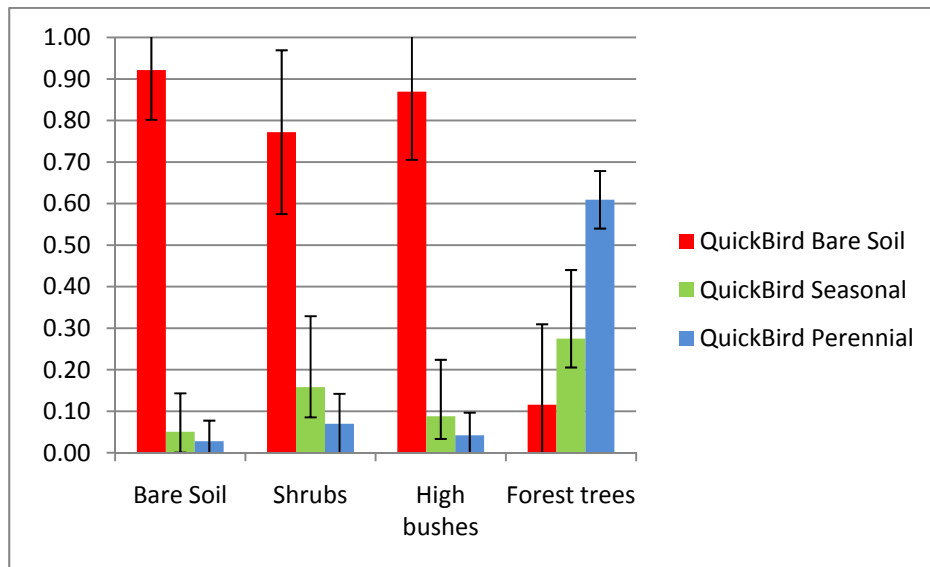
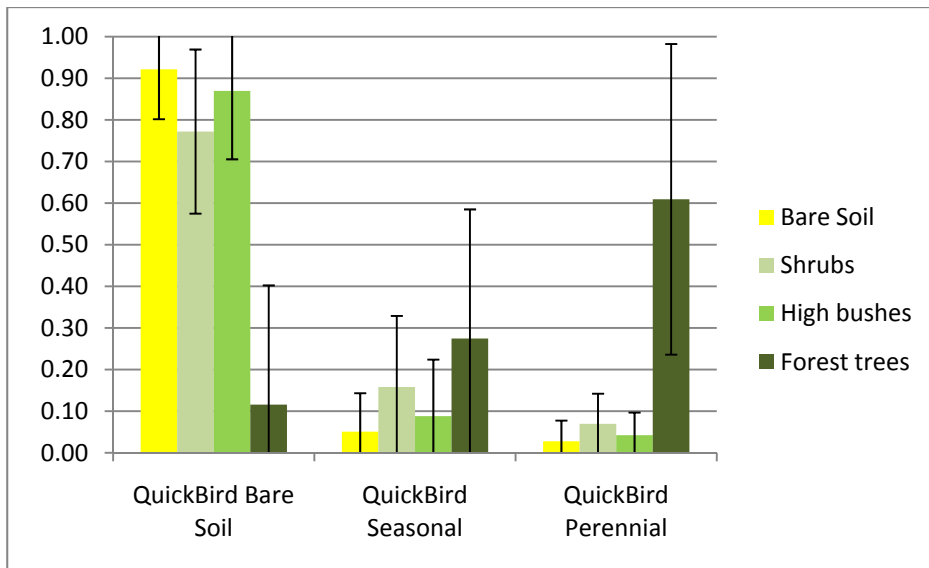


Figure 22: Percent coverage of bare soil, seasonal and perennial vegetation of five EBONE GHC categories: bare soil, shrubs, high bushes, and forest trees, in Avdat area



As we cannot detect height of vegetation using the QuickBird image we combined the shrubs and high bushes category into one category of shrubs.

Figure 23: Representation of percent coverage of bare soil, seasonal and perennial vegetation for each of three EBONE GHC categories: bare soil, shrubs and bushes, and forest trees, in Avdat area

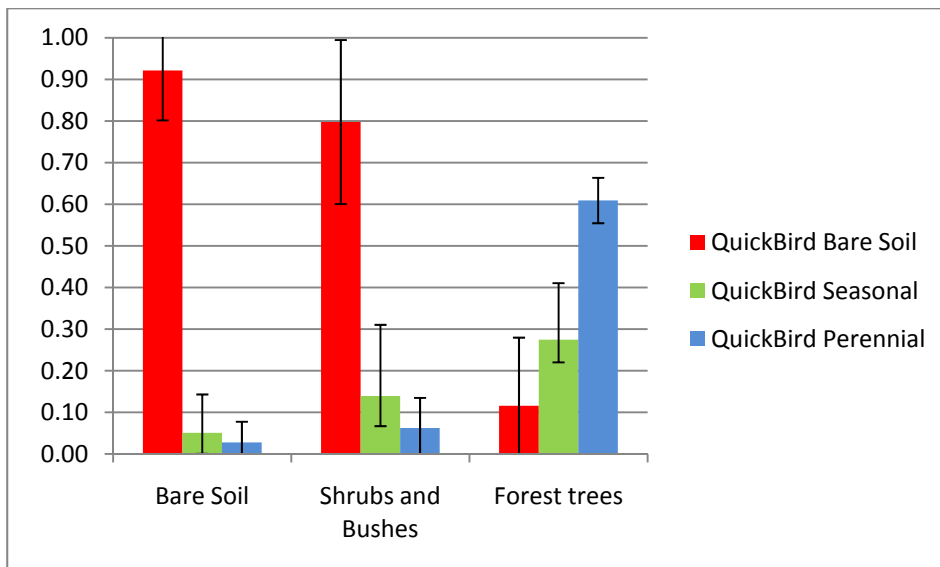


Figure 24: Percent coverage of bare soil, seasonal and perennial vegetation of three EBONE GHC categories: bare soil, shrubs and bushes, and forest trees, in Avdat area

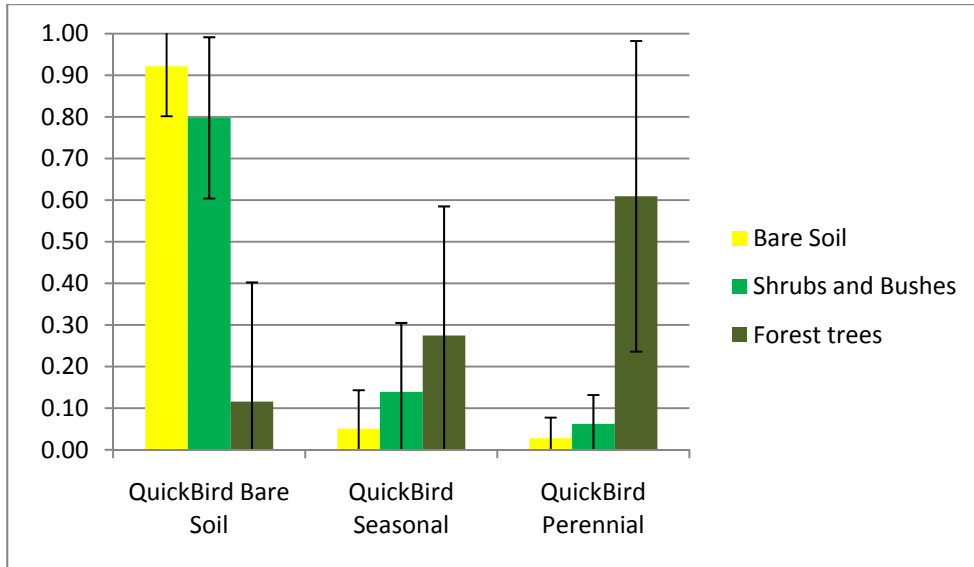


Table 23: Summary of the UnMixing classification results for Avdat area:

	Bare soil coverage	Seasonal vegetation coverage	Perennial vegetation coverage
Bare soil	high	very low	almost none
Shrubs	high	low	low
High bushes	high	low	almost none
Shrubs and high bushes	high	low	low
Forest trees	low	medium	high

Results of the UnMixing classification map show a good ability to map pixels based on their percent coverage of bare soil, seasonal and perennial vegetation per pixel and associate them with the combined EBONE GHC categories: bare soil, mixed shrubs (low and high bushes), and forest trees. Yet, there is an inconsistency with our expectations to have lower % coverage of bare soil associated with shrubs and higher % coverage of seasonal vegetation.

This can be related to seasonal vegetation on the ground that can be detected only on images acquired on appropriate dates. In addition there seem to be a need to redefine the characteristics of the bare soil category in the desert and add more categories representing different desert bare soil types.

6.4.2.1.2 Comparing the results of the UnMixing classification of the QuickBird images with the results of the UnMixing classification of the Landsat TM

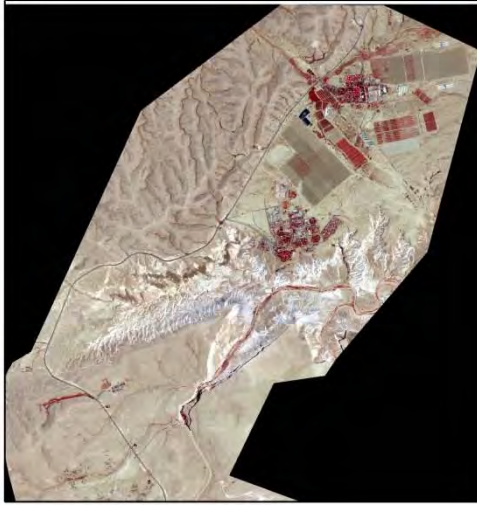
Table 24: Results of the correlation analyses of UnMixing classifications of the Landsat and QuickBird data in Lehavim forest area

	Bare Soil	Seasonal vegetation	Perennial vegetation
Correlation between Landsat and QuickBird data	0.42	0.28	0.39

Results of the correlation show a lower correlation between the the UnMixing classification results of the QuickBird and Landsat images, compared with the correlation observed at Ramat Ha'Nadiv area. Yet, the lower corelation does not necessarily show indicate an error in the classification, and can be due to various reasons that will be discussed in detail at the discussion section.

Figure 25: Example for UnMixing classification results of QuickBird images vs. Landsat images in Avdat area

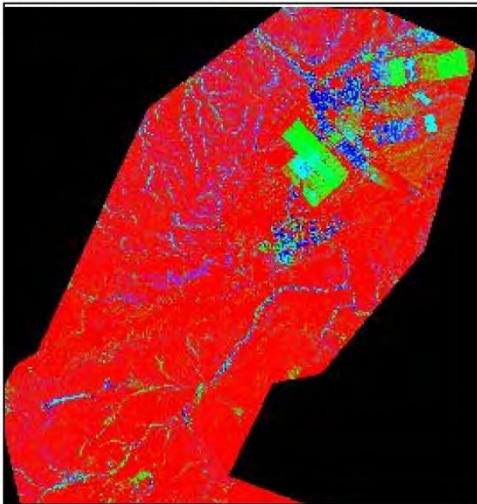
Subset of QuickBird image of
Avdat area: 15/7/2010



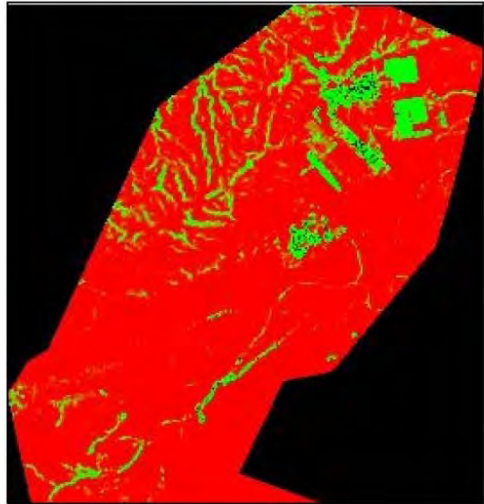
Subset of Landsat image of
Avdat area: 27/7/2001



UnMixing Classification of QuickBird
image: 5/4/2010 and 15/7/2010



UnMixing Classification of Landsat
image: 11/7/2001 and 8/3/2002



- R: Perennial vegetation
- G: Seasonal vegetation
- B: Bare soil

6.5. DISCUSSION

.... Discussion on the 4 methods

Results of the classification maps identify mistakes in the classification when compared with the ground data. Problems are associated both with mistakes in classifying the individual categories as well as differences in the total percent coverage of each category present on the map.

These mistakes are not necessarily errors in the classification and can be related to the following general reasons, applicable to the four classification methods used in the project:

1. Errors may be introduced due to spatial heterogeneity within natural vegetation, which is not captured in the polygonal presentation of EBONE GHC. Most polygons that are associated, in the field, with one dominant EBONE GHC category are on the ground heterogeneous polygons with small patches of vegetation categories. The supervised classification picks-up this heterogeneity.
2. Maquis and forest tree species may have similar reflectance values on the ground. Or on the contrary low-height forest tree species that are still growing may be classified in the field as shrubs although spectrally they look on the image as trees.
3. Problems in distinguishing herbaceous areas from bare soil might require adding the spring image to the classification process and analyzing these seasonal changes. This was achieved successfully with the UnMixing classification of the QuickBird images.

When analyzing specifically the errors associated with the UnMixing classification maps there are other reasons that need to be taken in consideration:

1. When analyzing the data and its results it is important to remember that the spring and summer QuickBird images were registered separately and have some error in their alignment. When linking the two images there is a small error and a pixel does not necessarily link to the exact same pixel on the other image. This can lead to some errors in the results although it is expected to affect only edges of polygons and contributes to a small degree of error.
2. A limiting factor in our ability to correctly classify these EBONE GHC categories is the high standard deviation. In most of the cases the standard deviation values are higher than the average values, which may lead to some mistakes if we base the classification of pixels to defined categories only on their average percent of coverage.

3. The difference in the spatial resolution of the images contributes to changes between the UnMixing classification of the Landsat and QuickBird images.
4. There is a difference in the acquisition year between landsat and QuickBird images. Some of the changes shown in the results of the UnMixing classification is a natural change due to natural vegetation changes occurring over the years (Table 16). Changes observed can be part of a method to monitor changes in the spatial distribution of mediterranean life forms, and to highlight areas where fieldwork is required to understand changes.
5. Seasonal differences because of the different dates of acquisition of the images (Table 25).

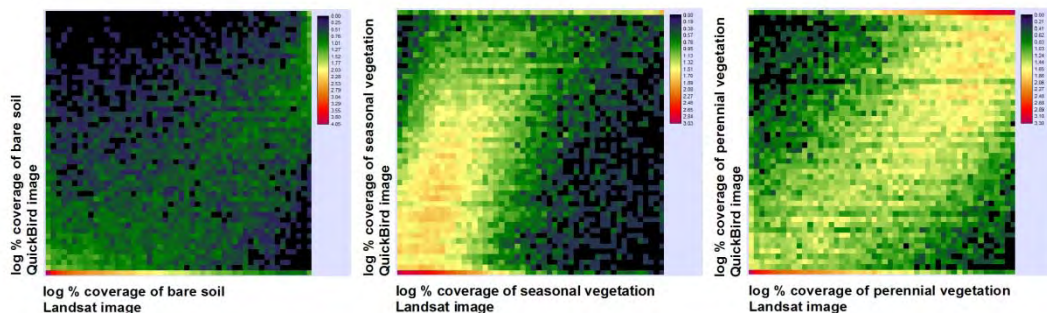
Table 25: List of acquiring dates of the QuickBird and Landsat images for the three study areas: Ramat Ha'Nadiv, Lehavim forest and Avdat

Study area	Season	QuickBird image	Landsat image
Ramat Ha'Nadiv	Spring	20/4/2010	24/3/2002
	Summer	26/7/2010	14/6/2000
Lehavim forest	Spring	22/3/2010	8/3/2002
	Summer	18/7/2010	11/7/2001
Avdat	Spring	5/4/2010	8/3/2002
	Summer	15/7/2010	27/7/2001

6. Lower detectability of sparse vegetation in the Landsat image

Add the scatter plots

Figure 26:



The segmentation classification process as done in the project is a preliminary analysis and needs more study in order to improve its. Additional layers such as: other seasonal QuickBird images, DEM, can be used to improve the classification.

7. Results - MODIS

7.1 Data preprocessing

MODIS product MOD13Q1 was downloaded from <https://wist.echo.nasa.gov/api/>. Altogether 249 images were downloaded of MODIS tiles 20/5, 21/5, 20/6 and 21/6, corresponding to the dates between 18/2/2000-4/3/2000 and 3/12/2010-18/12/2010. The four tiles were mosaicked and reprojected into Israel Transverse Mercator (ITM, also known as Israel New Grid) coordinate system at a spatial resolution of 250 m. The time series thus included four spectral bands (bands 1-3 and 7, corresponding to the red, NIR, blue, and MIR [2105-2155nm]) and the following variables: the normalized difference vegetation index (NDVI; Tucker, 1979), the enhanced vegetation index (EVI; Huete et al., 2002), MODIS pixel reliability flag and MODIS vegetation index quality flag (described in https://lpdaac.usgs.gov/lpdaac/products/modis_products_table/vegetation_indices/16_day_l3_global_250m/mod13q1). NDVI time series were smoothed using an Inverse Fourier transformation (with 20 harmonics) as applied in Idrisi Taiga Earth Trends Modeler. Trends were calculated on both the EVI and NDVI time series, using the raw and the smoothed time series. The following statistics were calculated using Idrisi Taiga Earth Trends Modeler:

- Linear correlation calculates the R of the least square correlation of the series with a linear trend. It maps out the Pearson Product-Moment linear correlation between the values of each pixel over time and a perfectly linear series. This is a commonly used form of trend analysis, but it is sensitive to noise in short series
- Linear trend calculates the intercept and slope of the least square correlation of the series with a linear trend.

- Median trend calculates the non-parametric Theil-Sen slope and intercept of the series. This is a robust non-parametric trend operator that is highly recommended for assessing the rate of change in short or noisy series (Hoaglin et al., 2000). It is calculated by determining the slope between every pairwise combination and then finding the median value.
- Monotonic trend calculates the non-parametric Mann-Kendall Tau correlation coefficient. It provides a non-linear trend indicator that measures the degree to which a trend is consistently increasing or decreasing. It has a range from -1 to +1. A value of +1 indicates a trend that continuously increases and never decreases. The opposite is true when it has a value of -1. A value of 0 indicates no consistent trend. It is calculated in a similar fashion to the median trend. All pairwise combinations of values over time are evaluated at each pixel and a tally is made of the number that are increasing or are decreasing with time. The Mann-Kendall statistic is simply the relative frequency of increases minus the relative frequency of decreases.
- Mann-Kendall significance calculates the z and p values of the significance of the monotonic trend.

While smoothing removes noises (e.g., due to clouds) thus enabling better detection of gradual trends and changes in vegetation cover, it may also remove sudden changes in vegetation due to disturbances such as fire. Therefore we identified fire scars using the raw unsmoothed spectral bands. Fire scars were mapped using the Relative differenced Normalized Burn Ratio (RdNBR; Miller and Thode, 2007), which is based on the Normalized Burn Ratio (NBR; Key and Benson, 1999), and was computed as following:

$$NBR = \frac{NIR - MIR}{NIR + MIR} \quad (2)$$

$$dNBR = \text{prefireNBR} - \text{postfireNBR} \quad (3)$$

$$RdNBR = \frac{dNBR}{\sqrt{|\text{prefireNBR}|}} \quad (4)$$

7.2 Results

7.2.1 Trends in NDVI values

Overall the trends identified using the EVI and NDVI time series, whether using the raw data or the smoothed times series, were quite similar. The following maps present the linear trends identified using smoothed NDVI time series, for those areas where the Mann-Kendall significance was less than 0.025 (Figure 1). The non-parametric Theil-Sen slope and Mann-Kendall TAU are shown in Figure 2.

Whereas there were areas with significant positive and negative trends in NDVI values, examining the slopes of the trends (expressing the change in NDVI values with time), the overall trend is of a decrease in NDVI values, especially in the transition zone south of Jerusalem-Ashdod.

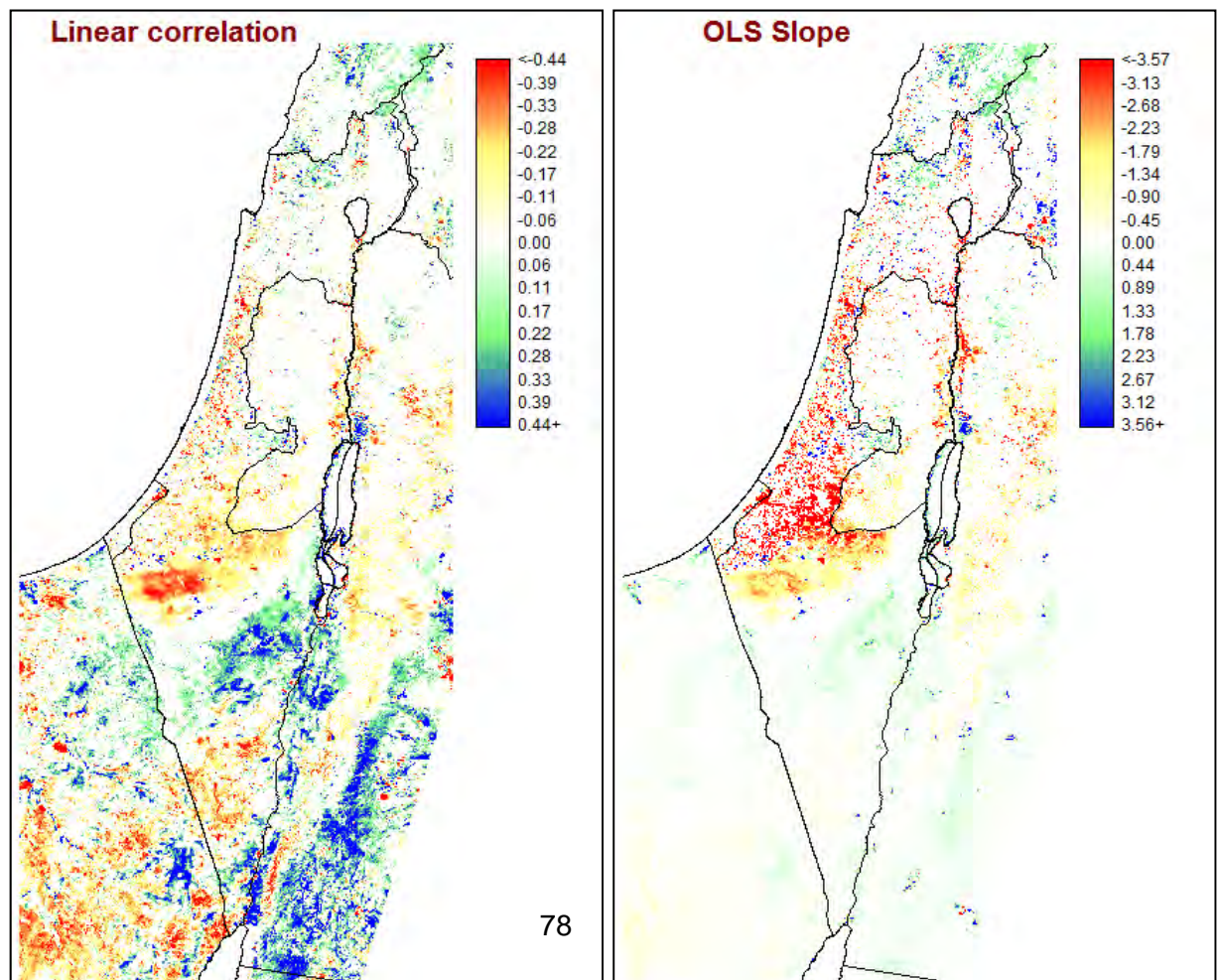


Figure 1: Linear trends in smoothed NDVI values

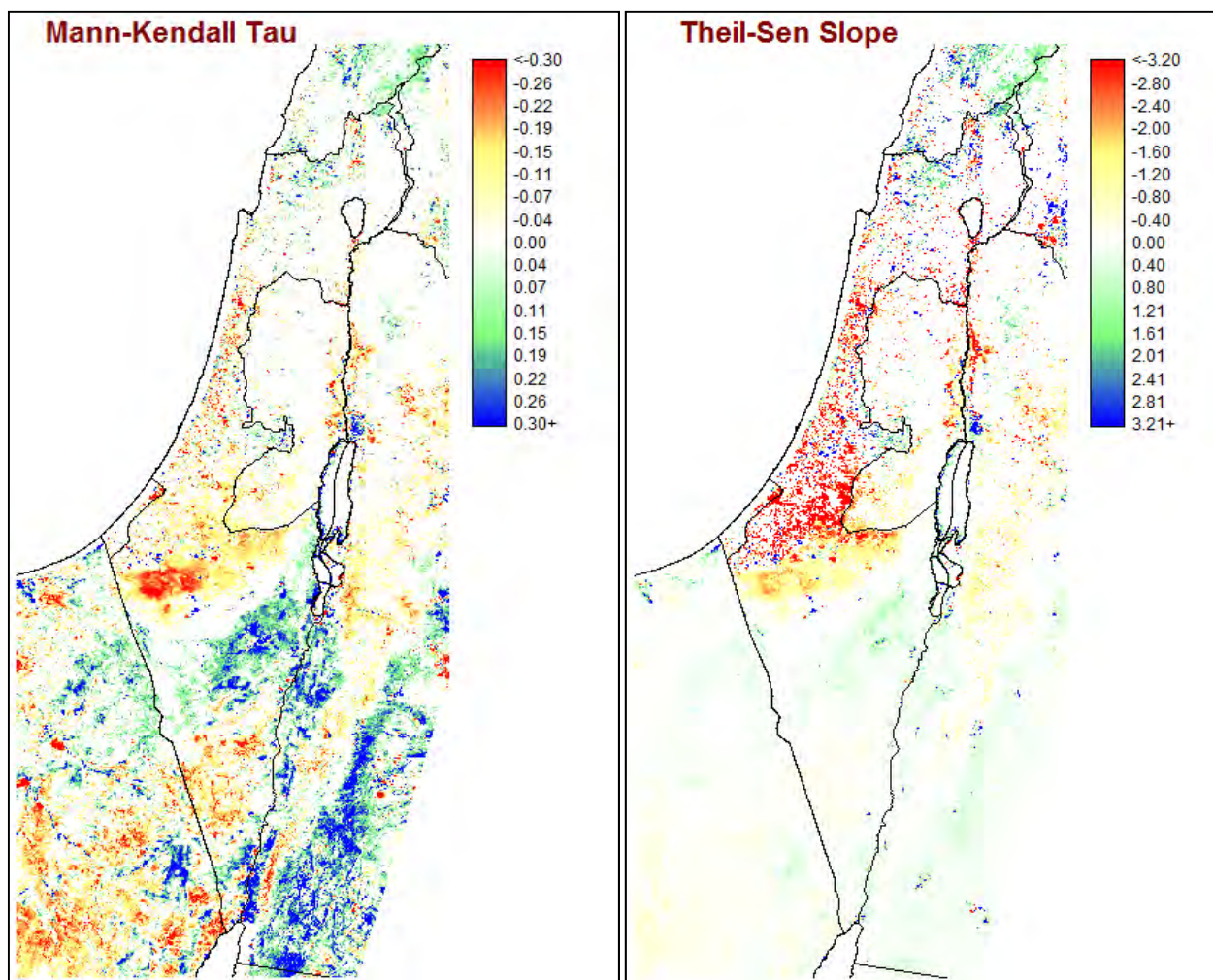


Figure 2: Non-parametric trends in smoothed NDVI values

Specific examples of gradual changes detected using these images are given below.

1. Decline in primary productivity as a function of decreasing rainfall

Within the transition zone between the Mediterranean and desert climate regions, two areas were selected in which a significant decrease in vegetation was detected: the Nizzana dunes in the west, and South Hebron mountains (Figure 3). The observed decrease in vegetation indices values seem to correspond well with lagged rainfall ($r = 0.73$, summed over a period of 2.5 months, for the Nizzana dunes area: Figure 4; $r = 0.77$, summed over a period of two months, for the South Hebron mountains area: Figure 5).

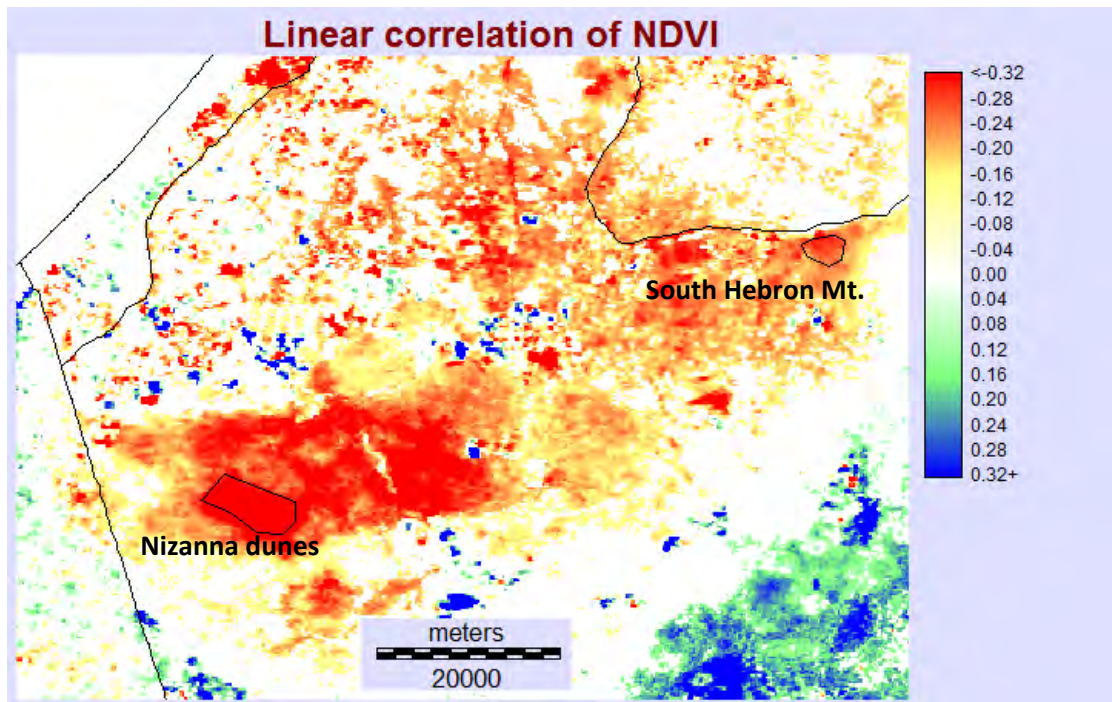


Figure 3: Linear correlation of NDVI values with time, 2000-2010.

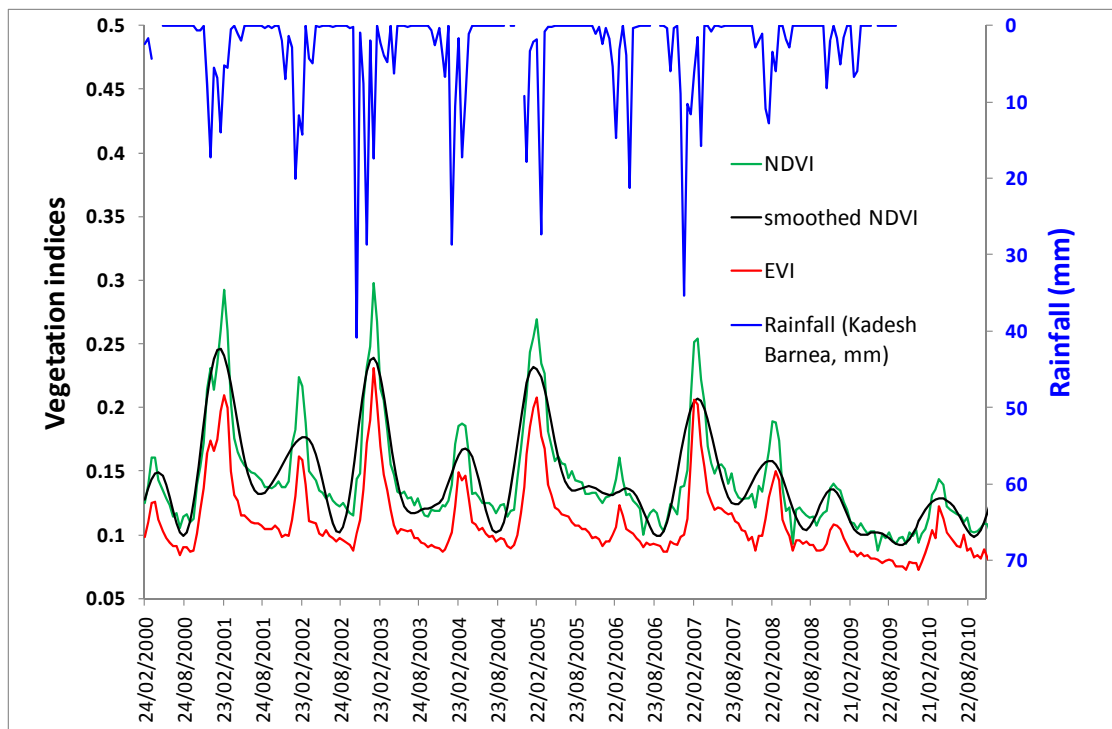


Figure 4: Changes in vegetation indices values and in rainfall in the Nizzana dunes area

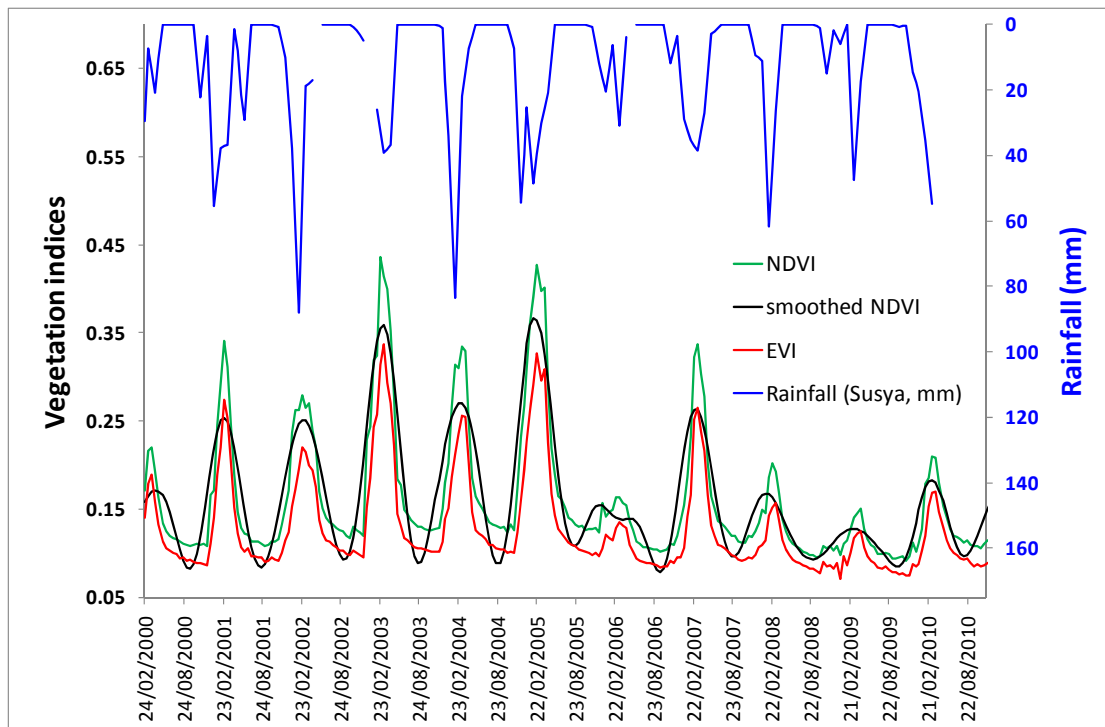


Figure 5: Changes in vegetation indices values and in rainfall in the South Hebron Mountains area

2. Vegetation recovery following fire.

Following forest fires vegetation recovers, and these trends are evident from time series of vegetation indices. In Figure 6 an area within the 1995 fire of Sha'ar ha Guy is delineated. NDVI values increased until 2005, ten years after the fire, and have since remained relatively stable, indicating that NDVI became saturated and cannot monitor vegetation recovery any longer for that area (Figure 7). Note that the EVI didn't perform well as the NDVI, and does not show an increase in vegetation cover. Similar patterns of vegetation recovery following fire were observed in other fire scars in Israel (not shown).

3. Vegetation recovery following the stop of grazing and cutting of vegetation

The Land of Israel was under centuries of human pressures of grazing, clearing (cutting of vegetation) and fire. These practices came to their ending with afforestation efforts and nature conservation, mostly after the establishment of the State of Israel (Carmel and Kadmon, 1999; Kadmon and Harari-Kremer, 1999; Levin et al., 2003). The Hermon mountain came under Israel control in 1967, and as evident from the vegetation indices time series, vegetation cover on the mountain at elevations higher than 1,000 meters.

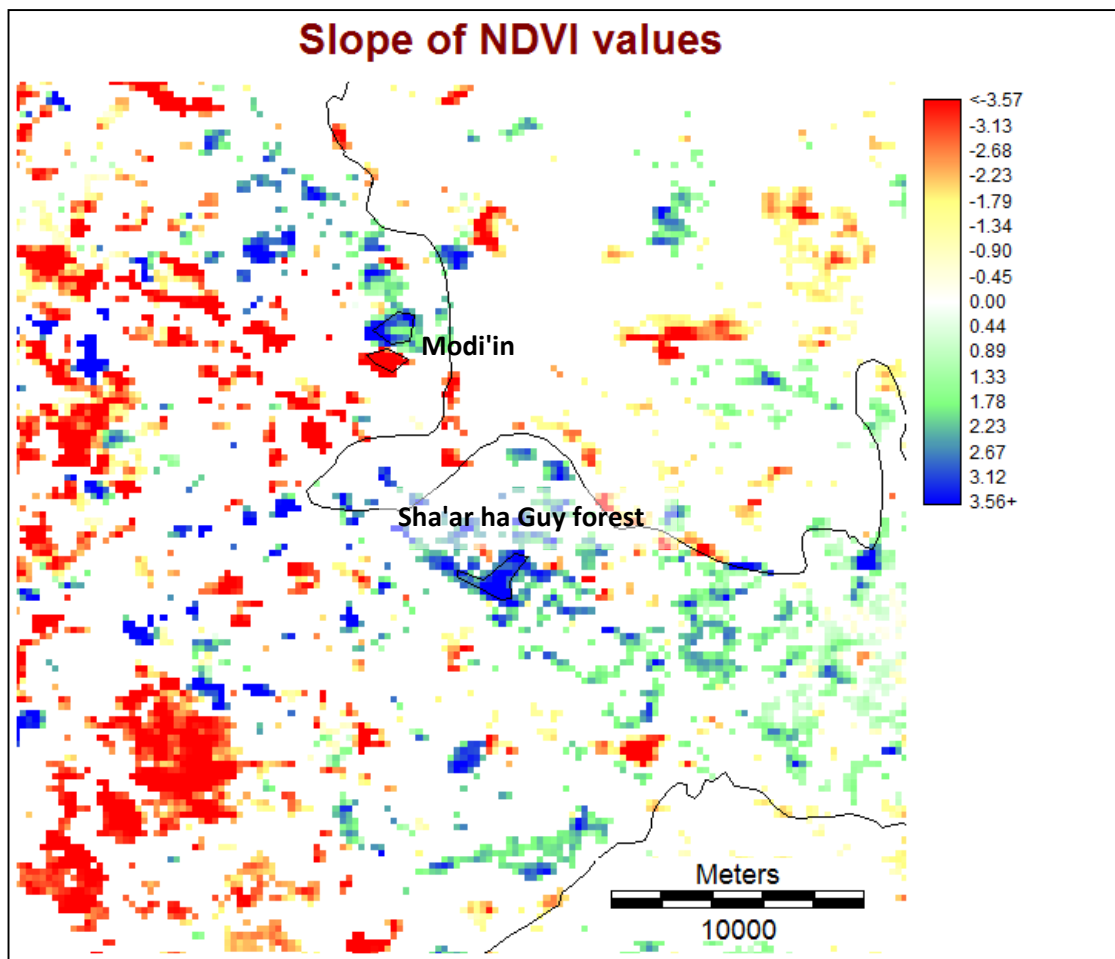


Figure 6: Regions of interest to the west of Jerusalem.

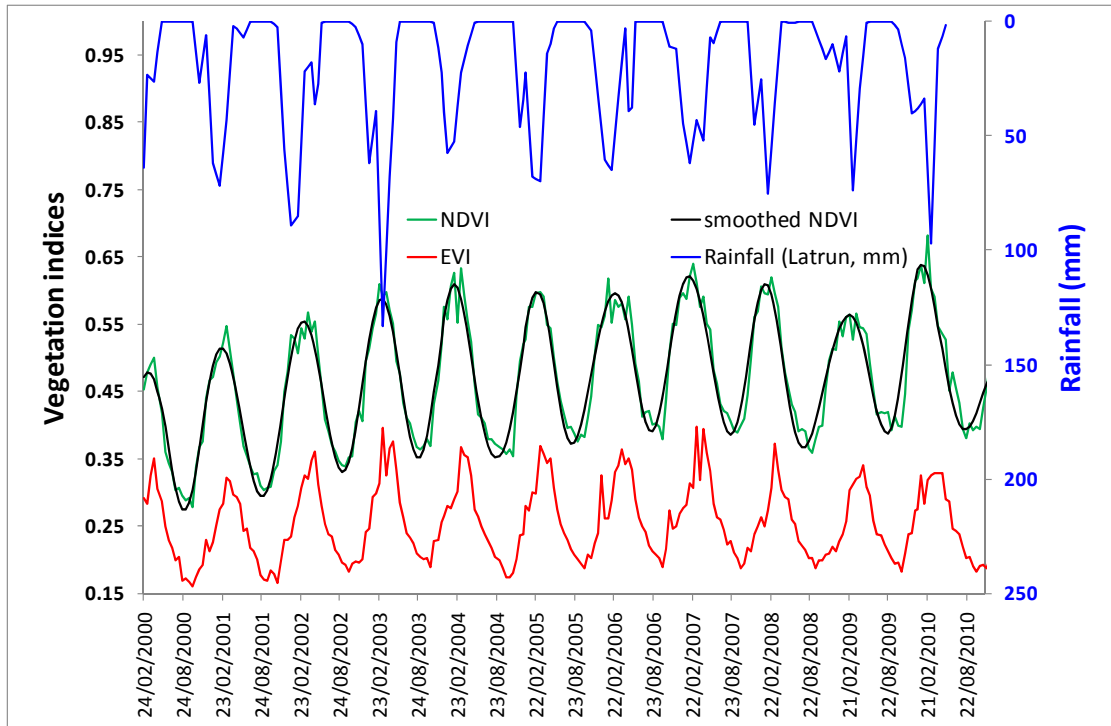


Figure 7: Changes in vegetation indices values and in rainfall in the area burnt during the forest fire of Sha'ar ha Guy, 1995

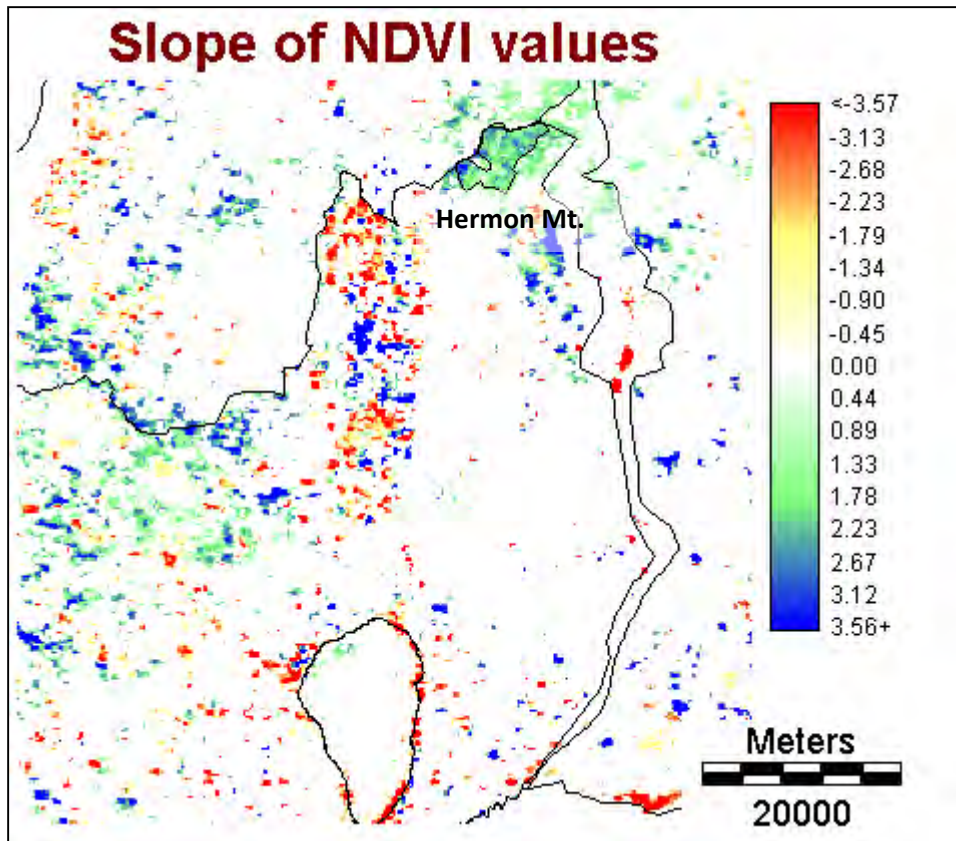


Figure 8: Hermon mountain region of interest.

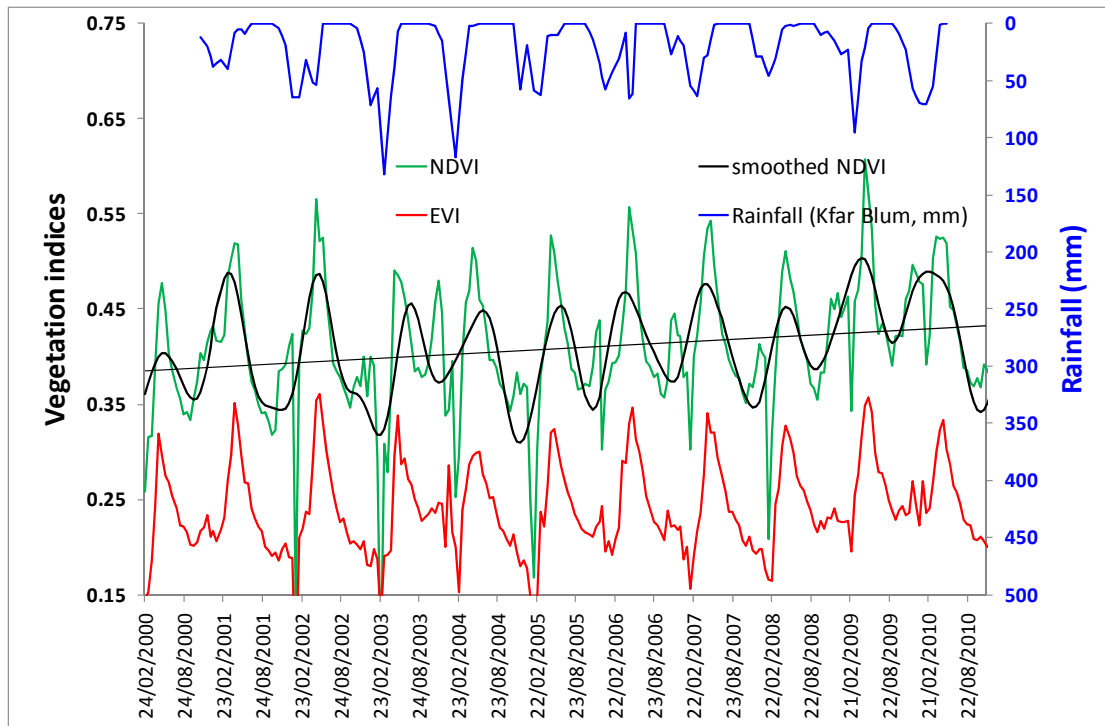


Figure 9: Changes in vegetation indices values and in rainfall in the higher elevations of the Hermon Mt.

4. Changes in vegetation cover due to development

Israel's population increases at a rapid rate (compared with OECD countries), and new towns and neighbourhoods are constantly built. The city of Modi'in, halfway between Tel-Aviv and Jerusalem, was founded in 1996. Within newly built-up areas two processes can be observed: at first, vegetation cover decreases abruptly, as natural vegetation is removed in order to build roads and buildings (southern part of Modi'in; Figure 6, 10). Later on, vegetation cover increases, as public and private gardens are developed (northern part of Modi'in; Figure 6, 11).

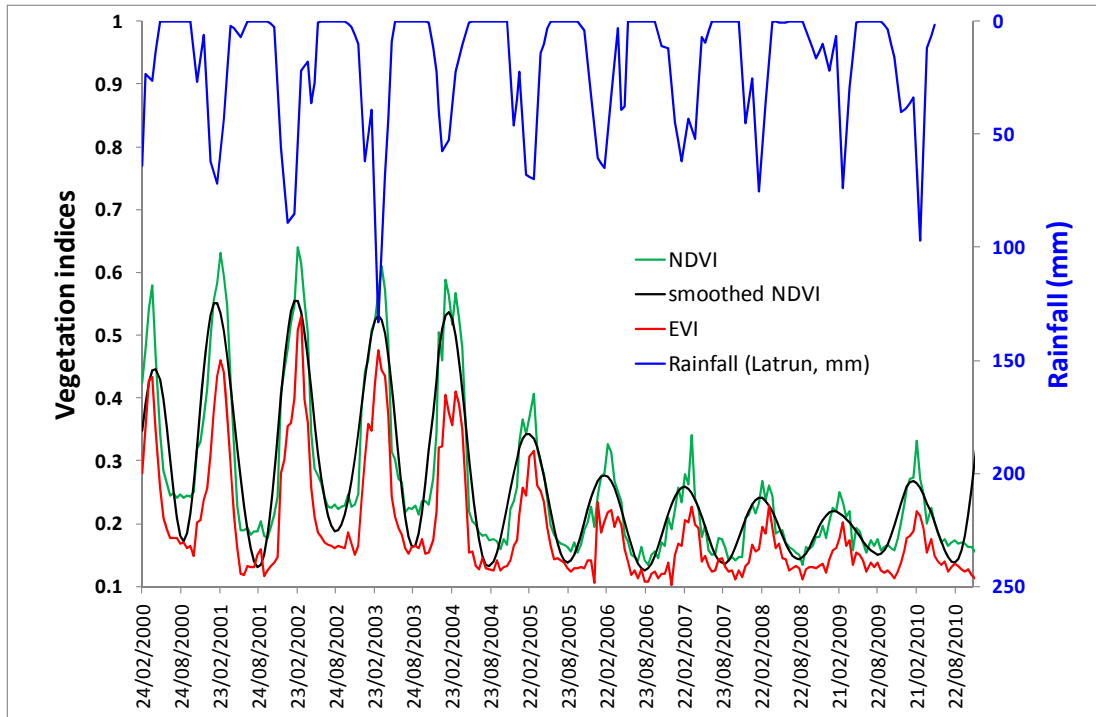


Figure 10: Southern part of Modi'in – a new neighbourhood whose development works started in 2004.

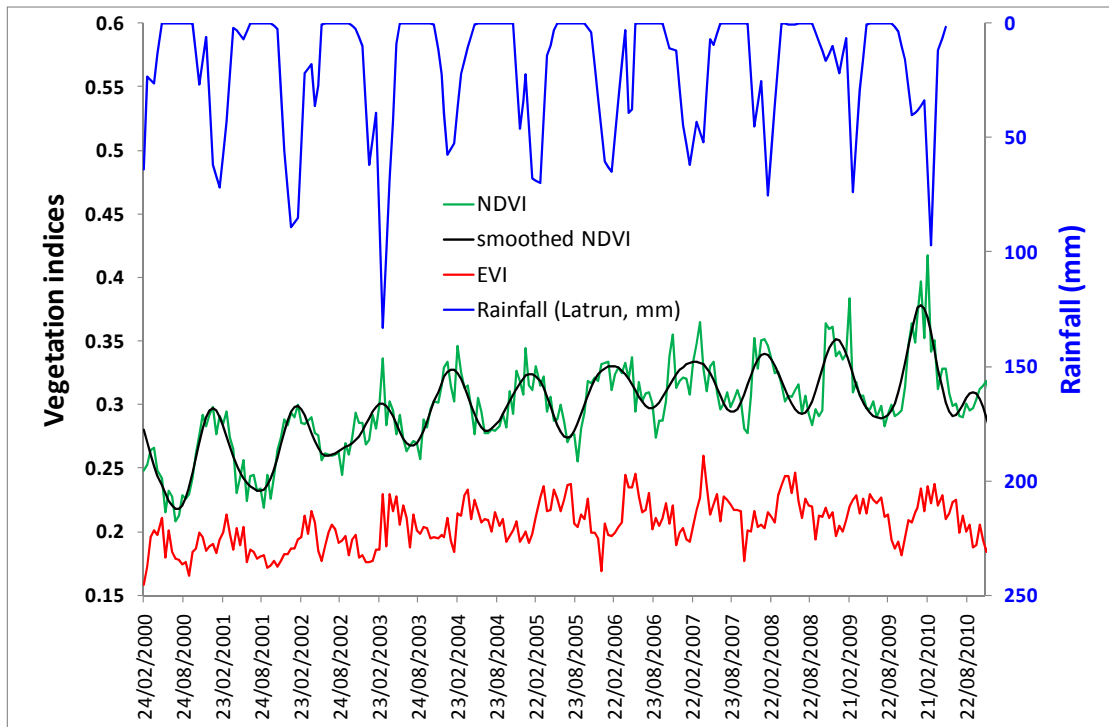


Figure 11: Northern part of Modi'in – gradual increase in vegetation cover within the new city.

7.3.2 Supervised classification of MODIS imagery

Following the approach of dynamic habitat approach of Duro et al. (reference), we calculated the minimum, mean, standard deviation and the coefficient of variation (CV) from the fourier denoised NDVI time series (Figure 12).

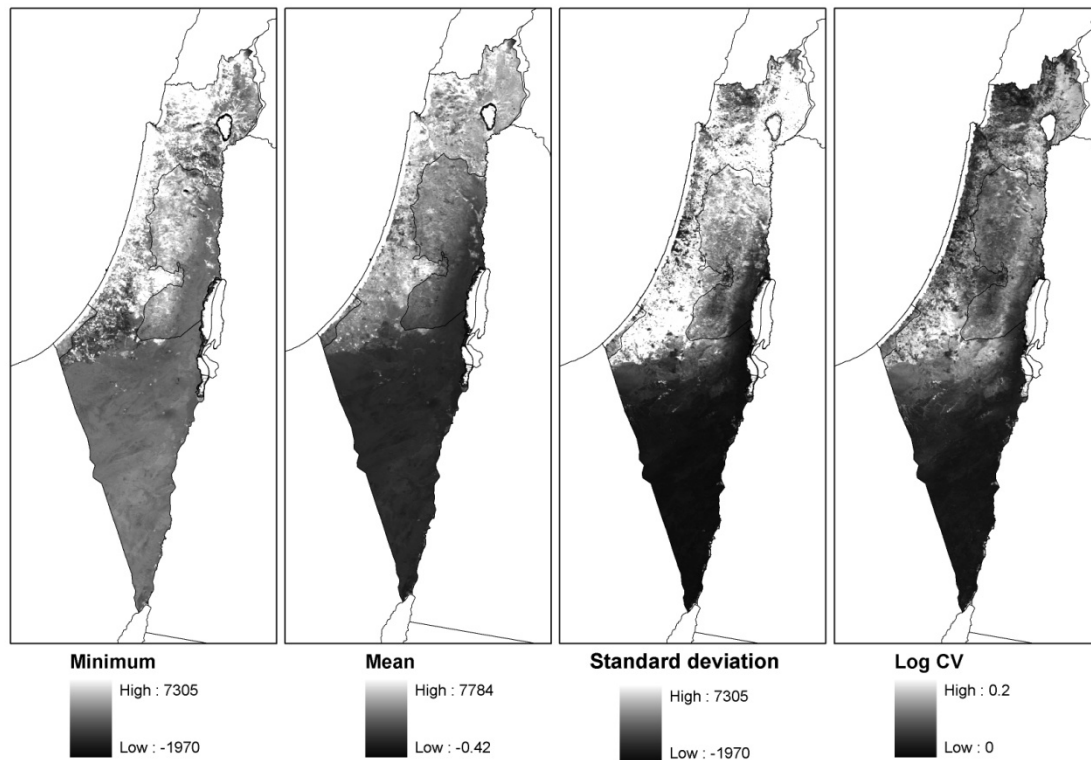


Figure 12: Basic statistics of the NDVI time series

We used these four layers within a Neural Network supervised classifier, using ten regions of interest, representing a broad classification of vegetation types in Israel, based on their seasonality. In seasonality we mean the temporal variability within and between years in NDVI values. Observing the average NDVI time series for the areas classified in Figure 15 are shown in Figure 13. The seasonal range of NDVI values may be similar between Mesic maquis and water bodies, however the mean NDVI values of the maquis are much higher than those of the water bodies. To simplify these time series, we calculated four statistics for each pixel: the mean, minimum and standard deviation of NDVI values. These are shown for the areas mapped in Figure 15 in the four barcharts of Figure 14. For example, extreme desert areas are characterized by low mean, minimum and standard deviation of NDVI values.

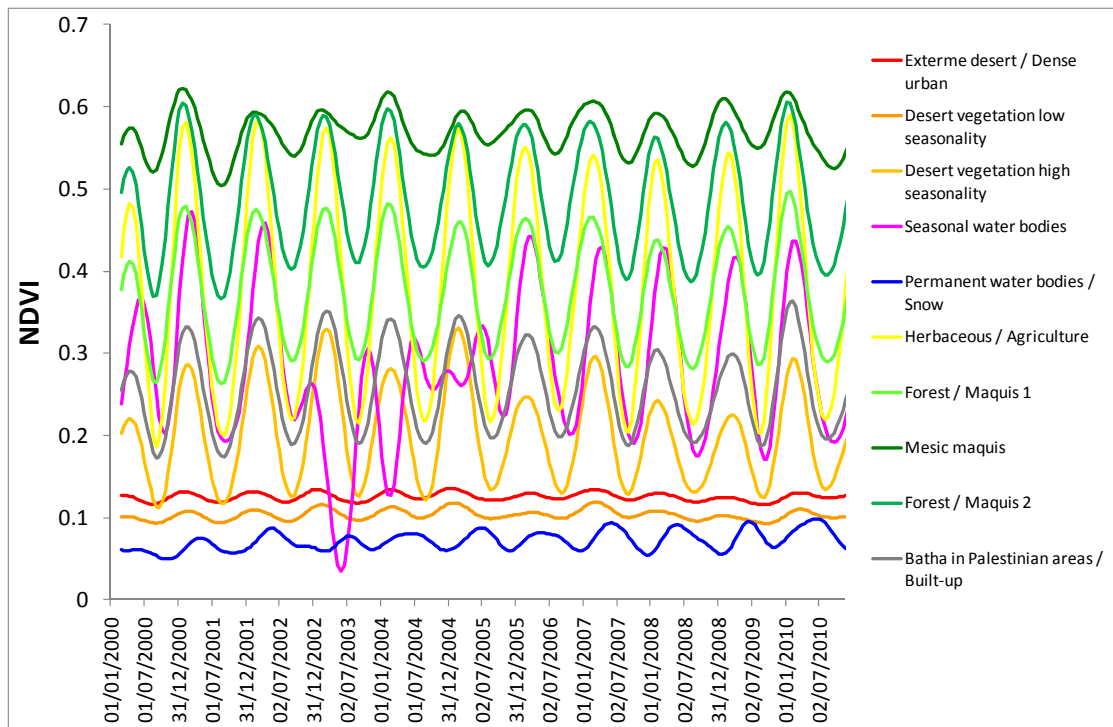


Figure 13: average NDVI time series for the areas classified in Figure 15.

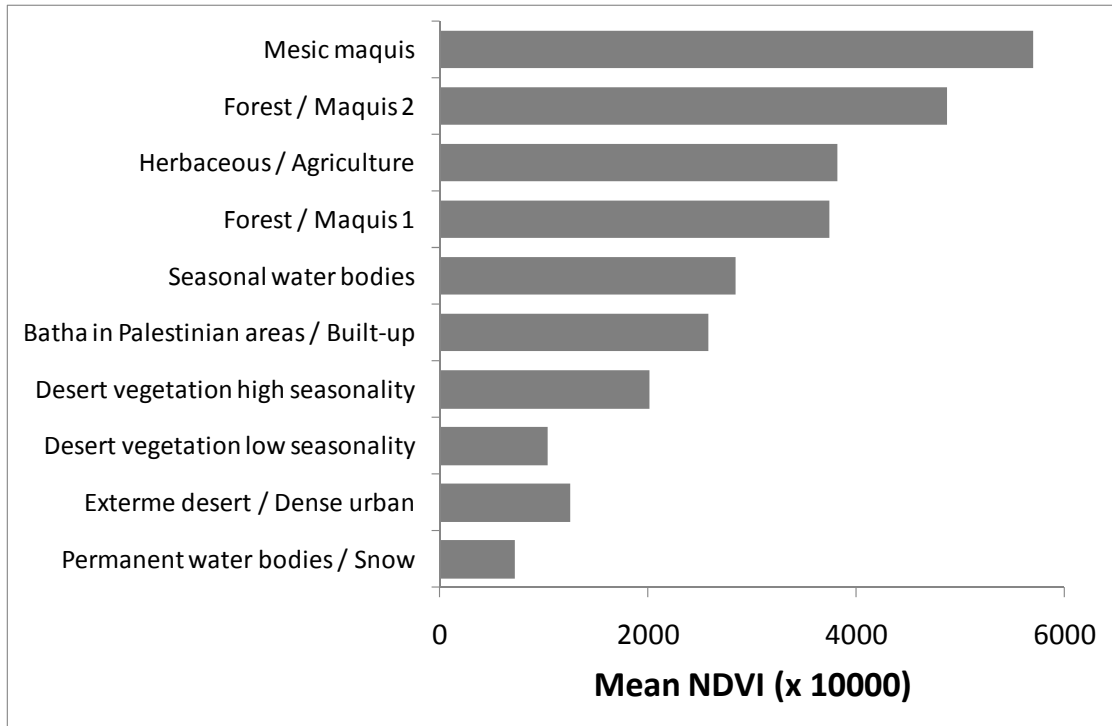


Figure 14a: Average Mean of NDVI values in the areas mapped on Figure 15.

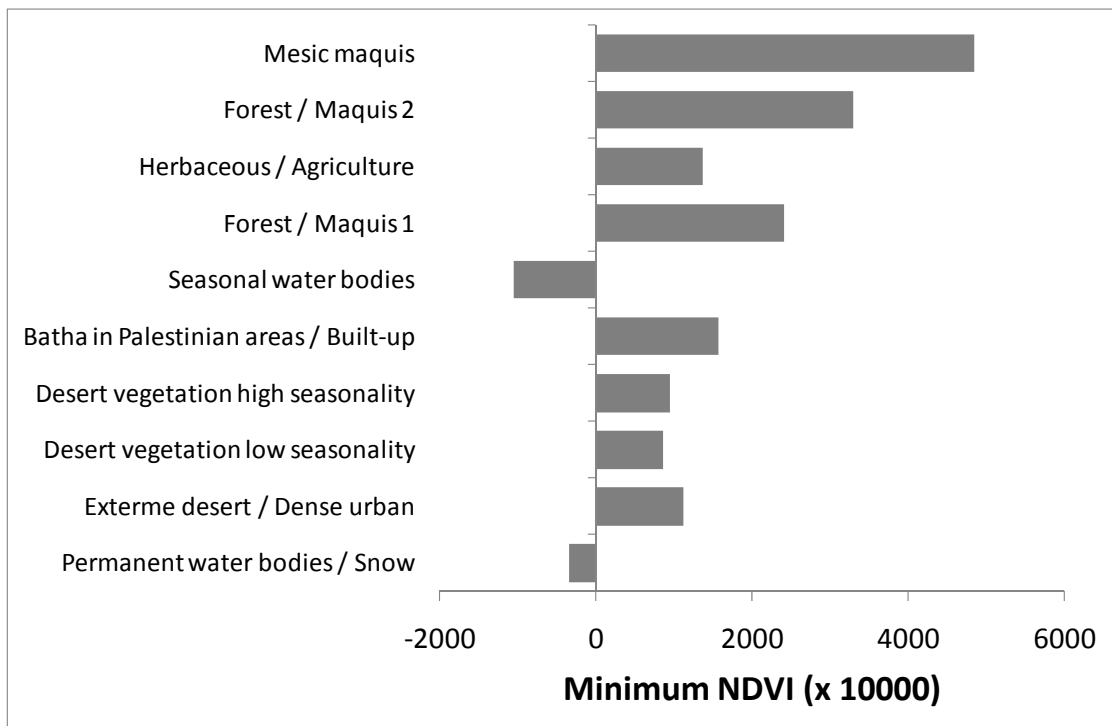


Figure 14b: Average Minimum of NDVI values in the areas mapped on Figure 15.

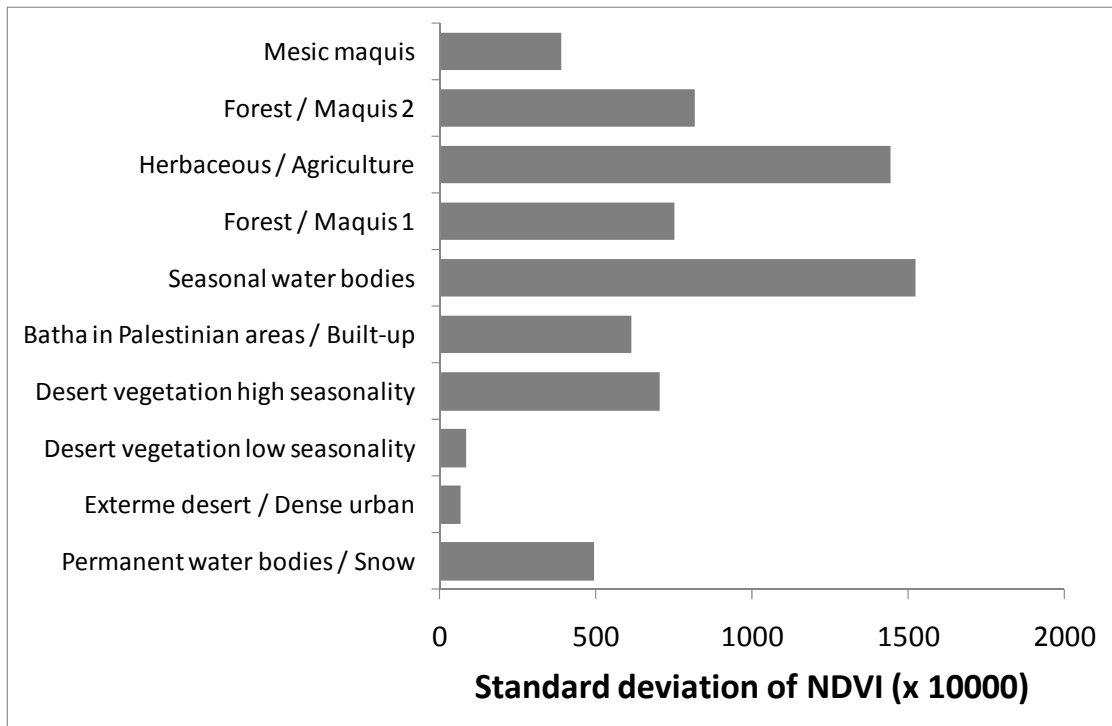


Figure 14c: Average Standard deviation of NDVI values in the areas mapped on Figure 15.

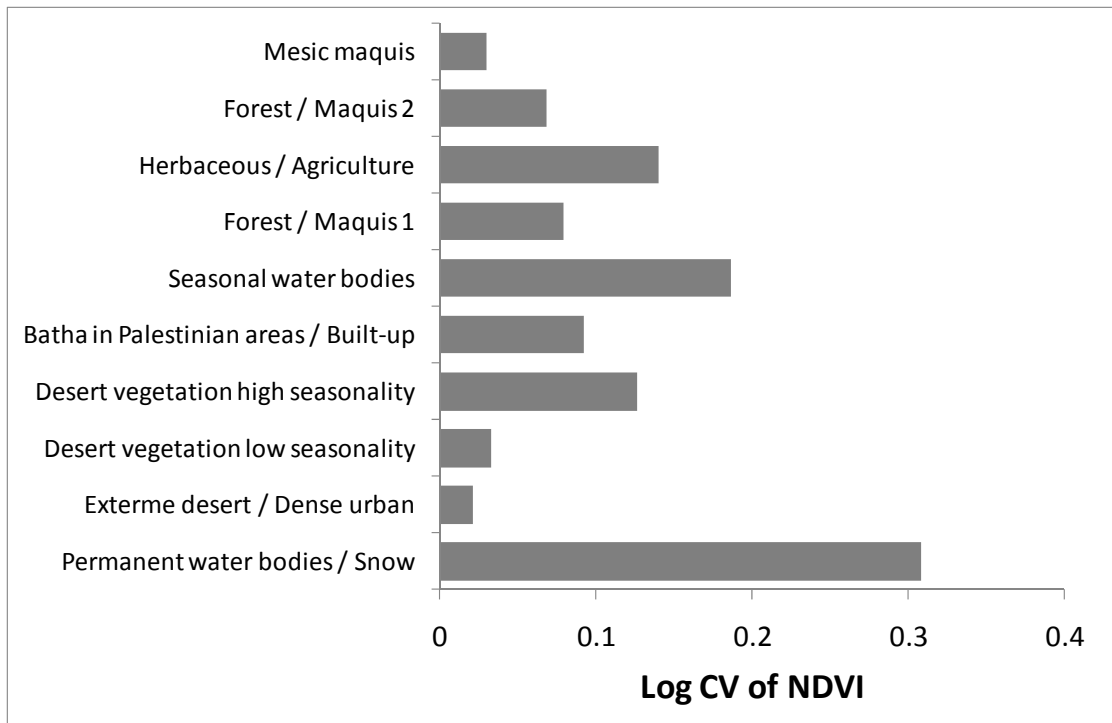


Figure 14d: Average Log CV of NDVI values in the areas mapped on Figure 15.

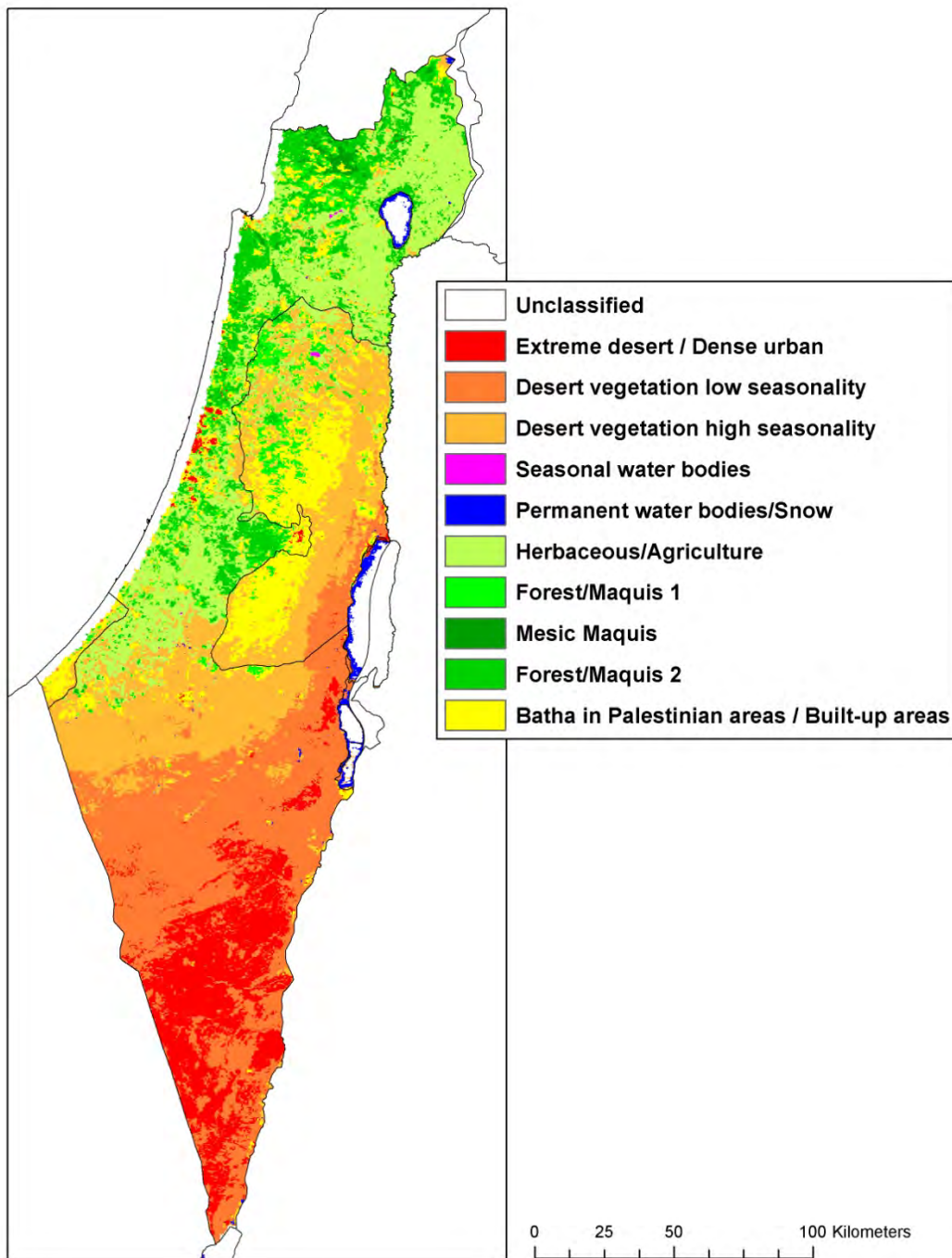


Figure 15: Neural Net classification of MODIS imagery based on four statistics: mean, minimum, standard deviation and Log CV of the denoised NDVI time series.

7.3.3 Differentiating between planted coniferous forests and Mediterranean maquis

One of the major aims of this study was to examine whether satellite imagery can enable us to differentiate between planted coniferous stands and Mediterranean maquis. We conducted this part of the study in the following steps:

3.3.1 Calibration layers

We used the JNF forest stands layer to identify all stands of coniferous planted forests. We used the INPA layer (reference to Amos Sabah) of natural vegetation to identify areas of natural vegetation (excluding coniferous trees). These two layers were intersected with our unmixed Landsat product (resampled to 250 m), leaving in the analysis only those pixels where perennial cover was greater than 75% (within a MODIS pixel). We then sieved out patches whose area was less than four MODIS pixels to reduce possible spectral mixing within pixels, so as to remain with areas where perennial cover is high. We then examined the average time series profiles within planted pine forests and within Mediterranean maquis in rainfall belts of 100 mm (using the rainfall layer used in Kadmon and Danin, 1997; Figure 22).

As can be seen in Figure 16 and 17, as rainfall increases, minimum NDVI values increase and the coefficient of variation decreases, especially for planted pine forests.

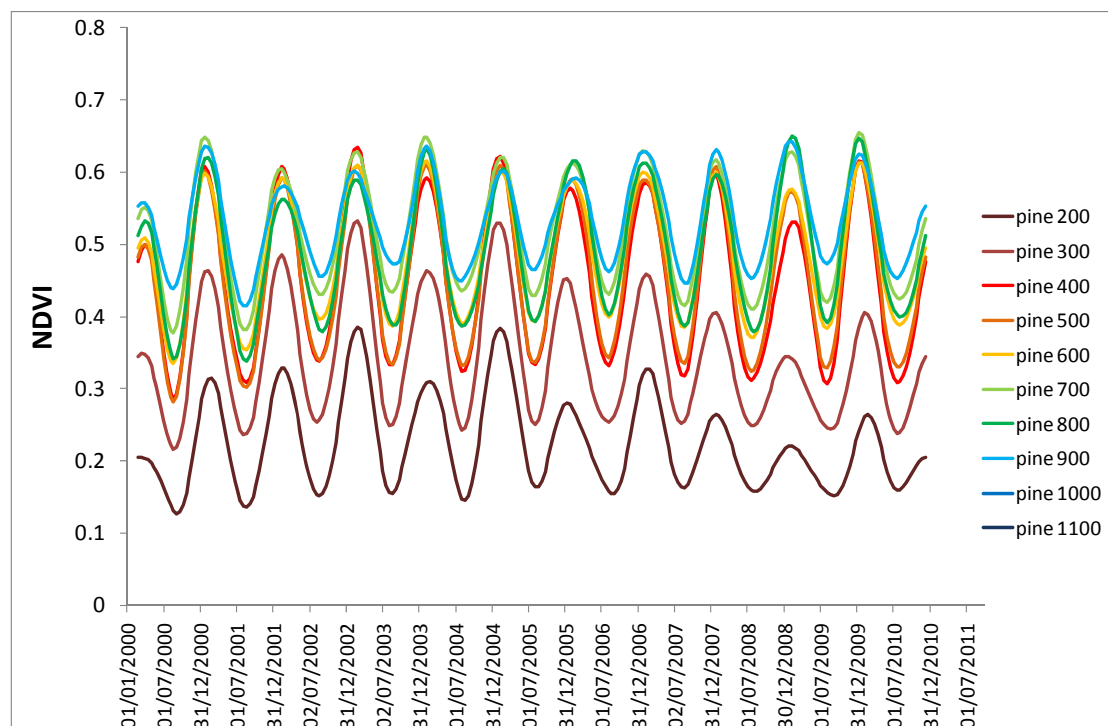


Figure 16: Time series profiles of NDVI within planted pine forests in 100mm rainfall belts

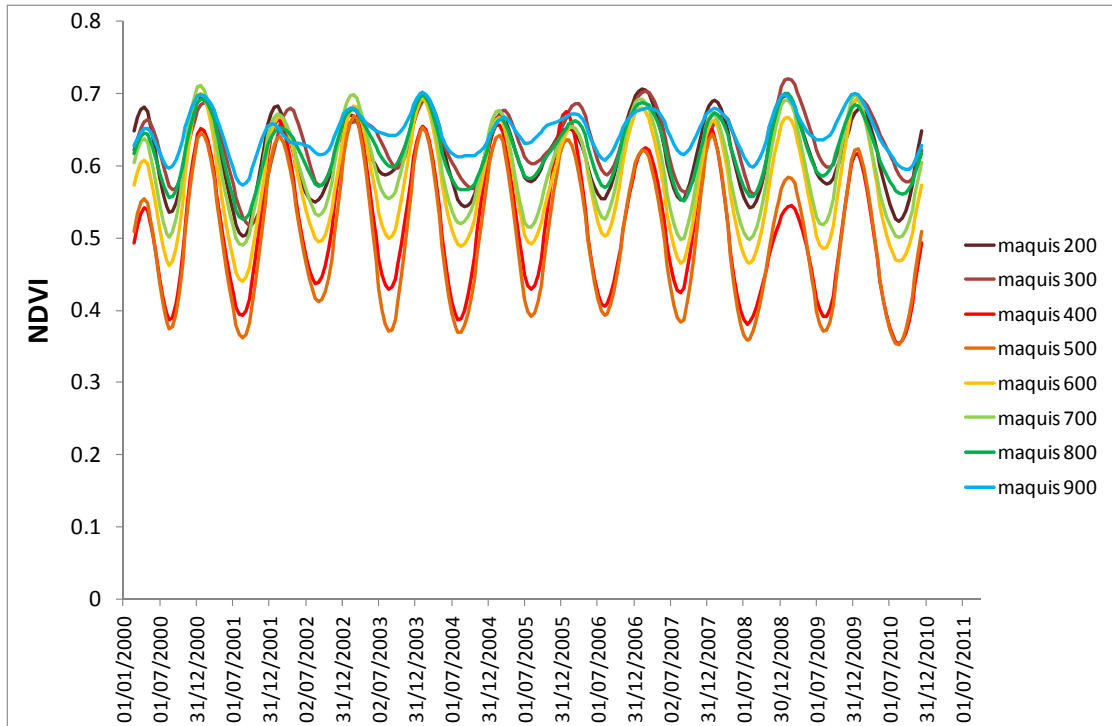


Figure 17: Time series profiles of NDVI within Mediterranean maquis in 100mm rainfall belts

In addition, we found that in all rainfall belts, the minimum NDVI values are higher in the maquis than in the pine stands, and the CV of NDVI values is lower in the maquis than in the pine stands (Figures 18-20).

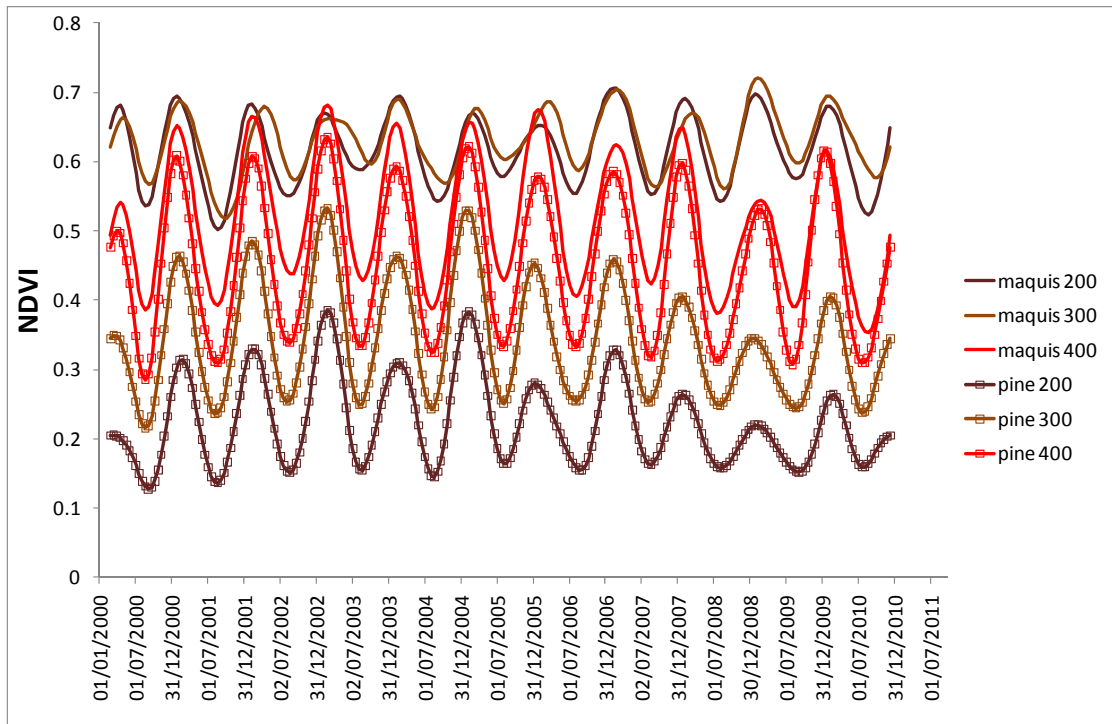


Figure 18: Comparison of time series profiles of NDVI between Mediterranean maquis and planted pins stands between 150-450 mm/year

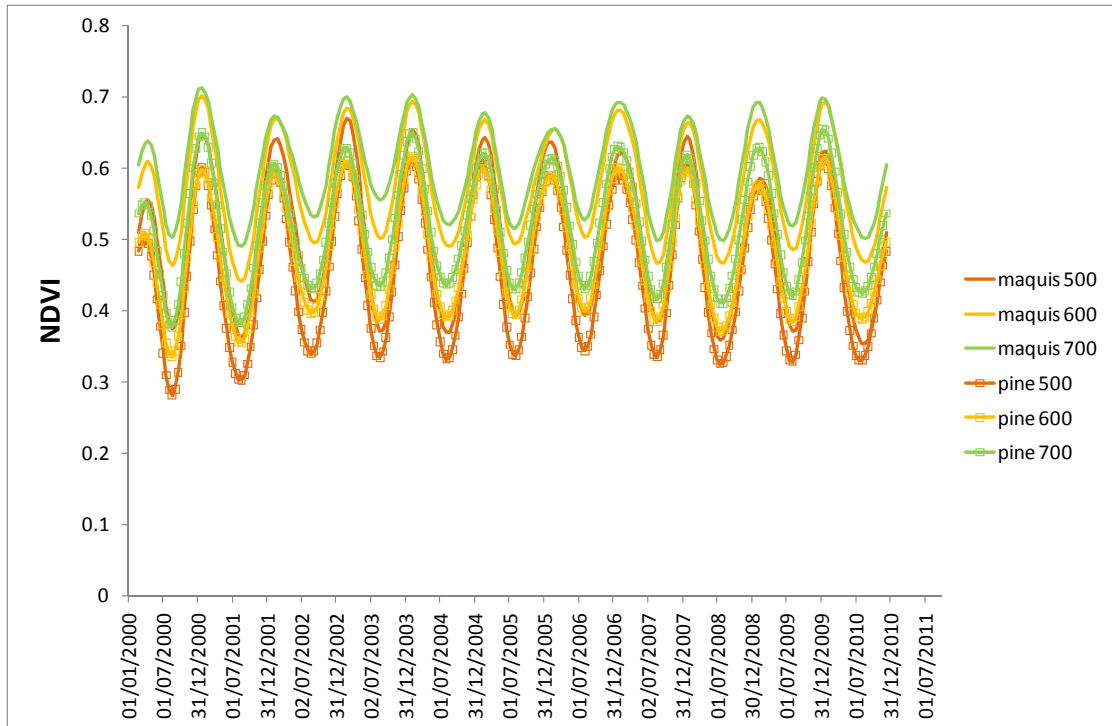


Figure 19: Comparison of time series profiles of NDVI between Mediterranean maquis and planted pins stands between 450-750 mm/year

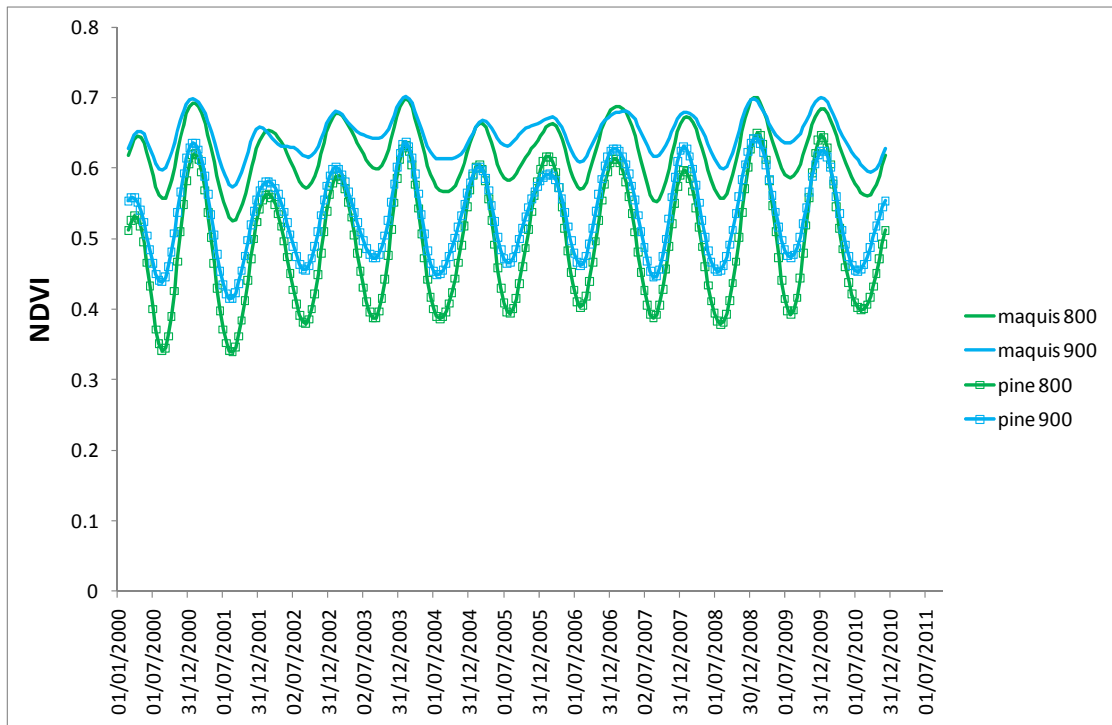


Figure 20: Comparison of time series profiles of NDVI between Mediterranean maquis and planted pins stands between 750-950 mm/year

7.3.3.2 Decision tree classification

We identified threshold values of minimum and CV of NDVI values within each rainfall belt, to differentiate between coniferous forest stands (mostly pines in Israel) and mediterranean maquis. These were applied within a decision tree in Envi (Figure 21).

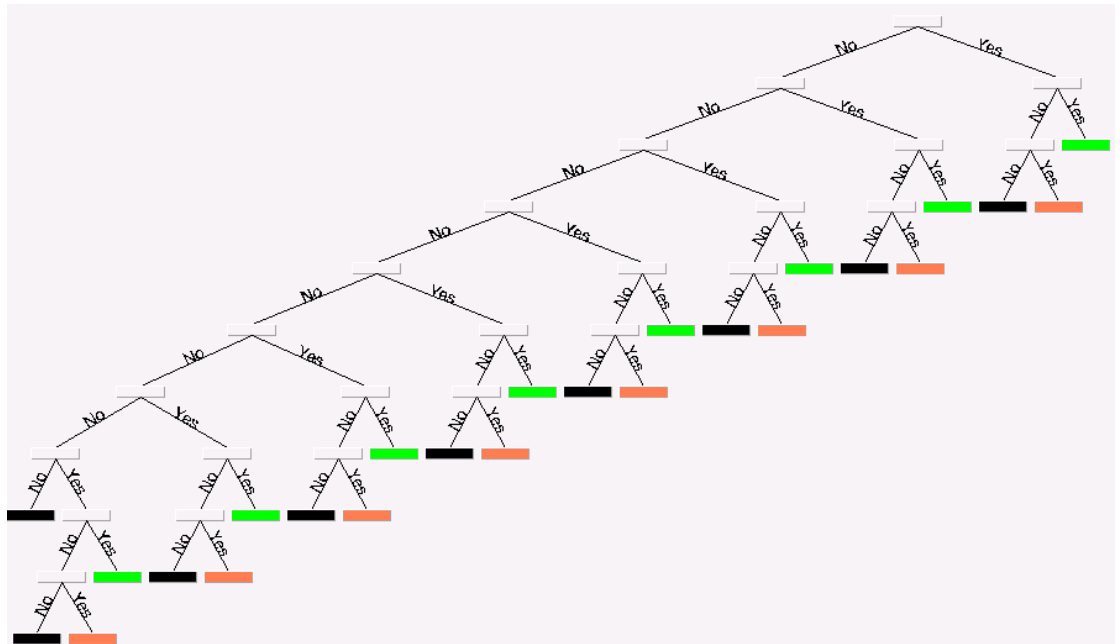


Figure 21: General scheme of the decision tree classification

The output map containing two classes was intersected with the forest areas as identified by the neural network supervised classification (shown in Figure 15). The resulting map is shown in Figure 22.

7.3.3.3 Accuracy assessment

The accuracy of the classified map of planted coniferous stands and Mediterranean maquis was estimated using GIS layers of the JNF and INPA as described above (Figure 22).

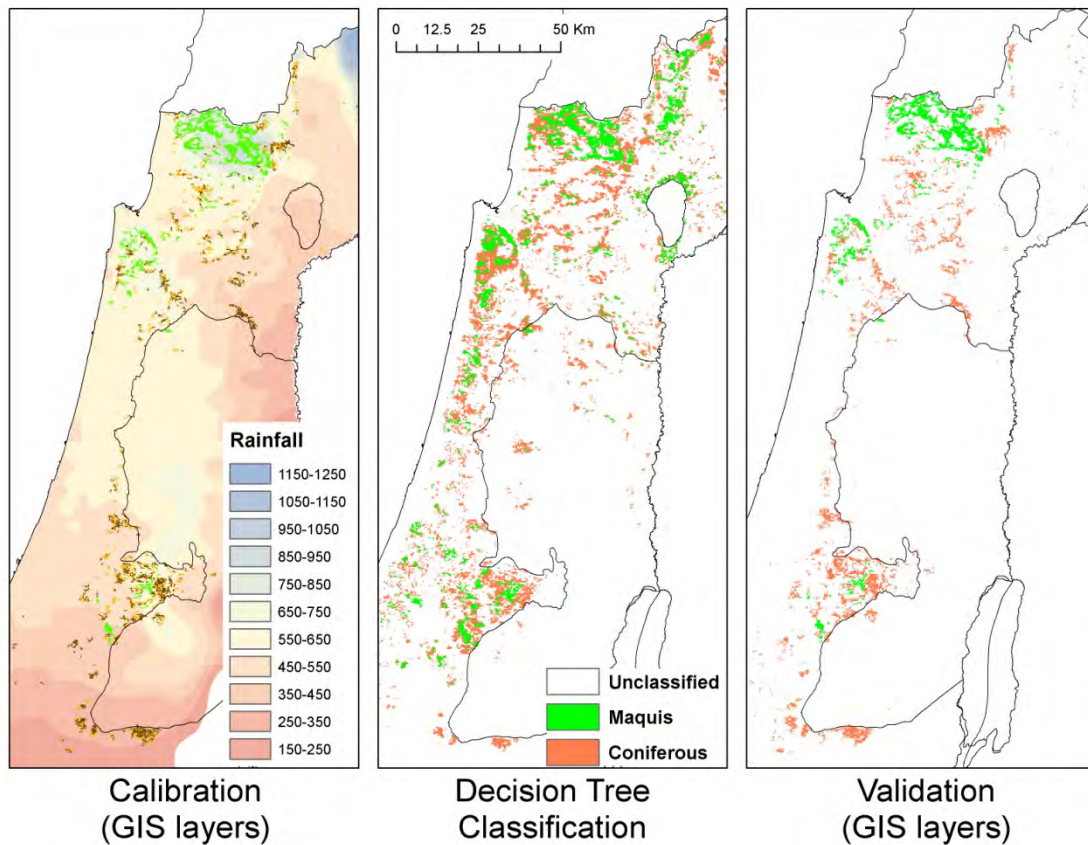


Figure 22: MODIS classification of Mediterranean maquis and planted coniferous trees.

The overall accuracy was 77% with a kappa coefficient of 0.53. While some of the errors may be related to misclassification of agricultural areas (e.g., in the northern Jordan Valley), it seems that using MODIS time series and rainfall data, coniferous trees can be separated from Mediterranean maquis.

7. 3.4 Fire mapping using MODIS

Fires were mapped from MODIS images using the RdNBR index as described in the methods above, and thresholds of dNBR, RdNBR and dNDVI values were used to create binary images of fire scars for each date. These images were further cleaned from noises using the 'closing' morphological filter (3x3) followed by a sieve operation leaving only fire scars larger than four MODIS pixels. Figure 23 presents an overview of 2010 fire scars in the Golan Heights. A visual comparison with two Landsat images from September and December 2010, in which fire scars appear in brown colors, indicates that fire scar mapping can be effectively done from MODIS imagery, for fire scars of at least 0.5 km². Further work is needed to refine and validate this methodology.

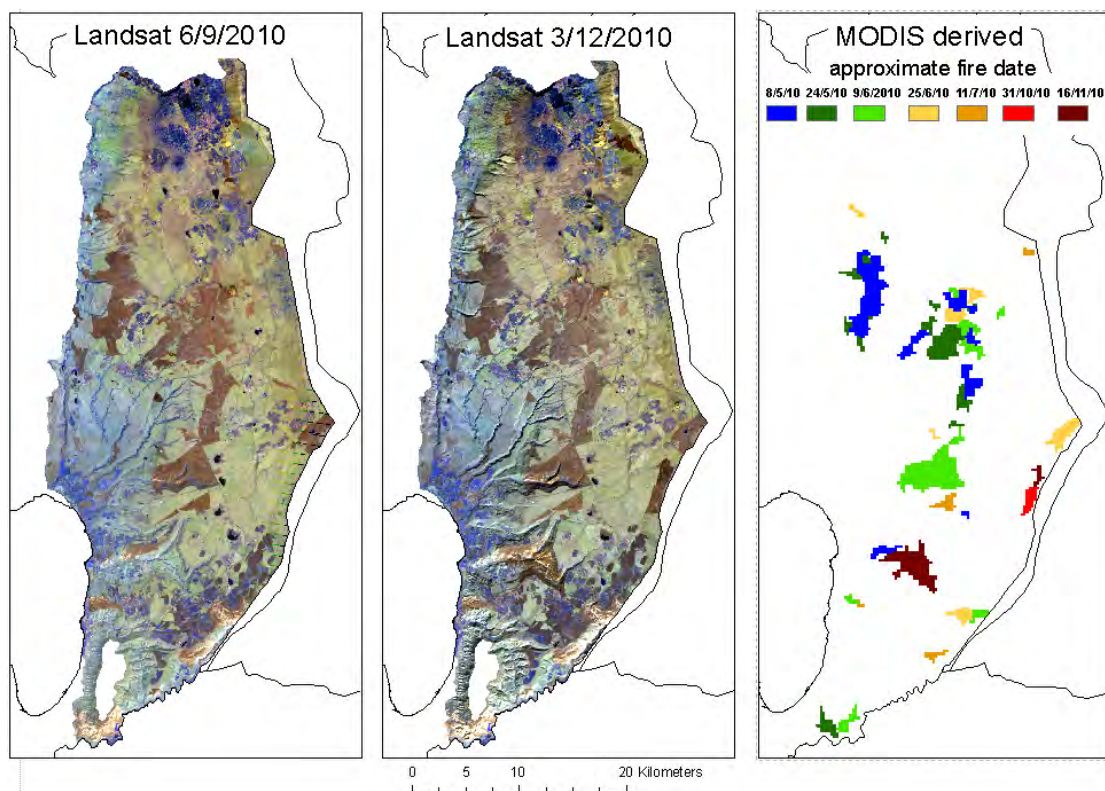


Figure 23: 2010 fire scars in the Golan Heights. The Landsat images are using a false color composite of bands 7, 5 and 4 (blue: vegetation, brown: fire scars).

8. Discussion

Overall remote sensing methods using operational passive sensors have been shown to enable the monitoring of gradual and abrupt changes in land cover and also enable mapping of broad types of Israel's land cover, at reasonable accuracies.

Within the Mediterranean regions the full breadth of EBONE classes was found to be too detailed to be replicated using passive remote sensing, and we therefore had to merge some EBONE classes prior to accuracy assessment so they better match with the remote sensing classifications. On the other hand, within the desert areas, EBONE methodology classified most of the areas as bare soil, whereas satellite imagery allowed the detection of seasonal green vegetation.

If vegetation height is an important consideration for land cover mapping, then LiDAR data should be acquired and used (as in Bar-Massada et al., in press). The disadvantage of LiDAR data, at present, is their high cost. LiDAR coverage is not available for all Israel, and was acquired once by Ofek Aerial Photography.

Using phenological data we have shown that perennial vegetation, seasonal vegetation and bare soil can be mapped at the sub-pixel level (following a modified version of the methodology of Shoshany and Svoray, 2002). This approach provides per pixel values of the percent cover of perennial vegetation, seasonal vegetation and bare soil, and can be used by INPA to create vegetation classes (e.g., areas with > 90% perennial vegetation whose areas is > 10 ha can be defined as forest/maquis stands). Applying the same methodology to previous or later images (e.g., from the 1990s or from 2010), changes in vegetation cover can be studied.

Using detailed time series from MODIS imagery, monitoring of changes can be achieved, and the spatial distribution of seasonal vegetation can be mapped, being of special interest in the transition zones and the desert, where rainfall is highly variable in space and in time. MODIS imagery provides near cloud-free images at no cost and a temporal resolution of 16 days (albeit at a spatial resolution of 250 m). Statistically significant trends in vegetation cover can then be identified, to direct areas where further research and field work may be done, so that the trends identified and the factors causing them can be understood.

One of the challenges in mapping Mediterranean vegetation is that of separating between maquis and coniferous planted trees. We have shown that using either high spatial resolution or detailed time series, maquis and coniferous trees can indeed be separated, at accuracies > 70%. Within QuickBird images, coniferous trees and especially cypress trees, were spectrally different from the maquis especially in the summer season. Further work is needed here, as maquis areas are also heterogeneous, and as the dominant species in maquis may change between areas, so the separability of maquis from coniferous stands may change. Maquis areas were found to possess less temporal variability in NDVI values, and to have higher NDVI values, especially in the summer, compared with coniferous trees. To separate between maquis and

coniferous trees on a national scale we used an ancillary layer of average annual rainfall, as the temporal profiles of NDVI change as rainfall increases. Additional ancillary layers may be further used to aid classification and to separate between different classes. For example, the slope can be calculated from a digital elevation model, so as enhance the mapping of agricultural areas that have a higher probability of being located in flat areas.

While promising, we would like to note on the following limitations of remote sensing, as well as sources for errors in the classifications. While cloud cover over Israel is less than in Europe, full coverage cloud-free satellite images of Israel are not common, and therefore our analysis of Landsat imagery was confined to the early 2000s. The acquisition problems of Landsat 7 since 2003 (scan line corrections) and low frequency of coverage of Israel by Landsat 5, didn't allow us to map land cover in the late 2000s. The Landsat Data Continuity Mission (LDCM, Landsat 8) is scheduled for launch in December 2012. If successful, it will allow cheap monitoring of land cover at a national scale at a medium spatial resolution. In the meanwhile, purchase of Landsat-type images (e.g., SPOT) may be necessary to offer national coverage at a reasonable price (compared with commercial satellites) at spatial resolutions of 10-30 m.

A critical issue when performing an accuracy assessment of classification results, is to have reliable reference data. Different data sets of collected by agencies in Israel provide a variety of land cover layers, using different classes and codes. While EBONE aims to create a uniform method for classification, it too has several limitations: (1) it is better suited for Mediterranean landscapes, leaving most of the desert areas classified as TER (bare soil); (2) being based on a polygonal characterization, within EBONE patches there is a lot of variability in vegetation cover; (3) EBONE classes are based on the highest vegetation type, even if it is not the dominant type in percent cover, whereas remote sensing methods are more affected by percent cover of area by a vegetation type, than by the height above ground. Segmentation techniques (as applied in this study as well as by Bar Massada et al., in press) allow an objective delineation of polygons and may be a useful aid in mapping vegetation classes in the field.

Additional errors in our mapping may be attributed to (1) Differences in dates, seasons and years of the available Landsat images that were used in the different areas (Landsat scenes) of Israel; (2) the time gap between the Landsat imagery (early 2000s) and the time of EBONE field mapping (2009); (3) imperfect preprocessing of the imagery, in terms of geometric, atmospheric and topographic corrections; (4) spatial differences in the phenology of a vegetation class (i.e. a specific tree species may start bloom in different dates as a function of local climatic conditions); (5) natural heterogeneity in vegetation cover, within the polygonal EBONE GHC reference sites, as well as errors in the delineation of the reference sites.

While further research is needed to improve our ability to spectrally separate between plant species (see Rud et al., 2006 for a preliminary work in this direction), a question to consider is what are the uses for which vegetation mapping is needed. For many uses, mapping of vegetation properties such as vegetation cover and height and monitoring these properties in time, maybe enough. No type of vegetation classification will satisfy all users and needs. Due to the heterogeneity of natural vegetation, vegetation classes are necessarily an arbitrary construct imposed by us (except in the case of homogeneous planted forest stands). One of the reasons for using polygonal mapping in a vector format is that it is easier to manage and to comprehend. Nature however is more complex, and monitoring of quantitative properties of vegetation seems to better correspond with real world objects.

9. Operational recommendations:

Following this work we recommend the following:

1. An annual tasking and acquisition of cloud-free images of all Israel using a Landsat type sensor, around March and October, capturing maximum and minimum greenness. This should be government funded, therefore allowing the free use of these images by all relevant government agencies.
2. An annual LiDAR coverage of Israel to be freely available for all government agencies, for monitoring of changes in vegetation height, coastal erosion (as well as urban uses).
3. Monitoring of large scale changes in vegetation cover in Israel using MODIS data, freely available for downloading. This can aid in detecting desertification, shrub encroachment, and for mapping disturbance events.
4. To employ within the GIS unit of INPA a remote sensing technician, that will be able to conduct analysis of satellite imagery.
5. Within the LTER sites, add to the EBONE classification also detailed descriptions of percent cover of vegetation types (e.g., perennial, seasonal) within 100×100 m quadrats.

10. References

- Alcaraz, D., Paruelo, J., Cabello, J. (2006) Identification of current ecosystem functional types in the Iberian Peninsula. *Global Ecology and Biogeography*, 2006, 15, 200-212.
- Bar Massada A., Kent R., Blank L., Perevolotsky A., Hadar L., Carmel Y. (in press). Automated segmentation of vegetation structure units in a Mediterranean landscape. *International Journal of Remote Sensing*.
- Barret E.C. and L.F. Curtis, 1992, *Introduction to environmental remote sensing*, Chapman and Hall, London, 426p.
- Ben-Dor, E., Kindel, B.C., and Patkin, K. A comparison between six model-based methods to retrieve surface reflectance and water vapor content from hyperspectral data: A case study using synthetic AVIRIS data. Presented at International Conference on Optics & Optoelectronics - ICOL 2005, Dehradun, India, 2005.
- Blaschke, T., (2010) Object based image analysis for remote sensing. *ISPRS Journal of Photogrammetry and Remote Sensing* 65, 2-16.
- Bunce, R.G.H., Groom, G.B., Jongman, R.H.G., and Padoa Schippa, E. (2005). *Handbook for Surveillance and Monitoring of European Habitats*, Alterra Report 1219, EU FP project EVK CT-2002-20018, 107 p.
- Bunce, R.G.H., Roche, P., Bogers, M.M. B., Walczak, M., de Blust, G., Geijzendorffer, I.R., and van den Borre J. 2010 *Handbook for Surveillance and Monitoring of Habitats, Vegetation and Selected Species*, ver 20100510. Alterra, 102 pp.
- Carlson TN, Ripley DA (1997) On the relation between NDVI, fractional vegetation cover, and leaf area index. *Remote Sensing of Environment* 62, 241-252.
- Carmel, Y., Kadmon, R., 1999. Effects of grazing and topography on long-term vegetation changes in a Mediterranean ecosystem in Israel. *Plant Ecology* 145, 243-254.
- Coops, N.C., Wulder, M.A., Duro, D.C., Han, T., and Berry, S. (2008). The development of a Canadian dynamic habitat index using multi-temporal satellite estimates of canopy light absorbance. *Ecological Indicators*, 8, 754-766.
- Duro, D.C., Coops, N.C., Wulder, M.A., and Han, T. (2007). Development of a large area biodiversity monitoring system driven by remote sensing. *Progress in Physical Geography*, 31, 235-260.
- Fernandez, N., Paruelo, J.M., Delibes, M. (2010). Ecosystem functioning of protected and altered Mediterranean environments: A remote sensing classification in Doñana, Spain. *Remote Sensing of Environment*, 114, 211-220.
- Guyot G., F. Baret, and S. Jacquemoud, 1992, *Imaging spectroscopy for vegetation studies*, in *Imaging spectroscopy: fundamentals and prospective applications*, Toselli F. and Bodechtel J. (eds.), pp. 145-165

- Hall, J. K. et al. 1999. Test of the accuracy of the DEM of Israel. Geological Survey of Israel, Jerusalem.
- Hoaglin, D.C., Mosteller, F., and Tukey, J.W., 2000, Understanding Robust and Exploratory Data Analysis, Wiley Classics Library Edition, (New York: Wiley).
- Huete A, Didan K, Miura T, Rodriguez EP, Gao X, Ferreira LG (2002) Overview of the radiometric and biophysical performance of the MODIS vegetation indices. *Remote Sensing of Environment* **83**, 195-213.
- Kadmon, R., Danin, A. 1997. Floristic variation in Israel: a GIS analysis. *Flora* 192: 341–345.
- Kadmon, R. & Harari-Kremer, R. 1999. Studying Long-Term Vegetation Dynamics Using Digital Processing of Historical Aerial Photographs. *Remote Sensing of Environment* 68:164-176.
- Karnieli, A., 2003, Natural vegetation phenology assessment by ground spectral measurements in two semi-arid environments, *International Journal of Biometeorology*, 47: 179-187.
- Kerr, J. T. and Ostrovsky, M. 2003. From space to species: ecological applications for remote sensing. *Trends in Ecology and Evolution*, 18, 299-305.
- Key CH, Benson NC (1999) Measuring and remote sensing of burn severity: the CBI and NBR. Poster abstract. In L.F. Neuenschwander and K. C. Ryan (Eds.), *Proceedings Joint Fire Science Conference and Workshop, Vol. II, Boise, ID, 15-17 June 1999. University of Idaho and International Association of Wildland Fire.* 284
- Levin, N., Ben-Dor, E., Kidron, G.J. 2003. The influence of human factors on the temporal changes in the stabilization rate of the Ashdod-Nizzanim dunes. *Horizons in Geography* 57-58:224-241.
- Levin N., Shmida A., Levanoni O., Tamari H., and Kark S., (2007). Predicting mountain plant richness and rarity from space using satellite-derived vegetation indices. *Diversity and Distributions*, 13, 692-703.
- Levin, N., McAlpine, C., Phinn, S., Price, P., Pullar, D., Law, B., and Kavanagh, R.P., (2009). Mapping forest patches and scattered trees from SPOT images and testing their ecological importance for woodland birds in a fragmented agricultural landscape. *International Journal of Remote Sensing*, 30, 3147-3169.
- Mallinis, G., Koutsias, N., Tsakiri-Stratim M., Karteris, M. (2008) Object-based classification using Quickbird imagery for delineating forest vegetation polygons in a Mediterranean test site. *ISPRS Journal of Photogrammetry & Remote Sensing* 63, 237–250.
- Miller JD Thode AE (2007) Quantifying burn severity in a heterogeneous landscape with a relative version of the delta Normalized Burn Ratio (dNBR). *Remote Sensing of Environment* **109**, 66–80.

- Pinker R.T. and A. Karnieli, 1995, Characteristic spectral reflectance characteristics of a semi-arid environment, *International Journal of Remote Sensing*, 16 (7): 1341-1363.
- Rast M., 1991, Imaging spectroscopy and its applications in spaceborne systems, European Space Agency, SP-1144, 143p.
- Richter, R. 1998. Correction of satellite imagery over mountainous terrain. *Applied Optics* 37: 4004-4015.
- Rozenstein, O., Karnieli, A. (2011). Comparison of methods for land-use classification incorporating remote sensing and GIS inputs. *Applied Geography*, 31, 533-544.
- Rud, R., Shoshany, M., Alchanatis, V., Cohen, Y. (2006) Application of spectral features' ratios for improving classification in partially calibrated hyperspectral imagery: a case study of separating Mediterranean vegetation species. *Journal of Real-Time Image Processing*, 1, 143-152.
- Schmidt H. and A. Karnieli, 2000, Remote sensing of the seasonal variability of vegetation in a semi-arid environment, *Journal of Arid Environments*, 45: 43-59
- Shoshany, M. (2000) Satellite remote sensing of natural Mediterranean vegetation: a review within an ecological context. *Progress in Physical Geography*, 24, 153-178.
- Shoshany, M., Svoray, T. (2002) Multidate adaptive unmixing and its application to analysis of ecosystem transitions along a climatic gradient. *Remote Sensing of Environment*, 82, 5-20.
- Smith, J.A., Lin, T.L., Ranson, K.J. (1980). The Lambertian assumption and Landsat data. *Photogrammetric Engineering and Remote Sensing*, 46, 1183-1189.
- Tueller P.T., 1987, Remote sensing science applications in arid environments, *Remote Sensing of Environment*, 23: 143-154.
- Tucker CJ (1979) Red and photographic infrared linear combinations for monitoring vegetation. *Remote Sensing of Environment* 8, 127–150

Annex-9

EBONE



European Biodiversity Observation Network:

Design of a plan for an integrated biodiversity observing system in space and time

5.2.2. The impact of spatial and thematic detail on change detection

Version 2.0

Document date: 2012-02-25

A contribution to Document Ref.: EBONE-D5.5-2.0

Authors:

L. Halada, F. Kohút, M. Mojses, J. Lieskovský (ILESAS, Slovakia)

Reviewer:

F. Gerard (Centre for Ecology and Hydrology, UK)



Contents

1. Executive Summary	5
2. The introduction and background	6
3. Material and methods	7
3.1 Case study sites	7
3.2 Remote sensing data	8
3.2.1 CORINE Land Cover standard data	8
3.2.2 More detailed land cover maps – BIOPRESS approach	8
3.3 EBONE habitat mapping data	9
4. Results	10
4.1 Spatial resolution	10
4.2 Thematic resolution	12
4.2.1 CORINE Land Cover (CLC)	12
4.2.2 General Habitat Categories (GHC)	13
4.3 Change detection and interpretation	15
4.3.1 Change detection	15
4.3.2. Changes interpretation	16
5. Conclusions	20
6. References	21
Annex 1: Corine Land Cover Legend	22
Annex 2: General Habitat Categories – full list	23

1. Executive Summary

In this report we assess

- 1) the consequences of implementing different spatial and thematic resolutions on the resulting data (in-situ or EO derived) for habitat monitoring and
- 2) the potential of the EBONE monitoring methodology for identifying and evaluating changes in habitat extent, management regime and other parameters recorded.

The assessment is based on a case study developed using eight test sites in Slovakia. Each of the eight test sites covers an area of 1 km x1 km. Changes in habitat extent were estimated for the period between 1949 and 2010 and derived from habitat maps produced using three different approaches: one approach is the EBONE method which has a minimal mapping unit of 400 m² (0.04ha) and uses the General habitat category nomenclature which potentially can describe 160 different habitat classes; a second approach is the BIOPRESS method which has a minimal mapping unit of 5,000 m² (0.5ha) and uses the CORINE Land Cover nomenclature describing 44 classes (CLC level 3); and a third approach is the CORINE land cover approach which also uses the CORINE Land Cover nomenclature but has a minimal mapping unit of 250,000 m² (25 ha). Because the field data mapped according to the EBONE protocol did not exist for 1949, it was simulated.

The results indicate that the EBONE approach produces more detailed maps (more classes and more polygons are being mapped) than the BIOPRESS approach. The EBONE approach identifies also more types of habitat changes. However, some changes identified by the BIOPRESS approach are not interpreted as change under the EBONE approach - e.g a change from CLC category 2.4.2 (complex cultivation patterns) to CLC category 2.1.1 (non-irrigated arable land) will remain classed as the GHC category 'Crops'. As this type of land cover change is quite common in the agricultural areas of Slovakia during the studied period, the BIOPRESS approach found more area changed than the EBONE approach.

We interpreted the observed changes in land cover/ habitat categories into generic processes of, amongst others intensification and afforestation, and found that for some sites the approaches would identify the same processes (usually in different quantity) as being dominant, whilst for other sites the approaches would identify different dominant processes. These differences arose mainly from the different nomenclature used and genuine class identification problems during the manual (visual) interpretation of air photos.

2. The introduction and background

In the EBONE project a system for the integrated monitoring of biodiversity in space and time is to be developed. This system should be based on existing monitoring methods and particular attention is given to the integration of *in-situ* and remote sensing based methods. In the EBONE Description of work (chapter “Concept and project objectives”) are formulated two targets:

1. *The provision of a sound scientific basis for the production of statistical estimates of stock and change of key indicators that can then be interpreted by policy makers responding to EU Directives regarding threatened ecosystems and species;*
2. *The development of a system for estimating past change but also for forecasting and testing policy options and designing mitigating management strategies for threatened ecosystems and species”.*

The methodology of habitats and landscape monitoring developed in EBONE has the ambition to serve as a scientific basis for the above mentioned statistical estimates. For each new methodology it is useful to evaluate its contribution through its comparison with other relevant available methods used in the same field and we tried to provide such evaluation in this report.

Both targets above foresee estimation of changes what requires to have results from at least two time layers. However, because the EBONE methodology was only developed and tested recently, two time layers mapped by the EBONE methodology are currently not available for any site. Therefore we decided to develop a case study enabling us to test the potential of the EBONE methodology for assessing change using simulated data.

The case study had the following main objectives:

- 1) to quantify improvement in spatial and thematic detail achieved using the EBONE field based approach by comparing the EBONE mapping results with land cover/habitat maps obtained through remote sensing;
- 2) to assess the potential of the EBONE methodology to identify and evaluate changes in habitat extent (general habitat categories, GHCs);
- 3) to compare the change detection achieved using the EBONE field based approach with changes identified through remote sensing.

We developed the case studies for 8 sites in Slovakia, in which we tested 1) EBONE monitoring approach using GHC maps produced on the basis of field mapping and 2) BioPress approach using CLC maps developed by manual interpretation of air photos. We selected a long time period 1949-2011 to study the landscape/habitat changes in order to guarantee the occurrence of significant changes and thus enable us to highlight differences between approaches.

3. Material and methods

3.1 Case study sites

For the case study we selected 8 sites located in 2 strata of the environmental stratification of Europe (Metzger et al. 2005) - in Pannonian (PAN2) and Continental stratum (CON2). Our selection we based on regular LUCAS grid 1x1 km covering whole Europe (Martino, Fritz 2008). In the first step, we overlaid the CORINE Land Cover (CLC) map 2006 by the LUCAS grid. In the next step, we excluded from selection squares where urban (CLC classes 1xx) is >10%; or forest (CLC 31x) is > 75 %; or intensive agriculture (CLC 211) > 30%; or water bodies (CLC 511, 512) > 75%. From remaining squares, 5 squares per environmental stratum were selected by random selection. Because of lack of time, field mapping was completed in 2011 for 4 sites per stratum, so finally we used 8 sites for the case study. The location of the sites is displayed in Figure 1, some details are provided in Table 1.

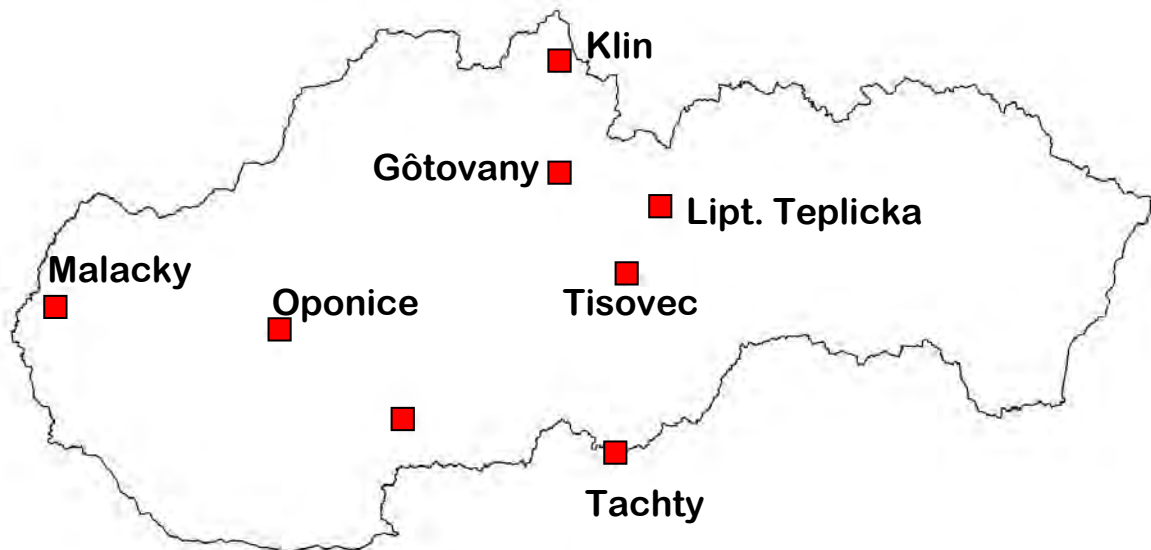


Fig. 1: Location of selected sites in Slovakia

Table 1: Basic information about test sites

No.	Code	Name	Geographic coordinates	
			N	E
1	CON2SK01	Klin	49° 25' 45''	19° 29' 25''
2	CON2SK03	Gotovany	49° 03' 53''	19° 30' 59''
3	CON2SK04	Liptovska Teplicka	48° 58' 45''	20° 04' 45''
4	CON2SK05	Tisovec	48° 44' 23''	19° 55' 13''
5	PAN2SK05	Tachty	48° 09' 01''	19° 55' 33''
6	PAN2SK04	Sudovce	48° 12' 57''	18° 50' 21''
7	PAN2SK02	Oponice	48° 27' 29''	18° 09' 37''

No.	Code	Name	Geographic coordinates	
			N	E
8	PAN2SK01	Malacky	48° 28' 20''	17° 02' 02''

3.2 Remote sensing data

3.2.1 CORINE Land Cover standard data

The standard CORINE Land Cover (CLC) maps were obtained from the European Environmental Agency (EEA) data service for year 2000. The CLC data are broadly used as the main information source about the land cover and represent thus certain standard. We used these data only for illustration of differences in spatial resolution (chapter 4.1) between standard CLC data and other 2 types of data described in chapters 3.2.2 and 3.2.3.

3.2.2 More detailed land cover maps – BIOPRESS approach

The land cover maps on the local level (resolution 0.5 ha what corresponds to the scale 1:10.000) represented the basic remote sensing data type for this case study. We developed such maps for years 1949 and 2003 using 2 different data sources: black-and-white aerial photographs from 1949 and ortho-photomaps in true colour from 2003.

In the first step we ortho-rectified the air photos from 1949. Then we proceed with the manual interpretation of air photographs. We followed the manual describing the CLC level 3 classes with respect to 1:10,000 and 1:25,000 scale photos (minimum mapping unit of 0.5 ha) and providing rules for change detection from photo-to-photo interpretation (Feranec et al. 2004). This manual was developed in the EU Framework (FP5) project BIOPRESS (Gerard et al., 2010). To ensure consistency of interpretation, all studied sites interpreted the same interpreter.

The approach adopted was to interpret the most recent aerial photographs first and then backdate them to year 1949. The year 1949 was selected because this is only year before 2000 from which the air photos are available for whole territory of Slovakia. The first interpretation has polygons labelled with the land cover of 2003 (CLC03). In the second interpretation, using the aerial photos of 1949 (CLC49), only new lines are added. The newly created polygons receive a label with the land cover of 1949 and also 2003. For polygons that did not change, the attributes of CLC03 are copied to CLC49. This ensured that the interpreter only added lines and created polygons if the land cover had changed. The results are polygons with multiple attributes which were used to produce change statistics (Gerard et al. 2010). Two land cover maps – from 2003 and 1949 – represent result of this task.

3.3 EBONE habitat mapping data

The habitat maps from the field mapping in 2010 and 2011 represented the basic data set. These maps were developed using the EBONE methodology for habitat monitoring (Bunce et al. 2011). The methodology is based on the General Habitat Categories (GHC) that are described below in chapter 4.2. The mapping procedure started with the manual interpretation of the aerial photographs (ortho-photomaps from 2003) aiming to delineate spatial units that probably represent one GHC or GHC combination. The result is the **potential GHC map** with minimum mapping unit 0,04 ha (400 m²) and minimal width of polygon 5 m as defined by the EBONE field monitoring methodology. This map was then used as a background for the field mapping - if necessary, the polygons were divided, merged, deleted or their boundaries were changed and both the GHCs and other attributes required by the EBONE methodology were recorded in the field forms. Based on these field data, **the final GHC map** was prepared in the form of the GIS layer with the attribute database.

Our aim was to test changes detection by the EBONE methodology, therefore we needed at least two time layers. However, as the EBONE methodology was recently developed, the field mapping did not provide yet the data for any site from two different years. Therefore we decided to **simulate** the older mapping. We selected year 1949 - the same year that was used in remote sensing part (chapter 3.2.2). The first step in development of the simulated GHC map for 1949m was similar to backdating of the land cover map (chapter 3.2.2) – we used the GHC map from 2003 as background and using the air photographs from 1949, we modified boundaries of spatial units that probably represent one GHC or GHC combination. Then the GHC unit was assigned to individual polygons on the basis of interpretation of the air photo from 1949. The expert knowledge was used for this step – the interpretation was done by the expert having both knowledge from the field EBONE mapping and experience with the historical air photo interpretation. No other attributes than the GHC unit were recorded – for addition of other attributes, the ancillary data are necessary. Two habitat (GHC) maps – from 2010(2011) and 1949 – represent result of this task.

4. Results

4.1 Spatial resolution

In this chapter we compare spatial resolution of 3 different products: standard CLC maps, spatially improved CLC maps (BioPress approach) and GHC maps (EBONE approach). The standard CLC product is developed for continental scale while two other products in question are focused to local scale. Thus it is not fully correct to compare CLC with other two product. We included CLC to this analysis only to set the scene – because the CLC is broadly used in Europe, it represents certain standard and it is good to show what improvement bring the other two products.

The CLC is based on satellite photos that are manually interpreted using a set of structural criteria to identify land cover classes defined in advance. The aim is to receive product consistent across Europe is reflected also by target scale (1:100.000), minimal size of mapping unit (25 ha) and minimal size of change identified (5 ha).

The BioPress project (5FP programme) used CLC approach as for legend and interpretation methodology, but different data source (air photos) and scale. Thus, we can consider this approach as the CLC modification to local scale. Because the EBONE approach is focused to local scale as well, we selected BioPress maps as suitable data for assessing improvement that brings EBONE approach to habitat monitoring against remote sensing based products at local scale. As mentioned above, the BioPress approach uses the CLC legend at 3-rd level (44 classes) and it is based on manual interpretation of air photos. The target scale is 1:10.000, minimum mapping unit is 0.5 ha.

The EBONE methodology uses the air photos for preparation of field mapping. The target scale is local, with minimum mapping unit 400 m² (0.04 ha). The summary of crucial features of three above mentioned products are in table 2.

Table 2: Spatial parameters of CORINE Land Cover, BioPress and EBONE maps

	CORINE Land Cover	Spatially improved CLC - BioPress	EBONE
Target scale	Continental	local	local
Data sources	Satellite	air photos	air photos, field
Min.mapping unit	25 ha	0.5 ha	0.04 ha
Mapped features	Polygons	polygons	polygons, lines, points

For spatial resolution assessment we used 4 indices: number of polygons (Nump), mean polygon size (MPS), edge Density (ED), and mean shape index (MSI). The calculation was done using the Fragstat software (McGarigal et Marks 1995). The results are in table 3. Significant differences between number of polygons identified by CLC and BioPress could be expected taking into account their big difference in target scale and resolution. The difference in spatial resolution between BioPress and EBONE approaches is smaller, but differences in number of identified polygons are big (see tab. 3, Fig. 2 and 3). The mean polygon size is negatively related to number of polygons, therefore we observed strong decrease in the average polygon size in direction from CLC to EBONE. The same pattern as for number of polygons occurred also for the edge density (tab. 3, fig. 4). These two measures are correlated, the EBONE mapping produced higher density

of boundaries than BioPress and much higher density than CLC. The mean shape index was lower for CLC than other 2 types of maps, the difference between BioPress and EBONE was not big, thus we can conclude that patches of CLC have more regular shape than other two products.

Table 3: Indices of spatial landscape structure calculated for CLC, BioPress and EBONE maps from 8 study sites

No.		1	2	3	4	5	6	7	8
Site name		Klin	Gôtovany	L. Teplička	Tisovec	Tachty	Súdovce	Oponice	Malacky
NUMP	CLC	2	3	5	5	10	7	7	5
NUMP	BioPress	11	19	10	26	34	31	28	15
NUMP	EBONE	90	49	73	65	79	88	61	80
MPS	CLC	49.987	33.320	19.992	19.991	9.996	14.281	14.280	19.994
MPS	BioPress	9.088	5.261	9.996	3.845	2.940	3.225	3.570	6.665
MPS	EBONE	1.111	2.040	1.377	1.538			1.639	1.254
ED	CLC	46.0	72.5	111.6	99.1	139.8	110.2	109.6	108.6
ED	BioPress	155.3	221.9	175.1	294.9	305.7	288.5	270.0	173.6
ED	EBONE	431.4	353.8	404.2	462.6			389.2	420.6
MSI	CLC	1.209	1.435	1.543	1.332	1.413	1.381	1.354	1.457
MSI	BioPress	1.625	1.699	1.823	1.849	1.801	1.641	1.681	1.681
MSI	EBONE	1.766	1.760	1.662	1.944	1.705	1.734	1.940	1.738

NUMP – number of polygons, MPS – mean polygon size /ha/, ED – edge density, MSI – mean shape index

Fig. 2: Habitat information obtained for site 8 (Malacky) when implementing the Corine Land Cover nomenclature at a 25 ha MMU, a 0.5 ha MMU and when implementing the General habitat categories nomenclature at a 0.04 ha MMU.



Fig. 3: Number of patches in 8 sites produced by different mapping methods

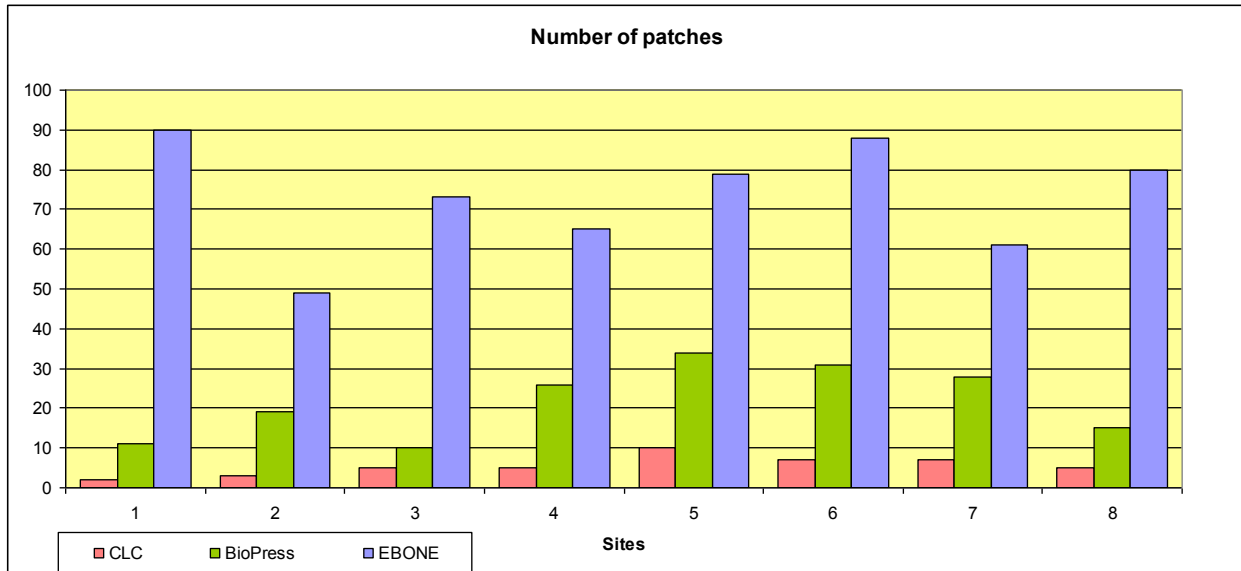
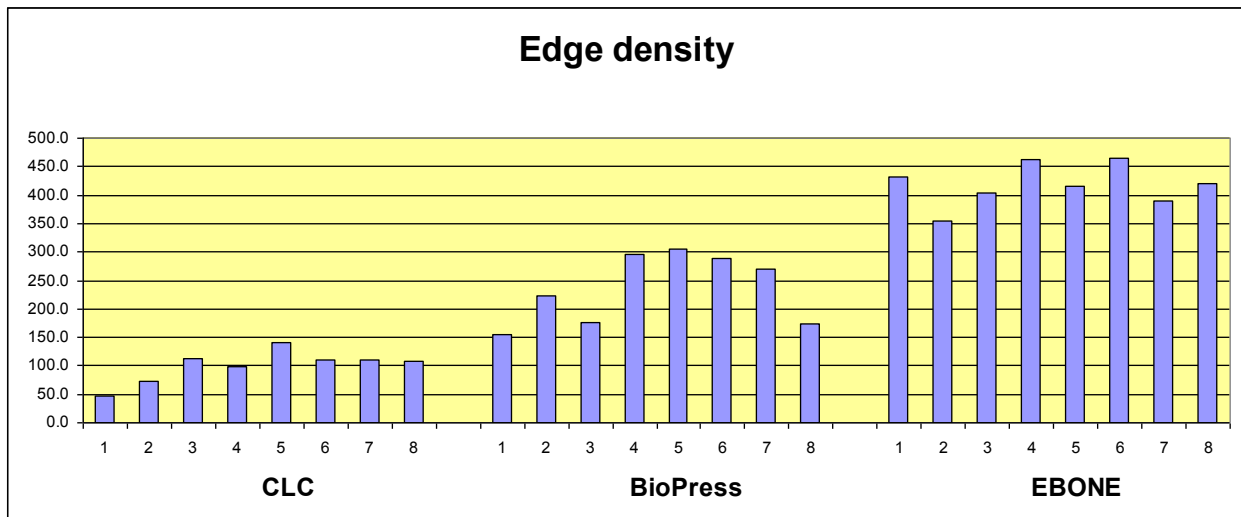


Fig. 4: Edge density in 8 sites obtained by different mapping methods



4.2 Thematic resolution

In this report, we are working with two different classifications: the land cover classification CORINE Land Cover (used in CLC and BioPress) and EBONE classification of habitat types based on General Habitat Categories (GHCs).

4.2.1 CORINE Land Cover (CLC)

CLC is hierarchical system of the land cover categories that distinguishes 5 classes in level 1 (artificial surfaces, agricultural areas, forests and semi-natural areas, wetlands, and water bodies). Level 2 includes 15 classes (table 5) and level 3 contains 44 classes (Annex I, Heymann et al.

1993). We worked with the CLC data at the level 3 with 44 classes individual classes are coded by digits – in third level, 3-digit codes are used.

Table 5: CORINE Land Cover units on levels 1 and 2

Level 1 units	Level 2 units and number of level 3 units
Artificial surfaces	Urban fabric (2), industrial, commercial and transport (4), mine, dump, construction (3), artificial vegetated (2)
Agricultural areas	Arable land (3), permanent crops (3), pastures (1), heterogeneous agricultural areas (4)
Forests and semi-natural areas	Forests (3), scrubs, herbaceous vegetation (4), open spaces with little or no vegetation (5)
Wetlands	Inland wetlands (2) maritime wetlands (3)
Water bodies	Inland waters (2), marine waters (3)

4.2.2 General Habitat Categories (GHC)

At European level, the General Habitat Categories (GHCs) have been developed as the primary structure for recording ecosystems or habitats (Bunce et al., 2012). The system of GHCs is mainly based on plant life forms (*sensu* Raunkiaer 1934), but it includes non-life form habitats as well in order to cover whole spectrum of habitats that need to be mapped. For coding of basic GHCs are used 3-character codes, for combinations of GHCs the combination of the basic codes is used (e.g. URB/ART – urban artificial). In total, 160 GHCs are identified by Bunce et al. (2011), their overview is in Tab. 6 and full list in Annex 2. From table 6 is visible that category trees/shrubs represent more than half of distinguished GHCs (81 categories). The main reason is that several criteria were used for division of this group: life form, height and character of leaves.

Table 6: Overview of the GHC system

GHC group	Basic GHC	Combinations
Urban	5: artificial, non-vegetated, crops, herbaceous, woody	10
Cultivated	3: bare ground, herbaceous crops, woody crops	1
Sparsely vegetated	5: sea, tidal, aquatic, terrestrial, ice and snow	6
Terrestrial	6: bare rock, boulders, stones, gravel, sand, earth/mud	15
Herbaceous wetland	3: submerged hydrophytes, emerged hydrophytes, helophytes	3
Herbaceous	6: leafy hemicryptophytes, caespitose hemicryptophytes, therophytes, geophytes, chamaephytes, cryptogams	15
Trees/shrubs	31 combinations	51
	6: dwarf chamaephytes, shrubby chamaephytes, low-, mid-, tall-, forest-, mega forest phanerophytes	

In previous paragraphs we reviewed quite high number of CLC and GHC categories/classes that could potentially occur in the landscape. In real landscapes, the number of occurring categories is much lower – depending mainly on climate, other biophysical parameters of landscape and

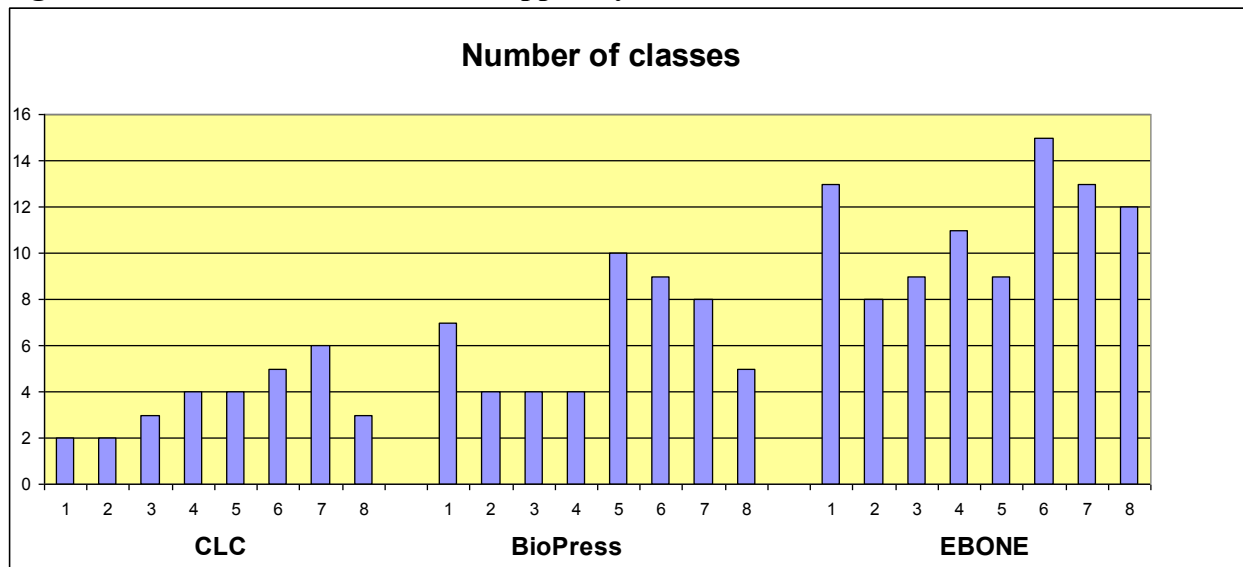
degree of habitats modification by activity of man. Based on much higher number of GHC categories (160) than CLC classes (44), it is possible to expect that in real mapping, the EBONE approach will identify higher number of classes than CLC mapping. Results of the case studies showed in table 7 and figure 5 generally confirm this expectation – CLC mapping produced lowest number of classes, followed by BioPress approach and the EBONE mapping used highest number of categories. There are some exceptions, e.g. in site 5 (Tachty) the BioPress approach identified higher number (10) classes than EBONE mapping (9).

Tab. 7: Thematic diversity indices in 8 sites obtained by different mapping methods

No.		1	2	3	4	5	6	7	8
Site name		Klin	Gôtovany	L. Teplička	Tisovec	Tachty	Súdovce	Oponice	Malacky
N_Class	CLC	2	2	3	4	4	5	6	3
N_Class	BioPress	7	4	4	4	10	9	8	5
N_Class	EBONE	13	8	9	11	9	15	13	12
SDI	CLC	0.413	0.608	0.964	1.359	1.263	1.535	1.488	1.037
SDI	BioPress	1.531	1.100	1.257	1.109	1.783	1.884	1.503	1.361
SDI	EBONE	1.922	1.690	1.432	1.832	1.739	1.987	2.024	1.833
SEI	CLC	0.596	0.877	0.877	0.981	0.911	0.954	0.831	0.944
SEI	BioPress	0.787	0.793	0.907	0.800	0.774	0.857	0.723	0.845
SEI	EBONE	0.749	0.813	0.652	0.764	0.792	0.734	0.789	0.738

N_Class – number of classes, SDI – Shannon’s Diversity Index, SEI - Shannon’s Eveness Index

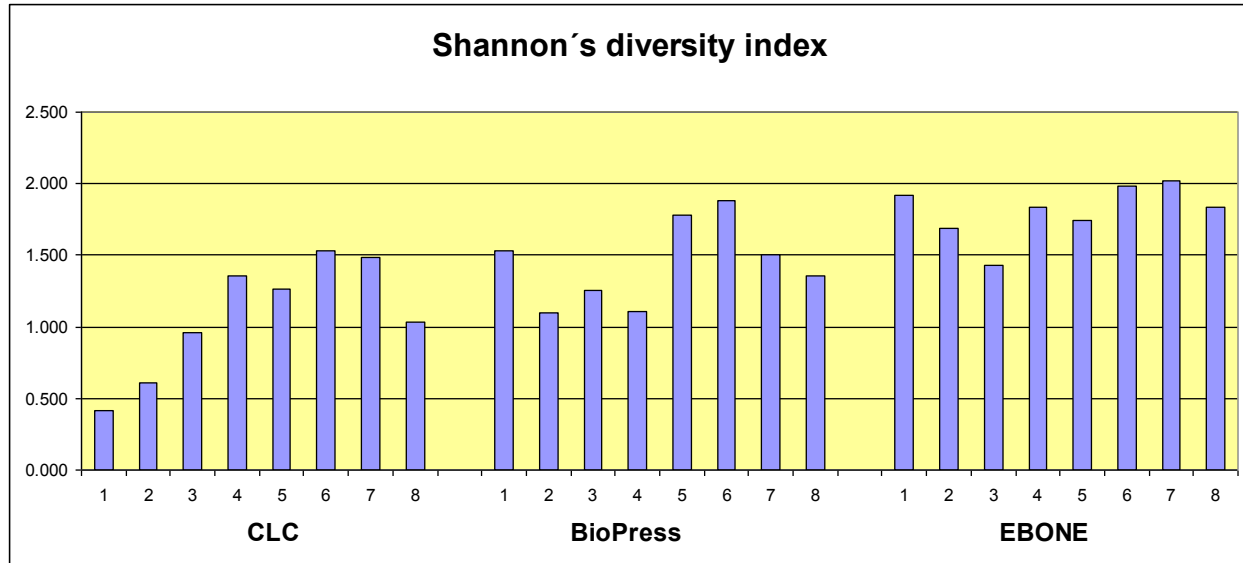
Fig. 5: Number of classes in 8 sites mapped by different methods



We calculated also two biodiversity indices – Shannon’s Diversity Index SDI and Shannon’s Eveness Index SEI. Although also SDI showed usually highest values for EBONE mapping and lowest for CLC, the differences were not so noticeable as the number of classes exhibited. In case

of SEI, in some sites we found relationship opposite to the SDI, but in some other sites other pattern was found.

Fig. 6: Shannon's diversity index in 8 sites mapped by different methodology



4.3 Change detection and interpretation

4.3.1 Change detection

Each transfer from one CLC class in 1949 to another CLC class in 2003 was considered as a change. For changes of GHCs between 1949 and 2010, we took into account the nature of data. While 2010 data were obtained by field mapping, 1949 data represent simulated maps – both delineation of patches and assignment of the GHC class to patches was done by manual interpretation of black-white air photos of not sufficient quality to distinguish some GHCs. Thus we did not consider as change any transfer among categories of herbaceous vegetation (caespitopse hemicryptophytes, leafy hemicryptophytes, and their combination) and among neighbouring height categories of shrubs and trees (low-medium-tall-forest phanerophytes).

The summary of change analysis are in table 8. While BioPress approach identified 6-24 change types per site (average 13.5 types), the EBONE approach identified 27-82 types of changes (average 49.75) for the same sites. These figures clearly demonstrate consequences of the higher thematic resolution of EBONE approach – the number of changes types identified is much higher (in average by 36.25) than number of change types identified by the BioPress approach.

Tab. 8: Summary of changes detected by BioPress and EBONE approaches

Site	No of change types			Changed area /%/		
	BioPress	EBONE	Difference	BioPress	EBONE	
1 Klin	7	27	20	93.07	47.99	45.08
2 Gôtovany	11	33	22	74.87	37.43	37.44
3. Lipt. Teplička	6	27	21	74.85	48.79	26.06
4. Tisovec	6	57	51	65.19	62.96	2.23
5. Tachty	22	51	29	73.54	63.32	10.22
6. Súdovce	24	82	58	79.03	61.21	17.82
7. Oponice	24	67	43	54.78	63.83	-9.05
8. Malacky	8	54	46	66.92	59.36	7.56
Average	13.5	49,75	36.25	72.78	55.61	17.17

When analysing changed area, the relationship between these two approaches are opposite. BioPress approach identified changes in 54.78-93.07 % of the area of studied sites (the average 72.78 %), the EBONE approach identified changes in 37.43-63.83 % of the area of studied sites (the average 55.61 %). The reason why we detected more changes by BioPress approach than by EBONE lies in nature of the dominant change and its different reflection by both approaches.

We studied changes of mainly agricultural landscape during quite long time period 1949-2010. The main change during this period was linked to the collectivisation of agricultural land that started in Slovakia in early 50-ties of XX. century. In this process the narrow strips of fields, grasslands and eventually permanent cultures were merged to larger fields of arable land (mainly) or grasslands. This process represents the change in the CLC classification – transfer from class 242 (Complex cultivation patterns) usually to class 211 (Non-irrigated arable land), eventually to class 231 (Pastures) or rarely to other class (e.g. 221 Vineyards or 222 Fruit trees and berry plantations).

Because of finer spatial resolution, EBONE approach usually allows to identify individual narrow strips or small patches as separate polygons (what is not case of the BioPress approach and CLC methodology). Using classification of EBONE, merging narrow fields of arable land to large blocks of arable land does not represent change – both narrow fields of arable land and large blocks of arable land are classified in one GHC category (cultivated/crops - CUL/CRO). The same is valid also for grasslands – narrow strips of grasslands and large blocks of grasslands are classified in the same way.

4.3.2. Changes interpretation

The changes that we identified could be linked to certain processes. We used similar approach as described in Gerard et al. (2010) and distinguished following processes:

Urbanisation: includes the transformation of non-urban classes to urban covers, but also to related covers (road systems, leisure areas, construction sites, etc).

De-urbanisation: is opposite process – transformation of urban classes to other land cover categories.

Agricultural intensification: includes conversion of non-agricultural classes to agricultural land cover classes, but also cases in which agricultural areas become transformed into classes of more intensive agricultural practice.

Agricultural extensification: includes agricultural areas that were transferred to classes of less intensive agricultural utilisation.

Land abandonment: includes the cropping cessation, grassland abandonment and conversion into early successional, herbaceous or woody habitats.

Afforestation: includes the conversion of open (more or less natural) habitats into forests.

Deforestation is conversion of forest areas to non-forest classes. We did not consider transformation of forest to shrub areas as deforestation – this change in Slovakia usually correspond to forestry management practice – clear-cutting of forest followed by natural or artificial reforestation.

Drainage: in a broad sense, includes all changes affecting aquatic or wetland habitats that are transformed into more terrestrial ones: disappearance of wetlands, but also changes in rivers and in estuarine areas.

Wetlands increase (Irrigation?) is the opposite process to drainage – transfer from terrestrial to more wet habitat – either wetlands or water bodies.

Not relevant change – transfer between classes that do not correspond to the above listed processes.

No change – the same class was recognised in both periods.

The classification of changes of the CORINE land cover classes to processes is summarized in table 9, similar classification for GHC units is in Annex 3.

Tab. 9: CORINE Land cover changes interpreted as processes

1949/2003	112	121	122	132	142	211	221	222	231	242	243	311	312	313	321	324	332	412	512	
112	U	U			DU	DU														
121		U			DU	DU														
122		U	U		DU	DU														
132	U	U	U	U		DU	DU													
142	U	U	U	U	U	DU	DU													
211	U	U	U	U	U	DU	Ex	Ex	Ex		Ex	Af	Af	Af	Ab	Ab	Ab	Ab	Ab	Ab
221	U	U	U	U	U	I			Ex		Ex	Af	Af	Af	Ab	Ab	Ab	Ab	Ab	Ab
222	U	U	U	U	U	I			Ex		Ex	Af	Af	Af	Ab	Ab	Ab	Ab	Ab	Ab
231	U	U	U	U	U	I	I	I			Ex	Af	Af	Af	Ab	Ab	Ab	Ab	Ab	Ab
242	U	U	U	U	U	I			Ex		Ex	Af	Af	Af	Ab	Ab	Ab	Ab	Ab	Ab
243	U	U	U	U	U	I	I	I	Ex			Af	Af	Af	Ab	Ab	Ab	Ab	Ab	Ab
311	U	U	U	De	U	De	De	De	De	De	De				De		De	De	De	De
312	U	U	U	De	U	De	De	De	De	De	De				De		De	De	De	De
313	U	U	U	De	U	De	De	De	De	De	De				De		De	De	De	De
321	U	U	U	U	U	I	I	I	I	I	I	Af	Af	Af		Af			Ir	Ir
324	U	U	U	U	U	I	I	I	I	I	I	Af	Af	Af	De		De	De	De	De
332	U	U	U	U	U	I	I	I	I	I	I	Af	Af	Af		Af				
333	U	U	U	U	U	I	I	I	I	I	I	Af	Af	Af		Af			Ir	Ir
412	U	U	U	U	U	I	I	I	Dr	I	I	Af	Af	Af	Dr	Dr	Dr	Dr	Dr	Dr
512	U	U	U	U	U	I	I	I	Dr	I	I	Af	Af	Af	Dr	Dr	Dr	Dr	Dr	Dr

U	Urbanisation	Ab	Agriculture abandonment	Ir	Irrigation?
DU	De-urbanisation	Af	Afforestation		No relevant change
I	Agriculture intensification	De	Deforestation		No changes
Ex	Agriculture extensification	Dr	Drainage		

The results of change interpretation in terms of processes are summarised in table 10. Very similar results provided both approaches in site 4 (Tisovec), but EBONE mapping identified much higher number of change types. Results achieved in sites 7 (Oponice) and 8 (Malacky) are quite similar. In other sites we recorded higher differences between results provided by BioPress mapping using remote sensing and EBONE mapping based on field survey.

The dominant intensification of agriculture identified by BioPress approach in site 1 (Klin) correspond to the change from complex cultivation patterns (242) to arable land (211) – this issues was discussed above in chapter 4.3.1. In site 2 (Gôtovany) main processes identified by BioPress approach are based on transition from complex cultivation patterns (242) to arable land (211 – classified as agriculture intensification) and to pastures (231 – classified as agriculture extensification). The EBONE approach did not identify change on main part of this area (classified either as crops or as grasslands in both periods). Afforestation was identified as the main process in site 3 (Liptovská Teplička) by both approaches, however, BioPress approach identified this process in much larger area. Main reason is that transfer from transitional woodland-shrub (324) to forest (here 312 – coniferous forest) is consider as change in BioPress

approach, but in EBONE classification both classes represent phanerophytes and thus no change is identified.

Table 10: Processes identified by BioPress and EBONE approaches

Process	1 Klin		2 Gôtovany		3 Gôtovany		3. Lipt. Teplička		4. Tisovec	
	BioPress	EBONE	BioPress	EBONE	BioPress	EBONE	BioPress	EBONE	BioPress	EBONE
Urbanisation	6.16	6.26		1.59		0.14				0.96
De-urbanisation		0.16								1.38
Agr. intensification	65.2	14.56	28.88	9.24		6.82				1.03
Agr. extensification	4.06	18.12	36.93	2.32						1.64
Agr. abandonment	0.82	1.14	4.53	13.78		3.2		7.98		0.39
Afforestation		5.94	4.53	8.7	41.45	16.8		56.19		56.32
Deforestation		0.17		0.5	0.08	0.09		1.02		
Drainage	14.24	1.65		1.18		1.05				0.2
Irrigation?				0.11						
No relevant change	2.59			0.01		20.69				1.05
No changes	6.89	52.01	25.13	62.57	58.47	51.21		34.81		37.04
Total changed	93.07	47.99	74.87	37.43	74.85	48.79		65.19		62.96

Tab. 10 continues

Process	5. Tachty		6. Súdovce		7. Oponice		8. Malacky	
	BioPress	EBONE	BioPress	EBONE	BioPress	EBONE	BioPress	EBONE
Urbanisation	1.65	2.14	2.48	6.15	2.21	2.45	3.49	2.69
De-urbanisation		1.14	0.14	1.48		1.2		
Agr. intensification	17.82	7.46	30.95	5.99	29.17	31.3	31.97	13.49
Agr. extensification	16.25	6.41	4.7	13.75	9.73	3.35		0.85
Agr. abandonment	1.82	1.41	1.77	0.19	3.05	1.95	1.19	2.31
Afforestation	20.06	34.93	29.62	24.26	10.19	10.2	29.52	24.88
Deforestation	1.15	0.07	1.62	0.02	0.43	0.67	0.74	1.21
Drainage		0.91				0.27		
Wetlands increase?	10.48	8.85						
No relevant change	4.3		5.38	9.36		12.44		13.93
No changes	26.46	36.68	23.34	38.79	45.22	36.17	33.08	40.64
Total changed	73.54	63.32	76.66	61.21	54.78	63.83	66.92	59.36

In site 5 (Tachty) both approaches identified afforestation as a main process, followed by other processes identified by both approaches: agriculture intensification, agriculture extensification and wetland increase. However, there are differences in area in which both approaches identified individual processes. In site 6 (Súdovce) the agriculture intensification identified as a main process by BioPress approach represent mainly transfer from complex cultivation patterns (242) to arable land – this transfer is not considered as change by EBONE approach as mentioned above. Afforestation - the second most abundant process – identified both approaches in similar amount.

We can summarise that the main differences in identification of processes by two different approaches arose mainly from different definition of classes in CLC and GHC classifications.

These differences are related mostly to class 242 Complex cultivation pattern that includes (together with 243) heterogeneous land cover classes. Identification problems during manual (visual) interpretation of air photo represent other sources of differences in assessment of processes – this is linked especially to problems to distinguish arable land from grasslands as well transitional woodland shrubs from forest types.

5. Conclusions

In this report, we tried to compare results of two different mapping methodologies: spatially refined CORINE Land Cover mapping operating on landscape level and EBONE mapping focused more to habitats. Our work in the case studies had several limitations, including quite low quality of historical black-white air photos from year 1949 and the lack of EBONE mapping data from 2 time horizon that led to necessity to “simulate” historical GHC map. Therefore the “change” part of this report (chapter 4.3.) should be considered as test of possible assessment of changes in land cover and habitat cover respectively in time. Nevertheless, we tried to keep our estimates as close to reality as possible.

We can conclude that the GHC (EBONE) approach produced spatially more detailed maps and distinguished more classes than CLC (BioPress) approach. Interpretation of changes and comparison of results needs knowledge of both CLC and GHC classifications and methodologies and in addition, also local knowledge of the site. When assessing the change detection, we can observe that GHC approach identified more types of changes than CLC approach. Changes detected by air photo interpretation (CLC) and EBONE field mapping (GHC) are often different and refer to different processes. The differences in thematic resolution, different definition of classes and limitations of manual air photo interpretation represent main reasons of differences in changes and processes identification.

Acknowledgements

The authors thank to Jana Špulerová, Robert Kanka, Veronika Piscová, Marta Dobrovodská and other colleagues from Institute of Landscape Ecology SAS who participated in the field mapping in the case study sites and contributed to this report by 2010-2011 GHC maps. We thank to Andrej Halabuk for comments to the methodology.

6. References

- Bossard, M., Feranec, J., Otahel, J., 2000: CORINE land cover technical guide - Addendum 2000. European Environment Agency, Copenhagen.
- Bunce, R.G.H., Bo 122 p.gers, M.M.B., Roche, P., Walczak, M., Geijzendorffer, I.R., Jongman, R.H.G., 2011: Manual for Habitat and Vegetation Surveillance and Monitoring: Temperate, Mediterranean and Desert Biomes. First edition. Wageningen, Alterra report 2154 . 106 pp.
- Estreguil, Ch., Mouton, C., 2009: Measuring and reporting on forest landscape pattern, fragmentation and connectivity in Europe: methods and indicators. – JRC Scientific and Technical Reports. Office for Official Publications of the European Communities, Luxembourg, 68 pp.
- EEA: <http://www.eea.europa.eu/data-and-maps>
- Feranec, J., Cebecauer, T., O’ahel’, J., 2004a: Manual of computer aided visual interpretation of aerial B&W photographs. Bratislava: Institute of Geography, Slovak Academy of Sciences.
- Feranec, J., Cebecauer, T., O’ahel’, J., 2004b: Photo-to-photo interpretation manual. Bratislava: Institute of Geography, Slovak Academy of Sciences.
- Gerard, F., Petit,S., Smith, G., Thomson, A., Brown, N., Manchester, S., Wadsworth, R., Bugar, G., Halada, L., Bezák, P., Boltiziar, M., De Badts, E., Halabuk, A., Mojses, M., Petrovic, F., Gregor, M., Hazeu, G., Múcher, C.A., Wachowicz, M., Huitu, H., Tuominen, S., Köhler, R., Olschofsky, K., Ziese, H., Kolar, J., Sustera, J., Luque, S., Pino, J., Pons, X., Roda, F., Roscher, M., Feranec, J., 2010: Land cover change in Europe between 1950 and 2000 determined employing aerial photography. – Progress in Physical Geography 34, 2: 183–205
- Heymann, Y., Steenmans, C., Croisille, G. and Bossard, M., 1993: CORINE land cover project: technical guide. Luxembourg: European Commission, Environment, Nuclear Safety and Civil Protection.
- Martino, L., Fritz, M., 2008: New insight into land cover and land use in Europe. Land Use/Cover Area frame statistical Survey: Methodology and Tools. - Statistics in Focus, 33/2008, 8 pp.
- McGarigal, K., and B.J. Marks. 1995. FRAGSTATS: spatial pattern analysis program for quantifying landscape structure. Gen. Tech. Report PNW-GTR-351, USDA Forest Service, Pacific Northwest Research Station, Portland, OR, 122 pp.
- Metzger, M., Bunce, R.G.H., Jongman, R.H.G., Múcher, C.A., Watkins, J.W., 2005: A climatic stratification of the environment of Europe. - Global Ecology and Biogeography 14: 549–563

Annex 1: Corine Land Cover Legend

LEVEL1	LEVEL2	LEVEL 3
1. ARTIFICIAL SURFACES	1.1 Urban fabric	1.1.1 Continuous urban fabric
		1.1.2 Discontinuous urban fabric
	1.2 Industrial, commercial and transport units	1.2.1 Industrial or commercial units
		1.2.2 Road and rail networks and associated land
		1.2.3 Port areas
		1.2.4 Airports
	1.3 Mine, dump and construction sites	1.3.1 Mineral extraction sites
		1.3.2 Dump sites
		1.3.3 Construction sites
	1.4 Artificial, non-agricultural vegetated areas	1.4.1 Green urban areas
		1.4.2 Sport and leisure facilities
	2. AGRICULTURAL AREAS	2.1 Arable land
2.1.2 Permanently irrigated land		
2.1.3 Rice fields		
2.2 Permanent crops		2.2.1 Vineyards
		2.2.2 Fruit trees and berry plantations
		2.2.3 Olive groves
2.3 Pastures		2.3.1 Pastures
2.4 Heterogeneous agricultural areas		2.4.1 Annual crops associated with permanent crops
		2.4.2 Complex cultivation patterns
		2.4.3 Land principally occupied by agriculture, with significant areas of natural vegetation
		2.4.4 Agro-forestry areas
3. FOREST AND SEMI-NATURAL AREAS		3.1 Forests
	3.1.2 Coniferous forest	
	3.1.3 Mixed forest	
	3.2 Scrub and/or herbaceous vegetation associations	3.2.1 Natural grasslands
		3.2.2 Moors and heathland
		3.2.3 Sclerophyllous vegetation
		3.2.4 Transitional woodland-shrub
	3.3 Open spaces with little or no vegetation	3.3.1 Beaches, dunes, sands
		3.3.2 Bare rocks
		3.3.3 Sparsely vegetated areas
		3.3.4 Burnt areas
		3.3.5 Glaciers and perpetual snow
4. WETLANDS	4.1 Inland wetlands	4.1.1 Inland marshes
		4.1.2 Peat bogs
	4.2 Maritime wetlands	4.2.1 Salt marshes
		4.2.2 Salines
		4.2.3 Intertidal flats
5. WATER BODIES	5.1 Inland waters	5.1.1 Water courses
		5.1.2 Water bodies
	5.2 Marine waters	5.2.1 Coastal lagoons
		5.2.2 Estuaries
		5.2.3 Sea and ocean

Annex 2: General Habitat Categories – full list

General Habitat Category	Code
URBAN	URB
Artificial	ART
Non Vegetated	NON
Crops	VEG
Herbaceous	GRA
Woody vegetation	TRE
Artificial / Non-Vegetated	ART/NON
Artificial / Crops	ART/VEG
Artificial / Herbaceous	ART/GRA
Artificial / Woody	ART/TRE
Non Vegetated / Crops	NON/VEG
Non Vegetated / Herbaceous	NON/GRA
Non Vegetated / Woody	NON/TRE
Crops / Herbaceous	VEG/GRA
Crops / Woody	VEG/TRE
Herbaceous / Woody	GRA/TRE
CULTIVATED	CUL
Bare Ground	SPA
Herbaceous Crops	CRO
Woody Crops	WOC
Herbaceous/Woody Crops	CROWOC
SPARSELY VEGETATED	SPV
Sea	SEA
Tidal	TID
Aquatic	AQU
Ice and Snow	ICE
Terrestrial	TER
Sea/Tidal	SEA/TID
Sea/Ice	SEA/ICE
Sea/Terrestrial	SEA/TER
Tidal/Aquatic	TID/AQU
Tidal/ Terrestrial	TID/TER
Aquatic/Terrestrial	AQU/TER
TERRESTRIAL	TER
Bare Rock	ROC
Boulders	BOU
Stones	STO
Gravel	GRV
Sand	SAN
Earth, Mud	EAR
Rock/Boulders	ROC/BOU
Rock/Stones	ROC/STO
Rock/Gravel	ROC/GRV
Rock/Sand	ROC/SAN

ANNEX-9

D5.2.2. The impact of spatial and thematic detail on change detection

General Habitat Category	Code
Rock/Earth	ROC/EAR
Boulders/Stones	BOU/STO
Boulders/Gravel	BOU/GRV
Boulders/Sand	BOU/GRV
Boulders/Earth	BOU/EAR
Stones/Gravel	STO/GRV
Stones/Sand	STO/SAN
Stones/Earth	STO/EAR
Gravel/Sand	GRV/SAN
Gravel/Earth	GRV/EAR
Sand/Earth	SAN/EAR
HERBACEOUS WETLAND	HER
Submerged Hydrophytes	SHY
Emergent Hydrophytes	EHY
Helophytes	HEL
Submerged Hydrophytes / Emergent Hydrophytes	SHY/EHY
Submerged Hydrophytes / Helophytes	SHY/HEL
Emergent Hydrophytes / Helophytes	EHY/HEL
HERBACEOUS	HER
Leafy Hemicryptophytes	LHE
Caespitose Hemicryptophytes	CHE
Therophytes	THE
Geophytes	GEO
Chamaephytes	HCH
Cryptogams	CRY
Leafy Hemicryptophytes / Caespitose Hemicryptophytes	LHE/CHE
Leafy Hemicryptophytes / Therophytes	LHE/THE
Leafy Hemicryptophytes / Geophytes	LHE/GEO
Leafy Hemicryptophytes / Herbaceous Chamaephytes	LHE/HCH
Leafy Hemicryptophytes / Cryptogams	LHE/CRY
Caespitose Hemicryptophytes / Therophytes	CHE/THE
Caespitose Hemicryptophytes / Geophytes	CHE/GEO
Caespitose Hemicryptophytes / Herbaceous Chamaephytes	CHE/HCH
Caespitose Hemicryptophytes / Cryptogams	CHE/CRY
Therophytes / Geophytes	THE/GEO
Therophytes / Herbaceous Chamaephytes	THE/HCH
Therophytes / Cryptogams	THE/CRY
Geophytes / Herbaceous Chamaephytes	GEO/HCH
Geophytes / Cryptogams	GEO/CRY
Chamaephytes / Cryptogams	HCH/CRY
TREES/SHRUBS	TRS
Dwarf Chamaephytes Winter Deciduous	DCH/DEC
Dwarf Chamaephytes Evergreen	DCH/EVR
Dwarf Chamaephytes Coniferous	DCH/CON
Dwarf Chamaephytes Winter Deciduous / Evergreen	DCH/DEC/EVR
Dwarf Chamaephytes Winter Deciduous / Coniferous	DCH/DEC/CON
Dwarf Chamaephytes Evergreen / Coniferous	DCH/EVR/CON

ANNEX-9

D5.2.2. The impact of spatial and thematic detail on change detection

General Habitat Category	Code
Shrubby Chamaephytes Winter Deciduous	SCH/DEC
Shrubby Chamaephytes Evergreen	SCH/EVR
Shrubby Chamaephytes Coniferous	SCH/CON
Shrubby Chamaephytes Non-Leafy Evergreen	SCH/NLE
Shrubby Chamaephytes Summer Deciduous and/or Spiny Cushion	SCH/SUM
Shrubby Chamaephytes Winter Deciduous / Evergreen	SCH/DEC/EVR
Shrubby Chamaephytes Winter Deciduous / Coniferous	SCH/DEC/CON
Shrubby Chamaephytes Winter Deciduous / Non-Leafy Evergreen	SCH/DEC/NLE
Shrubby Chamaephytes Winter Deciduous / Summer Deciduous	SCH/DEC/SUM
Shrubby Chamaephytes Evergreen / Coniferous	SCH/ EVR/CON
Shrubby Chamaephytes Evergreen / Non-Leafy Evergreen	SCH/EVR/NLE
Shrubby Chamaephytes Evergreen / Summer Deciduous	SCH/EVR/SUM
Shrubby Chamaephytes Coniferous / Non-Leafy Evergreen	SCH/CON/NLE
Shrubby Chamaephytes Coniferous / Summer Deciduous	SCH/CON/SUM
Shrubby Chamaephytes Non-Leafy Evergreen / Summer Deciduous	SCH/NLE/SUM
Low Phanerophytes Winter Deciduous	LPH/DEC
Low Phanerophytes Evergreen	LPH/EVR
Low Phanerophytes Coniferous	LPH/CON
Low Phanerophytes Non-Leafy Evergreen	LPH/NLE
Low Phanerophytes Summer Deciduous	LPH/SUM
Low Phanerophytes Winter deciduous / Evergreen	LPH/DEC/EVR
Low Phanerophytes Winter deciduous / Coniferous	LPH/DEC/CON
Low Phanerophytes Winter deciduous / Non-Leafy Evergreen	LPH/DEC/NLE
Low Phanerophytes Winter Deciduous Summer	LPH/DEC/SUM
Low Phanerophytes Evergreen / Coniferous	LPH/ EVR/CON
Low Phanerophytes Evergreen / Non-Leafy Evergreen	LPH/EVR/NLE
Low Phanerophytes Evergreen / Summer Deciduous	LPH/EVR/SUM
Low Phanerophytes Coniferous / Non-Leafy Evergreen	LPH/CON/NLE
Low Phanerophytes Coniferous / Summer Deciduous	LPH/CON/SUM
Low Phanerophytes Non-Leafy Evergreen / Summer Deciduous	LPH/NLE/SUM
Mid Phanerophytes Winter Deciduous	MPH/DEC
Mid Phanerophytes Evergreen	MPH/EVR
Mid Phanerophytes Coniferous	MPH/CON
Mid Phanerophytes Non Leafy Evergreen	MPH/NLE
Mid Phanerophytes Summer Deciduous and/or Spiny Cushion	MPH/SUM
Mid Phanerophytes Winter Deciduous / Evergreen	MPH/DEC/EVR
Mid Phanerophytes Winter Deciduous / Coniferous	MPH/DEC/CON
Mid Phanerophytes Winter Deciduous / Non-Leafy Evergreen	MPH/DEC/NLE
Mid Phanerophytes Winter Deciduous / Summer Deciduous	MPH/DEC/SUM
Mid Phanerophytes Evergreen / Coniferous	MPH/EVR/CON
Mid Phanerophytes Evergreen / Non-Leafy Evergreen	MPH/EVR/NLE
Mid Phanerophytes Evergreen / Broadleaved / Summer Deciduous	MPH/EVR/SUM
Mid Phanerophytes Coniferous / Non-Leafy Evergreen	MPH/CON/NLE
Mid Phanerophytes Coniferous / Summer Deciduous	MPH/CON/SUM
Mid Phanerophytes Non-Leafy Evergreen / Summer Deciduous	MPH/NLE/SUM
Tall Phanerophytes Winter Deciduous	TPH/DEC
Tall Phanerophytes Evergreen	TPH/EVR

ANNEX-9

D5.2.2. The impact of spatial and thematic detail on change detection

General Habitat Category	Code
Tall Phanerophytes Coniferous	TPH/CON
Tall Phanerophytes Non-Leafy Evergreen	TPH/NLE
Tall Phanerophytes Summer Deciduous	TPH/SUM
Tall Phanerophytes Winter Deciduous / Evergreen	TPH/DEC/EVR
Tall Phanerophytes Winter Deciduous / Coniferous	TPH/DEC/CON
Tall Phanerophytes Winter Deciduous / Non-Leafy Evergreen	TPH/DEC/NLE
Tall Phanerophytes Evergreen / Coniferous	TPH/EVR/CON
Tall Phanerophytes Evergreen / Non-Leafy Evergreen	TPH/EVR/NLE
Tall Phanerophytes Evergreen / Summer Deciduous	TPH/EVR/SUM
Tall Phanerophytes Coniferous / Non-Leafy Evergreen	TPH/CON/NLE
Tall Phanerophytes Coniferous / Summer Deciduous	TPH/CON/SUM
Forest Phanerophytes Winter Deciduous	FPH/DEC
Forest Phanerophytes Evergreen	FPH/EVR
Forest Phanerophytes Coniferous	FPH/CON
Forest Phanerophytes Summer Deciduous	FPH/SUM
Forest Phanerophytes Winter Deciduous / Evergreen	FPH/DEC/EVR
Forest Phanerophytes Winter Deciduous / Coniferous	FPH/DEC/CON
Forest Phanerophytes Evergreen / Coniferous	FPH/EVR/CON
Forest Phanerophytes Evergreen / Summer Deciduous	FPH/EVR/SUM
Forest Phanerophytes Coniferous/ Summer Deciduous	FPH/CON/SUM
Mega Forest Phanerophytes Deciduous	GPH/DEC
Mega Forest Phanerophytes Evergreen	GPH/EVR
Mega Forest Phanerophytes Conifer	GPH/CON
Mega Forest Phanerophytes Summer deciduous	GPH/SUM
Mega Forest Phanerophytes Winter Deciduous / Evergreen	GPH/DEC/EVR
Mega Forest Phanerophytes Winter Deciduous / Coniferous	GPH/DEC/CON
Mega Forest Phanerophytes Evergreen / Coniferous	GPH/EVR/CON
Mega Forest Phanerophytes Evergreen /Summer Deciduous	GPH/EVR/SUM
Mega Forest Phanerophytes Conifer /Summer Deciduous	GPH/CON/SUM

Annex 3: Changes of GHC interpreted as processes (continues on the next page)

1949/2010	URB/ART	URB/ART/GRA	URB/ART/TRE	URB/ART/VEG	URB/GRA	URB/GRA/TRE	URB/NON	URB/NON/GRA	URB/TRE	URB/VEG	CUL/CRO	CUL/SPA	CUL/WOC	SPV/AQU	SPV/EAR	HER/HEL	HER/CHE	HER/LHE	HER/LHE/CHE	TRS/LPH/DEC	TRS/MPH/DEC	TRS/TPH/CON	TRS/TPH/DEC	TRS/TPH/DEC/CON	TRS/FPH/CON	TRS/FPH/DEC	TRS/FPH/DEC/CON	
URB/ART	DU				DU	DU	DU	DU	DU	DU	DU	DU	DU	Ir	DU	Ir	DU	DU	DU	DU	DU	DU	DU	DU	DU	DU	DU	
URB/ART/GRA	U	DU			DU	DU	DU	DU	DU	DU	DU	DU	DU	Ir	DU	Ir	DU	DU	DU	DU	DU	DU	DU	DU	DU	DU	DU	DU
URB/ART/TRE	U		DU		DU	DU	DU	DU	DU	DU	DU	DU	DU	Ir	DU	Ir	DU	DU	DU	DU	DU	DU	DU	DU	DU	DU	DU	DU
URB/ART/VEG	U			DU	DU	DU	DU	DU	DU	DU	DU	DU	DU	Ir	DU	Ir	DU	DU	DU	DU	DU	DU	DU	DU	DU	DU	DU	DU
URB/GRA	U	U	U	U	DU						DU	DU	DU	Ir	DU	Ir	DU	DU	DU	DU	DU	DU	DU	DU	DU	DU	DU	DU
URB/GRA/TRE	U	U	U	U		DU					DU	DU	DU	Ir	DU	Ir	DU	DU	DU	DU	DU	DU	DU	DU	DU	DU	DU	DU
URB/NON	U	U	U	U			DU				DU	DU	DU	Ir	DU	Ir	DU	DU	DU	DU	DU	DU	DU	DU	DU	DU	DU	DU
URB/NON/GRA	U	U	U	U				DU			DU	DU	DU	Ir	DU	Ir	DU	DU	DU	DU	DU	DU	DU	DU	DU	DU	DU	DU
URB/TRE	U	U	U	U					DU		DU	DU	DU	Ir	DU	Ir	DU	DU	DU	DU	DU	DU	DU	DU	DU	DU	DU	DU
URB/VEG	U	U	U	U						DU	DU	DU	DU	Ir	DU	Ir	DU	DU	DU	DU	DU	DU	DU	DU	DU	DU	DU	DU
CUL/CRO	U	U	U	U	U	U	U	U	U	U				Ir	Ab	Ab	Ex	Ex	Ex	Ab	Ab	Af	Af	Af	Af	Af	Af	Af
CUL/SPA	U	U	U	U	U	U	U	U	U	U		DU		Ir	Ab	Ab	Ex	Ex	Ex	Ab	Ab	Af	Af	Af	Af	Af	Af	Af
CUL/WOC	U	U	U	U	U	U	U	U	U	U	I		DU	Ir	Ab	Ab	Ex	Ex	Ex	Ab	Ab	Af	Af	Af	Af	Af	Af	Af
SPV/AQU	U	U	U	U	U	U	U	U	U	U	Dr	Dr	Dr		Dr	Dr	Dr	Dr	Dr	Dr	Dr	Dr	Dr	Dr	Dr	Dr	Dr	Dr
SPV/EAR	U	U	U	U	U	U	U	U	U	U	I	I	I	Ir		Ir	I	I	I		Af	Af	Af	Af	Af	Af	Af	Af
SPV/EAR/CHE	U	U	U	U	U	U	U	U	U	U	I	I	I	Ir		Ir	I	I	I		Af	Af	Af	Af	Af	Af	Af	Af
HER/TRE	U	U	U	U	U	U	U	U	U	U	I	I	I	Ir		Ir	I	I	Ol		Af	Af	Af	Af	Af	Af	Af	Af
HER/HEL	U	U	U	U	U	U	U	U	U	U	Dr	Dr	Dr	Ir	Dr		Dr	Dr	Dr	Dr	Dr	Dr	Dr	Dr	Dr	Dr	Dr	Dr
HER/CHE	U	U	U	U	U	U	U	U	U	U	I	I	I	Ir	Ab	Ir				Ab	Ab	Af	Af	Af	Af	Af	Af	Af
HER/LHE	U	U	U	U	U	U	U	U	U	U	I	I	I	Ir	Ab	Ir				Ab	Ab	Af	Af	Af	Af	Af	Af	Af
HER/LHE/CHE	U	U	U	U	U	U	U	U	U	U	I	I	I	Ir	Ab	Ir				Ab	Ab	Af	Af	Af	Af	Af	Af	Af
TRS/LPH/CON	U	U	U	U	U	U	U	U	U	U	De	De	De	Ir	De	De	I	I	I			Af	Af	Af	Af	Af	Af	Af
TRS/LPH/DEC	U	U	U	U	U	U	U	U	U	U	De	De	De	Ir	De	De	I	I	I			Af	Af	Af	Af	Af	Af	Af
TRS/MPH/CON	U	U	U	U	U	U	U	U	U	U	De	De	De	Ir	De	De	I	I	I			Af	Af	Af	Af	Af	Af	Af
TRS/MPH/DEC	U	U	U	U	U	U	U	U	U	U	De	De	De	Ir	De	De	I	I	I			Af	Af	Af	Af	Af	Af	Af
TRS/TPH/CON	U	U	U	U	U	U	U	U	U	U	De	De	De	Ir	De	De	I	I	I									

ANNEX-9

D5.2.2. The impact of spatial and thematic detail on change detection

1949/2010	URB/ART	URB/ART/GRA	URB/ART/TRE	URB/ART/VEG	URB/GRA	URB/GRA/TRE	URB/NON	URB/NON/GRA	URB/TRE	URB/VEG	CUL/CRO	CUL/SPA	CUL/WOC	SPV/AQU	SPV/EAR	HER/HEL	HER/CHE	HER/LHE	HER/LHE/CHE	TRS/LPH/DEC	TRS/MPH/DEC	TRS/TPH/CON	TRS/TPH/DEC	TRS/TPH/DEC/CON	TRS/FPH/CON	TRS/FPH/DEC	TRS/FPH/DEC/CON
TRS/TPH/DEC	U	U	U	U	U	U	U	U	U	U	De	De	De	Ir	De	De	I	I	I								
TRS/TPH/DEC/CON	U	U	U	U	U	U	U	U	U	U	De	De	De	Ir	De	De	I	I	I								
TRS/FPH/CON	U	U	U	U	U	U	U	U	U	U	De	De	De	Ir	De	De	I	I	I								
TRS/FPH/DEC	U	U	U	U	U	U	U	U	U	U	De	De	De	Ir	De	De	I	I	I								
TRS/FPH/DEC/CON	U	U	U	U	U	U	U	U	U	U	De	De	De	Ir	De	De	I	I	I								